RECENT ADVANCES IN DIAGNOSIS AND MANAGEMENT OF UROTHELIAL CARCINOMA

EDITED BY: Ja Hyeon Ku and Woonyoung Choi
PUBLISHED IN: Frontiers in Oncology

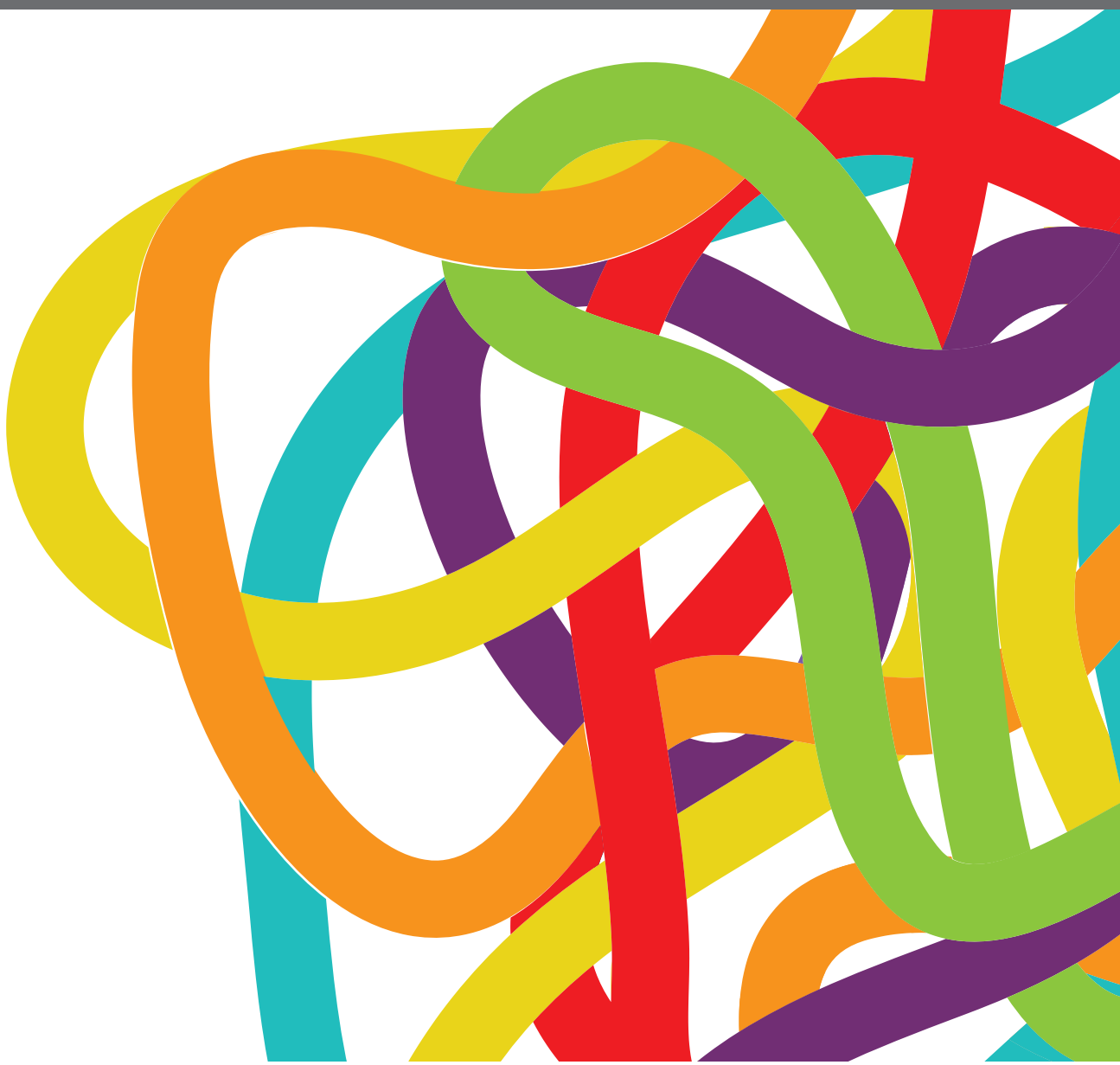

frontiers Research Topics

frontiers

ISSN 1664-8714
ISBN 978-2-88966-820-5
DOI 10.3389/978-2-88966-820-5

About Frontiers

Frontiers is more than just an open-access publisher of scholarly articles: it is a pioneering approach to the world of academia, radically improving the way scholarly research is managed. The grand vision of Frontiers is a world where all people have an equal opportunity to seek, share and generate knowledge. Frontiers provides immediate and permanent online open access to all its publications, but this alone is not enough to realize our grand goals.

Frontiers Journal Series

The Frontiers Journal Series is a multi-tier and interdisciplinary set of open-access, online journals, promising a paradigm shift from the current review, selection and dissemination processes in academic publishing. All Frontiers journals are driven by researchers for researchers; therefore, they constitute a service to the scholarly community. At the same time, the Frontiers Journal Series operates on a revolutionary invention, the tiered publishing system, initially addressing specific communities of scholars, and gradually climbing up to broader public understanding, thus serving the interests of the lay society, too.

Dedication to Quality

Each Frontiers article is a landmark of the highest quality, thanks to genuinely collaborative interactions between authors and review editors, who include some of the world's best academicians. Research must be certified by peers before entering a stream of knowledge that may eventually reach the public - and shape society; therefore, Frontiers only applies the most rigorous and unbiased reviews.
Frontiers revolutionizes research publishing by freely delivering the most outstanding research, evaluated with no bias from both the academic and social point of view. By applying the most advanced information technologies, Frontiers is catapulting scholarly publishing into a new generation.

What are Frontiers Research Topics?

Frontiers Research Topics are very popular trademarks of the Frontiers Journals Series: they are collections of at least ten articles, all centered on a particular subject. With their unique mix of varied contributions from Original Research to Review Articles, Frontiers Research Topics unify the most influential researchers, the latest key findings and historical advances in a hot research area! Find out more on how to host your own Frontiers Research Topic or contribute to one as an author by contacting the Frontiers Editorial Office: frontiersin.org/about/contact

RECENT ADVANCES IN DIAGNOSIS AND MANAGEMENT OF UROTHELIAL CARCINOMA

Topic Editors:
Ja Hyeon Ku, Seoul National University, South Korea
Woonyoung Choi, Johns Hopkins Medicine, United States

Citation: Ku, J. H., Choi, W., eds. (2021). Recent Advances in Diagnosis and Management of Urothelial Carcinoma. Lausanne: Frontiers Media SA.
doi: 10.3389/978-2-88966-820-5

Table of Contents

frontiers in Oncology

EDITORIAL
published: 29 March 2021
doi: 10.3389/fonc.2021.656974

Editorial: Recent Advances in Diagnosis and Management of Urothelial Carcinoma

Ja Hyeon Ku[1]* *and Woonyoung Choi*[2]

[1] Department of Urology, College of Medicine, Seoul National University, Seoul, South Korea, [2] The Johns Hopkins Hospital, Johns Hopkins Medicine, Baltimore, MD, United States

Keywords: urothelial carcinoma, bladder cancer, upper tract urothelial carcinoma, diagnosis, management

Editorial on the Research Topic

Recent Advances in Diagnosis and Management of Urothelial Carcinoma

INTRODUCTION

Bladder cancer (BC) is the fourth most common cancer in men in the United States. The American Cancer Society estimates that 80,470 new cases of BC will be diagnosed in the U.S. in 2019 and that 17,670 people will die of the disease (1). Upper urinary tract urothelial carcinoma (UC) is a rare urologic malignancy, accounting for only 5% to 10% of all UCs (2); however, it shows an aggressive nature with high recurrence and progression rates (3). UC remains a common malignancy with few treatment advances in the last 20 years despite its high prevalence.

This Research Topic aims to report on, but is not limited to, the latest results of current and emerging diagnostic and therapeutic modalities used in the treatment of UC as well as basic science.

Liu et al. explored the potential functions and mechanisms of miR-221 in the autophagy and tumorigenesis of BC. They demonstrated that the downregulation of miR-221 and HMGA1 mediates autophagy in BC, and both of them are valuable therapeutic targets for BC.

Zhu et al. studied the role of activity-dependent neuroprotective protein (ADNP) in BC. The authors found that ADNP is overexpressed in BC and promotes cancer growth partly through AKT pathways. These authors argued that ADNP is crucial in predicting the outcome of BC patients and may be a potential therapeutic target in BC.

Mencucci et al. analyzed alterations in E-cadherin expression and EMT-related events in BC, and identified Ephrin-B1 as a new marker of tumor aggressiveness.

To predict immunotherapeutic biomarkers and identify new therapeutic targets, Cao et al. screened and identified immune-related cells and genes in the tumor microenvironment of BC based on the Cancer Genome Atlas (TCGA) Database and bioinformatics. They described that his study provides a new approach for immunotherapy researchers to explore immunotherapeutic cells and gene targets for the first time.

To date, there are no markers can replace or even reduce the use of routine diagnostic tools (cytology and cystoscopy). Elamin et al. assessed the changes in blood gene expression in BC patients and to identified genes serving as biomarkers for BC diagnosis and progression

OPEN ACCESS

Edited and reviewed by:
Ronald M. Bukowski, Cleveland Clinic, United States

***Correspondence:**
Ja Hyeon Ku
kuuro70@snu.ac.kr

Specialty section:
This article was submitted to Genitourinary Oncology, a section of the journal Frontiers in Oncology

Received: *21 January 2021*
Accepted: *11 March 2021*
Published: *29 March 2021*

Citation:
Ku JH and Choi W (2021) Editorial: Recent Advances in Diagnosis and Management of Urothelial Carcinoma. Front. Oncol. 11:656974. doi: 10.3389/fonc.2021.656974

Song et al. investigated new urine biomarkers for high-grade BC and investigated how they promote high-grade BC progression and thus affect the prognosis based on large-scale sequencing data. They indicated that ECM1, CRYAB, CGNL1, and GPX3 are potential urine biomarkers and could be served as new diagnostic and prognostic makers for high-grade BC.

Hayashi et al. developed urinary cell-free DNA (cfDNA) analysis by droplet digital PCR (ddPCR) as a high-throughput and rapid assay for BC detection and prognosis. They reported that ddPCR analysis of urinary cfDNA is a simple and promising assay for the clinical setting, surpassing UroVysion for detection and prognosis determination in BC.

Zhu et al. described the genetics-based molecular subtyping of BC. These authors claimed molecular subtyping provides more abundant tumor biological information and is expected to assist or replace the traditional classification system in the future.

Jung et al. investigated the prognostic implications of immunohistochemical staining for CK14 and the transcriptional characteristics associated with CK14 expression in papillary non-muscle-invasive upper tract UC. Authors indicated that CK14-positive cancer is an aggressive subtype with basal/squamous-like (BASQ) molecular characteristics and dynamic proliferative activity. Authors in the same institute analyzed the association of immunohistochemically defined BASQ and non-BASQ subtypes with two PD-L1 assays in muscle-invasive BC (Kim et al.). They revealed that a high PD-L1 positive rate was significantly associated with the BASQ-subtype.

To predict lymph node metastasis preoperatively in patients with T1 high-grade UC, Ou et al. developed and validated a nomogram. This nomogram incorporated the tumor number, tumor size, lymphovascular invasion, fibrinogen, and monocyte-to-lymphocyte ratio, which showed favorable predictive accuracy for lymph node metastasis.

Fuhrman et al. took a first look at real world data of checkpoint inhibitors for the treatment of metastatic UC after chemotherapy since the data on real world experience is scarce. Authors demonstrated promising overall survival and a low incidence for severe adverse events.

Yuk and Ku summarized the role of various systemic inflammatory responses (SIRs) in the treatment of patients with UC. Authors reviewed various SIRs related to UC, including C-reactive protein, albumin-globulin ratio, albumin, Glasgow prognostic score, modified Glasgow prognostic score, neutrophil-lymphocyte ratio, and platelet-lymphocyte ratio.

Two meta-analyses were included in this Research Topic. Using the method of systematic review and meta-analysis, Liu et al. showed that thermal intravesical chemotherapy can reduce the recurrence rate without increasing incidence of adverse events in patients with non-muscle invasive BC, when compared with normal temperature intravesical chemotherapy. Wu et al. investigated the potential prognostic role of serum lactate dehydrogenase (LDH) in patients with UC and indicated that high level of pretreatment serum LDH was associated with inferior outcomes in patients with UC.

This Research Topic described the current status of information relevant to UC in a variety of basic and clinical categories. Our hope is that this Research Topic contributes to improve outcomes for UC.

AUTHOR CONTRIBUTIONS

JK and WC contributed to the writing and reviewing of this editorial. All authors contributed to the article and approved the submitted version.

REFERENCES

1. Siegel RL, Miller KD, Jemal A. Cancer statistics, 2018. *CA Cancer J Clin* (2018) 68:7–30. doi: 10.3322/caac.21442
2. Rouprêt M, Babjuk M, Compérat E, Zigeuner R, Sylvester RJ, Burger M, et al. European Association of Urology Guidelines on upper urinary tract urothelial carcinoma: 2017 update. *Eur Urol* (2018) 73:111–22. doi: 10.1016/j.eururo.2017.07.036
3. Petros FG. Epidemiology, clinical presentation, and evaluation of upper-tract urothelial carcinoma. *Transl Androl Urol* (2020) 9:1794–8. doi: 10.21037/tau.2019.11.22

Conflict of Interest: The authors declare that the research was conducted in the absence of any commercial or financial relationships that could be construed as a potential conflict of interest.

frontiers in Oncology

ORIGINAL RESEARCH
published: 09 January 2020
doi: 10.3389/fonc.2019.01484

A Specific Blood Signature Reveals Higher Levels of S100A12: A Potential Bladder Cancer Diagnostic Biomarker Along With Urinary Engrailed-2 Protein Detection

*Ayssar A. Elamin[1], Saskia Klunkelfuß[1], Susanne Kämpfer[1], Wulf Oehlmann[1], Matthias Stehr[1], Christopher Smith[2], Guy R. Simpson[2], Richard Morgan[3], Hardev Pandha[2] and Mahavir Singh[1]**

[1] LIONEX Diagnostics and Therapeutics GmbH, Brunswick, Germany, [2] Department of Oncology, Faculty of Health and Medical Sciences, University of Surrey, Guildford, United Kingdom, [3] Institute of Cancer Therapeutics, Faculty of Life Sciences, University of Bradford, Bradford, United Kingdom

OPEN ACCESS

Edited by:
Woonyoung Choi, The Johns Hopkins Hospital, Johns Hopkins Medicine, United States

Reviewed by:
Naveen Srinath Vasudev, University of Leeds, United Kingdom
Xin Xu, First Affiliated Hospital, College of Medicine, Zhejiang University, China

***Correspondence:**
Mahavir Singh
info@lionex.de

Specialty section:
This article was submitted to Genitourinary Oncology, a section of the journal Frontiers in Oncology

Received: *02 October 2019*
Accepted: *10 December 2019*
Published: *09 January 2020*

Citation:
Elamin AA, Klunkelfuß S, Kämpfer S, Oehlmann W, Stehr M, Smith C, Simpson GR, Morgan R, Pandha H and Singh M (2020) A Specific Blood Signature Reveals Higher Levels of S100A12: A Potential Bladder Cancer Diagnostic Biomarker Along With Urinary Engrailed-2 Protein Detection. Front. Oncol. 9:1484. doi: 10.3389/fonc.2019.01484

Urothelial carcinoma of the urinary bladder (UCB) or bladder cancer remains a major health problem with high morbidity and mortality rates, especially in the western world. UCB is also associated with the highest cost per patient. In recent years numerous markers have been evaluated for suitability in UCB detection and surveillance. However, to date none of these markers can replace or even reduce the use of routine tools (cytology and cystoscopy). Our current study described UCB's extensive expression profile and highlighted the variations with normal bladder tissue. Our data revealed that *JUP*, *PTGDR*, *KLRF1*, *MT-TC,* and *RNU6-135P* are associated with prognosis in patients with UCB. The microarray expression data identified also *S100A12*, *S100A8,* and *NAMPT* as potential UCB biomarkers. Pathway analysis revealed that natural killer cell mediated cytotoxicity is the most involved pathway. Our analysis showed that S100A12 protein may be useful as a biomarker for early UCB detection. Plasma S100A12 has been observed in patients with UCB with an overall sensitivity of 90.5% and a specificity of 75%. S100A12 is highly expressed preferably in high-grade and high-stage UCB. Furthermore, using a panel of more than hundred urine samples, a prototype lateral flow test for the transcription factor Engrailed-2 (EN2) also showed reasonable sensitivity (85%) and specificity (71%). Such findings provide confidence to further improve and refine the EN2 rapid test for use in clinical practice. In conclusion, S100A12 and EN2 have shown potential value as biomarker candidates for UCB patients. These results can speed up the discovery of biomarkers, improving diagnostic accuracy and may help the management of UCB.

Keywords: bladder, cancer, microarray, S100A12, plasma, EN2, lateral flow, urine

INTRODUCTION

Bladder cancer (- urothelial carcinoma of the urinary bladder, UCB) is the fourth and ninth most common cancer in men and women, respectively (1, 2). The global prevalence of UCB in Europe and North America has been estimated at 2.7 million (1, 2). UCB leads to significant mortality, with a survival rate of just 47–57% when linked to muscle-invasive disease (3). In addition to its effect on UCB patients, the disease poses a significant economic burden on healthcare systems with a mean treatment and monitoring cost of ∼200,000 USD per patient, rendering it the most expensive of all tumors to treat (4).

Generally, after haematuria, most patients experience a similar clinical process (5, 6). There were also several biomarkers used for diagnostic and monitoring purposes, but no marker has yet been shown to reduce the need for cystoscopy (6–11). This is especially problematic given the high recurrence rate, because of which lifelong surveillance is needed to detect any recurrence as early as possible (10). The development of reliable, non-invasive tests could therefore improve not only the UCB diagnosis itself but also the quality of life for patients with a disease history, and in this regard the detection of biomarkers in bodily fluids has shown a high potential (4–8, 10). The US Food and Drug Administration (FDA) has approved only a few urine-based tests, and there are currently no blood based tests (6, 10). Therefore, more novel biomarkers are urgently needed to detect UCB in general and especially in high-risk populations where the disease prevalence appears to be high (12, 13). The transcription factor Engrailed-2 (EN2) was previously shown to be a specific and potentially sensitive marker for bladder and prostate cancer (14–20). Using a standard ELISA method, we have previously shown that urinary EN2 could be detected and used as a UCB diagnosis biomarker, even in the early and non-invasive stages of the disease (15).

In addition to EN2, we have also investigated the diagnostic potential of S100 protein family members. The S100 family consists of 25 members, the expression of which have only been described in vertebrates (21). These proteins are characterized by a low molecular weight (9–13 kDa) and two Ca^{2+} binding sites in the form of EF-hands, one of which is unconventional (N-terminal) and has 100 times higher Ca^{2+} affinity than the canonical binding site in C-terminal. The S100 family members differ in length and sequence of the hinge region between the binding sites as well as the extension at C-terminal following the C-terminal EF-hand (22). The functions of S100 Proteins range from controlling protein phosphorylation, enzyme activity and transcription factors over the dynamics of cytoskeleton constituents, Ca^{2+} homeostasis and cell growth, and differentiation to an involvement in the inflammatory response (22, 23). They also mediate proinflammatory activity through binding the receptor for advanced glycation end-products (RAGE) on endothelial cells as well as recruitment of monocytes (23–27). Among the S100 group, S100A12, and S100P are unusual in that the coding gene can be found in the human genome but not in the mouse genome (28–30). S100A12 was recently shown to bind to CD36, a class B scavenger receptor, and this binding mediated translocation of CD36 to the membrane and where it can regulate lipid transport by direct interaction (31). Altered S100 protein levels have been linked to a variety of diseases, including cancer, neurodegenerative disorders, immune disorders, and inflammatory conditions (29). S100 genes also were shown to have roles in UCB progression and tumorigenesis (32). S100A8 and S100A9 were found to be increased in UCB patients and their expression related to stage and grade of the tumor (33). S100A12 RNA expression was shown to be increased in the tumors of transitional cell carcinoma (TCC) patients (34), and another study found that the urinary canine S100A8/A9 concentration relative ratio to S100A12 concentration maybe useful as a marker for canine TCC (35).

The main aim of this study was to assess the changes in blood gene expression in UCB patients and to identify genes serving as biomarkers for UCB diagnosis and progression. We identified elevated expression of the human S100A12 as a bladder cancer-enriched gene that is potentially a sensitive and specific diagnostic biomarker for UCB. Motivated by the fact that there is rapid growth in the demand for point-of-care tests based on lateral flow assays with high sensitivity, specificity and low cost, we also developed a lateral flow rapid test for detection of EN2 in urine samples. More than one hundred clinical samples were used to validate the rapid test which exhibited high sensitivity and specificity.

MATERIALS AND METHODS

Ethics Statement

All patients and healthy volunteers participating in the study gave written informed consent for sample donation and the collection. The protocol was approved by the local ethical committee of Faculty of Health and Medical Sciences, University of Surrey (Ref. 3/LO/0739).

Specimen, Data Collection, and Study Design

Patients selection was based on the following inclusion criteria: the patient was diagnosed with urothelial carcinoma of the urinary bladder (cystoscopic and histological evidence of Bladder Cancer). Recurrence-negative patients during monitoring have been defined as showing no cystoscopic or histological evidence of bladder cancer. Recurrence-positive patients during monitoring after treatment for *de novo* bladder cancer are identified as showing cystoscopic and histological evidence of bladder cancer. New patients were patients with bladder cancer without a history of UCB. Healthy volunteers had no previous history of bladder cancer or any other cancer (**Table 1**). The average age of positive cancer patients was 75.4 years and the average age of recurrence-negative patients was 70.5 years. The average age of new bladder cancer patients was 76.7 years and the average age of healthy volunteers was 68 years. Plasma from blood samples was collected from the same cohort of patients except 4 patients and one healthy volunteer were missed. Plasma was obtained using BD Vacutainer® Plasma Tubes (Heparin). Tubes containing 8–10 mL of blood were mixed for 30 min at RT and centrifuged at 1,600 g for 10 min at RT. Plasma was added to a fresh tube and centrifuged again at 1400 g for 10 min

TABLE 1 | Participant and specimen characteristics summary for microarray and plasma.

		No of TCC patient (transitional cell (urothelial) carcinoma)						Muscle invasive
Patients	**No of patients**	**Total No of TCC patient**	**G 1 pTa**	**G 2 pTa**	**G 2 pT1**	**G3 pTa**	**G3 T1**	**G3 T2a**
Risk group			**Low risk**	**Intermediate risk**	**Intermediate risk**	**High risk**	**High risk**	**High risk**
Recurrence-positive	17	15	4	9	1	0	1	2
Recurrence-negative	18	0	0	0	0	0	0	0
New Bladder Cancer patients	11	9	1	4	3	0	1	2
Health volunteers	29	0	0	0	0	0	0	0

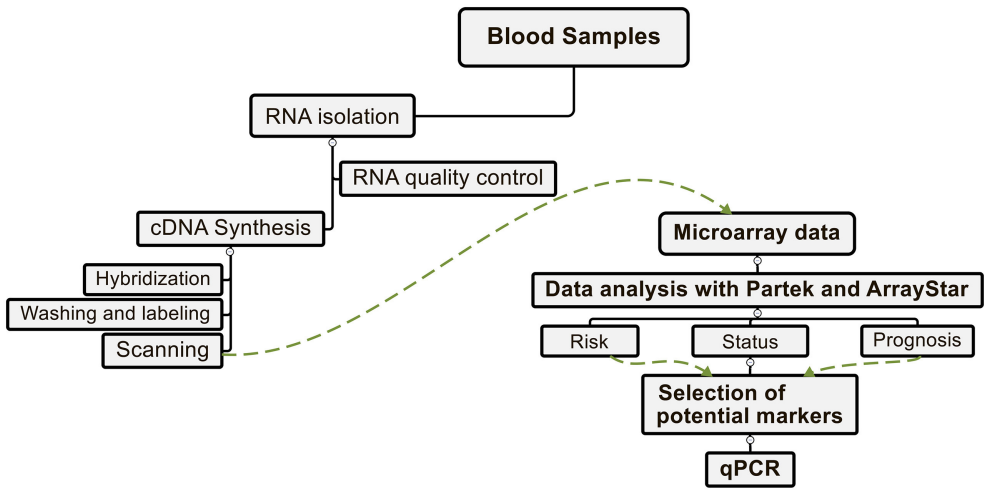

FIGURE 1 | Workflow scheme. From the blood samples, the total RNA was first isolated, subjected to a quality control, and converted to cDNA. Subsequently, after hybridization, labeling, and scanning of the microarray's chips were done. Data analysis in relation to the status of the disease, the risk group and the prognosis of the patients performed with two programs Partek® and ArrayStar®. From the differentially expressed genes the potential markers and verified their expression with a qPCR.

at RT. Plasma was then transferred to cryo-vials and stored at −80°C. Whole blood was collected using BD PAXgene™ Blood RNA Tubes. After the patient was bled the PAXgene™ Blood RNA Tubes were incubated at RT for 2 h and then chilled on ice for 10 min. The tubes were then incubated at −20°C overnight and then transferred to a storage box at −80°C. The workflow of the current microarray study from blood samples is illustrated in **Figure 1**. For EN2 detection using the lateral flow test, 62 urine samples from positive patients with cystoscopy and histological evidence of bladder cancer were used. This group in second analysis was grouped to different stages (Ta = 35 samples, T1 = 7, and T2-T3 = 9) and grades (36–38) (G1 = 11, G2 = 33, and G3 = 17) to evaluate the clinical sensitivity of the rapid test by tumor stage and grade. It was not possible to determine a stage (I) or a grade (II) for only one specimen. Forty-six negative samples were collected from healthy volunteers without any previous history and symptoms of bladder cancer or any other cancer. All urine samples were stored at −20°C.

RNA and Array Processing

Isolation of total RNA from clinical whole blood samples was performed according to the protocol of the manufacturer using the PAXgene® Blood RNA-Kit (PreAnalytiX). The total RNA was quantified by a Qubit™ Assay (Invitrogen) based on the manufacturer's standard protocols. The RNA integrity was determined by agarose gel electrophoresis. Using the manufacturer's protocol, the RNA samples were processed by the GeneChip® WT Plus Reagent Kit (Affymetrix). In summary, the total RNA firstly transcribed to double stranded cDNA, then transcribed to cRNA. The cRNA was then synthesized into single stranded cDNA, and then fragmented and biotinylated. Finally, the biotinylated single stranded cDNA has been hybridized onto the whole transcript Affymetrix® Human Gene 2.1 ST arrays, which cover a total of 40.716 annotated transcripts. The strips were then labeled using a streptavidin phycoerythrin conjugate, washed and scanned using the GeneAtlas® System (Affymetrix). Using the Command Console™ software (Affymetrix), the probe cell intensity data (CEL) files were created.

Gene and Exon Expression Analysis

For the gene and exon expression analysis, the CEL files are imported into Partek Genomics Suite version 6.6 (Partek Inc., St. Louis, MO, USA) and normalized using the Robust Multi-array Average (RMA) settings. A batch effects removal was performed to minimize the influence of external factors on the data using the tool in Partek software. The lists of differentially expressed genes were created using analysis of variance (ANOVA) with an fdr (false discovery rate) corrected $p < 0.05$ and a fold change >1.5 (39–42). The QC metrics table and QC graphical report was used to assess of the quality the experiments. The average linkage hierarchical clustering was conducted using spearman's correlation as a similarity matrix. Using the Partek Gene Ontology (GO) Enrichment tool, differentially expressed genes were grouped into functional categories ranked according to their *p*-values. Additionally, the differentially expressed genes were plotted in a volcano plot. The differentially expressed genes filter according to their fold-change were used for further functions analysis using Pathway analysis utilizing KEGG database (Partek® Pathway™). The significantly enriched pathways (using a Fisher's exact test) were determined and visualized by Partek Pathway. Enrichment Score (Fisher's Exact test) was used to sort the top enriched pathways out of differentially expressed genes). In the second analysis the CEL file were imported into DNASTAR® ArrayStar® (version 12.0) software (DNASTAR. Madison, WI) using again the RMA normalization. The lists of differentially expressed genes were generated using a Student's *t*-Test with a confidence interval >95% and a fold chance >1.5. Differentially expressed genes were grouped into their functional categories ranked according to their *p*-values using the Gene Ontology (GO) Enrichment tool. Unannotated and duplicate probe sets were removed from the lists.

Quantitative Real-Time PCR (qPCR)

Expression of selected genes was verified performing a quantitative PCR (qPCR) using the housekeeping gene GAPDH as reference. The primers used are described in **Table S1**. The analysis was performed in 20 µL containing each 10 µL 2x FastStart Essential DNA Master Mix (Roche), 2.4 µL H2O (PCR grade), 1.3 µL from 8 µM of the respective forward and reverse primers and 5 µL from 5 ng/µL template DNA. As template DNA the single strand cDNA generated for the microarrays was used. No template was included in the negative control. The following steps were included in the PCR Protocol: denaturation at 95°C followed by 9 touch-down cycles with the annealing temperature decreasing 1°C per cycle from 61° to 53°C. Then 31 cycles followed with 20 s at 95°C, 20 s at 53°C, and 20 s at 72°C. Finally, the DNA was denatured at 95°C for 20 s then at 55°C for 60 s and at 97°C for 1 s to generate the melting curves. The qPCR was performed on the Light Cycler® 96 (Roche) and the relative gene expression was determined using the Light Cycler® 96 software (version 1.1). Normalization was performed using the healthy samples as run calibrator. The normalized ratios were calculated as the ratio of the samples (target/reference) divided by the ratio of run calibrator (target/reference) using healthy samples.

Recombinant S100A12 Synthesis

The target gene was amplified using plasmid pENTR223.1 containing cDNA fragment of human S100A12 (Hölzel Diagnostika, Germany) as template and primers with the 5′-3′-sequences CGCGCGCCATGGTTACAAAACTTGAAGA GCATC and CGCGCGAAGCTTACTCTTTGTGGGTGTG GTAA, respectively. The ends of the PCR product were cleaved using FastDigest restriction endonucleases *NcoI* and *HindIII* (Thermo Scientific). By ligation to IPTG-inducible expression vector pLEXWO481 digested before with the same enzymes set the S100A12 reading frame was fused in frame with the N-terminal His-tag. *E. coli* DH5α (NEB) was transformed using ligation mixture. Afterwards plasmids were isolated from positive transformants and confirmed by sequencing. For production of biomass of recombinant *E. coli* DH5α cells we used previously described conditions (43).

Purification of His-Tagged Recombinant S100A12

All of the following purification steps were performed on ice or at 4°C. A cell pellet of 9.6 g in weight was thawed on ice and suspended in 20 mM Tris-HCl, 100 mM NaCl, pH 8.0 for 0.1 grams of cell pellet per mL. The cells were agitated gently for ∼1 h and homogenized (Miccra D-8). Cell lysis was performed by sonication (Bandelin Sonopuls GM 70, equipped with a UW 70 booster horn). Sonication was performed on ice for 5 × 30 sec. min. at 80% amplitude, with breaks between cycles to prevent warming of the mixture. The lysate was centrifuged at 27,000 × g, 8°C for 30 min to remove unlysed cells and insoluble cell debris. The supernatant (cleared lysate) was filtered through a fluted filter and the pellet was discarded. The following Ni-NTA affinity chromatography and gel filtration was performed with an Äkta prime plus chromatography system (GE Healthcare). The cleared lysate was applied on a column (HiScale 16, GE Healthcare) containing 5 mL Ni-NTA superflow resin that had been pre-equilibrated in 20 mM Tris-HCl, 100 mM NaCl, pH 8.0. After washing the column with 5 column volumes of 20 mM Tris-HCl, 100 mM NaCl, pH 8.0, a linear imidazole gradient from 0 to 1.0 M was applied over 20 column volumes. 2.5-mL fractions were collected over the gradient. The recombinant S100A12 protein was eluted with approximately 250 mM imidazole. Fractions containing S100A12 with a purity of 95% or higher were pooled. Buffer exchange against 10 mM NH_4HCO_3, pH 8.0 was performed using a prepacked desalting HiScale 16 column, filled with 40 mL Sephadex G-25 Medium (GE Healthcare). Protein-containing fractions were pooled and filtered through a 0.2 µM PES filter (Millex-GP, Merck Millipore).

Immunohistochemistry

The tissue array (Biomax BL802a), was subjected to deparaffinization in a series of alcohols and antigen retrieval in boiling in 0.01 M citrate buffer. Slides were blocked in normal horse serum (Vector Laboratories, UK) and Avidin/Biotin blocking kit (Vector Laboratories, UK). Sections were incubated with 1:1,000 S100A12 primary antibody (Sigma HPA002881) or PBS/0.1% BSA (negative control), before adding universal secondary antibody (Vector Laboratories, UK). ABC reagent (Vector Laboratories, UK) was dropped onto sections, followed

by DAB substrate solution (Vector Laboratories, UK). Sections were counterstained with haematoxylin (Vector Laboratories, UK), before being dehydrated in a series of alcohols, cover slipped with Vector mounting media (Vector Laboratories, UK), and visualized by light microscopy.

S100A12 Quantitation in Plasma Samples Using Biolayer Interferometry (BLI)

BLI experiments were conducted using an Octet QKe Instrument and high precision streptavidin biosensor (SAX), manufactured by ForteBio (Menlo Park, CA, USA). By measuring the light interference on the fiber optic sensor surface, and this is directly proportional to the thickness of the surface-bound molecules. Antibodies against S100A12 are chemically attached to the sensor surface using biotin-streptavidin interactions. Binding of S100A12 in the diluted plasma to the tethered antibodies results in surface thickening, which is monitored in real time. Purified rabbit anti-S100A12 polyclonal IgG were obtained from St. John's Laboratory (London, UK). Anti-S100A12 antibodies were biotinylated using Biotin Protein Labeling Kit (Roche) per the manufacturer's instructions. Sephadex G-25 columns (GE Healthcare) were then used to remove unreacted biotinylation reagent and buffer exchange into PBS. The biotinylated anti-S100A12 was immobilized on SAX biosensors at a single concentration of 10 μg/mL for 40 min (online). A solution of 0.1% BSA in PBS was used as blocking agent for 5 min to reduce the impact of non-specific binding to the surface of the sensor the sensors. The regeneration of the sensors was performed with 10 mM glycine buffer (pH = 2.2). All experiments were performed at 30°C with an agitation set at 1,000 rpm using solid black 96-well plates (Greiner Bio-One) with 10 min assay time (read time window) of dipping the prepared sensors in each well. The final volume for all the solutions was 200 μL/well. Different concentrations of recombinant S100A12 (from 1,857 ng/mL to 0 μg/mL) spiked in 1:12 diluted healthy human plasma to stablish the standard curve. The cohort plasma samples were all 1:12 diluted using PBS, pH 7.4 before applying in the assay plate. Data were analyzed with the Octet System Data Analysis software v7.1 (ForteBio, Menlo Park, CA, USA), and the S100A12 concentration in plasma samples was obtained using calibration curve which set up using the BLI response (binding rate) to the spiked rS100A12 concentration. Statistical analysis was performed using the GraphPad prism package. Unpaired *t*-test with Welch's correction was used to test the significance of differences between mean S100A12 concentrations in different patient groups. Receiver operator characteristics (ROC) curves were generated for the S100A12 and the unpaired *t*-test was used to test the area under the curve for significance. A combinatorial analysis of both S100A12 and EN2 as combi-biomarker and receiver operating characteristic (ROC) curve was carried out to using the CombiROC method (http://CombiROC.eu) (44).

Lateral Flow Prototype Development to Detect EN2 in Urine

The EN2 detection test is a membrane-based test for the qualitative detection of EN2 protein in urine through visual interpretation of color development in the test device. The test is based on the principle of Competitive Enzyme Immune Assay with a single test strip contained within a test cassette. This test strip consists of a proprietary EN2-binding IgG antibody (LIONEX GmbH) coupled to a colored conjugate, and a membrane with one test line and one control line. The test line contains EN2 recombinant protein (LIONEX GmbH), the control line consists of an antibody-binding protein (Rabbit anti mouse IgG, Thermo Scientific Fischer). The urine sample (60 μL) is pipetted into the sample well (S) followed by the diluent buffer (60 μL) 1 min later, the diluted sample passes through the conjugate and the EN2 protein in the sample binds to the conjugate. The EN2-conjugate complex migrates due to the capillary action to the site of the membrane where the recombinant EN2 protein is immobilized (test line) and the competition will take place between the sample EN2 and the coated EN2 on the membrane to the colored particle-labeled specific EN2 antibodies. If EN2 is absent or at a low concentration in the sample the labeled anti-EN2 attaches to the coated EN2 on the membrane and color intensity increases. If a high level of EN2 is in the sample, the EN2 is captured by the labeled anti-EN2 and the complex migrates through the membrane without attaching to the EN2 already coated on the test-region. In consequence the color of the test line appears weaker or no test line appears. The remaining complex migrates further across the membrane to the control zone ("C"). Again, a colored line appears, indicating that the test was performed correctly. After 15 min the intensity in the test line is compared to the Reference Scale card (**Figure S1**). For a positive result two colored lines appear in "T" and "C" or only one colored line appears in the control zone "C." The test line "T" can be absent or appears weak. The test will be considered as a negative result when two colored lines appear in "T" and "C"; the test line "T" appears strong. The test result is considered invalid if only the test line appears. The control line plays the role of an internal positive control for the lateral flow test and indicates successful test flow.

RESULTS

Gene Expression Analysis of UCB Patients

We carried out blood sample gene expression profiling in UCB cancer patient groups and/or in comparison to the healthy samples (**Table 1**). Comparing the expression profiles revealed a set of 14 differentially regulated genes. Of these, 5 were upregulated in bladder cancer while 9 were downregulated (**Figure 2**). The significance of regulated genes was set based on an fdr-corrected p- <0.05 and a fold change >1.5. This criterion was chosen to allow differentially expressed genes to simultaneously meet both fdr-controlled p-value and fold-change requirements even with arbitrarily small fold-changes (45–47). The most significantly upregulated genes included *RNASE2*, *RNU6-237P,* and *S100A12*, while the most significantly downregulated genes comprised *IGLV3-21*, *IGHV1-2,* and *TRAV13-1*.

Next, the UCB cohort patient samples were divided into different groups according to the prognosis of the patients. New UCB cases were labeled "new positive," in case of a recurrence

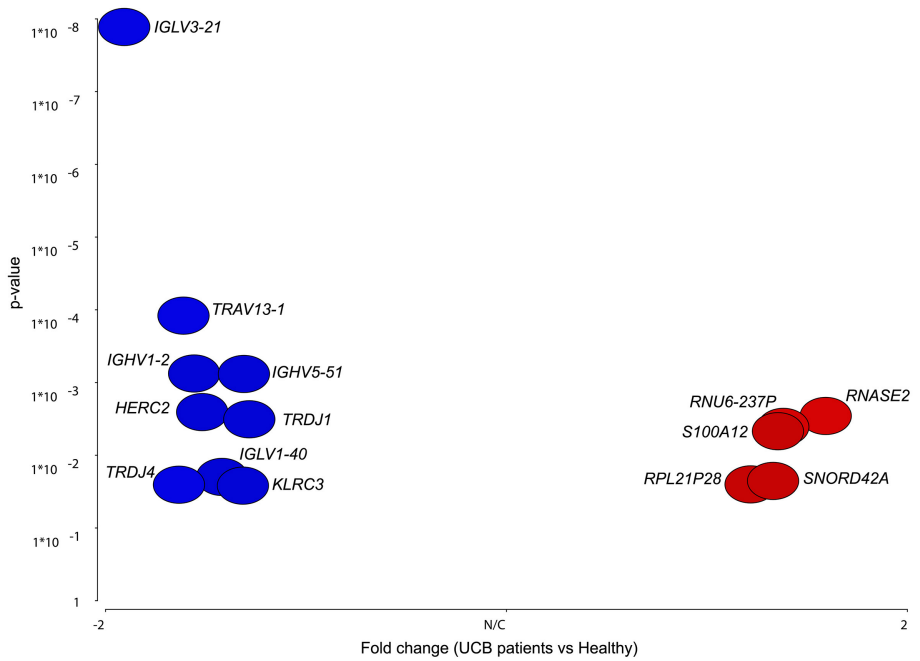

FIGURE 2 | Volcano plot of differentially expressed genes in UCB patients against probability. The figure shows data points of only differentially expressed genes lying above the fold change >1.5 and fdr-corrected p <0.05. Points to the right (red) represent candidates that were upregulated in UCB, while points to the left (blue) were downregulated.

of the disease within 5 years after treatment the samples were assigned to the group "recurrent" and patients with a bladder cancer history but negative at the time the sample was taken were placed in the "previously positive" group. The analysis of variance (ANOVA) was carried out between these groups and revealed a total of 127 differentially regulated genes (**Figure 3**). The comparison between the new positive samples and the negative control samples accounted for most of these genes showing 9 upregulated genes among the new positive patients and 38 downregulated genes. In total the comparison between the recurrent and the new positive samples revealed 38 differentially regulated genes. As shown in **Figure 3**, 18 of these genes were exclusively found in this comparison as possible prognostic markers to distinguish recurrent cases from new UCB cases (**Table S2**).

To identify a pattern of expression associated with UCB recurrence, we noticed that *PTGDR*, *KLRF1* and *MT-TC* genes were found to be significantly downregulated in new positive samples compared to negative and recurrent samples, while *RNU6-135P* was upregulated in new positive samples compared to previously positive and recurrent samples (**Table 2**). To further investigate the effects of risks groups in UCB, a model was built using healthy, previously positive patients and dividing samples into risk groups according to stage and grade of the disease as defined previously (48) (**Table 1**). ANOVA analysis carried out between these groups revealed no differentially regulated genes in the comparison between the low risk and negative samples. When comparing high risk and negative controls only the JUP gene was found to be significantly upregulated (fdr-corrected p <0.05; fold change >1.5) (**Table S3**), whilst a comparison of the intermediate risk group and negative controls revealed a total of 20 differentially regulated genes, 4 of which were upregulated while 16 were downregulated in the intermediate risk group. The most significantly upregulated genes were *RNU6-707P* and *S100A12*. *TRAJ29* and *TRAJ17* were the most significantly downregulated genes (**Table S3**).

Significantly enriched pathways are shown in **Table 3** from the Partek pathway analysis of UCB patients vs. healthy group sorted by the Enrichment Score (Fisher's exact test). This analysis showed that the genes significantly affected by bladder cancer are involved in the antigen processing and presentation, natural killer cell mediated cytotoxicity, and the ubiquitin mediated proteolysis pathways. By analyzing different combinations of the expression data in the prognostic and risk groups, the comparisons showed regulation in several pathways. It was noticeable, however, that the natural killer cell mediated cytotoxicity pathway repeatedly appeared in comparisons of different patient groups against the healthy and within the prognostic/risk groups (**Table 4**).

S100A12 Is UCB Relevant and Its Expression Is Elevated in High-Risk Patients

S100A12 was the only gene which was found to be differentially regulated in several analyses. This gene was significantly upregulated in the comparisons between patients and healthy volunteers as well as between intermediate risk patients and healthy volunteers. In both cases a fold change of 1.6 was

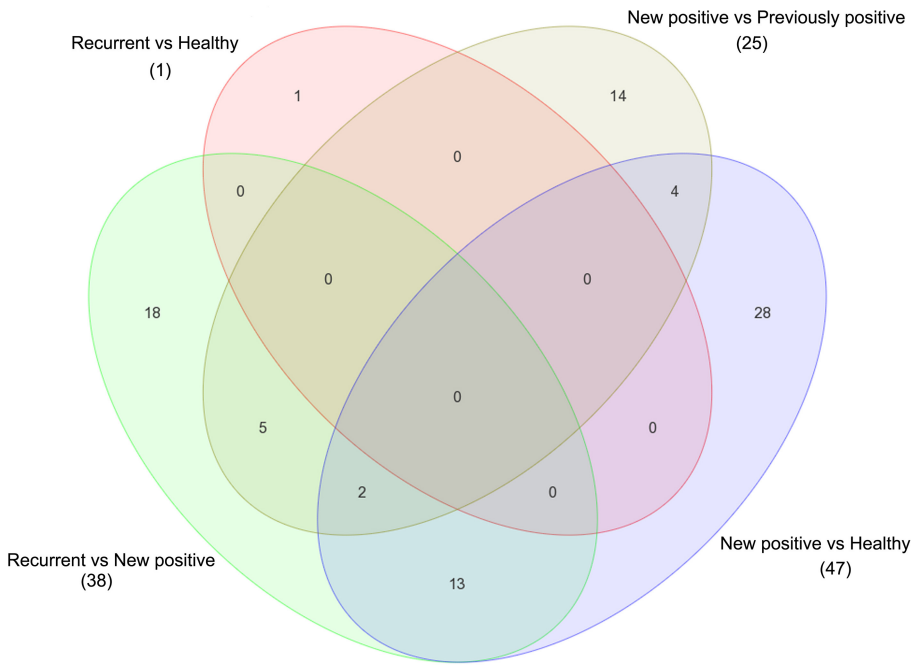

FIGURE 3 | Venn diagram shows the comparison and overlapping of regulated genes in different comparison of UCB according to their prognostic's groups. Significance was selected based on a fold change >1.5 with fdr-corrected p <0.05.

TABLE 2 | Selected potential prognostics biomarkers.

Gene	Fold change		
	New positive vs. Healthy	Recurrent vs. New positive	New positive vs. Previously positive
KLRF1 (Killer cell lectin-like receptor subfamily F member 1)	−1.87	1.97	−1.57
PTGDR (Prostaglandin D2 receptor)	−1.71	1.73	–
MT-TC (Mitochondrially encoded tRNA cysteine)	−1.91	2.04	−1.80
RNU6-135P (RNA, U6 small nuclear 135, pseudogene)	–	−2.65	1.98

TABLE 3 | The selected top pathways.

Pathway name	Database	Enrichment score	Enrichment p-value
Antigen processing and presentation	kegg	3.88856	0.0204748
Natural killer cell mediated cytotoxicity	kegg	3.29709	0.0369907
Ubiquitin mediated proteolysis	kegg	3.22929	0.0395856

The analysis done using Partek pathway and the data sorted by the Enrichment Score using Fisher's Exact test.

associated to this gene. In order to detect potential biomarkers, these results were checked by analyzing again the microarray raw data using DNAStar ArrayStar software. A student's t-test was applied with a confidence interval of 95% and a fold change >1.5. We identified a total of 141 differentially regulated genes, all of which were upregulated in UCB patients (**Table S4**). The top GO functions for disease effects were heavily weighted toward immune system process, regulation, inflammatory response, cellular homeostasis, and cell cycle genes. The list of the cellular homeostasis and cell cycle genes out of GO enrichment clustering was analyzed using ArrayStar, to gain insight into their biological relevance by supervised hierarchical clustering (**Figures S2**, **S3**). This analysis also showed a significant upregulation of *S100A12* in bladder cancer patients compared to healthy volunteers. In addition, the analysis of the different risk groups displayed an increasing expression pattern of *S100A12* among these groups (**Figure 4A**). The most significant upregulation was found among the high-risk patients with a fold change of 3.15. Among the intermediate risk patients, the fold change went down to 2.63 and dropped further to only 1.85 among the low risk patients. Interestingly, in the previously positive group *S100A12* also was found to be upregulated among prognosis group and higher than what seen in low risk individuals (2.15-fold) (**Figure 4A**). Moreover, in the ArrayStar analysis two genes from the S100 family were found to be differentially regulated in UCB patients compared to healthy volunteers. *S100A8* and *S100A9* were

TABLE 4 | Overview of genes differentially regulated in pathway analyses connected to natural killer cells.

Comparison	Pathway	Gene	Up or down regulated
Patient vs. healthy	Antigen processing and presentation	*KIR* (Killer-cell immunoglobulin-like receptor)	Down
	Natural killer cell mediated cytotoxicity	*NKG2C/E* (killer cell lectin-like receptor subfamily C)	Down
Intermediate risk vs. healthy	Antigen processing and presentation	*KIR* (Killer-cell immunoglobulin-like receptor)	Down
	Natural killer cell mediated cytotoxicity	*NKG2C/E* (killer cell lectin-like receptor subfamily C)	Down
New positive vs. healthy	Antigen processing and presentation	*CD8* (cluster of differentiation 8)	Down
	Antigen processing and presentation	*KIR* (Killer-cell immunoglobulin-like receptor)	Down
	Natural killer cell mediated cytotoxicity	*NKG2C/E* (killer cell lectin-like receptor subfamily C)	Down
	Natural killer cell mediated cytotoxicity	*NKG2D* (killer cell lectin-like receptor subfamily K)	Down
	Natural killer cell mediated cytotoxicity	*NKG2DL* (killer cell lectin-like receptor subfamily K ligand)	Down
	Natural killer cell mediated cytotoxicity	*Perforin*	Down
New positive vs. previously positive	Antigen processing and presentation	*KIR* (Killer-cell immunoglobulin-like receptor)	Down
	Antigen processing and presentation	*CD8* (cluster of differentiation 8)	Down
Recurrent vs. new positive	Natural killer cell mediated cytotoxicity	*Perforin*	Up

A pathway analysis was conducted with genes identified as differentially regulated by Partek.

significantly upregulated with a fold change of 1.92 and 1.56, respectively. Another interesting gene showing a significant upregulation in the ArrayStar analysis, which had not been found by Partek software analysis was *NAMPT* with a fold change of 2.05.

To validate the microarray analysis results, the expression of the following selected genes was checked by means of qPCR: *S100A12*, *S100A8*, *NAMPT*, *JUP*, *KLRF1,* and *PTGDR*. *S100A8* was included in this analysis, although this gene did not show a significant change among all groups in the ArrayStar analysis. However, it appears in the literature together with *S100A12* as a potential biomarker of bladder cancer in human and dogs (30, 32, 35). The real-time qPCR was performed using the housekeeping gene *GAPDH* as reference. The cDNA samples were pooled according to their risk and prognostic groups and the cDNA of each sample was present in equal amount. The analysis of the risk pools resulted in an expression pattern for *S100A12* similar to ArrayStar analysis and it could be confirmed that the expression increases with risk (**Figure 4B**). *S100A8* was shown to be 2-fold upregulated in intermediate risk patients, in high risk patients the fold change was 1.4 and in the low risk group it was 1.2. Surprisingly, *JUP* showed a significant increase among the high-risk group. Through the prognostic groups, the expression of *S100A12*, *S100A8,* and *NAMPT* in the new positive patients is significantly higher than that of previously positive and recurrent groups (**Figure 4C**). In contrast, the overexpression of *KLRF1* and *PTGDR* could not be demonstrated. Considering this profound microarray expression of *S100A12*, we screened a human bladder cancer tissue array using IHC with an antibody to S100A12. The tissue array contained, 1 squamous cell carcinoma, 2 adenocarcinoma, 57 cases of urothelial carcinoma, 10 normal bladder tissue and 10 each of adjacent normal bladder tissue, a single core per case. S100A12 appears to be mostly expressed in cells contained within the stroma and not in the tumor tissue. Necrotic areas showed non-specific staining which was therefore excluded from the analysis. **Figure S4** shows the percentages of cells that were positive for S100A12 in each tissue sample group (normal bladder, adjacent normal bladder tissue, T1-3 stage tumors and G1-3 grade tumors). The data shows normal bladder has the lowest expression of S100A12 and that expression rises with stage and grade. It is clear that the highest expression is present in the normal bladder tissue adjacent to the tumor suggesting immune infiltration by leukocytes (**Figure 5**).

Plasma S100A12 Concentrations Are Predictive for UCB

The presence of S100A12 in plasma would indicate that it could be a potential diagnostic marker, and indeed western blotting revealed that full-length protein S100A12 could be detected in the plasma of UCB patients (data not shown). To quantify the S100A12 concentration in UCB samples, the S100A12 was analyzed in plasma samples using biolayer interferometry (BLI). We assessed plasma S100A12 levels in the same microarray cohort of patients and controls. We found that S100A12 levels in those diagnosed with UCB were significantly higher than in healthy volunteers, $p < 0.0001$. The mean plasma S100A12 concentration in patients with UCB was 579.4 ± 30.58 ng/mL, whilst that for control subjects was 311.9 ± 37.03 ng/mL (**Figure 6A**). For test performance, the receiver operating characteristic (ROC) area under the curve (AUC) appeared to be 0.869 with standard error 0.05426 and $p < 0.0001$, with a sensitivity of 90.5% and a specificity of 75% (see **Figure 6B**). The ROC analysis study showed that the ideal cancer-vs.-control plasma concentration threshold of S100A12 was 350 ng/mL to maximize the test's sensitivity and specificity. The 95% confidence interval appeared to be 0.7627–0.9754. Higher risks and grade tumors (grades 2 and 3) were connected to higher mean plasma S100A12 concentrations (618.3 ± 60.59 ng/mL for grade 2 and 562.1 ± 88.46 ng/mL for grade 3) than grade 1 tumors (434.5 ± 38.92 ng/mL) (**Figure 7A**). Area under the ROC curve for high risk patients against healthy was 0.85 with standard error 0.067, and a 95% confidence interval of 0.7180 to 0.9820 (**Figure 7B**). Using an unpaired *t*-test the difference in the mean value for high risk vs. healthy was found

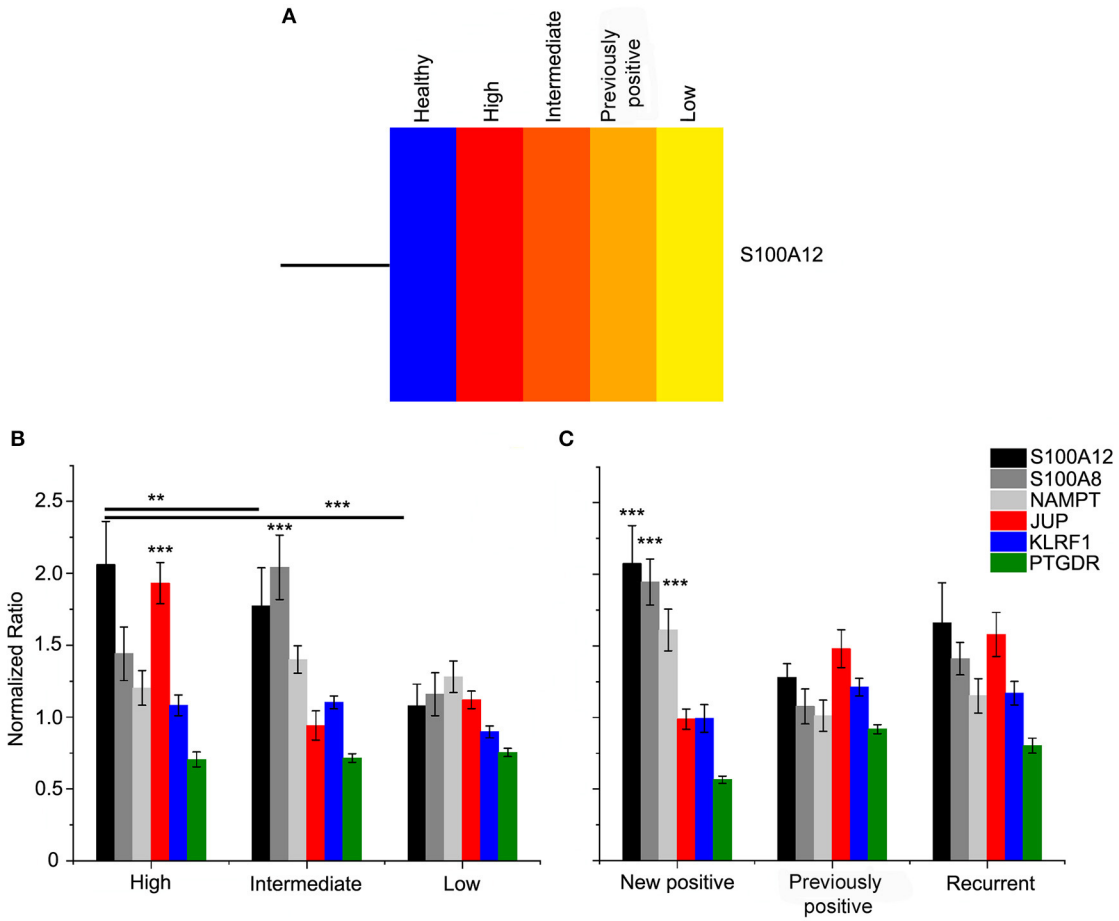

FIGURE 4 | (A) Heat map of S100A12 as most significantly regulated gene in risk groups. The gene and samples are clustered using Centroid linkage and Euclidean distance metric by ArrayStar software. The diagram row represents the S100A12 gene and the risk groups are presented in the columns. Color saturation reflects the differences in gene expression between tumor samples; red is higher than control group expression (blue). The intensity of color indicates the degree of gene expression from red (high expression fold) to yellow (low fold expression). qPCR validation of expression was done for selected genes. Normalized ratio ± ratio error determined for cDNA pools of study risk **(B)** and prognostic groups **(C)** by calculation of the ratio of the samples (target/reference) divided by the ratio of run calibrator (target/reference) (healthy samples). Quantitative PCR was performed for S100A12 (black), S100A8 (gray), NAMPT (light gray), JUP (red), KLRF1 (blue), and PTGDR (green). New positive, New UCB cases; recurrent, Cases with recurrence of the disease within 5 years after treatment; previously positive, Cases with UCB history but negative at the time the sample. $^{***}p \leq 0.0001$ and $^{**}p \leq 0.01$.

to be statistically significant ($p = 0.047$). The best cut-off in this comparison was found to be 306.9 ng/mL, which gives a sensitivity of 100% and specificity of 71.43%. The area under the curve rises when comparing intermediate risk group of cancer patients to healthy group (**Figure 7C**). The area under the ROC curve is 0.888 with standard error 0.052, $p < 0.001$ and a 95% confidence interval of 0.785 to 0.991. The *t*-test showed that difference in the mean value is statistically significant ($p \leq 0.0001$). The best cut-off in this contrast was found to be 372.7 ng/mL, which gives a sensitivity of 93.3% and specificity of 78.5%.

To test if S100A12 can also serve as a recurrence and prognostic marker, we performed a ROC analysis in the study prognostics groups. This indicated that the S100A12 concentration could differentiate the UCB-recurrent group and the previously positive group (recurrent-negative at sample) from the new positive UCB patients with an area under the curve of 0.793 and 0.725, respectively (**Figures 8A–C**). S100A12 also had diagnostic potential for new UCB patients in this analysis, with an area under the curve of 0.833 (**Figure 8D**), a standard error of 0.065 and p-value of 0.0002. The 95% confidence interval is 0.704–0.9623. Our results showed that best cut-off can be set to be 296.9 ng/mL, which gives a sensitivity of 100% and specificity of 71.43%.

EN2 Lateral Flow Prototype Validation

In this study, we also assessed the performance of the EN2 rapid test prototype in terms of the sensitivity and specificity of the test. This lateral flow based rapid test is intended as an *in-vitro*-diagnostic test, use of the device is not invasive. All urine samples are coded by an anonymous sample number. One hundred and seven coded urine sample, comprising sixty-two patients

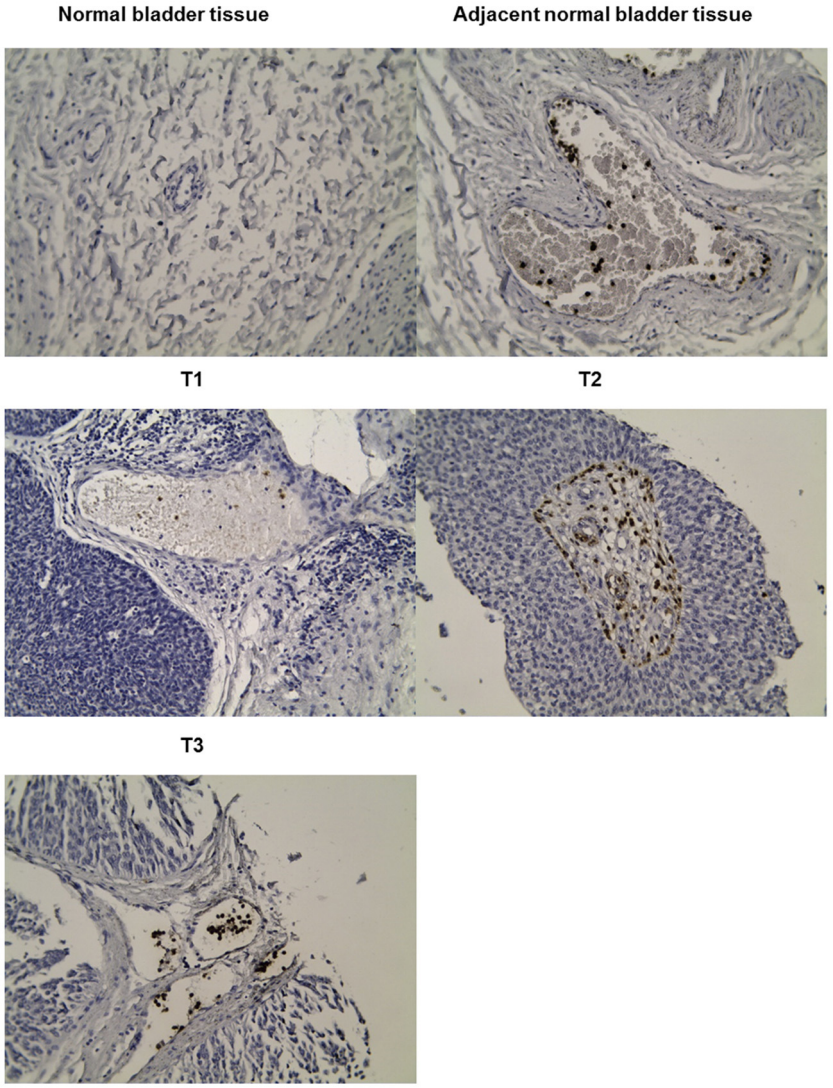

FIGURE 5 | Representative immunohistochemical analysis for tumors of T1, T2, and T3. IHC staining patterns for S100A12 in cancer tissue array tumors stained withanti-S100A12.

and forty-six healthy samples were used for the test prototypes. Each urine sample (60 μL) was applied without any dilution to the test device sample well. Sixty microliters of diluent buffer was applied after 120 s and the test was left for an additional 20 min. Test line intensity was interpreted visually after 15- and 20-min by comparing the test line to the reference card (**Figure S1**). Criterion for re-examination was that no control line appeared. The results of EN2 rapid tests were compared with cystoscopic and histological evidence of UCB. In the first analysis, the clinical specificity and sensitivity were determined for all positive samples with clinical evidence of bladder cancer vs. all negative samples from healthy volunteers with no history of non-bladder cancer, and active cancers (49–56). The results are summarized in **Table 5A**. In the second analysis, the clinical sensitivity of the lateral flow test was determined for tumor stage and grade using the positive urine specimens confirmed by means of cystoscopy and histology (62 positive samples). It was not possible to determine a stage or a grade for only one specimen. Stage and grade of the tumor, as well as its detection by the test, are presented in **Table 5B**. Overall, the sensitivity of the test was 85.48% (95% CI: 74.22–93.14%) at a specificity of 71.74% (95% CI: 56.54–84.01%). This result indicated that the test can potentially distinguish between cancer patients and healthy individuals.

DISCUSSION

Despite the large and growing list of candidate protein markers for UCB (5–11), as yet none have entered routine clinical use. There is no doubt that clinicians need better methods for individual patients' treatments and follow-up regimens selection.

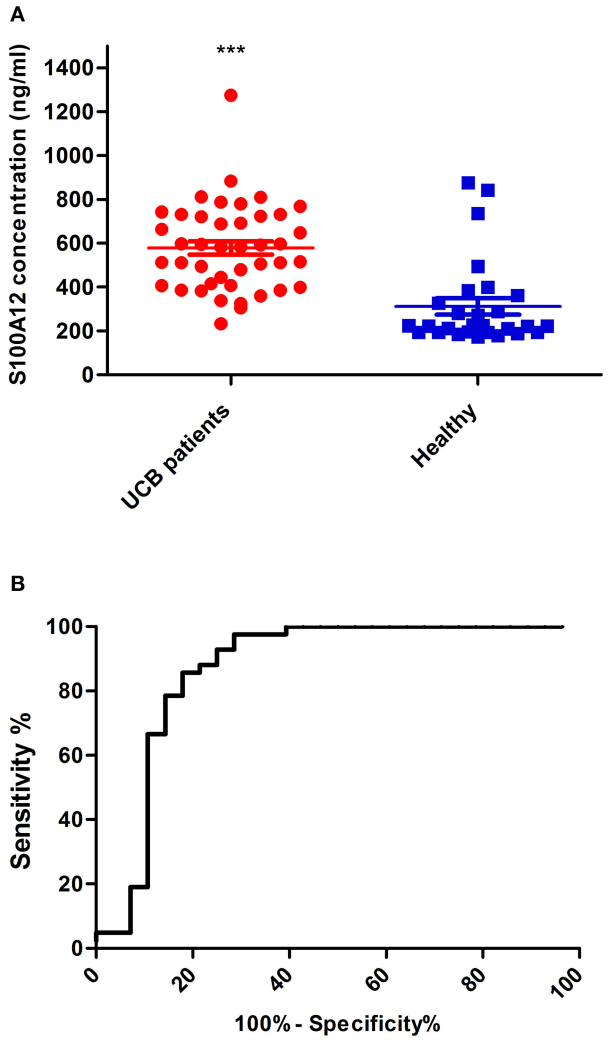

FIGURE 6 | Quantitation of S100A12 in UCB plasma samples by BLI **(A)**. The concentration of S100A12 was measured from plasma samples of each group (UCB patients and Healthy) using the biolayer interferometry (BLI). For each group, the mean value for of S100A12 is shown and standard error of the mean is represented by error bars. **(B)** A ROC analysis of plasma S100A12 concentrations in all UCB patients vs. all healthy in study cohort ***$p \leq 0.0001$.

It is therefore of paramount importance to recognize novel and validated UCB biomarkers for the detection of disease its recurrence. Using microarrays, different studies focused on UCB global expression profiling (11, 57–61). The main objective of the current study was identifying biomarkers that will predict the likelihood of progression in patients with high grade tumors. By utilizing gene expression profiling, we identified different genes as a signature biomarker for UCB and tumor progression using risk and prognostics grouping. In this study, we used a higher stringency fdr-corrected *p*-value score cut-off of <0.05 combined with batch effects removal to minimize any technical sources of variation (62–64).

Initial comparison was performed on UCB patients using the healthy group samples as control set. This comparison resulted in a set of 14 and 141 differentially regulated genes using Partek and ArrayStar software, respectively. Interestingly, *S100A12* is one of these genes which detected by both software packages to be upregulated in UCB patients (**Figure 2**). Further grouping of the UCB patients based on their prognosis resulted in a set of 127 differentially regulated genes. Among this multigene expression signature in UCB blood samples, we can identify new potential biomarkers for the prognosis of bladder cancer. *KLRF1* encodes the killer cell lectin-like receptor F member 1, which is expressed on human natural killer (NK) cells and different subsets of T cells (65). It has been shown that a ligand of this receptor (activation-induced C-type lectin, AICL) is produced by hematopoetic as well as non-hematopoetic tumor cells. Blocking of the interaction of AICL and *KLRF1* led to a partial inhibition of NK cell degranulation (65), showing that these receptors play a key role in the killing of tumor cell by NK-cells. A differential regulation of this gene in connection with cancer has not yet been described. Our microarray results however showed that the expression of this gene in new positive patients is considerably lower than in recurrent or previously positive bladder cancer patients. *PTGDR* is also expressed at a significantly lower level in new positive patients than in recurrent and previously positive patients. This gene codes for the prostaglandin D_2 receptor, which is expressed in different types of cells including immune system cells (NK cells, dendritic cells) as well as cells of central nervous system and smooth muscle cells (66). The receptor is activated by prostaglandin D_2 which is involved in a variety of different processes like sleep, regulation of body temperature and release of hormones. It also inhibits the aggregation of platelets and promotes relaxation of smooth muscles. It has been shown that the expression of this gene is downregulated in colorectal adenocarcinomas (67) and that there is a correlation between this dysregulation and disease progression as well as a hypermethylation of the gene. Similar hypermethylation patterns have also been demonstrated in the case of bladder cancer (68), although expression of the target gene itself was not been examined. As shown in **Table 2** our analysis also revealed other markers in UCB, including *MT-TC* (mitochondrial tRNA cysteine), and *RNU6-135P* (RNA U6 small nuclear 135). *MT-TC* has no known role in cancer, although the expression of tRNA genes in general as well *MT-TC* specifically are substantially upregulated in breast cancer (69). We therefore assumed that downregulation of each of the four genes or at least three of the four biomarkers, would be associated with a higher risk of disease recurrence as proposed for cell cycle regulators (p53, pRB, p21, and p27) (70–72). For searching expression patterns between UCB samples based on risk classification the UCB samples were sorted according to clinical risk score. Our microarray analysis revealed that *JUP* was significantly upregulated in samples of high-risk patients with high grade and stage bladder tumors. This gene encodes plakoglobin (also known as γ-catenin), which has been reported to be involved in the reduction of *in vitro* cell proliferation, invasion and migration (73) as well as the induction of apoptosis (74). Rieger-Christ et al. reported that *JUP* acts as bladder tumor suppressor and that silencing of this gene in late stage UCB is associated with tumor progression (75). It has however

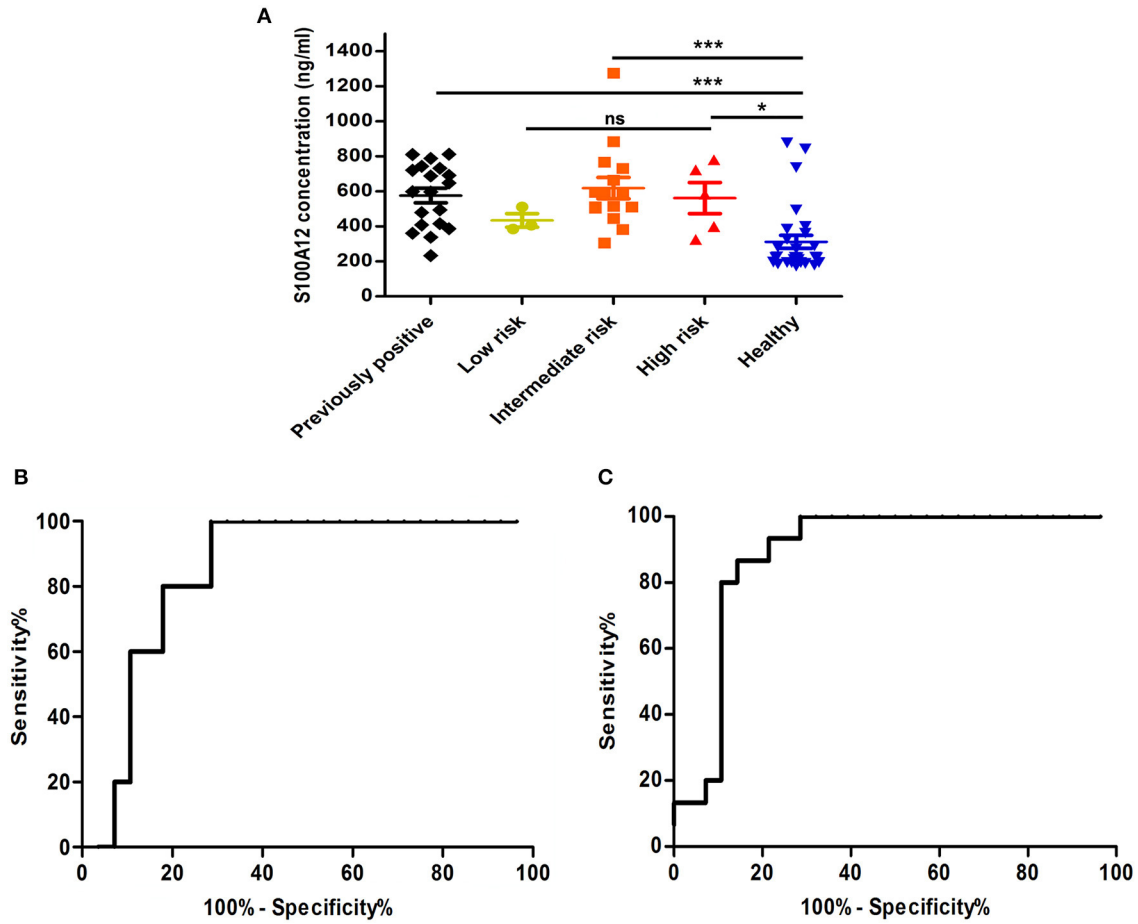

FIGURE 7 | A comparison of S100A12 concentrations in plasma within risk groups. **(A)** Comparison of plasma concentrations of S100A12 in UCB patients divided into groups according to their risk score. The standard error of the mean is represented by error bars. **(B)** A ROC analysis of plasma S100A12 concentrations in high risk UCB patients vs. healthy group. **(C)** A ROC analysis of plasma S100A12 concentrations of intermediate risk UCB patients against study healthy. ns, not significant, $^{***}p \leq 0.0001$ and $^{*}p \leq 0.05$.

also been demonstrated that wild-type and several mutated amino-terminal forms of plakoglobin transformed activity on RK3E epithelial cells (76). Importantly, when we carried out a pathway analysis for our dataset, the natural killer cell mediated cytotoxicity pathway appeared to play a major role in the context of UCB. This is supported by the finding that natural killer cells are essential for bladder cancer therapy with BCG (Bacillus Calmette-Guérin), which is frequently administered to treat superficial tumors (77). In addition, the genes listed in **Table 4** have been shown to be important for natural killer cell mediated cytotoxicity. The receptor *NKG2D* for example plays a central role in the recognition of UCB cells by natural killer cells (78). Here we show a downregulation of this receptor. This could be due to an interaction with its ligands, which has been shown previously to downregulate its expression (78). Furthermore, it has been shown that perforin, which was upregulated in this analysis, plays an important role in the lysis of UCB cells by natural killer cells (79).

Characteristics features of the effective biomarkers include cancer-specific expression and tumor release (15). One gene group that has been shown to have these properties recently is the S100 protein family and *S100A12* in particular (21, 24, 29, 32, 34, 35), which is expressed in different type of cancers. In our analysis, *S100A12* was found to be differentially expressed among UCB samples and between risk groups. For further analysis, *S100A12* and *S100A8* are selected based on the results of the UCB expression profile. A clear correlation between the qPCR assays and the microarray data is observed, especially in case of *S100A12* (**Figure 4**). Both genes were found to be independent and significant prognostic markers in UCB patients. Our results also indicated that, as molecular biomarkers, the products of these genes may be more robust in identifying the high mortality risk group than others with grade 1 disease, which may need to be confirmed with further investigations.

It is generally acknowledged that RNA expression level of a gene does not always reflect the protein expression level, and thus, in order to investigate the eligibility of S100A12 as candidate body fluids biomarker, we decided to measure the concentration of S100A12 in UCB plasma samples and compare it to healthy group samples. Using the 350 ng/mL as cut off,

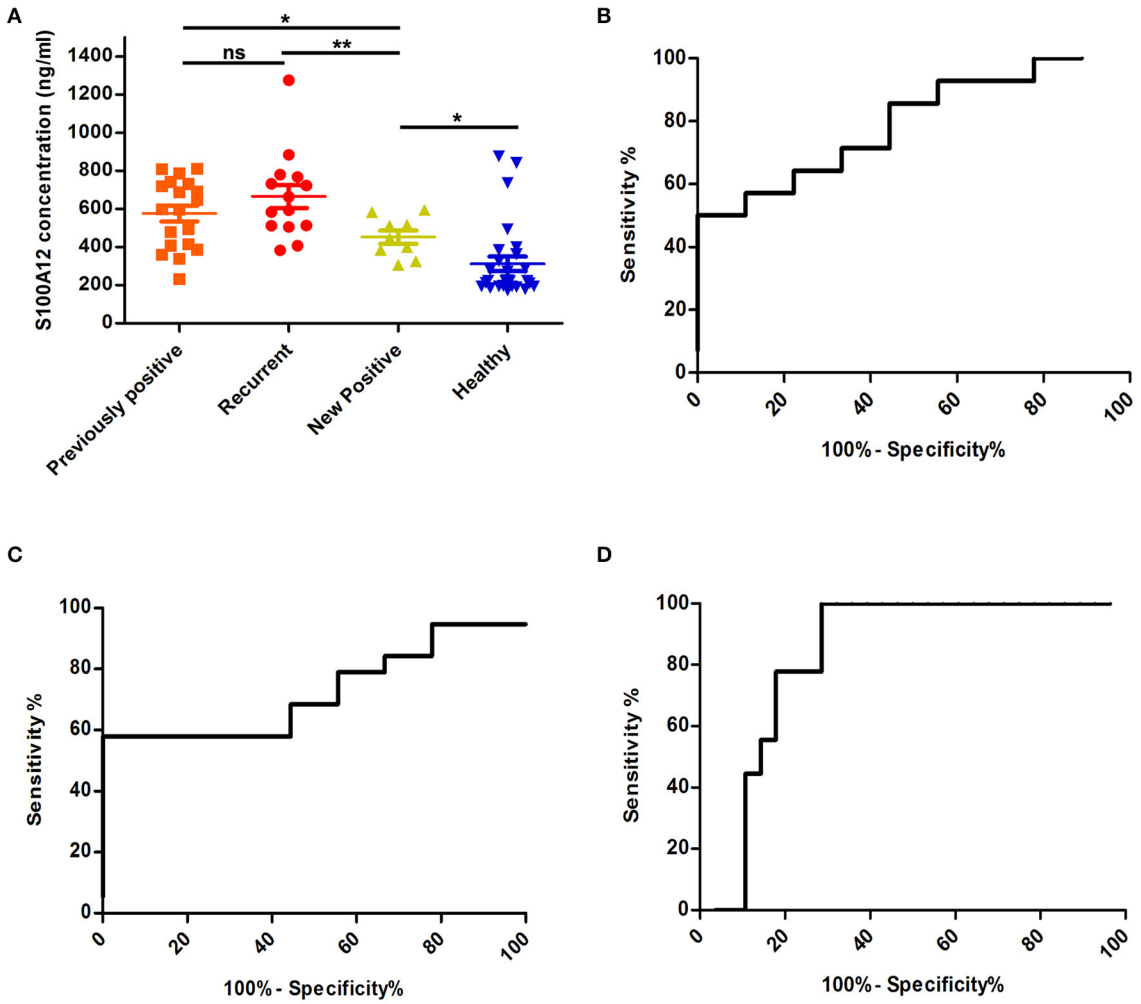

FIGURE 8 | Comparison of S100A12 levels in UCB patient prognostics groups. **(A)** S100A12 concentrations in plasma from UCB patients sorted according to their prognosis. The standard error of the mean is represented by error bars. **(B)** The ROC analysis of plasma S100A12 concentrations of recurrent group against new positive group of patients. The AUC is 0.793 with standard error 0.09, $p = 0.019$ and the 95% confidence interval appeared to be 0.6114–0.9759. The best cut-off in this comparison was found to be 512.5 ng/mL, giving 71.4% sensitivity and 66.67% specificity. **(C)** A ROC analysis of S100A12 concentration of previously positive group (recurrent-negative at sample) compared to new positive group. The AUC is 0.725 with standard error 0.095, $p = 0.058$ and 95% confidence interval between 0.5387 and 0.911. Using the cut-off 462.5 ng/mL the sensitivity is 68.4% and specificity will be 55.56%. **(D)** ROC analysis of S100A12 of new positive UCB patients against all healthy. ns, not significant, $^{**}p \leq 0.01$ and $^{*}p \leq 0.05$.

our data showed that S100A12 has a sensitivity of 90.5% and a specificity of 75%. The 100% specificity can be achieved using this assay, with a cut off at 880 ng/mL, the resulting sensitivity, however, is only 4.8%. The maximum sensitivity (100%) is obtained with a cut off at 230.4 ng/mL and this linked with 60% specificity. The cut off value of 350 ng/mL has been selected to provide high sensitivity and specificity. S100A12 could also serve as a prognostic biomarker because our study showed that overexpression of S100A12 protein was associated with recurrence of the disease as well as with high-grade/stage tumors (**Figures 7**, **8**). Unexpectedly, our data also showed that patients with a bladder cancer history, but negative at the sampling "previously positive" group had elevated S100A12 compared to healthy subjects. Similar findings were reported for p53 expression in 692 treated patients with advanced UCB (70) as well as for Ribonucleotide reductase subunit M1 (RRM1) as a prognostic biomarker (80). S100A12 has been shown to be secreted from important inflammatory effector cells such as neutrophils, monocytes, and macrophages (81) and is recognized as having a significant role in inflammation (24, 27, 30–32, 34, 35, 82, 83). A number of studies reported that S100A12 is markedly expressed in several inflammatory disorders such as atherosclerosis, inflammatory bowel disease, Kawasaki disease and coronary artery disease (84). S100B is expressed to differing degrees in normal tissue such as melanocytes, astrocytes, maturing oligodendrocytes, dendritic cells, Langerhans cells, kidney epithelial cells, and certain lymphocyte subpopulations (85). Similarly, S100A8/9 were reported to be markers for UCB

TABLE 5A | EN2 lateral flow test compared by results of clinical diagnosis (cystoscopy and histology method).

Group	Number of specimens	Clinical sensitivity in % (95% confidence interval)	Clinical specificity in % (95% confidence interval)
Patients (cystoscopy positive or/and evidence) (TP/FN)	62 (53/9)	85.48 (74.22–93.14)	71.74 (56.54–84.01)
Healthy (No history or evidence) (TN/FP)	46 (33/13)		

Exact Clopper-Pearson confidence intervals were used for sensitivity and specificity. TP, true positive; FN, false negative; TN, true negative and FP, false positive.

TABLE 5B | Sensitivity of EN2 lateral flow by tumor stage and grade.

Stage of the tumor (I)	Number of specimens	Clinical sensitivity in % (95% confidence interval)
Ta	35	88.57 (73.26–96.80)
T1	17	94.12 (71.31–99.85)
T2-T3	9	55.56 (21.20–86.30)
Grade of the tumor (II)	**Number of specimens**	**Clinical sensitivity in % (95% confidence interval)**
1	11	90.91 (58.72–99.77)
2	33	87.88 (71.80–96.60)
3	17	76.47 (50.10–93.19)

recurrence and grade, respectively (33). For UCB our data showed that expression of S100A12 found at the highest level in normal bladder tissue adjacent to the tumor and at much lower levels in tumor itself and normal tissue. S100A12 expression are in line with a previous study in squamous cell carcinoma (86). This could suggest that the S100A12 signal in bladder may be due to an immune infiltration by leukocytes such as neutrophils, monocytes, and macrophages. Further work is needed to be done to define which cell type is involved in this infiltrate. Although our samples are limited and S100A12 mRNA has been reported and linked with UCB (34, 87), to the best of our knowledge, the current study is the first to indicate an increased level of S100A12 protein and mRNA in human UCB and confirm the association between S100A12 and progression of UCB. Hence, we propose the utility of S100A12 at both the mRNA and protein level as a potential marker for UCB detection and prognosis. In addition, the relatively small number of samples had somewhat hampered our data. The current results do not comprise final validation of the clinical uses of S100A12 in UCB detection and prognosis. We have initiated further work using an additional validation cohort to confirm the diagnostic utility of this biomarker.

Additionally, we have previously shown that EN2 is also a potential diagnostic marker in UCB (15). Rapid lateral flow tests, although limited, might be more suitable for use due to their stability, user-friendliness, cost effectiveness, reproducibility, and rapidness (88). Our attempts to develop a prototype lateral flow for qualitative detection of EN2 in human urine were very successful. The sensitivity of the developed test was 85.48% (95% CI: 74.22–93.14%) at a specificity of 71.74% (95% CI: 56.54–84.01%). The test sensitivity varies depending on tumor stage and grade between 55.56 and 94.12% (**Table 5B**). Thus, the overall sensitivity and the specificity of the EN2 rapid test reaches or surpassed the sensitivity and specificity of many bladder cancer markers and tests on the market (38, 89, 90). These results may be useful for further development of a highly efficient non-invasive and improved diagnostic test. The usefulness of combing S100A12 and EN2 in a single test was assessed using CombiROC tool. Using a cut off 225 ng/mL as an optimal for S100A12, the area under curve (AUC) surprisingly rises to 0.93, and this associated with 92.5% sensitivity and a specificity of 83.1% (**Figure S5**). This shows that the combination of both biomarkers may equal or exceed the diagnostic performance of other promising UCB markers (5, 6, 8–10, 60, 72, 87).

In summary, in this study we examined the gene expression profile of UCB patients samples and identified several genes with potential diagnostic value by grouping and comparing UCB samples according to their clinical risk and prognostics scores. It is worth noting that these potential markers may be targets for protein and molecular-based clinical diagnosis and/or management of UCB. Importantly, our data revealed a significant increase in the UCB patients in the mRNA and protein expressions of S100A12. We conclude that S100A12 is an independent and significant prognostic marker for UCB patients, which may predict the disease course of UCB patients and facilitate the clinical management of this cancer. We report here also EN2 as diagnostic marker and its performance in prototype rapid lateral flow test assay looks very promising. The prototype performance encourages us to optimize the current design, perhaps adding S100A12 to improve sensitivity and specificity.

DATA AVAILABILITY STATEMENT

The datasets generated and analyzed in this study are available under the following link in the Gene Expression Omnibus (GEO): https://www.ncbi.nlm.nih.gov/geo/query/acc.cgi?acc=GSE138118.

ETHICS STATEMENT

The studies involving human participants were reviewed and approved by Faculty of Health and Medical Sciences, University of Surrey local ethical committee (Ref. 3/LO/0739). The patients/participants provided their written informed consent to participate in this study.

AUTHOR CONTRIBUTIONS

AE, SKl, SKä, WO, MSt, CS, and GS performed the laboratory experiments. AE, SKl, RM, HP, and MSi designed the study and wrote the paper. The final manuscript was reviewed and approved by all authors. All authors participated in data collection and analysis.

FUNDING

This work was funded by the Seventh Framework Program of the European Commission (FP7/ HEALTH.2012.1.2-1) under Grant Agreement No. 306157 (Project Name: DIPROMON).

ACKNOWLEDGMENTS

We would like to thank individuals in LIONEX GmbH and DIPROMON project consortium who provided suggestions or help, and all patients and healthy volunteers involved in the study.

SUPPLEMENTARY MATERIAL

The Supplementary Material for this article can be found online at: https://www.frontiersin.org/articles/10.3389/fonc.2019.01484/full#supplementary-material

REFERENCES

1. Ploeg M, Aben KK, Kiemeney LA. The present and future burden of urinary bladder cancer in the world. *World J Urol.* (2009) 27:289–93. doi: 10.1007/s00345-009-0383-3
2. Richters A, Aben KKH, Kiemeney L. The global burden of urinary bladder cancer: an update. *World J Urol.* (2019). doi: 10.1007/s00345-019-02984-4. [Epub ahead of print].
3. Jemal A, Siegel R, Xu J, Ward E. Cancer statistics, 2010. *CA Cancer J Clin.* (2010) 60:277–300. doi: 10.3322/caac.20073
4. Sievert KD, Amend B, Nagele U, Schilling D, Bedke J, Horstmann M, et al. Economic aspects of bladder cancer: what are the benefits and costs? *World J Urol.* (2009) 27:295–300. doi: 10.1007/s00345-009-0395-z
5. Herman MP, Svatek RS, Lotan Y, Karakiewizc PI, Shariat SF. Urine-based biomarkers for the early detection and surveillance of non-muscle invasive bladder cancer. *Minerva Urol Nefrol.* (2008) 60:217–35.
6. Budman LI, Kassouf W, Steinberg JR. Biomarkers for detection and surveillance of bladder cancer. *Can Urol Assoc J.* (2008) 2:212–21. doi: 10.5489/cuaj.600
7. Tilki D, Burger M, Dalbagni G, Grossman HB, Hakenberg OW, Palou J, et al. Urine markers for detection and surveillance of non-muscle-invasive bladder cancer. *Eur Urol.* (2011) 60:484–92. doi: 10.1016/j.eururo.2011.05.053
8. Riley RD, Sauerbrei W, Altman DG. Prognostic markers in cancer: the evolution of evidence from single studies to meta-analysis, and beyond. *Br J Cancer.* (2009) 100:1219–29. doi: 10.1038/sj.bjc.6604999
9. Parker J, Spiess PE. Current and emerging bladder cancer urinary biomarkers. *Sci World J.* (2011) 11:1103–12. doi: 10.1100/tsw.2011.104
10. Horstmann M. Currently available urine-based tumour markers in the detection of new and recurrent urothelial bladder cancer. *Nephrourol Mon.* (2012) 4:345–9. doi: 10.5812/numonthly.1841
11. Miremami J, Kyprianou N. The promise of novel molecular markers in bladder cancer. *Int J Mol Sci.* (2014) 15:23897–908. doi: 10.3390/ijms151223897
12. Lotan Y, Svatek RS, Sagalowsky AI. Should we screen for bladder cancer in a high-risk population?: a cost per life-year saved analysis. *Cancer.* (2006) 107:982–90. doi: 10.1002/cncr.22084
13. Zlotta AR, Roumeguere T, Kuk C, Alkhateeb S, Rorive S, Lemy A, et al. Select screening in a specific high-risk population of patients suggests a stage migration toward detection of non-muscle-invasive bladder cancer. *Eur Urol.* (2011) 59:1026–31. doi: 10.1016/j.eururo.2011.03.027
14. Morgan R, Boxall A, Bhatt A, Bailey M, Hindley R, Langley S, et al. Engrailed-2 (EN2): a tumor specific urinary biomarker for the early diagnosis of prostate cancer. *Clin Cancer Res.* (2011) 17:1090–8. doi: 10.1158/1078-0432.CCR-10-2410
15. Morgan R, Bryan RT, Javed S, Launchbury F, Zeegers MP, Cheng KK, et al. Expression of engrailed-2 (EN2) protein in bladder cancer and its potential utility as a urinary diagnostic biomarker. *Eur J Cancer.* (2013) 49:2214–22. doi: 10.1016/j.ejca.2013.01.019
16. Pandha H, Sorensen KD, Orntoft TF, Langley S, Hoyer S, Borre M, et al. Urinary engrailed-2 (EN2) levels predict tumour volume in men undergoing radical prostatectomy for prostate cancer. *BJU Int.* (2012) 110:E287–92. doi: 10.1111/j.1464-410X.2012.11208.x
17. Punia N, Primon M, Simpson GR, Pandha HS, Morgan R. Membrane insertion and secretion of the Engrailed-2 (EN2) transcription factor by prostate cancer cells may induce antiviral activity in the stroma. *Sci Rep.* (2019) 9:5138. doi: 10.1038/s41598-019-41678-0
18. Gómez-Gómez E, Jiménez-Vacas JM, Pedraza-Arévalo S, López-López F, Herrero-Aguayo V, Hormaechea-Agulla D, et al. Oncogenic role of secreted engrailed homeobox 2 (EN2) in prostate cancer. *J Clin Med.* (2019) 8:1400. doi: 10.3390/jcm8091400
19. Martin NL, Saba-El-Leil MK, Sadekova S, Meloche S, Sauvageau G. EN2 is a candidate oncogene in human breast cancer. *Oncogene.* (2005) 24:6890–901. doi: 10.1038/sj.onc.1208840
20. Konety BR, Getzenberg RH. Urine based markers of urological malignancy. *J Urol.* (2001) 165:600–11. doi: 10.1097/00005392-200102000-00081
21. Chen H, Xu C, Jin Q, Liu Z. S100 protein family in human cancer. *Am J Cancer Res.* (2014) 4:89–115.
22. Donato R. Intracellular and extracellular roles of S100 proteins. *Microsc Res Tech.* (2003) 60:540–51. doi: 10.1002/jemt.10296
23. Pietzsch J. S100 proteins in health and disease. *Amino Acids.* (2011) 41:755–60. doi: 10.1007/s00726-010-0816-8
24. Pietzsch J, Hoppmann S. Human S100A12: a novel key player in inflammation? *Amino Acids.* (2009) 36:381–9. doi: 10.1007/s00726-008-0097-7
25. Bierhaus A, Humpert PM, Morcos M, Wendt T, Chavakis T, Arnold B, et al. Understanding RAGE, the receptor for advanced glycation end products. *J Mol Med.* (2005) 83:876–86. doi: 10.1007/s00109-005-0688-7
26. Han SH, Kim YH, Mook-Jung I. RAGE: the beneficial and deleterious effects by diverse mechanisms of actions. *Mol Cells.* (2011) 31:91–7. doi: 10.1007/s10059-011-0030-x
27. Hofmann MA, Drury S, Fu C, Qu W, Taguchi A, Lu Y, et al. RAGE mediates a novel proinflammatory axis: a central cell surface receptor for S100/calgranulin polypeptides. *Cell.* (1999) 97:889–901. doi: 10.1016/S0092-8674(00)80801-6
28. Zimmer DB, Eubanks JO, Ramakrishnan D, Criscitiello MF. Evolution of the S100 family of calcium sensor proteins. *Cell Calcium.* (2013) 53:170–9. doi: 10.1016/j.ceca.2012.11.006
29. Bresnick AR, Weber DJ, Zimmer DB. S100 proteins in cancer. *Nat Rev Cancer.* (2015) 15:96–109. doi: 10.1038/nrc3893
30. Yao R, Davidson DD, Lopez-Beltran A, MacLennan GT, Montironi R, Cheng L. The S100 proteins for screening and prognostic grading of bladder cancer. *Histol Histopathol.* (2007) 22:1025–32. doi: 10.14670/HH-22.1025
31. Tondera C, Laube M, Pietzsch J. Insights into binding of S100 proteins to scavenger receptors: class B scavenger receptor CD36 binds S100A12 with high affinity. *Amino Acids.* (2016) 49:183–91. doi: 10.1007/s00726-016-2349-2
32. Yao R, Lopez-Beltran A, Maclennan GT, Montironi R, Eble JN, Cheng L. Expression of S100 protein family members in the pathogenesis of bladder tumors. *Anticancer Res.* (2007) 27:3051–8.

33. Minami S, Sato Y, Matsumoto T, Kageyama T, Kawashima Y, Yoshio K, et al. Proteomic study of sera from patients with bladder cancer: usefulness of S100A8 and S100A9 proteins. *Cancer Genom Proteom.* (2010) 7:181–9.
34. Khorramdelazad H, Bagheri V, Hassanshahi G, Karami H, Moogooei M, Zeinali M, et al. S100A12 and RAGE expression in human bladder transitional cell carcinoma: a role for the ligand/RAGE axis in tumor progression? *Asian Pac J Cancer Prev.* (2015) 16:2725–9. doi: 10.7314/APJCP.2015.16.7.2725
35. Heilmann RM, Wright ZM, Lanerie DJ, Suchodolski JS, Steiner JM. Measurement of urinary canine S100A8/A9 and S100A12 concentrations as candidate biomarkers of lower urinary tract neoplasia in dogs. *J Vet Diagn Invest.* (2014) 26:104–12. doi: 10.1177/1040638713516625
36. Kamat AM, Hahn NM, Efstathiou JA, Lerner SP, Malmström P-U, Choi W, et al. Bladder cancer. *Lancet.* (2016) 388:2796–810. doi: 10.1016/S0140-6736(16)30512-8
37. Babjuk M, Burger M, Comperat EM, Gontero P, Mostafid AH, Palou J, et al. European association of urology guidelines on non-muscle-invasive bladder cancer (TaT1 and carcinoma *in situ*) - 2019 update. *Eur Urol.* (2019) 76:639–57. doi: 10.1016/j.eururo.2019.08.016
38. Bellmunt J, Orsola A, Leow JJ, Wiegel T, De Santis M, Horwich A. Bladder cancer: ESMO practice guidelines for diagnosis, treatment and follow-up. *Ann Oncol.* (2014) 25(Suppl. 3):iii40–8. doi: 10.1093/annonc/mdu223
39. Bolstad BM, Irizarry RA, Astrand M, Speed TP. A comparison of normalization methods for high density oligonucleotide array data based on variance and bias. *Bioinformatics.* (2003) 19:185–93. doi: 10.1093/bioinformatics/19.2.185
40. Irizarry RA, Bolstad BM, Collin F, Cope LM, Hobbs B, Speed TP. Summaries of Affymetrix GeneChip probe level data. *Nucleic Acids Res.* (2003) 31:e15. doi: 10.1093/nar/gng015
41. Wu Z, Irizarry RA, Gentleman R, Martinez-Murillo F, Spencer F. A model based background adjustment for oligonucleotide expression arrays. *J Am Stat Assoc.* (2004) 99:909–17. doi: 10.1198/016214504000000683
42. Irizarry RA, Hobbs B, Collin F, Beazer-Barclay YD, Antonellis KJ, Scherf U, et al. Exploration, normalization, and summaries of high density oligonucleotide array probe level data. *Biostatistics.* (2003) 4:249–64. doi: 10.1093/biostatistics/4.2.249
43. Elamin AA, Stehr M, Oehlmann W, Singh M. The mycolyltransferase 85A, a putative drug target of Mycobacterium tuberculosis: development of a novel assay and quantification of glycolipid-status of the mycobacterial cell wall. *J Microbiol Methods.* (2009) 79:358–63. doi: 10.1016/j.mimet.2009.10.010
44. Mazzara S, Rossi RL, Grifantini R, Donizetti S, Abrignani S, Bombaci M. CombiROC: an interactive web tool for selecting accurate marker combinations of omics data. *Sci Rep.* (2017) 7:45477. doi: 10.1038/srep45477
45. Huggins CE, Domenighetti AA, Ritchie ME, Khalil N, Favaloro JM, Proietto J, et al. Functional and metabolic remodelling in GLUT4-deficient hearts confers hyper-responsiveness to substrate intervention. *J Mol Cell Cardiol.* (2008) 44:270–80. doi: 10.1016/j.yjmcc.2007.11.020
46. Patterson TA, Lobenhofer EK, Fulmer-Smentek SB, Collins PJ, Chu TM, Bao W, et al. Performance comparison of one-color and two-color platforms within the MicroArray quality control (MAQC) project. *Nat Biotechnol.* (2006) 24:1140–50. doi: 10.1038/nbt1242
47. Raouf A, Zhao Y, To K, Stingl J, Delaney A, Barbara M, et al. Transcriptome analysis of the normal human mammary cell commitment and differentiation process. *Cell Stem Cell.* (2008) 3:109–18. doi: 10.1016/j.stem.2008.05.018
48. Kulkarni JN, Bakshi GK. Staging of transitional cell carcinoma: has anything changed? *Ind J Urol.* (2008) 24:68–71. doi: 10.4103/0970-1591.38607
49. Altman DG, Bland JM. Diagnostic tests. 1: Sensitivity and specificity. *BMJ.* (1994) 308:1552.
50. Zweig MH, Campbell G. Receiver-operating characteristic (ROC) plots: a fundamental evaluation tool in clinical medicine. *Clin Chem.* (1993) 39:561–77.
51. Davidson M. The interpretation of diagnostic test: a primer for physiotherapists. *Aust J Physiother.* (2002) 48:227–32. doi: 10.1016/S0004-9514(14)60228-2
52. Baratloo A, Hosseini M, Negida A, El Ashal G. Part 1: simple definition and calculation of accuracy, sensitivity and specificity. *Emergency.* (2015) 3:48–9.
53. Gardner IA, Greiner M. Receiver-operating characteristic curves and likelihood ratios: improvements over traditional methods for the evaluation and application of veterinary clinical pathology tests. *Vet Clin Pathol.* (2006) 35:8–17. doi: 10.1111/j.1939-165X.2006.tb00082.x
54. Mercaldo ND, Lau KF, Zhou XH. Confidence intervals for predictive values with an emphasis to case-control studies. *Stat Med.* (2007) 26:2170–83. doi: 10.1002/sim.2677
55. Hanley JA, McNeil BJ. The meaning and use of the area under a receiver operating characteristic (ROC) curve. *Radiology.* (1982) 143:29–36. doi: 10.1148/radiology.143.1.7063747
56. Clopper CJ, Pearson ES. The use of confidence or fiducial limits illustrated in the case of the binomial. *Biometrika.* (1934) 26:404–13. doi: 10.1093/biomet/26.4.404
57. Sanchez-Carbayo M, Socci ND, Lozano J, Saint F, Cordon-Cardo C. Defining molecular profiles of poor outcome in patients with invasive bladder cancer using oligonucleotide microarrays. *J Clin Oncol.* (2006) 24:778–89. doi: 10.1200/JCO.2005.03.2375
58. Zaravinos A, Lambrou GI, Volanis D, Delakas D, Spandidos DA. Spotlight on differentially expressed genes in urinary bladder cancer. *PLoS ONE.* (2011) 6:e18255. doi: 10.1371/journal.pone.0018255
59. Dyrskjot L, Thykjaer T, Kruhoffer M, Jensen JL, Marcussen N, Hamilton-Dutoit S, et al. Identifying distinct classes of bladder carcinoma using microarrays. *Nat Genet.* (2003) 33:90–6. doi: 10.1038/ng1061
60. Zaravinos A, Lambrou GI, Boulalas I, Delakas D, Spandidos DA. Identification of common differentially expressed genes in urinary bladder cancer. *PLoS ONE.* (2011) 6:e18135. doi: 10.1371/journal.pone.0018135
61. Ying-Hao S, Qing Y, Lin-Hui W, Li G, Rong T, Kang Y, et al. Monitoring gene expression profile changes in bladder transitional cell carcinoma using cDNA microarray. *Urol Oncol.* (2002) 7:207–12. doi: 10.1016/S1078-1439(02)00192-8
62. McCarthy DJ, Smyth GK. Testing significance relative to a fold-change threshold is a TREAT. *Bioinformatics.* (2009) 25:765–71. doi: 10.1093/bioinformatics/btp053
63. Pusztai L, Hess KR. Clinical trial design for microarray predictive marker discovery and assessment. *Ann Oncol.* (2004) 15:1731–7. doi: 10.1093/annonc/mdh466
64. Luo J, Schumacher M, Scherer A, Sanoudou D, Megherbi D, Davison T, et al. A comparison of batch effect removal methods for enhancement of prediction performance using MAQC-II microarray gene expression data. *Pharmacogenomics J.* (2010) 10:278–91. doi: 10.1038/tpj.2010.57
65. Akatsuka A, Ito M, Yamauchi C, Ochiai A, Yamamoto K, Matsumoto N. Tumor cells of non-hematopoietic and hematopoietic origins express activation-induced C-type lectin, the ligand for killer cell lectin-like receptor F1. *Int Immunol.* (2010) 22:783–90. doi: 10.1093/intimm/dxq430
66. Garcia-Solaesa V, Sanz-Lozano C, Padron-Morales J, Hernandez-Hernandez L, Garcia-Sanchez A, Rivera-Reigada ML, et al. The prostaglandin D2 receptor (PTGDR) gene in asthma and allergic diseases. *Allergol Immunopathol.* (2014) 42:64–8. doi: 10.1016/j.aller.2012.12.002
67. Kalmar A, Peterfia B, Hollosi P, Galamb O, Spisak S, Wichmann B, et al. DNA hypermethylation and decreased mRNA expression of MAL, PRIMA1, PTGDR and SFRP1 in colorectal adenoma and cancer. *BMC Cancer.* (2015) 15:736. doi: 10.1186/s12885-015-1687-x
68. Reinert T, Modin C, Castano FM, Lamy P, Wojdacz TK, Hansen LL, et al. Comprehensive genome methylation analysis in bladder cancer: identification and validation of novel methylated genes and application of these as urinary tumor markers. *Clin Cancer Res.* (2011) 17:5582–92. doi: 10.1158/1078-0432.CCR-10-2659
69. Pavon-Eternod M, Gomes S, Geslain R, Dai Q, Rosner MR, Pan T. tRNA over-expression in breast cancer and functional consequences. *Nucleic Acids Res.* (2009) 37:7268–80. doi: 10.1093/nar/gkp787
70. Shariat SF, Bolenz C, Karakiewicz PI, Fradet Y, Ashfaq R, Bastian PJ, et al. p53 expression in patients with advanced urothelial cancer of the urinary bladder. *BJU Int.* (2010) 105:489–95. doi: 10.1111/j.1464-410X.2009.08742.x
71. Shariat SF, Chade DC, Karakiewicz PI, Ashfaq R, Isbarn H, Fradet Y, et al. Combination of multiple molecular markers can improve prognostication in patients with locally advanced and lymph node positive bladder cancer. *J Urol.* (2010) 183:68–75. doi: 10.1016/j.juro.2009.08.115

72. Ru Y, Dancik GM, Theodorescu D. Biomarkers for prognosis and treatment selection in advanced bladder cancer patients. *Curr Opin Urol.* (2011) 21:420–7. doi: 10.1097/MOU.0b013e32834956d6
73. Aktary Z, Pasdar M. Plakoglobin represses SATB1 expression and decreases *in vitro* proliferation, migration and invasion. *PLoS ONE.* (2013) 8:e78388. doi: 10.1371/journal.pone.0078388
74. Dusek RL, Godsel LM, Chen F, Strohecker AM, Getsios S, Harmon R, et al. Plakoglobin deficiency protects keratinocytes from apoptosis. *J Invest Dermatol.* (2007) 127:792–801. doi: 10.1038/sj.jid.5700615
75. Rieger-Christ KM, Ng L, Hanley RS, Durrani O, Ma H, Yee AS, et al. Restoration of plakoglobin expression in bladder carcinoma cell lines suppresses cell migration and tumorigenic potential. *Br J Cancer.* (2005) 92:2153–9. doi: 10.1038/sj.bjc.6602651
76. Kolligs FT, Kolligs B, Hajra KM, Hu G, Tani M, Cho KR, et al. Gamma-catenin is regulated by the APC tumor suppressor and its oncogenic activity is distinct from that of beta-catenin. *Genes Dev.* (2000) 14:1319–31.
77. Brandau S, Riemensberger J, Jacobsen M, Kemp D, Zhao W, Zhao X, et al. NK cells are essential for effective BCG immunotherapy. *Int J Cancer.* (2001) 92:697–702. doi: 10.1002/1097-0215(20010601)92:5<697::AID-IJC1245>3.0.CO;2-Z
78. Garcia-Cuesta EM, Lopez-Cobo S, Alvarez-Maestro M, Esteso G, Romera-Cardenas G, Rey M, et al. NKG2D is a key receptor for recognition of bladder cancer cells by IL-2-activated NK cells and BCG promotes NK cell activation. *Front Immunol.* (2015) 6:284. doi: 10.3389/fimmu.2015.00284
79. Brandau S, Suttmann H, Riemensberger J, Seitzer U, Arnold J, Durek C, et al. Perforin-mediated lysis of tumor cells by mycobacterium bovis bacillus calmette-guerin-activated killer cells. *Clin Cancer Res.* (2000) 6: 3729–38.
80. Harshman LC, Bepler G, Zheng Z, Higgins JP, Allen GI, Srinivas S. Ribonucleotide reductase subunit M1 expression in resectable, muscle-invasive urothelial cancer correlates with survival in younger patients. *BJU Int.* (2010) 106:1805–11. doi: 10.1111/j.1464-410X.2010.09327.x
81. Yndestad A, Damas JK, Oie E, Ueland T, Gullestad L, Aukrust P. Role of inflammation in the progression of heart failure. *Curr Cardiol Rep.* (2007) 9:236–41. doi: 10.1007/BF02938356
82. Realegeno S, Kelly-Scumpia KM, Dang AT, Lu J, Teles R, Liu PT, et al. S100A12 is part of the antimicrobial network against mycobacterium leprae in human macrophages. *PLoS Pathog.* (2016) 12:e1005705. doi: 10.1371/journal.ppat.1005705
83. Kontochristopoulos GJ, Stavropoulos PG, Krasagakis K, Goerdt S, Zouboulis CC. Differentiation between merkel cell carcinoma and malignant melanoma: an immunohistochemical study. *Dermatology.* (2000) 201:123–6. doi: 10.1159/000018454
84. He YY, Yan W, Liu CL, Li X, Li RJ, Mu Y, et al. Usefulness of S100A12 as a prognostic biomarker for adverse events in patients with heart failure. *Clin Biochem.* (2015) 48:329–33. doi: 10.1016/j.clinbiochem.2014.11.016
85. Donato R. S100: a multigenic family of calcium-modulated proteins of the EF-hand type with intracellular and extracellular functional roles. *Int J Biochem Cell Biol.* (2001) 33:637–68. doi: 10.1016/S1357-2725(01)00046-2
86. Funk S, Mark R, Bayo P, Flechtenmacher C, Grabe N, Angel P, et al. High S100A8 and S100A12 protein expression is a favorable prognostic factor for survival of oropharyngeal squamous cell carcinoma. *Int J Cancer.* (2015) 136:2037–46. doi: 10.1002/ijc.29262
87. Lee SJ, Lee EJ, Kim SK, Jeong P, Cho YH, Yun SJ, et al. Identification of pro-inflammatory cytokines associated with muscle invasive bladder cancer; the roles of IL-5, IL-20, and IL-28A. *PLoS ONE.* (2012) 7:e40267. doi: 10.1371/journal.pone.0040267
88. Koczula KM, Gallotta A. Lateral flow assays. *Essays Biochem.* (2016) 60:111–20. doi: 10.1042/EBC20150012
89. Abd El Gawad IA, Moussa HS, Nasr MI, El Gemae EH, Masooud AM, Ibrahim IK, et al. Comparative study of NMP-22, telomerase, and BTA in the detection of bladder cancer. *J Egypt Natl Cancer Inst.* (2005) 17:193–202.
90. Brown FM. Urine cytology. It is still the gold standard for screening? *Urol Clin North Am.* (2000) 27:25–37. doi: 10.1016/S0094-0143(05)70231-7

Conflict of Interest: AE, SKä, WO, MSt, and MSi are employed by LIONEX GmbH. SKl was employed during DIPROMON project by LIONEX GmbH. For uses of described biomarkers in this article, AE, SKl, WO, MSt, and MSi have filed a patent application No.: 16203695.8 and patent No.: 1405 under the title: Novel Human Bladder cancer Biomarkers and their Diagnostics use.

The remaining authors declare that the research was conducted in the absence of any commercial or financial relationships that could be construed as a potential conflict of interest.

frontiers in Oncology

ORIGINAL RESEARCH
published: 15 January 2020
doi: 10.3389/fonc.2019.01533

Screening and Identifying Immune-Related Cells and Genes in the Tumor Microenvironment of Bladder Urothelial Carcinoma: Based on TCGA Database and Bioinformatics

Jinlong Cao[1,2], *Xin Yang*[3], *Jianpeng Li*[1,2], *Hao Wu*[1,2], *Pan Li*[1,2], *Zhiqiang Yao*[1,2], *Zhichun Dong*[1,2] *and Junqiang Tian*[2]*

[1] Department of Urology, The Second Hospital of Lanzhou University, Lanzhou, China, [2] Key Laboratory of Urological Diseases of Gansu Provincial, Lanzhou, China, [3] Reproductive Medicine Center, The Second Hospital of Lanzhou University, Lanzhou, China

OPEN ACCESS

Edited by:
Woonyoung Choi,
The Johns Hopkins Hospital, Johns Hopkins Medicine, United States

Reviewed by:
Rasha Abu Eid,
University of Aberdeen, United Kingdom
Daniele Baiz,
University of Plymouth, United Kingdom

***Correspondence:**
Junqiang Tian
ery_tianjq@lzu.edu.cn

Specialty section:
This article was submitted to Genitourinary Oncology, a section of the journal Frontiers in Oncology

Received: 24 September 2019
Accepted: 19 December 2019
Published: 15 January 2020

Citation:
Cao J, Yang X, Li J, Wu H, Li P, Yao Z, Dong Z and Tian J (2020) Screening and Identifying Immune-Related Cells and Genes in the Tumor Microenvironment of Bladder Urothelial Carcinoma: Based on TCGA Database and Bioinformatics. Front. Oncol. 9:1533. doi: 10.3389/fonc.2019.01533

Bladder cancer is the most common cancer of the urinary system and its treatment has scarcely progressed for nearly 30 years. Advances in checkpoint inhibitor research have seemingly provided a new approach for treatment. However, there have been issues predicting immunotherapeutic biomarkers and identifying new therapeutic targets. We downloaded the gene expression profile and clinical data of 408 cases bladder urinary cancer from the Cancer Genome Atlas (TCGA) portal, and the abundance ratio of immune cells for each sample was obtained via the "Cell Type Identification by Estimating Relative Subsets of RNA Transcripts (CIBERSORT)" algorithm. Then, four survival-related immune cells were obtained via Kaplan-Meier survival analysis, and 933 immune-related genes were obtained via a variance analysis. Enrichment, protein-protein interaction, and co-expression analyses were performed for these genes. Lastly, 4 survival-related immune cells and 24 hub genes were identified, four of which were related to overall survival. More importantly, these immune cells and genes were closely related to the clinical features. These cells and genes may have research value and clinical application in bladder cancer immunotherapy. Our study not only provides cell and gene targets for bladder cancer immunotherapy, but also provides new ideas for researchers to explore the immunotherapy of various tumors.

Keywords: bladder urinary cancer, immunotherapy, tumor microenvironment, TCGA, bioinformatics

INTRODUCTION

Bladder cancer is the nineth most common malignant neoplasm in the world. It is mainly represented by bladder urothelial carcinoma (BUC), which accounts for >90% of bladder cancer, and smoking is recognized as the most common risk factor (1, 2). The traditional treatments for bladder cancer mainly include surgical resection and chemotherapy, but there is a high recurrence

rate, and the 5 year overall survival rate remains at 15–20% (3, 4). Owing to advancements in immuno-oncology and the introduction of checkpoint inhibitors in clinical practice for many cancers in recent years, there is hope for progress in the treatment of bladder cancer (5). Bacillus Calmette–Guérin is considered the earliest immunotherapeutic drug applied to bladder cancer, but its clinical application is limited due to low efficiency and high toxicity. Immunological checkpoint inhibitors are immunotherapeutic drugs that have emerged in recent years, and many clinical trials on these drugs are proceeding (6). A study from the Cancer Genome Atlas (TCGA) showed that bladder cancer is a disease with a large number of different genetic mutations, and may be sensitive to immunotherapy due to the high number of identifiable antigens (7). This finding suggests that immunotherapy may be beneficial in the treatment of bladder cancer. Many clinical trials of bladder cancer immunotherapy are currently in progress, but there are no results on efficacy, particularly compared to traditional cisplatin-based chemotherapy. Moreover, no approval has been given to any form of bladder cancer immunotherapy according to the Food and Drug Administration (6). The beneficiaries of immunotherapy are still limited to small-scale populations, and tumor-induced immune escape is a ubiquitous phenomenon. Many problems remain to be solved in BUC immunotherapy, especially in the field of predicting immunotherapeutic biomarkers and identifying new effective therapeutic targets.

Studies on the tumor microenvironment have been increasingly published in the field of cancer immunotherapy (8). The tumor microenvironment is the surrounding environment in which tumor cells reside, and consists of immune cells, mesenchymal cells, endothelial cells, inflammatory mediators, and extracellular molecules (9, 10). It is a powerful protective net for tumor cells formed in the fight between the tumor and the immune system, and it is also the premise and guarantee of tumor immune escape. Immune components in the tumor microenvironment have essential effects on gene expression by tumor tissues and the clinical outcome (11–13).

Cancer immunotherapy mainly works with some important proteins to enhance function or restore immune cells in the tumor microenvironment. Thus, we first explored survival-related immune cells in BUC, and then explored genes that are critical to the level of immune cell infiltration. In this study, the RNA-sequencing (RNA-Seq) gene expression profile and clinical data of 408 patients with BUC were downloaded from the TCGA database, and data extraction and analysis were performed with R software. A total of four survival-related immune cells and 24 hub genes were identified, four of which were related to survival. We validated the immune correlation through the online website "Tumor Immune Estimation Resource (TIMER)." Our study provides ideas and clues to BUC immunotherapy, and the cells and genes that were identified could be considered biomarkers for prognosis or targets for BUC therapy. Furthermore, this study also provides a new approach for immunotherapy researchers to explore immunotherapeutic cells and gene targets for the first time.

MATERIALS AND METHODS

Data Source and Pre-processing

The RNA-Seq gene expression profiles of patients with BUC, including the FPKM and count format, were downloaded from the TCGA database using the *gdc-client* download tool. Clinical data, such as gender, age, tumor grade, clinical stage, and survival time, were also downloaded from the TCGA portal. Then, R software (R Foundation for Statistical Computing, Vienna, Austria) was used for data extraction and sorting to obtain the gene expression matrices and clinical data. Subsequent analyses were conducted, and all analytical processes are shown in **Figure 1**.

Identifying Survival-Related Immune Cells

CIBERSORT is an analytical tool developed by Newman to provide an estimate of the abundance ratio of member cell types in a mixed cell population using gene expression data (14). We ran CIBERSORT locally in R software (15). The RNA-Seq (FPKM format) of BUC was analyzed to obtain the abundance ratio matrix of 22 immune cells. In total, 218 samples were selected with $P \leq 0.05$. Then, a correlation analysis was conducted among the contents of the 22 immune cells in the 218 samples. Next, the Kaplan-Meier analysis for overall survival was proceeded based on the abundance ratio of 22 immune cells whose cut-off level was set at the median value with the aid of R software and the Log-Rank was utilized to test. We identified survival-related immune cells according to the results of the Kaplan-Meier survival analysis.

Clinical Relationship With Survival-Related Immune Cells

The relationship between the abundance ratio of immune cells and tumor grade, clinical stage, stage T, and stage N was analyzed by combining the abundance ratio of immune cells and the clinical features in the 218 samples. Two variates used the independent sample *t*-test, while more variates used one-way ANOVA test. In this way, we could better understand the relevance of the clinical relationship with survival-related immune cells.

Identifying Immune-Related Genes

According to the grouping in step 2.2 and the survival-related cells identified, we analyzed and obtained the genes related to each immune cell infiltration level. The differentially expressed genes were analyzed with the edgeR R package and the condition that $|\log FC| > 1.5$ and $P < 0.05$. A Venn calculation and visualization were conducted via the online tool (http://bioinformatics.psb.ugent.be/webtools/Venn/) to obtain unique results for these genes.

Enrichment Analysis of Immune-Related Genes

Gene Ontology (GO) and Kyoto Encyclopedia of Genes and Genomes (KEGG) enrichment analyses were used to annotate

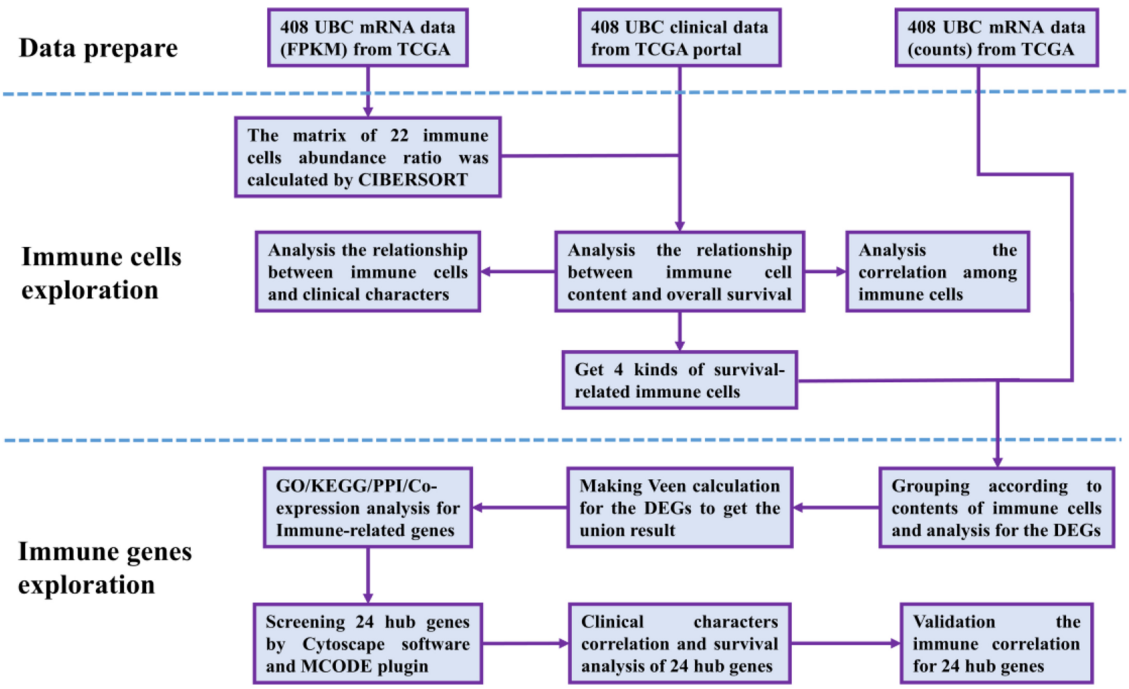

FIGURE 1 | Flow chart of data processing in this study. TCGA, The Cancer Genome Atlas (https://portal.gdc.cancer.gov/). FPKM and counts are the two different mRNA data formats in the TCGA database. CIBERSORT is a web tool to estimate the abundance ratios of member cell types in a mixed cell population, using gene expression data. DEGs, differentially expressed genes; GO, Gene Ontology; KEGG, Kyoto Encyclopedia of Genes, and Genomes; PPI, protein-protein interactions. Cytoscape is a network processing software, and MCODE is a plugin in Cytoscape.

the structure, functions, and pathways of the genes. The DAVID website (https://david.ncifcrf.gov/) is one of the most authoritative enrichment tools (16). We used DAVID to analyse immune-related genes in the GO and KEGG pathways. Counts $\geq$ 4 and $P < 0.05$ were set as the enrichment cut-offs to screen meaningful enrichment results. Counts indicate the number of genes enriched in one GO/KEGG term. *P*-value is the judgment of significance of enrichment results. The enrichment results were visualized via the ggplot2 R package.

Protein-Protein Interaction Network Construction, Hub Genes, and Modules Analysis

The 933 immune-related genes were imported into the STRING database (https://string-db.org/), a web tool used to explore protein-protein interactions, and the combined-score was set to $\geq$ 0.4 (17). The interaction network consisted of 829 nodes and 4,850 edges. This network was reconstructed via Cytoscape software and analyzed via the "molecular complex detection (MCODE)" plugin. In total, 29 modules were analyzed, including 24 *seed genes*, which were named hub genes. Then, we analyzed and obtained the 50 highest related genes to the 24 hub genes and the co-expression network of these genes via the cBioPortal online website (http://www.cbioportal.org/) (18, 19). For the co-expression analysis, the "TCGA provisional" dataset was selected and set as 7.5 in "Filter Neighbors by Alteration (%)." Lastly, we selected two modules with a gene number > 50 from MCODE and the co-expression network to perform GO/KEGG analysis via DAVID. The enrichment cut-off value was set to an adj. $P < 0.05$ and count $\geq$ 5.

Relationship Between Clinical Characteristics and Hub Genes

The relationship between hub genes and clinical characteristics was analyzed and visualized by the "Weighted Correlation Network analysis (WGCNA)" package in R. The 218 patients were grouped and analyzed for overall survival according to the expression level of the 24 hub genes, as for the Kaplan-Meier survival analysis of the immune cells.

Validation of the Immune Correlation

For validating the immune correlation of 24 hub genes, we employed the method of Pearson correlation analysis to analyse the correlation between these hub genes and 22 immune cells, which have got via the CIBERSORT in section identifying survival-related immune cells. The correlation index r and corresponding *p*-value are visualized via canvasXpress R package. TIMER (https://cistrome.shinyapps.io/timer/) is a comprehensive resource to systematically analyse immune infiltrates across diverse cancer types. The abundances of six immune cells (B cells, $CD4^+$ T cells, $CD8^+$ T cells, neutrophils,

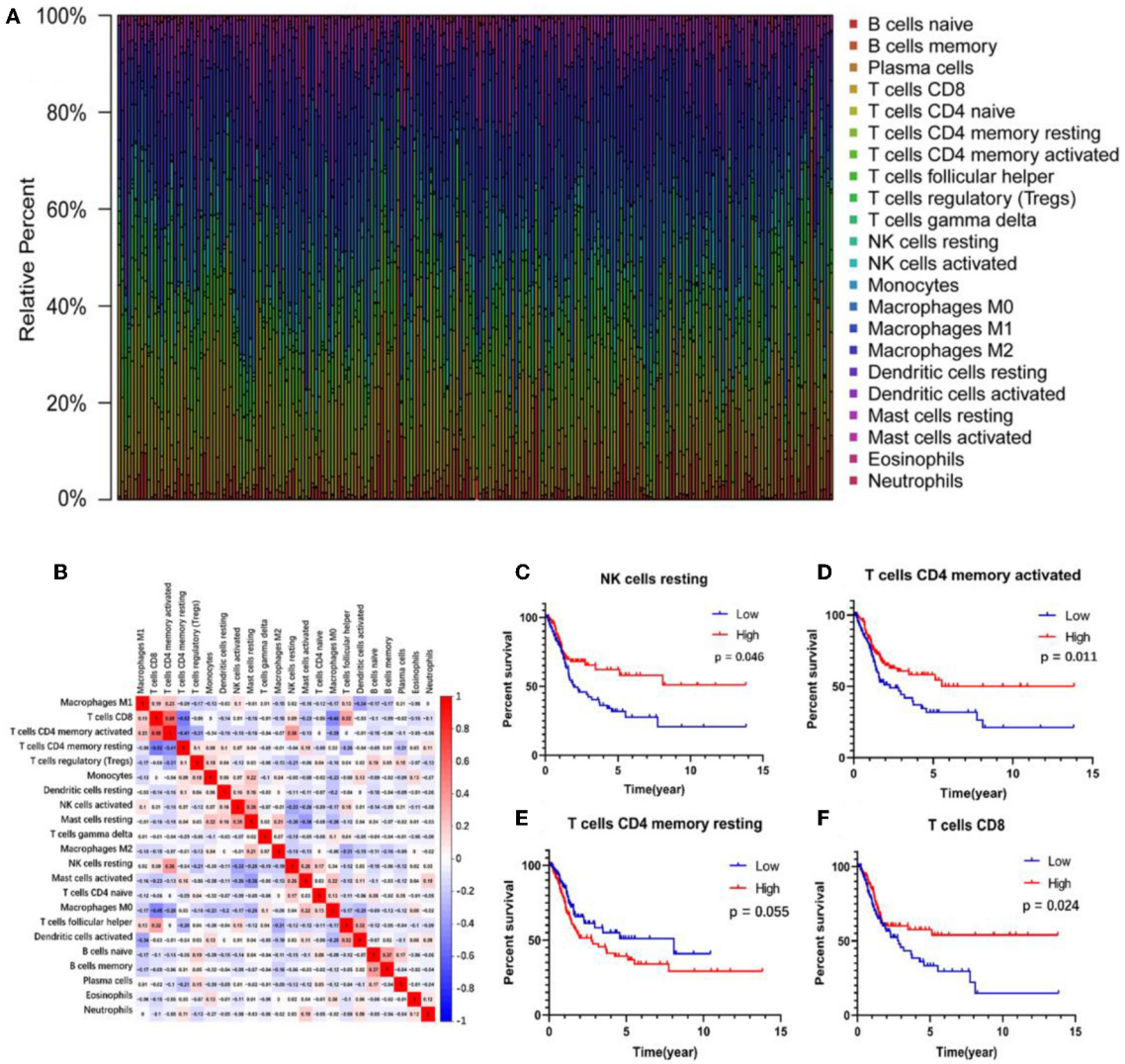

FIGURE 2 | The relationship between the abundance ratios of immune cells and overall survival. **(A)** The abundance ratio of immune cells in the 218 samples. Each column represents a sample, and each column with a different color and height indicates the abundance ratios of immune cells in this sample. **(B)** The relationship between the abundance ratios of various immune cells. The value represents the correlation value. Red represents a positive correlation, and the blue represents a negative correlation. **(C–F)** The survival analysis for the abundance ratios of the four immune cells. The red line indicates a high expressing group of immune cells, and the blue line indicates a low expressing group of immune cells.

macrophages, and dendritic cells [DCs]) were estimated by a special statistical method, which was validated using a pathological estimate and the results are reliable (20). Survival-related hub genes were also validated for immune correlation via TIMER.

RESULTS

Data Source and Pre-processing

The 408 cases of BUC data were downloaded and extracted into three matrices, including the RNA-Seq (FPKM and counts format) and clinical data. The subsequent analytical pre-processing for the study is shown in **Figure 1**.

Identifying Survival-Related Immune Cells

The abundance ratio of 22 immune cells in the 218 samples and their correlations were analyzed and are shown in **Figures 2A,B**. T cell CD4 memory activated and T cell CD8 contents were significantly correlated, while T cell CD4 memory resting was negatively correlated with T cell CD8 and T cell CD4 memory activated. Additionally, we analyzed the relationship between the abundance ratio of the 22 types of immune cells and overall survival via Kaplan-Meier analysis. The results in **Figures 2C–F** show that the abundance ratio of the four immune cells was related to survival, including T cell CD4 memory activated, T cell CD8, T cell CD4 memory resting, and natural killer (NK) cell resting.

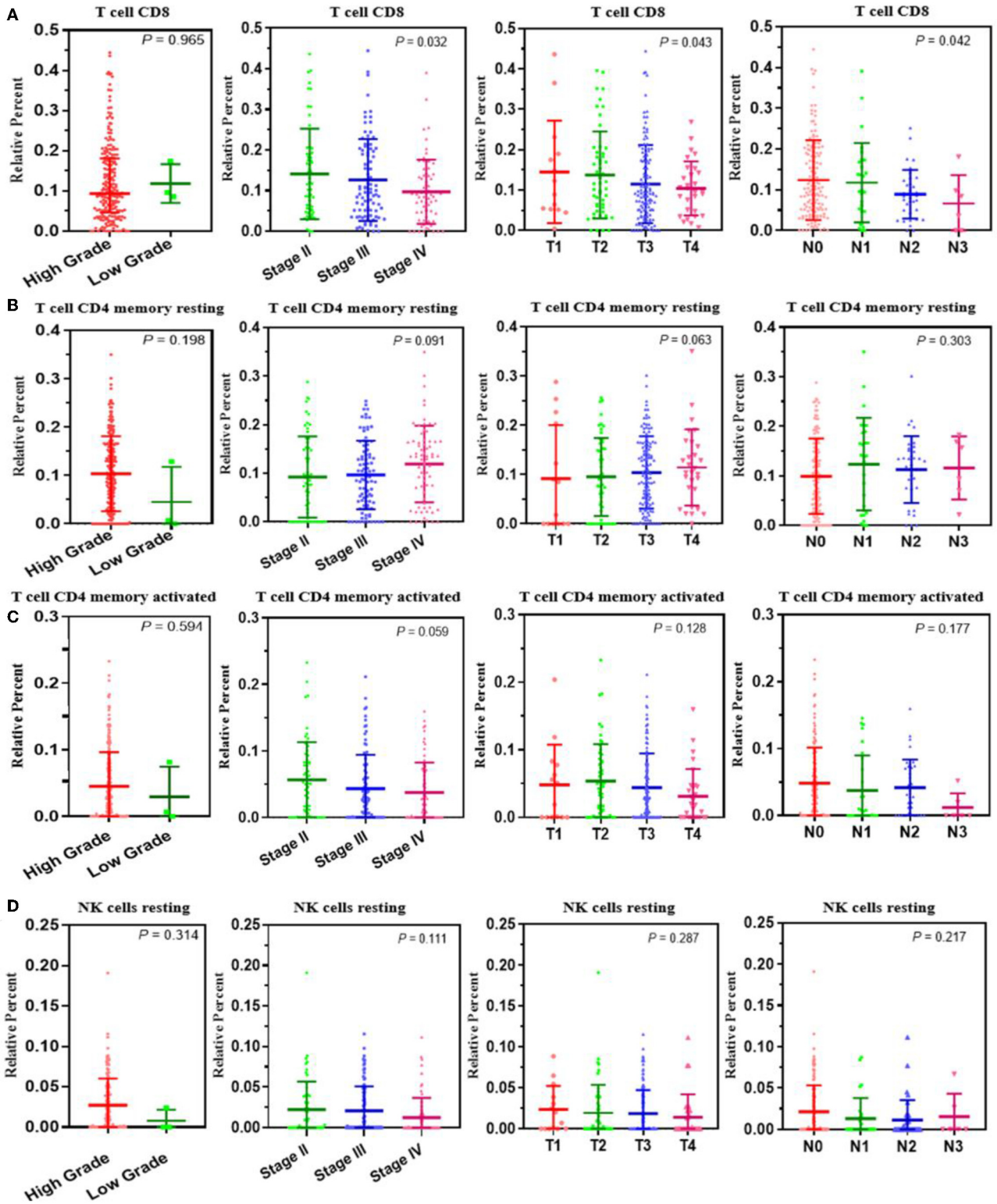

FIGURE 3 | The relationship between the abundance ratios of the immune cells and clinical characteristics. **(A–D)** The relationship between the abundance ratios of each immune cell and tumor grade, clinical stage, T stage, and N stage. Each dot signifies the abundance ratio of an immune cell in a sample. The three horizontal line in each picture means mean ± SD.

Clinical Relationship With Survival-Related Immune Cells

A correlation analysis was carried out between the contents of the four survival-related immune cells and the clinical characteristics (including stage T, stage N, clinical stage, and tumor grade) to determine the effect of the immune cell abundance ratio on BUC clinical features. As shown in **Figure 3**, the abundance ratio of T cell CD8, NK cell resting, and T cell CD4 memory resting decreased with the increase of stage T/stage N/clinical stage, while the abundance ratio of T cell CD4 memory activated increased in an opposite manner. Because there were only three cases of low-grade BUC, the relationship between BUC grade and survival-related immune cells was unclear.

Identifying Immune-Related Genes

We analyzed the genes related to the levels of the four survival-related immune cells and found that 514 genes were related to T cell CD8, 510 to NK cell resting, 560 to T cell CD4 memory resting, and 534 to T cell CD4 memory activated. Volcano plots were used to show the results in **Figures 4A–D**. The Venn map analysis shown in **Figure 4E** revealed 933 genes totally related to immune cells infiltration.

Enrichment Analysis of Immune-Related Genes

To investigate the biological classifications of immune-related genes, a GO/KEGG enrichment analysis was performed using the DAVID website, and the top 12 enrichment results for each term are plotted in **Figure 5**. GO analysis results showed that changes in the biological process (**Figure 5A**) of immune-related genes were significantly enriched in keratinization, peptide cross-linking, regulation of ion transmembrane transport, ion transmembrane transport, cell-cell signaling, etc. Changes in the molecular function (**Figure 5B**) were mainly enriched in keratin filament, extracellular region, intermediate filament, anchored component of membrane, Golgi lumen, acetylcholine-gated channel complex, etc. Changes in cellular component (**Figure 5C**) were mainly enriched in sequence-specific DNA binding, serine-type endopeptidase inhibitor activity, neuropeptide Y receptor activity, arachidonic acid epoxygenase activity, serotonin-activated cation-selective channel activity,

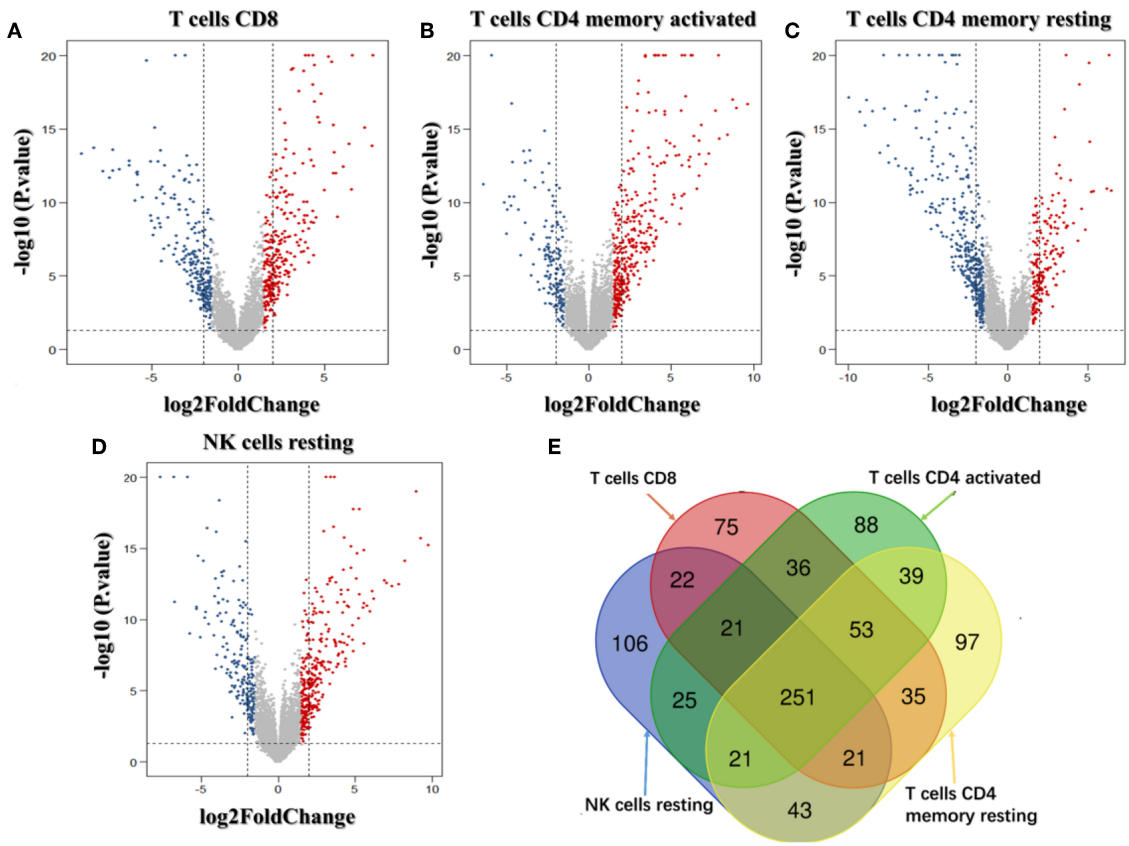

FIGURE 4 | Identification of genes related to immune cell infiltration. **(A–D)** Volcano plots of the bladder urinary cancer gene expression profiles grouping by T cells CD8, T cells CD4 memory activated, T cells CD4 activated and NK cells resting. Red/blue symbols classify the upregulated/downregulated genes according to the criteria: $|\log2FC| > 1.5$ and P-value < 0.05. **(E)** The Venn calculation result using the online tool (http://bioinformatics.psb.ugent.be/webtools/Venn/) to obtain genes involved in the infiltration of the four immune cells. The numbers in different color blocks represent the number of genes associated with immune cell infiltration. There are a total of 911 genes related to the infiltration of the four immune cells.

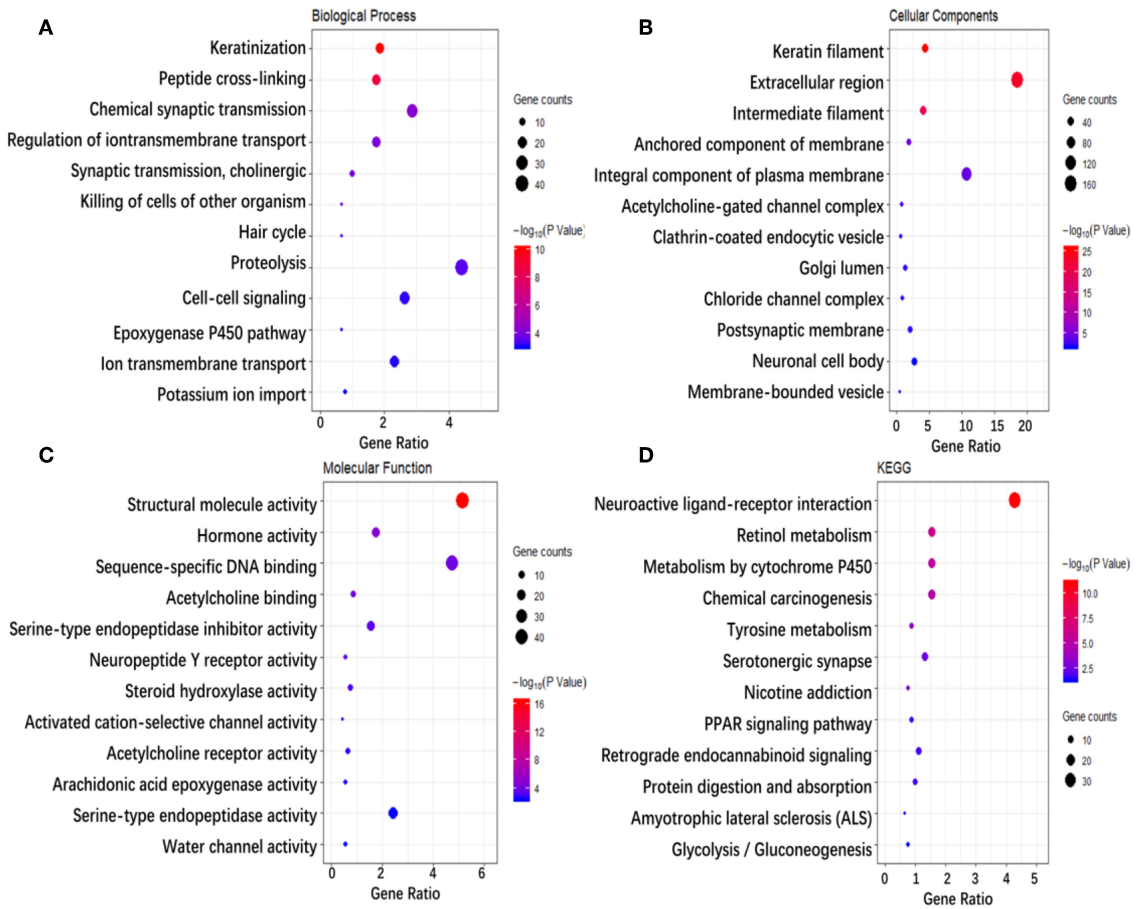

FIGURE 5 | Enrichment analysis of genes related to immune cell infiltration. **(A–D)** Represent the enrichment analysis results of genes involved in immune cell infiltration, namely biological processes, cellular components, molecular functions, and KEGG. The main 12 results of each term are shown, and the color indicates the significant degree of enrichment and the size indicates the number of genes enriched for each result.

etc. KEGG pathway analysis (**Figure 5D**) demonstrated that Metabolism of xenobiotics by cytochrome P450, Chemical carcinogenesis, Tyrosine metabolism, PPAR signaling pathway, etc. In brief, 933 immune-related genes were mainly involved in the transmission of various signaling pathways, as well as transportation and metabolism of nutrients.

Protein-Protein Interaction Network Construction, Hub Genes, and Module Analysis

To explore the interrelation of immune-related genes and obtain hub genes, we made a PPI and module analysis, and obtained 24 hub genes, 2 modules with genes >50, 50 co-expression genes, and the co-expression network. The information of the 24 hub genes is shown in **Table 1**, including the full gene names and primary functions. The two modules with genes >50 and the co-expression networks are shown in **Figures 6A–C**, respectively. According to the results of the enrichment analysis for three modules shown in **Table 2**, module 1 genes were mainly related to protein transport and metabolism, module 2 genes were mainly related to the composition of keratin and intermediate filaments, and the co-expression network genes were mainly related to various signaling pathways associated with cancer. Of the three modules, the most interesting and important one is the co-expression network. It is involved in many pathways related to cancer and immunity, such as G-protein coupled receptor signaling pathway, Wnt signaling pathway, regulation of phosphatidylinositol 3-kinase signaling, PI3K-Akt signaling pathway, ErbB signaling pathway, etc.

Relationship Between Clinical Characteristics and Hub Genes

The correlation analysis results of the clinical characteristics for the 24 hub genes are shown in **Figure 7A**. CDH7 was positively correlated with stage N, while CST4 was negatively correlated with stage T. The relationship between other hub genes and clinical characteristics can be easily found in the figure. The Kaplan-Meier survival analysis (**Figures 7B–E**) shows that four of the 24 hub genes strongly associated with clinical outcomes were CDH7, LUZP1, PSD2, and UGT2B15.

TABLE 1 | Functional roles of the 24 hub genes.

No.	Gene	Full name	Function
1	KRTAP19-6	Keratin associated protein 19-6	Developmental biology and keratinization
2	CHRM1	Cholinergic receptor muscarinic 1	Monoamine GPCRs and peptide ligand-binding receptors
3	AGTR2	Angiotensin II receptor type 2	Agents acting on the renin-angiotensin system pathway, pharmacodynamics and peptide ligand-binding receptors
4	SPRR2F	Small proline rich protein 2F	Cross-linked envelope protein of keratinocytes
5	GPR32	G protein-coupled receptor 32	Signaling by GPCR and G alpha (s) signaling events
6	UGT2B15	UDP glucuronosyltransferase family 2 member B15	Carbohydrate binding and glucuronosyltransferase activity
7	PSD2	Pleckstrin and Sec7 domain containing 2	Phospholipid binding and ARF guanyl-nucleotide exchange factor activity
8	MPPED1	Metallophosphoesterase domain containing 1	Hydrolase activity
9	STMN2	Stathmin 2	calcium-dependent protein binding and tubulin binding
10	CST4	Cystatin S	cysteine-type endopeptidase inhibitor activity
11	DGKK	Diacylglycerol kinase kappa	Glycerolipid metabolism and Signaling by GPCR
12	DMRTC2	DMRT like family C2	DNA-binding transcription factor activity and sequence-specific DNA binding
13	KRTAP2-3	Keratin associated protein 2–3	Developmental biology and keratinization
14	CSH1	Chorionic somatomammotropin hormone 1	Peptide ligand-binding receptors and Growth hormone receptor signaling
15	DSG4	Desmoglein 4	Developmental biology and keratinization
16	LIN28A	Lin-28 homolog A	Developmental biology and Wnt/hedgehog/notch
17	NKD1	NKD inhibitor of Wnt signaling pathway 1	Wnt/hedgehog/notch and wnt signaling pathway and pluripotency
18	KLK2	Kallikrein related peptidase 2	Agents acting on the renin-angiotensin system pathway, pharmacodynamics and signaling by Rho GTPases
19	FOXN4	Forkhead box N4	DNA-binding transcription factor activity and chromatin binding
20	UNC93A	Unc-93 homolog A	Toll-like receptor binding
21	LUZP1	Leucine zipper protein 1	chromosome 1p36 deletion syndrome
22	OTOG	Otogelin	Structural molecule activity and alpha-L-arabinofuranosidase activity
23	CDH7	Cadherin 7	ERK signaling and nanog in mammalian ESC pluripotency
24	TRIM51	Tripartite motif-containing 51	No data available

Validation of the Immune Correlation

The 24 hub genes are potential immunotherapeutic targets, and their relationship and interaction with immune cells are of great value for farther immune-related research. The correlation analysis results between the 24 hub genes and 22 immune cells are shown in **Figure 8A**. TIMER was used to validate the correlation between the four survival-related genes and the level of immune cell infiltration, and the results are shown in **Figure 8B**. Part of hub genes, including four survival-related genes, were significantly correlated with some certain immune cell infiltrate.

DISCUSSION

Bladder cancer is the most common tumor of the urinary system, and its treatment progress has been slow. In recent years, the discovery of immune checkpoints has pushed cancer immunotherapy to a new level, achieving specific blockade of immunosuppressive effects and enhancing the anti-tumor immune response. Accumulating clinical data show that cancer immunotherapy is a key step in clinical cancer management (10). The purpose of our study was to screen and identify cells and genes closely related to immune infiltration and clinical outcomes in the BUC microenvironment. Our study not only identified cell and gene targets for BUC immunotherapy, but also proposes a new research idea for immunotherapy of other tumors.

In this study, four kinds of immune cells were related to the survival of patients with bladder cancer, including T cell CD8, T cell CD4 memory resting, T cell CD4 activated, and NK cell resting. CD8+ T cells are a hot spot in cancer research. Programmed death-1 (PD-1) on the surface of CD8+

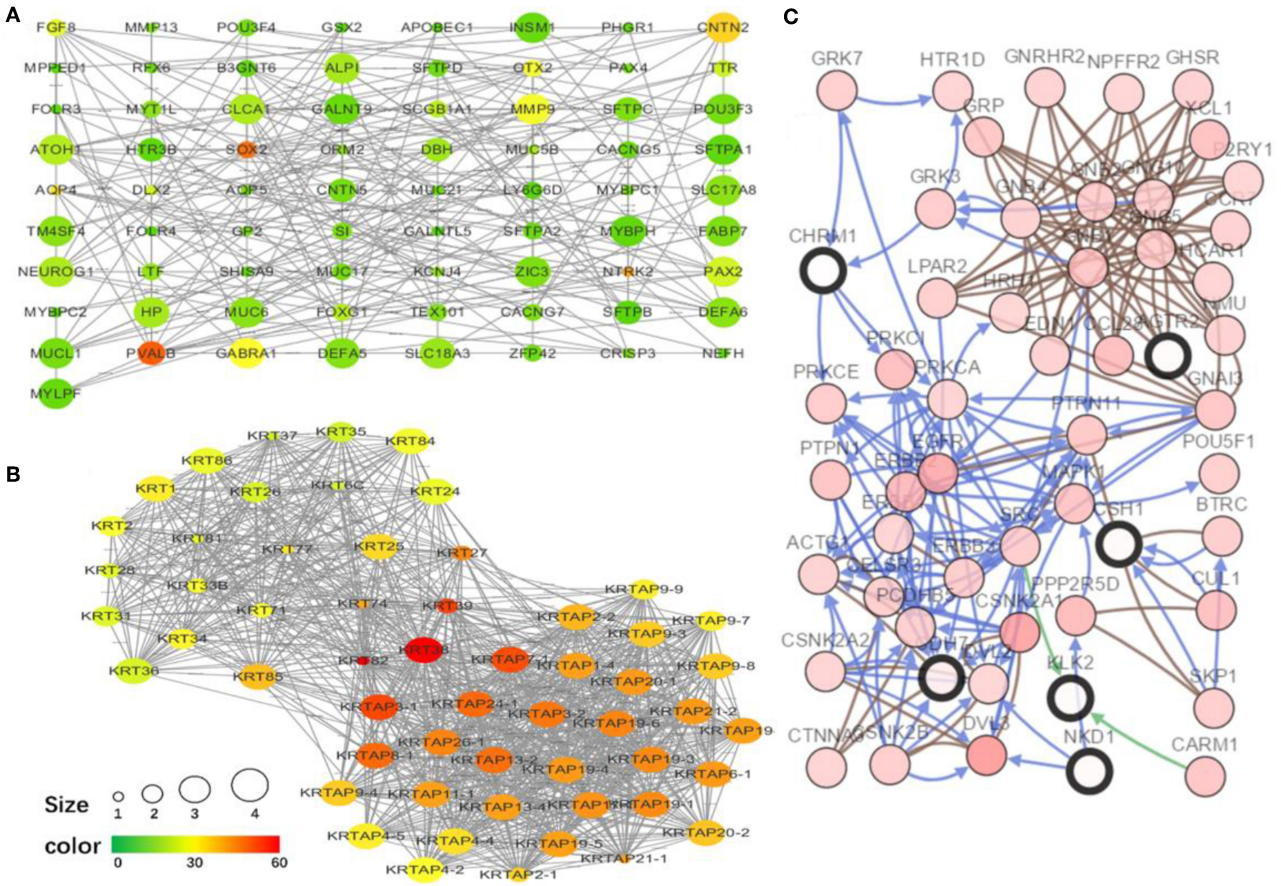

FIGURE 6 | The top two modules and co-expression network. **(A,B)** Two modules with more than 50 genes in MCODE. The size indicates the number of immune cells associated with the gene, ranging from 1 to 4. The color indicates the number of proteins interacting with the other proteins. A redder color indicates a higher number, while green indicates a lower number. **(C)** The co-expression network of the 24 hub genes and 50 co-expressed genes. The figure was obtained using the online tool (http://www.cbioportal.org/). White and red represent the hub and co-expressing genes, respectively.

T cells binds programmed death-ligand 1 (PD-L1) produced by tumor tissue, resulting in a limited host immune response. PD-L1 inhibitors increase the infiltration level of CD8+ T cells, which is an effective anti-tumor immune response (21). CD4+ memory T cells play an essential role in tumourigenesis and enlargement (22). CD4+ central memory T (TCM) cells maintain immune memory and exert immunoprotective effects during tumor metastasis (23, 24). CD4+ effector memory T (TEM) cells express adhesion molecules and chemokine receptors, which perform rapid functions (25). Both play a vital role in anti-tumor immunity, while TCM cells have more advantages than TEM cells (26). In the peripheral blood of patients with advanced cancer, the proportion of TCM cells decreases and TEM cells increases, presenting the typical T cell depletion status (27). In that study, patients with high T cell CD4 memory activated had shorter overall survival, while patients with high T cell CD4 memory resting had longer overall survival. This is consistent with the T cell depletion status theory. NK cells are an important part of the innate immune system, performing the function of memory antigen-specific immunity (28, 29). NK cells directly kill target cells, effectively remove diseased cells, and conduct immune surveillance. Some studies have shown that exercise-dependent mobilization of NK cells plays a crucial role in exercise-mediated protection against cancer (30–32). In summary, the four survival-related cells identified in this study are most likely to play an important role in immune infiltration as well as BUC immunotherapy, confirming that the analysis of immune-related genes based on the cells is credible.

The enrichment analysis of immune-related and co-expressed genes showed that these genes are mainly correlated with the transportation and metabolism of various nutrients (proteins, lipid, sugars, water, and ions) and various signaling pathways. By searching the signaling pathways enriched on the KEGG website (https://www.genome.jp/kegg/), we found that the PPAR signaling pathway, the epoxygenase P450 pathway, and the PI3K-Akt signaling pathway are involved in substance metabolism. The PI3K-Akt, Wnt, chemokine, and ErbB signaling pathways, as well as circadian rhythms and chemical carcinogenesis, are mainly associated with tumor cell metastasis, differentiation,

TABLE 2 | GO and KEGG pathway enrichment analysis of the top 2 modules and co-expression network.

Modules		Description	*P*.adjust	Count
Modules 1	BP terms	O-glycan processing	1.95E-04	7
		Cellular protein metabolic process	6.24E-04	8
		Respiratory gaseous exchange	0.0141	5
	CC terms	Lamellar body	1.47E-05	5
		Clathrin-coated endocytic vesicle	2.81E-04	5
		Extracellular region	0.00142	21
		Golgi lumen	0.001888	7
		Extracellular space	0.001995	19
Modules 2	CC terms	Intermediate filament	1.84E-60	35
		Keratin filament	2.16E-40	26
	MF terms	Structural molecule activity	1.61E-30	23
Co-expression	BP terms	Signal transduction	1.79E-06	22
		G-protein coupled receptor signaling pathway	5.32E-05	18
		Platelet activation	4.55E-04	8
		Wnt signaling pathway	9.23E-04	9
		Positive regulation of ERK1 and ERK2 cascade	0.007655	8
		Regulation of phosphatidylinositol 3-kinase signaling	0.01949	6
		Positive regulation of cytosolic calcium ion concentration	0.020014	7
	CC terms	Plasma membrane	3.47E-04	36
	MF terms	Protein kinase activity	0.016453	10
	KEGG pathway	Chemokine signaling pathway	6.32E-06	13
		Adherens junction	3.90E-05	9
		Wnt signaling pathway	6.02E-04	10
		Cholinergic synapse	0.001299	9
		Glutamatergic synapse	0.001592	9
		GABAergic synapse	0.002653	8
		Pathways in cancer	0.003451	14
		Morphine addiction	0.004209	8
		Circadian entrainment	0.005621	8
		Retrograde endocannabinoid signaling	0.008465	8
		Serotonergic synapse	0.015818	8
		PI3K-Akt signaling pathway	0.03281	12
		Dopaminergic synapse	0.040082	8
		ErbB signaling pathway	0.041677	7

survival, angiogenesis, and biological clocks. Metabolic change is an important feature of tumors. To meet the energy and biosynthetic demands of rapid proliferation, tumor cells use aerobic glycolysis for rapid energy supply (33). Different immune cell subsets also use different nutrients as an energy supply. Activated T cells, effector T (Teff) cells, including CD8+ T, CD4+ Th1, CD4+ Th2, and Th17, activated DCs, and activated M1 macrophages all use aerobic glycolysis, while the immunosuppressive cell subsets, such as regulatory T (Treg) cells, myeloid-derived suppressor cells, DC resting, and naive T cells use fatty acid oxidation to supply energy (34, 35). Thus, there is a competition between tumor cells and immune cells for energy. It has been shown that the severe nutrient deprivation in the tumor microenvironment allows Treg cells to use lactate as an energy substrate, while inhibiting lactate metabolism reduces Treg cell content (36). Similarly, promoting tryptophan degradation inhibits Teff cell function (37). These results indicate that the metabolic pattern of tumor tissue is related to immune cells, which can change the metabolism of specific substances to achieve different levels of immune cell infiltration and realize the treatment of tumors. Based on this evidence, we predict that these energy metabolism-related pathways act as an important bridge between immune infiltration and energy metabolism of BUC and are worthy of further study.

Of the enrichment analysis results, the PI3K-Akt signaling pathway is the clearest and important one to regulate immune environment. The general consensus is that the PI3K-Akt signaling pathway has the capacity to affect immune cell effector function and to regulate the immune-intrinsic features (38). Within the tumor microenvironment, a variety of immune cells co-exist in and interact with each other, and the activation

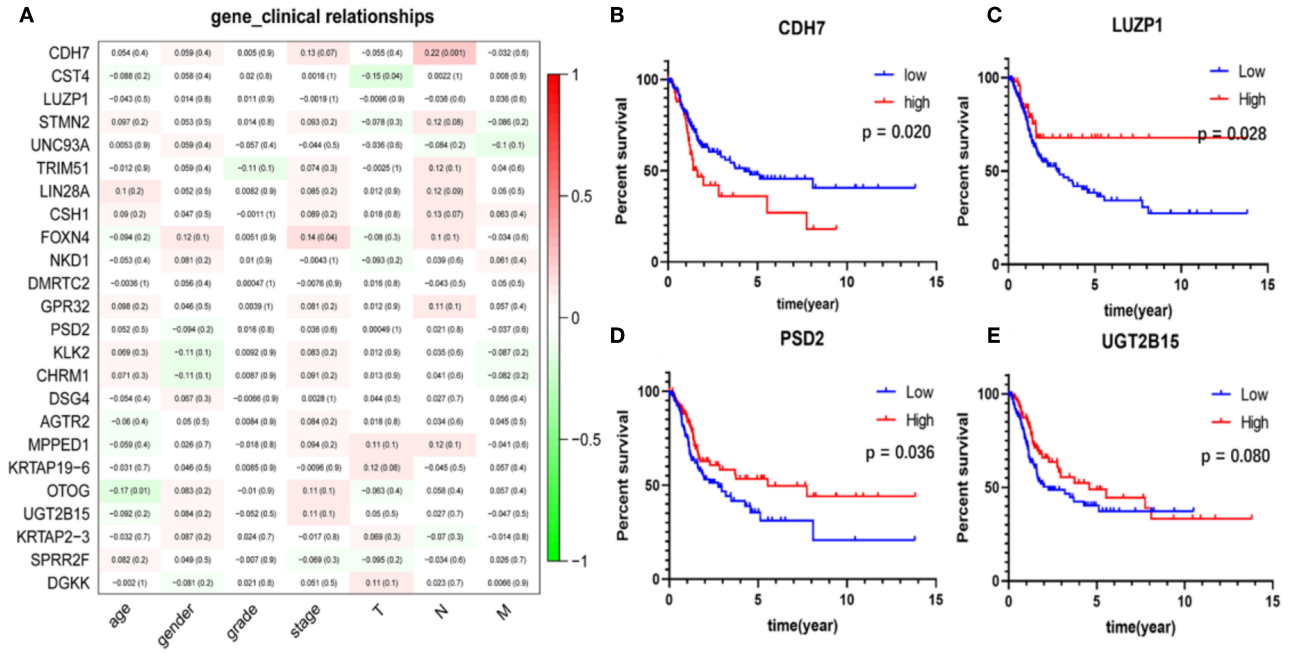

FIGURE 7 | Clinical features correlation and survival analyses of the hub genes. **(A)** The correlation between the 24 hub genes and clinical characteristics. The former numbers in each small rectangle indicate the correlation and the numbers in brackets indicate the *P*-value for the correlation. **(B–E)** Are the four genes significantly related to survival, in which the red line indicates the group with higher expression of this gene, and the blue line indicates the group with lower expression.

of most immune cells are affected by the PI3K-AKT signaling pathway (39, 40). AKT can balance the terminal differentiation and production of memory CD8+T cells via regulating TCR, IL-2 receptor, and IL-12 receptor, etc. (41). Peng (42) and Abu-Eid et al. (43) found that PI3K inhibitor /AKT inhibitor could significantly increase the infiltration of CD8+T cells in tumor tissues and significantly prolong survival time. Meanwhile, AKT inhibitors can even effectively enhance the differentiation of other memory T cells in tumor tissues (44, 45). Abu-Eid et al. (43) found that PI3K-Akt pathway inhibitors selectively inhibit Tregs with minimal effect on conventional T cells to enhance the antitumour immune response. Okkenhaug et al. (46) proved that the PI3K-AKT-m TOR signaling pathway contributes to the development and activity of lymphocytes. Additional immune microenvironment features, such as the expression of immune checkpoint PD-L1 and inflammation within the tumor, are also modulated by the PI3K-AKT pathway (38). Other signaling pathways, such as Wnt, chemokine, chemical carcinogenesis, etc. are also more or less related to immunity.

Finally, a total of 24 hub genes were identified, four of which were related to survival, namely CDH7, LUZP1, PSD2, and UGT2B15. Previous studies have failed to investigate the relationship between these four genes and immunity, and only a few studies have shown that these genes are involved in the development of certain tumors. CDH7 is a typical adhesion molecule, and some studies have shown that CDH7 is a melanoma inhibitory protein binding partner that affects the migration of malignant melanoma cells (47–49). LUZP1 is a basic component of many proteins as well as a significant component of the group of membrane proteins on the surface of NK cells. Upregulation of LUZP1 is associated with a poor prognosis of liver cancer (50). UGT2B15 is associated with gastric cancer, breast cancer, and prostate cancer. UGT2B15 may upregulate FOXA1 and activate the hippocampal-yap signaling pathway to promote the development of gastric cancer (51). In breast cancer, UGT2B15 is regulated by sex hormone signaling in estrogen receptor-positive breast cancer (52). In human prostate cancer cells, androgen glucuronidation catalyzed by glucuronyltransferase is one of the main pathways to inactivate androgens, and high androgen expression is essential in the pathogenesis of prostate cancer (53).

In conclusion, four survival-related immune cells and 24 hub genes were identified, and four of these genes were shown to be related to overall survival in patients with BUC. These cells and genes can be considered biomarkers for prognosis, or as markers for bladder cancer therapy, which can be a focus of immunotherapy for bladder cancer. However, the evidence of this study remains indirect, and from bioinformatics, as with other similar studies. Through further research on these cells and genes, a new understanding of the potential relationship between the tumor microenvironment and BUC immunotherapy as well as prognosis can be achieved.

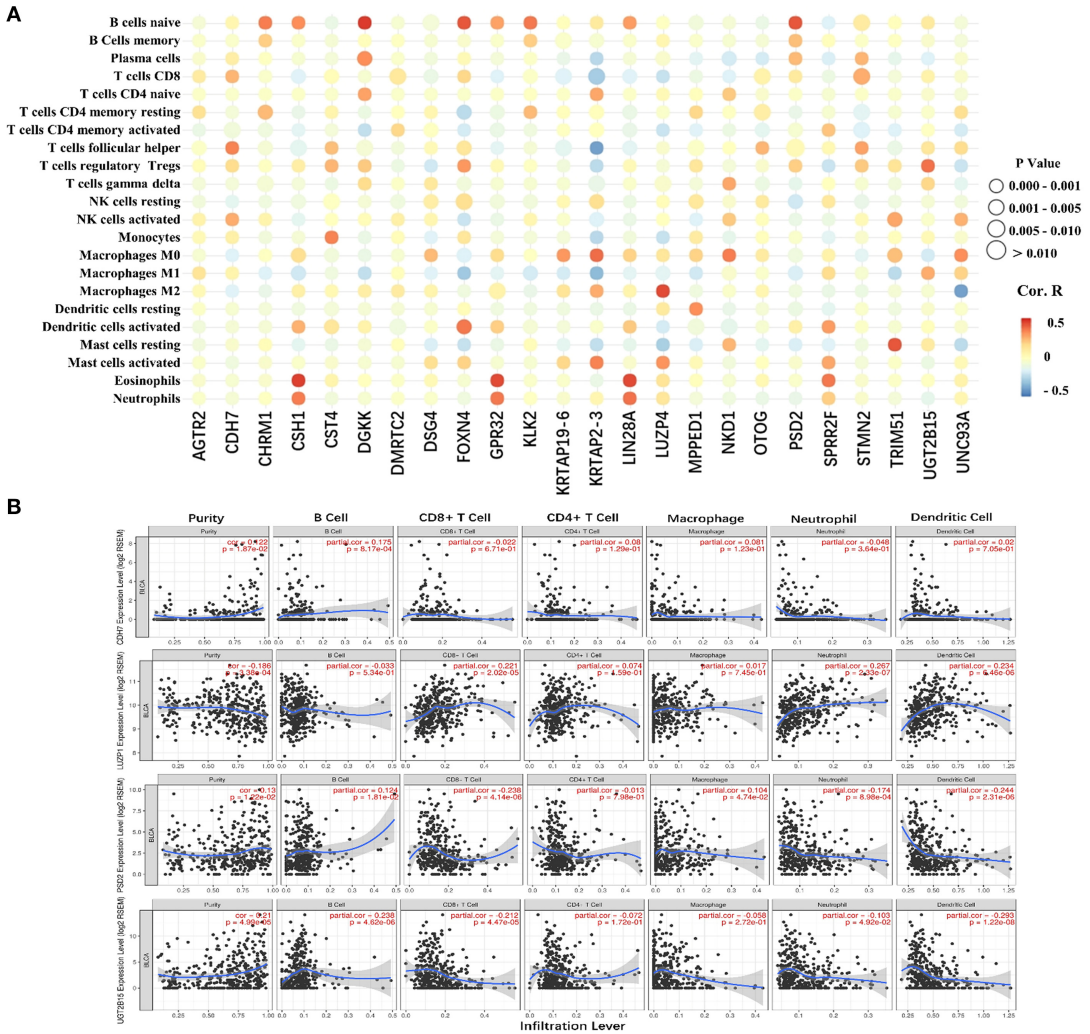

FIGURE 8 | The correlation between the hub genes and various immune cells. **(A)** Red represents positive correlation genes and blue represents a negative correlation. The point size represents *P*-value and shade of color represents Pearson correlation index r. The x axis indicates hub genes and y axis indicates immune cell types. **(B)** Each dot represents a sample, and the blue line represents the relationship between the expression level of each gene and immune cell contents.

DATA AVAILABILITY STATEMENT

Publicly available datasets were analyzed in this study, these can be found in The Cancer Genome Atlas (https://portal.gdc.cancer.gov/).

AUTHOR CONTRIBUTIONS

The study conception and design were performed by JC and JT. Material preparation, data collection, and analysis were performed by JC, XY, JL, HW, PL, and ZY. The first draft of the manuscript was written by JC, JL, and ZD. All authors commented on previous versions of the manuscript. All authors read and approved the final manuscript.

FUNDING

This work was supported by the Fundamental Research Funds for the Central Universities (Project number: 561219007), Doctoral Research Foundation of Lanzhou University Second Hospital (Project number: ynbskyjj2015-2-7), Cuiying Scientific and Technological Innovation Program of Lanzhou University Second Hospital (Project number: CY2017-BJ16), Cuiying Graduate Supervisor Applicant Training Program of Lanzhou University Second Hospital (Project number: 201704), Industry Planning Project of Health Department of Gansu Province (Project number: GWGL2013-30), and Science and Technology Project of Chengguan District, Lanzhou City, Gansu Province Science and Technology Bureau (Project number: 2017KJGG0052).

REFERENCES

1. Antoni S, Ferlay J, Soerjomataram I, Znaor A, Jemal A, Bray F. Bladder cancer incidence and mortality: a global overview and recent trends. *Eur Urol*. (2017) 71:96–108. doi: 10.1016/j.eururo.2016.06.010
2. Ferlay J, Soerjomataram I, Dikshit R, Eser S, Mathers C, Rebelo M, et al. Cancer incidence and mortality worldwide: sources, methods and major patterns in GLOBOCAN 2012. *Int J Cancer*. (2015) 136: E359–86. doi: 10.1002/ijc.29210
3. Bladder cancer: diagnosis and management of bladder cancer: (c) NICE (2015) Bladder cancer: diagnosis and management of bladder cancer. *BJU Int*. (2017) 120:755–65. doi: 10.1111/bju.14045
4. Aggen DH, Drake CG. Biomarkers for immunotherapy in bladder cancer: a moving target. *J Immunother Cancer*. (2017) 5:94. doi: 10.1186/s40425-017-0299-1
5. Bellmunt J, Orsola A, Leow JJ, Wiegel T, De Santis M, Horwich A. Bladder cancer: ESMO practice guidelines for diagnosis, treatment and follow-up. *Ann Oncol*. (2014) 25(Suppl. 3):iii40–8. doi: 10.1093/annonc/mdu223
6. Hindy JR, Souaid T, Kourie HR, Kattan J. Targeted therapies in urothelial bladder cancer: a disappointing past preceding a bright future? *Future Oncol*. (2019) 15:1505–24. doi: 10.2217/fon-2018-0459
7. Weinstein J, Akbani R, Broom B, Wang W, Verhaak R, McConkey D, et al. Comprehensive molecular characterization of urothelial bladder carcinoma. *Nature*. (2014) 507:315–22. doi: 10.1038/nature12965
8. Fidler IJ. The pathogenesis of cancer metastasis: the 'seed and soil' hypothesis revisited. *Nat Rev Cancer*. (2003) 3:453–8. doi: 10.1038/nrc1098
9. Hanahan D, Coussens LM. Accessories to the crime: functions of cells recruited to the tumor microenvironment. *Cancer Cell*. (2012) 21:309–22. doi: 10.1016/j.ccr.2012.02.022
10. Chen DS, Mellman I. Oncology meets immunology: the cancer-immunity cycle. *Immunity*. (2013) 39:1–10. doi: 10.1016/j.immuni.2013.07.012
11. Senbabaoglu Y, Gejman RS, Winer AG, Liu M, Van Allen EM, de Velasco G, et al. Tumor immune microenvironment characterization in clear cell renal cell carcinoma identifies prognostic and immunotherapeutically relevant messenger RNA signatures. *Genome Biol*. (2016) 17:231. doi: 10.1186/s13059-016-1092-z
12. Yoshihara K, Shahmoradgoli M, Martinez E, Vegesna R, Kim H, Torres-Garcia W, et al. Inferring tumour purity and stromal and immune cell admixture from expression data. *Nat Commun*. (2013) 4:2612. doi: 10.1038/ncomms3612
13. Cooper LA, Gutman DA, Chisolm C, Appin C, Kong J, Rong Y, et al. The tumor microenvironment strongly impacts master transcriptional regulators and gene expression class of glioblastoma. *Am J Pathol*. (2012) 180:2108–19. doi: 10.1016/j.ajpath.2012.01.040
14. Newman AM, Liu CL, Green MR, Gentles AJ, Feng W, Xu Y, et al. Robust enumeration of cell subsets from tissue expression profiles. *Nat Method*. (2015) 12:453–7. doi: 10.1038/nmeth.3337
15. Chen B, Khodadoust MS, Liu CL, Newman AM, Alizadeh AA. Profiling tumor infiltrating immune cells with CIBERSORT. *Methods Mol Biol*. (2018) 1711:243–59. doi: 10.1007/978-1-4939-7493-1_12
16. Huang DW, Sherman BT, Tan Q, Kir J, Liu D, Bryant D, et al. DAVID bioinformatics resources: expanded annotation database and novel algorithms to better extract biology from large gene lists. *Nucleic Acids Res*. (2007) 35:W169–75. doi: 10.1093/nar/gkm415
17. Szklarczyk D, Morris JH, Cook H, Kuhn M, Wyder S, Simonovic M, et al. The STRING database in 2017: quality-controlled protein-protein association networks, made broadly accessible. *Nucleic Acids Res*. (2017) 45:D362–8. doi: 10.1093/nar/gkw937
18. Gao J, Aksoy BA, Dogrusoz U, Dresdner G, Gross B, Sumer SO, et al. Integrative analysis of complex cancer genomics and clinical profiles using the cBioPortal. *Sci Signal*. (2013) 6:pl1. doi: 10.1126/scisignal.2004088
19. Cerami E, Gao J, Dogrusoz U, Gross BE, Sumer SO, Aksoy BA, et al. The cBio cancer genomics portal: an open platform for exploring multidimensional cancer genomics data. *Cancer Discov*. (2012) 2:401–4. doi: 10.1158/2159-8290.CD-12-0095
20. Li T, Fan J, Wang B, Traugh N, Chen Q, Liu JS, et al. TIMER: a web server for comprehensive analysis of tumor-infiltrating immune cells. *Cancer Res*. (2017) 77:e108–10. doi: 10.1158/0008-5472.CAN-17-0307
21. Tumeh PC, Harview CL, Yearley JH, Shintaku IP, Taylor EJ, Robert L, et al. PD-1 blockade induces responses by inhibiting adaptive immune resistance. *Nature*. (2014) 515:568–71. doi: 10.1038/nature13954
22. Sallusto F, Lenig D, Forster R, Lipp M, Lanzavecchia A. Two subsets of memory T lymphocytes with distinct homing potentials and effector functions. *Nature*. (1999) 401:708–12. doi: 10.1038/44385
23. Ludewig B, Oehen S, Barchiesi F, Schwendener RA, Hengartner H, Zinkernagel RM. Protective antiviral cytotoxic T cell memory is most efficiently maintained by restimulation via dendritic cells. *J Immunol*. (1999) 163:1839–44.
24. Wherry EJ, Teichgraber V, Becker TC, Masopust D, Kaech SM, Antia R, et al. Lineage relationship and protective immunity of memory CD8 T cell subsets. *Nat Immunol*. (2003) 4:225–34. doi: 10.1038/ni889
25. van Panhuys N, Perret R, Prout M, Ronchese F, Le Gros G. Effector lymphoid tissue and its crucial role in protective immunity. *Trends Immunol*. (2005) 26:242–7. doi: 10.1016/j.it.2005.03.005
26. Klebanoff CA, Gattinoni L, Torabi-Parizi P, Kerstann K, Cardones AR, Finkelstein SE, et al. Central memory self/tumor-reactive CD8+ T cells confer superior antitumor immunity compared with effector memory T cells. *Proc Natl Acad Sci USA*. (2005) 102:9571–6. doi: 10.1073/pnas.0503726102
27. Klebanoff CA, Gattinoni L, Restifo NP. CD8+ T-cell memory in tumor immunology and immunotherapy. *Immunol Rev*. (2006) 211:214–24. doi: 10.1111/j.0105-2896.2006.00391.x
28. Vivier E, Raulet DH, Moretta A, Caligiuri MA, Zitvogel L, Lanier LL, et al. Innate or adaptive immunity? The example of natural killer cells. *Science*. (2011) 331:44–9. doi: 10.1126/science.1198687
29. Sun JC, Beilke JN, Lanier LL. Adaptive immune features of natural killer cells. *Nature*. (2009) 457:557–61. doi: 10.1038/nature07665
30. Morvan MG, Lanier LL. NK cells and cancer: you can teach innate cells new tricks. *Nat Rev Cancer*. (2016) 16:7–19. doi: 10.1038/nrc.2015.5
31. Long EO, Kim HS, Liu D, Peterson ME, Rajagopalan S. Controlling natural killer cell responses: integration of signals for activation and inhibition. *Ann Rev Immunol*. (2013) 31:227–58. doi: 10.1146/annurev-immunol-020711-075005
32. Idorn M, Hojman P. Exercise-dependent regulation of NK cells in cancer protection. *Trends Mol Med*. (2016) 22:565–77. doi: 10.1016/j.molmed.2016.05.007
33. Palsson-McDermott EM, O'Neill LA. The Warburg effect then and now: from cancer to inflammatory diseases. *Bioessays*. (2013) 35:965–73. doi: 10.1002/bies.201300084
34. Pearce EL, Pearce EJ. Metabolic pathways in immune cell activation and quiescence. *Immunity*. (2013) 38:633–43. doi: 10.1016/j.immuni.2013.04.005
35. Michalek RD, Gerriets VA, Jacobs SR, Macintyre AN, MacIver NJ, Mason EF, et al. Cutting edge: distinct glycolytic and lipid oxidative metabolic programs are essential for effector and regulatory CD4+ T cell subsets. *J Immunol*. (2011) 186:3299–303. doi: 10.4049/jimmunol.1003613
36. Dhup S, Dadhich RK, Porporato PE, Sonveaux P. Multiple biological activities of lactic acid in cancer: influences on tumor growth, angiogenesis and metastasis. *Curr Pharm Des*. (2012) 18:1319–30. doi: 10.2174/138161212799504902
37. Fallarino F, Grohmann U, Vacca C, Bianchi R, Orabona C, Spreca A, et al. T cell apoptosis by tryptophan catabolism. *Cell Death Differ*. (2002) 9:1069–77. doi: 10.1038/sj.cdd.4401073
38. O'Donnell JS, Massi D, Teng MWL, Mandala M. PI3K-AKT-mTOR inhibition in cancer immunotherapy, redux. *Semin Cancer Biol*. (2018) 48:91–103. doi: 10.1016/j.semcancer.2017.04.015
39. Fridman WH, Pages F, Sautes-Fridman C, Galon J. The immune contexture in human tumours: impact on clinical outcome. *Nat Rev Cancer*. (2012) 12:298–306. doi: 10.1038/nrc3245
40. Okkenhaug K. Signaling by the phosphoinositide 3-kinase family in immune cells. *Ann Rev Immunol*. (2013) 31:675–704. doi: 10.1146/annurev-immunol-032712-095946
41. Kim EH, Suresh M. Role of PI3K/Akt signaling in memory CD8 T cell differentiation. *Front Immunol*. (2013) 1:4–20. doi: 10.3389/fimmu.2013.00020
42. Peng W, Chen JQ, Liu C, Malu S, Creasy C, Tetzlaff MT, et al. Loss of PTEN promotes resistance to T cell-mediated immunotherapy. *Cancer Discov*. (2016) 6:202–16. doi: 10.1158/2159-8290.CD-15-0283

43. Abu-Eid R, Samara RN, Ozbun L, Abdalla MY, Berzofsky JA, Friedman KM, et al. Selective inhibition of regulatory T cells by targeting the PI3K-Akt pathway. *Cancer Immunol Res*. (2014) 2:1080–9. doi: 10.1158/2326-6066.CIR-14-0095
44. van der Waart AB, van de Weem NM, Maas F, Kramer CS, Kester MG, Falkenburg JH, et al. Inhibition of Akt signaling promotes the generation of superior tumor-reactive T cells for adoptive immunotherapy. *Blood*. (2014) 124:3490–500. doi: 10.1182/blood-2014-05-578583
45. Lazarevic V, Glimcher Lh Fau—Lord GM, Lord GM. T-bet: a bridge between innate and adaptive immunity. *Nat Rev Immunol*. (2013) 13:777–89. doi: 10.1038/nri3536
46. Okkenhaug K, Turner M, Gold MR. PI3K Signaling in B cell and T cell biology. *Front Immunol*. (2014) 5:557. doi: 10.3389/fimmu.2014.00557
47. Kremmidiotis G, Baker E, Crawford J, Eyre HJ, Nahmias J, Callen DF. Localization of human cadherin genes to chromosome regions exhibiting cancer-related loss of heterozygosity. *Genomics*. (1998) 49:467–71. doi: 10.1006/geno.1998.5281
48. Winklmeier A, Contreras-Shannon V, Arndt S, Melle C, Bosserhoff AK. Cadherin-7 interacts with melanoma inhibitory activity protein and negatively modulates melanoma cell migration. *Cancer Sci*. (2009) 100:261–8. doi: 10.1111/j.1349-7006.2008.01048.x
49. Moore R, Champeval D, Denat L, Tan SS, Faure F, Julien-Grille S, et al. Involvement of cadherins 7 and 20 in mouse embryogenesis and melanocyte transformation. *Oncogene*. (2004) 23:6726–35. doi: 10.1038/sj.onc.1207675
50. Li G, Yuan L, Liu D, Liu J. Upregulation of leucine zipper protein mRNA in hepatocellular carcinoma associated with poor prognosis.*Technol Cancer Res Treat*. (2016) 15:517–22. doi: 10.1177/1533034615587432
51. Chen X, Li D, Wang N, Yang M, Liao A, Wang S, et al. Bioinformatic analysis suggests that UGT2B15 activates the HippoYAP signaling pathway leading to the pathogenesis of gastric cancer. *Oncol Rep*. (2018) 40:1855–62. doi: 10.3892/or.2018.6604
52. Hu DG, Selth LA, Tarulli GA, Meech R, Wijayakumara D, Chanawong A, et al. Androgen and estrogen receptors in breast cancer coregulate human UDP-Glucuronosyltransferases 2B15 and 2B17. *Cancer Res*. (2016) 76:5881–93. doi: 10.1158/0008-5472.CAN-15-3372
53. Grosse L, Paquet S, Caron P, Fazli L, Rennie PS, Belanger A, et al. Androgen glucuronidation: an unexpected target for androgen deprivation therapy, with prognosis and diagnostic implications. *Cancer Res*. (2013) 73:6963–71. doi: 10.1158/0008-5472.CAN-13-1462

Conflict of Interest: The authors declare that the research was conducted in the absence of any commercial or financial relationships that could be construed as a potential conflict of interest.

frontiers in Oncology

SYSTEMATIC REVIEW
published: 05 February 2020
doi: 10.3389/fonc.2020.00029

Thermal Intravesical Chemotherapy Reduce Recurrence Rate for Non-muscle Invasive Bladder Cancer Patients: A Meta-Analysis

*Kang Liu†, Jun Zhu†, Yu-Xuan Song, Xiao Wang, Ke-Chong Zhou, Yi Lu and Xiao-Qiang Liu**

Department of Urology, Tianjin Medical University General Hospital, Tianjin Medical University, Tianjin, China

OPEN ACCESS

Edited by:
Ja Hyeon Ku,
Seoul National University, South Korea

Reviewed by:
Chang Wook Jeong,
Seoul National University Hospital, South Korea
Donald Lee Lamm,
University of Arizona, United States
Fabio Campodonico,
Ente Ospedaliero Ospedali Galliera, Italy

***Correspondence:**
Xiao-Qiang Liu
xiaoqiangliu1@163.com

†*These authors share first authorship*

Specialty section:
This article was submitted to Genitourinary Oncology, a section of the journal Frontiers in Oncology

Received: *16 October 2019*
Accepted: *09 January 2020*
Published: *05 February 2020*

Citation:
Liu K, Zhu J, Song Y-X, Wang X, Zhou K-C, Lu Y and Liu X-Q (2020) Thermal Intravesical Chemotherapy Reduce Recurrence Rate for Non-muscle Invasive Bladder Cancer Patients: A Meta-Analysis. Front. Oncol. 10:29. doi: 10.3389/fonc.2020.00029

Background: Non-muscle invasive bladder cancer accounts for nearly 80% of newly diagnosed bladder cancer cases, which often recur and progress. This meta-analysis was evaluated by the adverse events and recurrence rate of thermal intravesical chemotherapy vs. normal temperature intravesical chemotherapy in the treatment of non-muscle invasive bladder cancer.

Methods: A systematic review and cumulative analysis of studies reporting adverse events and recurrence rate of thermal intravesical chemotherapy vs. normal temperature intravesical chemotherapy was performed through a comprehensive search of Pubmed, Embase, Cochranelibrary.com, CNKI, Wanfang Med Online database and VIP database. All analyses were performed using the Revman manager 5.

Result: Twelve studies (11 randomized controlled trials and 1 retrospective study) including 888 patients, 445 in the thermal intravesical chemotherapy group, and 443 in the normal temperature intravesical chemotherapy group, met the eligibility criteria. Patients in the thermal intravesical chemotherapy group had a lower risk of disease recurrence than those who had normal temperature intravesical chemotherapy (24 months follow-up group: RR = 0.30, 95% CI: 0.21–0.43, $P < 0.00001$, $I^2 = 0\%$; 36 months follow-up group: RR = 0.27, 95% CI: 0.14–0.54, $P = 0.0002$, $I^2 = 0\%$) while no significant difference in adverse events rate (RR = 0.89, 95% CI = 0.53–1.52; $P = 0.67$, $I^2 = 78\%$).

Conclusions: When compared with normal temperature intravesical chemotherapy, thermal intravesical chemotherapy can reduce the recurrence rate without increasing incidence of adverse events in patients with non-muscle invasive bladder cancer.

Keywords: thermal intravesical chemotherapy, normal temperature intravesical chemotherapy, hyperthermic intravesical chemotherapy, external thermal field thermotherapy, non-muscle invasive bladder cancer, meta-analysis

INTRODUCTION

Bladder cancer is one of the most common tumors in the urology system. In terms of its morbidity, it ranks the fourth among men and eleventh among women in all kinds of tumor, respectively (1). Last year, bladder cancer contributed more than 500,000 new cases and 190,000 deaths in 185 countries (2). Non-muscle invasive bladder cancer (NMIBC) makes up nearly 80% of newly diagnosed bladder carcinoma cases, of which Tis accounts for 10%, T1 for 30%, and Ta for 60% (3). Although the prognosis of patients with NMIBC have made great progress over the past decades, the recurrence and progression rate is still high. More than 60% of NMIBC patients will recur and more than 20% will progress into higher stages (4). Therefore, the economic burden created by intensive treatment and surveillance of NMIBC is very heavy for both individuals and governments.

Transurethral resection of bladder tumor (TURBT) is the most important diagnostic method and also the main treatment of NMIBC, but it could not prevent the recurrence and progression (5). Thus, adjuvant intravesical therapy came into being. It consists of bladder infusion chemotherapy and immunotherapy (6). One of the most effective intravesical therapy is bacillus Calmette-Guerin (BCG), which requires special care for its bio toxicity (7). And many other drugs, including mitomycin C (MMC), pirarubicin (THP), gemcitabine (GEM), hydroxycamptothecine (HCPT), etc. have been applied to intravesical chemotherapy (8). Despite all these efforts, the recurrence rate remains at 30% (9). In a word, preventing recurrence of NMIBC after TURBT still remains a challenge (10).

In recent years, thermal therapy has received increasing attention as a treatment for malignant tumors (11). High temperatures may enhance drug function by encouraging tumor cells to absorb more chemotherapeutic agents, redistributing their intracellular concentrations, altering metabolic patterns and/or inhibiting repair of DNA damage (12). Since NMIBC is prone to recurrence, thermal intravesical chemotherapy has been developed to improve the effectiveness of the treatment (13). It seems that thermal intravesical chemotherapy is good for patients with NMIBC (14). This meta-analysis is aimed to discuss whether thermal intravesical chemotherapy is associated with better efficacy with less or at least the same adverse events than normal temperature intravesical chemotherapy.

METHODS

Eligibility Criteria

Studies were suitable for inclusion if they meet the following criteria: (1) participants: NMIBC patients receiving TURBT; (2) intervention: thermal intravesical chemotherapy; (3) control: normal temperature intravesical chemotherapy; (4) containing both of the following outcomes: recurrence rate and adverse event; (5) study design: randomized controlled trials (RCTs) or retrospective studies. The adverse event is as follow: cystitis, bladder irritation, hematuria, urinary pain, lower urinary tract symptoms, urinary tract infection, anorexia, anxiety, insomnia, rash, lower abdomen skin redness, fatigue, myelosuppression, influenza-like symptoms, and abnormal blood biochemical indexes. Exclusion criteria are as follows: (1) thermal intravesical chemotherapy was discontinued during the treatment schedule; (2) data cannot be obtained even after contacting the author; (3) duplicated publications. When multiple studies were delivered by the same researcher based on similar patients, only the most comprehensive or largest one was included.

Study Search and Selection

Eligible studies focusing on the topic were identified through searching Pubmed, Embase, Cochranelibrary.com, CNKI, Wanfang Med Online database and VIP database. The search

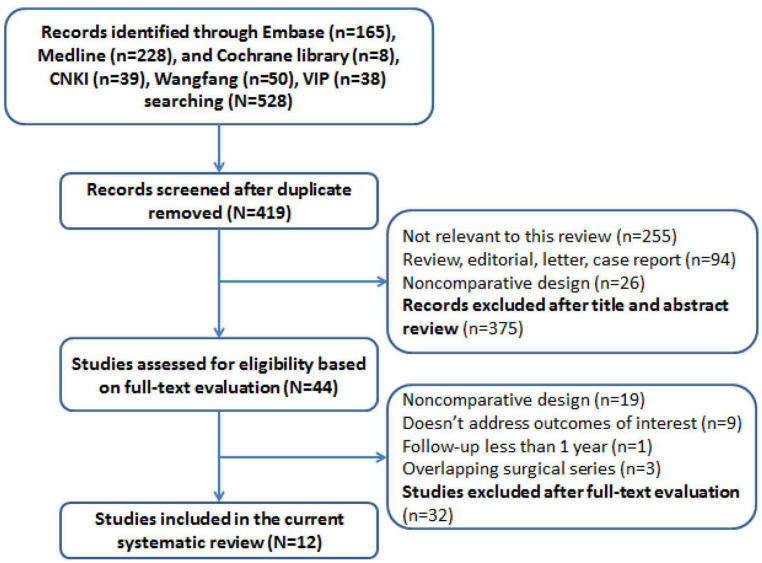

FIGURE 1 | Flow diagram of study selection in the meta-analysis.

TABLE 1 | Characteristics of the studies included in the meta-analysis.

Reference	Study period	Study design	Sample size	Clinical protocals	Number of patients	Age (yrs)	Median follow-up (month)	Tumor stage	Pathological grade	Significantly differ between groups	Previous intravesical treatment	Treatment device	Treatment schedule	Dose	Temperature (°C)	Duration (min)	Severity of AE	AE
Zhao et al. (15)	2011–2016	Single-center RCT	150	BCG	48	65.0 ± 7.1	24	NR	NR	No	NR	LR-2005 external thermal field treatment system (Guangzhou Laiwei Medical Devices Co., Ltd. Guangzhou, China)	**BCG:** 2 weeks after TURBT, BCG (150 mg) once a week for 6 weeks, then perfusion enhancement was performed at 3, 6, and 12 months, respectively. **ETFT-MMC:** 1 week after TURBT, MMC (30 mg) perfusion associated with ETFT once a week for 8 weeks, then once a month for 12 months. **MMC:** 1 week after TURBT, MMC (30 mg) once a week for 8 weeks, then once a month for 12 months.	–	NT	NR	Mild	Two influenza-like symptoms
				ETFT-MMC	49	67.0 ± 5.2	24							30 mg/30 ml	41∼43	60		Three lower abdomen skin redness
				MMC	48	66.0 ± 5.4	24							30 mg/30 ml	NT	NR		0
Colombo et al. (16)	1994–1999	Multicentre RCT	83	ETFT-MMC	39	≤95:>65 = 25:17	24.0	Ta:T1:CIS = 15:26;1	G1:G2:G3 = 4:27:11	No	Having not received either local or systemic chemotherapy or radiotherapy during the last 3 months.	Synergo101–1 (Medical Enterprises, Amsterdam, the Netherlands)	**ETFT-MMC:** 20–40 days after TURBT, an induction cycle of 8 weekly sessions and a subsequent maintenance regimen of 4 monthly sessions. **MMC:** 20–40 days after TURBT, an induction cycle of 8 weekly sessions and a subsequent maintenance regimen of 4 monthly sessions.	20 mg/50 ml	40∼44	40∼60	Various	Thirty-four have different side effects of different severity
				MMC	36	≤65:>65 = 16:25	24.0	Ta:T1 = 17:24	G1:G2:G3 = 1:33:7					20 mg/50 ml	NT	60		Twenty-one have different side effects of different severity
Gao et al. (17)	2009–2012	Single-center RCT	64	HIVEC-MMC	32	54.9 ± 8.1	36.0	T1	G1:G2 = 16:16	No	NR	NR	**HIVEC-MMC:** 1 week after TURBT, MMC (30mg) once a week for 6 weeks, then every 2 weeks for six rounds. **MMC:** 1week after TURBT, MMC (30mg) once a week for 6 weeks, then every 2 weeks for six rounds.	30 mg/500 ml	42∼43	120	Mild	Six bladder irritation

(Continued)

TABLE 1 | Continued

Reference	Study period	Study design	Sample size	Clinical protocals	Number of patients	Age (yrs)	Median follow-up (month)	Tumor stage	Pathological grade	Significantly differ between groups	Previous intravesical treatment	Treatment device	Treatment schedule	Dose	Temperature (°C)	Duration (min)	Severity of AE	AE
				MMC	32	56.5 ± 5.6	36.0		G1:G2 = 14:18					30 mg/500 ml	NT	NR		Seven bladder irritation
Guo et al. (18)	2013–2015	Single-center RCT	84	HIVEC-GEM	42	77.0 ± 6.0	24.0	Tis:TaG1/G2:G3:T1 = 3:20:11:8		No	NR	NR	**HIVEC-GEM:** Within 6 h after TURBT, GEM (1,000 mg) hyperthermic perfusion, then once a week for 8 weeks, after that every months for 1 year. **GEM:** Within 6 h after TURBT, GEM (1,000 mg) normal temperature perfusion, then once a week for 8 weeks, after that every months for 1 year.	1,000 mg/500 ml	42∼44	120	Mild	Two hematuria and three urinary pain and four cystitis and three anorexia and three anxiety and two insomnia and one rash
				GEM	42	76.0 ± 7.0	24.0	Tis:TaG1/G2:G3:T1 = 4:20:12:6						NR	NT	NR		Eight hematuria and 10 urinary pain and 11 cystitis and 4 anorexia and 3 anxiety and 3 insomnia and 1 rash
Guo et al. (19)	2014–2016	Single-center RCT	74	HIVEC-THP	38	75.9 ± 5.7	24.0	Ta:T1 = 20:18	G1:G2 = 23:15	No	NR	NR	**HIVEC-THP:** Within 6 h after TURBT, THP (40 mg) hyperthermic perfusion, then once a week for 8 weeks, after that every months for 1 year. **THP:** 1 week after TURBT, THP (40 mg) normal temperature perfusion, then once a week for 8 weeks, after that every months for 1 year.	40 mg/45 ml	42∼44	NR	Mild	Repeated calculation
				THP	36	75.0 ± 5.8	24.0	Ta:T1 = 19:17	G1:G2 = 24:12					40 mg/45 ml	NT	NR		
Li et al. (20)	2011–2014	Single-center RCT	90	HIVEC-MMC	45	58.4 ± 10.2	NR	T1	G1:G2 = 16:29	No	NR	BR-TRG-I type high-precision hyperthermic intraperitoneal perfusion treatment system	**HIVEC-MMC:** 3 days after TURBT, MMC (80 mg) hyperthermic perfusion, three times a day for four rounds. **MMC:** Within 24 h after TURBT, MMC normal temperature perfusion, then every 3 days for four rounds.	80 mg/600 ml	43	45	Mild	Ten bladder irritation

(Continued)

TABLE 1 | Continued

Reference	Study period	Study design	Sample size	Clinical protocals	Number of patients	Age (yrs)	Median follow-up (month)	Tumor stage	Pathological grade	Significantly differ between groups	Previous intravesical treatment	Treatment device	Treatment schedule	Dose	Temperature (°C)	Duration (min)	Severity of AE	AE
				MMC	45	60.4 ± 10.2	NR		G1:G2 = 14:31					NR	NT	45		Seven bladder irritation and one myelosuppression and one abnormal blood biochemical indexes
Liu et al. (21)	2009–2011	Single-center RCT	56	ETFT-THP	27	48.0~84.0	24.0	NR	low grade: high grade = 34:22	NR	No	ZD-2001 external thermal field treatment system	**ETFT-THP:** after TURBT, THP (40 mg) perfusion associated with ETFT once a week for 6 weeks, then THP (40 mg) only once every 2 weeks for 6 rounds, after that every months for six months. **THP:** after TURBT, THP (40 mg) once a week for 6 weeks, then once every 2 weeks for six rounds, after that every months for 6 months.	40 mg/40 ml	41~43	60	Mild	Five LUTS and two abnormal blood biochemical indexes
				THP	29		24.0							40 mg/40 ml	NT	30		13 LUTS and one abnormal blood biochemical indexes
Liu et al. (22)	2011–2014	Single-center RCT	40	HIVEC-MMC	20	51.5 ± 20.2	36.0	T1	G1:G2 = 18:22	No	NR	NR	**HIVEC-MMC:** 1 week after TURBT, MMC (30 mg) hyperthermic perfusion once a week for 6 weeks, then once every 2 weeks for six rounds. **MMC:** 1 week after TURBT, MMC (30 mg) once a week for 6 weeks, then once every 2 weeks for six rounds.	30 mg/500 ml	42~43	120	Mild	Four hematuria and 10 bladder irritation
				MMC	20		36.0							30 mg/500 ml	NT	NR		Two hematuria and eight bladder irritation
Peng et al. (23)	2010–2012	Single-center RCT	86	HIVEC-THP	44	42.0~68.0	22.3	Ta:T1 = 24:20	G1:G2 = 23:21	No	No	BR-TRG-I type high-precision hyperthermic intraperitoneal perfusion treatment system	**HIVEC-THP:** 1 week after TURBT, THP (40 mg) hyperthermia perfusion once a week for 8 weeks, after that every months for 8 months. **THP:** 1 week after TURBT, THP (40 mg) once a week for 8 weeks, after that every months for 8 months.	40 mg/600 ml	45	60	Mild	One gross hematuria

(Continued)

TABLE 1 | Continued

Reference	Study period	Study design	Sample size	Clinical protocals	Number of patients	Age (yrs)	Median follow-up (month)	Tumor stage	Pathological grade	Significantly differ between groups	Previous intravesical treatment	Treatment device	Treatment schedule	Dose	Temperature (°C)	Duration (min)	Severity of AE	AE
				THP	42		22.3	Ta:T1 = 23:19	G1:G2 = 10:32					40 mg/50 ml	NT	60		0
Su et al. (24)	2012–2014	Single-center RCT	76	HIVEC-MMC	38	50.2 ± 7.3	36.0	NR	NR	No	NR	NR	**HIVEC-MMC:** After TURBT, MMC (30 mg) hyperthermic perfusion once a week for 6 weeks, then twice a month for six rounds. **MMC:** After TURBT, MMC (30 mg) once a week for 6 weeks, then twice a month for six rounds.	30 mg/300 ml	45	120	Mild	One bladder irritation and one urinary tract infection
				MMC	38	50.5 ± 7.6	36.0							30 mg/500 ml	NT	NR		Four bladder irritation and four urinary tract infection and three fatigue
Zhao et al. (25)	2009–2014	Single-center RCT	83	ETFT-HCPT	39	65.0 ± 7.1	24.0	Ta:T1 = 15:27	G1:G2:G3 = 4:27:11	No	NR	LR-2005 external thermal field treatment system (Guangzhou Laiwei Medical Devices Co., Ltd. Guangzhou, China)	**ETFT-HCPT:** Within 24 h after TURBT, HCPT (20 mg) perfusion associated with ETFT, then once a week for 8 weeks, after that once a month for 6 months. **HCPT:** Within 24 h after TURBT, HCPT (20 mg) perfusion only, then once a week for 8 weeks, after that once a month for 6 months.	20 mg/40 ml	41∼43	60	Mild	Repeated calculation
				HCPT	37	67.0 ± 5.2	24.0	Ta:T1 = 17:24	G1:G2:G3 = 1:33:7					20 mg/40 ml	NT	60		
Wang et al. (26)	2010–2015	Single-center Retrospective	74	HIVEC-THP	37	62.2 ± 7.4	24.0	Ta:T1 = 19:18	low grade: high grade = 27:10	No	No	BR-TRG-I type high-precision hyperthermic intraperitoneal perfusion treatment system	**HIVEC-THP:** Within 24 h after TURBT, THP (30 mg) hyperthermic perfusion, then once a week for 8 weeks, after that once a month. **THP:** Within 24 h after TURBT, THP (30 mg) perfusion, then once a week for 8 weeks, after that once a month.	30 mg/1,500 ml	43	60	Mild	Five bladder irritation
				THP	37	61.5 ± 7.2	24.0	Ta:T1 = 21:16	low grade: high grade = 29:8					30 mg/50 ml	NT	60		Two bladder irritation

RCT, randomized controlled trial; ETFT, external thermal field thermotherapy; HIVEC, hyperthermic intravesical chemotherapy; MMC, mitomycin C; THP, pirarubicin; GEM, gemcitabine; HCPT, hydroxycamptothecine; NT, normal temperature; NR, not report.

strategy is given in **Appendix I**. We also browsed reference lists of systematic reviews on this topic to find any other qualified articles. All searches without language limits but limited to studies on humans.

Two independent reviewers (LK and ZJ) examined the titles and abstracts according to eligibility criteria mentioned before. Studies underwent full-text examination after removing duplicated, irrelevant, review, case report, letter, editorial and non-comparative design studies. Divergences were resolved by discussion with another reviewer (S-YX).

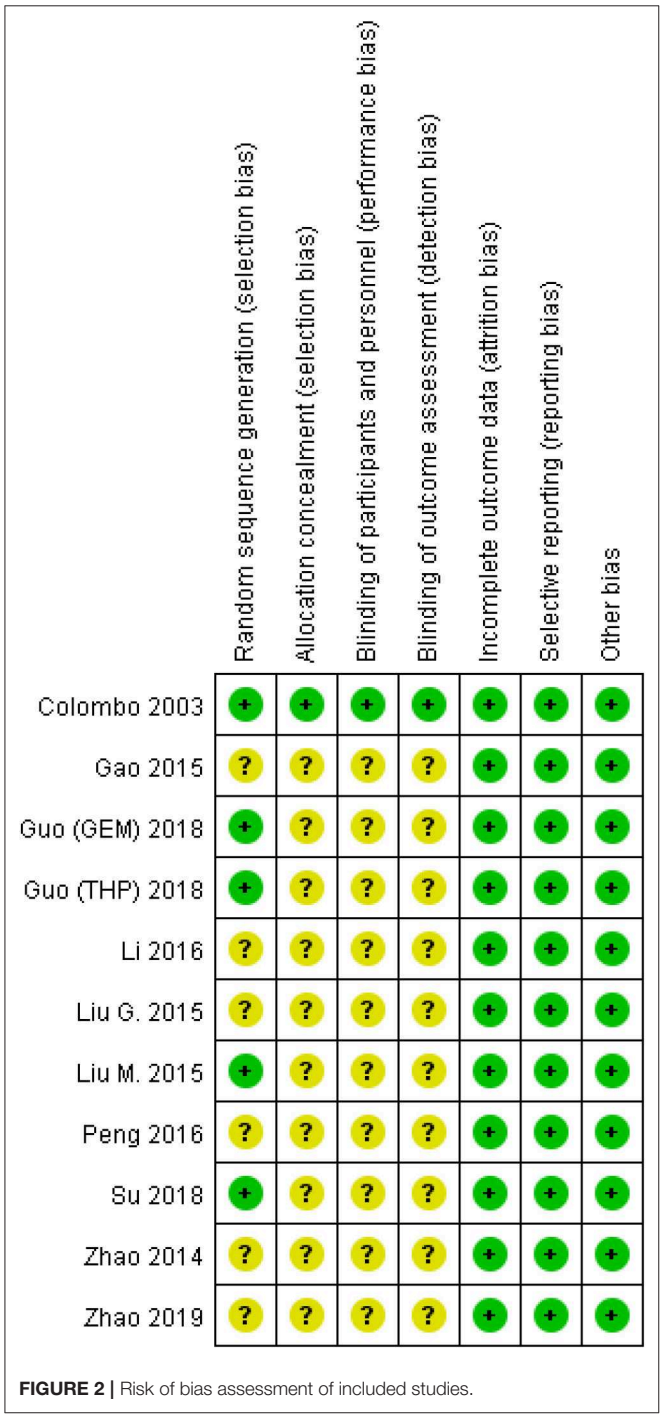

FIGURE 2 | Risk of bias assessment of included studies.

Quality Assessment and Data Extraction

The quality of all included RCTs was assessed using the "risk of bias" tool recommended by the Cochrane Collaboration. It consists of the following domains: random sequence generation, allocation concealment, blinding of participants and personnel, blinding of outcome assessment, incomplete outcome data, selective reporting and other bias. The Newcastle-ottawa quality scale was used to assess the quality of retrospective studies. Two reviewers (LK and ZJ) independently evaluated the quality of studies in these domains.

Data extraction was also executed by two reviewers (LK and ZJ) independently. The following information was extracted: first author's name, year of publication, study period, study design, sample size, clinical protocols, and number of patients who completed the study, age of participants, median follow-up, treatment schedule, and relevant data on outcomes. Disagreements were discussed and consensus was finally achieved.

Statistical Analysis

Relative risks (RR) with 95%CIs for the adverse events rate were calculated to evaluate the safety of thermal intravesical chemotherapy, as well as for the recurrence rate of different follow-up groups to assess the effectiveness. Chi-squared tests were used to detect heterogeneity between studies included in this meta-analysis. Considering that the statistical power of the heterogeneity test is generally low, a P-value of 0.10 was set as the significance threshold for the heterogeneity. The heterogeneity was considered significant if $P \leq 0.1$. We used I-squared (I^2) statistic to indicate the proportion of variation between the studies due to heterogeneity. The larger the I^2 value represented, the higher the heterogeneity was. And $I^2 > 50\%$ suggested substantial heterogeneity among the studies. Fixed effect model was adopted when no significant heterogeneity was detected ($P > 0.1$ and $I^2 < 50\%$), otherwise, random effect model would be used. We did subgroup analyses between two treatment regimens according to the clinical protocols of study (hyperthermic intravesical chemotherapy vs. external

TABLE 2 | Newcastle-ottawa quality scale.

	Wang et al.
Is the case definition adequate?	1
Representativeness of the cases	1
Selection of Controls	1
Definition of Controls	1
Comparability of cases and controls on the basis of the design or analysis	1
Ascertainment of exposure	1
Same method of ascertainment for cases and controls	1
Non-response rate	1
Total	8

thermal field thermotherapy), chemotherapeutic agent used in chemotherapy (MMC, THP, GEM, HCPT). All statistical analyses were performed using Revman software (version 5.3, The Cochrane Collaboration).

RESULTS

Study Selection

Five hundred and twenty-eight studies were identified from the aforementioned databases. One hundred and nine duplicated studies were first removed. Four hundred and nineteen studies were under screening titles and abstracts, among which 14 potentially relevant studies were obtained, and full texts were carefully checked for eligibility examination. Finally, 12 studies with a total of 888 participants were included in the meta-analysis. The process of study selection is shown in **Figure 1**.

Study Characteristics

The characteristics of the included studies are summarized in **Table 1**. These studies were published between 2003 and 2019, 11 studies with an RCT design and one, a retrospective study. A total of 888 participants were enrolled, with a median size of 74 (ranging from 40 to 150). All of the studies had enrolled patients with NMIBC. The median duration of follow-up across the studies was 24 months. Treatment schedules varied between these studies.

Quality Assessment

The "risk of bias" tool recommended by the Cochrane Collaboration was adopted to assess the quality of included RCTs (**Figure 2**). Five studies (16, 18, 19, 22, 24) described how random sequence was generated, and all RCTs except Colombo et al. didn't describe the allocation concealment and Blind method. No incomplete or selective outcome data was reported. Quality assessments of cohort studies were conducted according to the Newcastle-Ottawa Scale (NOS), which was developed to assess bias risk including three domains with eight items (**Table 2**).

Recurrence Rate

All studies were available, including 888 patients, 445 in the thermal intravesical chemotherapy group and 443 in the normal temperature intravesical chemotherapy group. The meta-analysis demonstrated a significant difference in recurrence rate between thermal intravesical chemotherapy with normal temperature intravesical chemotherapy in different follow-up groups (24 months follow-up group: RR = 0.30, 95% CI: 0.21–0.43, $P < 0.00001$, $I^2 = 0\%$; 36 months follow-up group: RR = 0.27, 95% CI: 0.14–0.54, $P = 0.0002$, $I^2 = 0\%$; **Figure 3**). The publishing bias are

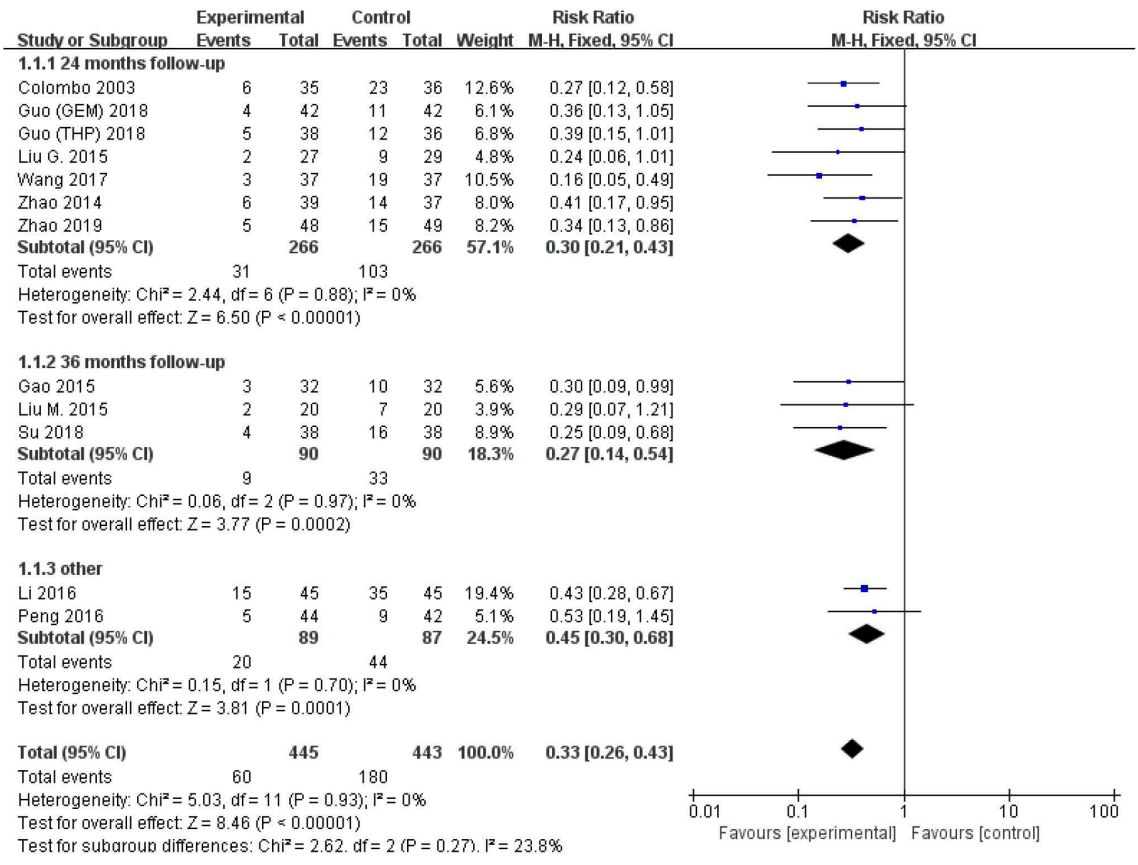

FIGURE 3 | Forest plot of recurrence rate comparing thermal intravesical chemotherapy with normal temperature intravesical chemotherapy in different follow-up groups.

limited ($P = 0.95$, $I^2 = 0\%$; **Figure 4**). Subgroup analysis shows that both HIVEC and ETFT vs. normal temperature intravesical chemotherapy confirm a significant difference statistically (RR = 0.34, 95% CI: 0.25–0.46, $P < 0.00001$ and RR = 0.31, 95% CI: 0.20–0.50, $P < 0.00001$; **Figure 5**). As for the different drugs used in the thermal intravesical chemotherapy, MMC and THP both can reduce the recurrence rate (RR = 0.33, 95% CI: 0.24–0.46, $P < 0.00001$ and RR = 0.30, 95% CI: 0.18–0.51, $P < 0.00001$; **Figure 6**).

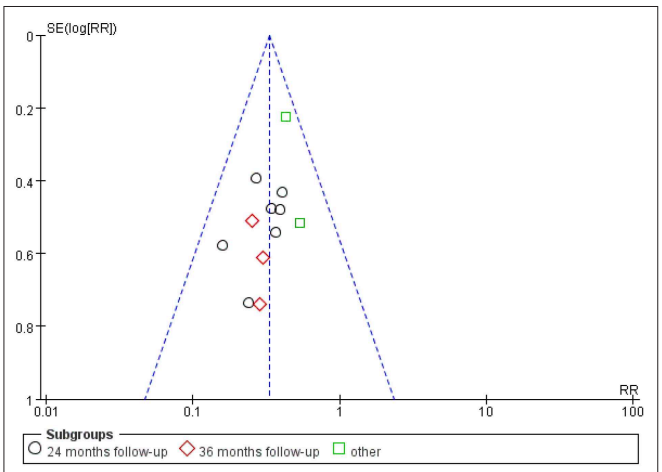

FIGURE 4 | Funnel plot of included studies.

Adverse Event Rate

The comparison of adverse events rate involved 10 studies ($n = 740$) because the other two studies were double-counted. Thermal intravesical chemotherapy seemed no more toxic than normal temperature intravesical chemotherapy (RR = 0.89, 95% CI: 0.53–1.51, $P = 0.67$; **Figure 7**). Subgroup analysis shows that the adverse events rate of thermal intravesical chemotherapy using different methods (HIVEC group: RR = 0.84, 95% CI: 0.46–1.54, $P = 0.57$; ETFT group: RR = 1.08, 95% CI: 0.31–3.80, $P = 0.90$; **Figure 8**) or different drugs (MMC group: RR = 1.12, 95% CI: 0.69–1.81, $P = 0.65$; THP group: RR = 1.04, 95% CI: 0.23–4.77, $P = 0.96$; **Figure 9**) was not statistically different from that at normal temperature.

DISCUSSION

The idea that thermal therapy can treat the tumor can be traced back to 1910 from Coley (27). And Rigatti et al. first applied thermal therapy to treat superficial bladder tumors in 1991 (28). Then Colombo et al. used a microwave device to make local bladder heating for intravesical chemotherapy, with a good overall response rate of 90.8% in 44 superficial bladder cancer patients (29). As the encouraging results were achieved, more and more urologists join to investigate thermal intravesical chemotherapy. Van der Heijden et al. reported 90 patients received combined treatment of MMC and local microwave hyperthermia. Finally, the risk of recurrence was 24.6% after a 2 year follow-up and no one suffered from stage

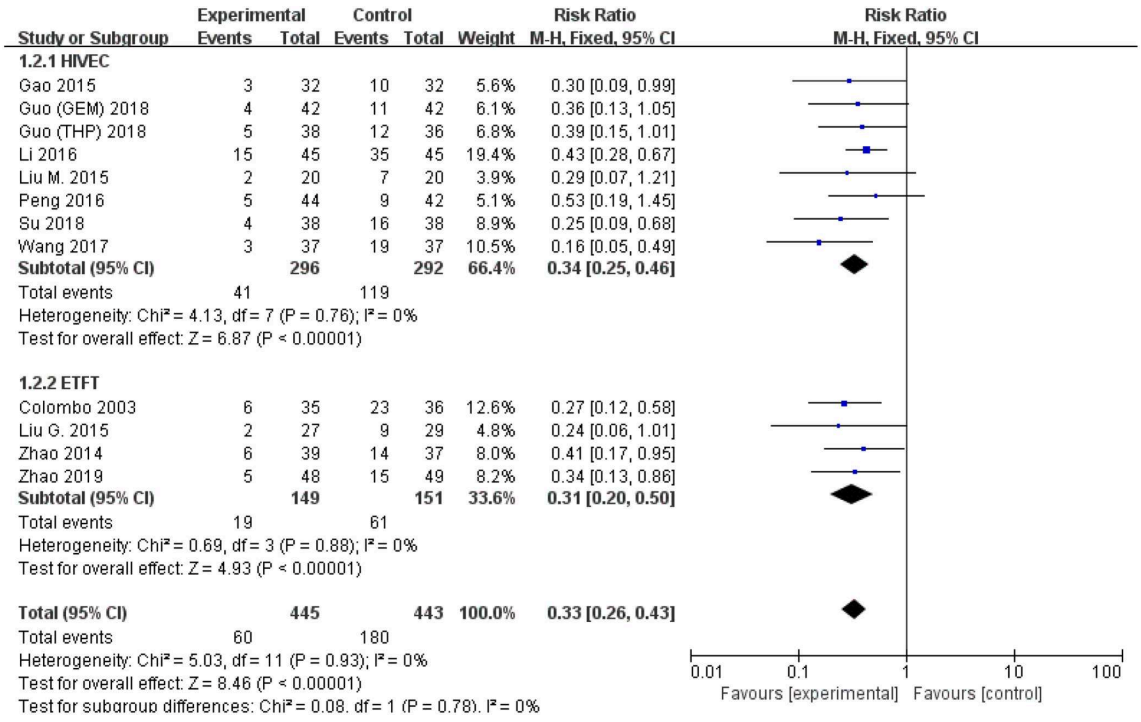

FIGURE 5 | Comparison on recurrence rate between thermal intravesical chemotherapy and normal temperature intravesical chemotherapy after subgroup analysis stratified by different approach used in thermal therapy.

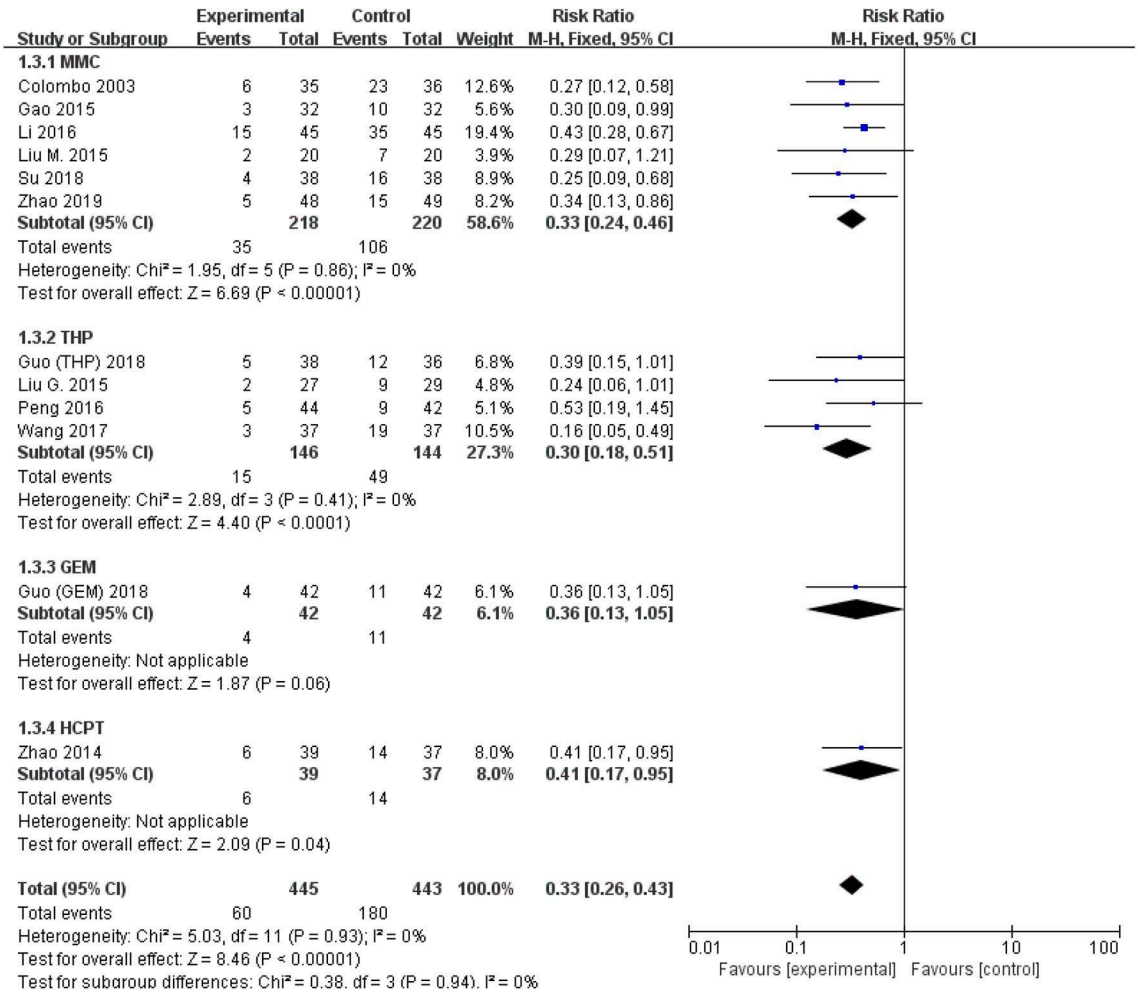

FIGURE 6 | Comparison on recurrence rate between thermal therapy and intravesical chemotherapy after subgroup analysis stratified by chemotherapeutic agent used in thermal intravesical chemotherapy.

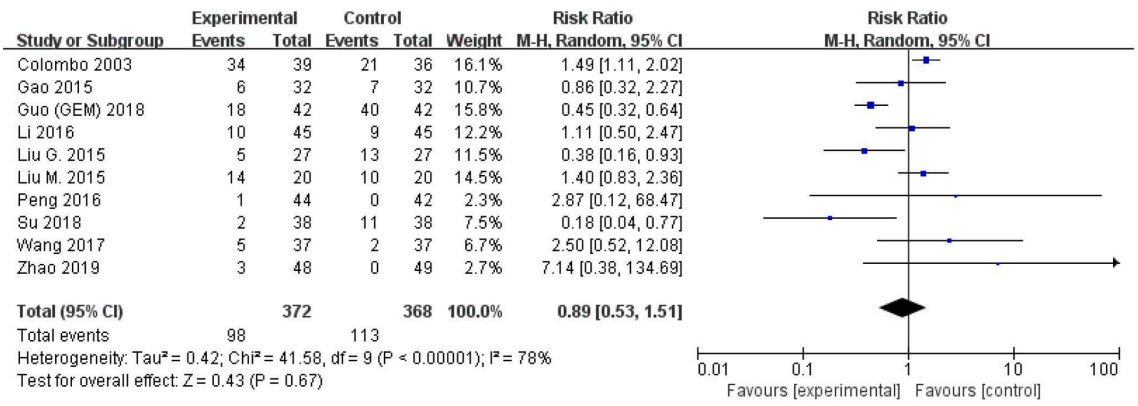

FIGURE 7 | Forest plot of adverse event rate comparing thermal intravesical chemotherapy with normal temperature intravesical chemotherapy.

or grade progression (30). Fifty-two patients with high-grade NMIBC treated by Gofrit et al. had chemo-thermotherapy, 86.5% of these patients preserved their bladder in the end of s 23 month follow-up (31). All these literature show the same point that thermal intravesical chemotherapy demonstrated a tumor cell killing effect which might be a good for NMIBC

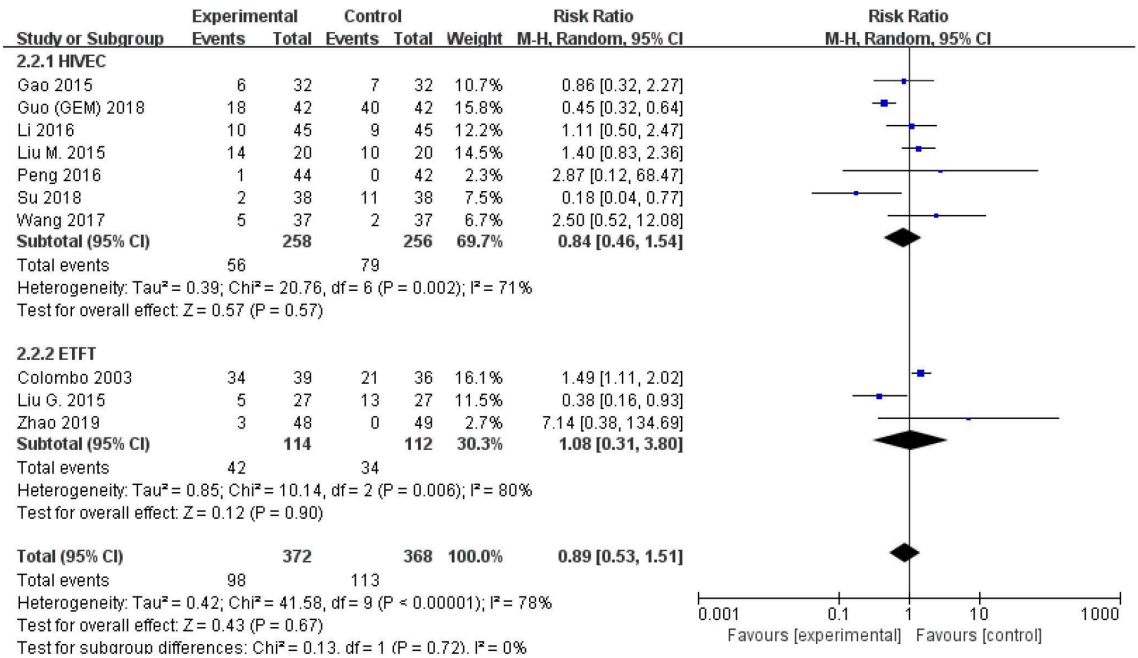

FIGURE 8 | Comparison on adverse event rate between thermal intravesical chemotherapy and normal temperature intravesical chemotherapy after subgroup analysis stratified by different approach used in thermal therapy.

patients. The meta-analysis aimed to figure out whether thermal intravesical chemotherapy is more effective and safer than normal temperature intravesical chemotherapy.

In the present study, the results of 12 eligible studies, include 11 RCTs and 1 retrospective study, were analyzed. Although the adverse events rate was not reduced, it highlighted that thermal intravesical chemotherapy was more advantageous than normal temperature intravesical chemotherapy in reducing risk of tumor recurrence among patients with NMIBC. Subgroup analyses of different chemotherapy approaches and drugs also indicated a significant reduction in recurrence rate without increasing adverse event rate.

The meta-analysis shows that the thermal intravesical chemotherapy can be tolerated relatively by patients. Most treatment adverse events were localized and transient as reporting. Of all the intake studies, only Zhao et al. (15, 25) and Colombo et al. (16) reported 12 and 8 patients' discontinuation, respectively. Reasons for withdrawal were various but mostly drug allergy, while Geijsen et al. (10) reported the oldest patients withdrew from complaints of improper hyperthermia treatment positioning. Our meta-analysis shows a lower withdrawal rate of 1.4%, which is close to 3.8% of Lammers's research (14).

There are two approaches to execute thermal intravesical chemotherapy. The first kind is called hyperthermic intravesical chemotherapy. In this way, chemotherapeutic agents dissolve in the solution and put it into a hyperthermic perfusion treatment machine connect with pipeline systems for infusion. The advantage of this method is obvious that we can control the temperature constantly. But still we cannot detect the temperature in the bladder wall since it became thinner during perfusion (27). Moreover, in consideration of single-use pipes, it may be too expensive to afford, especially for NMIBC patients who should generally receive more than six rounds intravesical chemotherapy. The second choice, as we called external thermal field thermotherapy, creates the local bladder heating by microwave. This method is more convenient and cheaper without pipeline systems (15). The weakness of ETFT is the intravesical temperature which could not be supervised with high-precision.

As for chemotherapeutic agents, there are four kinds of drugs used in thermal intravesical chemotherapy in our meta-analysis, including mitomycin C, pirarubicin, gemcitabine, hydroxycamptothecine. Only Zhao et al. compared the efficacy between thermal intravesical chemotherapy and normal temperature BCG perfusion (15), and the result turned out to be no difference in recurrence rate after the 2 years follow-up. BCG has been proved to be the most effective treatment for intermediate- and high-risk NMIBC since its first report in 1976 and became the standard management. Despite its efficacy, BCG perfusion therapy could cause a variety of adverse events, leading to the termination of the treatment in the end (7). More badly, BCG is scarce and expensive in China (15). So we have an urgent need to develop alternative therapy. MMC and THP are the main drugs applied in studies. MMC is an anti-metabolite drug identified from the products of a species of *Streptomyces caespitosus* (32). It destroys the structure and function of DNA, inhibits the replication of DNA, and kills tumor cells both in the proliferating and resting phase. The advantage of MMC is that normal mucosa of bladder is resistant to it. So patients who received MMC intravesical chemotherapy have fewer adverse

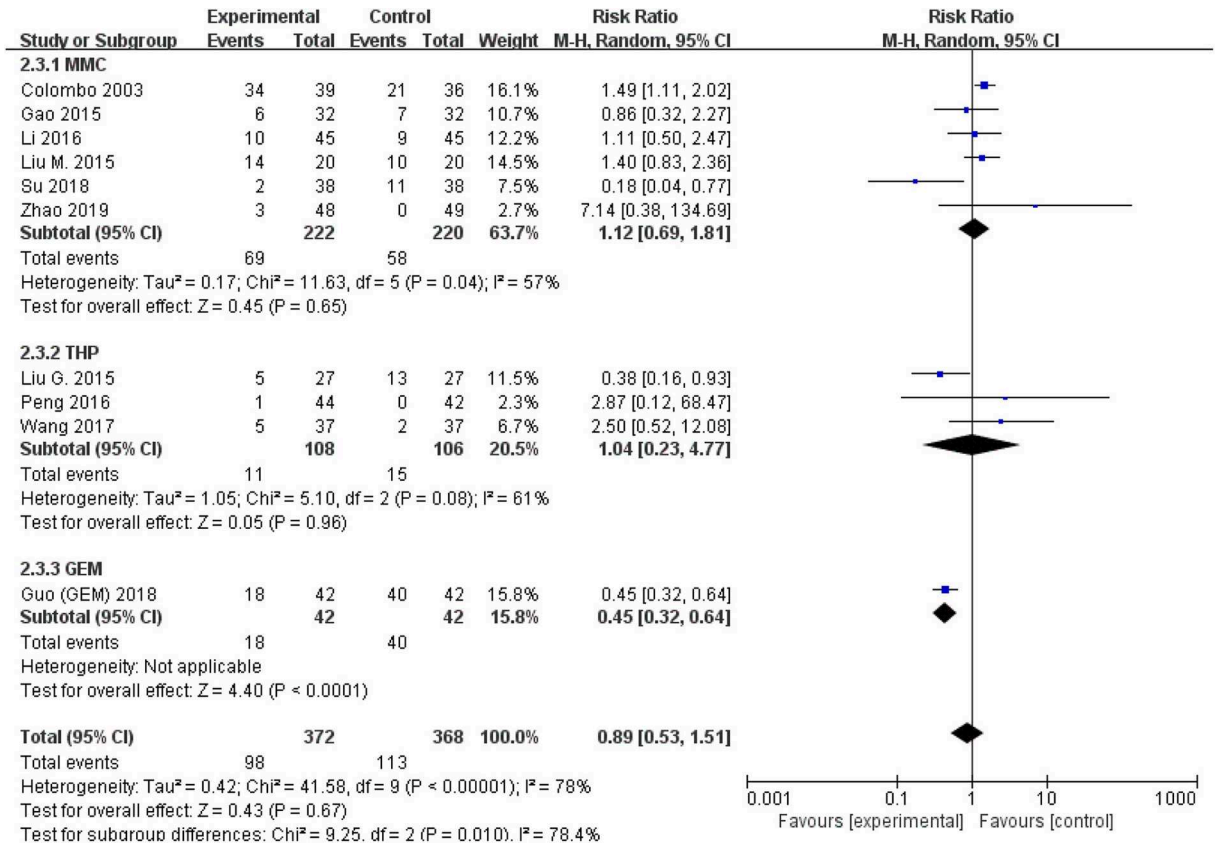

FIGURE 9 | Comparison on adverse event rate between thermal intravesical chemotherapy and normal temperature intravesical chemotherapy after subgroup analysis stratified by chemotherapeutic agent used in thermal intravesical chemotherapy.

events (33). THP can be absorbed into tumor cells quickly as it is one of the most effective agents for reducing recurrence of NMIBC (34). Although it shows no difference in the present meta-analysis, the study of the efficacy of the different thermal intravesical chemotherapeutics should be explored further.

As we all know, before thermal intravesical chemotherapy arises, intraperitoneal perfusion chemotherapy has already been widely used in the treatment of advanced ovarian and gastric cancer or peritoneal metastases. Zhu et al. reported patients after D2 dissection received intraperitoneal chemotherapy with whole abdominal hyperthermia, which reduced the recurrence and metastasis of peritoneal (35). Hotouras et al. systematically reviewed the literature of heated intraperitoneal chemotherapy (HIPEC) for recurrent ovarian cancer patients, and found that HIPEC is associated with benefits (36). Foreseeable, larger prospective studies will be carried out in all these fields.

In China, according to epidemiological investigation report published in 2018, bladder cancer has the highest morbidity among all kinds of urogenital neoplasms. The morbidity of male and female are 8.65 and 2.62 per 100,000 (37). The situation demands immediate action, especially treatment for NMIBC. In this meta-analysis, we found that thermal intravesical chemotherapy can reduce the recurrence rate of NMIBC. It indicates that thermal intravesical chemotherapy might be the next hot topic in academia.

LIMITATIONS

There are some limitations remaining, in spite of the eligibility criteria, that we had set to select published literature. First of all, treatment schedules and chemotherapeutic agents used in thermal intravesical chemotherapy are heterogeneous indeed. Second, risk levels among patients varied, which make it impossible to evaluate the difference in efficacy between thermal intravesical chemotherapy and normal temperature intravesical chemotherapy for patients at specific risk levels. These may bias the conclusions of this study. Beyond these limitations, this meta-analysis was strictly performed with setting reasonable eligibility criteria and reviewing all available publications' data, thus comparing efficacy between thermal intravesical chemotherapy and normal temperature intravesical chemotherapy.

CONCLUSIONS

In summary, compared with intravesical chemotherapy, thermal intravesical chemotherapy was associated with a lower recurrence rate without increasing adverse event rate among patients with NMIBC. Different approaches and drugs show the same effects of the efficacy. More high quality RCTs are still required to confirm those conclusions.

DATA AVAILABILITY STATEMENT

All datasets generated for this study are included in the article/**Supplementary Material**.

AUTHOR CONTRIBUTIONS

This meta-analysis was designed by X-QL and JZ. Searching of literature and data extraction was performed by KL and K-CZ. Data was rechecked by Y-XS and YL. Statistical analysis was performed by KL and XW. Writing of the manuscript was performed by KL and JZ. KL polished the article's English. X-QL reviewed the manuscript. All authors read and approved the final manuscript.

FUNDING

This work was supported by Zhao Yi-Cheng Medical Science Foundation. Name of granting agencies: Tianjin medical university general hospital (Grant no. ZYYFY2018031).

ACKNOWLEDGMENTS

We thank Dr. Yang Yong-Jiao for his help with English polishing.

SUPPLEMENTARY MATERIAL

The Supplementary Material for this article can be found online at: https://www.frontiersin.org/articles/10.3389/fonc.2020.00029/full#supplementary-material

REFERENCES

1. Dobruch J, Daneshmand S, Fisch M, Lotan Y, Noon AP, Resnick MJ, et al. Gender and bladder cancer: a collaborative review of etiology, biology, and outcomes. *Euro Urol*. (2016) 69:300–10. doi: 10.1016/j.eururo.2015.08.037
2. Bray F, Ferlay J, Soerjomataram I, Siegel RL, Torre LA, Jemal A. Global cancer statistics 2018: GLOBOCAN estimates of incidence and mortality worldwide for 36 cancers in 185 countries. *Cancer J Clin*. (2018) 68:394–424. doi: 10.3322/caac.21492
3. Huang J, Liu H. Current status of management of non-muscle invasive bladder cancer. *Chin J Urol*. (2019) 40:481–4.
4. Woldu SL, Bagrodia A, Lotan Y. Guideline of guidelines: non-muscle-invasive bladder cancer. *BJU Int*. (2017) 119:371–80. doi: 10.1111/bju.13760
5. Kamat AM, Colombel M, Sundi D, Lamm D, Boehle A, Brausi M, et al. BCG-unresponsive non-muscle-invasive bladder cancer: recommendations from the IBCG. *Nat Rev Urol*. (2017) 14:244–55. doi: 10.1038/nrurol.2017.16
6. Kamat AM, Bellmunt J, Galsky MD, Konety BR, Lamm DL, Langham D, et al. Society for immunotherapy of cancer consensus statement on immunotherapy for the treatment of bladder carcinoma. *J Immunother Cancer*. (2017) 5:68. doi: 10.1186/s40425-017-0271-0
7. Kawai K, Miyazaki J, Joraku A, Nishiyama H, Akaza H. Bacillus Calmette-Guerin (BCG) immunotherapy for bladder cancer: current understanding and perspectives on engineered BCG vaccine. *Cancer Sci*. (2013) 104:22–7. doi: 10.1111/cas.12075
8. Joice GA, Bivalacqua TJ, Kates M. Optimizing pharmacokinetics of intravesical chemotherapy for bladder cancer. *Nat Rev Urol*. (2019) 16:599–612. doi: 10.1038/s41585-019-0220-4
9. Abern MR, Owusu RA, Anderson MR, Rampersaud EN, Inman BA. Perioperative intravesical chemotherapy in non-muscle-invasive bladder cancer: a systematic review and meta-analysis. *J Natl Compr Cancer Netw*. (2013) 11:477–84. doi: 10.6004/jnccn.2013.0060
10. Geijsen ED, de Reijke TM, Koning CC, Zum Vorde Sive Vording PJ, de la Rosette JJ, Rasch CR, et al. Combining mitomycin C and regional 70 MHz hyperthermia in patients with nonmuscle invasive bladder cancer: a pilot study. *J Urol*. (2015) 194:1202–8. doi: 10.1016/j.juro.2015.05.102
11. Siddiqui J, Brown K, Zahid A, Young CJ. Current practices and barriers to referral for cytoreductive surgery and HIPEC among colorectal surgeons: a binational survey. *Euro J Surg Oncol*. (2019) 46: 166–72. doi: 10.1016/j.ejso.2019.09.007
12. Ekin RG, Akarken I, Cakmak O, Tarhan H, Celik O, Ilbey YO, et al. Results of intravesical chemo-hyperthermia in high-risk non-muscle invasive bladder cancer. *Asian Pac J Cancer Prev*. (2015) 16:3241–5. doi: 10.7314/APJCP.2015.16.8.3241
13. Tan WS, Kelly JD. Intravesical device-assisted therapies for non-muscle-invasive bladder cancer. *Nat Rev Urol*. (2018) 15:667–85. doi: 10.1038/s41585-018-0092-z
14. Lammers RJ, Witjes JA, Inman BA, Leibovitch I, Laufer M, Nativ O, et al. The role of a combined regimen with intravesical chemotherapy and hyperthermia in the management of non-muscle-invasive bladder cancer: a systematic review. *Euro Urol*. (2011) 60:81–93. doi: 10.1016/j.eururo.2011.04.023
15. Zhao Z, Zhao G, Zheng D, Chen S, Li J, Lin S. Clinical analysis of adjuvant hyperthermic intravesical chemotherapy for treating non-muscle invasive bladder cancer. *Int J Urol Nephrol*. (2019) 39:450–3.
16. Colombo R, Da Pozzo LF, Salonia A, Rigatti P, Leib Z, Baniel J, et al. Multicentric study comparing intravesical chemotherapy alone and with local microwave hyperthermia for prophylaxis of recurrence of superficial transitional cell carcinoma. *J Clin Oncol*. (2003) 21:4270–6. doi: 10.1200/JCO.2003.01.089
17. Gao F, Wang G. Intravesical mitomycin hyperthemal perfusion combined withItransurethral resection for treating bladder cancer in 32 cases. *Chin Pharm*. (2015) 24:85–6.
18. Guo X, Wang M, Shi L, Bai Y. Clinical observation of immediate intravesical instillation of gemcitabine hyperthermic perfusion and normal temperature perfusion after TURBt in elderly patients with high risk non-muscle invasive bladder cancer. *J Clin Urol*. (2018) 33:821–4.
19. Guo X, Wang M, Shi L, Bai Y. Clinical observation of immediately hyperthermic intravesical chemotherapy with pirarubicin versus traditional intravesical instillation with pirarubicin after transurethral resection of the bladder tumor in elderly patients with superficial bladder cancer. *Pract Geriatr*. (2018) 32:524–6.
20. Li B, Xia T. Effect of BR-TRG-I body cavity hyperthermic perfusion instrument on intravesical chemotherapy. *J Clin Urol*. (2016) 31:419–21.
21. Liu G, Teng D, Huang G, Cao J, Sun W. Clinical application of thermochemotherapy for bladder cancer. *Med Inf*. (2015) 28:87.
22. Liu M, Zhang Y. Curative effect comparative analysis of hyperthermic perfusion therapy and mitomycin perfusion chemotherapy after transurethral resection of bladder tumor. *Chin Foreign Med Res*. (2015) 13:17–8.
23. Peng Y, Feng Z, Huang Q, Qiu G. Efficacy of pirobicin in the prevention of recurrence of superficial bladder cancer after TURBT. *China Prac Med*. 2016;11(1):176-8.
24. Su X, Pan X, Liu Y. Observation on the efficacy of mitomycin hyperthermic intravesical chemotherapy combined with TURBT in patients with non-muscle invasive bladder cancer. *Chin J Mod Drug Appl*. (2018) 12:105–6.
25. Zhao Z, Hu W, Zheng D, Zhao G, Chen S, Chen H, et al. Preventing recurrence of superficial bladder cancer with intravesical chemotherapy of HCPT combined with external electric field hyperthermia. *J Mod Urol*. (2014) 19:508–12.
26. Wang Y, Li Y, Hong J, Li W, Zheng S, Wu K. The primary clinical application of hyperthermic intravesical chemotherapy in the prevention of non-muscle-invasive bladder cancer recurrence after transurethral resection of bladder tumor. *J Mod Urol*. (2017) 22:903–6.
27. Coley WB. The treatment of inoperable sarcoma by bacterial toxins (the mixed toxins of the *Streptococcus erysipelas* and the *Bacillus*

prodigiosus). *Proc R Soc Med*. (1910) 3:1–48. doi: 10.1177/003591571000301601
28. Rigatti P, Lev A, Colombo R. Combined intravesical chemotherapy with mitomycin C and local bladder microwave-induced hyperthermia as a preoperative therapy for superficial bladder tumors. A preliminary clinical study. *Euro Urol*. (1991) 20:204–10. doi: 10.1159/000471701
29. Colombo R, Lev A, Da Pozzo LF, Freschi M, Gallus G, Rigatti P. A new approach using local combined microwave hyperthermia and chemotherapy in superficial transitional bladder carcinoma treatment. *J Urol*. (1995) 153(3 Pt 2):959–63. doi: 10.1016/S0022-5347(01)67613-4
30. van der Heijden AG, Kiemeney LA, Gofrit ON, Nativ O, Sidi A, Leib Z, et al. Preliminary European results of local microwave hyperthermia and chemotherapy treatment in intermediate or high risk superficial transitional cell carcinoma of the bladder. *Euro Urol*. (2004) 46:65–71. doi: 10.1016/j.eururo.2004.01.019
31. Gofrit ON, Shapiro A, Pode D, Sidi A, Nativ O, Leib Z, et al. Combined local bladder hyperthermia and intravesical chemotherapy for the treatment of high-grade superficial bladder cancer. *Urology*. (2004) 63:466–71. doi: 10.1016/j.urology.2003.10.036
32. Serretta V, Scalici Gesolfo C, Alonge V, Di Maida F, Caruana G. Mitomycin C from birth to adulthood. *Urologia*. (2016) 83(Suppl 2):2–6. doi: 10.5301/uro.5000195
33. Bosschieter J, Nieuwenhuijzen JA, van Ginkel T, Vis AN, Witte B, Newling D, et al. Value of an immediate intravesical instillation of mitomycin C in patients with non-muscle-invasive bladder cancer: a prospective multicentre randomised study in 2243 patients. *Euro Urol*. (2018) 73:226–32. doi: 10.1016/j.eururo.2017.06.038
34. Kang M, Jeong CW, Kwak C, Kim HH, Ku JH. Single, immediate postoperative instillation of chemotherapy in non-muscle invasive bladder cancer: a systematic review and network meta-analysis of randomized clinical trials using different drugs. *Oncotarget*. (2016) 7:45479–88. doi: 10.18632/oncotarget.9991
35. Zhu L, Xu Y, Shan Y, Zheng R, Wu Z, Ma S. Intraperitoneal perfusion chemotherapy and whole abdominal hyperthermia using external radiofrequency following radical D2 resection for treatment of advanced gastric cancer. *Int J Hyperther*. (2019) 36:403–7. doi: 10.1080/02656736.2019.1579372
36. Hotouras A, Desai D, Bhan C, Murphy J, Lampe B, Sugarbaker PH. Heated IntraPEritoneal Chemotherapy (HIPEC) for patients with recurrent ovarian cancer: a systematic literature review. *Int J Gynecol Cancer*. (2016) 26:661–70. doi: 10.1097/IGC.0000000000000664
37. He Y, Li D, Liang D, Zheng R, Zhang S, Zeng H, et al. Incidence and mortality of bladder cancer in China, 2014. *Chin J Oncol*. (2018) 40:647–52. doi: 10.3760/cma.j.issn.0253-3766.2018.09.002

Conflict of Interest: The authors declare that the research was conducted in the absence of any commercial or financial relationships that could be construed as a potential conflict of interest.

frontiers in Oncology

REVIEW
published: 07 February 2020
doi: 10.3389/fonc.2020.00102

Traditional Classification and Novel Subtyping Systems for Bladder Cancer

Shaoming Zhu[1†], *Weimin Yu*[1†], *Xiao Yang*[2], *Cheng Wu*[1] *and Fan Cheng*[1*]

[1] *Department of Urology, Renmin Hospital of Wuhan University, Wuhan, China,* [2] *Department of Gynaecology and Obstetrics, Renmin Hospital of Peking University, Beijing, China*

Bladder cancer is the most common tumor in the urinary system, with approximately 420,000 new cases and 160,000 deaths per year. The European Organization for Research and Treatment of Cancer (EOTRC) classifies non-muscular invasive bladder cancer (NMIBC) into low-risk, medium-risk and high-risk groups based on a comprehensive analysis of NMIBC pathological parameters and the risk of recurrence and progression to muscular invasive bladder cancer (MIBC). Traditional classification systems are based on pathologic grading, staging systems, and clinical prognosis. However, the pathological parameters of the tumor cannot fully reflect the "intrinsic characteristics" of bladder cancer, and tumors with a similar pathology exhibit different biological behaviors. Furthermore, although the traditional classification system cannot accurately predict the risk of recurrence or the progression of bladder cancer patients (BCs) individually, this method is widely used in clinical practice because of its convenient operation. With the development of sequencing and other technologies, the genetics-based molecular subtyping of bladder cancer has become increasingly studied. Compared with the traditional classification system, it provides more abundant tumor biological information and is expected to assist or even replace the traditional typing system in the future.

Keywords: bladder cancer, molecular subtypes, EOTRC, clinical prognosis, multiomics

OPEN ACCESS

Edited by:
Ja Hyeon Ku,
Seoul National University, South Korea

Reviewed by:
Ari Adamy,
Santa Casa Hospital, Brazil
Mohamed Saad Zaghloul,
Cairo University, Egypt

***Correspondence:**
Fan Cheng
urology1969@163.com

†These authors have contributed equally to this work

Specialty section:
This article was submitted to Genitourinary Oncology, a section of the journal Frontiers in Oncology

Received: *02 August 2019*
Accepted: *20 January 2020*
Published: *07 February 2020*

Citation:
Zhu S, Yu W, Yang X, Wu C and Cheng F (2020) Traditional Classification and Novel Subtyping Systems for Bladder Cancer. Front. Oncol. 10:102. doi: 10.3389/fonc.2020.00102

INTRODUCTION

Bladder cancer (BC) is the most common urinary tract tumor, with approximately 420,000 new cases and 160,000 deaths per year, and the incidence ratio of men:women ranges from 6:1 to 2:1 (1, 2). There are many risk factors for bladder cancer, including occupational and environmental factors [metal processing, dyes, rubber, plastics and exposure to other aromatic compounds (3)], living environment factors (arsenic in water, chlorine disinfectants, and nitrate) (2, 3), personal/dietary factors [coffee, smoking (4)], infection of pathogenic microorganisms (schistosomiasis and urinary tract bacteria) (2, 5), drugs (pioglitazone was recently shown to not be significantly associated with the risk of bladder cancer), patient age, gender, race, and socioeconomic status (2).

Bladder cancer is divided into non-muscular invasive bladder cancer (NMIBC) and muscular invasive bladder cancer (MIBC) according to the European Association of Urology (EAU) guidelines. Bladder cancer can also be divided into several types—urothelial carcinoma, squamous epithelial carcinoma, and adenocarcinoma—among which over 90% are urothelial carcinomas

(6). In 2006, Sylvester et al. comprehensively analyzed the pathological parameters and risk of recurrence and progression of 2,596 NMIBC patients (NMIBCs) with Ta and T1 stage bladder cancer (7). The risk of recurrence and progression can be directly calculated and predicted by the pathological parameters in the corresponding software system (https://www.eortc.be/tools/bladdercalculator/). The European Organization for Research and Treatment of Cancer (EORTC) prediction system is mainly based on the following pathological parameters: previous recurrence rate (primary, recurrence $\leq$1 per year, recurrence $>$ 1 per year), number (1, 2–7, 8 or more), diameter ($<$3 cm, $\geq$3 cm), T stage (Ta, T1), grading (WHO 1973) (grade 1, 2, 3), and whether or not it is combined with carcinoma *in situ* (CIS). According to the differences among these pathological parameters, recurrence and progression, EAU guidelines further classify NMIBC into low-risk, medium-risk and high-risk groups (6). Due to the classification system, pathological information is easy to obtain, the system is simple to operate, and the prediction is relatively accurate; therefore, it is widely used in the clinic.

TRADITIONAL CLASSIFICATION AND MOLECULAR SUBTYPING SYSTEMS

The traditional classification system for bladder cancer is mainly based on pathological parameters (8, 9). Under similar pathological staging and grading, the recurrence and progression of bladder cancer vary greatly among different individuals and directly affect the optimal monitoring and treatment schedules (10, 11). For example, according to the EORTC software system calculation (https://www.eortc.be/tools/bladdercalculator/), primary Ta grade 3 bladder cancer is a high-risk bladder cancer, with a 5 years recurrence rate of 46% and a 5 years progression risk of 6%, which indicates that 94% of patients will not progress to MIBC within 5 years. Thus, the following question arises: why are all patients monitored and treated with the same program? Despite their similar pathological parameters, the biological behaviors of tumors are quite different. Some patients were pathologically classified as low-risk, but the actual tumor showed highly invasive biological characteristics and early metastasis, leading to the following question: can conventional conservative treatment be administered to all low-risk patients? Some high-risk patients do not respond to BCG, while others are sensitive to BCG (Bacillus Calmette-Guerin) (12, 13). However, the traditional classification system cannot predict this response. Therefore, it is difficult for doctors to choose schedules for BCG perfusion, radical cystectomy or another treatment according to the traditional prediction system. Some tumors are less likely to metastasize and need only local resection, while other tumors are highly invasive and need radical cystectomy and/or another treatment. Unfortunately, there is still no effective means to distinguish the two. Moreover, the traditional classification system can only predict the risk of recurrence and progression of NMIBC but not the risk of MIBC. After radical cystectomy, some muscle invasive bladder cancer patients (MIBCs) benefit from neoadjuvant chemotherapy (NAC), while others do not (14–16), which cannot be predicted by the traditional classification system. The pathological parameters of the tumor cannot fully reflect the "intrinsic characteristics" of bladder cancer. Therefore, it is difficult for doctors to provide individual and precise supervision and treatment for bladder cancer.

With the rapid development of sequencing, mass spectrometry and other techniques, studies based on genomics and transcriptome (17), epigenetics (18), proteomics (19) and other omics (20–22) will provide a new direction for the accurate diagnosis and treatment of bladder cancer. A good classification system should meet the following criteria: I. It should provide an accurate prediction for the risk of recurrence and progression of bladder cancer and help develop individualized monitoring, conservative treatment, surgical schemes, adjuvant therapies and follow-up schedules. II. It should be able to accurately identify individuals with tolerance to chemotherapy, targeted therapy, immunotherapy and help develop individualized adjuvant treatment plans. III. It should provide not only important information for predicting the recurrence and prognosis of bladder cancer but also effective molecular information for the study of molecular mechanisms, such as tumor development, progression, chemotherapy and immunotherapy tolerance. IV. It should also aid in the development of personalized new molecular diagnoses and treatments. In particular, the study of molecular subtyping based on genetics has made rapid progress in the study of bladder cancer and has attracted increasing attention (23–25). The development of molecular subtyping based on genomics and transcriptomes, etc., provides a new way to understand bladder cancer.

Molecular subtyping was not first applied in the study of bladder cancer; initially, molecular subtyping was widely conducted in acute leukemia (26), breast cancer (27), colorectal cancer (28), hepatocellular and intrahepatic cholangiocarcinoma (29), and gastric cancer (30). The basic method of molecular subtyping is to detect gene expression in tumor tissues by sequencing, microarray and other technologies and then perform a cluster analysis of the different genes based on the gene expression level and genes involved in the biological process. Eventually, BCs are divided into several subtypes, and different molecular subtypes reflect different intrinsic and clinical characteristics of the tumors. For example, patients with basal-like or *HER-2*-enriched breast tumors have a poor clinical prognosis (31). Although patients with basal-like or *HER-2*-enriched breast cancer have a poor clinical prognosis, they are sensitive to neoadjuvant chemotherapy (NAC), which can benefit patients with this subtype (31). For the two major types of bladder cancer, NMIBC and MIBC, the molecular subtyping of bladder cancer can be divided into early BC subtyping, NMIBC subtyping, MIBC subtyping, etc. (**Table 1**; **Figure 1**).

EARLY MOLECULAR SUBTYPING OF BC

Lund 2012 Five Subtyping System

The earliest representative study on the molecular subtyping of bladder cancer was conducted by Sjodahl et al. at the University of Lund in 2012 (Lund 2012) (32). In this study, the transcriptome data of 308 bladder cancer samples were collected to analyze the expression levels of 13,953 genes, the biological processes

TABLE 1 | Major molecular subtyping systems.

Subtyping systems	Abbreviation	Cases of the studies	Subtypes
Early BC subtyping (including NMIBC and MIBC)	Lund 2012 five subtyping system (32)	$n = 308$	Urobasal A, genomically unstable, infiltrated, urobasal B, and SSC-like
NMIBC subtyping	UROMOL 2016 three subtyping system (33)	$n = 460$	Class 1, Class 3, and Class 2
	Van Kessel et al. (34)	$n = 1,239$	Reclassify EAU high-risk NMIBCs into good, moderate, and poor subtypes
MIBC subtyping	UNC 2014 two subtyping system (31)	$n = 262$	Basal-like (including claudin-low), and luminal
	MDA 2014 three subtyping system (35)	$n = 73$	Luminal, p53-like, basal
	TCGA 2014 four subtyping system (36)	$n = 129$	Clusters I, II, III, and IV (Luminal, luminal-infiltrated, basal squamous, basal)
	TCGA 2017 five subtyping system (37)	$n = 412$	Luminal, luminal-infiltrated, basal-squamous, neural, and luminal-papillary
BC subtyping (including NMIBC and MIBC)	BOLD 2018 six subtyping system (38)	$n = 2411$	Neural-like, luminal-like, papillary-like, HER2-like, Squamous-cell carcinoma-like and mesenchymal-like
Subtyping based on adjuvant chemotherapy	GSC 2017 four subtyping system (39)	$n = 343$	Claudin-low, basal, luminal-infiltrated, and luminal
	Seiler 2018 four subtyping system (40)	$n = 116$	CC1, CC2, CC3, and CC4 (Basal, luminal, immune, scar-like)

BC, Bladder cancer; NMIBC, non-muscle invasive bladder cancer; MIBC, muscle invasive bladder cancer; SSC, squamous cell carcinoma; GSC, single-sample genomic subtyping classifier; CC, consensus clusters.

involved in these genes (including immunological characteristics, cell cycle, cytokeratins/uroplakins, FGFR3 characteristics, etc.), and mutations in the *FGFR3*, *PIK3CA*, and *TP53* genes. BC was divided into five subtypes: urobasal A, genomically unstable, urobasal B, squamous cell carcinoma like (SSC-like), and infiltrated (**Table 1**). The urobasal A subtype exhibits an elevated expression of genes related to the early cell cycle, uroplakins, the FGFR3 signature, cell adhesion and other biological processes, while the genomically unstable subtype is characterized by immune characteristics and an elevated expression of genes related to the late cell cycle. The urobasal B, SSC-like, and infiltrated subtypes all highly expressed immunological signature genes, whereas the urobasal B and SSC-like subtypes highly expressed genes involved in the late cell cycle and cell adhesion (**Figure 2**).

An analysis of the prognoses associated with the five subtypes revealed that the prognoses of the five subtypes were significantly different. The urobasal A and infiltrated subtypes have a relatively better prognosis, while the SSC-like and urobasal B subtypes have the worst prognosis. By subtyping the tumors classified as grade 3, it was found that urobasal A has the best prognosis, while urobasal B has the worst prognosis, suggesting that even in the same pathological classification, clinical characteristics differ from their intrinsic molecular subtypes. The authors further explored the relationship between molecular subtypes and histopathologic classification and found that tumors in the Ta stage are mainly composed of the urobasal A subtype. In the T1 stage, tumors are mainly composed of urobasal A and genomically unstable subtypes. All subtypes of MIBC account for a certain proportion. Urobasal A is the main tumor subtype in G1 and G2 BC. G3 is similar to MIBC in that all subtypes account for a certain proportion. The above results indicate that there is a certain consistency between the molecular subtypes and pathological classification. In tumors with good stages and grades, the urobasal A subtype is the main component, while in those with a poor clinical prognosis, the proportion of the urobasal A subtype decreases significantly, and all subtypes account for a certain proportion.

MOLECULAR SUBTYPING OF NMIBC

Compared with the number of MIBC molecular subtyping studies, the number of NMIBC molecular subtyping studies is low, which may be because partial bladder cancer specimens are not easy to obtain, especially Ta BC, with single and small-sized tumors. Therefore, there may be some missing data, resulting in publication bias. Representative studies include UROMOL 2016 subtyping (33) and Van Kessel 2018 high-risk NMIBC subtyping (34). Thus, far, these two studies have the largest number of experimental cases in NMIBC molecular subtyping studies.

UROMOL 2016 Three Subtyping System

Hedegaard et al. (33) performed a transcriptome sequencing analysis of 476 samples (460 NMIBC, 16 MIBC) from multiple centers. Based on the expression levels of 8,074 genes and biological processes involved in the early cell cycle, the late cell cycle, keratins, uroplakins, epithelial-mesenchymal transformation, differentiation-related genes, etc., NMIBC patients can be classified into three categories according to the results of the cluster analysis: Class 1, Class 3, and Class 2.

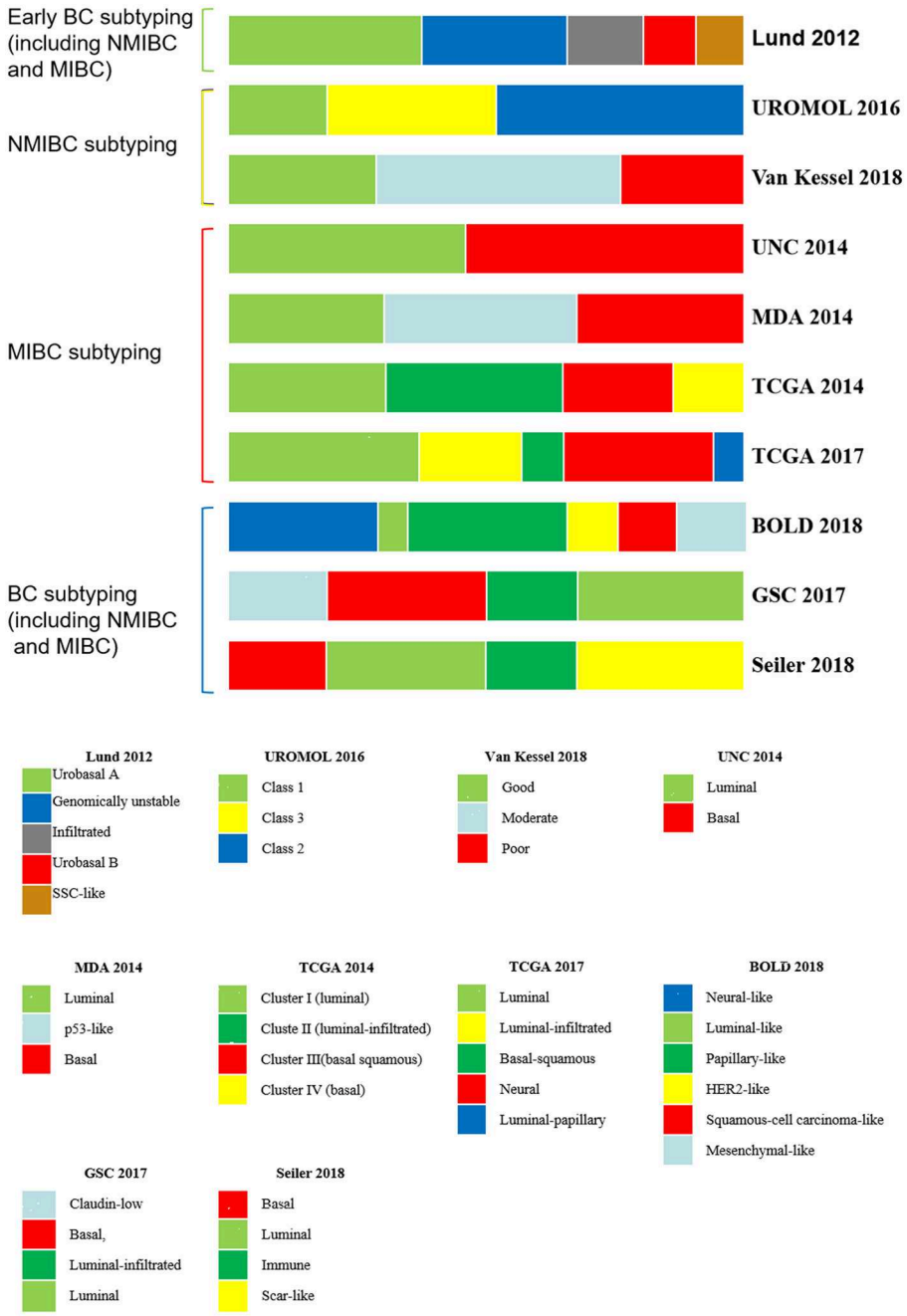

FIGURE 1 | BC molecular subtyping systems. BC, bladder cancer; NMIBC, non-muscular invasive bladder cancer; MIBC muscular invasive bladder cancer.

The Class 1 subtype highly expresses early cell cycle-related genes, and the clinical prognosis is the best. The late cell cycle-related genes of the Class 2 subtype are highly expressed, and the clinical prognosis is poor. The Class 1 and Class 2 subtypes both highly expressed uroplakins, while Class 3 shows undifferentiation. In addition, by analyzing the genes of bladder cancer stem cell markers, it was found that Class 3 is enriched in stem cells and the basal cell marker *CD44* gene. Compared with Class 1 and Class 3, Class 2 is enriched in EMT (epithelial-mesenchymal transition)-related genes.

The team used 117 major genes from the subtype analysis to classify 130 BCs (85 Ta, 37 T1, 8 MIBC) and eight normal samples and analyzed the relationship between the molecular subtyping system and pathological classification. High-risk bladder cancer with a high stage and a high grade mainly consists of Class 2 and 3 subtypes. The main components of normal or Ta BC are Class 1, and the Class 2 subtype is most likely to progress to MIBC. Subsequently, these 117 genes were used to classify the data of 306 NMIBCs in the Lund 2012 study. It was found that 306 NMIBCs are mainly composed of Classes 1 and 2, and only

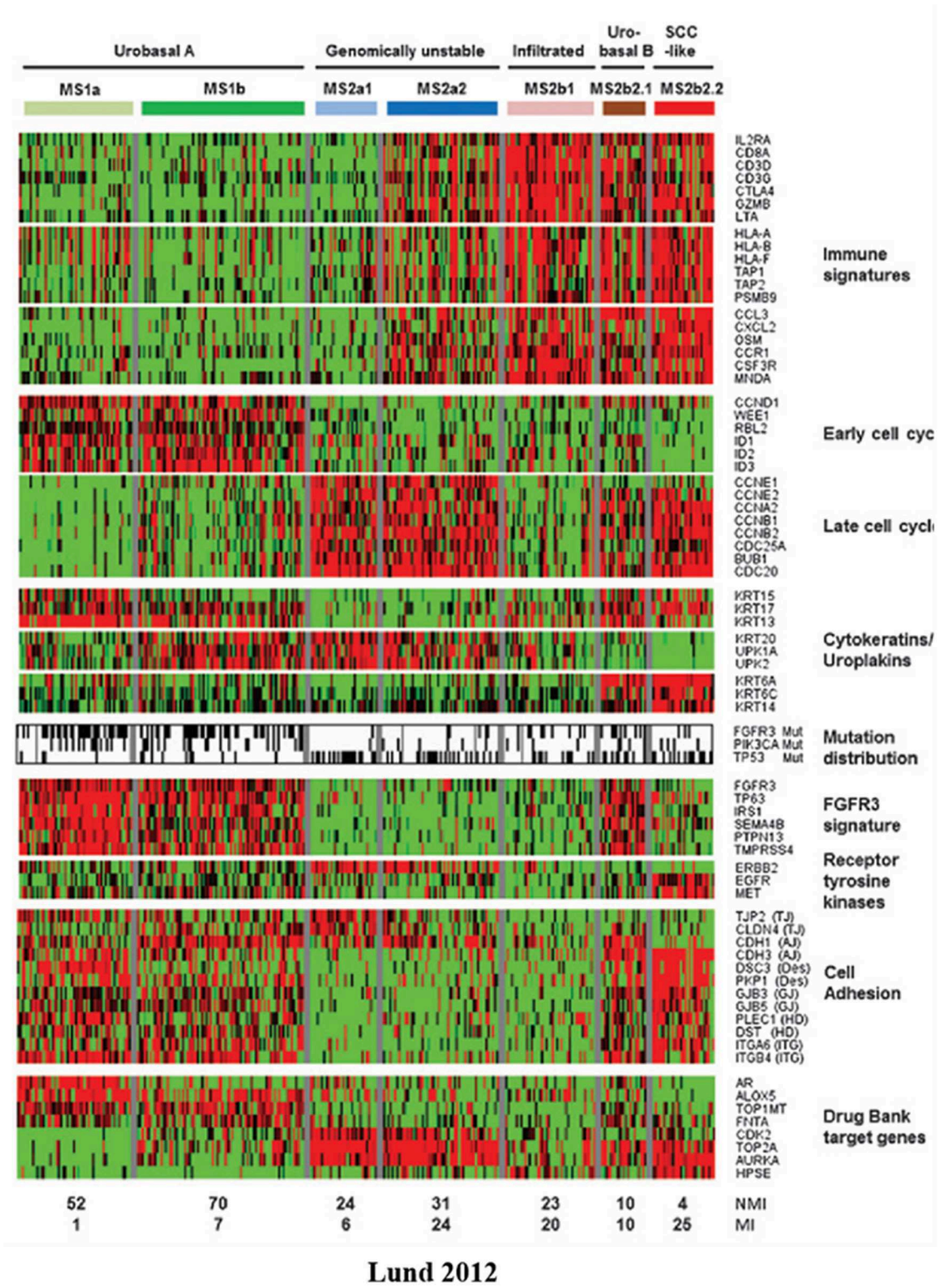

FIGURE 2 | Heatmap of mRNA-seq data from the Lun 2012 molecular subtyping system. BCs are divided into five subtypes according to their genetic expression profiles (32). Red, high expression; green, low expression; black; mutation; white, wild-type; gray, no mutation data. SSC, squamous cell carcinoma; FGFR3, fibroblast growth factor receptor 3.

5% are composed of Class 3. The team also analyzed 408 MIBCs in the TCGA (The Cancer Genome Atlas) database, and the Class 3 subtype was not found. The above results suggest that the Class 3 subtype mainly exists in the NMIBC group, which is less than that of Class 1 and Class 2, and has a poor clinical prognosis. Class 1 is similar to the urobasal A subtype in the Lund 2012 system and the papillary subtype in the MIBC TCGA 2014 system (**Figure 3**).

The team further analyzed the genomic mutations and found that the median number of single nucleotide polymorphisms (SNPs) per patient was 218 (ranging from 1 to 863). The most common mutations were *PIK3CA* ($n = 108$) and *FGFR3* ($n = 279$). The mutated genes are mainly related to cell structure, cytoskeletal function, chromatin organization and chromatin remodeling. Chromatin remodeling gene mutations were found in 86% of the samples, mainly in the Class 2 subtype, and were concentrated in DNA damage repair, *MAPK*/*ERK*, and *ERBB* family genes. *APOBEC* family gene mutations were found in all tumor subtypes.

In conclusion, the Class 1 subtype in NMIBC mainly includes tumors with a low grade, a low stage, and a good clinical prognosis. However, Class 3 mainly includes NMIBC in a low proportion and is enriched in stem cell and basal cell markers, similar to the phenotype of CIS (carcinoma *in situ*). Moreover, Class 2 is mainly a highly malignant tumor enriched in uroplakins with a poor clinical prognosis, and the mutated genes are mainly involved in chromatin remodeling.

High-Risk NMIBC Subtyping

Van Kessel et al. (34) found that the methylation status of *GATA2*, *TBX2*, *TBX3,* and *ZIC4* and mutations in *FGFR3*, *TERT*, *PIK3CA,* and *RAS* are correlated with the progression of NMIBC (41, 42). Then, the research team detected and analyzed frozen tumor tissues of 1,239 patients with NMIBC from 6 European countries (276 patients were classified as low-risk, 273 as medium-risk and 555 as high-risk according to the EAU guidelines); ultimately, the high-risk NMIBCs were divided into three subtypes.

A total of 57 NMIBCs (4.6%) progressed to MIBCs, with a median follow-up time of 27 months (0–81 months) and a PIR (rate of progression per 100 patients-year) of high-risk NMIBCs = 4.25. Wild-type *FGFR3* and *GATA2* and *TBX3* methylation were significantly correlated with NMIBC progression (HR 0.34, 2.53, and 2.64, respectively). The high-risk NMIBC group was reclassified as a good class (PIR = 0.86, 26.2%), a moderate class (PIR = 4.32, 49.7%), and a poor class (PIR = 7.66, 24.0%) according to *FGFR3* mutations and the *GATA2* methylation status. The classification method was validated and analyzed with another 362 patients who were classified as high-risk NMIBCs according to the EUA guidelines. A total of 30 NMIBCs developed to MIBCs, with a progression rate of 8.3%. All NMIBCs were divided into the good class (95), moderate class (180), or poor class (87). Moreover, 2 of 95 patients in the good class (2.1%), 15 of 180 patients in the moderate class (8.3%), and 13 of 87 patients in the poor class (14.9%) progressed to MIBC. Therefore, this subtyping method combined with the EUA guideline pathological classification system can further classify high-risk NMIBCs into three subtypes with a low, medium and high risk of progression and different clinical prognoses. Therefore, the traditional pathological classification system combined with molecular subtyping greatly improves the prediction ability of the traditional classification system and guides the selection of clinical supervision and treatment schemes.

MOLECULAR SUBTYPING OF MIBC

There are an increasing number of molecular subtyping systems on MIBCs, including the UNC (University of North Carolina) two subtyping system, the MDA (MD Anderson) three subtyping system and the TCGA subtyping system. The TCGA database contains a series of genomic, transcriptomic and other data on tumor samples from MIBCs. As the number of patients increased, the subtyping methods developed rapidly, from the original four-subtype system (129 MIBCs) in 2014 to the five-classification system (412 MIBCs) in 2017. Combined with the characteristics of each subtype and its clinical information, the comprehensive analysis provides important information for the diagnosis, treatment and prognosis of bladder cancer.

UNC Two Subtyping System

Damrauer et al. (31) analyzed 262 high-grade MIBCs by extracting data from four published studies. According to the expression levels related to the differentiation of the urinary epithelium (such as keratin and CD44), MIBCs are divided into two subtypes. As these two molecular subtypes are similar to the expression profiles of the luminal and basal subtypes of breast cancer, they are named luminal-like and basal-like subtypes, respectively, and the basal-like subtype also contains a "claudin-low" subtype.

The disease-specific and overall survival rates of the luminal-like subtype are significantly higher than those of the basal-like subtype (*P*-values are 0.019 and 0.008, respectively). The genome of this subtype is enriched in *FGFR3* (fibroblast growth factor receptor 3) and *TSC1* (tubercular sclerosis 1) mutations, as well as changes in the RB1 pathway, including *RB1* deletion mutations and the amplification of *CCND1* (cyclin D1), *E2F3* (E2F transcription factor 3), and *CCNE1* (cyclin E1). The basal-like and luminal-like subtypes have similar characteristics to breast cancer, and subtypes of breast cancer with claudin-low characteristics can also be found in MIBCs. Moreover, the claudin-low subtype belongs to the basal-like subtype, but there is no significant difference in the disease-specific survival rate or overall survival rate between the two. The claudin-low subtype expresses low levels of claudin-binding protein and high levels of EMT and stem-like marker genes.

MDA Three Subtyping System

In 2014, a research team from the MD Anderson Cancer Center analyzed the mRNA of 73 MIBC patients' tumors. Their molecular profiles are similar to those of breast cancer and were subtyped as the luminal, p53-like and basal subtypes (35). The luminal subtype is enriched with epithelial markers, activated *PPAR-*γ, estrogen receptor, *FGFR3* mutations, and high *FGFR3* expression, suggesting possible sensitivity to FGFR blockers. The mRNA profiles of the p53-like and luminal subtypes are

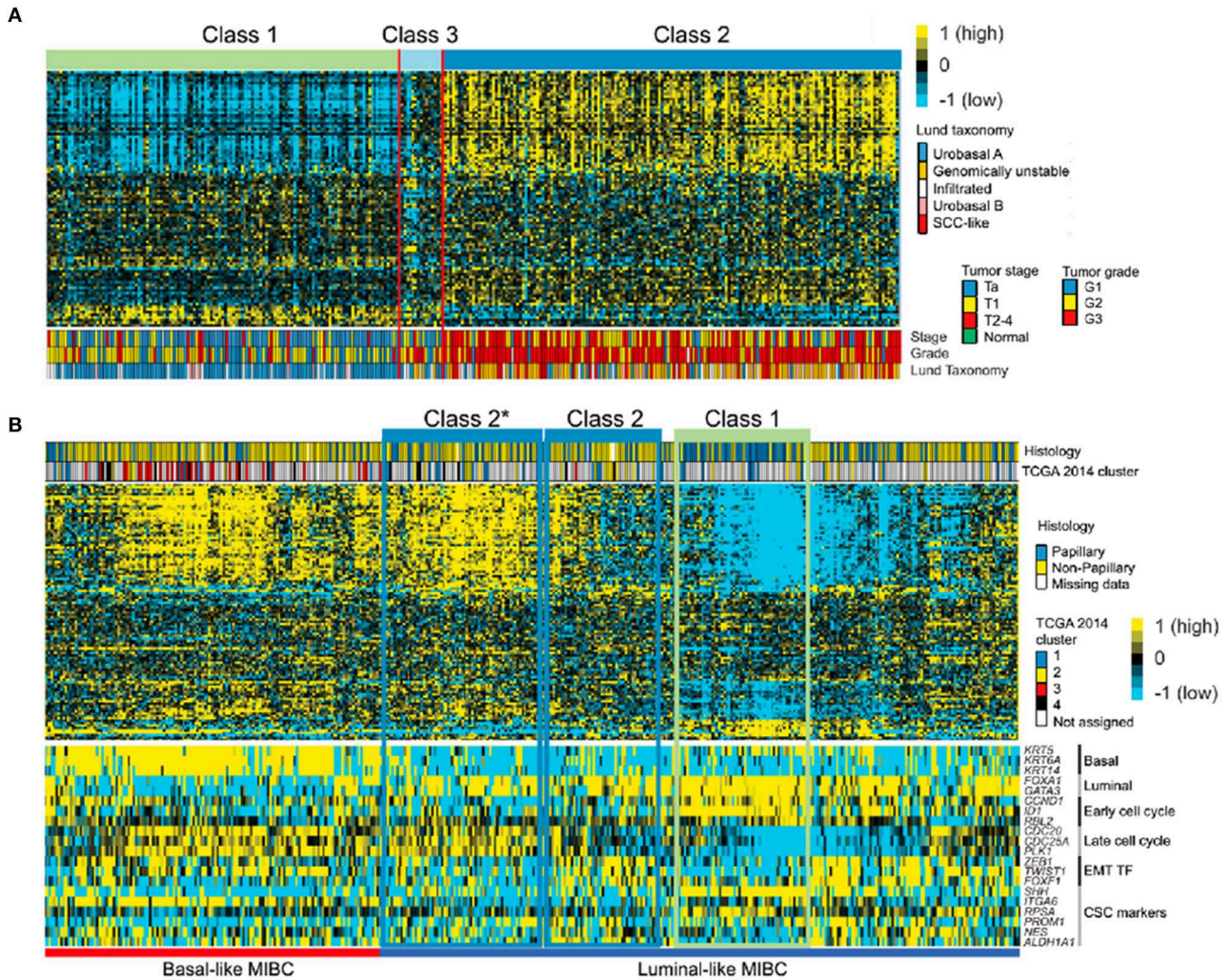

FIGURE 3 | The correlation among UROMOL 2016 and other molecular subtyping systems (33). **(A)** The UROMOL 2016 subytping system analyzed the microarray data from 306 tumors from the Lund group based on 95 of 117 classifier genes (33). The Class 1 subtype is highly similar to the urobasal A subtype, and Class 1 subtypes mainly consist of low-risk NMIBC, while high-risk NMIBC tends to be concentrated in the Class 3 and Class 2 subtypes. **(B)** UROMOL 2016 was used to subtype the TCGA database (33). Heatmap of mRNA-seq data from 408 MIBC samples from TCGA based on 107 of the 117 classifier genes. Class 1 and Class 2 tumors are highlighted based on expression profile similarities to original classes. Class 2*: tumors with high similarity to Class 2 but with differences in EMT and CSC marker expression (33). Yellow, high expression; blue, low expression. SSC, squamous cell carcinoma; EMT, endothelial-mesenchymal transformation; CSC: cancer stem cell.

similar, but the wild-type *p53* gene is significantly activated in the p53-like subtype; therefore, these MIBCs are classified into the p53-like subtype (the TP53 mutation frequency is similar in all subtypes). The p53-like subtype is resistant to neoadjuvant chemotherapy drugs, and all drug-resistant MIBCs become the p53-like subtype after chemotherapy, suggesting that the *p53* gene may play an important role in chemotherapy. Basal MIBCs highly express squamous cell differentiation markers and *p63* and are more invasive and associated with a poor prognosis compared with other subtypes.

Furthermore, the team aimed to determine the relationship among these molecular subtyping systems and others. The Lund 2012 "urobasal A" subtype can be divided into the MDA "luminal" subtype. The Lund 2012 "infiltrated" and MDA "p53-like" subtypes are enriched in extracellular matrix markers. The basal/SCC-like subtype in Lund 2012 and the MDA basal subtype are both enriched in squamous cell differentiation markers. The luminal, p53-like and basal subtypes exist not only in MIBC but also in NMIBC. The luminal subtype is enriched in epithelial markers, showing activated *PPAR-γ* and *FGFR3* mutations, and has a good clinical prognosis. The p53-like subtype belongs to the luminal subtype, but its wild-type *p53* gene is significantly activated and tolerant to chemotherapy. The basal subtype is enriched in squamous cell differentiation markers and activated *p63* and is more invasive and has a poor clinical prognosis.

TCGA Subtyping System

The Cancer Genome Atlas (TCGA) project was sponsored by The National Cancer Institute and The National Human Genome Institute (USA) to study information related to the human cancer genome. With the increasing number of patients and the development of various detection technologies, biological databases have become increasingly abundant. Therefore, various molecular subtyping systems are being constantly updated and improved. In 2014, the genetic data of 129 MIBCs were analyzed, and it was found that the signature of the molecular subtypes is similar to that of breast cancer, but the name is conservative, and these subtypes were named Cluster I, Cluster II, Cluster III, and Cluster IV (36). Subsequently, TCGA was updated to include 208 MIBCs, which were subtyped into the luminal, immune undifferentiated, luminal immune, and basal subtypes based on their genetic expression signature, which included uroplakins and immune infiltration (43). When the number of MIBCs reaches 412, they can be classified into five subtypes—luminal, luminal-infiltrated, basal-squamous, neural, and luminal-papillary—based on their genetic signature (37).

The TCGA 2014 (36) subtyped MIBCs into Cluster I, II, III, and IV subtypes. Cluster I MIBCs mainly include papilloma pathological phenotypes enriched in *FGFR3* gene mutations; Clusters I and II highly express *GATA3*, *FOXA1*, *UPK3A* and luminal and uroplakin genes and are enriched in *RBB2* mutations and estrogen receptor beta (ESR2). Cluster III highly expresses epithelial and precursor or progenitor cells and keratin, and some include squamous cell pathological phenotypes. The most frequent mutations in the MIBC genome are *TP53* (49%), *FGFR3* (12%), *ERCC2* (12%), *RB1* (13%), *CDKN1A* (14%), *EP300* (15%), and *PIK3CA* (20%). The most frequent deletions or amplifications in the genome are *CDKN2A* (47%), *NCOR1* (25%), *YWHAZ* (22%), and *E2F3/SOX4* (20%). Changes in genes or mRNAs involved in the PI3K/mTOR and FGFR3/RTK/RAS signaling pathways may represent potential targets for targeted therapy.

TCGA 2017 (37) then classified 412 MIBCs into five different subtypes: luminal, luminal-infiltrated, basal-squamous, neural, and luminal-papillary. The luminal, luminal-infiltrated, and luminal-papillary subtypes highly express luminal marker genes (*KTT20*, *GATA3*, *UPK1A*, *UPK2*, *FGFR3*, etc.), and the luminal-infiltrated subtype highly expresses ECM (extracellular matrix) and smooth muscle genes. The luminal-papillary subtype is mainly a papillary pathological phenotype. Basal marker genes (*KRT5*, *KRT6A*, *CD44*, etc.), squamous epithelium-like genes (*GSDMC*, *TGM1*, etc.), and immune marker genes (*CXCL11*, *L1CAM*, etc.) are highly expressed in basal squamous cells. The neural subtype highly expresses neural differentiation genes.

BC MOLECULAR SUBTYPING SYSTEM

BOLD 2018 Six Subtyping System

Robertson et al. (38) analyzed the published data of 2411 BCs from TCGA, UROMOL, and IMvigor 210 publication studies, and BCs were reclassified into six subtypes: neural-like (neural 22.7%), luminal-like (LUM 22.7%), papillary-like (PAP 22.7%), HER2-like (HER2L 22.7%), squamous cell carcinoma-like (SCC) (22.7%) and mesenchymal-like (MES 22.7%). Survival analysis was performed on 541 patients with BC. The median overall survival time of the neural, luminal, SCC-like, and mesenchymal subtypes was 87, 91, 107, 20, and 86 months, respectively (the data of the papillary subtype were not available) and that of the six subtypes of 280 MIBCs was 43, 16, 23, 102, 16, and 79 months, respectively. The genes involved in these subtypes are different from those involved in basal, ECM, luminal/uroplakins, immune/infiltration, proliferation, neural differentiation, squamous cell differentiation and other biological processes.

The correlation between BOLD 2018 and the traditional pathological classification showed that the LUM and PAP subtypes are dominant in NMIBCs, while the neural, MES and SCC subtypes are dominant in MIBCs. The proportion of the HER2L subtype in NMIBCs and MIBCs is relatively even. Ta is mainly composed of PAP, while T1 BCs are mainly composed of the LUM and HER2L subtypes, and only a few NMIBCs (20%) are of the neural, MES and SCC subtypes. The HER2L, MES and SCC subtypes are enriched in advanced and high-grade tumors, which are prone to lymph node metastasis and have a poor clinical prognosis.

Moreover, the LUM and HER2L subtypes of NMIBCs have progressive characteristics, while the neural, SCC and MES subtypes of MIBC have progressive characteristics. PAP NMIBCs have a better prognosis and therefore require less supervision. However, the HER2L, LUM, MES and SCC subtypes have a higher risk of progression and therefore require frequent monitoring and aggressive treatment. The tolerance of the MES subtype to chemotherapy is similar to that of the claudin-low subtype. High PD1 and CTLA4 expression signals in the neural, MES and SCC subtypes may be a potential therapeutic target for immune checkpoints.

Intratumoral Heterogeneity in BC

Molecular subtyping plays an important role in predicting the prognosis and treatment response of bladder cancer patients. However, current subtyping studies are mainly based on detecting the DNA or RNA of tumor tissues or cells. However, traditional sequencing technology is based on whole tumor tissue rather than a single cell; therefore, intratumoral heterogeneity may be an important factor affecting the accuracy of molecular subtyping. Warrick et al. (44) conducted a pathological examination on 309 bladder cancer markers and found that 83 of them exhibited intratumoral variation in BC tumor tissues. Then, these 83 specimens were subtyped with the Lund subtyping system, and 39% exhibited molecular heterogeneity. Eventually, these 83 samples were divided into urothelial-like, genomically unstable, basal-squamous, mesenchymal-like, and neuroendocrine-like subtypes. The basal-squamous subtype shows the greatest variability; approximately 78% of these tumors simultaneously exhibit the genomically unstable or urothelial-like subtype. Heterogeneity in bladder cancer is common, which leads to variation in molecular subtypes and affects the prognosis and treatment response of patients and therefore should be a focus of attention.

MOLECULAR SUBTYPING BASED ON ADJUVANT CHEMOTHERAPY

Molecular Subtyping Used to Predict the Response and Prognosis to Neoadjuvant Chemotherapy (NAC)

Seiler et al. (39) used molecular subtyping to predict the response and prognosis to NAC. A total of 343 MIBCs were analyzed by transcriptome sequencing before NAC, and the GSC [single-sample genomic subtyping classifier (GSC)] was developed by comprehensively analyzing the outcomes of NAC BCs in previously published molecular subtyping studies (UNC, MDA, TCGA, Lund, etc.) Then, the MIBCs were divided into four subtypes: claudin-low, basal, luminal, and luminal. Basal tumors were divided into basal and claudin-low subtypes based on the expression of EMT and immune infiltration genes. A comparative analysis of 223 published non-NAC MIBCs' overall survival (OS) found that the predicted accuracy of GSC was 83%. In another 82 validated MIBCs, the accuracy of GSC was 73%, which was significantly higher than that of other major published molecular subtyping systems (37%).

The 3 years overall survival (OS) rate of the GSC basal subtype in the non-NAC group was 49.2% (95% CI 39.5–61.2%; $P < 0.001$) vs. 77.8% (95% CI 67.2–90.0%) in the NAC group; $P < 0.001$). In the non-NAC group, patients with the GSC basal subtype had a risk ratio of 2.22 relative to those with the GSC luminal subtype. The basal and luminal subtypes of GSC in the NAC group were not significantly different. These results indicate that EMT and immune infiltration play an important role in the response to adjuvant chemotherapy and patient prognosis and that patients with the GSC basal subtype benefit from neoadjuvant chemotherapy.

Adjuvant Chemotherapy Affects Molecular Subtyping

NAC affects the biological signature of a tumor, and the traditional molecular subtyping system is inconsistent before and after NAC treatment. Seiler's research team (40) examined the genes in 133 pre- and post-NAC MIBCs, 116 of which were pre-NAC and post-NAC paired samples. By analyzing the genetic expression signature, cisplatin-resistant bladder cancer patients were divided into four major subtypes: CC1-basal, CC2-luminal, CC3-immune, and CC4-scar-like. NAC does not affect the phenotype of the CC1-basal and CC2-luminal subtypes, which are manifested as a basal and a luminal phenotype pre-NAC, respectively. Basal and luminal markers are lost in the CC3-immune subtype, which is characterized by the highest immune activity after NAC. After NAC, the CC4-scar-like subtype highly expresses wound healing/Scar-related genes, and its prognosis is the best.

Liu et al. (45) conducted full exon sequencing analysis of MIBCs pre- and post-NAC and found that chemotherapy did not increase the overall mutation load of the tumors but increased the mutations of some subclonal tumors. After chemotherapy, these subclonal MIBCs are associated with poor OS, and the genes involved in the cell cycle and immune checkpoint regulation are significantly altered. Cisplatin-based chemotherapy affects the genetic signature of bladder cancer; therefore, studying the altered genes before and after chemotherapy and the effects of these changes may provide important information for the study of chemotherapy resistance mechanisms.

DISCUSSION

The traditional classification system is based on a comprehensive analysis of the pathological characteristics, recurrence, progression, and prognosis of NMIBCs and then predicts the risk of recurrence and progression of NMIBCs (46, 47). The molecular subtyping system mainly uses cluster analysis to examine the genome and the expression levels of genes and their involved biological processes (25). Compared with the traditional classification system, molecular subtyping reflects the intrinsic characteristics of the tumors, and it not only predicts the prognosis and treatment response of NMIBCs but also MIBCs (48).

Obtaining high-quality samples is the first key step to establish molecular subtyping, but unfortunately, many factors can easily affect the quality of samples, resulting in distortion of the results. NIMBC, especially in the early stage, has a very small tumor size, and it is difficult to obtain enough sample for pathological, genomic, and transcriptometric diagnoses to be performed at the same time. In contrast, the volume of the MIBC tumors is often larger and has enough samples for all of the above testing. This may be one of the reasons why NIMBC molecular typing has developed slowly in recent years, while MIBC molecular typing has developed rapidly. Surgery also affects the quality of tumor samples. Transurethral resection of bladder tumor (TURBT) resects tumor tissue by electrocision, and the length of burning time and the depth of cutting directly affect the quality of tumor tissue. In addition, the longer the operation time is, the more serious the mRNA degradation.

mRNA in resected tumor tissues is easily degraded; a longer cut-off time leads to more serious degradation. However, the surgical time for TURBT or radical cystectomy often varies greatly depending on the operator's experience, so both the surgical method and surgical time are factors that cannot be ignored, as both affect the quality of the specimens. mRNA in frozen samples is relatively stable, while that in formalin-fixed, paraffin-embedded specimens is often severely degraded (49). Because the TME contains a large number of other components, such as stromal cells and immune cells, the inappropriate purification of tissues can also affect the results of molecular subtyping (23). Of course, bladder cancer is a highly heterogeneous tumor, and even if the samples are collected from different sites of the same tumor tissue, its molecular subtyping results may be different (44). Therefore, the establishment of a more reasonable specimen collection and management procedure is the first step to ensure the accuracy of molecular typing results.

NMIBC Molecular Subtyping

The early molecular classification system subdivided BC into luminal and non-luminal subtypes, mainly according to

whether there was high expression of urothelial differentiation biomarkers. Although there are an increasing number of molecular subtyping systems, they are basically built from these two basic subtypes. It should be noted that the basal subtype is just one subtype of the non-luminal type. Due to the high proportion of non-luminal subtype tumors, studies often mistake non-luminal as basal subtype (23). In addition, luminal and basal subtypes are not the exclusive subtypes of MIBC, and these two subtypes also exist in NMIBC. However, it cannot be considered that luminal and basal subtypes in MIBC transform from luminal and basal subtypes in NMIBC, respectively. According to UROMOL 2016, 460 NMIBCs were divided into Class 1 (luminal-like), Class 3 (basal-like) and Class 2 (high-risk luminal-like) subtypes. Class 1 highly expresses luminal-like biomarkers, which is highly similar to urobasal A in the Lund 2012 classification (**Figure 3**). Class 1 subtypes mainly consist of low-risk NMIBC, while high-risk NMIBC tends to be concentrated in the Class 3 and Class 2 subtypes. Although Class 3 has the characteristics of MIBC basal-like, Jakob Hedegaard thought that Class 3 subtypes could not be considered precursors of MIBC basal-like subtypes. Compared with Class 2 subtypes, the proportion of Class 3 in MIBC was very small, so the team speculated that Class 3 gradually shifted into the Class 2 subtype in progression (33). Second, in addition to the luminal differentiation feature, luminal subtypes highly expressed cell adhesion, early cell cycle, metabolism, and FGFR3 genes. Late cell cycle, CSC markers and EMT-related genes tend to be highly expressed in Class 2 (high-risk luminal-like tumors). In addition, extracellular matrix organization, immune response and other changes were also observed. However, late cell cycle, CSC markers and EMT-related genes tend to be highly expressed in partial non-luminal subtypes; extracellular matrix organization, immune response and other changes were also observed in non-luminal subtypes (32, 33). Third, further research is needed on which genes drive NMIBC to MIBC. Gottfrid Sjödahl's team (50) followed up 357 urothelial bladder cancer patients (UBCs) and analyzed the genes of 73 patients who transformed from NMIBCs to MIBCs. They found that although *FGFR3*, *PIK3CA*, or *TERT* were the most common mutations of NMIBC, they were not associated with progression, while *TP53* was a common mutation in advanced UBC and highly associated with highly invasive subtypes, suggesting that *TP53* may be a key factor driving the progression of NMIBC (41). The methylation state of *GATA2* may be related to the progression of NMIBC. Van Kessel analyzed the *GATA2* methylation status and *FGFR3* mutation status of high-risk NMIBC and found that NMIBC with *GATA2* methylation and *FGFR3* wild type was more likely to progress into MIBC (34). Although it is not clear which genes drive the transformation of NMIBC into MIBC, molecular typing provides important clues. Molecular subtyping is also helpful to monitor and manage the recurrence and progression of NMIBC, especially high-risk NMIBC. High-risk NMIBC was further classified into good, moderate and poor subtypes, which increased the accuracy of its prediction of the risk of NMIBC progression (34). Therefore, novel molecular subtyping has the potential for implementation in the traditional NMIBC guidelines. As mentioned above, compared with the molecular subtyping of MIBC, the molecular subtyping of NMIBC is developing slowly at present, with relatively few reports in the literature; further study is needed.

MIBC Molecular Subtyping

During progression, not only the intrinsic characteristics of bladder cancer cells but also the tumor microenvironment (TME) change. Early MIBC molecular classification systems tended to focus on the molecular classification of tumor cells themselves, such as luminal, basal and other subtypes (31, 35). With a deeper understanding of BC cells and their TME, molecular subtyping efforts began to focus more on heterogeneity, the extracellular matrix (ECM) and immune infiltration, promoting further refinement of BC typing. More systematic and comprehensive molecular subtyping has deepened the comprehensive understanding of the characteristics of BC, thus promoting the development of new targeted therapies and immunotherapies in the treatment of bladder cancer. The more systematic and comprehensive molecular subtyping not only deepens the understanding of the characteristics but also promotes the development of novel targeted therapies and immunotherapies in the treatment of bladder cancer. TCGA 2017 subdivided luminal into luminal, luminal-papillary and luminal subtypes and subdivided non-luminal into basal squamous and neural subtypes according to their pathological and genetic characteristics (37). BOLD 2018 also include neural-like, luminal-like, papillary-like, squamous-cell carcinoma-like subtypes and added HER2-like and mesenchymal-like subtypes (38). Recently, Kamoun established and verified a comprehensive network based on six classification systems and divided MIBC into luminal-papillary, luminal non-specified, luminal instability, stroma-rich, basal/squamous, and neurostable-like (51). This classification system considers not only the heterogeneity of BC tumor cells themselves but also the influence of infiltrated immune cells and stromal cells on the clinical characteristics and prognosis of tumors. Therefore, the new subtyping systems partially retain the classical subtypes of the previous subtyping system as well as propose some new subtypes.

First, the prognosis of each subtype is different, and the response to neoadjuvant chemotherapy is also different. Luminal subtypes with relatively mature differentiation tend to have a better prognosis, while basal and neural-like subtypes with poor differentiation have a worse prognosis (23, 33, 38, 51). Although the prognosis of the luminal-papillary subtype is good, it is not sensitive to neoadjuvant chemotherapy (NAC) (37). Although basal/squamous LumNS (luminal non-specified) has a poor prognosis, they may benefit from NAC. In conclusion, not all people can benefit from NAC, and molecular subtyping is beneficial to select patients with specific subtypes that are sensitive to NAC, which could help avoid the toxicity of unnecessary chemotherapy and optimize the therapeutic strategy, a task that is difficult for traditional typing.

Second, based on the comprehensive analysis of the genome, transcriptome, and non-coding RNA of BC, molecular subtyping provides a new direction for personal and precise treatment. Genetic alterations in BC include point mutations, gene fusion, gene amplification, and deletion. The most common genetic

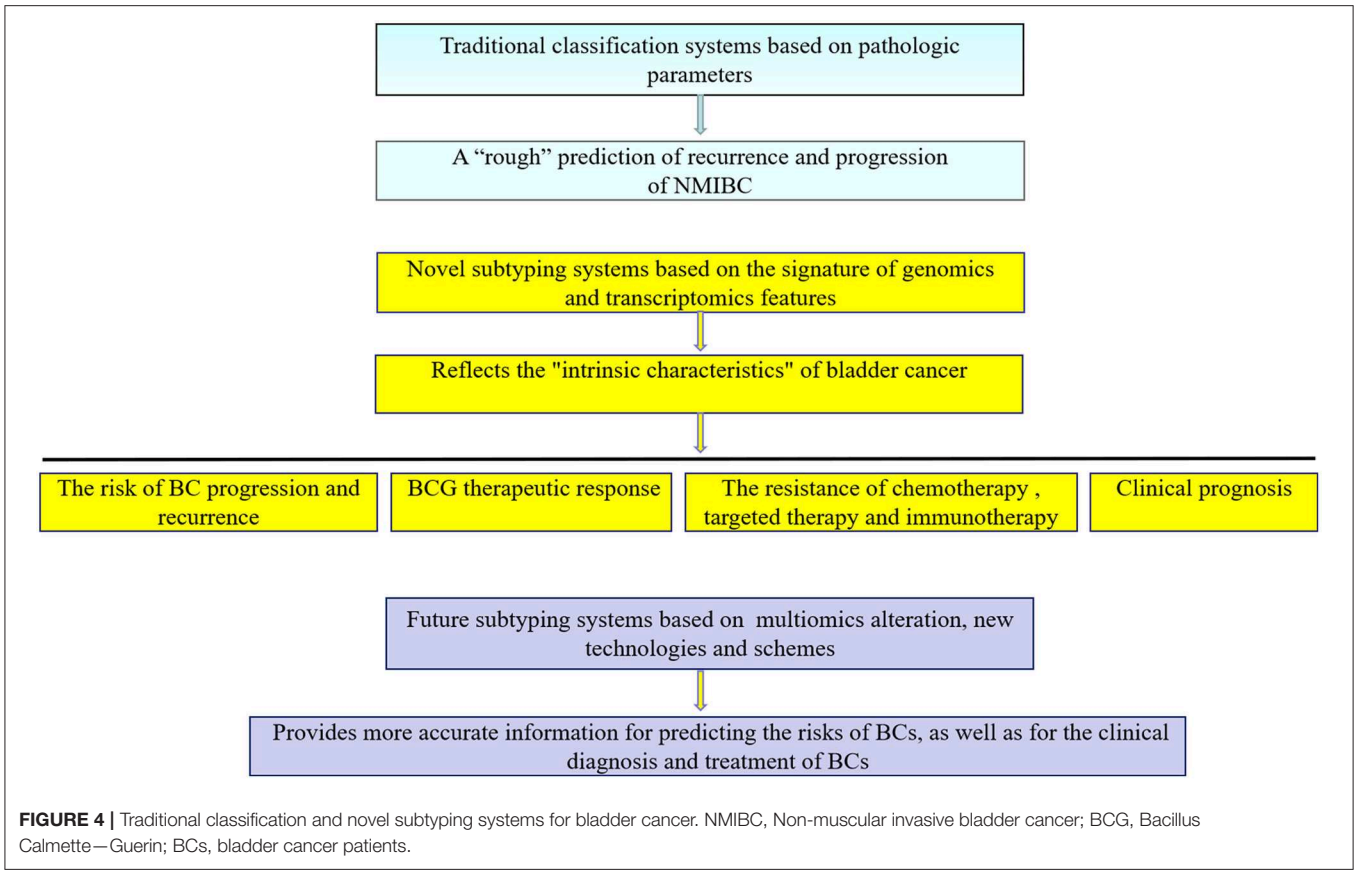

FIGURE 4 | Traditional classification and novel subtyping systems for bladder cancer. NMIBC, Non-muscular invasive bladder cancer; BCG, Bacillus Calmette—Guerin; BCs, bladder cancer patients.

changes in NMIBC include *FGFR3*, *KDM6A*, *PIK3CA*, and *KMT2D*, while the most common mutations in MIBC include *TP53*, *KMT2D*, *KDM6A*, and *RB1*. In addition, APOBEC-mediated mutagenesis may be an important factor in driving genetic mutations in NMIBC and MIBC (1). These altered genes are involved in a number of important biological processes, including TP53/cell cycle, RTK/RAS/PI3K, FGFR3, EGFR, chromatin modifiers, DNA damage, etc. It is the in-depth study of these processes that has promoted the development of BC targeted therapy and accurate diagnostic and treatment approaches. *FGFR3* is one of the most common amplification mutation genes in luminal subtypes, and targeted FGFR has become a promising treatment. FGFR1-4 alterations UC patients respond well to the FGFR inhibitors erdafitinib and rogaratinib (52, 53), and these drugs are undergoing UC II/III clinical trials. Similarly, *PIK3CA* is also a common activated mutant gene, and targeting the PI3K pathway has achieved a good therapeutic effect *in vivo* and *in vitro* preclinical BC treatment (54). In addition to the above targeted therapies, other targeted signaling pathways, such as ERBB2 and TSC1, are undergoing preclinical testing.

Third, molecular subtyping provides guidance for BC immunotherapy. Anti-programmed death 1 (PD-1), programmed death-ligand 1 (PD-L1), and cytotoxic t-lymphocyte antigen 4 (CTLA4) are important second-line therapies for MIBCs with NAC failure. Unfortunately, not all patients can benefit from immunotherapy. The luminal-infiltrated subtype in the TCGA 2017 subtyping system moderately expressed PD-L1 and CTLA-4. In particular, although this subtype is not sensitive to NAC, it has a good response to anti-PD-L1, PD-1 and CTLA-4 treatment. In addition, the basal/squamous subtype is sensitive not only to NAC but also to anti-PD-L1, PD-1, and CTLA-4 (37).

Compared to the traditional BC classification, molecular subtyping provides more information for precise treatment. For example, in the classification system established by Kamoun et al. (51), the luminal papillon (LumP) subtype highly expressed the *FGFR3* gene, and targeted FGFR3 therapy was effective. LumNS (luminal non-specified) and stroma-rich were rich in infiltrated stromal and immune cells. Both of these subtypes highly expressed panfibroblast TGF-β and showed resistance to PD-1 or PD-L1 treatment. Similar to TCGA 2017, the neuroauction (NE) subtype highly expressed cell cycle- and DNA replication-related genes and was sensitive to NAC therapy. The basal/squamous subtype showed good responsiveness to immunotherapy but was not sensitive to radiotherapy.

There are an increasing number of molecular subtyping systems that are being constantly updated and provide important information for clinical diagnosis and treatment. However, BC molecular subtyping still has some limitations: (I). In the traditional pathological classification system, it is relatively easy to obtain pathological parameters, it is convenient to operate, and the prediction results are approximate, which is suitable for clinical applications. (II) Molecular subtyping is mainly based on "static" research, especially in NMIBC, and enables a one-time

detection and analysis of tumor specimens rather than "dynamic" tracking. For example, during the monitoring and follow-up of NMIBCs, primary, recurrent and progressive tumors should be collected and analyzed to identify a better risk prediction system by integrating the information and data in the whole diagnosis and treatment process. (III) Currently, molecular subtyping is mainly focused on genome and transcriptome research, whereas the proteomics and immune status of tumors are also closely related to their development. Therefore, multiomics should be included in the study of molecular subtyping. (IV) Bladder cancer often exhibits intratumor heterogeneity. There may be multiple molecular subtypes in the same tumor, which may be an important factor affecting the accuracy of the molecular subtyping prediction system. With the rapid development of single-cell high-throughput sequencing (46, 55, 56), mass spectrometric detection (57), immune analysis (58, 59), and other technologies, the accuracy of the molecular subtyping prediction system will be further improved (**Figure 4**). Compared with traditional pathological classification, molecular subtyping offers a more comprehensive analysis of the genome, transcriptome and non-coding RNA, providing important guidance for BC adjuvant chemotherapy, targeted therapy and immunotherapy. In the future, these classifications will become an important complementary approach to traditional pathological classification.

AUTHOR CONTRIBUTIONS

SZ and WY drafted the manuscript. FC, XY, and CW revised the content and approved the manuscript for publication.

REFERENCES

1. Hurst C, Rosenberg J, Knowles M. SnapShot: bladder cancer. *Cancer Cell.* (2018) 34:350. doi: 10.1016/j.ccell.2018.07.013
2. Cumberbatch M, Jubber I, Black PC, Esperto F, Figueroa JD, Kamat AM, et al. Epidemiology of bladder cancer: a systematic review and contemporary update of risk factors in 2018. *Eur Urol.* (2018) 74:784–95. doi: 10.1016/j.eururo.2018.09.001
3. Czerniak B, Dinney C, McConkey D. Origins of bladder cancer. *Annu Rev Pathol.* (2016) 11:149–74. doi: 10.1146/annurev-pathol-012513-104703
4. Gruber K. Coffee consumption and bladder cancer are linked, analysis shows. *Bmj.* (2015) 350:h1477. doi: 10.1136/bmj.h1477
5. Markowski MC, Boorjian SA, Burton JP, Hahn NM, Ingersoll MA, Maleki VS, et al. The microbiome and genitourinary cancer: a collaborative review. *Eur Urol.* (2019) 75: 637–46. doi: 10.1016/j.eururo.2018.12.043
6. EAU Guidelines. *Edn. presented at the EAU Annual Congress Copenhagen 2018.* ISBN 978–94-92671–01-1.
7. Sylvester RJ, van der Meijden AP, Oosterlinck W, Witjes JA, Bouffioux C, Denis L, et al. Predicting recurrence and progression in individual patients with stage Ta T1 bladder cancer using EORTC risk tables: a combined analysis of 2,596 patients from seven EORTC trials. *Eur Urol.* (2006) 3:465–6. doi: 10.1016/j.eururo.2005.12.031
8. Zamboni S, Moschini M, Simeone C, Antonelli A, Mattei A, Baumeister P, et al. Prediction tools in non-muscle invasive bladder cancer. *Transl Androl Urol.* (2019) 8:39–45. doi: 10.21037/tau.2019.01.15
9. Zhang G, Steinbach D, Grimm MO, Horstmann M. Utility of the EORTC risk tables and CUETO scoring model for predicting recurrence and progression in non-muscle-invasive bladder cancer patients treated with routine second transurethral resection. *World J Urol.* (2019) 37:2699–705. doi: 10.1007/s00345-019-02681-2
10. Zhang L, Wu B, Zha Z, Qu W, Zhao H, Yuan J. Clinicopathological factors in bladder cancer for cancer-specific survival outcomes following radical cystectomy: a systematic review and meta-analysis. *BMC Cancer.* (2019) 19:716. doi: 10.1186/s12885-019-5924-6
11. Lopez-Beltran A, Henriques V, Montironi R, Cimadamore A, Raspollini MR, Cheng L. Variants and new entities of bladder cancer. *Histopathology.* (2019) 74:77–96. doi: 10.1111/his.13752
12. Meng MV, Gschwend JE, Shore N, Grossfeld GD, Mostafid H, Black PC. Emerging immunotherapy options for BCG-unresponsive non-muscle-invasive bladder cancer. *J Urol.* (2019) 202:1111–9. doi: 10.1097/JU.0000000000000297
13. Pettenati C, Ingersoll MA. Mechanisms of BCG immunotherapy and its outlook for bladder cancer. *Nat Rev Urol.* (2018) 15:615–25. doi: 10.1038/s41585-018-0055-4
14. Pederzoli F, Bandini M, Briganti A, Plimack ER, Niegisch G, Yu EY, et al. Incremental utility of adjuvant chemotherapy in muscle-invasive bladder cancer: quantifying the relapse risk associated with therapeutic effect. *Eur Urol.* (2019) 76:425–9. doi: 10.1016/j.eururo.2019.06.032
15. Martini A, Jia R, Ferket BS, Waingankar N, Plimack ER, Crabb SJ, et al. Tumor downstaging as an intermediate endpoint to assess the activity of neoadjuvant systemic therapy in patients with muscle-invasive bladder cancer. *Cancer.* (2019) 125:3155–63. doi: 10.1002/cncr.32169
16. Waingankar N, Jia R, Marqueen KE, Audenet F, Sfakianos JP, Mehrazin R, et al. The impact of pathologic response to neoadjuvant chemotherapy on conditional survival among patients with muscle-invasive bladder cancer. *Urol Oncol.* (2019) 37:572.e21–8. doi: 10.1016/j.urolonc.2019.04.027
17. Boormans JL, Zwarthoff EC, Black PC, Goebell PJ, Kamat AM, Nawroth R, et al. New horizons in bladder cancer research. *Urol Oncol.* (in press). doi: 10.1016/j.urolonc.2018.12.014
18. Kim S, Kim Y, Kong J, Kim E, Choi JH, Yuk HD, et al. Epigenetic regulation of mammalian Hedgehog signaling to the stroma determines the molecular subtype of bladder cancer. *Elife.* (2019) 8:37. doi: 10.7554/eLife.43024.037
19. Stroggilos R, Mokou M, Latosinska A, Makridakis M, Lygirou V, Mavrogeorgis E, et al. Proteome-based classification of Non-muscle Invasive Bladder Cancer. *Int J Cancer.* (2019) 146:281–94. doi: 10.1002/ijc.32556
20. Witzke KE, Grosserueschkamp F, Jutte H, Horn M, Roghmann F, von Landenberg N, et al. Integrated fourier transform infrared imaging and proteomics for identification of a candidate histochemical biomarker in bladder cancer. *Am J Pathol.* (2019) 189:619–31. doi: 10.1016/j.ajpath.2018.11.018
21. Grossman HB, Bellmunt J, Black PC. Can biomarkers guide the use of neoadjuvant chemotherapy in t2 bladder cancer? *Eur Urol Oncol.* (2019) 2:597–602. doi: 10.1016/j.euo.2019.06.002
22. Loras A, Suarez-Cabrera C, Martinez-Bisbal MC, Quintas G, Paramio JM, Martinez-Manez R, et al. Integrative metabolomic and transcriptomic analysis for the study of bladder cancer. *Cancers.* (2019) 11:686. doi: 10.3390/cancers11050686
23. Sjodahl G, Jackson CL, Bartlett JM, Siemens DR, Berman DM. Molecular profiling in muscle-invasive bladder cancer: more than the sum of its parts. *J Pathol.* (2019) 247:563–73. doi: 10.1002/path.5230
24. Morera DS, Lahorewala SS, Belew D, Ghosh S, Klaassen Z, Jordan AR, et al. Clinical parameters outperform molecular subtypes for predicting outcome in bladder cancer: results from multiple cohorts including TCGA. *J Urol.* (2019) 203:62–72. doi: 10.1097/JU.0000000000000351.
25. Choi W, Ochoa A, McConkey DJ, Aine M, Hoglund M, Kim WY, et al. Genetic alterations in the molecular subtypes of bladder cancer: illustration in the cancer genome atlas dataset. *Eur Urol.* (2017) 72:354–65. doi: 10.1016/j.eururo.2017.03.010
26. Rose D, Haferlach T, Schnittger S, Perglerova K, Kern W, Haferlach C. Subtype-specific patterns of molecular mutations in acute myeloid leukemia. *Leukemia.* (2017) 31:11–7. doi: 10.1038/leu.2016.163
27. Plevritis SK, Munoz D, Kurian AW, Stout NK, Alagoz O, Near AM, et al. Association of screening and treatment with breast cancer mortality by

molecular subtype in US women, 2000–2012. *Jama.* (2018) 319:154–64. doi: 10.1001/jama.2017.19130
28. Lenz HJ, Ou FS, Venook AP, Hochster HS, Niedzwiecki D, Goldberg RM, et al. Impact of consensus molecular subtype on survival in patients with metastatic colorectal cancer: results from CALGB/SWOG 80405 (Alliance). *J Clin Oncol.* (2019) 37:1876–85. doi: 10.1200/JCO.18.02258
29. Xue R, Chen L, Zhang C, Fujita M, Li R, Yan SM, et al. Genomic and transcriptomic profiling of combined hepatocellular and intrahepatic cholangiocarcinoma reveals distinct molecular subtypes. *Cancer Cell.* (2019) 35:932–47. doi: 10.1016/j.ccell.2019.04.007
30. Cristescu R, Lee J, Nebozhyn M, Kim KM, Ting JC, Wong SS, et al. Molecular analysis of gastric cancer identifies subtypes associated with distinct clinical outcomes. *Nat Med.* (2015) 21: 449–56. doi: 10.1038/nm.3850
31. Damrauer JS, Hoadley KA, Chism DD, Fan C, Tiganelli CJ, Wobker SE, et al. Intrinsic subtypes of high-grade bladder cancer reflect the hallmarks of breast cancer biology. *Proc Natl Acad Sci USA.* (2014) a111: 3110–5. doi: 10.1073/pnas.1318376111
32. Sjodahl G, Lauss M, Lovgren K, Chebil G, Gudjonsson S, Veerla S, et al. A molecular taxonomy for urothelial carcinoma. *Clin Cancer Res.* (2012) 18: 3377–86. doi: 10.1158/1078-0432.CCR-12-0077-T
33. Hedegaard J, Lamy P, Nordentoft I, Algaba F, Hoyer S, Ulhoi BP, et al. Comprehensive transcriptional analysis of Early-Stage urothelial carcinoma. *Cancer Cell.* (2016) 30: 27–42. doi: 10.1016/j.ccell.2016.05.004
34. van Kessel K, van der Keur KA, Dyrskjot L, Algaba F, Welvaart N, Beukers W, et al. Molecular markers increase precision of the european association of urology Non-Muscle-Invasive bladder cancer progression risk groups. *Clin Cancer Res.* (2018) 24:1586–93. doi: 10.1158/1078-0432.CCR-17-2719
35. Choi W, Porten S, Kim S, Willis D, Plimack ER, Hoffman-Censits J, et al. Identification of distinct basal and luminal subtypes of muscle-invasive bladder cancer with different sensitivities to frontline chemotherapy. *Cancer Cell.* (2014) 25:152–65. doi: 10.1016/j.ccr.2014.01.009
36. Comprehensive molecular characterization of gastric adenocarcinoma. *Nature.* (2014) 513:202–9. doi: 10.1038/nature13480
37. Robertson AG, Kim J, Al-Ahmadie H, Bellmunt J, Guo G, Cherniack AD, et al. Comprehensive molecular characterization of Muscle-Invasive bladder cancer. *Cell.* (2018) 174:1033. doi: 10.1016/j.cell.2018.07.036
38. Tan TZ, Rouanne M, Tan KT, Huang RY, Thiery JP. Molecular Subtypes of urothelial bladder cancer: results from a meta-cohort analysis of 2,411 tumors. *Eur Urol.* (2019) 75: 423–32. doi: 10.1016/j.eururo.2018.08.027
39. Seiler R, Ashab H, Erho N, van Rhijn B, Winters B, Douglas J, et al. Impact of molecular subtypes in muscle-invasive bladder cancer on predicting response and survival after neoadjuvant chemotherapy. *Eur Urol.* (2017) 72:544–54. doi: 10.1016/j.eururo.2017.03.030
40. Seiler R, Gibb EA, Wang NQ, Oo HZ, Lam HM, van Kessel KE, et al. Divergent biological response to neoadjuvant chemotherapy in muscle-invasive bladder cancer. *Clin Cancer Res.* (2018) 25:5082–93. doi: 10.1158/1078-0432.CCR-18-1106
41. Kandimalla R, van Tilborg AA, Kompier LC, Stumpel DJ, Stam RW, Bangma CH, et al. Genome-wide analysis of CpG island methylation in bladder cancer identified TBX2, TBX3, GATA2, and ZIC4 as pTa-specific prognostic markers. *Eur Urol.* (2012) 61:1245–56. doi: 10.1016/j.eururo.2012.01.011
42. Beukers W, Kandimalla R, Masius RG, Vermeij M, Kranse R, van Leenders GJ, et al. Stratification based on methylation of TBX2 and TBX3 into three molecular grades predicts progression in patients with pTa-bladder cancer. *Mod Pathol.* (2015) 28:515–22. doi: 10.1038/modpathol.2014.145
43. Kim J, Akbani R, Creighton CJ, Lerner SP, Weinstein JN, Getz G, et al. Invasive bladder cancer: genomic insights and therapeutic promise. *Clin Cancer Res.* (2015) 21:4514–24. doi: 10.1158/1078-0432.CCR-14-1215
44. Warrick JI, Sjodahl G, Kaag M, Raman JD, Merrill S, Shuman L, et al. Intratumoral heterogeneity of bladder cancer by molecular subtypes and histologic variants. *Eur Urol.* (2019) 75:18–22. doi: 10.1016/j.eururo.2018.09.003
45. Liu D, Abbosh P, Keliher D, Reardon B, Miao D, Mouw K, et al. Mutational patterns in chemotherapy resistant muscle-invasive bladder cancer. *Nat Commun.* (2017) 8:2193. doi: 10.1038/s41467-017-02320-7
46. Cambier S, Sylvester RJ, Collette L, Gontero P, Brausi MA, van Andel G, et al. EORTC nomograms and risk groups for predicting recurrence, progression, and disease-specific and overall survival in Non-Muscle-invasive stage Ta-T1 urothelial bladder cancer patients treated with 1–3 years of maintenance bacillus Calmette-Guerin. *Eur Urol.* (2016) 69:60–9. doi: 10.1016/j.eururo.2015.06.045
47. Rieken M, Shariat SF, Kluth L, Crivelli JJ, Abufaraj M, Foerster B, et al. Comparison of the EORTC tables and the EAU categories for risk stratification of patients with non-muscle-invasive bladder cancer. *Urol Oncol.* (2018) 36:8–17. doi: 10.1016/j.urolonc.2017.08.027
48. McConkey DJ, Choi W, Ochoa A, Siefker-Radtke A, Czerniak B, Dinney CP. Therapeutic opportunities in the intrinsic subtypes of muscle-invasive bladder cancer. *Hematol Oncol Clin North Am.* (2015) 29:377–94. doi: 10.1016/j.hoc.2014.11.003
49. Meeks JJ, McConkey DJ. Limited upstaging in luminal subtype tumors: ready for clinical practice? *Eur Urol.* (2019) 76:207–8. doi: 10.1016/j.eururo.2019.05.025
50. Sjodahl G, Eriksson P, Patschan O, Marzouka NA, Jakobsson L, Bernardo C, et al. Molecular changes during progression from nonmuscle invasive to advanced urothelial carcinoma. *Int J Cancer.* (2019) doi: 10.1002/ijc.32737. [Epub ahead of print].
51. Kamoun A, de Reynies A, Allory Y, Sjodahl G, Robertson AG, Seiler R, et al. Consensus molecular classification of muscle-invasive bladder cancer. *Eur Urol.* (2019). doi: 10.1016/j.eururo.2019.09.006. [Epub ahead of print].
52. Loriot Y, Necchi A, Park SH, Garcia-Donas J, Huddart R, Burgess E, et al. Erdafitinib in locally advanced or metastatic urothelial carcinoma. *N Engl J Med.* (2019) 381:338–48. doi: 10.1056/NEJMoa1817323
53. Casadei C, Dizman N, Schepisi G, Cursano MC, Basso U, Santini D, et al. Targeted therapies for advanced bladder cancer: new strategies with FGFR inhibitors. *Ther Adv Med Oncol.* (2019) 11:432461971. doi: 10.1177/1758835919890285
54. Zeng SX, Zhu Y, Ma AH, Yu W, Zhang H, Lin TY, et al. The phosphatidylinositol 3-Kinase pathway as a potential therapeutic target in bladder cancer. *Clin Cancer Res.* (2017) 23:6580–91. doi: 10.1158/1078-0432.CCR-17-0033
55. Zhang X, Zhang M, Hou Y, Xu L, Li W, Zou Z, et al. Single-cell analyses of transcriptional heterogeneity in squamous cell carcinoma of urinary bladder. *Oncotarget.* (2016) 7:66069–76. doi: 10.18632/oncotarget.11803
56. Yang Z, Li C, Fan Z, Liu H, Zhang X, Cai Z, et al. Single-cell sequencing reveals variants in ARID1A, GPRC5A and MLL2 driving self-renewal of human bladder cancer stem cells. *Eur Urol.* (2017) 71:8–12. doi: 10.1016/j.eururo.2016.06.025
57. Wu Z, Wang S, Jiang F, Li Q, Wang C, Wang H, et al. Mass spectrometric detection combined with bioinformatic analysis identified possible protein markers and key pathways associated with bladder cancer. *Gene.* (2017) 626:407–13. doi: 10.1016/j.gene.2017.05.054
58. Liu Y, Yang W, Zhao L, Liang Z, Shen W, Hou Q, et al. Immune analysis of expression of IL-17 relative ligands and their receptors in bladder cancer: comparison with polyp and cystitis. *BMC Immunol.* (2016) 17:36. doi: 10.1186/s12865-016-0174-8
59. Singh P, Black P. Emerging role of checkpoint inhibition in localized bladder cancer. *Urol Oncol.* (2016) 34:548–55. doi: 10.1016/j.urolonc.2016.09.004

Conflict of Interest: The authors declare that the research was conducted in the absence of any commercial or financial relationships that could be construed as a potential conflict of interest.

frontiers in Oncology

ORIGINAL RESEARCH
published: 27 March 2020
doi: 10.3389/fonc.2020.00394

Gene Expression Profiles Identified Novel Urine Biomarkers for Diagnosis and Prognosis of High-Grade Bladder Urothelial Carcinoma

Yuxuan Song[1†], Donghui Jin[2†], Ningjing Ou[1†], Zhiwen Luo[3], Guangyuan Chen[4], Jingyi Chen[5], Yongjiao Yang[6] and Xiaoqiang Liu[1]*

[1] Department of Urology, Tianjin Medical University General Hospital, Tianjin, China, [2] Department of Cardiothoracic Surgery, Tianjin Medical University General Hospital, Tianjin, China, [3] Department of Hepatobiliary Surgery, National Cancer Center/National Clinical Research Center for Cancer/Cancer Hospital, Chinese Academy of Medical Sciences and Peking Union Medical College, Beijing, China, [4] The Second Clinical Medical School, Nanchang University, Nanchang, China, [5] Department of Gastroenterology and Institute of Clinical Molecular Biology, Peking University People's Hospital, Beijing, China, [6] Department of Urology, The Second Hospital of Tianjin Medical University, Tianjin, China

OPEN ACCESS

Edited by:
Woonyoung Choi,
Johns Hopkins Medicine,
United States

Reviewed by:
Chien-Feng Li,
Chi Mei Medical Center, Taiwan
Fangjian Zhou,
Sun Yat-sen University, China

***Correspondence:**
Xiaoqiang Liu
liutjykdx@163.com

[†]These authors have contributed equally to this work

Specialty section:
This article was submitted to Genitourinary Oncology, a section of the journal Frontiers in Oncology

Received: 02 December 2019
Accepted: 05 March 2020
Published: 27 March 2020

Citation:
Song Y, Jin D, Ou N, Luo Z, Chen G, Chen J, Yang Y and Liu X (2020) Gene Expression Profiles Identified Novel Urine Biomarkers for Diagnosis and Prognosis of High-Grade Bladder Urothelial Carcinoma. Front. Oncol. 10:394. doi: 10.3389/fonc.2020.00394

Bladder urothelial carcinoma (BC) has been identified as one of the most common malignant neoplasm worldwide. High-grade bladder urothelial carcinoma (HGBC) is aggressive with a high risk of recurrence, progression, metastasis, and poor prognosis. Therefore, HGBC clinical management is still a challenge. We performed the present study to seek new urine biomarkers for HGBC and investigate how they promote HGBC progression and thus affect the prognosis based on large-scale sequencing data. We identified the overlapped differentially expressed genes (DEGs) by combining GSE68020 and The Cancer Genome Atlas (TCGA) datasets. Subsequent receiver operating characteristic (ROC) curves, Kaplan-Meier (KM) curves, and Cox regression were conducted to test the diagnostic and prognostic role of the hub genes. Chi-square test and logistic regression were carried out to analyze the associations between clinicopathologic characteristics and the hub genes. Ultimately, we performed gene set enrichment analysis (GSEA), protein-protein interaction (PPI) networks, and Bayesian networks (BNs) to explore the underlying mechanisms by which ECM1, CRYAB, CGNL1, and GPX3 are involved in tumor progression. Immunohistochemistry based on The Human Protein Atlas and quantitative real-time polymerase chain reaction based on urine samples confirmed the downregulation and diagnostic values of the hub genes in HGBC. In conclusion, our study indicated that CRYAB, CGNL1, ECM1, and GPX3 are potential urine biomarkers of HGBC. These four novel urine biomarkers will have attractive applications to provide new diagnostic methods, prognostic predictors and treatment targets for HGBC, which could improve the prognosis of HGBC patients, if validated by further experiments and larger prospective clinical trials.

Keywords: urine, biomarker, bladder urothelial cancer, diagnosis, prognosis, TCGA, GEO

INTRODUCTION

Bladder urothelial carcinoma (BC) has been identified as the ninth most common malignant neoplasm all over the world (1, 2). More than 199,000 people died of it and over 549,000 cases were newly diagnosed in 2018 (1, 2). Although the age standardized incidence and number of deaths are decreasing in the past 20 years, the number of BC incident cases is growing globally and the BC burden may ascend in the future as a result of aged tendency of population and polluted environment (3, 4). BC is classified as high-grade bladder urothelial carcinoma (HGBC) and low-grade bladder urothelial carcinoma (LGBC) based on how cancer cells histologically differ from normal bladder cells (5). HGBC is aggressive and has a high risk of recurrence, progression, metastasis and poor prognosis, while LGBC is a kind of tumor with low malignancy and comparatively good prognosis (5). In addition, treatments for HGBC and LGBC are quite different. HGBC patients should receive radical cystectomy with or without postoperative chemotherapy; LGBC patients are most commonly treated with transurethral resection of bladder tumor (6, 7). Hence, an early and accurate diagnosis of BC, particularly differential diagnosis between HGBC and LGBC, is a critical factor for clinical management of BC.

At present, cystoscopy and urine cytology are commonly acknowledged as the gold standard methods for BC diagnosis (8). However, cystoscopy may sometimes miss HGBC, particularly carcinoma *in situ* (CIS). Besides, as an invasive method, cystoscopy may cause damage to surrounding organs and even lead to tumor metastasis caused by improper human operation (9, 10). Although urine cytology is a non-invasive examination, it is costly with poor sensitivity and specificity. What's more, urine cytology is subjective and varies from different pathologists' experience. The above factors contribute to the challenges and high cost associated with BC clinical management.

Recently, many urine-based tests have been carried out to explore potential biomarkers for HGBC. However, most of these urine biomarkers lack of enough sensitivity and specificity and should be used alongside cystoscopy (11). Besides, very few of these biomarkers could be utilized to predict tumor progression, metastasis and prognosis or served as potential therapeutic targets. Therefore, powerful urine biomarkers are still required to improve the diagnosis and prognosis of HGBC.

As a consequence, we conducted a series of analyses based on gene expression profile of high-throughput sequencing data obtained from Gene Expression Omnibus (GEO) and The Cancer Genome Atlas (TCGA) in order to seek potential urine biomarkers for HGBC. In the present study, we first identified the key differentially expressed genes (DEGs) by combining GEO and TCGA datasets. Then we found that ECM1 (extracellular matrix protein 1), CRYAB (alpha B-crystallin), CGNL1 (cingulin-like 1), and GPX3 (glutathione peroxidase 3) are correlated with diagnosis, progression, metastasis and prognosis of HGBC. Ultimately, we performed gene set enrichment analysis (GSEA), protein-protein interaction (PPI) networks and Bayesian networks (BNs) to explore the underlying mechanisms by which the four hub genes are involved in tumor progression. Immunohistochemistry based on The Human Protein Atlas (THPA) and quantitative real-time polymerase chain reaction (qRT-PCR) based on urine samples were utilized to validate the hub genes and their diagnostic values. In summary, this study indicated that ECM1, CRYAB, CGNL1, and GPX3 could be served as new diagnostic and prognostic urine biomarkers for HGBC.

MATERIALS AND METHODS

GEO Data Source

The gene expression profiling dataset of GSE68020 was obtained from GEO (http://www.ncbi.nlm.nih.gov/geo/) database. Fifty urine samples including HGBC patients ($n = 30$) and non-tumor healthy controls ($n = 20$) were evaluated for BC via urine cytology. RNA was isolated and measured by microarray (Platform: GPL10558 Illumina HumanHT-12 V4.0 expression beadchip).

TCGA Data Source

TCGA BLCA (Bladder Urothelial Carcinoma) dataset contained normal bladder samples ($n = 19$) and BC samples ($n = 411$) which included HGBC samples ($n = 380$). The RNA-sequencing data and clinical data were downloaded from TCGA (http://tcga-data.nci.nih.gov/tcga/database).

RNA Data Processing and Identification of Differentially Expressed Genes

We mainly used R software (v.3.5.3 and v.3.4.4: http://www.r-project.org) to analyze and deal with RNA data. To identify DEGs in GSE68020 and TCGA BLCA datasets between BC patients and non-tumor healthy controls, we utilized limma R package (12). The cut-off criteria of adjusted *P*-value (*adj. P*-value) was set as 0.05 and the criterion of Fold change was set as $|\log FC| \geq 1$. For the identified DEGs from GSE68020 and TCGA BLCA datasets, we generated volcano plots using limma R package. For DEGs from GSE68020, we generated a heat map using pheatmap R package.

Then, an online tool, venny 2.1 (http://bioinfogp.cnb.csic.es/tools/venny/index.html) was applied to identify overlapped DEGs in the two gene expression microarrays. The upregulated and downregulated DEGs were calculated, respectively.

Receiver Operating Characteristic Curves for Diagnostic Value

To measure the diagnostic values of the 5 hub genes for HGBC, receiver operating characteristic (ROC) curves were plotted and area under the curve (AUC) values were also calculated. Statistical analysis was performed with GraphPad Prism 7.0. $P < 0.05$ was considered as statistically significant difference.

Survival and Statistical Analysis

Based on TCGA BLCA dataset, univariate and multivariate Cox regression, Kaplan-Meier (KM) method and log-rank test were used to compare the influence of expression levels of the 5 hub genes on overall survival (OS) along with other clinical characteristics. Clinical characteristics included Union for International Cancer Control (UICC) stage, histological grade,

pathological T (pT) stage, pathological N (pN) stage, pathological M (pM) stage, age and gender. We utilized survival and survminer R packages to perform these analyses. What' more, we also used Gene Expression Profiling Interactive Analysis (GEPIA) (http://gepia.cancer-pku.cn/) for further calculating disease free survival (DFS) with the 5 hub genes on the basis of TCGA BLCA dataset (13). The correlations between clinicopathologic characteristics and expression of hub genes were analyzed with the chi-square test and logistic regression. The cut-off values of the 5 hub genes expression were determined by their median values. $P < 0.05$ was considered as statistically significant difference.

Gene Set Enrichment Analysis

GSEA is a computational method that assesses whether a priori defined a set of genes shows statistically significant, concordant differences between two biological states (14). In the present study, GSEA firstly generated an ordered list of all genes according to their correlation with expression of hub genes, GSEA was carried out to elucidate the significant survival difference observed between high expression and low expression groups. Gene set permutations were performed 1,000 times for each analysis. The expression level of hub genes was used as a phenotype label. To illustrate the roles of ECM1, CRYAB, CGNL1, and GPX3, we carried out GSEA to analyze the enrichment of HGBC patients in TCGA BLCA dataset. False discovery rate (FDR) < 25% and nominal $P < 0.05$ were regarded as the cut-off criteria of sorting Gene Ontology (GO) functional enrichment and KEGG pathway enrichment.

Protein-Protein Interactions Network and Module Analysis

To better understand the metabolism and molecular mechanisms of carcinoma, the functional interactions between proteins become necessary. String online server (version 11.0: http://string-db.org/) was designed and adopted to collect and integrate the information by consolidating known and predicted protein-protein association data for a large number of organisms (15). ECM1, CRYAB, CGNL1 and GPX3 were, respectively, put into the tool to construct and visualize the PPI networks about each protein. Interaction score of 0.400 was set as the threshold. Besides, Cytoscape software (Cytoscape_v.3.6.1) was applied to plot the PPI networks.

Construction of Bayesian Networks

In order to further clarify the roles of the CRYAB, ECM1, GPX3, and CGNL1 with HGBC, we constructed BNs to dissect the complex regulatory relationships among the four hub genes. BN is a graphical model that encodes probabilistic relationships among variables of interest (16). In the present study, we allowed these items as the nodes fed into the BNs: histological grade, UICC stage, pN stage and expression of the four hub genes based on TCGA BLCA dataset. Hence, we constructed three BNs and the nodes were described as follows: (1) BN1: BC histological grade+ CRYAB + ECM1 + GPX3 + CGNL1; (2) BN2: BC UICC stage + CRYAB + ECM1 + GPX3 + CGNL1; and (3) BN3: BC pN + CRYAB + ECM1 + GPX3 + CGNL1.

The conditional likelihood of the variables given their parents is represented in a BN by using Gaussian conditional densities. Under the assumption of parameter independence, an initial BN structure is learned from the training data. From this initial network, greedy search algorithm with random restarts is performed to get the highest score posterior network to avoid local maxima. Finally, an optimized BN that maximizes the Bayesian factor is obtained using heuristic search of the network space in a specified domain. The three BNs were carried out using deal R package.

Immunohistochemistry From the Human Protein Atlas

Immunohistochemistry was obtained from The Human Protein Atlas (THPA) (http://www.proteinatlas.org/) (17). THPA is a Swedish-based program initiated in 2003 with the aim to map all the human proteins in cells, tissues and organs using integration of various omics technologies, including antibody-based imaging, mass spectrometry-based proteomics, transcriptomics and systems biology. All the data in the knowledge resource is open access to allow researchers to freely access the data for exploration of the human proteome. The Tissue Atlas and Pathology Atlas showed the distribution of the proteins across all major tissues, organs and tumors in the human body.

We evaluated expression levels of CRYAB, ECM1, GPX3, CGNL1, and CRNN (cornulin) between normal bladder tissues and HGBC tissues from THPA. Staining intensity was scored as follows: absent staining, 0; mild staining, 1; moderate staining, 2; marked staining, 3. Percentages of positive cells were categorized as follows: <5% of positive cells, 0; 5–25%, 1; 26–50%, 2; 51–75%, 3; 76–100%, 4. For each case, the two scores were multiplied to produce a total staining score. According to the total staining scores, we divided the expression into four levels: negative (-, score 0); weakly positive (+, scores 1–4); positive (++, scores 5–8); strongly positive (+ + +, scores 9–12).

Differences of immunohistochemistry between normal bladder tissues and HGBC tissues were compared with Mann-Whitney U test and Fisher's Exact test. $P < 0.05$ was considered as statistically significant difference. Detailed characteristics of immunohistochemistry data are in **Supplementary Table 1**.

Urine Samples in Tianjin Validation Cohort, RNA Extraction and Quantitative Real-Time Polymerase Chain Reaction (qRT-PCR)

The study was approved by the Ethics Committee of Tianjin Medical University General Hospital. All recruited participants volunteered to participate and signed informed consent before being enrolled in our study.

A total of 30 patients who were pathologically and clinically diagnosed with BC were enrolled from Tianjin Medical University General Hospital. None of the BC patients had received any surgery, chemotherapy or radiotherapy before collecting urine samples. Clinical and pathological data of patients including age, gender, tumor UICC stage and histological grade were recorded. We also enrolled 30 healthy

TABLE 1 | Primer sequences used to amplify target genes by quantitative real-time polymerase chain reaction (qRT-PCR).

Gene name		Primer sequences
GPX3	Forward	5′-GAAGGCTCCCCGCCAGAT-3′
	Reverse	5′-TCAATGGTGAGGGCTCCGTA-3′
ECM1	Forward	5′-AGCACCCCAATGAACAGAAGG-3′
	Reverse	5′-CTGCATTCCAGGACTCAGGTT-3′
CRYAB	Forward	5'-TGGATAGAAGGGGGACAAGGAG-3′
	Reverse	5′-CATGGAGACTTGTGATCCGGG-3′
CGNL1	Forward	5'-TACGGTGTCAGTATTCGGGTC-3′
	Reverse	5′-GCTGGGCGTATGGGTTTTC-3′
CRNN	Forward	5′-GGGATCATCGAGGCCTTCAG-3′
	Reverse	5′-CTGGATCGTGGGGTTTCACA-3′
GAPDH	Forward	5′-AGAAGGCTGGGGCTCATTTG-3′
	Reverse	5′-AGGGGCCATCCACAGTCTTC-3′

controls matched by age and sex. Urine was collected from the healthy individuals to be used as the healthy control specimens. All the 30 BC patients and 30 controls (Tianjin validation cohort) are Asians.

A single and naturally voided midstream urine sample was obtained from all recruited participants. Approximately 50 ml of urine was collected and put on ice immediately, then the samples were centrifuged as soon as possible (not later than 1 h later) at 3,000 rpm for 7 min at 4°C. Total RNA from urine samples were extracted using RNeasy kit (Qiagen, Valencia, CA). The first chain of cDNA was synthesized by reverse transcription with TaqMan® Reverse Transcription Reagents (Applied Biosystems, Grand Island, NY). GAPDH was used as internal control. The sequences of the primers were displayed in **Table 1**. qRT-PCR was performed using the CFX96 Touch PCR system (Bio-Rad). The relative mRNA expressions of CRYAB, ECM1, GPX3, CGNL1, and CRNN were calculated by $2^{-\Delta\Delta Ct}$ method. In addition, ROC curves were plotted and AUC values were calculated based on the qRT-PCR results by GraphPad Prism 7.0. $P < 0.05$ was considered as statistically significant difference.

RESULTS

Workflow for this study was displayed in **Figure 1A**.

Identification of Differentially Expressed Genes

The GSE68020 dataset was processed with limma R package. According to the criteria mentioned above, a total of 17 DEGs including 5 upregulated and 12 downregulated genes were selected for further analyses as shown in the volcano plot and heat map (**Figures 1B,D**).

The TCGA BLCA dataset was also analyzed with limma R package. After differential expression analysis, 1617 DEGs were screened out to meet the requirements, among which 536 were upregulated and 1,081 were downregulated (**Figure 1C**).

To validate the reliability of DEGs, we adopted Venn diagram to obtain overlapped DEGs of the two datasets. Ultimately, 5 DEGs including CRYAB, ECM1, CGNL1, GPX3, and CRNN were confirmed to be appeared in both datasets as shown in Venn diagram (**Figure 1E**). All of the 5 hub genes were downregulated genes.

Diagnostic Value of the 5 Hub Genes in GSE68020 and TCGA BLCA Datasets

ROC curves were applied to measure the diagnostic value of the 5 hub genes in HGBC. Based on TCGA BLCA dataset, we found that CRYAB (AUC = 0.9326, $P < 0.001$), ECM1 (AUC = 0.6782, $P = 0.009$), CGNL1 (AUC = 0.9314, $P < 0.001$), and GPX3 (AUC = 0.8480, $P < 0.001$) are effective in distinguishing HGBC tissues and normal para-carcinoma tissues (**Figure 2A**). However, CRNN (AUC = 0.5057, $P = 0.933$) proved to be no diagnostic capability for HGBC. Similar results were found in GEO dataset (**Figure 2B**).

In addition, we also evaluated whether the 5 hub genes have the potential to be used in differential diagnosis between HGBC and LGBC. We identified that CRYAB (AUC = 0.7472, $P < 0.001$), ECM1 (AUC = 0.8100, $P < 0.001$) and GPX3 (AUC = 0.6714, $P = 0.010$) can be applied in differential diagnosis between HGBC and LGBC, while CRNN (AUC = 0.5891, $P = 0.179$) and CGNL1 (AUC = 0.5411, $P = 0.536$) can't (**Figure 2C**).

Survival Analysis of Hub Genes in TCGA BLCA Dataset

To explore whether the 5 hub genes are associated with BC and HGBC survival time, we utilized log-rank test and drew KM curves. As shown in **Figures 3A,B**, we identified that higher expression levels of CRYAB and ECM1 are associated with worse OS time of BC and HGBC ($P < 0.05$), while GPX3, CGNL1 and CRNN can't influence the OS time. Furthermore, higher CRYAB expression can also lead to a poor DFS time of BC ($P < 0.05$) (**Figure 3C**).

Correlations Between Expression Levels of the 5 Hub Genes and Clinical Outcomes in TCGA BLCA Dataset

To ensure whether expression levels of the 5 hub genes may influence the clinical outcomes of BC, we performed chi-square test and logistic regression. As shown in **Figure 4** and **Table 2**, higher expression levels of CRYAB and ECM1 are observed in HGBC and advanced UICC stage (stage III and stage IV) BC ($P < 0.05$). In addition, higher expression levels of CRYAB, ECM1 and CGNL1 may predict lymph node metastasis of BC ($P < 0.05$). However, higher GPX3 expression level is an indicator for early UICC stage (stage I) ($P < 0.05$).

In order to further confirm the prognostic value of the 5 hub genes, we performed univariate and multivariate Cox regression to calculate hazard ratios (HRs). Among 411 BC samples from TCGA BLCA dataset, 165 BC samples were enrolled in Cox regression analyses since they contained a record of complete information of UICC stage, histological grade, pT stage, pN stage, pM stage, age and gender.

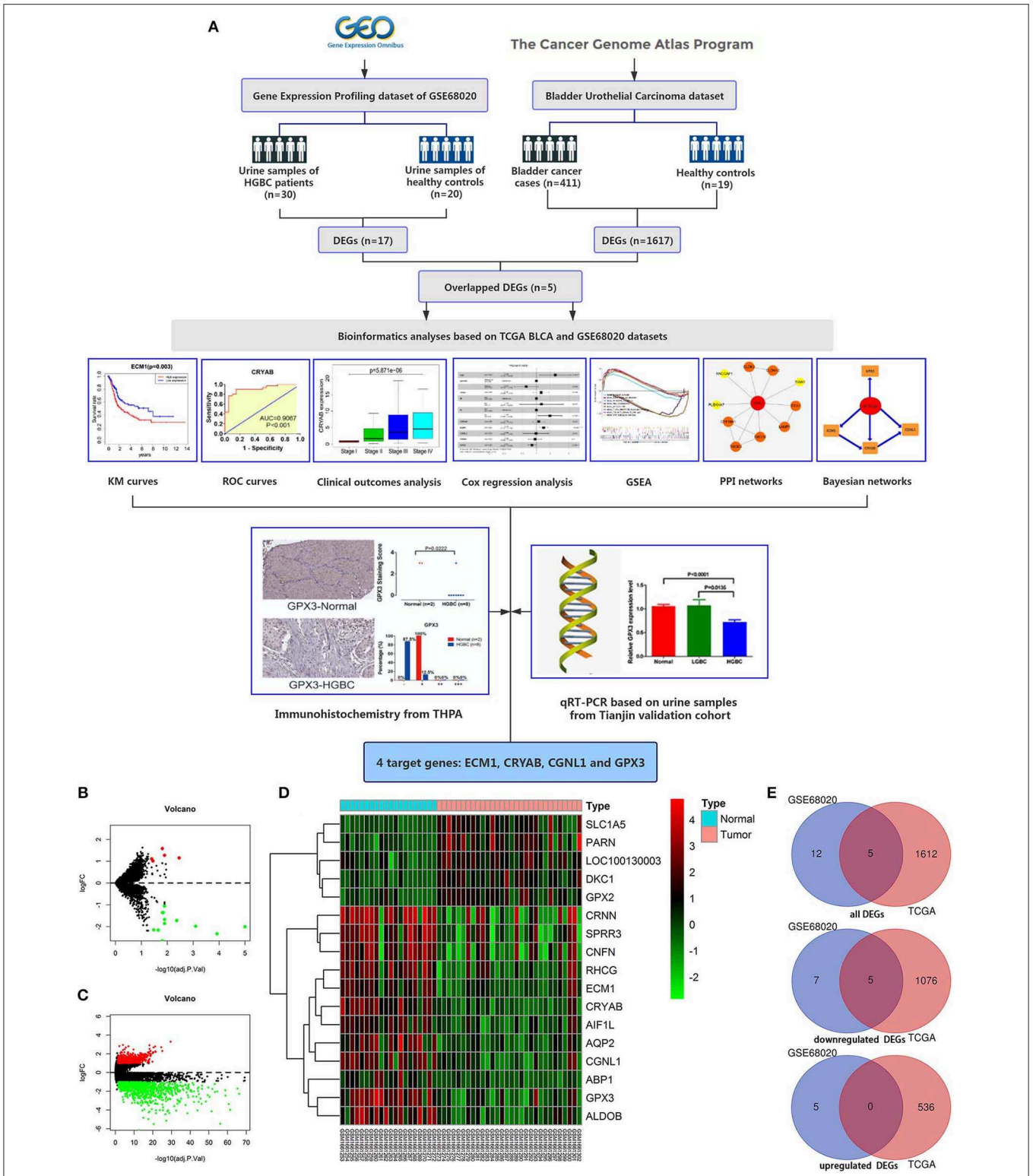

FIGURE 1 | Workflow of this study and identification of differentially expressed genes (DEGs) based on GEO GSE68020 and TCGA BLCA datasets. **(A)** Workflow of this study; **(B)** Volcano plot for GSE68020 dataset; **(C)** Volcano plot for TCGA BLCA dataset; **(D)** Heat map for DEGs of TCGA BLCA dataset; and **(E)** Venn diagram for overlapped DEGs. Permissions to use the logo of GEO (Gene Expression Omnibus) have been obtained from the copyright holders of GEO. GEO, Gene Expression Omnibus; TCGA, The Cancer Genome Atlas; BLCA, Bladder Urothelial Carcinoma; KM, kaplan-Meier; ROC, receiver operating characteristic; GSEA, gene set enrichment analysis; PPI, protein-protein interaction; THPA, The Human Protein Atlas; qRT-PCR, quantitative real-time polymerase chain reaction.

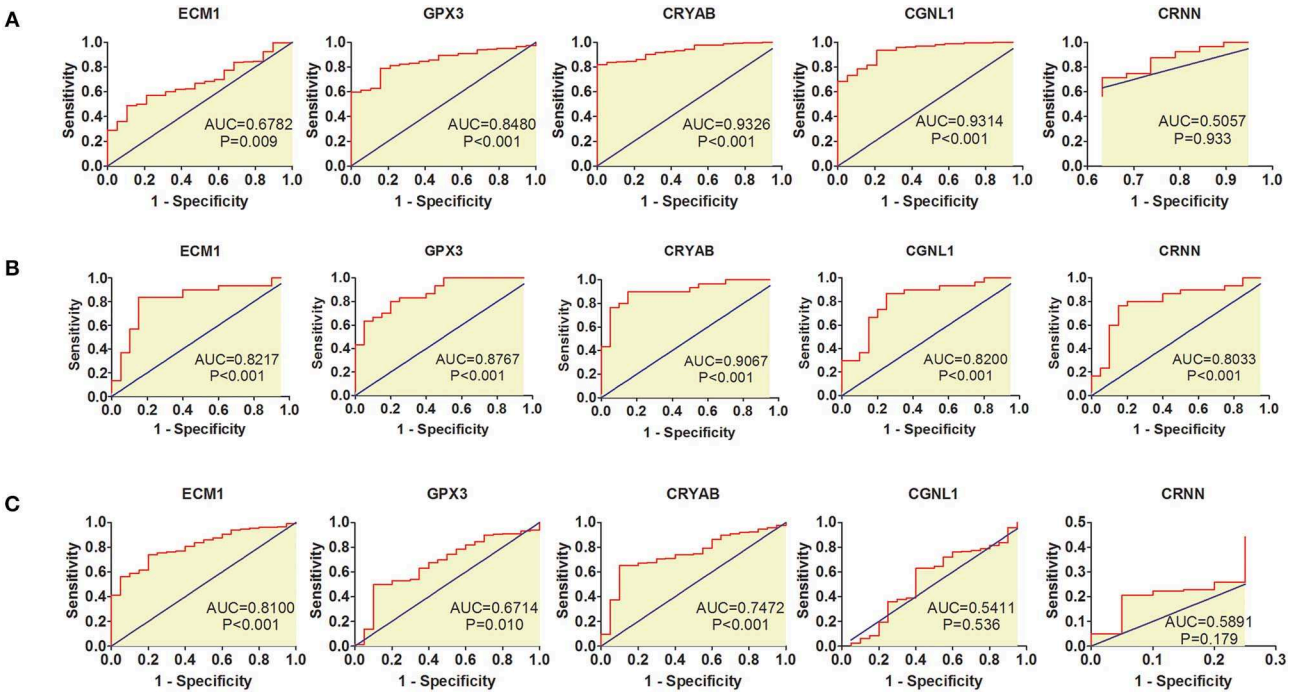

FIGURE 2 | Receiver operating characteristic (ROC) curves for diagnostic values of ECM1, GPX3, CRYAB, CGNL1, and CRNN. **(A)** ROC curves of diagnostic value for high-grade bladder urothelial carcinoma (HGBC) based on TCGA BLCA dataset; **(B)** ROC curves of diagnostic value for HGBC based on GSE68020 dataset; and **(C)** ROC curves for differential diagnosis between HGBC and low-grade bladder urothelial carcinoma (LGBC) based on TCGA BLCA dataset. AUC, area under the curve.

Univariate Cox regression revealed that UICC stage (HR = 1.51, $P = 0.024$), pN stage (HR = 2.18, $P = 0.003$), age (HR = 2.30, $P = 0.029$) along with CRYAB (HR = 1.26, $P = 0.026$), and ECM1 (HR = 1.42, $P < 0.001$) expression status are significantly associated to OS of BC patients, while other factors including histological grade, pT stage, pM stage and gender don't have effects on OS (**Table 3**).

Multivariate Cox regression was carried out with every gene, respectively. We demonstrated that higher ECM1 expression (HR = 1.44, $P = 0.001$), lymph node metastasis (HR = 1.97, $P = 0.026$), and advanced age (HR = 2.58, $P = 0.018$) might be considered as independent poor prognostic indicators of OS. However, higher GPX3 expression might be an independent good prognostic indicator (HR = 0.81, $P = 0.043$) (**Table 3**).

GSEA Revealed Biological Function of Hub Genes in BC (GO and KEGG Pathway Analysis)

To explore the underlying mechanisms by which CRYAB, ECM1, GPX3, and CGNL1 are involved in BC progression, GSEA was carried out between high expression and low expression groups on the basis of TCGA BLCA dataset. Both KEGG pathway analysis and GO functional enrichment were performed.

We identified pathways that are differentially activated in HGBC. Upregulation of CRYAB, ECM1, GPX3, and CGNL1 were enriched in pathways which are vital in tumorigenesis and progression, such as vascular endothelial growth factor (VEGF), TGF-β (transforming growth factor-β), Wnt and MAPK signaling pathways. Downregulation of the four genes can have effects on spliceosome (**Figures 5A,C,E,G**).

GO functional enrichment was also conducted and we found that the CRYAB, ECM1, GPX3, and CGNL1 are enriched in biological process (BP) including extracellular matrix structural constituent, glycosaminoglycan binding and cytokine binding. With regard to molecular function (MF), they are enriched in collagen containing extracellular matrix and collagen trimer. As for cell component (CC) analysis, they are located in extracellular structure organization and regulation of vasculature development. Based on the 3 genes, the top five significant GO terms for BP, CC, and MF are shown in **Figures 5B,D,F,H**.

PPI Network Analyses and Module Functional Enrichment

To further detect the interaction between the proteins encoded by CRYAB, ECM1, GPX3, and CGNL1, the four genes were put into String separately. Based on the String database, we constructed four PPI network modules in **Figure 6**. Besides, functional enrichments of the four modules were shown in **Table 4**.

Construction of Bayesian Networks

We constructed three BNs as described in Materials and methods section. Since chi-square test and logistic regression show that CRYAB, ECM1, CGNL1, and GPX3 are significantly associated with histological grade, UICC stage and pN stage ($P < 0.05$), we combined the four hub genes with histological grade, UICC stage

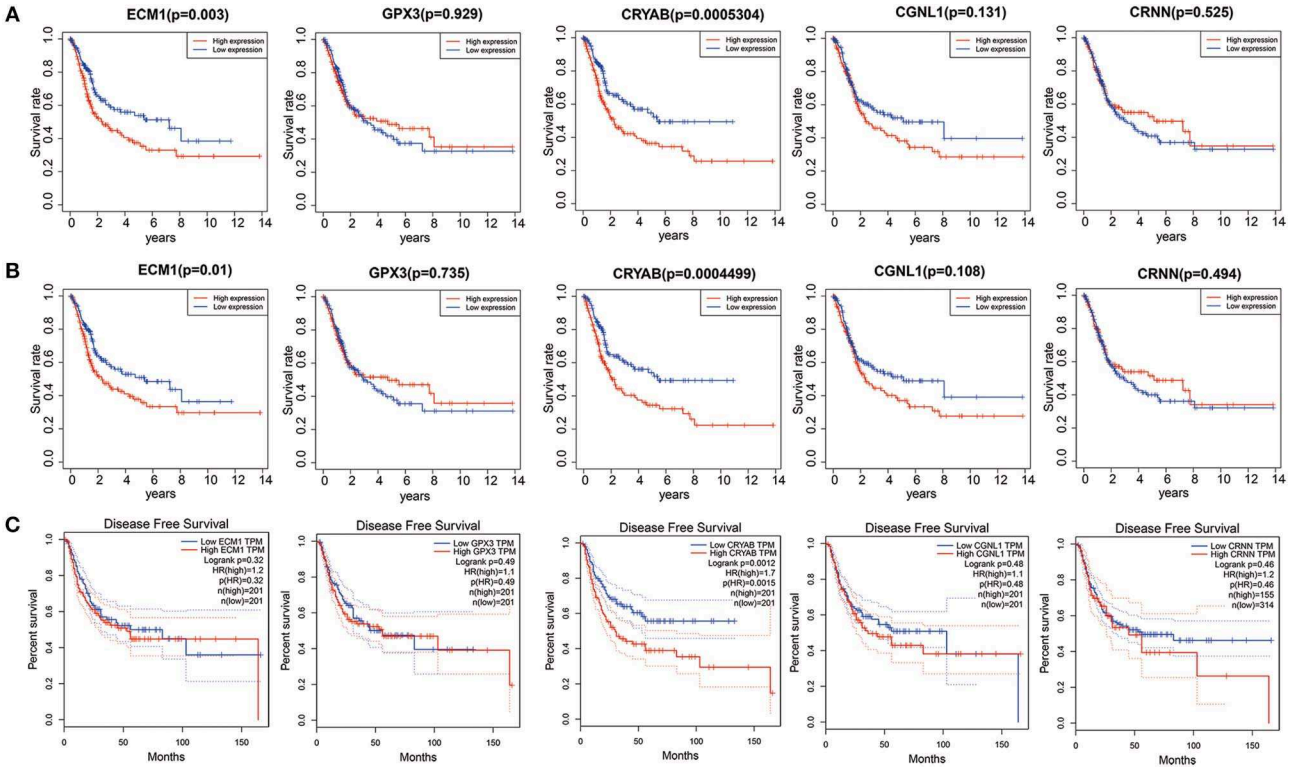

FIGURE 3 | Kaplan-Meier (KM) curves for prognostic values of ECM1, GPX3, CRYAB, CGNL1, and CRNN. **(A)** Overall survival (OS) based on TCGA BLCA dataset; **(B)** OS based on high-grade bladder urothelial carcinoma in TCGA BLCA dataset; and **(C)** Disease free survival (DFS) based on Gene Expression Profiling Interactive Analysis (GEPIA).

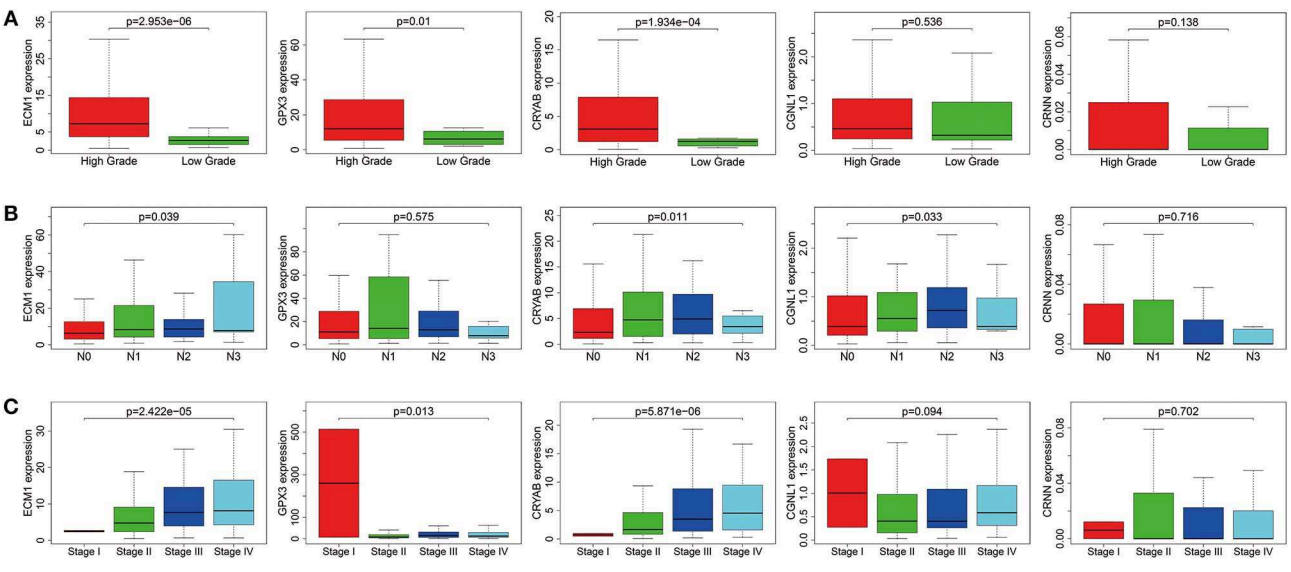

FIGURE 4 | Expression levels of ECM1, GPX3, CRYAB, CGNL1, and CRNN in different clinicopathologic characteristics. **(A)** Histological grade; **(B)** pN (pathological N) stage; and **(C)** UICC (Union for International Cancer Control) stage.

and pN stage, respectively, to construct the three BNs in **Figure 7**. In each of BNs, an edge specified as node1→ node2 means that node2 is a direct cause of node1.

From **Figure 7**, we identified that CRYAB, ECM1, CGNL1, and GPX3 are all direct factors of BC histological grade, UICC stage and pN stage. This discovery is consistent with

TABLE 2 | Relationship between expression of the five DEGs and clinicopathological characteristics in BC patients from TCGA.

Clinical characteristics	Total (N)	CRYAB expression		*P*-value	ECM1 expression		*P*-value	GPX3 expression		*P*-value	CGNL1 expression		*P*-value	CRNN expression		*P*-value
(A)		**High**	**Low**		**High**	**Low**		**High**	**Low**		**High**	**Low**		**High**	**Low**	
Histological grade																
High grade	380	198 (52.1%)	182 (47.9%)	**<0.001**	199 (52.4%)	181 (47.6%)	**<0.001**	196 (51.6%)	184 (48.4%)	**0.006**	190 (50.0%)	190 (50.0%)	0.383	192 (50.5%)	188 (49.5%)	0.176
Low grade	20	2 (10.0%)	18 (90.0%)		1 (00.3%)	19 (05.0%)		4 (20.0%)	16 (80.0%)		8 (40.0%)	12 (60.0%)		7 (35.0%)	13 (65.0%)	
UICC stage																
Stage I+II	130	43 (33.1%)	87 (66.9%)	**<0.001**	47 (12.4%)	83 (21.8%)	**<0.001**	52 (40.0%)	78 (60.0%)	**0.006**	57 (43.8%)	73 (56.2%)	0.094	71 (54.6%)	59 (45.4%)	0.189
Stage III+IV	271	158 (58.3%)	113 (41.7%)		153 (40.3%)	118 (31.1%)		148 (54.6%)	123 (45.4%)		143 (52.8%)	128 (47.2%)		129 (47.6%)	142 (52.4%)	
pT stage																
T1	4	0 (0.0%)	4 (100.0%)	0.052	1 (00.3%)	3 (00.8%)	0.356	2 (50.0%)	2 (50.0%)	1.000	2 (50.0%)	2 (50.0%)	1.000	3 (75.0%)	1 (25.0%)	0.623
T2+T3+T4	367	193 (52.6%)	174 (47.4%)		191 (50.3%)	176 (46.3%)		189 (51.5%)	178 (48.5%)		184 (50.1%)	183 (49.9%)		184 (50.1%)	183 (49.9%)	
pM stage																
No (M0)	193	78 (40.4%)	115 (59.6%)	0.988	72 (18.9%)	121 (31.8%)	0.409	77 (39.9%)	116 (60.1%)	0.215	84 (43.5%)	109 (56.5%)	0.686	91 (47.2%)	102 (52.8%)	0.485
Yes (M1)	11	5 (45.5%)	6 (54.5%)		6 (01.6%)	5 (01.3%)		7 (63.6%)	4 (36.4%)		6 (54.5%)	5 (45.5%)		4 (36.4%)	7 (63.6%)	
pN stage																
No (N0)	234	108 (46.2%)	126 (53.8%)	**<0.001**	109 (28.7%)	125 (32.9%)	**0.029**	116 (49.6%)	118 (50.4%)	0.430	103 (44.0%)	131 (56.0%)	**0.002**	125 (53.4%)	109 (46.6%)	0.106
Yes (N1+N2+N3)	128	84 (65.6%)	44 (34.4%)		75 (19.7%)	53 (13.9%)		69 (53.9%)	59 (46.1%)		78 (60.9%)	50 (39.1%)		57 (44.5%)	71 (55.5%)	
Age (years)																
≤60	106	39 (36.8%)	67 (63.2%)	**0.002**	48 (12.6%)	58 (15.3%)	0.271	44 (41.5%)	62 (58.5%)	**0.045**	50 (47.2%)	56 (52.8%)	0.516	58 (54.7%)	48 (45.3%)	0.246
>60	297	162 (54.5%)	135 (45.5%)		153 (40.3%)	144 (37.9%)		157 (52.9%)	140 (47.1%)		151 (50.8%)	146 (49.2%)		143 (48.1%)	154 (51.9%)	
gender																
Female	105	55 (52.4%)	50 (47.6%)	0.551	55 (14.5%)	50 (13.2%)	0.551	55 (52.4%)	50 (47.6%)	0.551	51 (48.6%)	54 (51.4%)	0.756	57 (54.3%)	48 (45.7%)	0.293
Male	298	146 (49.0%)	152 (51.0%)		146 (38.4%)	152 (40.0%)		146 (49.0%)	152 (51.0%)		150 (50.3%)	148 (49.7%)		144 (48.3%)	154 (51.7%)	
(B)		**OR (95%CI)**			**OR (95%CI)**			**OR (95%CI)**			**OR (95%CI)**			**OR (95%CI)**		
Histological grade (high vs. low)	400	9.79 (2.77, 62.14)		**0.002**	20.89 (4.27, 377.21)		**0.003**	4.26 (1.53, 15.08)		**0.011**	1.50 (0.61, 3.91)		0.386	2.38 (0.90, 7.43)		0.100
UICC stage (III+IV vs. I+II)	401	2.83 (1.83, 4.41)		**0.000**	2.30(1.49.3.54)		**0.000**	1.80 (1.18, 2.77)		**0.006**	1.43 (0.94, 2.18)		0.095	0.85 (0.56, 1.29)		0.440
pN stage (N1+N2+N3 vs. N0)	362	2.23 (1.43, 3.50)		**0.000**	1.62 (1.05, 2.52)		**0.029**	1.19 (0.77, 1.84)		0.431	1.98 (1.28, 3.09)		**0.002**	0.76 (0.49, 1.18)		0.222
pM stage (M1 vs. M0)	204	1.23 (0.34, 4.22)		0.741	2.02 (0.59, 7.22)		0.261	2.64 (0.77, 10.35)		0.132	1.56(0.45, 5.57)		0.477	0.74 (0.19, 2.54)		0.642
Age (>60 vs. ≤60)	403	2.06(1.31, 3.27)		**0.002**	1.28 (0.82, 2.01)		0.271	1.58 (1.01, 2.48)		**0.046**	1.16 (0.74, 1.81)		0.516	0.86 (0.55, 1.34)		0.498
Gender (male vs. female)	403	0.87 (0.56, 1.36)		0.551	0.87(0.56, 1.36)		0.551	0.87 (0.56, 1.36)		0.551	1.07 (0.69, 1.68)		0.756	0.68 (0.43, 1.06)		0.091

A, chi-square test; B, logistic regression; DEGs, differentially expressed genes; TCGA, The Cancer Genome Atlas; UICC, Union for International Cancer Control; pT, pathological T; pN, pathological N; pM, pathological M. Bold values meant P-value < 0.05.

TABLE 3 | Univariate and multivariate Cox analyses between expression levels of the five DEGs and patient survival based on TCGA.

Items	Univariate Cox	*P*-value	Multivariate Cox	*P*-value
Histological grade	-	0.996	-	-
UICC stage	**1.51 (1.06, 2.15)**	**0.024**	1.27 (0.85, 1.9)	0.245
pT stage	-	0.997	-	-
pM stage	2.09 (0.75, 5.80)	0.158	1.29 (0.44, 3.8)	0.641
pN stage	**2.18 (1.30, 3.66)**	**0.003**	1.97 (1.08, 3.58)	**0.026**
Age	**2.30 (1.09, 4.85)**	**0.029**	2.58 (1.18, 5.64)	**0.018**
Gender	0.59 (0.34, 1.03)	0.062	0.61 (0.34, 1.09)	0.095
CRYAB	**1.26 (1.03, 1.55)**	**0.026**	1.12 (0.83, 1.52)	0.443
ECM1	**1.42 (1.18, 1.71)**	**<0.001**	**1.44 (1.17, 1.78)**	**0.001**
CGNL1	1.19 (0.71, 1.98)	0.511	0.98 (0.52, 1.85)	0.957
CRNN	1.16 (0.86, 1.57)	0.339	0.94 (0.68, 1.3)	0.700
GPX3	0.97 (0.82, 1.15)	0.716	**0.81 (0.65, 0.99)**	**0.043**

DEGs, differentially expressed genes; TCGA, The Cancer Genome Atlas; UICC, Union for International Cancer Control; pT, pathological T; pN, pathological N; pM, pathological M. Bold values meant P-value < 0.05.

the results of chi-square test and logistic regression. It is worth noting that CGNL1 is a direct cause of CRYAB for BC histological grade as shown in BN1. In the meantime, it is interesting to note that CRYAB is a direct cause of CGNL1 for BC UICC stage as shown in BN2. Furthermore, with regard to BC pN stage, BN3 illustrated that CGNL1 is a direct cause of CRYAB and CRYAB is a direct cause of ECM1.

Immunohistochemistry From the Human Protein Atlas

To further validate our above findings, we evaluated expression levels of CRYAB, ECM1, GPX3, CGNL1 and CRNN between normal bladder tissues and HGBC tissues based on immunohistochemistry from THPA. As shown in **Figure 8A**, Mann-Whitney *U* test suggested that normal bladder tissues have higher staining scores of GPX3 ($P = 0.0222$) and ECM1 ($P = 0.0021$) than HGBC tissues. However, there is no difference for the staining scores of CRYAB, CGNL1 and CRNN between the two groups ($P > 0.05$).

In addition, we divided the expression into four levels: negative (–), weakly positive (+), positive (++) and strongly positive (+ + +). Distributions of the four expression levels for each gene were demonstrated in **Figure 8B**. Fisher's Exact test showed that normal bladder tissues have higher expression level of GPX3 ($P = 0.016$) and ECM1 ($P = 0.001$) than HGBC tissues, while no differences were found for expression levels of CRYAB, CGNL1 and CRNN ($P > 0.05$) (**Table 5**).

The results of immunohistochemistry confirmed that GPX3 and ECM1 are differentially expressed between HGBC tissues and normal bladder tissues, which is consistent with the results of TCGA BLCA dataset. **Figure 8C** showed the expression levels of the 5 genes in TCGA BLCA dataset.

Expression of GPX3, ECM1, CRYAB, CGNL1, and CRNN in Tianjin Validation Cohort

We recruited 30 BC patients and 30 controls from Tianjin Medical University General Hospital for further validation. Clinical characteristics of enrolled BC patients and controls in Tianjin validation cohort are displayed in **Table 6**. The chi-square test revealed that the patients and controls are matched for age ($P = 0.602$) and gender ($P = 0.438$). Among the 30 BC patients, 13 were LGBC patients and 17 were HGBC.

To investigate and confirm whether the five genes were detectable and altered in urine samples of BC patients compared with healthy controls, we performed qRT-PCR to detect the expression levels of GPX3, ECM1, CRYAB, CGNL1 and CRNN at mRNA level, respectively. As shown in **Figure 9A**, the relative expressions of GPX3, ECM1, CRYAB, and CGNL1 are significantly lower in urine of HGBC patients than in controls ($P < 0.05$), while no difference were revealed in CRNN expression ($P > 0.05$).

Figure 9B displayed the ROC curves performed to investigate the diagnostic value of the five genes for HGBC. The results suggested that expressions of GPX3 (AUC = 0.8794, $P = 0.0001$), ECM1 (AUC = 0.9794, $P < 0.0001$), CRYAB (AUC = 0.9216, $P < 0.0001$), and CGNL1 (AUC = 0.9765, $P < 0.0001$) have good predictive power for diagnosis of HGBC, indicating that they may be used as an urine biomarker for HGBC.

Figure 9C showed the ROC curves conducted to evaluate the predictive value of differential diagnosis between HGBC and LGBC. We identified that GPX3 (AUC = 0.7692, $P = 0.0128$), ECM1 (AUC = 0.7330, $P = 0.0312$), CRYAB (AUC = 0.9457, $P < 0.0001$), and CGNL1 (AUC = 0.8190, $P = 0.0032$) can be applied in differential diagnosis between HGBC and LGBC, while CRNN (AUC = 0.5136, $P = 0.9001$) can't.

The results of qRT-PCR confirmed that GPX3, ECM1, CRYAB and CGNL1 are lower in urine of HGBC patients than controls, which is consistent with the results of GSE68020 dataset. **Figure 9D** showed the expression levels of the 5 genes in GSE68020 dataset.

DISCUSSION

Accumulating evidence suggests that bioinformatics analysis would be an effective method to find novel molecular biomarkers in early diagnosis, therapeutic process monitoring and prognostic evaluation of cancer (18). Although previous investigations have identified various biomarkers for BC, most of biomarkers have not been applied in clinical practice for their inconsistent performance in terms of specificity and/or sensitivity (19). Besides, very few of the studies have focused on biomarkers for HGBC. In the present study, TCGA BLCA dataset, a large-scale prospective cohort research, and GSE68020 dataset from GEO were exploited in order to explore potential urine biomarkers for HGBC.

Our findings indicated that CRYAB, ECM1, CGNL1, and GPX3 are effective urine biomarkers for HGBC diagnosis, of which CRYAB, ECM1 and GPX3 are also urine biomarkers

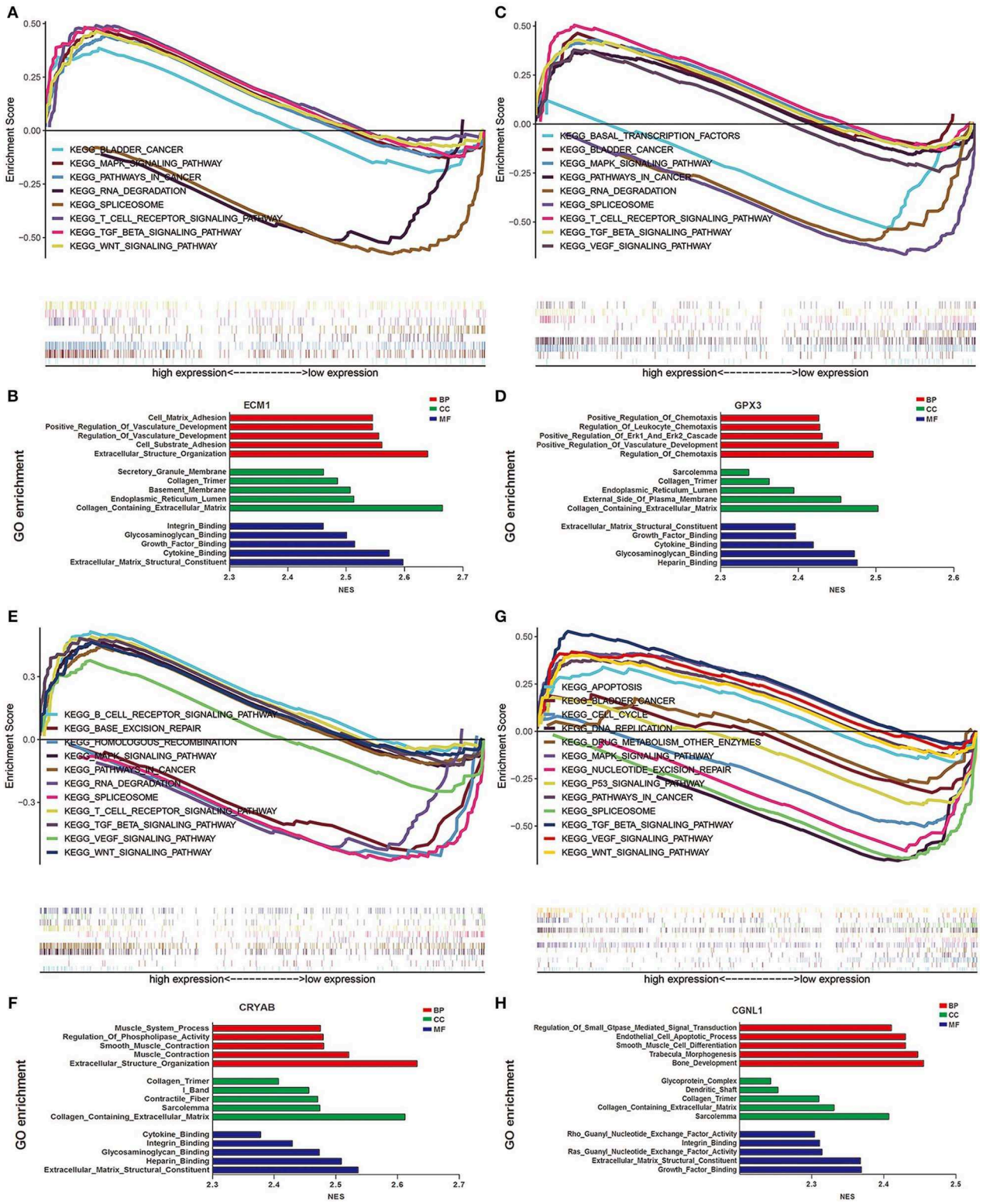

FIGURE 5 | Gene set enrichment analysis (GSEA) analysis of ECM1, GPX3, CRYAB, and CGNL1. **(A)** KEGG pathway enrichment for ECM1; **(B)** Gene Ontology (GO) enrichment for ECM1; **(C)** KEGG pathway enrichment for GPX3; **(D)** GO enrichment for GPX3; **(E)** KEGG pathway enrichment for CRYAB; **(F)** GO enrichment for CRYAB; **(G)** KEGG pathway enrichment for CGNL1; and **(H)** GO enrichment for CGNL1. BP, biological process; CC, cell component; MF, molecular function; NES, Normalized Enrichment Score.

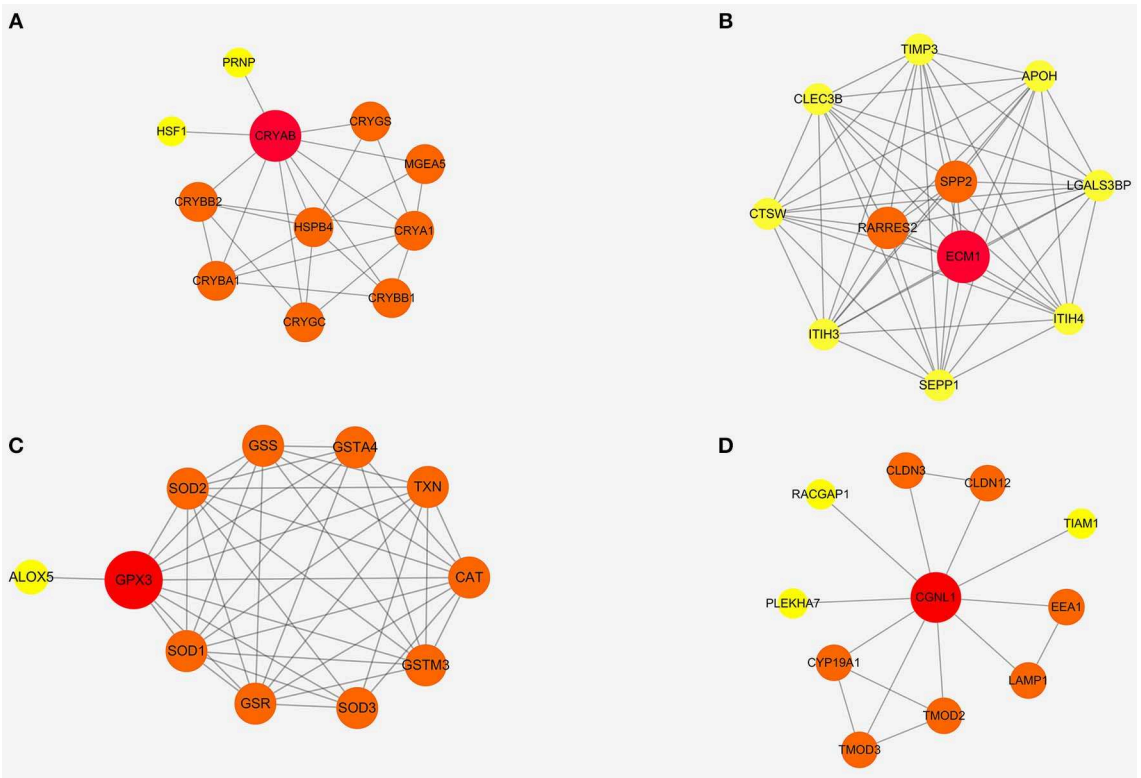

FIGURE 6 | Protein-protein interaction (PPI) networks of four modules based on ECM1, GPX3, CRYAB, and CGNL1. **(A)** CRYAB module PPI network; **(B)** ECM1 module PPI network; **(C)** GPX3 module PPI network; and **(D)** CGNL1 module PPI network.

for differential diagnosis between HGBC and LGBC. Besides, CRYAB, ECM1, and GPX3 are potential urine prognostic factors for HGBC; ECM1 and GPX3 might be considered as independent prognostic indicators for HGBC. According to clinicopathologic characteristics, we identified that CRYAB, ECM1, GPX3, and CGNL1 may predict histological grade, UICC stage and lymph node metastasis. In order to further validate these findings, we extracted immunohistochemistry of normal bladder tissues and HGBC tissues for these hub genes from THPA. In addition, we also performed qRT-PCR of these hub genes based on the urine samples from 30 BC patients and 30 controls in Tianjin validation cohort. The results confirmed the different expression levels of CRYAB, ECM1, CGNL1, and GPX3 between HGBC patients and controls, and their diagnostic values were also proved. The above findings could provide new diagnostic methods, prognostic predictor and treatment targets for HGBC, which could improve the prognosis of HGBC patients.

Till now, the role of CRYAB in BC has not been reported. It is the first time that our study found CRYAB plays a vital role in diagnosis, metastasis and prognosis of HGBC patients. Both OS and DFS are worse in cases with lower CRYAB expression. CRYAB could enhance tumorigenesis by regulating the VEGF and conferring anti-VEGF resistance in breast cancer (20, 21). In addition, CRYAB participates in anti-apoptosis through activating the Akt signaling pathway, enhancing PI3K activity and inhibiting calcium-activated Raf/MEK/ERK signaling pathway (22–24). As a consequence, we hypothesized that CRYAB promotes tumorigenesis and resist cell apoptosis of HGBC via these signaling pathways. Subsequent GSEA analysis identified that CRYAB is associated with B cell receptor, T cell receptor, VEGF, MAPK, Wnt, and TGF-β signaling pathways, which supports our hypothesis and previous studies.

Previous investigation identified that upregulated ECM1 is associated with BC growth, migration, apoptosis and postoperative recurrence, which was in agreement with our results (25). However, the biological function of ECM1 in different tumors remains controversial. Wang' s study indicated that ECM1 might enhance cell proliferation and invasiveness by regulating the expression of glucose transporter 1, lactate dehydrogenase and hypoxia-inducible factor 1α (25). There is also evidence that ECM1 potentiates the phosphorylation of epidermal growth factor receptor (EGFR) and extracellular signal-regulated kinase through physical interaction with EGFR and activation of EGFR signaling in breast cancer development (26). Besides, studies based on pancreatic ductal adenocarcinoma suggested that increased ECM1 expression abrogated the anti-tumor effect exerted by miR-23a-5p (27). The present study indicated that ECM1 is as an independent prognostic indicator for HGBC and high ECM1 expression can also predict lymph node metastasis. Both GSEA and functional enrichments of

TABLE 4 | GO functional and KEGG pathway enrichments of PPI networks based on the four gene modules.

CGNL1			GPX3			ECM1			CRYAB		
GOterm/ pathway	**Description**	**FDR**	**GOterm/ pathway**	**Description**	**FDR**	**GOterm/ pathway**	**Description**	**FDR**	**GOterm/ pathway**	**Description**	**FDR**
BP (GO)											
GO:0051694	Pointed-end actin filament capping	0.0067	GO:1990748	Cellular detoxification	3.60E-14	GO:0002576	Platelet degranulation	6.94E-22	GO:0007601	Visual perception	5.15E-07
GO:0031032	Actomyosin structure organization	0.0067	GO:0098869	Cellular oxidant detoxification	3.53E-12	GO:0010466	Negative regulation of peptidase activity	7.33E-06	GO:0051260	Protein homooligomerization	0.00011
GO:0030036	Actin cytoskeleton organization	0.0135	GO:0006749	Glutathione metabolic process	9.98E-09	GO:0030162	Regulation of proteolysis	4.12E-05	GO:0003008	System process	0.00013
GO:0016338	Calcium-independent cell-cell adhesion via plasma membrane cell-adhesion molecules	0.0135	GO:0006979	Response To Oxidative Stress	3.25E-08	GO:0010951	Negative regulation of endopeptidase activity	0.00021	GO:0050877	Nervous system process	0.00018
GO:0007015	Actin filament organization	0.0172	GO:0034599	Cellular response to oxidative stress	9.65E-08	GO:0051336	Regulation of hydrolase activity	0.00059	GO:0032387	Negative regulation of intracellular transport	0.00051
MF (GO)											
GO:0005523	Tropomyosin binding	0.0027	GO:0016209	Antioxidant activity	7.12E-13	GO:0004866	Endopeptidase inhibitor activity	8.89E-05	GO:0005212	Structural constituent of eye lens	1.02E-19
GO:0008092	Cytoskeletal protein binding	0.0426	GO:0016491	Oxidoreductase activity	2.24E-08	GO:0030234	Enzyme regulator activity	0.0011	GO:0051082	Unfolded protein binding	0.00069
GO:0005515	Protein binding	0.0426	GO:0004784	Superoxide dismutase activity	2.19E-07	GO:0004867	Serine-type endopeptidase inhibitor activity	0.0087	GO:0042802	Identical protein binding	0.0031
—	—	—	GO:0003824	Catalytic Activity	1.87E-05	GO:0002020	Protease binding	0.0137	GO:0001540	Amyloid-beta binding	0.0074
—	—	—	GO:0043295	Glutathione binding	0.00033	GO:0008201	Heparin binding	0.0173	—	—	—
CC (GO)											
GO:0043296	Apical junction complex	0.00015	GO:0031970	Organelle envelope lumen	0.0016	GO:0031089	Platelet dense granule lumen	6.28E-32	—	—	—
GO:0005911	Cell-cell junction	0.00015	GO:1904813	Ficolin-1-rich granule Lumen	0.0472	GO:0005576	Extracellular region	7.36E-10	—	—	—
GO:0005923	Bicellular tight junction	0.0023	GO:0044444	Cytoplasmic part	0.0472	GO:0044421	Extracellular region part	7.40E-06	—	—	—
GO:0044430	Cytoskeletal part	0.0024	GO:0044429	Mitochondrial part	0.0472	GO:0005615	Extracellular space	4.37E-05	—	—	—
GO:0019897	Extrinsic component of plasma membrane	0.0024	GO:0044421	Extracellular region part	0.0472	GO:0031012	Extracellular matrix	0.0012	—	—	—
KEGG											
hsa04530	Tight junction	0.0018	hsa00480	Glutathione metabolism	1.92E-09	—	—	—	hsa04141	Protein processing in endoplasmic reticulum	0.0216
hsa05152	Tuberculosis	0.0265	hsa04213	Longevity regulating pathway-multiple species	7.82E-05	—	—	—	—	—	—
hsa04145	Phagosome	0.0265	hsa04146	Peroxisome	0.00012	—	—	—	—	—	—
—	—	—	hsa05418	Fluid shear stress and atherosclerosis	0.00038	—	—	—	—	—	—
—	—	—	hsa05014	Amyotrophic lateral sclerosis	0.0022	—	—	—	—	—	—

Go, Gene Ontology; BP, biological process; CC, cell component; MF, molecular function; FDR, false discovery rate.

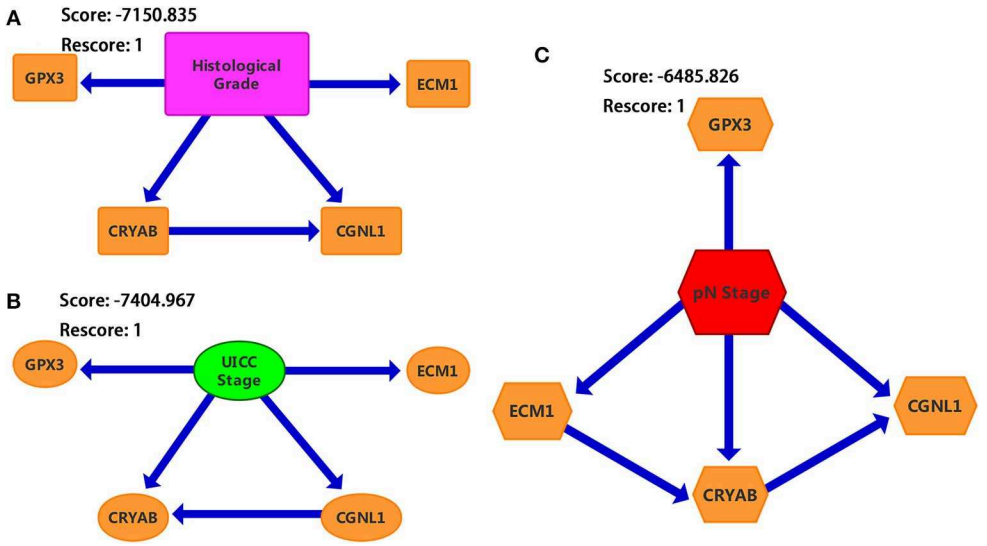

FIGURE 7 | Bayesian networks (BNs) based on ECM1, GPX3, CRYAB, and CGNL1 with bladder urothelial carcinoma (BC). **(A)** Histological grade; **(B)** UICC (Union for International Cancer Control) stage; and **(C)** pN (pathological N) stage.

ECM1 module showed that ECM1 expression is related to cell adhesion, extracellular matrix structural constituent and extracellular structure organization, which may be used to explain the metastasis of HGBC.

GPX3 is a member of a family of selenoproteins with vital antioxidant roles (28). It is reported that GPX3 is related to many malignancies including including head and neck, ovarian, and colon tumors (29, 30). Hypermethylation of the GPX3 promoter reduces GPX3 expression (31, 32). Furthermore, decreased GPX3 expression could inhibit clonogenicity and anchorage-independent cell survival in ovarian cancer progression (33). In addition, interactions between GPX3 and the p53-inducible gene 3 (PIG3) protein leads to activation of the apoptosis in prostate cancer cells (34). A retrospective study based on 40 BC patients reported that high GPX3 expression level in plasma might be predictive indicator for BC diagnosis and recurrence after transurethral resection (35). However, based on 405 BC samples, our results demonstrated that higher GPX3 expression level may predict an early UICC stage and better prognosis. Thus, the exact biological role of GPX3 and its potential mechanism for the progression and recurrence of BC are still unclear. Although our study contained a sufficient capacity, studies based on cells and a larger sample size are required to explore the relationship between GPX3 and BC. Functional enrichments showed that GPX3 plays a role in cellular detoxification and glutathione binding and metabolism. GSEA revealed that upregulated expression of GPX3 may act on extracellular matrix structure and positive regulation of vasculature development. We assumed that GPX3 is involved in the progression and recurrence of HGBC by participating in toxic metabolic process.

CGNL1, an endothelial junction complex protein, promotes GTPase mediated angiogenesis by strengthening adherens junctions via Rac1 activation, which further makes new blood vessels stable and extendable (36). What's more, CGNL1 is also involved in cell-cell junction assembly through regulating the activity of GTPases and Rac (37). Previous studies demonstrated that CGNL1 gene expression is associated with endometrial cancer survival (38). Our results showed that CGNL1 is a diagnostic factor for HGBC and can predict lymph node metastasis. GSEA and functional enrichments showed that CGNL1 may participate in HGBC progression by regulating cell-cell junction, tight junction, cytoskeletal protein binding, tropomyosin binding and growth factor binding, which confirms the findings of previous studies. However, further *in vitro* and *in vivo* studies are warranted to validate these mechanisms in BC.

Based on the networks of Bayesian analysis, we observed that the interaction of CRYAB and CGNL1 plays a key role in histological grade, UICC stage and pN stage of BC. Hence, we put CRYAB and CGNL1 into String online server to find the underlying mechanism of interaction. Functional enrichments showed that the two genes may have a combined effect on actin cytoskeleton (GO: 0015629, $P = 0.039$). In addition, GSEA of KEGG pathway analysis revealed that both genes are enriched in VEGF, MAPK, Wnt, and TGF-β signaling pathways.

Lymph node metastasis is a key indicator to predict poor prognosis of BC (39). In the present study, multivariate Cox regression showed that lymph node metastasis is an independent poor prognostic indicator of OS, which is consistent with previous research.

In the meantime, several limitations remained in our research. Firstly, although immunohistochemistry based on THPA and qRT-PCR based on urine samples confirmed the downregulation of CRYAB, ECM1, CGNL1, and GPX3 in HGBC and their diagnostic values, the exact molecular mechanisms of the these hub genes have not been investigated in the present

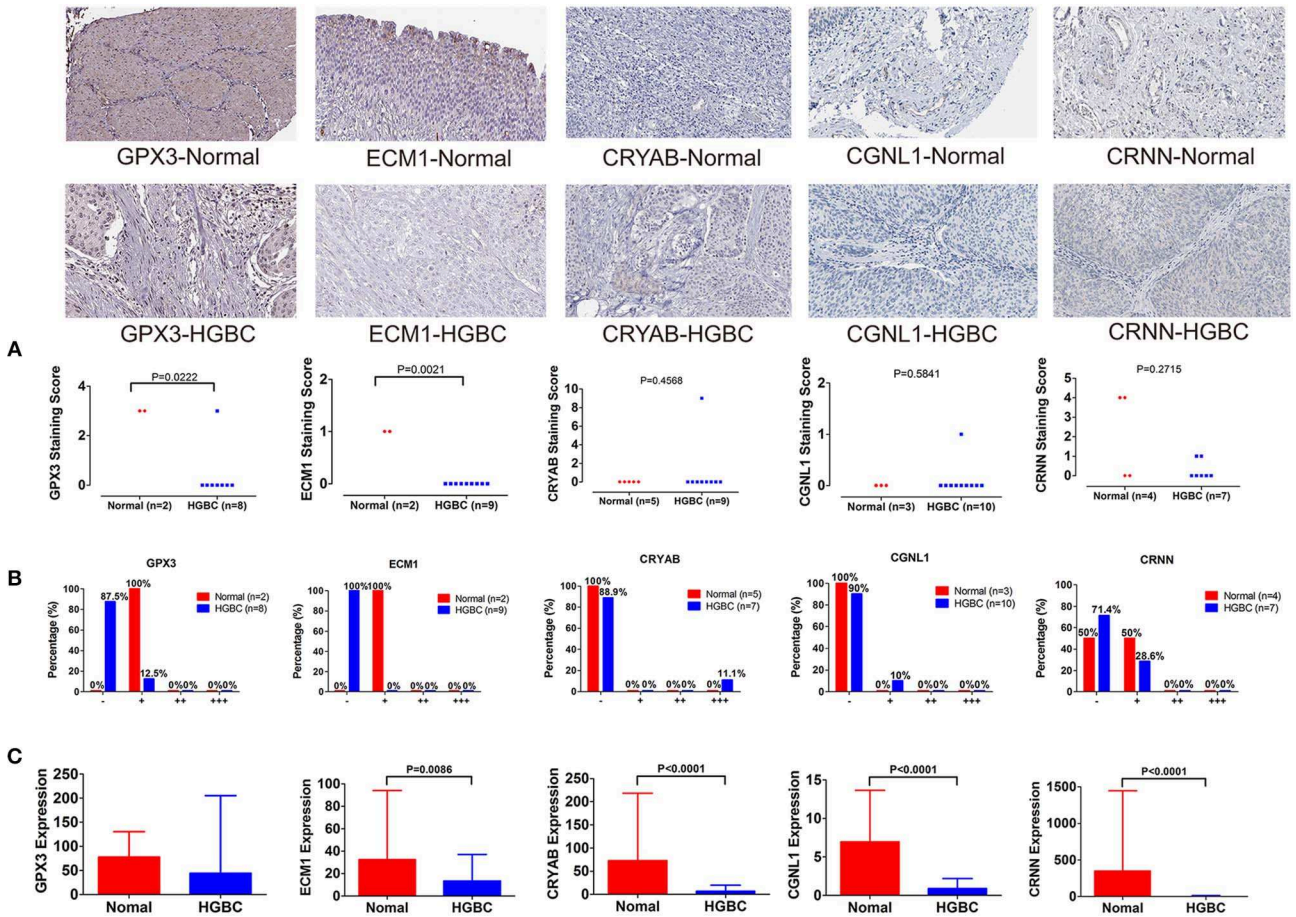

FIGURE 8 | Immunohistochemistry from The Human Protein Atlas (THPA) confirmed the downregulation of GPX3 and ECM1 in high-grade bladder urothelial carcinoma (HGBC) tissues by Mann-Whitney U test ($P < 0.05$). **(A)** Mann-Whitney *U* test compared the staining scores of immunohistochemistry between normal bladder tissues and HGBC tissues; **(B)** Distributions of the four expression levels [negative (–), weakly positive (+), positive (++) and strongly positive (+ + +)] of immunohistochemistry; and **(C)** Expressions of the 5 genes in TCGA BLCA dataset.

TABLE 5 | Comparison of immunohistochemistry expression level between normal bladder and HGBC by Fisher's Exact test from The Human Protein Atlas.

Gene name		*N*	Immunohistochemistry expression level				*P*-value
			Negative (–)	Weakly positive (+)	Positive (++)	Strongly positive (+ + +)	
GPX3	Normal bladder tissue	2	0	2	0	0	**0.016**
	HGBC tissue	8	7	1	0	0	
ECM1	Normal bladder tissue	2	0	2	0	0	**0.001**
	HGBC tissue	9	9	0	0	0	
CRYAB	Normal bladder tissue	5	5	0	0	0	0.439
	HGBC tissue	9	8	0	0	1	
CGNL1	Normal bladder tissue	3	3	0	0	0	0.569
	HGBC tissue	10	9	1	0	0	
CRNN	Normal bladder tissue	4	2	2	0	0	0.477
	HGBC tissue	7	5	2	0	0	

Immunohistochemistry expression level: the expression of immunohistochemistry was divided into four levels: negative (–), weakly positive (+), positive (++) and strongly positive (+++); HGBC, high-grade bladder urothelial carcinoma. Bold values meant P-value < 0.05.

study, and their prognostic values have not been proved by external validation. Secondly, immunohistochemistry was extracted from THPA. Even if we used Mann-Whitney U test and Fisher's Exact test to confirm the statistical significance, the number and information from THPA are still limited. Therefore, further studies based on a larger sample size and

other racial types or regions are still required to verify these hypotheses and to make these results more convincible in the future.

TABLE 6 | Characteristics of enrolled participants from Tianjin validation cohort.

	BC patients ($n = 30$)	Controls ($n = 30$)	chi-square	*P-value*
Age (years)				
≤60	14 (46.67%)	12 (40.00%)	0.271	0.602
>60	16 (53.33%)	18 (60.00%)		
Gender				
Male	13 (43.33%)	16 (53.33%)	0.601	0.438
Female	17 (56.67%)	14 (46.67%)		
UICC stage				
Stage I	7 (23.33%)			
Stage II	8 (26.67%)			
Stage III	9 (30.00%)			
Stage IV	6 (20.00%)			
Histological grade				
Low grade	13 (43.33%)			
High grade	17 (56.67%)			

CONCLUSIONS

In general, our findings indicated that CRYAB, CGNL1, ECM1, and GPX3 are potential urine biomarkers of HGBC. All the four genes have the capability to be diagnostic indicators for HGBC. Furthermore, CRYAB, ECM1, and GPX3 are potential urine prognostic factors for HGBC, among which ECM1 and GPX3 might be considered as independent prognostic indicators for HGBC and new treatment targets as well. The four genes can also predict histological grade, UICC stage and lymph node metastasis. Immunohistochemistry and qRT-PCR were used to confirm the downregulation of the hub genes and their diagnostic values in HGBC. Among the four hub genes, CRYAB and CGNL1 have not been reported the relationship with HGBC before and the results of Bayesian analysis suggested that the interaction of CRYAB and CGNL1 plays a key role in HGBC. In addition, we used bioinformatics methods to explore the underlying mechanisms. These four novel urine biomarkers will have attractive applications to provide new diagnostic methods, prognostic predictors and treatment targets for HGBC, which could improve the prognosis of HGBC patients, if validated by further experiments and larger prospective clinical trials.

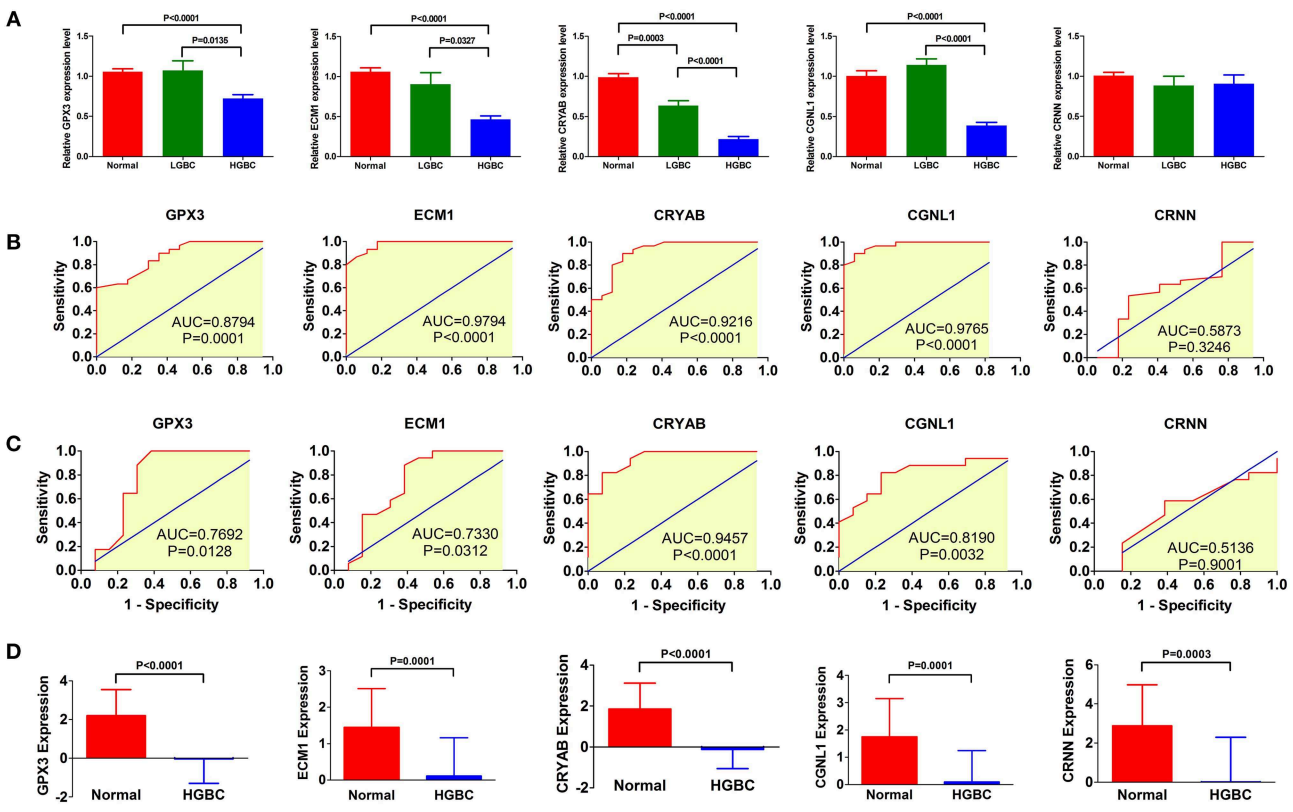

FIGURE 9 | qRT-PCR of urine samples from Tianjin validation cohort. Relative expressions of GPX3, ECM1, CRYAB, and CGNL1 are significantly lower in urine of high-grade bladder urothelial carcinoma (HGBC) patients than in controls ($P < 0.05$). **(A)** qRT-PCR of urines samples from controls, low-grade bladder urothelial carcinoma (LGBC) and HGBC; **(B)** Receiver operating characteristic (ROC) curves of diagnostic value for HGBC based on qRT-PCR; **(C)** ROC curves for differential diagnosis between HGBC and LGBC based on qRT-PCR; and **(D)** Expressions of the 5 genes in GSE68020 dataset. AUC, area under the curve.

DATA AVAILABILITY STATEMENT

Publicly available datasets were analyzed in this study. The data can be found in Gene Expression Omnibus (GEO: http://www.ncbi.nlm.nih.gov/geo/), The Cancer Genome Atlas (TCGA: http://tcga-data.nci.nih.gov/tcga/), and The Human Protein Atlas (THPA: http://www.proteinatlas.org/). GSE68020 dataset was from GEO; BLCA (Bladder Urothelial Carcinoma) dataset was from TCGA; and immunohistochemistry was from THPA. All the data are open access. Summarized detailed characteristics of immunohistochemistry data from THPA are in **Supplementary Table 1**.

ETHICS STATEMENT

The studies involving human participants were reviewed and approved by the Ethics Committee of Tianjin Medical University General Hospital. The patients/participants provided their written informed consent to participate in this study.

AUTHOR CONTRIBUTIONS

YS, JC, and DJ: research design. NO, YS, ZL, GC, and JC: data extraction and meta-analysis. YS, YY, and XL: drafting of the manuscript and modification.

FUNDING

This work was supported by Zhao Yi-Cheng Medical Science Foundation (ZYYFY2018031).

SUPPLEMENTARY MATERIAL

The Supplementary Material for this article can be found online at: https://www.frontiersin.org/articles/10.3389/fonc.2020.00394/full#supplementary-material

REFERENCES

1. Antoni S, Ferlay J, Soerjomataram I, Znaor A, Jemal A, Bray F. Bladder cancer incidence and mortality: a global overview and recent trends. *Eur Urol.* (2017) 71:96–108. doi: 10.1016/j.eururo.2016.06.010
2. Bray F, Ferlay J, Soerjomataram I, Siegel RL, Torre LA, Jemal A. Global cancer statistics 2018: GLOBOCAN estimates of incidence and mortality worldwide for 36 cancers in 185 countries. *CA Cancer J Clin.* (2018) 68:394–424. doi: 10.3322/caac.21492
3. Ebrahimi H, Amini E, Pishgar F, Moghaddam SS, Nabavizadeh B, Rostamabadi Y, et al. Global, regional and national burden of bladder cancer, 1990 to 2016: results from the GBD study 2016. *J Urol.* (2019) 201:893–901. doi: 10.1097/JU.0000000000000025
4. Yang Y, Cheng Z, Jia X, Shi N, Xia Z, Zhang W, et al. Mortality trends of bladder cancer in China from 1991 to 2015: an age-period-cohort analysis. *Cancer Manag Res Vol.* (2019) 11:3043–51. doi: 10.2147/CMAR.S189220
5. Humphrey PA, Moch H, Cubilla AL, Ulbright TM, Reuter VE. The 2016 WHO classification of tumours of the urinary system and male genital organs—part B: prostate and bladder tumours. *Eur Urol.* (2016) 70:106–19. doi: 10.1016/j.eururo.2016.02.028
6. Kirkali Z, Chan T, Manoharan M, Algaba F, Busch C, Cheng L, et al. Bladder cancer: epidemiology, staging and grading, and diagnosis. *Urology.* (2005) 66:4–34. doi: 10.1016/j.urology.2005.07.062
7. Goebell PJ, Legal W, Weiss C, Fietkau R, Wullich B, Krause S. Multimodale therapien zum blasenerhalt bei high-grade-blasentumoren. *Der Urologe.* (2008) 47:838–45. doi: 10.1007/s00120-008-1715-4
8. Babjuk M, Burger M, Zigeuner R, Shariat SF, van Rhijn BWG, Compérat E, et al. EAU guidelines on non–muscle-invasive urothelial carcinoma of the bladder: update 2013. *Eur Urol.* (2013) 64:639–53. doi: 10.1016/j.eururo.2013.06.003
9. Konety BR. Molecular markers in bladder cancer: a critical appraisal. *Urol Oncol.* (2006) 24:326–37. doi: 10.1016/j.urolonc.2005.11.023
10. Tilki D, Burger M, Dalbagni G, Grossman HB, Hakenberg OW, Palou J, et al. Urine markers for detection and surveillance of non–muscle-invasive bladder cancer. *Eur Urol.* (2011) 60:484–92. doi: 10.1016/j.eururo.2011.05.053
11. Tan WS, Tan WP, Tan M, Khetrapal P, Dong L, DeWinter P, et al. Novel urinary biomarkers for the detection of bladder cancer: a systematic review. *Cancer Treat Rev.* (2018) 69:39–52. doi: 10.1016/j.ctrv.2018.05.012
12. Ritchie ME, Phipson B, Wu D, Hu Y, Law CW, Shi W, et al. limma powers differential expression analyses for RNA-sequencing and microarray studies. *Nucleic Acids Res.* (2015) 43:e47. doi: 10.1093/nar/gkv007
13. Tang Z, Li C, Zhang K, Yang M, Hu X. GE-mini: a mobile APP for large-scale gene expression visualization. *Bioinformatics.* (2017) 33:941–3. doi: 10.1093/bioinformatics/btw775
14. Subramanian A, Kuehn H, Gould J, Tamayo P, Mesirov JP. GSEA-P: a desktop application for gene set enrichment analysis. *Bioinformatics.* (2007) 23:3251–3. doi: 10.1093/bioinformatics/btm369
15. Szklarczyk D, Morris JH, Cook H, Kuhn M, Wyder S, Simonovic M, et al. The STRING database in 2017: quality-controlled protein–protein association networks, made broadly accessible. *Nucleic Acids Res.* (2017) 45:D362–8. doi: 10.1093/nar/gkw937
16. Neil M, Fenton N, Tailor M. Using bayesian networks to model expected and unexpected operational losses. *Risk Analysis.* (2005) 25:963–72. doi: 10.1111/j.1539-6924.2005.00641.x
17. Uhlen M, Oksvold P, Fagerberg L, Lundberg E, Jonasson K, Forsberg M, et al. Towards a knowledge-based human protein atlas. *Nat Biotechnol.* (2010) 28:1248–50. doi: 10.1038/nbt1210-1248
18. Milan T, Wilhelm BT. Mining cancer transcriptomes: bioinformatic tools and the remaining challenges. *Mol Diagn Ther.* (2017) 21:249–58. doi: 10.1007/s40291-017-0264-1
19. Olkhov-Mitsel E, Savio AJ, Kron KJ, Pethe VV, Hermanns T, Fleshner NE, et al. Epigenome-wide DNA methylation profiling identifies differential methylation biomarkers in high-grade bladder cancer. *Transl Oncol.* (2017) 10:168–77. doi: 10.1016/j.tranon.2017.01.001
20. Ruan Q, Han S, Jiang WG, Boulton ME, Chen ZJ, Law BK, et al. B-crystallin, an effector of unfolded protein response, confers anti-VEGF resistance to breast cancer via maintenance of intracrine VEGF in endothelial cells. *Mol Cancer Res.* (2011) 9:1632–43. doi: 10.1158/1541-7786.MCR-11-0327
21. Chen W, Lu Q, Lu L, Guan H. Increased levels of alphaB-crystallin in vitreous fluid of patients with proliferative diabetic retinopathy and correlation with vascular endothelial growth factor. *Clin Exp Ophthalmol.* (2017) 45:379–84. doi: 10.1111/ceo.12891
22. Pasupuleti N, Matsuyama S, Voss O, Doseff AI, Song K, Danielpour D, et al. The anti-apoptotic function of human αA-crystallin is directly related to its chaperone activity. *Cell Death Dis.* (2010) 1:e31. doi: 10.1038/cddis.2010.3
23. Liu ES, Raimann A, Chae BT, Martins JS, Baccarini M, Demay MB. c-Raf promotes angiogenesis during normal growth plate maturation. *Development.* (2016) 143:348–55. doi: 10.1242/dev.127142
24. Zhang J, Liu J, Wu J, Li W, Chen Z, Yang L. Progression of the role of CRYAB in signaling pathways and cancers. *OncoTargets Therapy Vol.* (2019) 12:4129–39. doi: 10.2147/OTT.S201799
25. Wang Z, Zhou Q, Li A, Huang W, Cai Z, Chen W. Extracellular matrix protein 1 (ECM1) is associated with carcinogenesis potential of

human bladder cancer. *Onco Targets Ther Volume.* (2019) 12:1423–32. doi: 10.2147/OTT.S191321
26. Lee K, Nam K, Oh S, Lim J, Kim Y, Lee JW, et al. Extracellular matrix protein 1 regulates cell proliferation and trastuzumab resistance through activation of epidermal growth factor signaling. *Breast Cancer Res.* (2014) 16:479. doi: 10.1186/s13058-014-0479-6
27. Huang W, Huang Y, Gu J, Zhang J, Yang J, Liu S, et al. miR-23a-5p inhibits cell proliferation and invasion in pancreatic ductal adenocarcinoma by suppressing ECM1 expression. *Am J Transl Res.* (2019) 11:2983–94.
28. Brigelius-Flohé R. Tissue-specific functions of individual glutathione peroxidases. *Free Radic Biol Med.* (1999) 27:951–65. doi: 10.1016/S0891-5849(99)00173-2
29. Saga Y, Ohwada M, Suzuki M, Konno R, Kigawa J, Ueno S, et al. Glutathione peroxidase 3 is a candidate mechanism of anticancer drug resistance of ovarian clear cell adenocarcinoma. *Oncol Rep.* (2008) 20:1299–303.
30. Chen B, Rao X, House MG, Nephew KP, Cullen KJ, Guo Z. GPx3 promoter hypermethylation is a frequent event in human cancer and is associated with tumorigenesis and chemotherapy response. *Cancer Lett.* (2011) 309:37–45. doi: 10.1016/j.canlet.2011.05.013
31. Zmorzynski S, Swiderska-Kołacz G, Koczkodaj D, Filip AA. Significance of polymorphisms and expression of enzyme-encoding genes related to glutathione in hematopoietic cancers and solid tumors. *Biomed Res Int.* (2015) 2015:1–6. doi: 10.1155/2015/853573
32. Pelosof L, Yerram S, Armstrong T, Chu N, Danilova L, Yanagisawa B, et al. GPX3 promoter methylation predicts platinum sensitivity in colorectal cancer. *Epigenetics.* (2017) 12:540–50. doi: 10.1080/15592294.2016.1265711
33. Worley BL, Kim YS, Mardini J, Zaman R, Leon KE, Vallur PG, et al. GPx3 supports ovarian cancer progression by manipulating the extracellular redox environment. *Redox Biol.* (2018) 128:D76. doi: 10.1016/j.freeradbiomed.2018.10.166
34. Wang H, Luo K, Tan L, Ren B, Gu L, Michalopoulos G, et al. p53-induced gene 3 mediates cell death induced by glutathione peroxidase 3. *J Biol Chem.* (2012) 287:16890–902. doi: 10.1074/jbc.M111.322636
35. Wieczorek E, Jablonowski Z, Tomasik B, Gromadzinska J, Jablonska E, Konecki T, et al. Different gene expression and activity pattern of antioxidant enzymes in bladder cancer. *Anticancer Res.* (2017) 37:841–8. doi: 10.21873/anticanres.11387
36. Chrifi I, Hermkens D, Brandt MM, van Dijk CGM, Bürgisser PE, Haasdijk R, et al. Cgnl1, an endothelial junction complex protein, regulates GTPase mediated angiogenesis. *Cardiovasc Res.* (2017) 113:1776–88. doi: 10.1093/cvr/cvx175
37. Ijssennagger N, Janssen AWF, Milona A, Ramos Pittol JM, Hollman DAA, Mokry M, et al. Gene expression profiling in human precision cut liver slices in response to the FXR agonist obeticholic acid. *J Hepatol.* (2016) 64:1158–66. doi: 10.1016/j.jhep.2016.01.016
38. Li W, Wang S, Qiu C, Liu Z, Zhou Q, Kong D, et al. Comprehensive bioinformatics analysis of acquired progesterone resistance in endometrial cancer cell line. *J Transl Med.* (2019) 17:58. doi: 10.1186/s12967-019-1814-6
39. Sharma M, Goto T, Yang Z, Miyamoto H. The impact of perivesical lymph node metastasis on clinical outcomes of bladder cancer patients undergoing radical cystectomy. *BMC Urol.* (2019) 19:77. doi: 10.1186/s12894-019-0507-z

Conflict of Interest: The authors declare that the research was conducted in the absence of any commercial or financial relationships that could be construed as a potential conflict of interest.

frontiers in Oncology

ORIGINAL RESEARCH
published: 27 March 2020
doi: 10.3389/fonc.2020.00283

Ephrin-B1 Is a Novel Biomarker of Bladder Cancer Aggressiveness. Studies in Murine Models and in Human Samples

*María Victoria Mencucci[1†], Lara Lapyckyj[1†], Marina Rosso[1], María José Besso[1], Denise Belgorosky[2], Mariana Isola[3], Silvia Vanzulli[4], Catalina Lodillinsky[2], Ana María Eiján[2], Juan Carlos Tejerizo[5], Matías Ignacio Gonzalez[5], María Ercilia Zubieta[5] and Mónica Hebe Vazquez-Levin[1]**

[1] Laboratorio de Estudios de la Interacción Celular en Reproducción y Cáncer, Instituto de Biología y Medicina Experimental (IBYME; CONICET-FIBYME), Buenos Aires, Argentina, [2] Research Area, Instituto de Oncología Angel H. Roffo, Universidad de Buenos Aires, Buenos Aires, Argentina, [3] Departamento de Anatomía Patológica, Hospital Italiano de Buenos Aires, Buenos Aires, Argentina, [4] Academia Nacional de Medicina, Buenos Aires, Argentina, [5] Departamento de Urología, Hospital Italiano de Buenos Aires, Buenos Aires, Argentina

OPEN ACCESS

Edited by:
Woonyoung Choi,
Johns Hopkins Medicine,
United States

Reviewed by:
Kouji Izumi,
Kanazawa University, Japan
Hiroaki Matsumoto,
Yamaguchi University, Japan

***Correspondence:**
Mónica Hebe Vazquez-Levin
mhvazquez@ibyme.conicet.gov.ar;
mhvazl@gmail.com

[†]These authors have contributed equally to this work

Specialty section:
This article was submitted to Genitourinary Oncology, a section of the journal Frontiers in Oncology

Received: 12 November 2019
Accepted: 18 February 2020
Published: 27 March 2020

Citation:
Mencucci MV, Lapyckyj L, Rosso M, Besso MJ, Belgorosky D, Isola M, Vanzulli S, Lodillinsky C, Eiján AM, Tejerizo JC, Gonzalez MI, Zubieta ME and Vazquez-Levin MH (2020) Ephrin-B1 Is a Novel Biomarker of Bladder Cancer Aggressiveness. Studies in Murine Models and in Human Samples. Front. Oncol. 10:283. doi: 10.3389/fonc.2020.00283

Bladder cancer (BC) is the ninth most common cancer worldwide, but molecular changes are still under study. During tumor progression, Epithelial cadherin (E-cadherin) expression is altered and β-catenin may be translocated to the nucleus, where it acts as co-transcription factor of tumor invasion associated genes. This investigation further characterizes E-cadherin and β-catenin associated changes in BC, by combining bioinformatics, an experimental murine cell model (MB49/MB49-I) and human BC samples. In *in silico* studies, a DisGeNET (gene-disease associations database) analysis identified *CDH1* (E-cadherin gene) as one with highest score among 130 BC related-genes. COSMIC mutation analysis revealed *CDH1* low mutations rates. Compared to MB49 control BC cells, MB49-I invasive cells showed decreased E-cadherin expression, E- to P-cadherin switch, higher β-catenin nuclear signal and lower cytoplasmic p-Ser33-β-catenin signal, higher Ephrin-B1 ligand and EphB2 receptor expression, higher Phospho-Stat3 and Urokinase-type Plasminogen Activator (UPA), and UPA receptor expression. MB49-I cells transfected with Ephrin-B1 siRNA showed lower migratory and invasive capacity than control cells (scramble siRNA). By immunohistochemistry, orthotopic MB49-I tumors had lower E-cadherin, increased nuclear β-catenin, lower pSer33-β-catenin cytoplasmic signal, and higher Ephrin-B1 expression than MB49 tumors. Similar changes were found in human BC tumors, and 83% of infiltrating tumors depicted a high Ephrin-B1 stain. An association between higher Ephrin-B1 expression and higher stage and tumor grade was found. No association was found between abnormal E-cadherin signal, Ephrin-B1 expression or clinical-pathological parameter. This study thoroughly analyzed E-cadherin and associated changes in BC, and reports Ephrin-B1 as a new marker of tumor aggressiveness.

Keywords: bladder cancer, epithelial cadherin, beta-catenin, Ephrin-B1, biomarker

INTRODUCTION

Bladder cancer (BC) is one of the ten solid tumors with highest incidence and mortality worldwide, with 549,393 new cases and 199,922 deaths reported in 2018, and with an increase of 50% expected for 2040 (International Agency for Research on Cancer; WHO[1]). Clinically, it is classified as non-muscle-invasive (NMIBC) and muscle-invasive (MIBC) or infiltrating BC, being the latter highly aggressive. Urothelial tumors represent >90% of the cases; while 75% are limited to the mucosa or submucosa at the time of diagnosis, 10–30% NMIBC patients progress to MIBC and 50–70% have tumor recurrence (1). Thus, muscle invasion is a key event in BC, being important to identify MIBC biomarkers for accurate treatment and understanding the underlying mechanisms to prevent tumor progression and aggressiveness.

Among molecular changes associated to BC, a decreased expression of epithelial cadherin (E-cadherin) has long been reported (2). In a systematic review and meta-analysis, reduced E-cadherin was associated with poor BC prognosis (3); however, the underlying mechanisms have not been fully characterized. E-cadherin is the founder member of the cadherin superfamily (4). It is a 120 kDa transmembrane glycoprotein encoded by the *CDH1* gene; its extracellular domain mediates cell-cell adhesion, while the cytoplasmic domain binds to β-catenin that links E-cadherin to the actin cytoskeleton, and is involved in signal transduction (5). E-cadherin decrease/loss expression is a hallmark of Epithelial-to-Mesenchymal Transition (EMT) that promotes cell motility/invasive behavior, cancer progression and metastasis (6, 7). Alterations in E-cadherin expression during EMT are accompanied by increased expression of transcriptional represors, β-catenin loss at the cell membrane, and filamentous actin (F-actin) belt replacement by a network of stress fibers. Also, it is tipically characterized by an increased expression of neural (N-cadherin) and, in some cases, by placental (P-cadherin) cadherin, a phenomenon called cadherin switch. Some evidence of EMT-related events has been reported in BC (8–10).

This report further characterizes alterations in E-cadherin expression and EMT-related events in BC with the aim to identify novel markers of BC progression. Studies were addressed in the MB49 and MB49-I murine model of tumor progression (11, 12), and in BC patient tissue samples.

MATERIALS

Chemicals were of analytical and tissue culture grade and purchased from BioRad (Richmond, CA, USA), ThermoFisher Scientific (Carlsbad, CA, USA), and Sigma Chemical Co. (St. Louis, MO, USA), unless specifically indicated. Primary antibodies used were: Anti-E-cadherin: (1) 610181 (BD Biosciences, San Diego, CA, USA), (2) HECD-1 (Thermo); Anti-β-catenin (610153; BD); Anti-phospho-Ser33-β-catenin (pSer33-β-catenin; Ser33-R; SCB); Anti-N-cadherin (H-63, SCB); Anti-P-cadherin (H-105, SCB); Anti-Ephrin-B1 (A-20, SCB); Anti-EphB2 (H-80, SCB); Anti-Signal transducer and activator of transcription 3 (STAT3) (B-7, SCB); Anti-phospho-STAT3 (pSTAT3) (C-20, SCB); Anti-Proliferating cell nuclear antigen (PCNA) (PC10, SCB), Anti-actin (I-19, SCB); Anti-β-tubulin (D-66, Sigma). Secondary antibodies used were Cy3-labeled anti-mouse or anti-rabbit (Sigma) and FITC-labeled anti-mouse (Vector Lab. Inc., Burlingame, CA, USA) IgGs for fluorescence immunocytochemistry, Anti-mouse (Vector) or Anti-rabbit (Sigma) IgGs coupled to horseradish peroxidase for Western immunoblotting. In control experiments, primary antibodies were replaced by purified mouse or rabbit IgGs, as required.

Murine Cell Lines and Tumors

Established MB49 and MB49-I mouse cell lines were used as experimental models. The MB49 cell line was generated from an *in vitro* neoplastic transformation of mouse bladder epithelium primary cultures (13). The MB49-I cell line was originated after *in vivo* successive passages of a primary tumor obtained by subcutaneous inoculation of MB49 cells in C57Bl/6J males (11).

Murine bladder tumors were generated by orthotopic inoculation of MB49 and MB49-I cells into C57BL/6 mice bladder (11). Mice were handled in accordance with the international procedure for Care and Use of Laboratory Animals; a protocol was approved by the Institute of Oncology Angel H. Roffo Review Board (#2012/02).

Human Tumor Samples

Human BC tissue samples were obtained from patients diagnosed with urothelial BC at Hospital Italiano of Buenos Aires, between 2012 and 2016. The project was approved by Ethics Committees of Hospital Italiano and IBYME (Protocol #C004-1/2012); patients signed a written informed consent. Ten fresh biopsies (non-tumor and tumor sections, 1 cm^3 each) from patients diagnosed with infiltrating BC were collected from the surgical piece, placed in RNA Later® and subjected to RNA extraction and subsequent quantitative real-time PCR analysis. In addition, 38 paraffin-embedded tissue samples from patients diagnosed with BC and subjected to transurethral resection or radical cystectomy, were included in the study and analyzed by immunohistochemistry; **Supplementary Table 1** summarizes available information on patient gender, age, tumor stage and grade, as well as evidence of metastasis.

PCR Primers

Primers were designed for endpoint (analytical) and quantitative real time PCR protocols using Primer-BLAST tool (http://www.ncbi.nlm.nih.gov/tools/primer-blast); sequences and expected PCR fragment sizes are listed in **Supplementary Table 2**. Some primers were previously reported (14, 15).

[1]International Agency for Research on Cancer; World Health Organization. http://globocan.iarc.fr.

METHODS

Bioinformatics

To perform text mining on BC gene-disease associations, the DisGeNET discovery platform (http://www.disgenet.org/) was used. DisGeNET integrates information on human diseases and their genes from expert-curated databases and scientific literature found by means of text-mining approaches (16). Gene-disease associations are ranked according to DisGeNET score, and annotated with DisGeNET gene-disease association type ontology. A set of search terms related to BC was selected to browse all DisGeNET databases and to search for *CDH1* among the output list. The DisGeNET version containing 628,685 associations between 17,549 genes and 24,166 diseases was used in the present study (March, 2019).

Listed somatic mutations in the *CDH1* (E-cadherin) and *CTNNB1* (β-catenin) genes in BC were retrieved from the COSMIC (http://cancer.sanger.ac.uk/cosmic) catalog of public domain data tool. COSMIC provides information about mutations affecting tumor-associated genes, and establishes a hierarchy of the 20 most commonly mutated genes in a specific tumor, as well as number of cases in which a mutation was reported. For each mutation, information is available on position and type of change, as well as amino acid(s) involved; in case of substitutions, it provides information on the specific change that occurs with the mutation. The COSMIC v88 used in this study includes over 6 million coding mutations across than >1.4 million tumor samples curated from >26,000 publications (17). Information was filtered to obtain data from samples of patients diagnosed with transitional cell carcinoma of the bladder, which were 5,774 of the total 8,359 BC samples (March, 2019).

MB49 and MB49-I Cell Culture and Orthotopic Tumors

MB49 and MB49-I cell lines were cultured as previously reported (11). At 70–80% confluence, cells were harvested and processed for RNA and protein (Western immunoblotting/immunocytochemistry) analyses.

MB49 and MB49-I orthotopic tumors were generated as previously described (11). Basically, orthotopic cell injection in C57BL/6 female mice was performed by placing a catheter into the urethra. Previously, focal electrocautery was performed to induce punctual damage to the bladder wall. MB49 and MB49-I suspensions from subconfluent cell culture monolayers were instilled in 100 µl RPMI 1640 medium. Mice were monitored twice weekly for hematuria and by bladder palpation. Two weeks after tumor cell inoculation, the animals were sacrificed and tumors included in paraffin for subsequent immunohistochemical analysis.

Transient Transfection Assays

MB49-I cells transient transfection was performed using Lipofectamine® 2000 (Thermo) and 100 pmol/ml of a specific small interfering Ephrin-B1 RNA (siRNA) (#39437, SCB; pool of 3 target-specific 19–25 nt siRNAs designed to knock down gene expression) following a standard procedure (18). Control assays with scramble siRNA (#37007, SCB) were included.

RNA Extraction, cDNA Synthesis, Standard, and Quantitative Real Time PCR

Cell and tissue total RNA was isolated and processed for complementary DNA (cDNA) synthesis (14, 15, 18). PCR samples were prepared with SYBR Green® PCR Master Mix (Thermo) mixture and run in CFX96 Touch™ (BioRad) PCR unit. Triplicate samples and negative controls (no template) were always included. Dissociation curves were run to confirm signal specificity. GAPDH was selected as endogenous control and MB49 cells as reference. The calculation describing these relations is $2^{-\Delta\Delta Ct}$, where $\Delta\Delta Ct$ = [ΔCt test sample – ΔCt reference sample], and ΔCt = [Ct gene under study – Ct endogenous gene]. Alternatively, calculations were done using $2^{-\Delta Ct}$ method, where ΔCt = [Ct gene under study – Ct endogenous gene]. Primer sequences and expected PCR fragment sizes are listed in **Supplementary Table 2**.

Protein Extraction and Western Immunoblotting Protocols

Protein extraction and analysis was done essentially as previously described (14, 15, 18). Basically, cell monolayers were incubated with PBS on ice, followed by protein extraction with RIPA (20 mM Tris-HCl, pH = 7.5, 150 mM NaCl, 1% NP-40, 1% sodium deoxycholate, and standard protease inhibitors cocktail) buffer. For Stat3 and phospho-Stat3 detection, buffer was supplemented with 1 mM orthovanadate, 10 mM β-glycerol phosphate, and 25 mM sodium fluoride (phosphatase inhibitors). Cells were harvested using a scrapper, and lysis was completed by physical rupture with a 22G needle syringe. Cell lysates were centrifuged at 13,000 × *g* for 30 min, pellets were discarded, and protein content was quantified using the Bradford method with a commercial reagent (BioRad) following manufacturer's instructions.

The NE-PER Nuclear and Cytoplasmic Extraction Reagents (Pierce Protein Research Products (Thermo) commercial kit was used to obtain MB49 and MB49-I cell cytoplasmic and nuclear extracts.

Proteins were separated by electrophoresis in 10% Sodium Dodecyl Sulfate-PolyAcrylamide Gel Electrophoresis (SDS-PAGE) followed by Western immunoblotting. Proteins were immunodetected using standardized protocols and specific antibodies. Protein bands obtained in development plates (AGFA, Belgium) were digitized using a scanner (Hewlett-Packard, USA) and, in some cases, the signal density was quantified with the Image J software (Wright Cell Imaging Facility; Toronto, ON, Canada), and normalized with loading controls.

Fluorescence Immunocytochemical Analysis

Cells grown on glass coverslips were fixed and subjected to immunocytochemical analysis (14, 15, 18). Cell nuclei were stained with 1 µg/ml Hoechst 33342 or 5 µg/ml propidium iodide (BD Pharmigen) in PBS for 5 min, as specifically indicated. Negative controls were done placing purified mouse or rabbit IgG at the same concentration of primary antibody. Presence

of filamentous actin (F-actin) was detected with AlexaFluor 488 phalloidin (Thermo). Stained cells were observed in a fluorescence microscope (Nikon-C2, excitation filters 488 nm/544 nm, emission filters 523–530 nm/570-lp nm); when required, images were analyzed using the Image J software.

Immunohistochemical Analysis

Immunohistochemical analysis was performed in paraffin-embedded sections from orthotopic tumors of MB49 and MB49-I cell lines, normal C57BL/6 mice bladder and human bladder tumors. Five μm-tissue sections were stained with hematoxylin/eosin for cell morphology analysis or subjected to immunohistochemistry of E-cadherin, β-catenin, pSer33-β-catenin, and Ephrin-B1. In negative controls, primary antibody was replaced by IgG added at the same concentration of primary antibodies. Signal was developed with LSAB+System-HRP (Dako) colorimetric system. Ephrin-B1 staining was scored by two anatomo-pathologists, according to the percentage of stained cells (0, no stained cells, 1, 1 to 29%, 2, 30 to 69%, 3, 70 100% stained cells) and the intensity of the signal (0, without staining; 1: weak; 2: moderate; 3: strong), and a total score was calculated ($\geq$3, "high" Ephrin-B1; <3 "low" Ephrin-B1). E-cadherin staining score was normal ($\geq$1–29% cells with a membrane signal) or abnormal (low or high signal, but without membrane localization).

Cell Migration and Invasion Assays

Cell migration and invasion assays were run in MB49-I cells transiently transfected with a siRNA toward Ephrin-B1 and Control (scramble SiRNA). The procedure was done basically as previously reported (18) (8 h to assess migration and 40 h to evaluate invasion). In the lower part of the device, medium with 10% FBS was placed to act as chemoattractant. Cells were fixed and stained with 0.5% violet crystal solution in 20% methanol. Images from six different fields were recorded and cells counted using the Image J software.

Statistical Analysis

All experiments were run in triplicates. Results are expressed as mean ± SEM. Statistical analysis was done using GraphPad Prism software, version 5.01 (GraphPad Software, USA) and InfoStat, version 2015 (InfoStat Group, Argentina). For assays involving two groups, the Mann Whitney or Wilcoxon test was performed, as required; for assays involving >2 groups, the Kruskal Wallis test followed by multiple decompositions according to Dunn was run. Analysis of Ephrin-B1 and E-cadherin immunohistochemistry results was done using the Pearson Chi-Square test. A $P < 0.05$ was considered statistically significant.

RESULTS AND DISCUSSION

Bioinformatics Survey of BC and E-Cadherin

A bioinformatics analysis was done to retrieve a list of BC-associated genes. To perform this analysis, the DisGeNET database was surveyed to identify genes annotated to the terms "Malignant neoplasm of urinary bladder," "Bladder Neoplasm," "Transitional cell carcinoma of bladder," "Carcinoma *in situ* of bladder," and "Carcinoma of bladder." One hundred and thirty genes were identified; *CDH1* was among genes with highest score (*CDH1*, *CDKN2A*, *ERCC2*, *FGFR3*, *GSTP1*, *HRAS*, *NQO1*, *TP53*, *TSC1*), specifically when only the term "Bladder neoplasm" was surveyed. **Figure 1** shows a graphical representation of both networks, and **Supplementary Table 3** lists genes retrieved from DisGeNet survey, with their association type and score.

In addition, a search of *CDH1* somatic mutations in BC was done using the COSMIC bioinformatics tool. As a result, *CDH1* mutations were found in 17/587 (2.90%) tested BC samples, 15 of which were located in exonic sequences of different protein segments [residues 9, 27, 28, 150, 159, 210, 240, 248, 357, 638 (twice), 641, 677, 731, 785]. **Table 1** lists the identified mutations.

Altogether, these studies showed evidence of *CDH1*/E-cadherin involvement in BC, which was related only in few cases to mutations in the *CDH1* gene. Results of these surveys encouraged authors to further investigate changes in E-cadherin and related molecules, and the underlying mechanisms in BC.

Expression of E-Cadherin and EMT-Related Markers in MB49 and MB49-I Murine BC Cell Lines

Initial studies were focused on evaluating the expression of E-cadherin and some EMT-related genes in MB49 and MB49-I *in vitro* cell cultures (**Figure 2A**). While in standard RT-PCR assays E-cadherin mRNA was detected in both cell lines, quantitative real-time PCR analyses revealed a 30% decrease ($P < 0.05$) in E-cadherin transcript levels in MB49-I cells compared to MB49 parental cells (**Figure 2B**). In agreement with these findings, E-cadherin protein analysis by Western immunoblotting revealed significant lower expression levels of the 120 KDa full-length adhesion full-length protein form in MB49-I cells, representing <10% of those found in MB49 cells (**Figures 2C,D**). These findings are consistent with early studies done in human samples, in which lower E-cadherin levels were found in infiltrating than in superficial bladder tumors (2, 19, 20). In any case, while a 30% decrease in the *CDH1* transcript was found in MB49-I compared to MB49 cells, a sharp decrease to undetectable protein levels was determined. Differences observed between both cell lines in E-cadherin transcript and protein levels may relate to expression levels of the adhesion protein present in these cell lines and methodologies used to detect them. Both cell lines depict low E-cadherin mRNA expression levels (around Ct 36), but the quantitative real time PCR procedure can accurately measure low transcript levels in both cell lines. On the other hand, expression levels of the adhesion protein may be close to the limit of detection, resulting in a very poor/absent signal in MB49-I cells, even when using sensitive detection systems. Alternatively, differences between RNA and protein levels in the murine cell lines may result from selective regulatory post-transcriptional, translational and post-translational mechanisms, i.e., pre-mRNA splicing, polyadenylation, capping, and mRNA transport, turnover, storage, and translation (21). Some post-transcriptional mechanisms have been shown to critically influence EMT (22–24). Among mechanisms determining

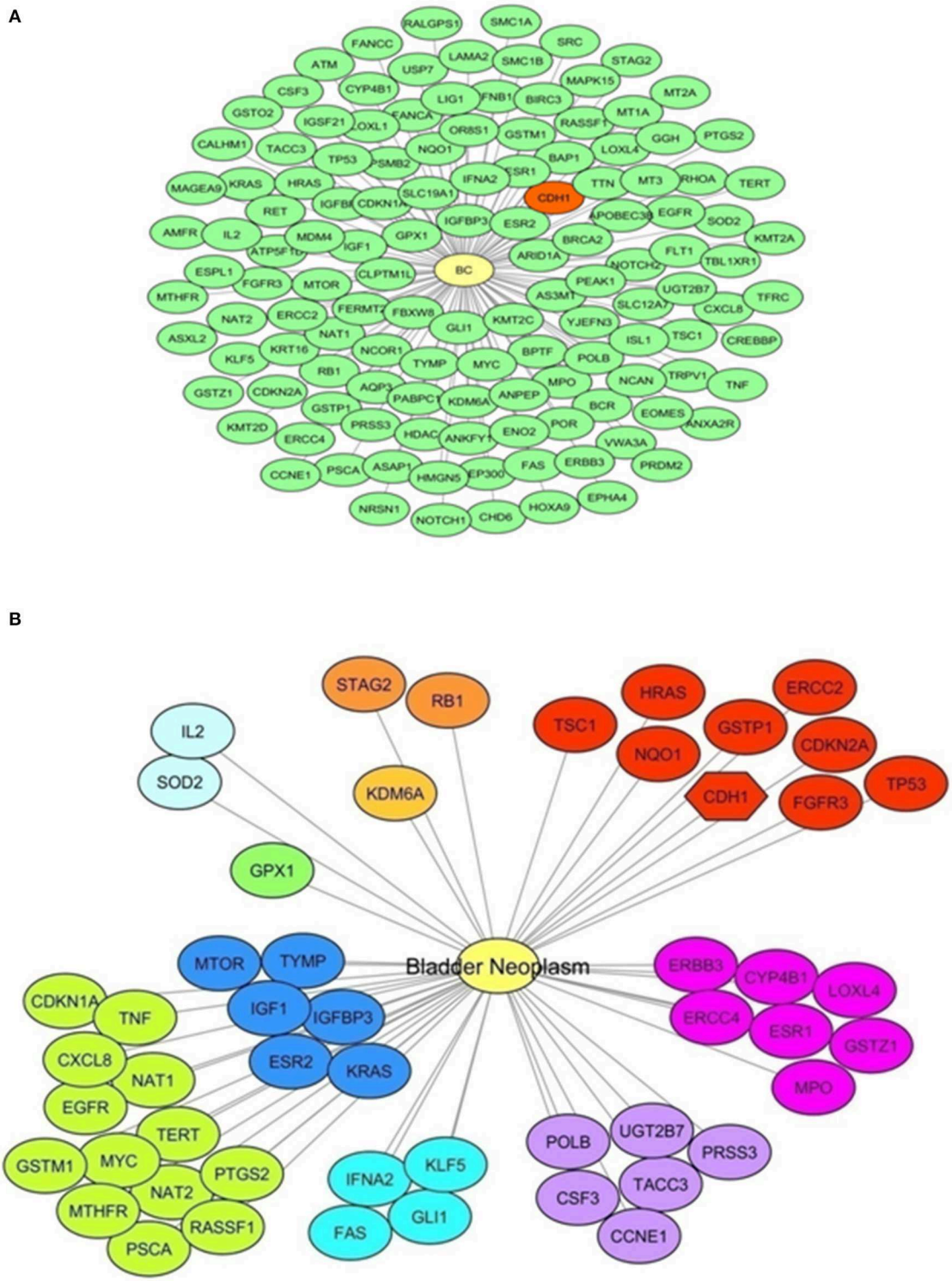

FIGURE 1 | E-cadherin and Bladder Cancer. A bioinformatics survey. **(A)** Network representation of genes annotated to the terms "Malignant neoplasm of urinary bladder," "Bladder Neoplasm," "Transitional cell carcinoma of bladder," "Carcinoma *in situ* of bladder," and "Carcinoma of bladder" obtained with DisGeNET using Cytoscape. A yellow node represents the "Bladder Cancer" disease node. Green nodes represent disease-related genes (130 genes). In red, the *CDH1* gene is highlighted. **(B)** Network representation of genes annotated to the term "Bladder Neoplasm" obtained with DisGeNET using Cytoscape. A yellow node represents the Bladder Cancer disease node. Other nodes represent disease-related genes, showing same colors for equal score. Red colored nodes depict the highest score (0.6); the *CDH1* gene is among these genes and highlighted with a different node shape. Information on the score and association type is presented in **Supplementary Table 3**.

TABLE 1 | *CDH1* somatic mutations and BC.

Transcript	Sample ID	AA mutation	CDS mutation
ENST00000261769	2727096	p.S9*	c.26C > A
ENST00000261769	2726284	p.P27fs*27	c.79_85delCCCTGCC
ENST00000261769	2725343	p.C28fs*1	c.84_85delCC
ENST00000261769	2721157	p.R150K	c.449G > A
ENST00000261769	2720314	p.P159 > HT	c.475_476insATA
ENST00000261769	2714567	p.E210Q	c.628G > C
ENST00000261769	2721980	p.I248N	c.743T > A
ENST00000261769	2719872	p.?	c.1320 + 2T > G
ENST00000261769	2772700	p.?	c.1320 + 5G > A
ENST00000261769	2719775	p.K557N	c.1671G > C
ENST00000261769	2724773	p.W638*	c.1914G > A
ENST00000261769	2097275	p.W638*	c.1914G > A
ENST00000261769	2722509	p.Q677*	c.2029C > T
ENST00000261769	2097330	p.L731F	c.2191C > T
ENST00000261769	992969	p.N785N	c.2355C > T
ENST00000261769	1995691	p.N240Xfs*10	c.?
ENST00000261769	2395174	p.Q641*	c.?

A bioinformatics analysis using COSMIC. Data retrieved from the COSMIC database (GRCh38 · COSMIC v90).

mRNA turnover by ribonucleoproteins, HuR is one of the best-studied regulators of cytoplasmic mRNA fate (21), and evidence supports its interaction with the 3'-untranslated region of E-cadherin mRNA and regulation of E-cadherin translation (25). In BC, HuR appears to regulate the expression of many urinary tumors-associated molecules (26), and a significant association between positive cytoplasmic HuR signal and high tumor grade, pT stage and micro-vessel density has been reported in BC (27). Differences found between E-cadherin expression levels in both cell lines and between mRNA and protein levels found may be, at least in part, related to the expression of HuR in the murine cell model and modulation of E-cadherin mRNA and protein stability. Mouse cells have been reported to conserve consensus sequences and mechanisms found in humans for these regulations (28). In addition to this regulatory mechanism, the translated E-cadherin protein may be subjected to proteolytic cleavage, catalyzed by matrix metalloproteinases (MMP-3, MMP-7, MMP-9, and MT1-MMP), A-disintegrin-and-metalloproteinases (ADAM10 and ADAM15), plasmin, and kallikrein 7, releasing the 86 KDa ectodomain fragment and a 38 KDa fragment associated to the membrane, which is degraded to smaller fragments (5, 29). Since MMP9 has been previously reported in BC (30) and in the MB49-I cell model (11), part of the lower signal may be the result of E-cadherin processing; E-cadherin cellular fragments may not be resolved in 10% SDS-PAGE gels, are below the limit of the detection, or lack the antibody epitope, and are not shown in the profile.

Since transcriptional repression is one mechanism associated to decreased E-cadherin (5), expression of Snail, Slug, Zeb1, and Twist transcriptional repressors was analyzed in both cell lines. As shown in **Figure 2E**, an increased expression ($P < 0.05$) of Snail and Slug transcripts was observed in MB49-I cells compared to MB49 cells. On the other hand, while lower levels ($P < 0.05$) of Zeb1 mRNA were detected in MB49-I cells compared to those in MB49 cells, no detectable levels of Twist were found in either BC cell line. Findings in the present report are in line with a previous study by Gou et al. (31), describing a relationship between a higher Snail expression, and the presence of advanced tumors among 332 human samples from patients with superficial BC evaluated by immunohistochemistry; in the same report, Snail was a predictor of disease recurrence and progression. Moreover, a higher expression of Slug was also previously reported in infiltrating tumors, in a study of 47 patients diagnosed with BC (32). Finally, Tang et al. (33) reported significantly lower expression levels of Twist1 mRNA in 13 paired urothelial bladder cancer specimens than the non-tumor mucosas.

The cadherin switching phenomenon represents an important aspect of the EMT, and it has been typically described as a process by which E-cadherin expression is replaced by N-cadherin expression (34, 35). However, later studies found an abnormal expression of other members of the superfamily as part of the cadherin switch (36). Thus, the E-cadherin to N-cadherin and/or P-cadherin switch phenomenon was analyzed in the *in vitro* murine BC model. Regarding N-cadherin, mRNA expression analysis revealed significant lower levels of this transcript in MB49-I compared to MB49 cells (**Figure 2F**). In line with these findings, fluorescence immunocytochemistry revealed a lower signal for N-cadherin in MB49-I compared to MB49 cells (**Figure 2G**). Previous studies have reported ∼40% of bladder tumors depicting a positive signal for this protein (37–39). This percentage was found in either NMIBC (37) or MIBC (40) tumor cohorts, showing that not all invasive tumors show increased expression of N-cadherin. While some of these studies showed an association between increased N-cadherin expression and recurrence-free survival (37, 38), others failed to find a relationship between N-cadherin expression with clinicopathological parameters (39, 41). In line with the results of the present report, a study by Jäger et al. (42) found a positive N-cadherin expression in superficial (Ta/T1) cases to be a risk factor, and a lack of expression in MIBC cases correlated with reduced patient survival. Moreover, they reported 14% (13/92) N-cadherin-negative (2 × T2, 8 × T3, and 3 × T4) MIBC, and 12/13 patients died of BC within 18 months; the average survival time in this group was 3.5-fold lower than in MIBC cases expressing N-cadherin. In another study, the N-cadherin-negative muscle-invasive tissue samples ("high risk") depicted a 2-fold higher expression level of the VEGF angiogenic factor than N-cadherin-positive muscle invasive cancers (43), highlighting the association between negative N-cadherin expression in BC and tumor aggressiveness.

With regard to P-cadherin assessment, transcript (**Figure 2H**) and protein (**Figure 2I**) levels were higher ($P < 0.05$) in MB49-I cells compared to MB49 cells. Results from this report agree with several studies that show P-cadherin expression in association with BC progression. Rieger-Christ et al. (44) described P-cadherin in over 90% of the cases in a cohort of ∼100 tumors; authors also reported N-cadherin expression, absent in normal urothelium but localized to the membrane in focal areas of the tumor mass in invasive tumors. Later, Bryan et al. (45) studied

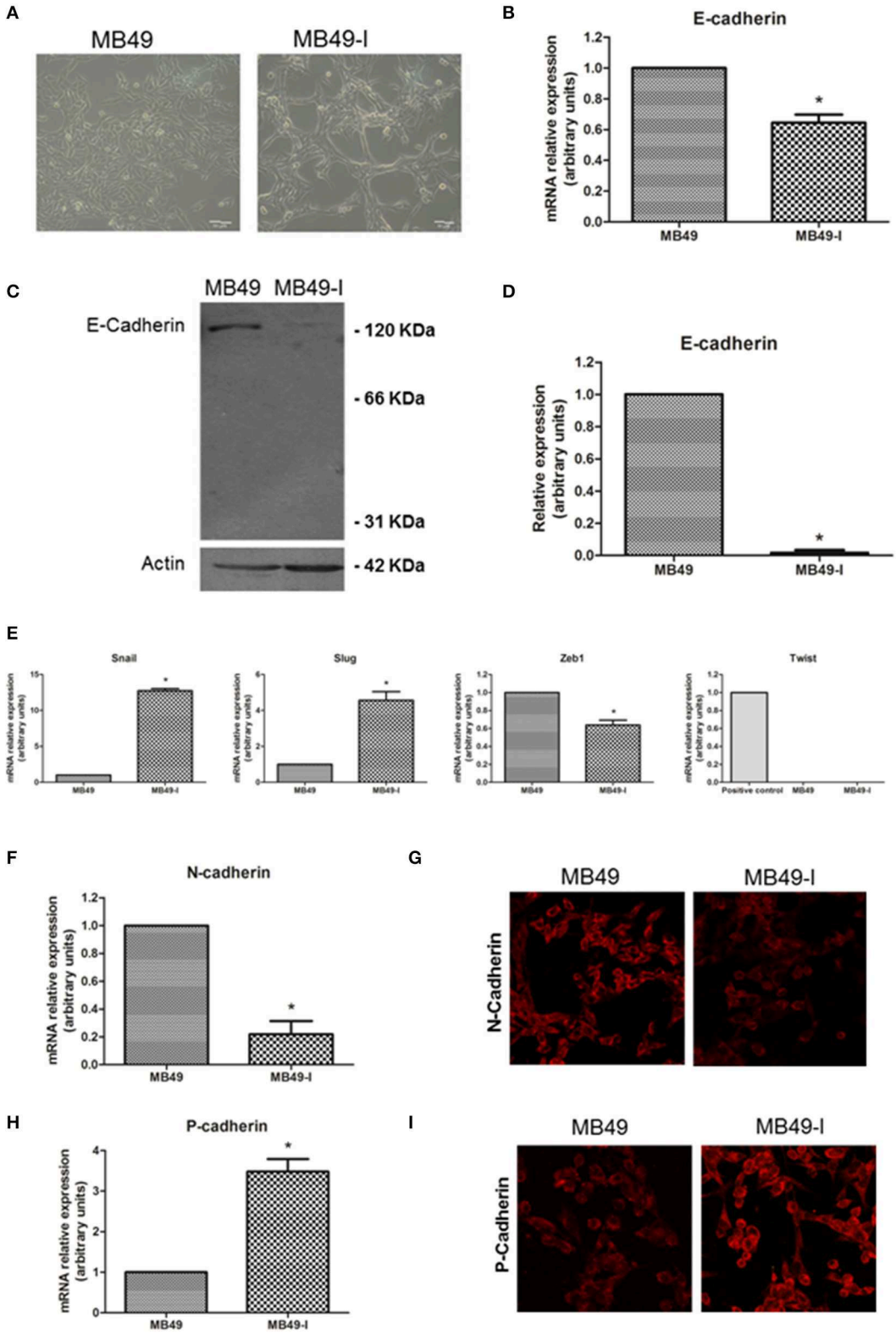

FIGURE 2 | EMT molecules and BC. Studies in the MB49 and MB49-I cell murine models. **(A)** Phase contrast microscopy of MB49 and MB49-I cells. Graph Bar = 20 μm. **(B)** Quantitative analysis of E-cadherin mRNA in MB49 and MB49-I cells by real-time PCR. Results are plotted as mean relative expression with Standard Error

(Continued)

FIGURE 2 | of the Mean (SEM); *$P < 0.05$. **(C)** Immunodetection of E-cadherin protein forms in total protein extracts of MB49 and MB49-I cells after performing 10% polyacrylamide gel electrophoresis (SDS-PAGE) followed by Western immunoblotting with anti E-cadherin antibody (610181; 2.5 μg/ml). Actin (I-19; 2 μg/ml) was used as loading control. References indicate the molecular weight standards of 66 and 31 KDa and the 120 KDa E-cadherin full length form. **(D)** Densitometric analysis of results obtained by Western Immunoblotting for the expression of E-cadherin performed with the ImageJ program; results are shown as percentage of the expression level of CadE in line MB49-I. Assessments of 3 replicates were included in the analysis. Data is shown as mean ± SEM. **(E)** Quantitative analysis by real-time PCR of Snail, Slug, Zeb1, and Twist mRNA expression in MB49 and MB49-I cells. For Twist, mouse testis was used as a positive control. ns, not significant; *$P < 0.05$. **(F)** Quantitative analysis by real-time PCR of N-cadherin mRNA expression in MB49 and MB49-I cells. **(G)** Fluorescence immunocytochemistry analysis by confocal laser microscopy of N-cadherin (H-63; 2 μg/ml) in MB49 and MB49-I cells. Negative controls are shown on the right, and cell nucleae were visualized using HOESCHT 33342. **(H)** Quantitative analysis by real-time PCR of P-cadherin mRNA expression in MB49 and MB49-I cells, *$P < 0.05$. In all cases, relative expression levels of each mRNA was calculated using actin as endogenous gene and the MB49 cell line as reference. **(I)** Fluorescence immunocytochemistry analysis by confocal laser microscopy of P-cadherin (H-105; 2 μg/ml) in MB49 and MB49-I cells. Negative controls are shown on the right, and cell nucleae were visualized using HOESCHT 33342.

over 150 bladder tumors, finding increased membranous P-cadherin expression in almost half of all MIBC, accompanied by significantly lower expression of E-cadherin. Increased P-cadherin expression was associated with worse BC-specific survival, and P-cadherin status was an independent prognostic factor (alongside grade and stage). Moreover, functional *in vitro* experiments showed that altering the balance of E- and P-cadherin in favor of P-cadherin expression enhanced anchorage-independent growth, and P-cadherin alone was unable to mediate normal cell–cell adhesion. Authors concluded that P-cadherin expression promoted a more malignant and invasive phenotype of BC, even in the presence of E-cadherin. The same year Mandeville et al. (46) reported the expression of P-cadherin in BC, and found that P-cadherin overexpression induced an increase in migratory capacity in *in vitro* models. Van Marck et al. (47) later showed that stable knockdown of P-cadherin in RT-112 BC cells diminished invasion and migration, and promoted intercellular adhesion, supporting a P-cadherin transformation promoting role in BC. Mandeville et al. (46) suggested P-cadherin to have a role in regulating migration of basal cells to the intermediate cell layer in normal urothelium as well as a role in neoplastic progression, while Bryan et al. (45) suggested that P-cadherin may be induced in BC to reduce cell-cell adhesion and to enable cell-matrix interactions as a first step to invasion in a similar fashion to N-cadherin. In Jäger's report (42), high P-cadherin gene expression proved to be an independent favorable prognostic factor of cancer-related survival, and a risk factor of recurrence in superficial cancers after tumor resection. In 2014, Wang et al. (48) reported a correlation between P-cadherin high expression and tumor progression. Finally, using a molecular approach, a thorough report by Choi and collaborators described the identification of distinct basal and luminal subtypes of MIBC with different sensitivities to frontline; in the study, *CDH3*, the gene encoding P-cadherin was listed among gene classifiers for muscle invasive progression and muscle invasive overall survival (49).

Protein Assessment of the Adherent Complex Members. β-Catenin Expression Analysis

Considering the relevance of the adhesion complex integrity upon cell-cell adhesiveness, and the decreased E-cadherin mRNA and protein levels found in MB49-I cells, subcellular localization of some members of the adherent complex was evaluated. Localization of E-cadherin and β-catenin was determined in both cell lines by fluorescence immunocytochemistry, while evaluation of the actin cytoskeleton organization was performed by Filamentous actin (F-actin) staining with Alexa488-phalloidin. As shown in **Figure 3A** (top panels), immunolocalization analysis of E-cadherin in whole cells revealed a signal in the cytoplasm of both cell lines, but ∼50% less intense in MB49-I cells, in line with the results of mRNA and total E-cadherin protein expression analysis described above (**Figure 2C**). On the other hand, β-catenin immunolocalization analysis revealed striking differences between both cell lines; while in MB49 cells the β-catenin signal was localized mainly in the cytoplasm, in MB49-I cells it was stronger and distributed in the cytoplasm and nucleus (**Figure 3A**, middle panel). F-actin fluorescence distribution evidenced stress fibers in both lines (**Figure 3A**, bottom panels).

To confirm a higher expression of β-catenin protein in MB49-I cells, Western immunoblotting of total protein extracts from both cell lines was done. In agreement with the immunocytochemistry results, higher levels of β-catenin were detected in MB49-I cells compared to MB49 cells (**Figures 3B,C**). These changes could not be attributed to an increase in mRNA expression (MB49: 1; MB49-I: 0.978±0.043; ns). Based on these findings, β-catenin subcellular distribution was quantified, finding nuclear localization in ∼80% of MB49-I cells and in ∼10% of MB49 cells (**Figure 3D**). This evaluation was also done in cytoplasmic and nuclear protein extracts (β-tubulin cytoplasmic marker; PCNA nuclear marker). As shown in **Figure 3E,** β-catenin signal in MB49-I cells was weaker in the cytoplasmic fraction and stronger in the nuclear fraction, when compared to MB49 cells.

In normal cells, β-catenin localizes at the cell membrane in a complex with E-cadherin; cytoplasmic β-catenin is maintained at low levels, being constitutively captured by a destruction complex that facilitates its N-term phospho targeting, ubiquitination and destruction in the proteasome. The adenomatous polyposis coli (APC) and Axin are structural components of the destruction complex, while CK1 casein kinases and 3 glycogen synthase kinase-3β (GSK-3β) are recruited to serine phosphorylate β-catenin. Under certain conditions, β-catenin accumulates in the cytosol and is shuttled to the nucleus, where it binds and forms complexes with transcription factors of the lymphoid enhancer factor (Lef)/T-cell factor (TCF) family, and activates target

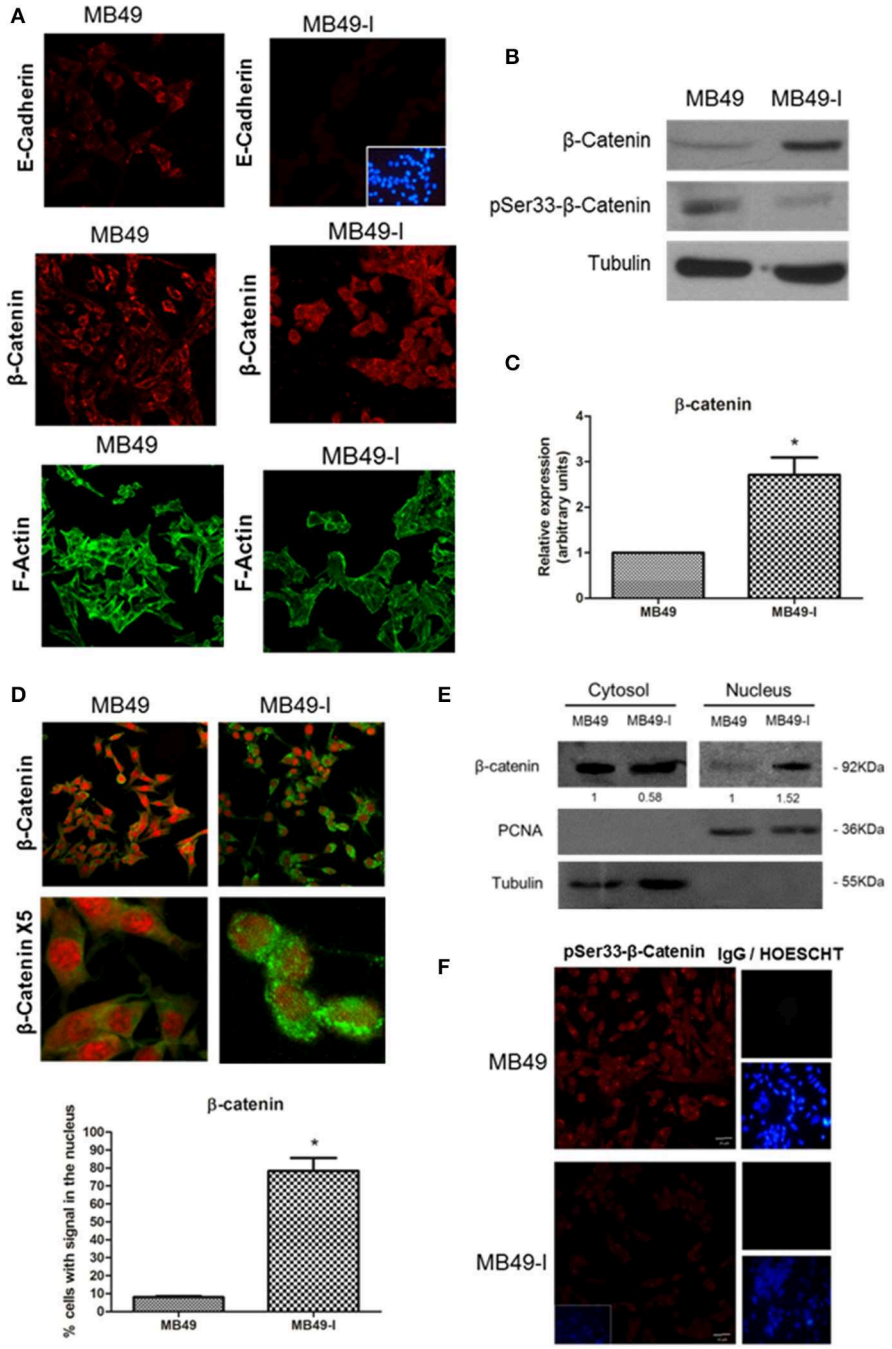

FIGURE 3 | Evaluation of adherent complex members in MB49 and MB49-I cells. **(A)** Fluorescence immunocytochemistry of E-cadherin (610181; 2.5 μg/ml), (top panels) and β-catenin (610153; 2.5 μg/ml) (middle panels) and analysis by confocal microscopy. Bar indicates 20 μm (Magnification 40×). Negative controls are shown on the right; cell nucleae were visualized using HOESCHT 33342. Confocal laser microscopy analysis of actin cytoskeleton organization by visualization of filamentous actin (F-actin) labeled with phalloidin-Alexa488 in MB49 and MB49-I cells (bottom panels). **(B)** Immunodetection of β-catenin (610153; 2.5 μg/ml) and pSer33-β-catenin (Ser33-R; 4 μg/ml) after performing 10% SDS-PAGE followed by Western immunoblotting of MB49 and MB49-I cell extracts. Loading controls were done using a specific antibody toward β-tubulin (D-66; 0.05 μg/ml). **(C)** Densitometric quantification analysis of β-catenin in MB49 and MB49-I cells using the Image J software; $^*P < 0.05$. **(D)** Fluorescence immunocytochemistry of β-catenin (610153; 2.5 μg/ml) and analysis by confocal microscopy in MB49 and MB49-I cells. Cell nuclei were visualized using Propidium Iodide. Bar = 20 μm (Magnification 40×). MB49-I cells with nuclear localization of β-catenin are indicated with an arrow. Graphic representation of the percentage of MB49 and MB49-I cells with β-catenin signal in the nucleus; $^*P < 0.05$. **(E)** Detection of β-catenin (610153; 2.5 μg/ml) after 10% SDS-PAGE followed by Western immunoblotting of cytoplasmic and nuclear fractions of MB49 and MB49-I cell extracts. Cell fraction loading and purity: β-tubulin (positive in the cytoplasmic fraction; D-66, 0.05 μg/ml), PCNA (positive in the nuclear fraction; PC10, 0.2 μg/ml). **(F)** Fluorescence immunocytochemistry and confocal laser microscopy analysis in MB49 and MB49-I cells of pSer33-β-catenin (Ser33-R; 4 μg/ml). Negative controls shown on the right; cell nucleus visualized using HOESCHT 33342.

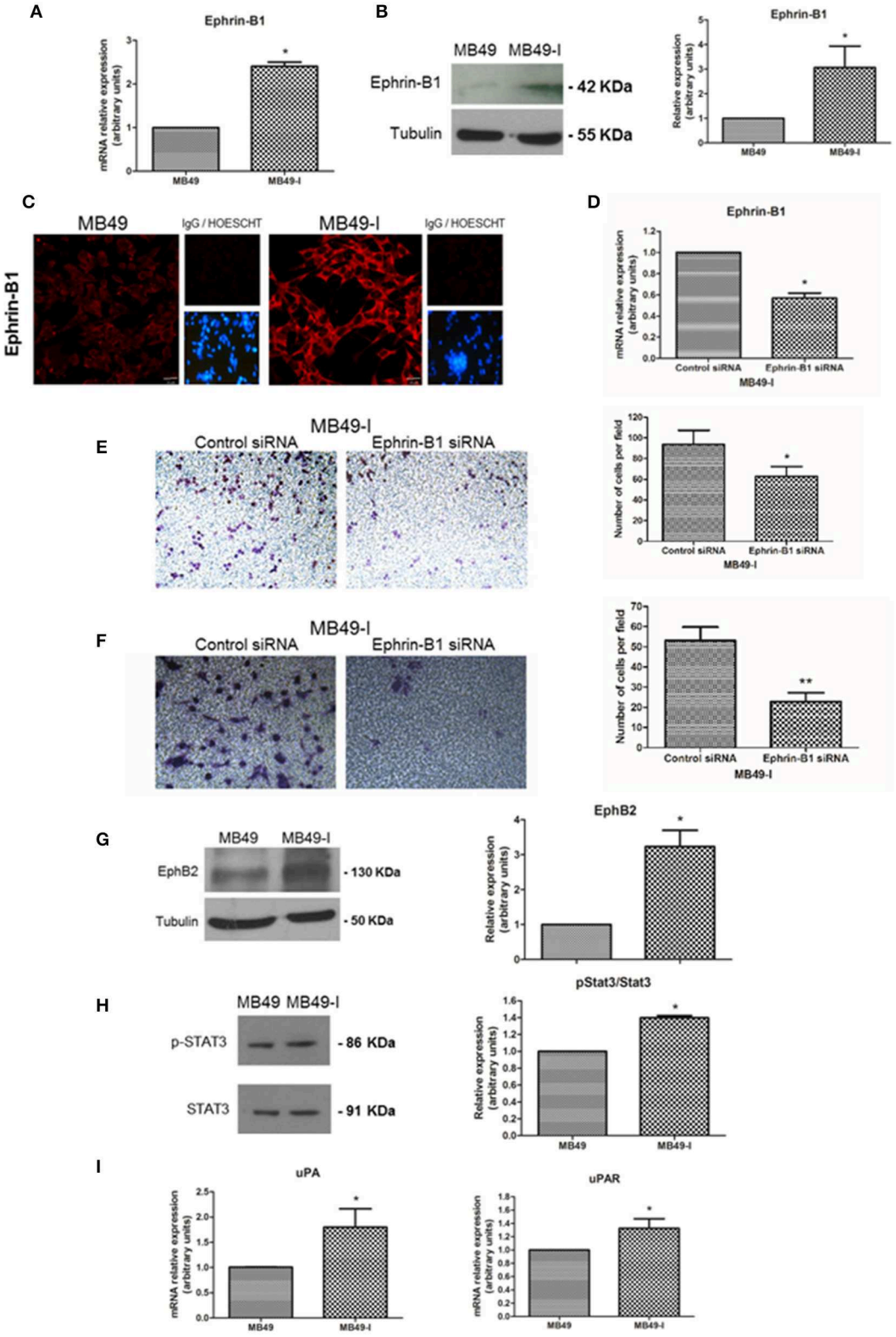

FIGURE 4 | Expression analysis of Ephrin-B1 and related proteins in the MB49 and MB49-I cell murine models. **(A)** Quantitative expression analysis of Ephrin-B1 mRNA in MB49 and MB49-I cells by real-time PCR. (**B**, Left) Immunodetection of Ephrin-B1 (A-20; 2 μg/ml) after 10% SDS-PAGE of MB49 and MB49-I cells protein

(Continued)

FIGURE 4 | extracts followed by Western Immunoblotting. β-tubulin (D-66, 0.05 μg/ml) used as loading control. (Right) Densitometric analysis of Ephrin-B1 immunodetection; *$P < 0.05$. **(C)** Fluorescence immunocytochemistry and analysis by confocal laser microscopy of Ephrin-B1 (A-20; 2 μg/ml) in MB49 and MB49-I cells. (Right) Negative controls; cell nucleae were visualized using HOESCHT 33342. **(D)** Quantitative analysis of Ephrin-B1 mRNA by real-time PCR in cells transiently transfected with an Ephrin-B1specific siRNA (cells MB49-I siRNA Ephrin-B1) or control siRNA (MB49-I siRNA Control cells); *$P < 0.05$. (**E**, Left) Representative images of the migration assay obtained by phase contrast microscopy (Magnification 20×). (Right) Graphical representation of the migration assay results in siRNA MB49-I Ephrin-B1 and siRNA control MB49-I cells. The average number of cells in each of the evaluated fields is plotted; *$P < 0.05$. **(F**, Left). Representative images of the invasion assay obtained by phase contrast microscopy (Magnification 20×). (Right) Graphic representation of the invasion assay results. The average number of cells in each of the evaluated fields is plotted; **$P < 0.001$. (**G**, Left) Immunodetection of EphB2 (H-80; 2 μg/ml) in MB49 and MB49-I cells protein extracts after 10% SDS-PAGE/Western Immunoblotting. Immunodetection of β-tubulin was carried out as loading control. (Right) Densitometric analysis of EphB2; *$P < 0.05$. (**H**, Left) Immunodetection of pStat3 (C-20; 2 μg/ml) and Stat3 (B-7; 2 μg/ml) of protein extracts of MB49 and MB49-I cells, after 10% SDS-PAGE/Western Immunoblotting. Loading control: β-tubulin (D-66, 0.05 μg/ml). (Right) Densitometric analysis of phospho-Stat3 immunodetection. Signal intensity of this molecule was normalized using Stat3 signal intensity and MB49 cells as reference; *$P < 0.05$. **(I)** Quantitative analysis of uPA and uPAR mRNA by real-time PCR in MB49 and MB49-I cells; *$P < 0.05$.

genes, which are regulators of cell proliferation and involved in tumorigenesis. N-terminal β-catenin phosphorylation is required for its degradation and for attenuating its effect on transcription (50–52). β-catenin nuclear localization has been related to tumor progression and aggressiveness in several tissues (i.e., breast, renal, and colorectal cancer); in particular, there are reports describing an aberrant localization of β-catenin in the cell cytoplasm and nucleus in BC (53, 54).

Taking into account that β-catenin is phosphorylated in the degradation complex by GSK-3β in Ser33, Ser37, and Ser41 (52, 55), presence and localization of pSer33-β-catenin were assessed in MB49 cells and MB49-I cells, both by Western immunoblotting and fluorescent immunocytochemistry using a commercial antibody. As result, lower levels of P-Ser33-β-catenin were found in MB49-I cells compared to MB49 cells (**Figures 3B,F**, respectively), in agreement with β-catenin localization found in the MB49-I cell nucleus. In line with these findings, Roy et al. (56) reported the results of next generation sequence analysis done in 15 primary bladder adenocarcinomas, in which mutations were found in *CTNNB1* (encoding β-catenin) (3/15, 20%), including activating missense mutations at known hotspots (p.D32N and p.S45F) and amplification; in the study, the immunohistochemistry analysis revealed β-catenin nuclear localization in mutated samples. In addition to these findings, the COSMIC database lists 10/29 mutations (all missense) around Ser33, Ser41, and adjacent residues, from 764 samples of transitional cell carcinoma of the bladder evaluated. The list is shown in **Supplementary Table 4**.

Expression Analysis of Ephrin-B1 and Related Proteins in MB49 and MB49-I Cells

Studies have identified Ephrin-B1 as a target gene of β-catenin nuclear transcriptional activity (57–59). Moreover, Ephrin-B1 expression has been associated to tumor progression and invasion in cell models (60, 61) and in different cancer types [hepatocarcinoma: (62), ovarian: (63), gastric: (64)]. Other members of the Ephrin family have been studied in BC. Among them, a higher expression of Ephrin-A1 and EphA2 receptor was found in BC cell lines and in advancing tumor compared to controls, as well as an association between their expression and tumor stage (65). Moreover, a high expression of arterial Ephrin-B2 and venous EphB4 receptor was reported in BC, and proposed to contribute to tumor angiogenesis (66).

Based on this background information, Ephrin-B1 mRNA and protein levels were determined in both cell lines, finding significantly higher expression of Ephrin-B1 transcript in MB49-I cells than in MB49 cells (**Figure 4A**). In agreement with these results, a stronger signal for Ephrin-B1 was found in MB49-I than in MB49 protein cell extracts (**Figure 4B**). This increase was also evidenced by fluorescence immunocytochemistry, with an Ephrin-B1 signal >300% higher in MB49-I cells than in MB49 cells (**Figure 4C**). To evaluate the association between Ephrin-B1 expression and an invasive cellular behavior, MB49-I cells were transfected with Ephrin-B1 (MB49I-siRNAEphrin-B1 cells) or scramble (MB49I-siRNAControl) siRNA. The effectiveness of the procedure was confirmed by a decrease in Ephrin-B1 mRNA levels (**Figure 4D**). MB49-I siRNA Ephrin-B1 treated cells depicted lower migratory and invasive capacity than control cells (**Figures 4E,F**).

Co-expression of Ephrin-B1 and the EphB2 receptor has been observed in small cell lung cancer (67), gastric cancer (64) as well as in medulloblastoma (61). Also, their co-expression was related to metastasis by immunohistochemistry in a study done in 50 cholangiocarcinoma samples (68). Based on these findings, EphB2 expression was evaluated in total protein cell extracts, finding 3 times higher levels in MB49-I cells than in MB49 cells (**Figure 4G**). These findings are in agreement with the association reported between high EphB2 expression and EMT induction and progression of human cervical cancer (69), although they contrast with a report describing its decrease in human BC samples (70).

Among several signal transduction mechanisms, Ephrin-B1 interaction with EphB2 receptor results in its activation, which is followed by Stat3 recruitment, phosphorylation and enhanced transcriptional activation (71). Deregulation of Stat3 signaling has been reported in several solid tumors, among them BC (72), and its activation has been associated to tumor invasion and metastasis (73). Thus, the expression of Stat3 and the Tyr705-phospho Stat3 (pStat3) activated form was analyzed in both cell lines, finding a 35% increase in pStat3/Stat3 ratio in MB49-I cells (**Figure 4H**). Moreover, the expression of Stat3 target genes, specifically Urokinase-type Plasminogen Activator (uPA) and its receptor uPAR (Urokinase-type Plasminogen Activator Receptor) was evaluated, finding higher levels of both transcripts in MB49-I cells compared to

MB49 cells (**Figure 4I**). In line with these findings, uPA activity was previously reported in MB49-I cells conditioned media (11). These molecules play a fundamental role in tissue remodeling during invasion and metastasis, and their expression was related to BC poor prognosis (74). uPA and uPAR expression has been related to β-catenin transcriptional activity in colorectal tumors (75).

Expression Analysis of E-cadherin, β-catenin, and Ephrin-B1 in Murine and Human Bladder Tumors

Taking into account findings obtained in cell cultures of the BC murine model, orthotopic tumors were derived from both cell lines, and immunodetection of E-cadherin, β-catenin, pSer33-β-catenin, and Ephrin-B1 was done in paraffin-embedded tissue

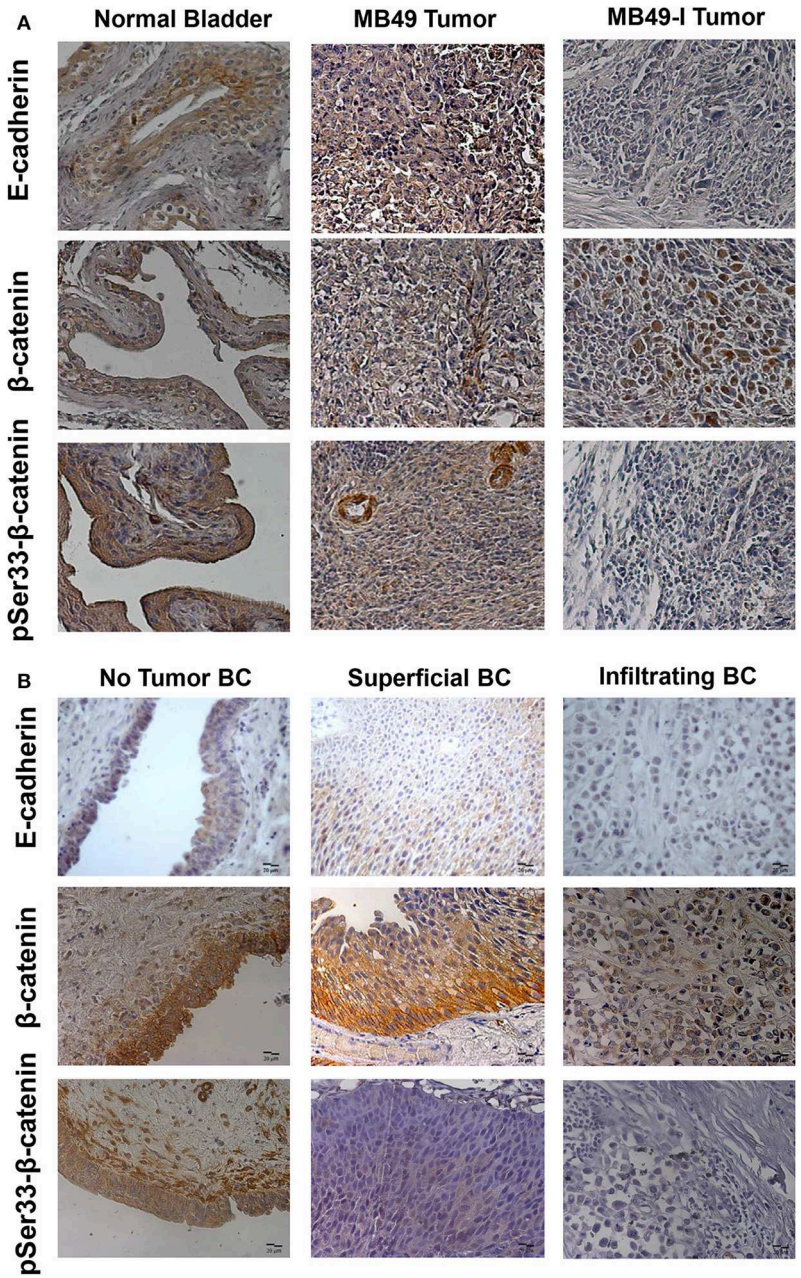

FIGURE 5 | Immunohistochemical analysis of E-cadherin, β-catenin and pSer33-β-catenin in murine and human bladder tissues. **(A)** Colorimetric immunohistochemistry of: Top: E-cadherin (610181; 2 μg/ml), Middle: β-catenin (610153; 2 μg/ml) and pSer33-β-catenin (Ser33-R; 2 μg/ml) in paraffin sections of normal bladder (left), MB49 tumors (middle), and MB49-I tumors (right). Bar = 20 μm (Magnification 40×). Contrast staining was performed using hematoxylin. **(B)** Colorimetric immunohistochemistry of E-cadherin (HECD-1; 0.6 μg/ml), β-catenin (610153; 2 μg/ml), and pSer33-β-catenin (Ser33-R; 2 μg/ml) in paraffin sections of bladder tissue from patients with superficial or infiltrating BC. In addition, a non-tumor section of bladder from patients with infiltrating BC after cystectomy is included. Bar = 20 μm (Magnification 40×). Contrast staining was performed using hematoxylin.

sections; for all proteins evaluated, murine bladder C57BL/6 mice bladders were included as controls (non-tumor). E-cadherin was immunolocalized at the cell membrane and cytoplasm in normal bladder; contrasting, a cytoplasm signal was mainly found in MB49 tumors, and a low intensity or undetectable signal in MB49-I tumors (**Figure 5A**, top). β-catenin was

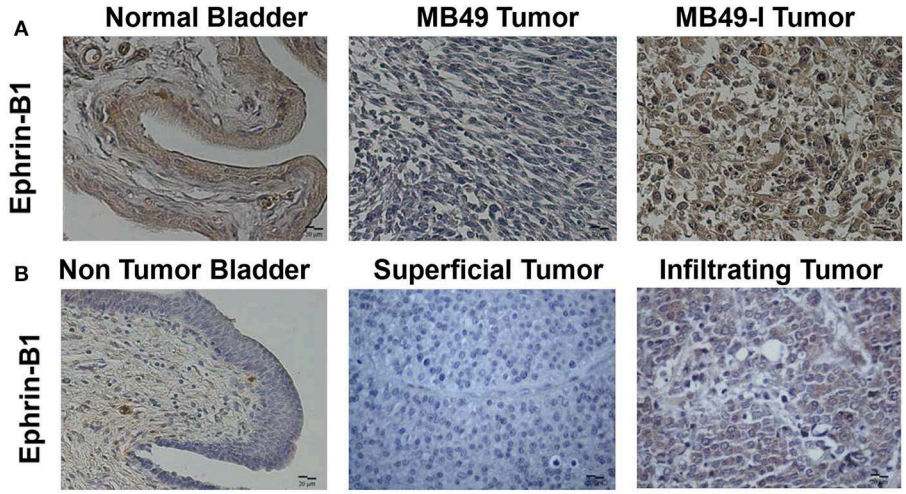

C

	n	Ephrin-B1 Low (%)	Ephrin-B1 High (%)	*P*
Stage				
T1	20	10 (50.0)	10 (50.0)	***0.031**
T2-T4	18	3 (16.6)	15 (83.4)	
Grade				
Low	10	7 (70.0)	3 (30.0)	***0.005**
High	28	6 (21.0)	22 (79.0)	
Metastasis				
No	27	10 (37.0)	17 (63.0)	0.565
Yes	11	3 (27.0)	8 (73.0)	
E-cadherin staining				
normal	*19*	*8 (42.0)*	*11 (58.0)*	*0.305*
abnormal	*19*	*5 (26.0)*	*14 (74.0)*	

FIGURE 6 | Immunohistochemical analysis of Ephrin-B1 in murine and human bladder tissues. **(A)** Colorimetric immunohistochemistry of Ephrin-B1 (A-20; 2 μg/ml) in paraffin sections of normal bladder (left), MB49 tumors (middle), and MB49-I tumors (right). Bar = 20 μm (Magnification 40×). Contrast staining was performed using hematoxylin. **(B)** Colorimetric immunohistochemistry of Ephrin-B1 (A-20; 2 μg/ml) in paraffin sections of bladder tissue from patients with superficial or infiltrating BC. In addition, a non-tumor section corresponding to bladder of a patient diagnosed with infiltrating BC and undergoing cystectomy is included. Bar = 20 μm (Magnification 40×). Contrast staining was performed using hematoxylin. **(C)** Analysis of the relationship between Ephrin-B1 expression and different clinico-pathological parameters in a set of BC samples. Ephrin-B1 staining analysis was performed assigning a score according to the percentage of stained cells (0, no stained cells, 1:1–29%, 2:30–69%, 3:70–100%) and the intensity of the signal (0, no staining; 1: weak; 2: moderate; 3: strong). The total score was calculated after adding both scores. The *P*-value was calculated using Pearson's Chi square test. *$P < 0.05$.

immunolocalized at the cell membrane and cytoplasm of normal bladders and MB49 tumors, while MB49-I tumors showed a signal in the nucleus in a high proportion of cells (**Figure 5A**, middle). Moreover, pSer33-β-catenin immunodetection revealed a strong signal in both normal bladder and MB49 tumors, but very weak in MB49-I tumors (**Figure 5A**, bottom). In all cases, protein subcellular localization and signal intensity was comparable to that found in both cells growing in monolayers.

A similar analysis done in human tumor samples from patients diagnosed with BC, revealed a strong signal for E-cadherin in the cell membrane of sections of the tumor classified as non-tumor tissue, and a weaker signal in the cytoplasm of tumor sections from superficial and infiltrating tumors, with lowest intensity in the latter (**Figure 5B**, top), in agreement with previous reports in human BC (2, 19, 20). β-catenin was immunodetected at the cell membrane of non-tumor bladder and superficial tumors, but alterations in its expression and localization were observed as previously reported (19, 20). In particular, a cytoplasmic and nuclear signal was found in a subset of infiltrating tumors evaluated (**Figure 5B**, middle). This localization of β-catenin was similar to that reported in 87% (26/30) of MIBC evaluated, which was associated it with poor prognostic parameters, among them tumor grade, stage, microvessel density, vascular invasion, and lymph node metastasis (53). For pSer33-β-catenin, a cytoplasmic staining was observed in non-tumoral bladder and superficial tumors, although with less intensity, while no signal was detected in infiltrating tumors (**Figure 5B**, bottom).

Regarding Ephrin-B1 immunodetection, MB49-I tumors depicted a stronger signal compared to normal bladders and MB49 tumors (**Figure 6A**). To assess Ephrin-B1 expression in human BC, two studies were done. First, fresh biopsies of tumor and non-tumor mucosa were obtained from 10 patients during radical cystectomy. Transcript expression assessed by real-time PCR revealed higher ($P < 0.05$) Ephrin-B1 levels in tumor vs. non-tumor samples (Non tumor $= 0.001446 \pm 0.0006982$, Tumor $= 0.003612 \pm 0.001740$).

Ephrin-B1 immunohistochemical analysis was done in superficial and infiltrating tumors; normal bladder tissue sections found in tumor pieces were also evaluated. A faint or absent signal was observed in the urothelium of the non-tumoral section, while a signal was detected in all tumors (**Figure 6B**). A low or high Ephrin-B1 score was assigned, according to the percentage of stained cells and the signal intensity. As result, a positive association ($P = 0.031$) was found between Ephrin-B1 expression and tumor stage (**Figure 6C**), with a high proportion of infiltrating tumors (15/18, 83.4%) depicting a high score. Half of superficial tumors (10/20; 50%) showed a weak signal for Ephrin-B1, but 10 superficial tumors depicted a strong signal, 6 of which were high grade, and other 2 were large tumors with multifocal sites. A positive association was also found between Ephrin-B1 expression and tumor grade ($P = 0.005$), with 79% high-grade tumors depicting a high score. Likewise, 70% low-grade tumors had a low score. No significant relationship was found between Ephrin-B1 staining and the occurrence of metastasis.

E-cadherin expression was also analyzed in the 38 samples, and compared with Ephrin-B1 results, finding 74% tumors depicting an abnormal E-cadherin expression and high Ephrin-B1 expression, although no significant relationship was found between both proteins (**Figure 6C**). No significant relationship was also found between E-cadherin signal and tumor stage, grade, or metastasis (**Supplementary Table 5**).

Altogether, findings reported in this investigation further characterized changes in E-cadherin and EMT-related molecules in BC. Using a combination of bioinformatics, a murine model of tumor aggressiveness and BC patient samples, the expression of Ephrin-B1 and related proteins is reported for the first time in association to BC progression/aggressiveness, gaining knowledge on the underlying mechanisms of BC. Evaluation of Ephrin-B1 in a multicenter study with a large cohort of patients will help confirming its role as a biomarker of BC aggressiveness. Since antibodies, recombinant proteins, and peptides developed to target the Ephrin/Eph ligand-receptor system have been reported to reduce tumor growth in breast, prostate, colon, head, and neck cancer animal models and some molecules are under investigation in clinical trials (76), additional studies with these molecules in BC will contribute to determine Ephrin-B1 role as therapeutic target of disease progression.

DATA AVAILABILITY STATEMENT

The raw data supporting the conclusions of this article will be made available by the authors, without undue reservation, to any qualified researcher.

ETHICS STATEMENT

The studies involving human participants were reviewed and approved by Ethics Committees of Hospital Italiano and IBYME (Protocol #C004-1/2012). The patients/participants provided their written informed consent to participate in this study. The animal study was reviewed and approved by Institute of Oncology Angel H. Roffo Review Board (#2012/02).

AUTHOR CONTRIBUTIONS

MV-L, LL and MM were involved in study conception and design and drafted the manuscript. MM, LL, MR, MB, DB, MI, SV, CL, AE, JT, MG, MZ and MV-L participated in data collection. MM, LL, MR, MB, and MV-L participated in data analysis. MV-L was responsible of grants that supported this study, coordinating and supervising the entire project. All authors read and accepted the final version.

FUNDING

Studies were supported by grants to MV-L from the Agencia Nacional de Promoción Científica y Tecnológica de Argentina Grant PICTSU-1072, Consejo Nacional de Investigaciones

Científicas y Técnicas (CONICET) Grant PIP740 and PIP887, Instituto Nacional del Cáncer Grant INC 2014–2015 and INC 2016–2017, as well as JT and MV-L personal funds. Special thanks to Fundación R. Barón and Fundación Williams for institutional (IBYME) support.

SUPPLEMENTARY MATERIAL

The Supplementary Material for this article can be found online at: https://www.frontiersin.org/articles/10.3389/fonc.2020.00283/full#supplementary-material

REFERENCES

1. Kamat AM, Hahn NM, Efstathiou JA, Lerner SP, Malmström PU, Choi W, et al. Bladder cancer. *Lancet*. (2016) 388:2796–810. doi: 10.1016/S0140-6736(16) 30512-8
2. Bringuier PP, Umbas R, Schaafsma HE, Karthaus HF, Debruyne FM, Schalken JA. Decreased E-cadherin immunoreactivity correlates with poor survival in patients with bladder tumors. *Cancer Res.* (1993) 53:3241–5.
3. Xie Y, Li P, Gao Y, Gu L, Chen L, Fan Y, et al. Reduced E-cadherin expression is correlated with poor prognosis in patients with bladder cancer: a systematic review and meta-analysis. *Oncotarget*. (2017) 8:62489–99. doi: 10.18632/oncotarget.19934
4. Angst BD, Marcozzi C, Magee AI. The cadherin superfamily: diversity in form and function. *J Cell Sci*. (2001) 114(Pt 4):629–641.
5. van Roy F, Berx G. The cell-cell adhesion molecule E-cadherin. *Cell Mol Life Sci*. (2008) 65:3756–88.doi: 10.1007/s00018-008-8281-1
6. Thiery JP, Acloque H, Huang RY, Nieto MA. Epithelial-mesenchymal transitions in development and disease. *Cell*. (2009) 139:871–90. doi: 10.1016/j.cell.2009.11.007
7. Lamouille S, Xu J, Derynck R. Molecular mechanisms of epithelial-mesenchymal transition. *Nat Rev Mol Cell Biol*. (2014) 15:178–96. doi: 10.1038/nrm3758
8. McConkey DJ, Choi W, Marquis L, Martin F, Williams MB, Shah J, et al. Role of epithelial-to-mesenchymal transition (EMT) in drug sensitivity and metastasis in bladder cancer. *Cancer Metastasis Rev*. (2009) 28:335–44. doi: 10.1007/s10555-009-9194-7
9. Yun SJ, Kim WJ. Role of the epithelial-mesenchymal transition in bladder cancer: from prognosis to therapeutic target. *Korean J Urol*. (2013) 54:645–50. doi: 10.4111/kju.2013.54.10.645
10. Singh R, Ansari JA, Maurya N, Mandhani A, Agrawal V, Garg M. Epithelial-to-mesenchymal transition and its correlation with clinicopathologic features in patients with urothelial carcinoma of the bladder. *Clin Genitourin Cancer*. (2017) 15:e187–97. doi: 10.1016/j.clgc.2016.07.021
11. Lodillinsky C, Rodriguez V, Vauthay L, Sandes E, Casabé A, Eiján AM. Novel invasive orthotopic bladder cancer model with high cathepsin B activity resembling human bladder cancer. *J Urol*. (2009) 182:749–55. doi: 10.1016/j.juro.2009.03.076
12. Belgorosky D, Langle Y, Prack McCormick B, Colombo L, Sandes E, Eiján AM. Inhibition of nitric oxide is a good therapeutic target for bladder tumors that express iNOS. *Nitric Oxide*. (2014) 36:11–8. doi: 10.1016/j.niox.2013.10.010
13. Summerhayes IC, Franks LM. Effects of donor age on neoplastic transformation of adult mouse bladder epithelium *in vitro*. *J Natl Cancer Inst*. (1979) 62:1017–23.
14. Lapyckyj L, Castillo LF, Matos ML, Gabrielli NM, Lüthy IA, Vazquez-Levin MH. Expression analysis of epithelial cadherin and related proteins in IBH-6 and IBH-4 human breast cancer cell lines. *J Cell Physiol*. (2010) 222:596–605. doi: 10.1002/jcp.21974
15. Rosso M, Majem B, Devis L, Lapyckyj L, Besso MJ, Llauradó M, et al. E-cadherin: a determinant molecule associated with ovarian cancer progression, dissemination and aggressiveness. *PLoS ONE*. (2017) 12:e0184439. doi: 10.1371/journal.pone.0184439. eCollection 2017
16. Piñero J, Queralt-Rosinach N, Bravo À, Deu-Pons J, Bauer-Mehren A, Baron M, et al. DisGeNET: a discovery platform for the dynamical exploration of human diseases and their genes. *Database*. (2015) 2015:bav028. doi: 10.1093/database/bav028
17. Forbes SA, Beare D, Bindal N, Bamford S, Ward S, Cole CG, et al. COSMIC: high-resolution cancer genetics using the catalogue of somatic mutations in cancer. *Curr Protoc Hum Genet*. (2016) 91:10.11.1–37. doi: 10.1002/cphg.21
18. Matos ML, Lapyckyj L, Rosso M, Besso MJ, Mencucci MV, Briggiler CI, et al. Identification of a novel human E-cadherin splice variant and assessment of its effects upon EMT-related events. *J Cell Physiol*. (2017) 232:1368–86. doi: 10.1002/jcp.25622
19. Garcia del Muro X, Torregrosa A, Muñoz J, Castellsagué X, Condom E, Vigués F, et al. Prognostic value of the expression of E-cadherin and beta-catenin in bladder cancer. *Eur J Cancer*. (2000) 36:357–362. doi: 10.1016/s0959-8049(99)00262-2
20. Nakopoulou L, Zervas A, Gakiopoulou-Givalou H, Constantinides C, Doumanis G, Davaris P, et al. Prognostic value of E-cadherin, beta-catenin, P120ctn in patients with transitional cell bladder cancer. *Anticancer Res*. (2000) 20:4571–8.
21. Brennan CM, Steitz JA. HuR and mRNA stability. *Cell Mol Life Sci*. (2001) 58:266–77. doi: 10.1007/PL00000854
22. Aparicio LA, Abella V, Valladares M, Figueroa A. Posttranscriptional regulation by RNA-binding proteins during epithelial-to-mesenchymal transition. *Cell Mol Life Sci*. (2013) 70:4463–77. doi: 10.1007/s00018-013-1379-0
23. Bebee TW, Cieply BW, Carstens RP. Genome-wide activities of RNA binding proteins that regulate cellular changes in the epithelial to mesenchymal transition (EMT). *Adv Exp Med Biol*. (2014) 825:267–302. doi: 10.1007/978-1-4939-1221-6_8
24. Warzecha CC, Carstens RP. Complex changes in alternative pre-mRNA splicing play a central role in the epithelial-to-mesenchymal transition (EMT). *Semin Cancer Biol*. (2012) 22:417–27. doi: 10.1016/j.semcancer.2012.04.003
25. Yu TX, Gu BL, Yan JK, Zhu J, Yan WH, Chen J, et al. CUGBP1 and HuR regulate E-cadherin translation by altering recruitment of E-cadherin mRNA to processing bodies and modulate epithelial barrier function. *Am J Physiol Cell Physiol*. (2016) 310:C54–65. doi: 10.1152/ajpcell.00112.2015
26. Zhang F, Cai Z, Lv H, Li W, Liang M, Wei X, et al. Multiple functions of HuR in urinary tumors. *J Cancer Res Clin Oncol*. (2019) 145:11–8. doi: 10.1007/s00432-018-2778-2
27. Fus LP, Pihowicz P, Koperski L, Marczewska JM, Górnicka B. High cytoplasmic HuR expression is associated with advanced pT stage, high grade and increased microvessel density in urothelial bladder carcinoma. *Ann Diagn Pathol*. (2018) 33:40–4. doi: 10.1016/j.anndiagpath.2017.12.002
28. Winter J, Roepcke S, Krause S, Müller EC, Otto A, Vingron M, et al. Comparative 3'UTR analysis allows identification of regulatory clusters that drive Eph/ephrin expression in cancer cell lines. *PLoS One*. (2008) 3:e2780. doi: 10.1371/journal.pone.0002780
29. David JM, Rajasekaran AK. Dishonorable discharge: the oncogenic roles of cleaved E-cadherin fragments. *Cancer Res*. (2012) 72:2917–23. doi: 10.1158/0008-5472.CAN-11-3498
30. Slaton JW, Karashima T, Perrotte P, Inoue K, Kim SJ, Izawa J, et al. Treatment with low-dose interferon-alpha restores the balance between matrix metalloproteinase-9 and E-cadherin expression in human transitional cell carcinoma of the bladder. *Clin Cancer Res*. (2001) 7:2840–53.
31. Gou Y, Ding W, Xu K, Wang H, Chen Z, Tan J, et al. Snail is an independent prognostic indicator for predicting recurrence and progression in non-muscle-invasive bladder cancer. *Int Urol Nephrol*. (2015) 47:289–93. doi: 10.1007/s11255-014-0874-z
32. Wu K, Zeng J, Zhou J, Fan J, Chen Y, Wang Z, et al. Slug contributes to cadherin switch and malignant progression in muscle-invasive bladder cancer development. *Urol Oncol*. (2013) 31:1751–60. doi: 10.1016/j.urolonc.2012.02.001
33. Tang X, Xing J, Li W, Wu Z, Zhang K, Zheng J. Expression of transcription factor Twist1 in bladder urothelial carcinoma and its clinical significance. *J BUON*. (2013) 18:211–9.

34. Wheelock MJ, Shintani Y, Maeda M, Fukumoto Y, Johnson KR. Cadherin switching. *J Cell Sci*. (2008) 121(Pt 6):727–35. doi: 10.1242/jcs.000455
35. Loh CY, Chai JY, Tang TF, Wong WF, Sethi G, Shanmugam MK, et al. The E-cadherin and N-cadherin switch in epithelial-to-mesenchymal transition: signaling, therapeutic implications, and challenges. *Cells*. (2019) 8:E1118. doi: 10.3390/cells8101118
36. Yu W, Yang L, Li T, Zhang Y. Cadherin signaling in cancer: its functions and role as a therapeutic target. *Front Oncol*. (2019) 9:989. doi: 10.3389/fonc.2019.00989
37. Abufaraj M, Shariat SF, Haitel A, Moschini M, Foerster B, Chłosta P, et al. Prognostic role of N-cadherin expression in patients with non-muscle-invasive bladder cancer. *Urol Oncol*. (2017) 35:264–71. doi: 10.1016/j.urolonc.2017.01.012
38. Muramaki M, Miyake H, Terakawa T, Kumano M, Sakai I, Fujisawa M. Expression profile of E-cadherin and N-cadherin in non-muscle-invasive bladder cancer as a novel predictor of intravesical recurrence following transurethral resection. *Urol Oncol*. (2012) 30:161–6. doi: 10.1016/j.urolonc.2010.01.005
39. Liu B, Miyake H, Nishikawa M, Fujisawa M. Expression profile of epithelial-mesenchymal transition markers in non-muscle-invasive urothelial carcinoma of the bladder: correlation with intravesical recurrence following transurethral resection. *Urol Oncol*. (2015) 33:110.e11–e18. doi: 10.1016/j.urolonc.2014.08.012
40. Abufaraj M, Haitel A, Moschini M, Gust K, Foerster B, Özsoy M, et al. Prognostic role of N-cadherin expression in patients with invasive bladder cancer. *Clin Genitourin Cancer*. (2017) 2017: e73–8. doi: 10.1016/j.clgc.2017.07.001
41. Baumgart E, Cohen MS, Silva Neto B, Jacobs MA, Wotkowicz C, Rieger-Christ KM, et al. Identification and prognostic significance of an epithelial-mesenchymal transition expression profile in human bladder tumors. *Clin Cancer Res*. (2007) 13:1685–94. doi: 10.1158/1078-0432.CCR-06-2330
42. Jäger T, Becker M, Eisenhardt A, Tilki D, Tötsch M, Schmid KW, et al. The prognostic value of cadherin switch in bladder cancer. *Oncol Rep*. (2010) 23:1125–32. doi: 10.3892/or_00000741
43. Szarvas T, Jäger T, Tötsch M, vom Dorp F, Kempkensteffen C, Kovalszky I, et al. Angiogenic switch of angiopietins-Tie2 system and its prognostic value in bladder cancer. *Clin Cancer Res*. (2008) 14:8253–62. doi: 10.1158/1078-0432.CCR-08-0677
44. Rieger-Christ KM, Cain JW, Braasch JW, Dugan JM, Silverman ML, Bouyounes B, et al. Expression of classic cadherins type I in urothelial neoplastic progression. *Hum Pathol*. (2001) 32:18–23. doi: 10.1053/hupa.2001.21140
45. Bryan RT, Atherfold PA, Yeo Y, Jones LJ, Harrison RF, Wallace DM, et al. Cadherin switching dictates the biology of transitional cell carcinoma of the bladder: *ex vivo* and *in vitro* studies. *J Pathol*. (2008) 215:184–94. doi: 10.1002/path.2346
46. Mandeville JA, Silva Neto B, Vanni AJ, Smith GL, Rieger-Christ KM, Zeheb R, et al. P-cadherin as a prognostic indicator and a modulator of migratory behaviour in bladder carcinoma cells. *BJU Int*. (2008) 102:1707–14. doi: 10.1111/j.1464-410X.2008.08115.x
47. Van Marck V, Stove C, Jacobs K, Van den Eynden G, Bracke M. P-cadherin in adhesion and invasion: opposite roles in colon and bladder carcinoma. *Int J Cancer*. (2011) 128:1031–44. doi: 10.1002/ijc.25427
48. Wang P, Lin SL, Zhang LH, Li Z, Liu Q, Gao JX, et al. The prognostic value of P-cadherin in non-muscle-invasive bladder cancer. *Eur J Surg Oncol*. (2014) 40:55–9. doi: 10.1016/j.ejso.2013.12.018
49. Choi W, Porten S, Kim S, Willis D, Plimack ER, Hoffman-Censits J, et al. Identification of distinct basal and luminal subtypes of muscle-invasive bladder cancer with different sensitivities to frontline chemotherapy. *Cancer Cell*. (2014) 25:152–65. doi: 10.1016/j.ccr.2014.01.009
50. Thievessen I, Seifert HH, Swiatkowski S, Florl AR, Schulz WA. E-cadherin involved in inactivation of WNT/beta-catenin signalling in urothelial carcinoma and normal urothelial cells. *Br J Cancer*. (2003) 88:1932–8. doi: 10.1038/sj.bjc.6601031
51. Henderson BR, Fagotto F. The ins and outs of APC and beta-catenin nuclear transport. *EMBO Rep*. (2002) 3:834–9. doi: 10.1093/embo-reports/kvf181
52. Voronkov A, Krauss S. Wnt/beta-catenin signaling and small molecule inhibitors. *Curr Pharm Des*. (2013) 19:634–64. doi: 10.2174/138161213804581837
53. Elserafy FA, Elbaky TMA, Elsherif EAR, Nor-Eldin-Elkady NM, Dawood MM, Ei Gharabawy MS. Evaluation of β-Catenin expression in muscle-invasive urothelial bladder carcinoma. *Menoufia Med J*. (2015) 27:507–13. doi: 10.4103/1110-2098.145491
54. Maurya N, Singh R, Goel A, Singhai A, Singh UP, Agrawal V, et al. Clinicohistopathological implications of phosphoserine 9 glycogen synthase kinase-3β/ β-catenin in urinary bladder cancer patients. *World J Clin Oncol*. (2019) 10:166–82. doi: 10.5306/wjco.v10.i4.166
55. Liu C, Li Y, Semenov M, Han C, Baeg GH, Tan Y, et al. Control of beta-catenin phosphorylation/degradation by a dual-kinase mechanism. *Cell*. (2002) 108:837–47. doi: 10.1016/s0092-8674(02)00685-2
56. Roy S, Pradhan D, Ernst WL, Mercurio S, Najjar Y, Parikh R, et al. Next-generation sequencing-based molecular characterization of primary urinary bladder adenocarcinoma. *Mod Pathol*. (2017) 30:1133–43. doi: 10.1038/modpathol.2017.33
57. Batlle E, Henderson JT, Beghtel H, van den Born MM, Sancho E, Huls G, et al. Beta-catenin and TCF mediate cell positioning in the intestinal epithelium by controlling the expression of EphB/ephrinB. *Cell*. (2002) 111:251–63. doi: 10.1016/s0092-8674(02)01015-2
58. Boitard M, Bocchi R, Egervari K, Petrenko V, Viale B, Gremaud S, et al. Wnt signaling regulates multipolar-to-bipolar transition of migrating neurons in the cerebral cortex. *Cell Rep*. (2015) 10:1349–61. doi: 10.1016/j.celrep.2015.01.061
59. Tice DA, Szeto W, Soloviev I, Rubinfeld B, Fong SE, Dugger DL, et al. Synergistic induction of tumor antigens by Wnt-1 signaling and retinoic acid revealed by gene expression profiling. *J Biol Chem*. (2002) 277:14329–35. doi: 10.1074/jbc.M200334200
60. Tanaka M, Sasaki K, Kamata R, Sakai R. The C-terminus of ephrin-B1 regulates metalloproteinase secretion and invasion of cancer cells. *J Cell Sci*. (2007) 120(Pt 13):2179–2189. doi: 10.1242/jcs.008607
61. Sikkema AH, den Dunnen WF, Hulleman E, van Vuurden DG, Garcia-Manero G, Yang H, et al. EphB2 activity plays a pivotal role in pediatric medulloblastoma cell adhesion and invasion. *Neuro Oncol*. (2012) 14:1125–35. doi: 10.1093/neuonc/nos130
62. Sawai Y, Tamura S, Fukui K, Ito N, Imanaka K, Saeki A, et al. Expression of ephrin-B1 in hepatocellular carcinoma: possible involvement in neovascularization. *J Hepatol*. (2003) 39:991–996. doi: 10.1016/s0168-8278(03)00498-7
63. Castellvi J, Garcia A, de la Torre J, Hernandez J, Gil A, Xercavins J, et al. Ephrin B expression in epithelial ovarian neoplasms correlates with tumor differentiation and angiogenesis. *Hum Pathol*. (2006) 37:883–9. doi: 10.1016/j.humpath.2006.02.021
64. Kataoka H, Tanaka M, Kanamori M, Yoshii S, Ihara M, Wang YJ, et al. Expression profile of EFNB1, EFNB2, two ligands of EPHB2 in human gastric cancer. *J Cancer Res Clin Oncol*. (2002) 128:343–8. doi: 10.1007/s00432-002-0355-0
65. Abraham S, Knapp DW, Cheng L, Snyder PW, Mittal SK, Bangari DS, et al. Expression of EphA2 and Ephrin A-1 in carcinoma of the urinary bladder. *Clin Cancer Res*. (2006) 12:353–60. doi: 10.1158/1078-0432.CCR-05-1505
66. Ozgür E, Heidenreich A, Dagtekin O, Engelmann U, Bloch W. Distribution of EphB4 and EphrinB2 in normal and malignant urogenital tissue. *Urol Oncol*. (2011) 29:78–84. doi: 10.1016/j.urolonc.2008.12.020
67. Tang XX, Brodeur GM, Campling BG, Ikegaki N (1999). Coexpression of transcripts encoding EPHB receptor protein tyrosine kinases and their ephrin-B ligands in human small cell lung carcinoma. *Clin Cancer Res.* 5:455–460.
68. Khansaard W, Techasen A, Namwat N, Yongvanit P, Khuntikeo N, Puapairoj A, et al. Increased EphB2 expression predicts cholangiocarcinoma metastasis. *Tumour Biol*. (2014) 35:10031–41. doi: 10.1007/s13277-014-2295-0
69. Gao Q, Liu W, Cai J, Li M, Gao Y, Lin W, et al. EphB2 promotes cervical cancer progression by inducing epithelial-mesenchymal transition. *Hum Pathol*. (2014) 45:372–81. doi: 10.1016/j.humpath.2013.10.001
70. Li X, Choi WW, Yan R, Yu H, Krasnoperov V, Kumar SR, et al. The differential expression of EphB2 and EphB4 receptor kinases in normal

bladder and in transitional cell carcinoma of the bladder. *PLoS ONE*. (2014) 9:e105326. doi: 10.1371/journal.pone.0105326
71. Bong YS, Lee HS, Carim-Todd L, Mood K, Nishanian TG, Tessarollo L, et al. ephrinB1 signals from the cell surface to the nucleus by recruitment of STAT3. *Proc Natl Acad Sci USA*. (2007) 104:17305–10. doi: 10.1073/pnas.0702337104
72. Kamran MZ, Patil P, Gude RP. Role of STAT3 in cancer metastasis and translational advances. *Biomed Res Int*. (2013) 2013:421821. doi: 10.1155/2013/421821
73. Santoni M, Conti A, Piva F, Massari F, Ciccarese C, Burattini L, et al. Role of STAT3 pathway in genitourinary tumors. *Future Sci OA*. (2015) 1:FSO15. doi: 10.4155/fso.15.13
74. Dohn LH, Illemann M, Høyer-Hansen G, Christensen IJ, Hostmark J, Litlekalsoy J, et al. Urokinase-type plasminogen activator receptor (uPAR) expression is associated with T-stage and survival in urothelial carcinoma of the bladder. *Urol Oncol*. (2015) 33:165.e15–24. doi: 10.1016/j.urolonc.2014.12.001
75. Hiendlmeyer E, Regus S, Wassermann S, Hlubek F, Haynl A, Dimmler A, et al. Beta-catenin up-regulates the expression of the urokinase plasminogen activator in human colorectal tumors. *Cancer Res*. (2004) 64:1209–14. doi: 10.1158/0008-5472.can-3627-2
76. Lodola A, Giorgio C, Incerti M, Zanotti I, Tognolini M. Targeting Eph/ephrin system in cancer therapy. *Eur J Med Chem*. (2017) 142:152–62. doi: 10.1016/j.ejmech.2017.07.029

Conflict of Interest: The authors declare that the research was conducted in the absence of any commercial or financial relationships that could be construed as a potential conflict of interest.

frontiers in Oncology

ORIGINAL RESEARCH
published: 24 April 2020
doi: 10.3389/fonc.2020.00623

CK14 Expression Identifies a Basal/Squamous-Like Type of Papillary Non-Muscle-Invasive Upper Tract Urothelial Carcinoma

Minsun Jung[1], *Insoon Jang*[2], *Kwangsoo Kim*[2] *and Kyung Chul Moon*[1,3]*

[1] Department of Pathology, Seoul National University Hospital, Seoul, South Korea, [2] Division of Clinical Bioinformatics, Biomedical Research Institute, Seoul National University Hospital, Seoul, South Korea, [3] Medical Research Center, Kidney Research Institute, Seoul National University College of Medicine, Seoul, South Korea

Object: CK14 expression is an important marker of basal/squamous-like (BASQ)-type muscle-invasive bladder carcinoma, and this molecularly defined subtype has a poor prognosis and a distinct response to chemotherapy. However, CK14 expression and its clinicopathological and molecular significance in papillary non-muscle-invasive upper tract urothelial carcinoma (NMIUTUC) remain unknown. Herein, we investigated the prognostic implications of immunohistochemical (IHC) staining for CK14 and the transcriptional characteristics associated with CK14 expression in papillary NMIUTUC.

Materials and Methods: IHC staining for CK14 was conducted in 204 papillary NMIUTUC specimens. Positive CK14 IHC staining was defined as a positive signal in >0% of tumor cells. RNA sequencing data were analyzed from 8 papillary high-grade NMIUTUC specimens consisting of 4 CK14-positive and 4 CK14-negative tumors.

Results: CK14 positivity was associated with a high TNM stage ($p < 0.001$) and a high World Health Organization grade ($p = 0.003$). Survival analysis showed that CK14 positivity was significantly associated with poor progression-free survival ($p = 0.015$; hazard ratio [HR] = 2.990; 95% confidence interval [CI] = 1.180–7.580) and was marginally associated with poor cancer-specific survival ($p = 0.052$; HR = 3.77; 95% CI = 0.900–15.780). Gene set enrichment analysis demonstrated that the CK14-positive tumors were associated with a basal subtype of breast cancer, squamous cell carcinoma development, p40, tumor necrosis factor α-nuclear factor-κB, and p53 pathways, and embryonic stem cells; these characteristics are reminiscent of the BASQ subtype. In addition, with a $p < 0.05$ and |fold change| ≥2 as the cutoffs, we identified 178 differentially expressed genes when comparing CK14-positive and CK14-negative tumors. Functional analysis of these genes revealed several networks and gene ontology terms related to the positive regulation of cellular proliferation in CK14-positive tumors. Consistent with these results, we demonstrated that the mean Ki-67 proliferative index was higher in CK14-positive tumors than it was in CK14-negative tumors (2.3 vs. 0.8%, respectively, $p = 0.002$).

OPEN ACCESS

Edited by:
Woonyoung Choi,
The Johns Hopkins Hospital,
United States

Reviewed by:
Felix KH Chun,
University Medical Center Hamburg-Eppendorf, Germany
Anirban P. Mitra,
University of Southern California,
United States

***Correspondence:**
Kyung Chul Moon
blue7270@gmail.com

Specialty section:
This article was submitted to Genitourinary Oncology, a section of the journal Frontiers in Oncology

Received: *16 January 2020*
Accepted: *03 April 2020*
Published: *24 April 2020*

Citation:
Jung M, Jang I, Kim K and Moon KC (2020) CK14 Expression Identifies a Basal/Squamous-Like Type of Papillary Non-Muscle-Invasive Upper Tract Urothelial Carcinoma. Front. Oncol. 10:623. doi: 10.3389/fonc.2020.00623

Conclusion: CK14-positive papillary NMIUTUC is an aggressive subtype with BASQ-like molecular characteristics and dynamic proliferative activity. We propose that CK14 IHC staining can be a useful biomarker of BASQ-type papillary NMIUTUC that can be applied in daily practice with the aim of precision oncology.

Keywords: Cytokeratin 14, carcinoma, transitional cell, upper tract urothelial carcinoma, prognosis, gene expression profiling, high-throughput nucleotide sequencing, basal/squamous-like

INTRODUCTION

Muscle-invasive bladder carcinoma (MIBC) is broadly classified into basal and luminal subtypes based on transcription profiles (1–5). The basal subtype shows basal/squamous/stem cell-like features: high expression of basal-type genes (*KRT5*, *KRT6*, *KRT14*, *CD44*, *CDH3*, *TGM1*, *DSC3*, *MYC*, and *EGFR*), low levels of luminal-type genes (*KRT20*, *PPARG*, *GATA3*, *FOXA1*, *ERBB2*, and *UPK*s), active signaling pathways [p63, c-myc, signal transducer and activator of transcription 3, and nuclear factor-κB (NF-κB)], and frequent squamous differentiation (1, 4, 6). In addition, basal-type MIBC has a worse prognosis than the luminal subtype, but it may respond well to cytotoxic chemotherapies (1, 7). Recently, it was also suggested that genetic subtypes of MIBC may determine susceptibility to immune checkpoint inhibitors (8, 9). However, the basal subtypes defined by various independent studies contain a diversity in detailed molecular and phenotypic characteristics. In an attempt to explore the common ground, therefore, a consensus was reached regarding the existence and the definition of the common basal/squamous-like (BASQ) subtype: MIBC with high expression of CK14 and CK5/6 but low expression of GATA3 and FOXA1 (10). Immunohistochemical (IHC) staining for these markers is a readily accessible technique that helps to standardize the assessment of the BASQ subtype (11, 12).

On the other hand, accumulating evidence demonstrates that non-muscle-invasive urothelial carcinoma has a clinical-pathological-genetic association that is distinct from (and occasionally even contradictory to) what has been characterized in MIBC. For example, Hedegaard and colleagues (13) demonstrated that the luminal-like (e.g., high *KRT20*/*UPK*s and low *KRT5*/*CD44*) gene expression cluster of non-muscle-invasive bladder carcinoma (NMIBC) had worse clinical outcomes than what was observed in the basal-like cluster. Different studies further support the association between luminal-like type and either advanced pathological states or short survival durations in NMIBC using CK5/6 (*KRT5/KRT6)* and CK20 (*KRT20*) as surrogate protein or mRNA markers (14–16). In line with these results when studying the urinary bladder, we previously reported that papillary non-muscle-invasive upper tract urothelial carcinoma (NMIUTUC) with luminal-like, CK5/6-negative/CK20-positive, or CD44-negative/CK20-positive, immunophenotypes had distinctly poor prognoses that were probably associated with altered cell adhesion and late cell cycle/proliferation functions (17, 18).

Despite these conflicting results observed regarding some of the subtype-defining markers in early urothelial carcinoma, high *KRT14* levels were independently prognostic of poor survival both in NMIBC and in MIBC (19). CK14 is a type I acidic keratin that is expressed in mitotically active basal cells of the stratified epithelium, where it promotes proliferation, and differentiation and in turn supports structural integrity (20). As CK14-positive basal cells differentiate into umbrella cells in the normal urothelium, CK14 expression is reduced and replaced by CK20. Consistent with this observation, Volkmer et al. (19) and Ho et al. (21) demonstrated that CK14 defined the most primitive/least differentiated basal-type urothelial carcinoma, which preceded the emergence of cancer cells expressing CK5 (intermediately differentiated) or CK20 (well-differentiated); further, CK14 expression marked the highly tumorigenic stem cell population. The increase in CK14 immunoreactivity was also observed at an early carcinogenesis stage, initiating the appearance of malignant lesions of the urinary bladder in a rat model (22). Moreover, CK14-positive urothelial carcinoma cells might have a predilection for chemoresistance (23). In addition, CK14 was associated with a poor prognosis of other malignancies, including breast cancer, squamous cell carcinoma, and salivary gland carcinoma, because it triggers proliferation, dedifferentiation, invasion, and metastasis of these cancers (24–26). However, how CK14 overexpression regulates the progression of urothelial carcinoma has not been fully elucidated. Furthermore, because of the rarity of upper tract urothelial carcinoma, which accounts for only 5–10% of the total urothelial carcinoma (27), CK14 expression and its clinicopathological and molecular significance in papillary NMIUTUC has not been studied. Herein, we investigated the prognostic implications of IHC staining for CK14 in 204 papillary NMIUTUC specimens. In addition, we analyzed the transcriptional characteristics associated with CK14 expression in papillary NMIUTUC.

MATERIALS AND METHODS

The clinical and prognostic significance of CK14 expression was determined in a prognosis cohort using IHC staining of tissue microarray (TMA) slides. Transcriptional characteristics associated with CK14 expression were evaluated in the high-grade GEP cohort composed of fresh-frozen NMIUTUC samples. As supplement, we subsidiarily assembled the low-grade NMIBC cohort using Lund urinary bladder data. This study was approved by the regional Institutional Review Board (H-1911-029-1077), and informed consent was waived by the Review Board.

Prognosis Cohort and TMA

Formalin-fixed paraffin-embedded blocks of 204 NMIUTUC specimens (195 radical nephroureterectomy and 9 ureterectomy) were collected from the pathologic archive of Seoul National

University Hospital (prognosis cohort). Clinicopathological and follow-up data were obtained from medical records. The staging and grading evaluation followed the American Joint Committee on Cancer 8th TNM staging system and World Health Organization (WHO) 2004/2016 classification, respectively (28). Triplicate 2 mm cores of tumor area were utilized for TMA experiments (Superbiochips Laboratories, Seoul, Republic of Korea).

Immunohistochemical Staining

IHC staining for CK14 (1:300; LL002; Cell Marque Cat# 314M-14, RRID:AB_1159418, Rocklin, CA, US) and Ki-67 (1:100; MIB-1; Agilent Cat# M7240, RRID:AB_2142367, Santa Clara, CA, US) was conducted on 4-μm-thick TMA sections with a Benchmark autostainer (Ventana, Tucson, AZ, US), according to the manufacturer's instructions. IHC staining revealed that CK14 expression was variable and included the following patterns: absent, focal staining in a few tumor cells, immunoreactivity confined to the basal layer, or diffuse staining with or without occasional strong signal detected in the basal layer (**Supplementary Figure 1**). Because CK14 and Ki-67 stains are routinely conducted for diagnostic purposes in various organs and the staining protocols are firmly established, we did not use positive or negative controls. Considering the prognostic significance and sample distribution, immunoreactivity in >0% of tumor cells was defined as positive CK14 IHC staining (**Supplementary Figure 2**). Two pathologists (MJ and KCM) read the CK14 IHC slides. Intra/inter-observer variability was minimal due to the clear and straightforward staining result. The mean Ki-67 proliferative index (%) was quantitatively measured using QuPath (version 0.1.2) (29) on TMA slides that were virtually scanned (Aperio AT2, Leica Biosystem, Wetzlar, Germany). For 189 patients, IHC profiles for CK5/6 and CK20 were retrieved from our previous study (17). Briefly, positive CK5/6 and CK20 IHC staining was defined as >20 and >1%, respectively. CK5/6-other staining referred to either a positive expression or CK5/6 expression confined to the basal layer. CK20-other staining referred to either a negative reaction or CK20 expression that was restricted to umbrella cells.

Gene Expression Profile (GEP) Cohorts

GEP analysis in the context of CK14 protein expression was determined from RNA sequencing and CK14 IHC staining data from independent high-grade papillary NMIUTUC specimens, which were generated previously (18). In short, surgically resected fresh tumors were cut in half: one half was subjected to RNA sequencing using a HiSeq 2500 platform (Illumina, San Diego, CA, US), and the other half was embedded in paraffin blocks for evaluation of CK14 immunoexpression. According to the same cutoff criteria used for CK14 positivity (>0%), 4 CK14-positive and 4 CK14-negative high-grade papillary NMIUTUC samples were assembled as the high-grade GEP cohort.

In our RNA sequencing depository, there were too few CK14-positive low-grade papillary NMIUTUC specimens to analyze. Therefore, we used Lund urinary bladder carcinoma mRNA data (GSE32894) to determine GEP related to CK14 expression in papillary low-grade early urothelial carcinoma (5). Clinicopathological details and CK14 IHC expression of these samples were obtained from another source, as summarized in **Supplementary Table 1** (30). The previous annotation "urothelial-like histology," indicating clear separation between tumor and stroma and well-arranged tumor cells with homogenous nuclei, was tentatively accepted as a papillary architecture in NMIBC (30). Consequently, a low-grade NMIBC cohort (6 CK14-positive and 25 CK14-negative NMIBCs) was created with the following inclusion criteria: (1) stage Ta or T1, (2) grade 1 [WHO 1999 guideline (28)], and (3) "urothelial-like histology." CK14 positivity (IHC tumor cell score >0) and negativity (IHC tumor cell score = 0) were designated as above (30). For these 31 cases, gene expression data were preprocessed according to previous methods (5). Differentially expressed genes (DEG)s between CK14-positive and CK14-negative tumors were analyzed in both the high-grade GEP cohort and low-grade NMIBC cohort.

Functional Enrichment and Network Analysis

Gene set enrichment analysis (GSEA) was performed against public gene sets (31). The networks and functional analyses were generated through the use of Ingenuity Pathway Analysis with a Benjamini-Hochberg false discovery rate (FDR) <0.05 as the cutoff (32). Based on the knowledge database, IPA determines local networks and functional terms that are particularly enriched for the input DEG sets. Gene ontology (GO) (33, 34) and Kyoto encyclopedia of genes and genomes (KEGG) (35) analyses were also performed. In addition, a Metascape membership search of GO themes was conducted, as previously described (36).

Statistics

The association between clinicopathological variables and IHC results was analyzed by Pearson's $\chi 2$-test with Yate's correction or Fisher's exact test. Progression-free survival (PFS) was defined as the interval between surgery and upper urinary tract recurrence or distant metastasis, or the last follow-up visit. Cancer-specific survival (CSS) was defined as the interval between surgery and cancer-related death or the last follow-up visit. Overall survival (OS) was calculated as the term between surgery and death or the last follow-up visit. Kaplan-Meier analyses with log-rank tests were used to compare survival. A Cox proportional hazards regression model was used to calculate the hazard ratio (HR) and confidence interval (CI) in univariate and multivariate analyses. A two-tailed $p < 0.05$ was considered statistically significant. All statistical analyses were performed with SPSS 25 (IBM, Armonk, NY) or R.

RESULTS

Clinicopathological Association of CK14 IHC Staining

Clinicopathological details of patients in the prognosis cohort and their association with CK14 expression are summarized in **Table 1**. Briefly, the median age was 67 years (range, 29–95) at diagnosis, and the male-to-female sex ratio was 4.1:1. IHC staining for CK14 was positive in 139 (68.1%) patients and

TABLE 1 | Clinicopathological details of the prognosis cohort associated with CK14 expression.

Variables	CK14-negative (n = 139, %)	CK14-positive (n = 65, %)	Total (N = 204, %)	P
Age				0.190
<67	73 (52.5)	27 (41.5)	100 (49.0)	
≥67	66 (47.5)	38 (58.5)	104 (51.0)	
Sex				0.775
Female	26 (18.7)	14 (21.5)	40 (19.6)	
Male	113 (81.3)	51 (78.5)	164 (80.4)	
Multifocality				0.685
Absent	128 (92.1)	58 (89.2)	186 (91.2)	
Present	11 (7.9)	7 (10.8)	18 (8.8)	
TNM stage				<0.001
0	61 (43.9)	9 (13.8)	70 (34.3)	
≥I	78 (56.1)	56 (86.2)	134 (65.7)	
WHO grade				0.003
Low	86 (61.9)	25 (38.5)	111 (54.4)	
High	53 (38.1)	40 (61.5)	93 (45.6)	
CK5/6-CK20*				0.001
Neg-Other	22 (16.9)	12 (20.3)	34 (18.0)	
Neg-Pos	31 (23.8)	27 (45.8)	58 (30.7)	
Other-Other	34 (26.2)	3 (5.1)	37 (19.6)	
Other-Pos	43 (33.1)	17 (28.8)	60 (31.7)	

Data are available in 189 patients.

CK, cytokeratin; IVR, intravesical recurrence; TNM, tumor-node-metastasis; WHO, World Health Organization; Neg, negative; Pos, positive.

negative in 65 (31.9%) patients. CK14 positivity was associated with high (≥I) TNM stage ($p < 0.001$) and high WHO grade ($p = 0.003$). In addition, CK14 positivity was related to combined CK5/6-CK20 expression ($p = 0.001$), where CK5/6-negative/CK20-positive expression was more prevalent in CK14-positive tumors (45.8 vs. 23.8%).

Prognostic Implications of CK14 IHC Staining

In the survival analysis, CK14 positivity was significantly associated with poor PFS ($p = 0.015$; HR = 2.990; 95% CI = 1.180–7.580) and was marginally associated with poor CSS ($p = 0.052$; HR = 3.77; 95% CI = 0.900–15.780) and OS ($p = 0.275$; HR = 1.44; 95% CI = 0.750–2.760) (**Figure 1**). However, when adjusted for TNM stage, WHO grade and multifocality, CK14 expression failed to show significant association with PFS, while WHO grade and multifocality were independent prognostic factors of papillary NMIUTUC (**Table 2**).

Transcriptional Characteristics Associated With CK14 Expression

The median age of the high-grade GEP cohort was 67 years (range, 56–78) with a male-to-female sex ratio of 1.7:1. The renal pelvis/calyx (50%) and ureter (50%) were equally affected. One tumor was in stage pTa, and the other 7 tumors were in pT1. After exclusion of genes with 0 fragments in any sample, 15,395 genes were identified across the high-grade GEP cohort (**Supplementary Data 1**). GSEA demonstrated that CK14-positive tumors were associated with a basal subtype of breast cancer (FDR = 0.0), tumorigenesis of squamous cell

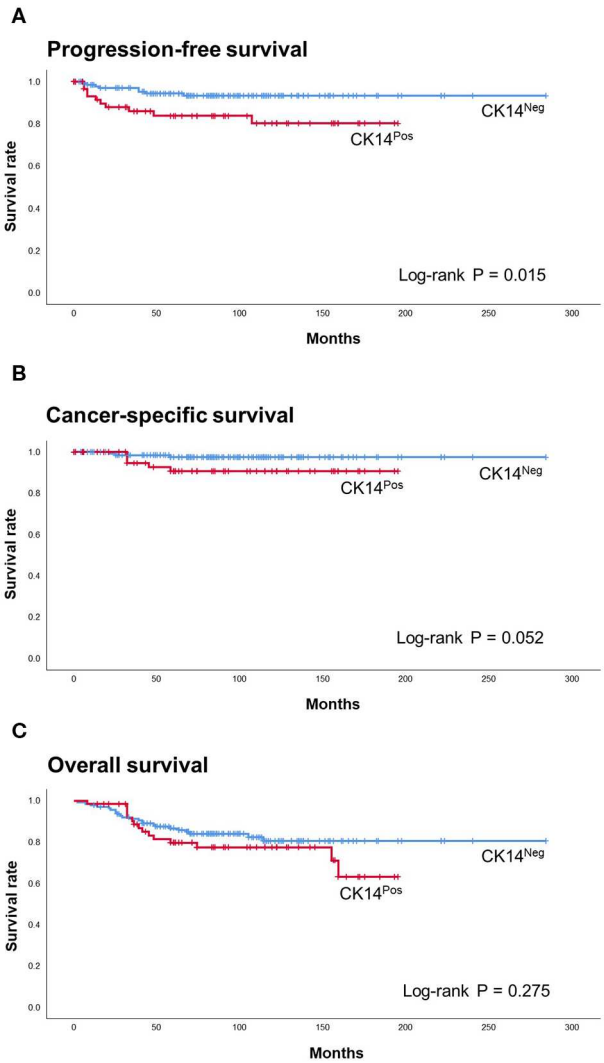

FIGURE 1 | Kaplan-Meier with log-rank test of CK14 IHC staining in PFS **(A)**, CSS **(B)**, and OS **(C)** of the prognosis cohort.

TABLE 2 | Multivariate analysis of progression-free survival.

	Adjusted HR	95% CI	P
CK14			
Positive vs. negative	1.995	0.731–5.448	0.178
TNM stage			
≥I vs. 0	1.308	0.442–3.867	0.628
WHO grade			
High vs. low	6.300	1.742–22.784	0.005
Multifocality			
Present vs. absent	3.515	1.130–10.934	0.030

HR, hazard ratio; CI, confidence interval; CK, cytokeratin.

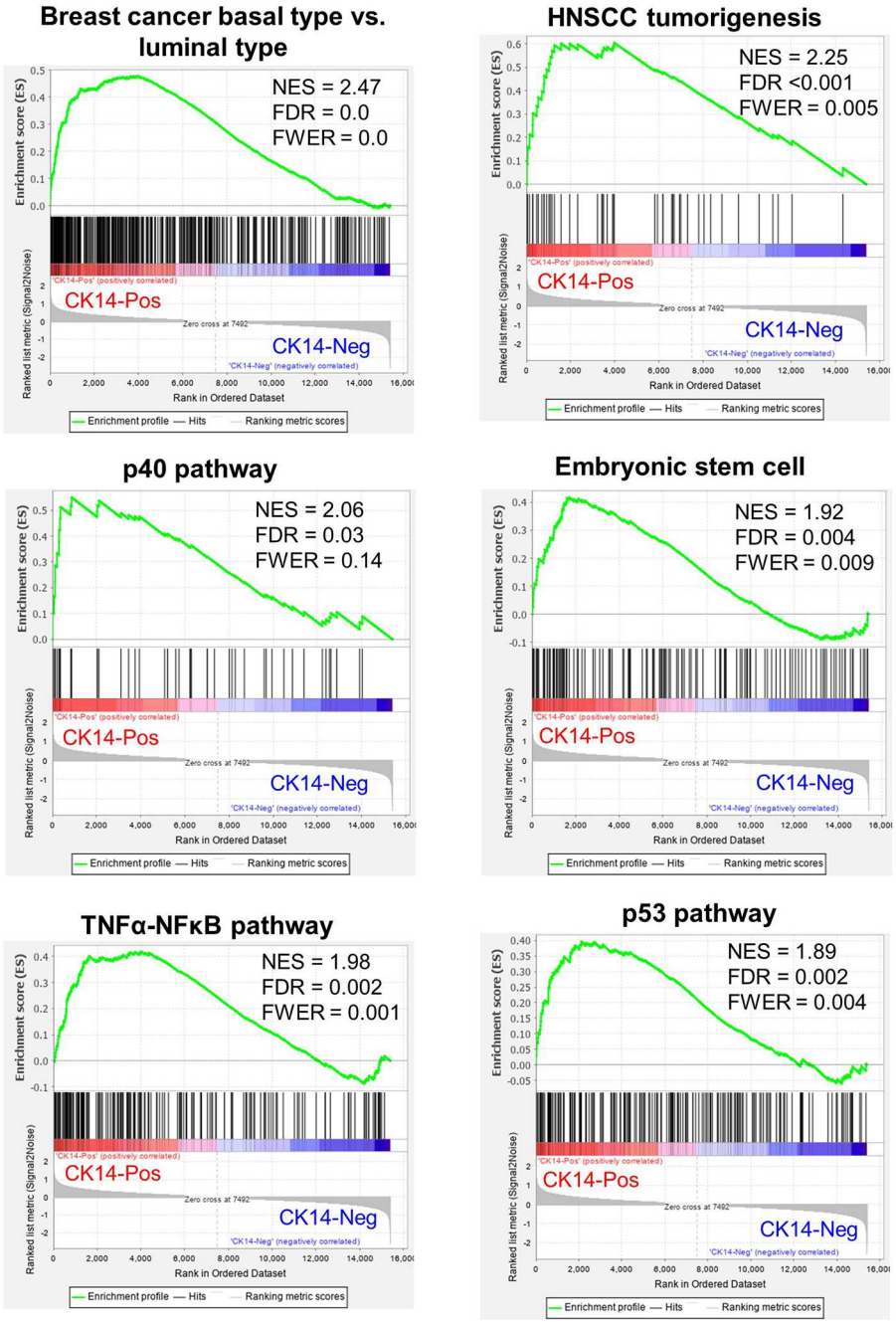

FIGURE 2 | Representative GSEA results enriched in CK14-positive tumors in the high-grade GEP cohort. NES, normalized enrichment score; FDR, false discovery rate; FWER, family-wise error rate; HNSCC, head and neck squamous cell carcinoma.

carcinoma (FDR <0.001), the p40 (ΔNp63) pathway (FDR = 0.03), embryonic stem cell activities (FDR = 0.004), the tumor necrosis factor-α-NF-κB pathway (FDR = 0.002) and the p53 pathway (FDR = 0.002) (**Figure 2**). In addition, a poorly differentiated state of squamous cell carcinoma (FDR = 0.0), c-myc (FDR = 0.002), EGFR (FDR = 0.004), Wnt (FDR = 0.004), and mammalian target of rapamycin complex 1 (mTORC1) (FDR = 0.025) cascades, cell migration (FDR <0.001) and epithelial-mesenchymal transition (EMT) (FDR = 0.025) were also significantly associated with CK14 expression in high-grade papillary NMIUTUC.

With a $p < 0.05$ and $|\text{fold change}| \geq 2$ as the cutoffs, we identified 178 DEGs in the high-grade GEP cohort; of those identified, 103 and 75 genes were highly and

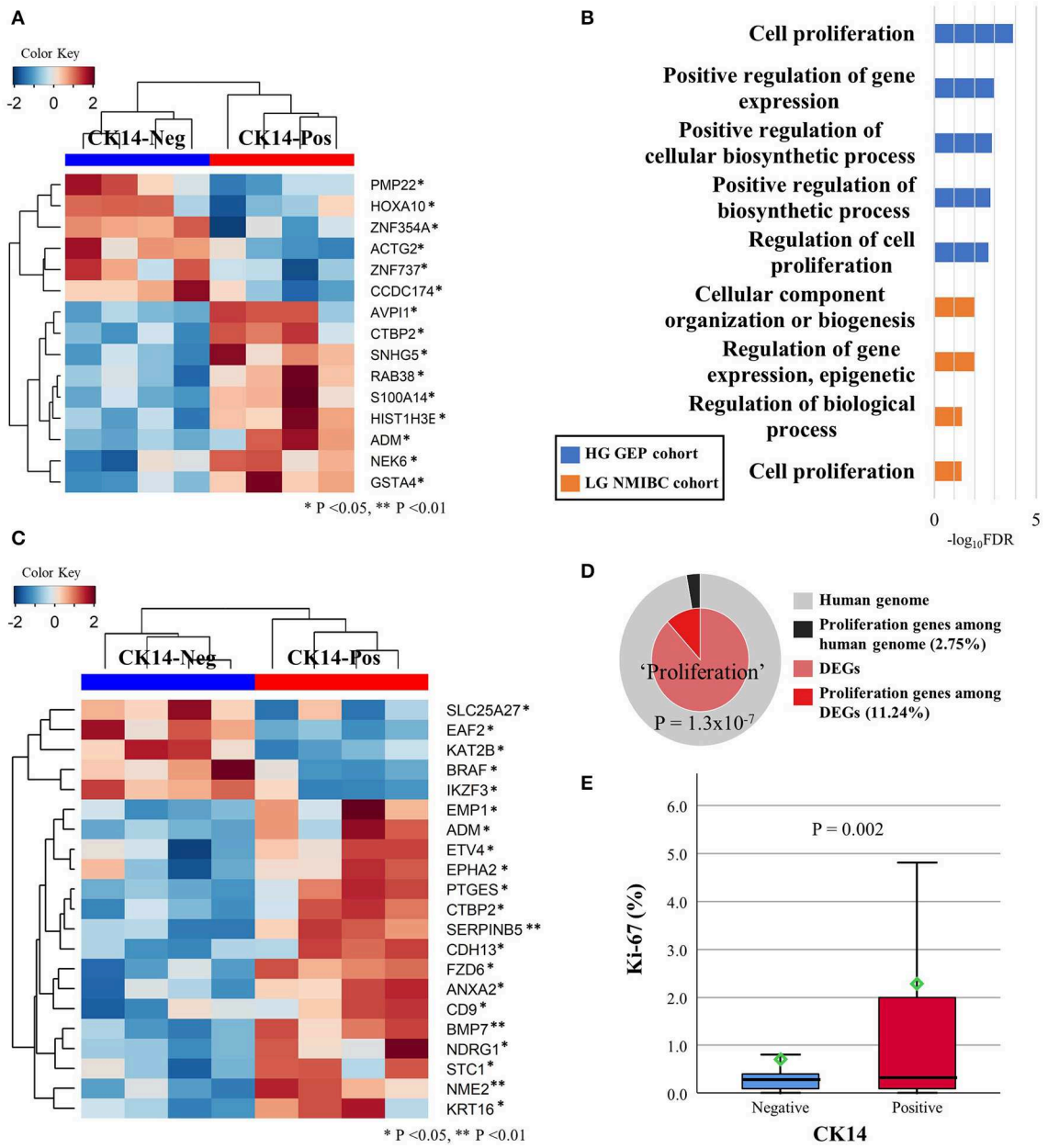

FIGURE 3 | DEGs in the high-grade GEP cohort that are involved in cellular growth and proliferation network, as revealed by IPA **(A)**. Several GO-biologic process terms associated with proliferation were identified in the high-grade GEP cohort (blue) and the low-grade NMIBC cohort (orange) **(B)**. Unsupervised clustering analysis of the DEGs included in the "cell proliferation" (GO: 0008283) GO term in the high-grade GEP cohort **(C)**. Membership search of proliferation-related GO signatures enriched in the high-grade GEP cohort **(D)**. The Ki-67 proliferative index is much higher in CK14-positive tumors than it is in CK14-negative tumors in the prognosis cohort **(E)**.

lowly expressed, respectively, in CK14-positive tumors (**Supplementary Figure 3A**). *KRT14* gene was highly expressed in CK14-positive tumors compared to CK14-negative tumors (fold change = 40.2, p = 0.035). IPA identified "cellular growth and proliferation" as one of the highest scored networks specifically related to CK14 expression (**Figure 3A**, **Supplementary Figure 4**). Other network-associated functions that were influenced by CK14 expression mainly included "cellular movement" and "cancer" (**Table 3**). IPA also identified significant enrichment of cellular movement/invasion and cell death functions, which were upregulated and downregulated, respectively, in CK14-positive tumors (**Table 4**). Consistent with these results, several GO and KEGG terms related to cell proliferation and cell component biosynthesis (e.g., "cell proliferation," FDR <0.001; "positive regulation of gene

expression," FDR = 0.001), cell death (e.g., "cell death" and "apoptotic process"; both, FDR <0.001), adhesion (e.g., "cell adhesion" and "biologic adhesion"; both, FDR <0.001) and "pathways in cancer" (FDR <0.001) were identified (**Figures 3B,C**, **Supplementary Table 2**). Furthermore, GO themes related to proliferation ("cell proliferation," "positive regulation of cell proliferation," "epithelial cell proliferation," and "regulation of epithelial cell proliferation") were particularly enriched within the DEGs when compared to their representation within the human genome ($p = 1.3 \times 10^{-7}$) (**Figure 3D**).

A similar comparison of the low-grade NMIBC cohort identified 26 DEGs between CK14-positive and CK14-negative tumors. In unsupervised clustering analysis, all CK14-positive tumors and 3 CK14-negative tumors (UC_0041_2, UC_0240_1 and UC_0414_1) were grouped together by these DEGs (**Supplementary Figure 3B**). There was one gene (*CLCA4*) that was upregulated in CK14-positive tumors both in the high-grade GEP cohort and the low-grade NMIBC cohort. In agreement with the high-grade GEP cohort, cellular growth and proliferation overrepresented the biological functions associated with CK14 expression in the low-grade NMIBC cohort, as revealed by the IPA network search (**Table 3**, **Supplementary Figure 5**) and GO analysis (**Figure 3B**, **Supplementary Table 2**).

Next, we tried to validate the difference in cellular proliferation between CK14-positive and CK14-negative papillary NMIUTUC using Ki-67 IHC staining. CK14-positive tumors displayed a 2.3 ± 5.36% proliferative index (mean ± standard deviation), which was higher than 0.8 ± 2.06% index of CK14-negative tumors in the prognosis cohort (Mann-Whitney U, $p = 0.002$) (**Figure 3E**).

DISCUSSION

In this study, we demonstrated that positive IHC staining for CK14 was associated with high-risk phenotypes of papillary NMIUTUC and was predictive for unfavorable survival rates. We compared CK14-positive and CK14-negative high-grade papillary NMIUTUC at the mRNA level to define a molecular framework underlying CK14 expression in papillary NMIUTUC. We found that CK14 positivity in papillary high-grade NMIUTUC marked transcriptional characteristics reminiscent of those in BASQ-type MIBC, including signatures of basal/stem cell and squamous cell carcinoma. This CK14-positive BASQ-like subtype was characterized by high proliferative functions in high-grade papillary NMIUTUC as well as in low-grade papillary NMIBC. IHC staining for Ki-67 verified a much higher

TABLE 4 | Functional enrichment in CK14-positive tumors in the high-grade GEP cohort as assessed by Ingenuity Pathway Analysis.

Category	Function	Activation z-score*	FDR
Cellular Movement	Invasion of tumor cell lines	1.491	0.00251
	Cell movement of tumor cell lines	1.947	0.00255
	Invasion of cells	1.674	0.00255
	Migration of tumor cell lines	2.185	0.0058
	Migration of cells	1.975	0.0169
	Cell movement	1.658	0.0182
Cell death and survival	Necrosis	−1.246	0.00218
	Apoptosis	−1.159	0.00316
	Cell death of tumor cell lines	−1.361	0.00393
	Apoptosis of tumor cell lines	−1.658	0.0274

GEP, gene expression profile; FDR, false discovery rate (Benjamini Hochberg).
**z-scores indicate activation (>0) or inhibition (<0) of the predicted function based on the fold change of the DEGs (upregulation or downregulation) and its agreement with the functions.*

TABLE 3 | Networks associated with CK14 positivity as assessed by Ingenuity Pathway Analysis.

Network	DEGs	Score
High-grade GEP cohort		
Digestive system development and function, gastrointestinal disease, organ morphology	*NIPAL2*, *AIFM3*, *EMP1*, *PLK2*, *TBC1D3*, *CAPN2*, *ARHGAP32*, *NPIPA8*, *BRAF*, *MPZL2*, *LMO7*, *SERPINB5*, *PERP*, *COL17A1*, *KRT14*, *ERCC5*	22
Cellular growth and proliferation, cellular development, gene expression	*PMP22*, *HOXA10*, *ZNF354A*, *ACTG2*, *ZNF737*, *CCDC174*, *AVPI1*, *CTBP2*, *SNHG5*, *RAB38*, *S100A14*, *HIST1H3E*, *ADM*, *NEK6*, *GSTA4*	20
Cellular movement, cancer, organismal injury and abnormalities	*SPINK5*, *SALL2*, *ANKS1A*, *ATP2B4*, *SERPINB5*, *EPHA2*, *ACSM3*, *PON3*, *ANO1*, *CLDND1*, *AHNAK*, *TAGLN*, *ACTA2*, *PSIP1*, *EPOR*	20
Cellular movement, cellular development, tissue development	*ITGA6*, *ALDH161*, *CD9*, *PTGFRN*, *CHAF1A*, *PTGES*, *POU5F1*, *KAT2B*, *BAG3*, *BRAF*, *KRT16*, *CD56*, *NDUFC2*, *RPL10A*, *RND3*	20
Cellular growth and proliferation, connective tissue development and function, tissue development	*KCNK1*, *RELB*, *MPZL2*, *MAP3K8*, *USP6NL*, *RAD54B*, *SLC2A1*, *PERP*, *NDRG1*, *GPR87*, *PLK2*, *ETHE1*, *ATIC*, *EAF2*	18
Low-grade NMIBC cohort		
Cellular growth and proliferation, cell cycle, cellular development	*IGF2*, *IL20RB*, *COL7A1*, *HIST1H2AC*, *HIST1H2BG*, *HIST2H2BE*, *HIST2H2AA3*, *HIST2H2AA4*, *TRNP1*, *IL1A*, *RND3*	24

DEGs, differentially expressed genes; NMIUTUC, non-muscle-invasive upper tract urothelial carcinoma; NMIBC, non-muscle-invasive bladder carcinoma.

proliferative activity in CK14-positive tumors than what was seen in CK14-negative papillary NMIUTUC.

There have been several seminal studies that uncovered genetically heterogeneous subclasses within MIBC via transcriptional clustering (1–5, 37). Of the subclasses, a common subtype, named the BASQ subtype, harbors a high level of basal-type genes, squamous-like features, and an aggressive phenotype (10). Although the BASQ subtype is a good foundation for MIBC evaluation, the applicability of BASQ markers (CK14, CK5/6, GATA3, FOXA1) to NMIUTUC or NMIBC has been questioned by us and others (13, 14, 16–18). For instance, CK5/6-negative/CK20-positive luminal-like papillary NMIUTUC had worse survival and was enriched with motility- and proliferation-associated genes (17, 18). In the same way, "class 2" NMIBC defined by Hedegaard and coworkers (13) was characterized by luminal-like genetic attributes, including low *KRT*5, *KRT6,* and *CD44* expression and high *GATA3*, *FOXA1,* and *KRT20* expression, but it had far worse survival than the other types of NMIBC. Moreover, this "class 2" subtype highly expressed *KRT14* and genetic signatures related to late cell cycle, cancer stem cell phenotype and EMT, which was in accord with another report that found high CK14/*KRT14* to be a determinant of poor NMIBC prognosis (19). In contrast to "class 2," basal-like subtype "class 3" NMIBC was paradoxically shown to have a favorable prognosis, which probably reflected a dormant state (13). Consistent with these reports, we showed that CK14 positivity was associated with poor PFS in papillary NMIUTUC, which was in agreement with the characteristics of CK14-positive BASQ-type MIBC. Although the overall good prognosis of papillary NMIUTUC hindered the statistical significance of CK14 IHC staining in predicting CSS and OS in our study, Kaplan-Meier plots suggested that CK14 positivity also reached worse outcomes in CSS and OS. In addition, we demonstrated that CK14-positive papillary NMIUTUC had BASQ-like genetic features that were similar to those of basal-type breast cancer and those of squamous cell carcinoma (1, 2, 4, 38). Furthermore, CK14-positive papillary NMIUTUC shared other molecular hallmarks of BASQ-type MIBC: activated p40, c-myc, EGFR, and NF-κB pathways, which mediate growth and squamous differentiation of urothelial carcinoma. These observations further support the genetic similarity between CK14-positive papillary NMIUTUC and BASQ-type MIBC (1, 6, 38).

Network and functional enrichment analyses as well as Ki-67 IHC staining demonstrated that cellular growth and proliferative functions are particularly upregulated in CK14-positive papillary NMIUTUC, in accordance with previously reported high-risk phenotypes of NMIBC (13) and NMIUTUC (18). The DEGs associated with this function involved several oncogenes [e.g., *CTBP2* (39), *SNHG5* (40), *RAB38* (41), *ADM* (42), *ETV4* (43), *EPHA2* (44), *PTGES* (45), *FZD6* (46), *ANXA2* (47), and *STC1* (48)] and tumor-suppressor genes [e.g., *EAF2* (49) and *IKZF3* (50)], which were upregulated and downregulated, respectively, in CK14-positive tumors. Dysregulation of these genes modulates proliferation, survival, migration, EMT, or metastasis of urothelial carcinoma, and other malignancies, leading to poor prognoses of these tumors. Interestingly, some of these genes, such as *ETV4*, *PTGES*, *CTBP2*, *FZD6*, *EAF2,* and *IKZF6*, have not been implicated in urothelial carcinoma; thus, these genes are potential candidates for diagnostic, prognostic, and therapeutic biomarkers of urothelial carcinoma. In addition to cellular proliferation, functional analyses suggested that CK14-positive papillary NMIUTUC had increased invasion and migration activities. In early urothelial neoplasms, CK14 expression denotes a stem cell population of basal cells that harbor high mitotic activities and have self-renewal, tumorigenesis, and stromal invasion potential (21, 51). Likewise, varied transcription activators and activation pathways (e.g., p40, c-myc, NF-κB, EGFR, Wnt, and mTORC1 signaling pathways) that were enriched in CK14-positive papillary NMIUTUC are linked to proliferation and/or malignant transformation of basal cells and embryonal stem cells (21). For example, silencing of p40 inhibited c-myc-mediated proliferation of urothelial carcinoma, and high p63 expression was associated with poor prognosis in NMIBC (6, 21). Both EGFR-dependent cell growth and EGFR inhibitor-induced growth restriction were specific to the BASQ subtype in MIBC (38). CK14 expression may regulate the treatment response to cancer therapeutics, including chemotherapy, immunotherapy, and Bacillus Calmette-Guérin in urothelial carcinoma (1, 7–10, 19, 21, 52). Therefore, we hypothesize that CK14-positive papillary NMIUTUC is highly populated with proliferative cancer stem cells, which will potentially impact the treatment strategy.

Normal urothelium has a hierarchical structure of basal, intermediate, and umbrella cells with sequential differentiation that involve gradual changes in keratin profiles from CK14 to CK5 and/or to CK20; thus, these cells that are in different states supposedly can give rise to urothelial carcinomas with poor (CK14-positive/CK5-negative/CK20-negative), moderate (CK14-negative/CK5-positive/CK20-negative), and well (CK14-negative/CK5-negative/CK20-positive) differentiation, respectively (19, 21). The BASQ-like molecular subtypes defined in different studies, including the TCGA cluster III/IV, the Lund "urothelial-like B" subtype and the Lund "squamous cell carcinoma-like" subtype, exhibited poorly differentiated gene expression characteristics (10). Interestingly, poorly differentiated properties associated with CK14 positivity might be partially opposed by our finding that CK14 positivity was associated with luminal-like CK5/6-negative/CK20-positive expression in papillary NMIUTUC (17). The Lund "genomically unstable" subtype, which corresponds to a high-risk group of NMIBC, expresses low CK5 and high CK20, and is enriched with genetic signatures typical of urothelial differentiation and disrupted adhesion (5, 10, 14, 30). Similarly, low CK5/6 and high CK20 expression profiles were associated with high-risk phenotypes of both papillary NMIUTUC and NMIBC that exhibited altered adhesion, migration, and proliferation (13, 17, 18). Both CK14 and CK20 were suggested to direct the aggravation of early urothelial carcinoma via the carcinoma *in situ*-driven pathway (13, 17, 21). In an animal model, altered expression of CK14 and CK20 corresponded to an early tumorigenic step of papillary urothelial carcinoma (22). Taken together, it would be reasonable to speculate that CK5/6-negative/CK20-positive expression may represent a "second

hit" to a primitive and aggressive CK14-positive papillary NMIUTUC. In other words, this putative CK14-positive/CK5/6-negative/CK20-positive expression might mirror a highly progressive CK14-positive urothelial carcinoma progeny, which remains to be explored (19). Furthermore, CK14, CK5/6, and CK20 expression would be valuable prognostic biomarkers in papillary NMIUTUC that appear to complement one another.

This study has some limitations. The number of patients included in the prognosis cohort was not enough to statistically discriminate CSS and OS in survival analysis. Second, the high-grade GEP cohort was relatively small, which introduced a risk of a biased estimation regarding molecular characteristics. Nevertheless, transcriptional profiles of CK14-positive papillary NMIUTUC were similar to those reported for the BASQ subtype, underscoring the appropriate representation of the high-grade GEP cohort. Finally, we applied array-based NMIBC mRNA data to infer transcriptional changes influenced by CK14 IHC staining in low-grade tumors. It is known that urothelial carcinoma of the upper and lower tract has high amount of overlap in transcriptomes, especially within early-staged tumors (53). However, the differences in tumor locations and analytic platforms prohibited deeper comparison of the high-grade GEP cohort and the low-grade NMIBC cohort. Further study incorporating enough samples of both low-grade and high-grade papillary NMIUTUC that exhibits positive CK14 IHC staining will be required.

In conclusion, CK14 positivity represents an aggressive BASQ-like subtype in papillary NMIUTUC that is enriched with brisk proliferative activity. CK14 IHC staining is a promising biomarker that can be applied in the management of non-muscle-invasive urothelial carcinoma in daily practice, with the aim of precision oncology.

DATA AVAILABILITY STATEMENT

Publicly available datasets were analyzed in this study, these can be found in the NCBI Gene Expression Omnibus (GSE32894). The datasets generated for this study can be found in the Sequence Read Archive (SRA), PRJNA609154.

ETHICS STATEMENT

The studies involving human participants were reviewed and approved by Institutional Review Board of Seoul National University Hospital. Written informed consent for participation was not required for this study in accordance with the national legislation and the institutional requirements.

AUTHOR CONTRIBUTIONS

MJ and KM designed and performed the experiments. IJ, KK, and MJ analyzed the data. MJ wrote the manuscript. KM supervised the entire process.

FUNDING

This research was supported by the Basic Science Research Program through the National Research Foundation of Korea (NRF) funded by the Ministry of Education (grant number 2018R1D1A1B07045763).

SUPPLEMENTARY MATERIAL

The Supplementary Material for this article can be found online at: https://www.frontiersin.org/articles/10.3389/fonc.2020.00623/full#supplementary-material

REFERENCES

1. Choi W, Porten S, Kim S, Willis D, Plimack ER, Hoffman-Censits J, et al. Identification of distinct basal and luminal subtypes of muscle-invasive bladder cancer with different sensitivities to frontline chemotherapy. *Cancer Cell*. (2014) 25:152–65. doi: 10.1016/j.ccr.2014.01.009
2. Damrauer JS, Hoadley KA, Chism DD, Fan C, Tiganelli CJ, Wobker SE, et al. Intrinsic subtypes of high-grade bladder cancer reflect the hallmarks of breast cancer biology. *Proc Natl Acad Sci USA*. (2014) 111:3110–5. doi: 10.1073/pnas.1318376111
3. Robertson AG, Kim J, Al-Ahmadie H, Bellmunt J, Guo G, Cherniack AD, et al. Comprehensive molecular characterization of muscle-invasive bladder cancer. *Cell*. (2017) 171:540–56.e25. doi: 10.1016/j.cell.2017.09.007
4. The Cancer Genome Atlas Research Network. Comprehensive molecular characterization of urothelial bladder carcinoma. *Nature*. (2014) 507:315–22. doi: 10.1038/nature12965
5. Sjodahl G, Lauss M, Lovgren K, Chebil G, Gudjonsson S, Veerla S, et al. A molecular taxonomy for urothelial carcinoma. *Clin Cancer Res*. (2012) 18:3377–86. doi: 10.1158/1078-0432.CCR-12-0077-T
6. Choi W, Shah JB, Tran M, Svatek R, Marquis L, Lee IL, et al. p63 expression defines a lethal subset of muscle-invasive bladder cancers. *PLoS ONE*. (2012) 7:e30206. doi: 10.1371/journal.pone.0030206
7. Seiler R, Ashab HAD, Erho N, van Rhijn BWG, Winters B, Douglas J, et al. Impact of molecular subtypes in muscle-invasive bladder cancer on predicting response and survival after neoadjuvant chemotherapy. *Eur Urol*. (2017) 72:544–54. doi: 10.1016/j.eururo.2017.03.030
8. Rosenberg JE, Hoffman-Censits J, Powles T, van der Heijden MS, Balar AV, Necchi A, et al. Atezolizumab in patients with locally advanced and metastatic urothelial carcinoma who have progressed following treatment with platinum-based chemotherapy: a single-arm, multicentre, phase 2 trial. *Lancet*. (2016) 387:1909–20. doi: 10.1016/S0140-6736(16)00561-4
9. Sharma P, Retz M, Siefker-Radtke A, Baron A, Necchi A, Bedke J, et al. Nivolumab in metastatic urothelial carcinoma after platinum therapy (CheckMate 275): a multicentre, single-arm, phase 2 trial. *Lancet Oncol*. (2017) 18:312–22. doi: 10.1016/S1470-2045(17)30065-7
10. Lerner SP, McConkey DJ, Hoadley KA, Chan KS, Kim WY, Radvanyi F, et al. Bladder cancer molecular taxonomy: summary from a consensus meeting. *Bladder Cancer*. (2016) 2:37–47. doi: 10.3233/BLC-150037
11. Yuk HD, Jeong CW, Kwak C, Kim HH, Moon KC, Ku JH. Clinical outcomes of muscle invasive bladder cancer according to the BASQ classification. *BMC Cancer*. (2019) 19:897. doi: 10.1186/s12885-019-6042-1
12. Sjodahl G, Eriksson P, Lovgren K, Marzouka NA, Bernardo C, Nordentoft I, et al. Discordant molecular subtype classification in the basal-squamous subtype of bladder tumors and matched lymph-node metastases. *Mod Pathol*. (2018) 31:1869–81. doi: 10.1038/s41379-018-0096-5

13. Hedegaard J, Lamy P, Nordentoft I, Algaba F, Hoyer S, Ulhoi BP, et al. Comprehensive transcriptional analysis of early-stage urothelial carcinoma. *Cancer Cell*. (2016) 30:27–42. doi: 10.1016/j.ccell.2016.05.004
14. Patschan O, Sjodahl G, Chebil G, Lovgren K, Lauss M, Gudjonsson S, et al. A molecular pathologic framework for risk stratification of stage T1 urothelial carcinoma. *Eur Urol*. (2015) 68:824–32. doi: 10.1016/j.eururo.2015.02.021
15. Desai S, Lim SD, Jimenez RE, Chun T, Keane TE, McKenney JK, et al. Relationship of cytokeratin 20 and CD44 protein expression with WHO/ISUP grade in pTa and pT1 papillary urothelial neoplasia. *Mod Pathol*. (2000) 13:1315–23. doi: 10.1038/modpathol.3880241
16. Breyer J, Wirtz RM, Otto W, Erben P, Kriegmair MC, Stoehr R, et al. In stage pT1 non-muscle-invasive bladder cancer (NMIBC), high KRT20 and low KRT5 mRNA expression identify the luminal subtype and predict recurrence and survival. *Virchows Arch*. (2017) 470:267–74. doi: 10.1007/s00428-017-2064-8
17. Jung M, Kim B, Moon KC. Immunohistochemistry of cytokeratin (CK) 5/6, CD44 and CK20 as prognostic biomarkers of non-muscle-invasive papillary upper tract urothelial carcinoma. *Histopathology*. (2019) 74:483–93. doi: 10.1111/his.13763
18. Jung M, Lee JH, Kim B, Park JH, Moon KC. Transcriptional analysis of immunohistochemically defined subgroups of non-muscle-invasive papillary high-grade upper tract urothelial carcinoma. *Int J Mol Sci*. (2019) 20:570. doi: 10.3390/ijms20030570
19. Volkmer JP, Sahoo D, Chin RK, Ho PL, Tang C, Kurtova AV, et al. Three differentiation states risk-stratify bladder cancer into distinct subtypes. *Proc Natl Acad Sci USA*. (2012) 109:2078–83. doi: 10.1073/pnas.1201493109
20. Alam H, Sehgal L, Kundu ST, Dalal SN, Vaidya MM. Novel function of keratins 5 and 14 in proliferation and differentiation of stratified epithelial cells. *Mol Biol Cell*. (2011) 22:4068–78. doi: 10.1091/mbc.e10-08-0703
21. Ho PL, Kurtova A, Chan KS. Normal and neoplastic urothelial stem cells: getting to the root of the problem. *Nat Rev Urol*. (2012) 9:583–94. doi: 10.1038/nrurol.2012.142
22. Gil da Costa RM, Oliveira PA, Vasconcelos-Nobrega C, Arantes-Rodrigues R, Pinto-Leite R, Colaco AA, et al. Altered expression of CKs 14/20 is an early event in a rat model of multistep bladder carcinogenesis. *Int J Exp Pathol*. (2015) 96:319–25. doi: 10.1111/iep.12145
23. Kurtova AV, Xiao J, Mo Q, Pazhanisamy S, Krasnow R, Lerner SP, et al. Blocking PGE2-induced tumour repopulation abrogates bladder cancer chemoresistance. *Nature*. (2015) 517:209–13. doi: 10.1038/nature14034
24. Cheung KJ, Padmanaban V, Silvestri V, Schipper K, Cohen JD, Fairchild AN, et al. Polyclonal breast cancer metastases arise from collective dissemination of keratin 14-expressing tumor cell clusters. *Proc Natl Acad Sci USA*. (2016) 113:E854–63. doi: 10.1073/pnas.1508541113
25. Gao XL, Wu JS, Cao MX, Gao SY, Cen X, Jiang YP, et al. Cytokeratin-14 contributes to collective invasion of salivary adenoid cystic carcinoma. *PLoS ONE*. (2017) 12:e0171341. doi: 10.1371/journal.pone.0171341
26. Dmello C, Sawant S, Alam H, Gangadaran P, Mogre S, Tiwari R, et al. Vimentin regulates differentiation switch via modulation of keratin 14 levels and their expression together correlates with poor prognosis in oral cancer patients. *PLoS ONE*. (2017) 12:e0172559. doi: 10.1371/journal.pone.0172559
27. Siegel RL, Miller KD, Jemal A. Cancer statistics, (2017) *CA Cancer J Clin*. (2017) 67:7–30. doi: 10.3322/caac.21387
28. Cheng L, MacLennan GT, Lopez-Beltran A. Histologic grading of urothelial carcinoma: a reappraisal. *Hum Pathol*. (2012) 43:2097–108. doi: 10.1016/j.humpath.2012.01.008
29. Bankhead P, Loughrey MB, Fernandez JA, Dombrowski Y, McArt DG, Dunne PD, et al. QuPath: open source software for digital pathology image analysis. *Sci Rep*. (2017) 7:16878. doi: 10.1038/s41598-017-17204-5
30. Sjodahl G, Lovgren K, Lauss M, Patschan O, Gudjonsson S, Chebil G, et al. Toward a molecular pathologic classification of urothelial carcinoma. *Am J Pathol*. (2013) 183:681–91. doi: 10.1016/j.ajpath.2013.05.013
31. Subramanian A, Tamayo P, Mootha VK, Mukherjee S, Ebert BL, Gillette MA, et al. Gene set enrichment analysis: a knowledge-based approach for interpreting genome-wide expression profiles. *Proc Natl Acad Sci USA*. (2005) 102:15545–50. doi: 10.1073/pnas.0506580102
32. Kramer A, Green J, Pollard J Jr, Tugendreich S. Causal analysis approaches in ingenuity pathway analysis. *Bioinformatics*. (2014) 30:523–30. doi: 10.1093/bioinformatics/btt703
33. Ashburner M, Ball CA, Blake JA, Botstein D, Butler H, Cherry JM, et al. Gene ontology: tool for the unification of biology. the gene ontology consortium. *Nat Genet*. (2000) 25:25–9. doi: 10.1038/75556
34. The Gene Ontology C. The gene ontology resource: 20 years and still going strong. *Nucleic Acids Res*. (2019) 47:D330–D8. doi: 10.1093/nar/gky1055
35. Kanehisa M, Goto S. KEGG: kyoto encyclopedia of genes and genomes. *Nucleic Acids Res*. (2000) 28:27–30. doi: 10.1093/nar/28.1.27
36. Zhou Y, Zhou B, Pache L, Chang M, Khodabakhshi AH, Tanaseichuk O, et al. Metascape provides a biologist-oriented resource for the analysis of systems-level datasets. *Nat Commun*. (2019) 10:1523. doi: 10.1038/s41467-019-09234-6
37. Aine M, Eriksson P, Liedberg F, Sjodahl G, Hoglund M. Biological determinants of bladder cancer gene expression subtypes. *Sci Rep*. (2015) 5:10957. doi: 10.1038/srep10957
38. Rebouissou S, Bernard-Pierrot I, de Reynies A, Lepage ML, Krucker C, Chapeaublanc E, et al. EGFR as a potential therapeutic target for a subset of muscle-invasive bladder cancers presenting a basal-like phenotype. *Sci Transl Med*. (2014) 6:244ra91. doi: 10.1126/scitranslmed.3008970
39. Liu X, Yao N, Qian J, Huang H. High expression and prognostic role of CAP1 and CtBP2 in breast carcinoma: associated with E-cadherin and cell proliferation. *Med Oncol*. (2014) 31:878. doi: 10.1007/s12032-014-0878-7
40. Ma Z, Xue S, Zeng B, Qiu D. lncRNA SNHG5 is associated with poor prognosis of bladder cancer and promotes bladder cancer cell proliferation through targeting p27. *Oncol Lett*. (2018) 15:1924–30. doi: 10.3892/ol.2017.7527
41. Tian DW, Liu SL, Jiang LM, Wu ZL, Gao J, Hu HL, et al. RAB38 promotes bladder cancer growth by promoting cell proliferation and motility. *World J Urol*. (2019) 37:1889–97. doi: 10.1007/s00345-018-2596-9
42. Liu AG, Zhang XZ, Li FB, Zhao YL, Guo YC, Yang RM. RNA interference targeting adrenomedullin induces apoptosis and reduces the growth of human bladder urothelial cell carcinoma. *Med Oncol*. (2013) 30:616. doi: 10.1007/s12032-013-0616-6
43. Sizemore GM, Pitarresi JR, Balakrishnan S, Ostrowski MC. The ETS family of oncogenic transcription factors in solid tumours. *Nat Rev Cancer*. (2017) 17:337–51. doi: 10.1038/nrc.2017.20
44. Abraham S, Knapp DW, Cheng L, Snyder PW, Mittal SK, Bangari DS, et al. Expression of EphA2 and Ephrin A-1 in carcinoma of the urinary bladder. *Clin Cancer Res*. (2006) 12:353–60. doi: 10.1158/1078-0432.CCR-05-1505
45. Wang T, Jing B, Sun B, Liao Y, Song H, Xu D, et al. Stabilization of PTGES by deubiquitinase USP9X promotes metastatic features of lung cancer via PGE2 signaling. *Am J Cancer Res*. (2019) 9:1145–60.
46. Corda G Sala A. Non-canonical WNT/PCP signalling in cancer: Fzd6 takes centre stage. *Oncogenesis*. (2017) 6:e364. doi: 10.1038/oncsis.2017.69
47. Liu X, Ma D, Jing X, Wang B, Yang W, Qiu W. Overexpression of ANXA2 predicts adverse outcomes of patients with malignant tumors: a systematic review and meta-analysis. *Med Oncol*. (2015) 32:392. doi: 10.1007/s12032-014-0392-y
48. Cai S, Liu L, Wang C, Zhang H, Wu W, Yang H, et al. Stanniocalcin-1 relates to tumor recurrence and unfavorable prognosis of urothelial bladder cancer. *Int J Clin Exp Pathol*. (2016) 9:5429–36.
49. Guo W, Keener AL, Jing Y, Cai L, Ai J, Zhang J, et al. FOXA1 modulates EAF2 regulation of AR transcriptional activity, cell proliferation, and migration in prostate cancer cells. *Prostate*. (2015) 75:976–87. doi: 10.1002/pros.22982
50. Wu YM, Hu W, Wang Y, Wang N, Gao L, Chen ZZ, et al. Exploring novel targets of basal-like breast carcinoma by comparative gene profiling and mechanism analysis. *Breast Cancer Res Treat*. (2013) 141:23–32. doi: 10.1007/s10549-013-2664-1

51. Chan KS, Espinosa I, Chao M, Wong D, Ailles L, Diehn M, et al. Identification, molecular characterization, clinical prognosis, and therapeutic targeting of human bladder tumor-initiating cells. *Proc Natl Acad Sci USA*. (2009) 106:14016–21. doi: 10.1073/pnas.0906549106
52. Chen M, Hildebrandt MA, Clague J, Kamat AM, Picornell A, Chang J, et al. Genetic variations in the sonic hedgehog pathway affect clinical outcomes in non-muscle-invasive bladder cancer. *Cancer Prev Res*. (2010) 3:1235–45. doi: 10.1158/1940-6207.CAPR-10-0035
53. Sanford T, Porten S, Meng MV. Molecular analysis of upper tract and bladder urothelial carcinoma: results from a microarray comparison. *PLoS ONE*. (2015) 10:e0137141. doi: 10.1371/journal.pone.0137141

Conflict of Interest: The authors declare that the research was conducted in the absence of any commercial or financial relationships that could be construed as a potential conflict of interest.

frontiers in Oncology

ORIGINAL RESEARCH
published: 12 May 2020
doi: 10.3389/fonc.2020.00589

Downregulation of HMGA1 Mediates Autophagy and Inhibits Migration and Invasion in Bladder Cancer via miRNA-221/TP53INP1/p-ERK Axis

Xiaoqiang Liu[1,2†], Zhengtao Zhou[1†], Yibing Wang[3†], Ke Zhu[1,2], Wen Deng[1], Yulei Li[1], Xiaochen Zhou[1], Luyao Chen[1], Yu Li[1], An Xie[2], Tao Zeng[4], Gongxian Wang[1,2] and Bin Fu[1,2]*

[1] Department of Urology, The First Affiliated Hospital of Nanchang University, Nanchang, China, [2] Jiangxi Institute of Urology, Nanchang, China, [3] Department of Emergency, The Second Affiliated Hospital of Nanchang University, Nanchang, China, [4] Department of Urology, The People's Hospital of Jiangxi Province, Nanchang, China

OPEN ACCESS

Edited by:
Ja Hyeon Ku,
Seoul National University, South Korea

Reviewed by:
Dario Palmieri,
The Ohio State University, United States
Luigi M. Terracciano,
University of Basel, Switzerland

***Correspondence:**
Bin Fu
urofubin@sina.com

[†] These authors have contributed equally to this work

Specialty section:
This article was submitted to Genitourinary Oncology, a section of the journal Frontiers in Oncology

Received: 04 December 2019
Accepted: 31 March 2020
Published: 12 May 2020

Citation:
Liu X, Zhou Z, Wang Y, Zhu K, Deng W, Li Y, Zhou X, Chen L, Li Y, Xie A, Zeng T, Wang G and Fu B (2020) Downregulation of HMGA1 Mediates Autophagy and Inhibits Migration and Invasion in Bladder Cancer via miRNA-221/TP53INP1/p-ERK Axis. Front. Oncol. 10:589. doi: 10.3389/fonc.2020.00589

MicroRNAs (miRNAs) have been implicated in regulating the development and metastasis of human cancers. MiR-221 is reported to be an oncogene in multiple cancers, including bladder cancer (BC). Deregulation of autophagy is associated with multiple human malignant cancers. Whether and how miR-221 regulates autophagy and how miR-221 has been regulated in BC are poorly understood. This study explored the potential functions and mechanisms of miR-221 in the autophagy and tumorigenesis of BC. We showed that the downregulation of miR-221 induces autophagy via increasing TP53INP1 (tumor protein p53 inducible nuclear protein 1) and inhibits migration and invasion of BC cells through suppressing activation of extracellular signal-regulated kinase (ERK). Furthermore, the expression of miR-221 is regulated by high-mobility group AT-hook 1 (HMGA1) which is overexpressed in BC. And both miR-221 and HMGA1 are correlated with poor patient survival in BC. Finally, the downregulation of HMGA1 suppressed the proliferative, migrative, and invasive property of BC by inducing toxic autophagy via miR-221/TP53INP1/p-ERK axis. Collectively, our findings demonstrate that the downregulation of miR-221 and HMGA1 mediates autophagy in BC, and both of them are valuable therapeutic targets for BC.

Keywords: high-mobility group AT-hook 1 (HMGA1), bladder cancer, autophagy, miR-221, TP53INP1

INTRODUCTION

Bladder cancer (BC) is the fourth most common cancer in men in the United States with an estimated 62,380 new cases and 12,520 deaths in 2018 (1). Approximately 75% of cases are non-muscle-invasive BC (Ta, T1), which has a good prognosis, with 94% of patients surviving ≥5 years and is usually treated by transurethral resection and intravesical chemotherapy (2). However, approximately half of these patients will experience cancer recurrence, and 20% will progress to muscle-invasive BC (MIBC), which requires additional surgical interventions and chemotherapy (3). Although few patients are initially diagnosed with MIBCs, the 5-year survival of patients with MIBC is low: nearly 50.1% for regional stage and 10.2% for distant stage (4). Despite the crucial advances in BC research this year, the mortality rate of BC has remained unchanged due to the lack of specific targets (5).

Autophagy, which is a cellular self-degradative process mobilizing intracellular nutrient resources, plays an important role in cell survival under stress conditions. However, hyperactivated autophagy can lead to non-apoptotic programmed cell death (6). The deregulation of this process is associated with multiple human diseases, including cancer (7). In cancer, autophagy has a complex role and shows either an oncogenic or tumor suppressor activity (8). A feasible strategy to treat cancer is to reprogram cancerous cells to undergo toxic autophagy (9).

MicroRNAs (miRNAs) are an abundant class of single-stranded non-coding small RNAs that negatively regulate gene expression through inducing the degradation of target messenger RNAs (mRNAs) or translation repression by binding to the 3′ untranslated region (3′-UTR) of mRNAs (10). Emerging evidence indicates that the dysregulation of miRNA expression is involved in tumor initiation, proliferation, invasion, and metastasis (11). Thus, the identification of specific molecules that target miRNAs and its upstream transcription factors may be an effective approach to eradicate BC. MiR-221 has been frequently identified as deregulated across different cancer types, including BC (12). Nevertheless, the role of miR-221 in autophagy and the molecular mechanism of miR-221 being regulated in BC are still unclear.

High-mobility group A (HMGA) protein family consists of four members (HMGA1a, HMGA1b, HMGA1c, and HMGA2), which preferentially binds to the minor groove of AT-rich regions in double-stranded DNA and thereby modulates the transcription of several genes through direct protein-protein interactions with transcription factors by modifying its conformation and enhancing the affinity of its binding to DNA (13). They are encoded by two genes, *HMGA1* and *HMGA2*. *HMGA1* gene gives rise to three HMGA1 isoforms (HMGA1a, HMGA1b, and HMGA1c) through alternative splicing (14). HMGA1 has been reported to play an important role in many types of cancers, including lung cancer (15), colorectal cancer (16), breast cancer (17), cervical cancer (18), and BC (19). HMGA1 contributes to tumor formation and progression through several mechanisms: inactivation of the apoptotic function of p53 (20), enhancement of the expression of genes involved in stem cell and inflammatory pathway (21), and modulation of the expression of miRNAs and genes involved in cell cycle and epithelial-mesenthymal transition (13). However, the role of HMGA1 in BC remains unknown.

In this study, we investigated the role of miR-221 and HMGA1 and demonstrated that the downregulation of HMGA1 inhibits migration and invasion partly via miRNA-221/TP53INP1/p-ERK axis-mediated toxic autophagy in BC.

MATERIALS AND METHODS

Cell Culture and Treatment

Human BC cells of the 5637, J82, EJ, UM-UC-3, and T24 lines, the SV-HUC-1 human immortalized uroepithelium cell line, and 293T cells were purchased from the Cell Bank of Type Culture Collection of Chinese Academy of Sciences, Shanghai Institute of Cell Biology (Shanghai, China). 5637, J82, and EJ cells were maintained in RPMI-1640 (Gibco; Thermo Fisher Scientific, Inc.). T24, UM-UC-3, and 293T cells were cultured in Dulbecco's modified Eagle's medium (DMEM; Gibco), and SV-HUC-1 cells were cultured in F-12K medium (Gibco). Media were supplemented with 10% heat-inactivated fetal bovine serum (FBS; Hyclone), 100 U/ml penicillin, and 100 μg/ml streptomycin at 37°C in a humidified incubator with 5% CO_2.

Luciferase Reporter Assay

The segments of wild-type (WT) TP53INP1 3′UTR and mutant (MUT) TP53INP1 3′UTR were PCR amplified and inserted into the Renilla luciferase gene (psi-CHECK-2 vector; Promega) to generate the TP53INP1 WT plasmids and TP53INP1 MUT plasmids. 5637 cells and 293T cells were transfected using Lipofectamine™ 2000 (Invitrogen) in accordance with the recommendations of the manufacturer. Luciferase vectors (100 ng) (TP53INP1 WT, TP53INP1 MUT, and the empty vectors) were individually transfected into 5637 cells and 293T along with 100 nM hsa-miR-221-3p mimics (RiboBio, Guangzhou, China) or 100 nM negative control (NC) (RiboBio, Guangzhou, China). At 48 h after transfection, luciferase assays were performed using the Dual-Luciferase Reporter Assay System (Promega). For each transfection, the luciferase activity of three replicates was considered.

Lentiviral Vector Construction

Recombinant lentiviral expression plasmids (pLV-IRES-BSD-GFP-miR-221/pLV-IRES-BSD-GFP-sh-miR-221) and pLV-IRES-BSD-GFP-shTP53INP1 were constructed, and their identity was confirmed by DNA sequencing. To generate lentiviral particles, the recombinant expression plasmids were co-transfected with a packaging plasmid system into 293T cells, and the resultant viral particles were harvested at 48 h after transfection. 5637 cells were infected with the miR-221 lentiviral vector or with an NC vector, and T24 cells were infected with the sh-miR-221 lentiviral vector or with an NC vector, at a multiplicity of infection (MOI) of 50 and with polybrene (8 mg/ml) for 2 days. Infection efficiency was assessed in each experiment by observing the green fluorescent protein (GFP) expression under a fluorescence microscope.

Transfection

Cells of the 5637 and T24 lines were plated in six-well plates at 2×10^5 per well. The hsa-miR-221-3p mimic/inhibitor, NC, and HMGA1 siRNA were obtained from RiboBio (Guangzhou, China). The sequences of miR-221-3p mimics and miR-221-3p inhibitor were 5′-AGCUACAUUGUCUGCUGGGUUUC-3′ and 5′-GAAACCCAGCAGACAAUGUAGCU-3′, respectively. The following siRNA sequences were used: HMGA1 siRNA (5′-GGACAAGGCUAACAUCCCATT-3′), ATG5 siRNA (5′-GGATGAGATAACTGAAAG-3′), and NC siRNA (5′-UUCUCCGAACGUGUCACGUTT-3′). StarBase v2.0 (http://starbase.sysu.edu.cn/) was used to identify the predicted target of miR-221-3p. 5637 and T24 cells grown to 70–80% confluence were transfected using the Lipofectamine™ 2000 transfection reagent (Invitrogen, USA) and Opti-MEM medium (Gibco) in accordance with the instructions of the manufacturer. Six hours

after transfection, the medium was replaced with fresh medium containing 10% FBS.

RNA Extraction and Real-Time Quantitative PCR Analysis

Total RNAs were extracted from BC cell lines (5637, T24, J82, EJ, UM-UC-3) and SV-HUC-1 human immortalized uroepithelium cell line transfected with or without miRNA mimic/inhibitor or siRNA using TRIzol reagent (Invitrogen). cDNA was synthesized using a Takara PrimeScript RT reagent Kit (Takara) and specific miR-221 primers from the Bulge-Loop™ hsa-miR-221-3p RT-qPCR Primer Set (RiboBio, Guangzhou, China) for quantitative miRNA analysis. Quantitative real-time PCR was conducted on the ABI PRISM 7500 real-time PCR system (Applied Biosystems, USA). Real-time PCR results were normalized against an internal control U6. Relative expression levels were evaluated using the $2^{-\Delta\Delta Ct}$ method and then expressed as fold changes. For RT-qPCR, 400 ng of total RNA was used in a Takara PrimeScript RT reagent Kit (Takara) in accordance with the manufacturer's instructions, and PCR was performed on the ABI PRISM 7500 real-time PCR system (Applied Biosystems). The expression level of glyceraldehyde-3-phosphate dehydrogenase (GAPDH) was used as the internal control. All reactions were performed at least in triplicate. The oligonucleotide sequences of the RT-qPCR primers for *HMGA1*, *TP53INP1*, and *GAPDH* were as follows: HMGA1-forward, 5′-GCTGGTAGGGAGTCAGAAGGA-3′, and HMGA1-reverse, 5′-TGGTGGTTTTCCGGGTCTTG-3′; TP53INP1-forward, 5′-GACTTCATAGATACTTGCAC-3′, and TP53INP1-reverse, 5′-ATTGGACATGACTCAAACTG-3′; GAPDH-forward, 5′-CATGAGAAGTATGACAACAGCCT-3′, and GAPDH-reverse, 5′- AGTCCTTCCACGATACCAAAGT-3′.

Western Blot Analysis

Total proteins from cells were prepared using radioimmunoprecipitation assay (RIPA) lysis buffer (Beyotime, Jiangsu, China). Protein was quantified using a Pierce BCA Protein Assay Kit (Thermo Fisher Scientific), followed by Western blot analysis. Once transferred to a polyvinylidene fluoride (PVDF) membrane, antibodies targeting GAPDH (Abcam, ab8245, 1:1,000), TP53INP1 (Abcam, ab32131, 1:1,000), HMGA1 (Abcam, ab32131, 1:1,000), ERK1/2 (CST, 3195, 1:1,000), p-ERK1/2 (CST, 9523, 1:1,000), LC3B (CST, 79424, 1:1,000), poly (ADP-ribose) polymerase (PARP, CST, 9532, 1:1,000), Beclin1 (CST, 3495, 1:1,000), ATG5 (CST, 12994, 1:1,000), and p62 (CST, 79424, 1:1,000) were used with a secondary antibody horseradish peroxidase-labeled goat anti-rabbit (1:4,000; 1.5 h of incubation at room temperature; Abcam, ab6721). GAPDH served as an internal control. Protein bands were visualized by enhanced chemiluminescence.

Cell Viability Assay

The effects of siHMGA1 on the viability of T24 cells were assessed using a Cell Counting Kit-8 (CCK-8) detection kit (Nanjing Keygen Biotech Co., Ltd., Nanjing, China) as described in Liu et al. (22). T24 cells were transfected with siHMGA1 and NC siRNA as described before. The cells were incubated at 37°C for 24, 48, 72, and 96 h. Absorbance was measured at 450 nm. Cell viability was expressed as a percentage of absorbance in the siHMGA1-transfected wells compared with that of the NC siRNA wells. Each experiment was performed in triplicate and repeated at least three times.

Colony Formation Assay

To perform the colony formation assays, the cells were transfected with siHMGA1 and/or miR-221-3p mimic as described before. After 24 h of transfection, the cells were trypsinized, counted, and replated to the six-well plate in equal numbers (200 cells). After 9–13 days of culture, the cells were fixed in methanol for 30 min, stained with crystal violet (C3886, Sigma-Aldrich) for 30 min, washed several times with phosphate buffered saline (PBS), and then photographed.

Cell Migration and Transwell Assay

Cell migration was determined using a wound healing assay. 5637 and T24 cells were seeded in six-well plates and transfected with pLV-IRES-BSD-GFP-miR-221/pLV-IRES-BSD-GFP-sh-miR-221, HMGA1 siRNA, or non-target control for 48 h. A wound was created by scratching the monolayer with a 200-μl pipette tip. The wounded monolayer was then washed three times with PBS to remove cell debris. After scratching, the area of the cell-free scratch was photographed with Olympus CKX41 inverse microscope at 0 and 24 h. Cell invasion capacities were measured by a transwell assay (Corning, Toledo, OH, USA). 5637 and T24 cells were transfected with pLV-IRES-BSD-GFP-miR-221/pLV-IRES-BSD-GFP-sh-miR-221, miR-221 mimic, HMGA1 siRNA, or non-target control for 48 h and then seeded in the upper chamber of the transwell system. The upper chamber of the insert was precoated with 0.1 ml (300 μg/ml) of Matrigel matrix (Corning) for the invasion assay. Invaded cells on the underside of the membrane were counted. In this assay, prepared cells were seeded in the upper chamber with a serum-free medium, and the medium of the lower chamber was supplemented with 10% FBS as a chemoattractant. After 24 h of incubation, the cells were fixed with 4% formaldehyde. Cells that did not invade through the pores were removed with a cotton swab. Cells that had migrated or invaded the lower surface of the membrane were stained with crystal violet. Finally, five representative fields for each well were randomly imaged at 100× magnification and quantified using Olympus CKX41 inverse microscope.

Tissue Microarray and Immunohistochemistry

Human BC tissue microarrays (TMAs) containing 48 pairs of tumors and matched adjacent tissues and 16 tumors were purchased from Xi'an Alenabio Biotech Co., Ltd. (Xi'an, China). The immunohistochemical staining of TMAs using primary antibodies against HMGA1 (Abcam, ab32131) was performed as previously described (23). Briefly, after dewaxing, rehydration, antigen retrieval, and blocking, the arrays were incubated overnight at 4°C with HMGA1 antibody. Color detection was performed by 3,3′-diaminobenzidine (DAB) and hematoxylin counterstaining. Stained tumor and adjacent normal tissues were

classified into two groups (low and high) in accordance with the staining intensity of each tissue.

Autophagic Vacuoles Staining

Autophagosome formation was analyzed using a Cyto-ID autophagy detection kit (Enzo Life Sciences) according to the manufacturer's instruction (24) and LC3 antibody staining. Briefly, for Cyto-ID autophagy detection kit staining, cells were stained with Cyto-ID autophagy detection dye and Hoechst 33342 for 30 min at 37°C. For LC3 antibody staining, cells were fixed with methanol for 10 min and blocked with 2.5% BSA for 30 min, incubated with an anti-LC3B antibody (1:200; CST) at 4°C overnight, washed three times with PBS, and incubated with an Alexa Fluor 488-conjugated secondary antibody (1:500; Invitrogen) for 1 h. Slides were imaged under a microscope (Nikon).

Statistical Analysis

All data were presented as the means ± SD in at least three replicates per group. Statistical analysis was performed to determine the significance of the difference between groups using ANOVA or Student's *t*-test. All statistical analyses were performed using GraphPad/Prism software for Windows. $p < 0.05$ was considered statistically significant.

RESULTS

Downregulation of miR-221 Promotes Autophagy in Bladder Cancer Cells

Our previous study showed that miR-221 mediates the immune evasion of BC cells (25). However, the molecular mechanism of miR-221 action in BC remains unclear. To further investigate the role of miR-221 in BC cells, we first examined the expression level of miR-221 in a panel of five BC cell lines (5637, J82, T24, EJ, and UM-UC-3) and the human immortalized uroepithelium cell line (SV-HUC-1). We showed that miR-221 was significantly upregulated or unchanged in invasive BC lines (T24, J82, EJ, UM-UC-3) but downregulated in the non-invasive BC cell line (5637) (**Figure 1A**), which indicated that the overexpression of miR-221 might be specifically correlated to MIBC. Moreover, we performed Kaplan–Meier analysis in the database (http://kmplot.com/analysis/) and found that patients with BC with high miR-221 expression had worse prognosis and shorter survival time than those with low miR-221 expression (**Figure 1B**).

Autophagy is a vital regulator of invasion and migration in cancer (26). Previous studies have revealed that miR-221 inhibits autophagy and promotes heart failure by modulating the p27/CDK2/mTOR axis and inhibits hypoxia/reoxygenation-induced autophagy through the DDIT4/mTORC1 and TP53INP1/p62 pathways (27, 28). Given that our previous study showed that the downregulation of miR-221 inhibits the migration and invasion of BC cells, we investigated whether miR-221 could influence autophagy of BC cells. We transfected the non-invasive BC cell line 5637 and invasive BC cell line T24 with miR-221 mimic and miR-221 inhibitor and verified the expression of miR-221 by RT-qPCR (**Figure 1C**). Immunoblotting analysis showed that the downregulation of miR-221 increased the LC3-II/LC3-I expression ratio and decreased the p62 expression in T24 cells. And lysosomal inhibitor chloroquine (CQ) could further promote LC3-II accumulation compared to miR-221 inhibitor action alone (**Figure 1D**). We further analyzed the ultrastructure of T24 BC cells by using transmission electron microscopy (TEM). Representative TEM images are shown in **Figure 1E**. Typical autolysosomes were observed in T24 cells, whereas the few autolysosomes were observed in control cells after transfection with the miR-221 inhibitor. Moreover, we detected autophagic flux by using Cyto-ID staining and LC3 antibody staining as reported (29, 30). As presented in **Figure 1F**, we found that the suppression of miR-221 expression induced the formation and accumulation of autophagosomes (green fluorescence) in T24 cells (**Figure 1F**). Thus, our results indicated that the suppression of miR-221 expression promoted autophagy in BC cells.

Downregulation of miR-221 Induces Autophagy and Inhibits Invasion and Migration of Bladder Cancer Cells *in vitro* via TP53INP1/p-ERK Axis

To further illustrate the mechanism underlying the autophagy-regulating effect of miR-221, we screened for the candidate autophagy-related targets of miR-221 using StarBase v2.0 (http://starbase.sysu.edu.cn/) and literature search. MiR-221 inhibits hypoxia/reoxygenation-induced autophagy through TP53INP1/p62 pathways (28). Thus, we speculated that miR-221 could modulate autophagy and then regulate the invasion and migration of BC cells by targeting TP53INP1. Interestingly, consistent with this prediction, miR-221 suppressed TP53INP1 expression in 5637 cells, and the suppression of miR-221 expression increased the expression of TP53INP1 in T24 cells (**Figure 2A**). Although Beclin1 was identified as a target of miR-221, we did not detect a significant change in the expression of BC cells transfected with the miR-221 mimic or inhibitor. Previous studies have revealed that the downregulation of TP53INP1 could activate a p73-dependent DUSP10/ERK signaling pathway to promote the metastasis of hepatocellular carcinoma (31). Western blot analyses showed that the phosphorylation of ERK1/2 was significantly repressed after suppressing the expression of miR-221, and the expression of total ERK1/2 was unchanged in T24 cells (**Figure 2A**).

We constructed a luciferase reporter to further validate whether miR-221 directly targets the 3′UTR of TP53INP1. The predicted binding sites of TP53INP1 are shown in **Figure 2B**. Luciferase reporter assays confirmed that miR-221 could reduce the luciferase activity in the cells transfected with the plasmid harboring WT *TP53INP1* 3′UTR (*TP53INP1* WT) but did not affect luciferase activity in the cells transfected with plasmids harboring mutant *TP53INP1* (*TP53INP1* MUT) (**Figure 2B**).

Next, we determined whether suppression of miR-221 promoted autophagy and inhibited invasion and migration of BC cells via increasing TP53INP1. We found that the

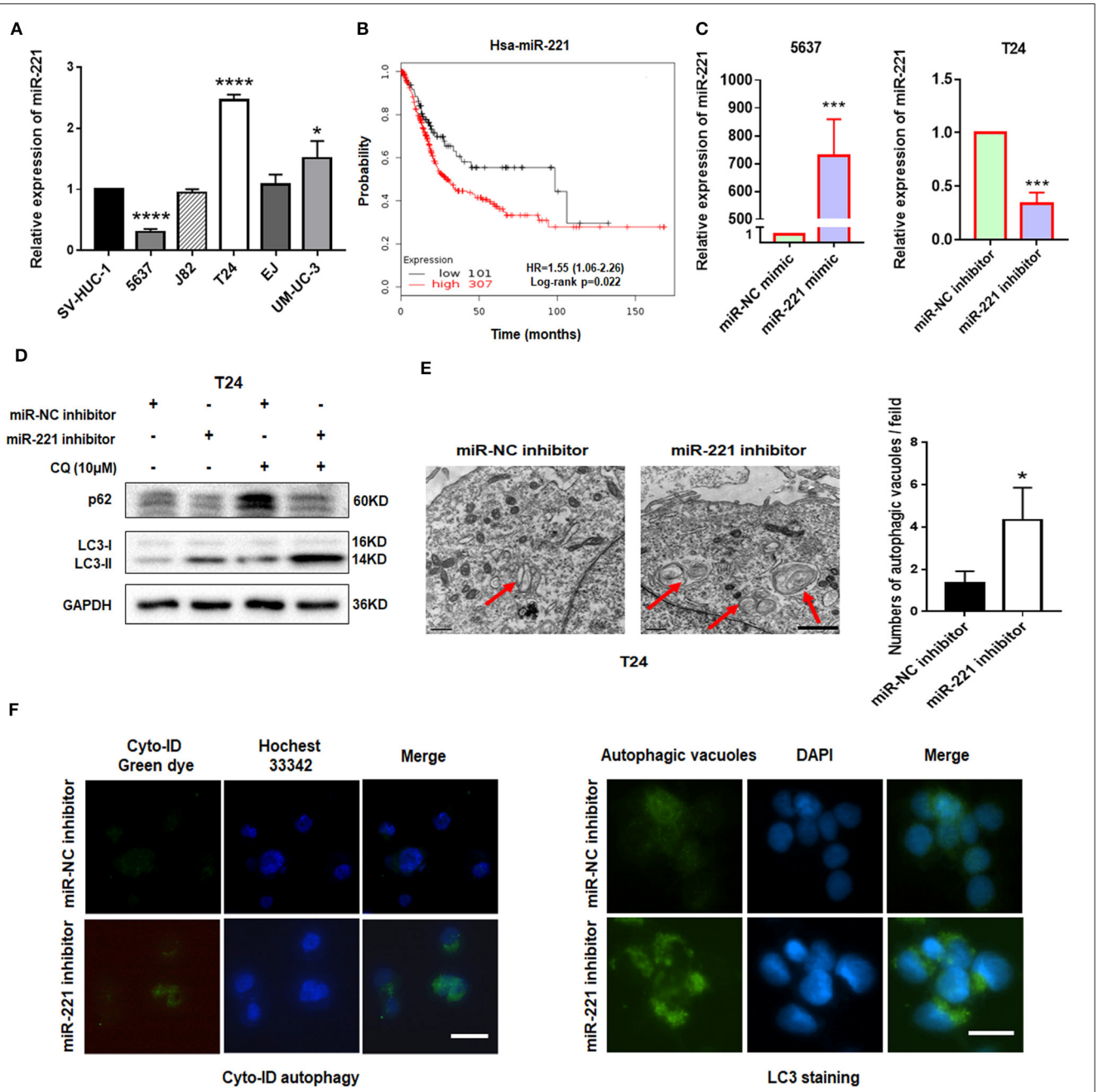

FIGURE 1 | Downregulation of miR-221 induces autophagy in bladder cancer (BC) cells. **(A)** The expression of miR-221 was determined by RT-qPCR in BC cell lines. SV-HUC-1 was used as a normal control. **(B)** The Kaplan–Meier survival analysis of low and high level of miR-221 from The Cancer Genome Atlas (TCGA) database. **(C)** Relative expression of miR-221 after knockdown and overexpression of miR-221 examined by RT-qPCR. **(D)** T24 cells were transfected with miR-221 inhibitor or miR-NC inhibitor for 24 h, followed by exposure to 10 mM chloroquine (CQ). **(E)** Two representative transmission electron microscopy (TEM) images were identified to show the autophagosome after knockdown of miR-221 for 24 h. Red arrows indicate autolysosome. Scale bar, 1 μm. **(F)** T24 cells were transfected with miR-221 inhibitor for 48 h and then stained with Cyto-ID Autophagy Detection Kit (left) and LC3 antibody (right). Scale bar, 50 μm. *$p < 0.05$, ***$p < 0.001$, and ****$p < 0.0001$.

downregulation of miR-221-induced autophagy could be partially blocked by knockdown of TP53INP1 (**Figure 2C**). Furthermore, the downregulation of miR-221-induced decrease of ERK phosphorylation was largely blocked by TP53INP1 knockdown (**Figure 2C**). On the other hand, the inhibition of invasion and migration induced by miR-221 suppression could be partly blocked by TP53INP1 knockdown (**Figures 2D,E**). Taken together, the downregulation of miR-221 could induce autophagy and inhibit invasion and migration of BC cells *in vitro* through the TP53INP1/p-ERK axis.

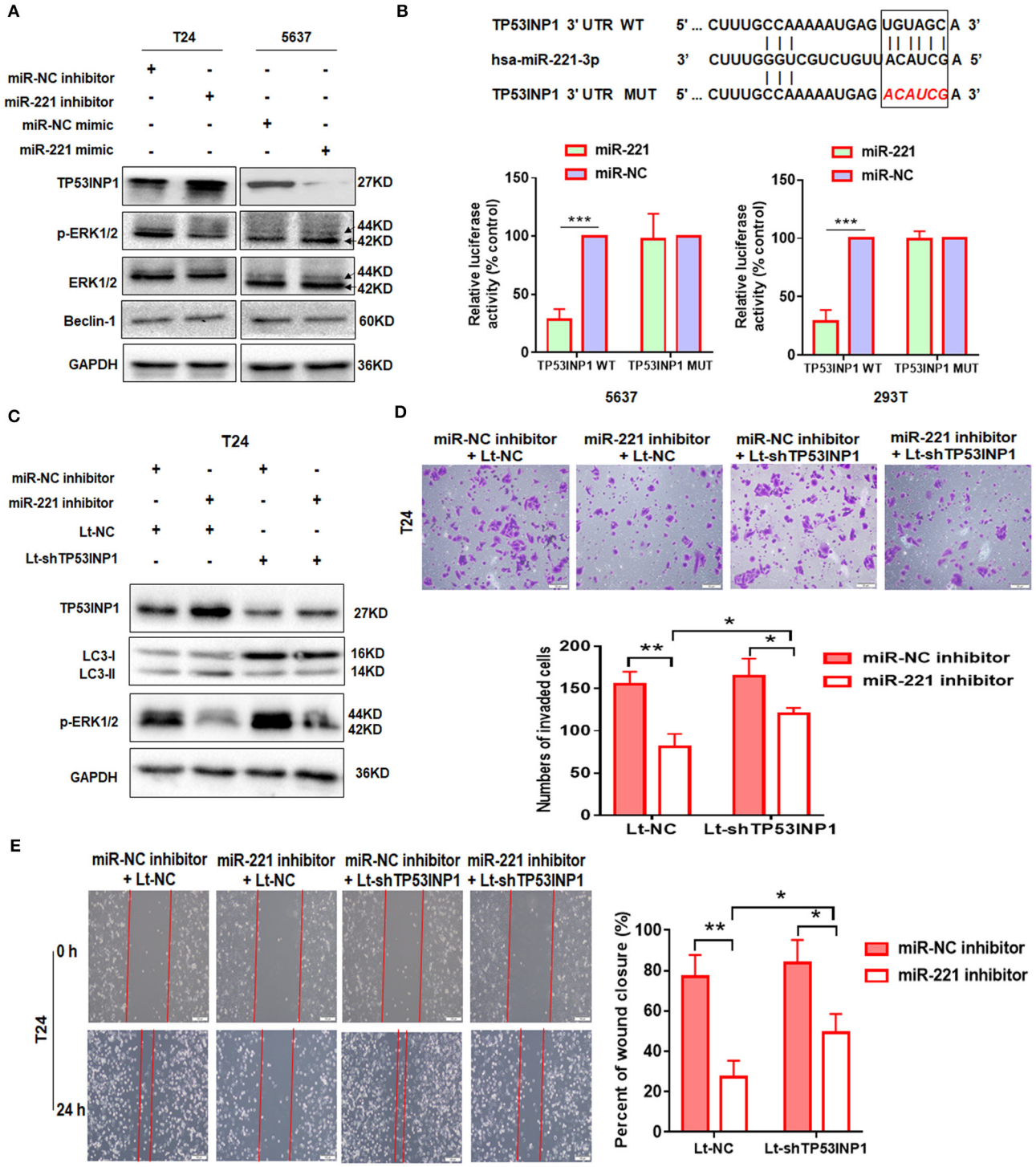

FIGURE 2 | TP53INP1 is the direct target of miR-221. **(A)** The protein expression of p62, LC3, TP53INP1, p-ERK1/2, and ERK1/2 in T24 cells treated by miR-221 inhibitor and 5637 cells treated by miR-221 mimic. Glyceraldehyde-3-phosphate dehydrogenase (GAPDH) was used for normalization. **(B)** Schematic illustration of the sequence of hsa-miR-221 and its complementary sequence in 3′UTR of TP53INP1 mRNA, in which the letters in red represent the five nucleotides we mutated. Luciferase activity assays using luciferase reporters with wild-type TP53INP1 3′UTR (TP53INP1 WT) or mutant TP53INP1 3′UTR (TP53INP1 MUT) were performed with co-transfection of miR-221 mimics or negative control into 5637 bladder cancer (BC) cells and 293T cells. Data represent the mean ± SD of triplicates. **(C–E)** T24 cells were transfected with miR-221 inhibitor or Lt-TP53INP1 for 48 h. A portion of the cells were harvested for IB analysis **(C)**. The other portion of cells were seeded in the upper chamber of the transwell system **(D)** or plated into six-well plates for 24 h, followed by wound healing assay **(E)**. Scale bar, 50 μm **(D)**, 100 μm **(E)**. $^{*}p < 0.05$, $^{**}p < 0.01$, and $^{***}p < 0.001$.

The Oncogenic Effect of miR-221 Is Extracellular Signal-Regulated Kinase Pathway-Dependent, and miR-221 Suppression-Induced Inhibition of Invasion and Migration Is Autophagy-Dependent

To further investigate the role of miR-221 in BC, we transfected the non-invasive BC line 5637 with a lentiviral vector encoding the human *MIR221* gene, while invasive BC cell line T24 was transfected with a specific *MIR221*-shRNA lentivirus. The transfection efficiency and expression of miR-221 were verified by RT-qPCR (**Figure 3A**). Subsequent Western blot analysis showed that the ectopic overexpression of miR-221 decreased TP53INP1 expression and enhanced the phosphorylation of ERK1/2 in 5637 cells. By contrast, the suppression of endogenous miR-221 expression increased the expression of TP53INP1 and repressed the phosphorylation of ERK1/2 in T24 cells (**Figure 3B**). Transwell and wound-healing assays showed that the ectopic overexpression of miR-221 could remarkably promote the invasive and migratory capacity of 5637 BC cells (**Figure 3D**), whereas the suppression of endogenous miR-221 expression could impede the invasive and migratory capacity of T24 BC cells (**Figure 3E**). To further validate the role of p-ERK1/2 signaling in miR-221-regulated invasion and migration of BC cells, we analyzed the impact of introducing an ERK inhibitor (U0126) into 5637 cells with stable miR-221 overexpression. As presented in **Figure 3D**, the introduction of U0126 attenuated *in vitro* cell migration and invasion abilities, suggesting that ERK signaling is needed to drive invasion and migration in BC cells with ectopic miR-221 overexpression.

Furthermore, to investigate whether the effects of miR-221 suppression on cellular invasion and migration were due to autophagy induction, we determined the effect of ATG5 knockdown (**Figure 3C**). We found that ATG5 knockdown partly blocked miR-221 suppression-induced inhibition of invasion and migration (**Figure 3E**).

Thereafter, we determine the impact of miR-221 on BC progression *in vivo*. We established a xenograft model by the subcutaneous implantation of T24-sh-miR-221 cells and their control cells into the posterior hip of nude mice, which were killed after 30 days. We found that the implantation of sh-miR-221 cells significantly impacted the BC cell proliferation *in vivo* (**Figure 3F**). Overall, these results suggested that the oncogenic effect of miR-221 is ERK pathway-dependent, and the effects of miR-221 suppression on cell invasion and migration are autophagy-dependent.

High-Mobility Group AT-Hook 1 Was Upregulated in Bladder Cancer and Correlated With miR-221

Thereafter, we investigated how miR-221 was upregulated in invasive BC cells. Previously, miR-221 is targeted and regulated by transcriptional factor HMGA1 during cervical cancer (18). In addition, as a key regulator of the autophagic pathway in cancer cells, HMGA1 might contribute to cancer progression (6). And HMGA1 mRNA was upregulated in BC and correlated with the prognosis of BC patients (19). However, the role of HMGA1 in BC remains unclear. It was unknown whether the miR-221-mediated autophagy, migration, and invasion of BC cells were regulated by HMGA1. We further evaluated the correlation between HMGA1 and miR-221 in The Cancer Genome Atlas (TCGA) database by LinkedOmics (32), in which we observed a strong and positive correlation between miR-221 and HMGA1 and a negative correlation between miR-221 and TP53INP1, HMGA1, and TP53INP1 in 402 BC tissues (**Figure 4A**). Given that HMGA1 might act as upstream of miR-221 and was overexpressed in BC, HMGA1 expression was silenced by siRNA transfection in the human BC T24 and 5637 cells (**Figure 4B**). We first evaluated the effect of HMGA1 silencing on the expression of miR-221 and TP53INP1 by RT-qPCR, observing a strong reduction of miR-221 and an increase of TP53INP1 (**Figure 4B**). Altogether, these data suggest that HMGA1 is correlated with miR-221 in BC.

We first chose to evaluate the expression of HMGA1 in TCGA database by Gene Expression Profiling Interactive Analysis (GEPIA) for exploring the function of HMGA1 in the progression of BC (33). Notably, HMGA1 expression was significantly increased in BC tissues and cell lines (**Figures 4C,E**). Furthermore, consistent with a previous study, the present study found that the high expression of HMGA1 was correlated with poor prognosis of patients with BC as revealed by provisional TCGA database analysis in the database (http://kmplot.com/analysis/) (**Figure 4D**). Next, we tested the HMGA1 level in 64 BC tissues and paired 48 adjacent non-tumor tissues by immunohistochemistry. As presented in **Figure 4F**, HMGA1 was highly expressed in 45/64 (70.31%) BC and 12/48 (25%) paracancer tissues ($p < 0.001$).

Downregulation of High-Mobility Group AT-Hook 1 Inhibits the Proliferation, Colony Formation, Invasion, and Migration of Bladder Cancer Cells by Promoting Autophagy

Next, we investigated the effect of HMGA1 on the proliferation of BC cell lines. CCK8 assays showed that HMGA1 silencing inhibited the proliferative capacities of T24 cells (**Figure 5A**). Consistent with the abovementioned results, the colony formation assays showed that the suppression of HMGA1 decreased colony formation (**Figure 5D**), and the transwell invasion and wound healing assays indicated that HMGA1 silencing significantly inhibited cell migration and invasion (**Figures 5E,F**).

To further illustrate the molecular mechanisms underlying the downregulation of the HMGA1-induced inhibition on BC cell proliferation, invasion, and migration, autophagy and apoptosis-related proteins were examined through Western blot analysis after HMGA1 knockdown in BC cells. We silenced HMGA1 expression in T24 cells by transfecting T24 cells with HMGA1 siRNA and examined the HMGA1 protein expression by Western blot analysis. As expected, the HMGA1 protein level was strikingly reduced in the siHMGA1 group compared with that in the siNC group. Consistent with a

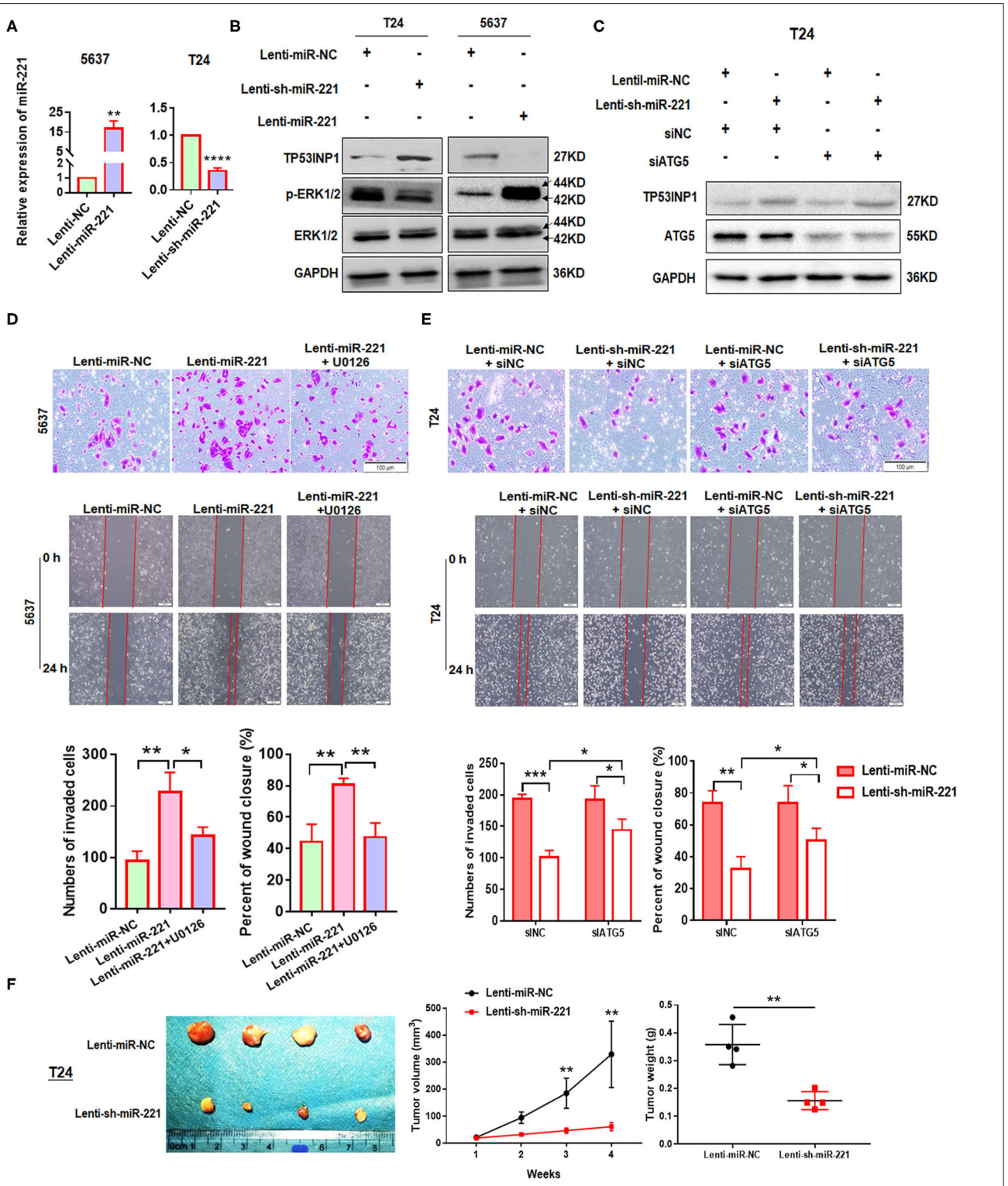

FIGURE 3 | MiR-221 suppression-induced inhibition of invasion and migration is autophagy dependent. **(A)** Relative expression of miR-221 after overexpression and knockdown of miR-221 in 5637 and T24 cells detected by RT-qPCR. **(B)** Validation of the expression of TP53INP1, p-ERK1/2, and ERK1/2 using Western blot analysis. Glyceraldehyde-3-phosphate dehydrogenase (GAPDH) was detected as loading control. **(C)** T24 cells were transfected with Lenti-sh-miR-221 or siRNA targeting ATG5 (siATG5). **(D,E)** Transwell invasion assays and wound healing assay of 5637 cells treated with Lenti-miR-221 and ERK inhibitor U0126 and T24 cells treated with Lenti-sh-miR-221 or siRNA targeting ATG5. Scale bar, 100 μm. **(F)** For the *in vivo* analyses, 5×10^6 T24-sh-miR-221 cells were injected subcutaneously into the posterior hip of nude mice. The mice were continuously observed for 30 days. Images of the tumors generated by T24-sh-miR-221 cells ($n = 4$). Tumor volume was monitored every week. Tumor weight was evaluated in T24-sh-miR-221 or miR-NC treated mice. $^*p < 0.05$, $^{**}p < 0.01$, $^{***}p < 0.001$, and $^{****}p < 0.0001$.

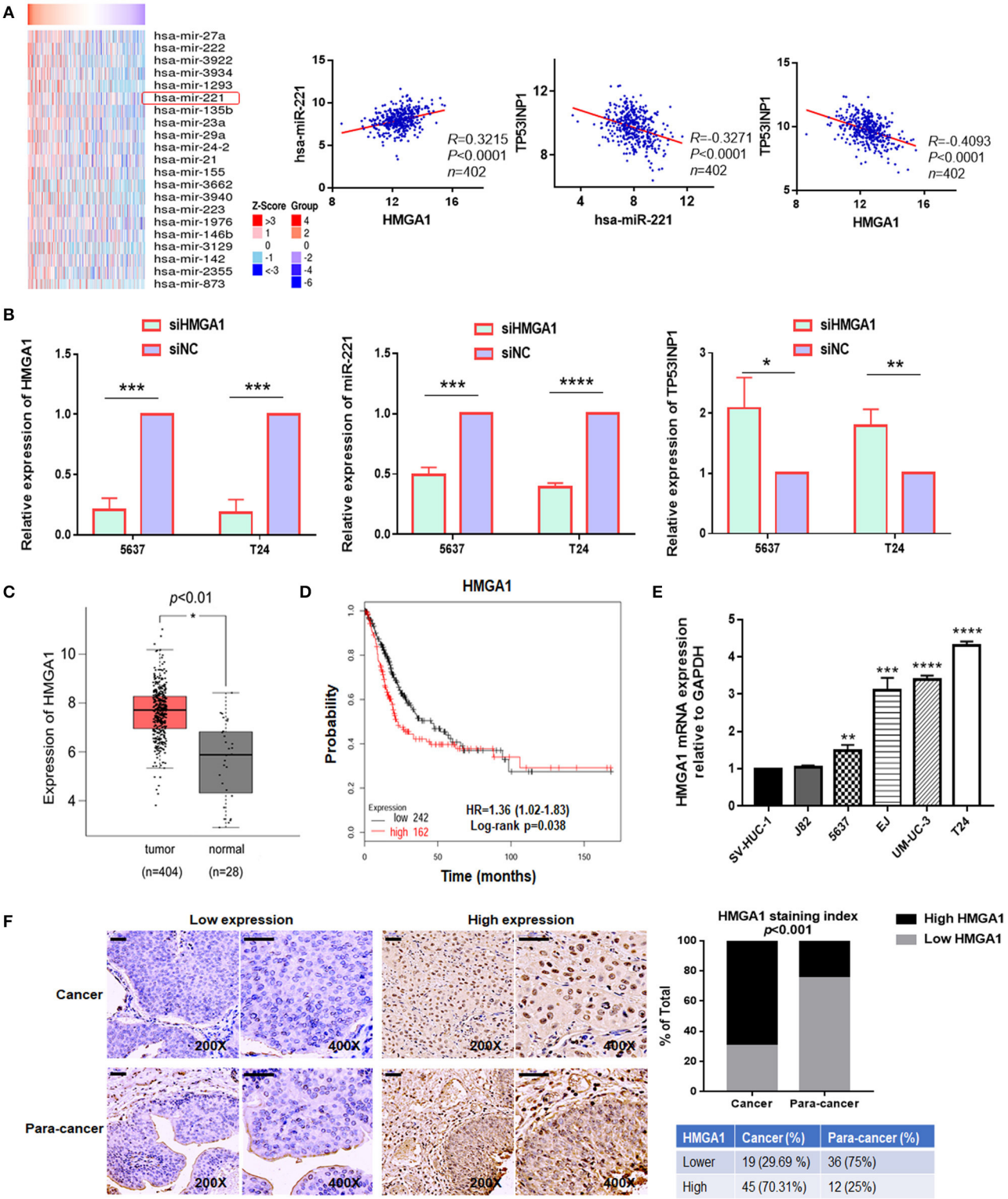

HMGA1	Cancer (%)	Para-cancer (%)
Lower	19 (29.69 %)	36 (75%)
High	45 (70.31%)	12 (25%)

FIGURE 4 | The expression of high-mobility group AT-hook 1 (HMGA1) and its correlation with miR-221 in bladder cancer (BC). **(A)** Heatmap diagram of differential miRNAs which were positively correlated with HMGA1 in The Cancer Genome Atlas (TCGA) database (left). The correlation between HMGA1 and miR-221, miR-221 and TP53INP1, and HMGA1 and TP53INP1 were examined in 402 cases of BC samples in the TCGA database (right). **(B)** The effects of siHMGA1 on the expression of HMGA1, miR-221, and TP53INP1 in 5637 and T24 cells were determined by RT-qPCR. **(C)** Expression of HMGA1 in BC samples (red box) and adjacent tissues (gray box). **(D)** The Kaplan–Meier survival analysis of low and high level of HMGA1 from the TCGA database. **(E)** The expression of HMGA1 was determined by RT-qPCR in BC cell lines. SV-HUC-1 was used as a normal control. **(F)** Immunohistochemistry (IHC) staining of HMGA1 in 64 BC tissues and paired 48 adjacent non-tumor tissues obtained from patients with BC. Scale bar, 50 μm. $^{*}p < 0.05$, $^{**}p < 0.01$, $^{***}p < 0.001$, and $^{****}p < 0.0001$.

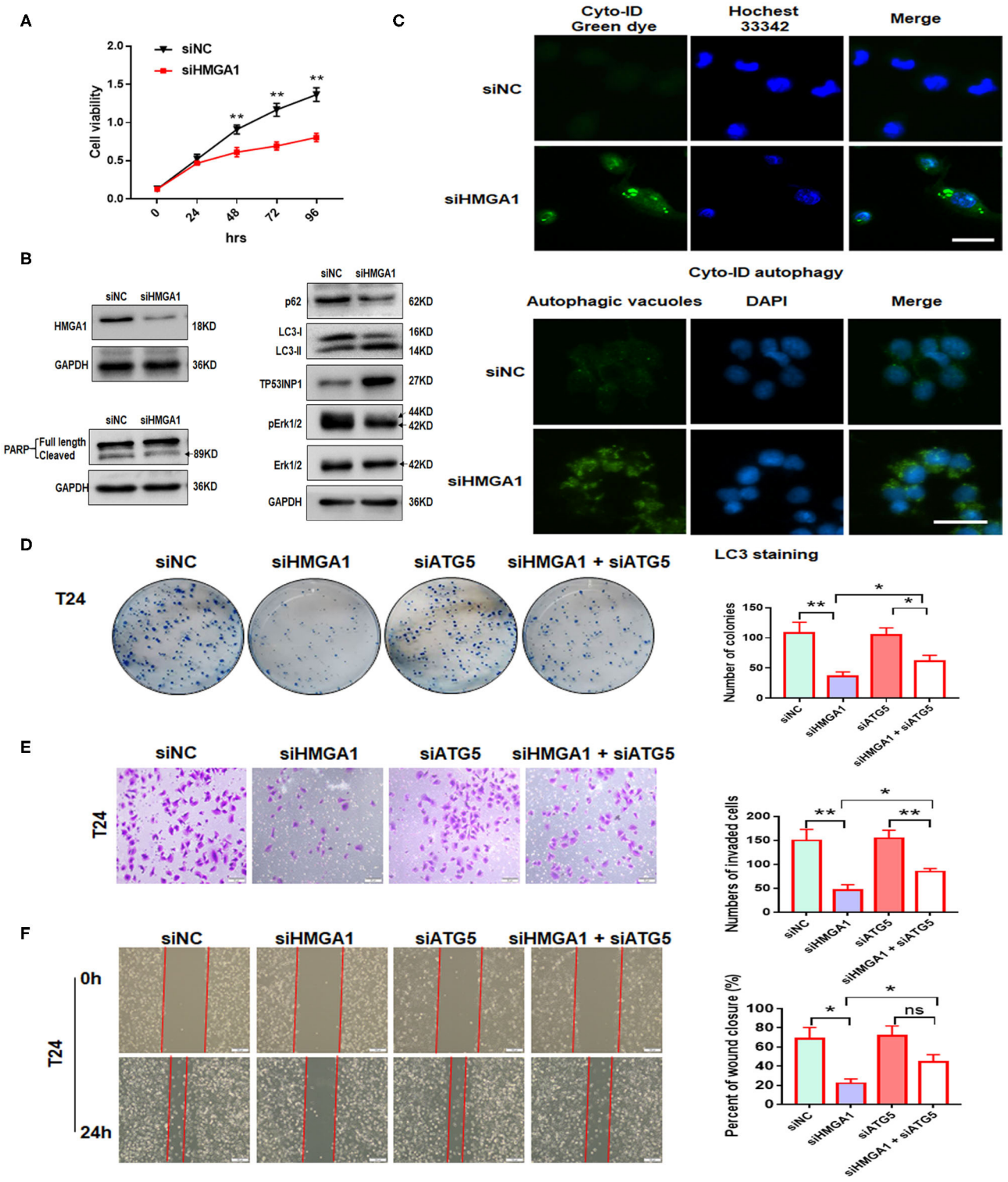

FIGURE 5 | The effect of high-mobility group AT-hook 1 (HMGA1) knockdown on autophagy and growth, invasion, and migration of bladder cancer (BC) cells. **(A)** Cell Counting Kit-8 (CCK-8) cell viability assay of T24 cells treated with siHMGA1. **(B)** The protein expression of HMGA1, poly (ADP-ribose) polymerase (PARP), p62, LC3, TP53INP1, p-ERK1/2, and ERK1/2 in T24 cells transfected with HMGA1 siRNA. **(C)** T24 cells were transfected with HMGA1 siRNA for 48 h and then stained with Cyto-ID Autophagy Detection Kit and LC3 antibody. Scale bar, 50 μm. **(D)** Cell clone numbers were counted when HMGA1 or ATG5 was silenced in T24. **(E)** The effect of HMGA1 or ATG5 knockdown on the invasive ability of T24 cells as detected by transwell invasion assay. Scale bar, 50 μm. **(F)** The effect of HMGA1 or ATG5 silencing on cell migration of T24 cells performed by wound healing assay. Scale bar, 100 μm. $^{*}p < 0.05$, $^{**}p < 0.01$ and ns, no statistical significance.

previous study (6), HMGA1 silencing significantly increased LC3-II protein levels and reduced p62 protein levels but did not induce apoptosis in T24 cells, as assessed by measuring the cleavage of PARP (**Figure 5B**). Interestingly, HMGA1 knockdown increased TP53INP1 expression and repressed the phosphorylation of ERK1/2 in T24 cells (**Figure 5B**). In addition, HMGA1 knockdown induced the formation and accumulation of autophagosomes (green fluorescence) in T24 cells (**Figure 5C**).

Furthermore, to investigate whether the effects of HMGA1 knockdown on cellular proliferation, invasion, and migration were due to autophagy induction, we knocked down ATG5 to abrogate autophagy. We found that ATG5 knockdown partly blocked HMGA1 silencing-induced inhibition of colony formation, invasion, and migration (**Figures 5D–F**). Overall, these results indicated that HMGA1 could modulate autophagy and contribute to the proliferation, invasion, and migration of BC cells.

MiR-221 Rescues the Impact of High-Mobility Group AT-Hook 1 Downregulation

We performed a colony formation assay, transwell invasion assay, and wound healing assay to further investigate the relationship between miR-221 and the effect induced by HMGA1 silencing. We found that miR-221 mimics could partly increase the efficiency of BC cell colony formation inhibited by the knockdown of HMGA1 (**Figure 6A**). Moreover, HMGA1 knockdown markedly inhibited cell invasion and migration, and miR-221 could rescue their invasive and migratory potential (**Figures 6B,C**).

Downregulation of High-Mobility Group AT-Hook 1 Modulates Autophagy Partly by miR-221/TP53INP1 Axis

Given that miR-221 was regulated by HMGA1 and positively correlated with HMGA1 expression in BC, we hypothesized that the regulation of miR-221 may account for the effects on autophagy caused by HMGA1 silencing. Subsequent Western blot analyses showed that the downregulation of HMGA1 increased the LC3-II/LC3-I expression ratio and decreased the p62 expression in T24 cells, whereas the miR-221 mimic significantly reversed the effect of HMGA1 silencing (**Figure 7A**). Furthermore, the miR-221 mimic significantly antagonized the increase in TP53INP1 expression and reduction in ERK1/2 phosphorylation mediated by HMGA1 silencing (**Figure 7A**). Overall, these data suggested that the downregulation of HMGA1 modulated autophagy partly through the miR-221/TP53INP1 axis (**Figure 7B**).

DISCUSSION

Recent studies have indicated that miR-221 acts as an oncogene in the tumorigenesis and progression of various cancers (18, 34, 35). Our study revealed that high expression of miR-221 was correlated with poor prognosis of BC patients, and downregulation of miR-221 strongly impeded BC cell invasion and migration by inducing autophagy via modulating TP53INP1/p-ERK1/2 axis. The suppression of miR-221 prevented BC proliferation *in vivo*. Moreover, we found that miR-221 was regulated by HMGA1. HMGA1 silencing induced a reduction of miR-221 and autophagy and inhibited the proliferative, invasive, and migratory capacities of BC cells by loss-of-function experiments, and overexpression of miR-221 rescues the effect of HMGA1 downregulation. In these contexts, our study supports that miR-221 and HMGA1 are potential therapeutic targets for BC.

MiR-221 acts as an important regulator of autophagy balance and cardiac remodeling by modulating the p27/CDK2/mTOR axis, and miR-221 has been implicated as a therapeutic target in heart failure (27). Moreover, miR-221 is downregulated by the overexpression of *mda-7*/IL-24 in a cancer cell-specific manner, and downregulation of miR-221 can cause toxic autophagy and cancer cell-specific death (36). In this study, we confirmed that miR-221 acts as an oncogene in BC. Through gain- or loss-of-function studies, we found that the downregulation of miR-221 could promote autophagy in BC. In addition, TP53INP1, which acts as a tumor suppressor by inducing cell death via caspase-dependent autophagy (37), was identified as a target of miR-221 through luciferase reporter assay (**Figure 2B**). TP53INP1 knockdown could in part abrogate the effect of miR-221 suppression-induced autophagy and inhibition of cell invasion and migration (**Figures 2C–E**).

The activation of mitogen-activated protein kinase (MAPK)/ERK plays a critical role in tumor progression and invasion (38). TP53INP1 downregulation can activate the ERK pathway in a p73-dependent DUSP10 manner (31). We now show that TP53INP1 is a target of miR-221, and the overexpression of miR-221 can promote cancer cell migration and invasion through the TP53INP1/p-ERK1/2 axis.

MiRNAs have been shown to be regulated by the upstream transcription factors (39). However, the transcriptional regulation of miR-221 in BC has not been reported. MiR-221 and miR-222 are highly homologous miRNAs that are significantly overexpressed in many human cancers (12). MiR-222 was reported to be regulated by HMGA1 which can promote cell proliferation through binding to the promoter of miR-222 in lung cancer (15). Moreover, HMGA1 can accelerate migration/invasion in cervical cancer via regulating the transcription of miR-221/222 (18). Bioinformatics mining in TCGA dataset showed that miR-221 was positively correlated with the expression of HMGA1 in BC samples (**Figure 4A**). This positive correlation indicated that HMGA1 might regulate its expression in BC. This relationship has been confirmed by HMGA1 silencing which resulted in the downregulation of miR-221 and the upregulation of TP53INP1 (**Figure 4B**). HMGA1 silencing also resulted in the downregulation of miR-222 (data not shown). But TP53INP1 did not increase when the miR-222 inhibitor was transfected into T24 and 5637 BC cells (data not shown).

HMGA1 is reported to have critical roles in the tumorigenesis and progression of various cancers (13). However, the role of HMGA1 in BC remains unknown. We now demonstrate that HMGA1 is overexpressed in BC cell lines and tissues, and HMGA1 high expression was associated with poor prognosis in BC. Moreover, our study showed that HMGA1 silencing

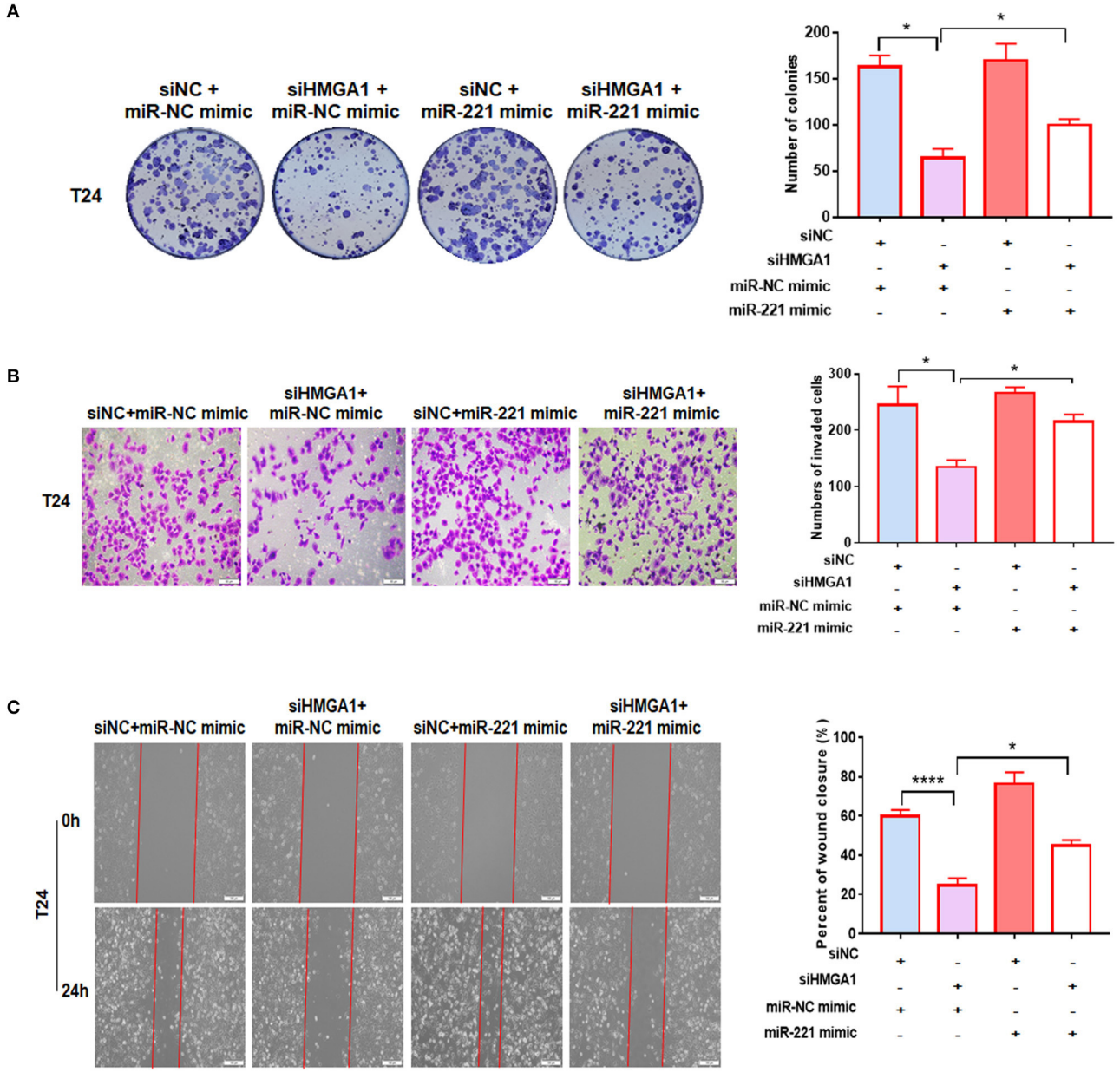

FIGURE 6 | MiR-221 reversed the high-mobility group AT-hook 1 (HMGA1) silencing-induced decrease in proliferation, migration, and invasion in bladder cancer (BC) cells. **(A)** Colony formation assay indicated that HMGA1 silencing inhibited cell proliferation of BC cells, and the effect was abolished by miR-221 mimics. **(B)** Transwell invasion assay demonstrated that downregulation of HMGA1 decreased the invasive capacity of BC cells, and this effect was eliminated by miR-221 mimics. Scale bar, 50 μm. **(C)** Wound healing assay revealed that HMGA1 silencing diminished the migratory ability of BC cells, and this effect was abrogated by miR-221 mimics. Scale bar, 100 μm. $^{*}p < 0.05$ and $^{****}p < 0.0001$.

could induce autophagy but not apoptosis in BC cells. HMGA1 silencing could inhibit the proliferative, invasive, and migratory capacities of BC cells, and these effects are autophagy-dependent. The previous study reported that HMGA1 inhibits autophagy through negatively regulating ULK1 transcriptional activity (6). HMGA1 has also been demonstrated to activate phosphoinositide 3-kinase (PI3K)/AKT and mammalian target of rapamycin complex 1 (mTORC1) pathway (40), which strongly inhibits autophagy in cancer cells (41). We have shown here that HMGA1 is involved in autophagy through regulating the miR-221/TP53INP1 axis. As a transcriptional factor, HMGA1 may have dozens of targets. HMGA1 may modulate autophagy through other mechanisms. But our results revealed that HMGA1 silencing could downregulate the expression of miR-221 and upregulate the levels of TP53INP1, which could interact with LC3 and promote autophagy-dependent

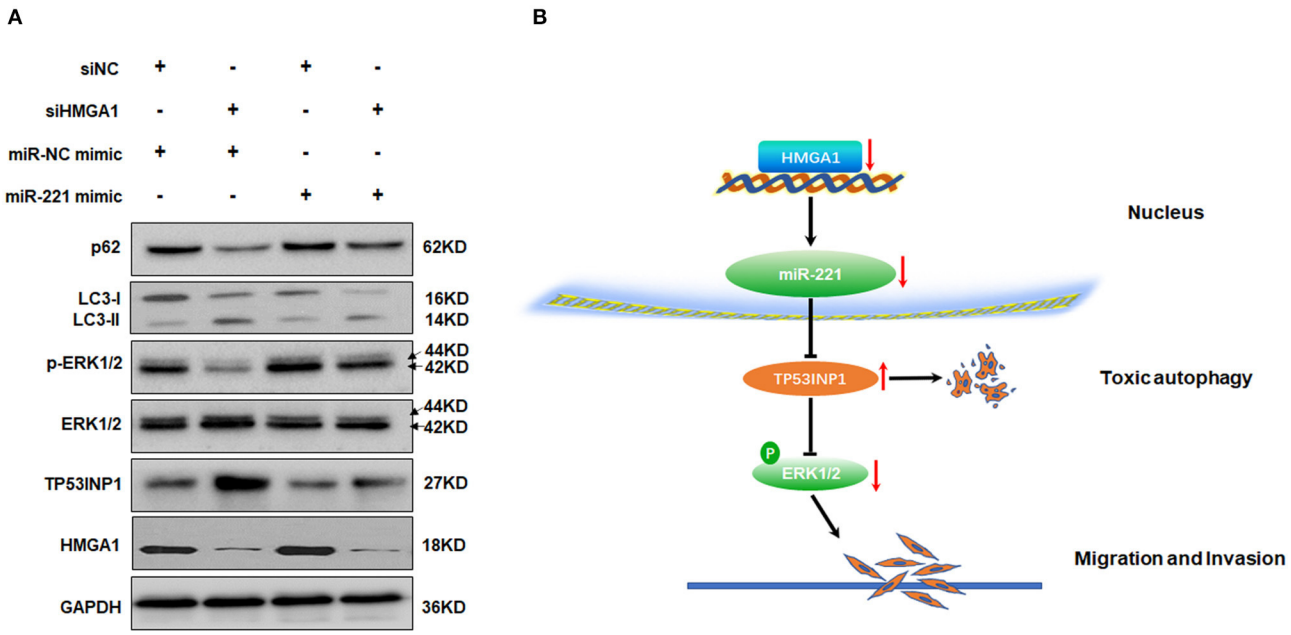

FIGURE 7 | MiR-221 antagonized the downregulation of high-mobility group AT-hook 1 (HMGA1)-mediated autophagy and the proposed model of the role of HMGA1 in autophagy and bladder cancer (BC) migration and invasion. **(A)** Immunoblotting analysis of p62, LC3, TP53INP1, ERK1/2, phosphorylated-ERK1/2, and HMGA1 protein expression in T24 cells transfected with siRNA targeting HMGA1 (siHMGA1) and/or miR-221 mimic for 48 h. Glyceraldehyde-3-phosphate dehydrogenase (GAPDH) was used for normalization. **(B)** Downregulation of HMGA1 mediates reduction of MiR-221 which increases the level of autophagy by directly targeting TP53INP1, followed by inhibition of the extracellular signal-regulated kinase (ERK) pathway, and results in the suppression of migration and invasion in BC.

cell death (37). Furthermore, the overexpression of miR-221 could inhibit HMGA1 downregulation-induced autophagy and partly reinstate the biological effect of HMGA1 downregulation. Therefore, the miR-221/TP53INP1 axis is regulated by HMGA1, and HMGA1 plays a vital role in BC progression.

In summary, this study highlights MiR-221 is regulated by HMGA1 and can target TP53INP1/p-ERK1/2 axis to inhibit autophagy and promote migration and invasion in BC cells. MiR-221 and HMGA1 are correlated with poor patient survival in BC and are valuable therapeutic targets.

DATA AVAILABILITY STATEMENT

The datasets generated for this study are available on request to the corresponding author.

ETHICS STATEMENT

The studies involving human participants were reviewed and approved by the first affiliated hospital of Nanchang university. The patients/participants provided their written informed consent to participate in this study. This animal study was reviewed and approved by the first affiliated hospital of Nanchang University.

AUTHOR CONTRIBUTIONS

XL, ZZ, and YW performed the experiments and generated data. XL, WD, KZ, YulL, XZ, LC, YuL, and AX analyzed data. TZ, GW, and BF designed the experiments. XL and BF wrote the manuscript. All authors reviewed and approved the manuscript.

FUNDING

This study was supported by the National Natural Science Foundation of P.R. China (Grant Nos. 81560419, 81960512, and 81602256), the Natural Science Foundation of Jiangxi (Grant No. 20151BAB205047), and the Jiangxi Provincial Graduate Innovation Special Fund Project (Grant No. YC2018-B019).

REFERENCES

1. Siegel RL, Miller KD, Jemal A. Cancer statistics, 2018. *CA Cancer J Clin*. (2018) 68:7–30. doi: 10.3322/caac.21442
2. Brausi M, Witjes JA, Lamm D, Persad R, Palou J, Colombel M, et al. A review of current guidelines and best practice recommendations for the management of nonmuscle invasive bladder cancer by the international bladder cancer group. *J Urol*. (2011) 186:2158–67. doi: 10.1016/j.juro.2011.07.076
3. Burger M, Catto JWF, Dalbagni G, Grossman HB, Herr H, Karakiewicz P, et al. Epidemiology and risk factors of urothelial bladder cancer. *Eur Urol*. (2013) 63:234–41. doi: 10.1016/j.eururo.2012.07.033

4. Abdollah F, Gandaglia G, Thuret R, Schmitges J, Tian Z, Jeldres C, et al. Incidence, survival and mortality rates of stage-specific bladder cancer in United States: a trend analysis. *Cancer Epidemiol*. (2013) 37:219–25. doi: 10.1016/j.canep.2013.02.002
5. Kobayashi T, Owczarek TB, McKiernan JM, Abate-Shen C. Modelling bladder cancer in mice: opportunities and challenges. *Nat Rev Cancer*. (2015) 15:42–54. doi: 10.1038/nrc3858
6. Conte A, Paladino S, Bianco G, Fasano D, Gerlini R, Tornincasa M, et al. High mobility group A1 protein modulates autophagy in cancer cells. *Cell Death Differ*. (2017) 24:1948–62. doi: 10.1038/cdd.2017.117
7. Mah LY, Ryan KM. Autophagy and cancer. *Cold Spring Harb Perspect Biol*. (2012) 4:a008821. doi: 10.1101/cshperspect.a008821
8. Levine B. Cell biology: autophagy and cancer. *Nature*. (2007) 446:745–7. doi: 10.1038/446745a
9. Thorburn A, Thamm DH, Gustafson DL. Autophagy and cancer therapy. *Mol Pharmacol*. (2014) 85:830838. doi: 10.1124/mol.114.091850
10. Bartel DP. MicroRNAs: genomics, biogenesis, mechanism, and function. *Cell*. (2004) 116:281–97. doi: 10.1016/S0092-8674(04)00045-5
11. Gebert LFR, MacRae IJ. Regulation of microRNA function in animals. *Nat Rev Mol Cell Biol*. (2019) 20:21–37. doi: 10.1038/s41580-018-0045-7
12. Ravegnini G, Cargnin S, Sammarini G, Zanotti F, Bermejo JL, Hrelia P, et al. Prognostic role of miR-221 and miR-222 expression in cancer patients: a systematic review and meta-analysis. *Cancers*. (2019) 11:970. doi: 10.3390/cancers11070970
13. Wang Y, Hu L, Zheng Y, Guo L. HMGA1 in cancer: cancer classification by location. *J Cell Mol Med*. (2019) 23:2293–2302. doi: 10.1111/jcmm.14082
14. Fusco A, Fedele M. Roles of HMGA proteins in cancer. *Nat Rev Cancer*. (2007) 7:899–910. doi: 10.1038/nrc2271
15. Zhang Y, Ma T, Yang S, Xia M, Xu J, An H, et al. High-mobility group A1 proteins enhance the expression of the oncogenic miR-222 in lung cancer cells. *Mol Cell Biochem*. (2011) 357:363–71. doi: 10.1007/s11010-011-0907-1
16. Liang L, Li X, Zhang X, Lv Z, He G, Zhao W, et al. MicroRNA-137, an HMGA1 target, suppresses colorectal cancer cell invasion and metastasis in mice by directly targeting FMNL2. *Gastroenterology*. (2013) 144:624–35. doi: 10.1053/j.gastro.2012.11.033
17. Méndez O, Peg V, Salvans C, Pujals M, Fernández Y, Abasolo I, et al. Extracellular HMGA1 promotes tumor invasion and metastasis in triple-negative breast cancer. *Clin Cancer Res*. (2018) 24:6367–82. doi: 10.1158/1078-0432.CCR-18-0517
18. Fu F, Wang T, Wu Z, Feng Y, Wang W, Zhou S, et al. HMGA1 exacerbates tumor growth through regulating the cell cycle and accelerates migration/invasion via targeting miR-221/222 in cervical cancer. *Cell Death Dis*. (2018) 9:594. doi: 10.1038/s41419-018-0683-x
19. Lin R, Shen W, Zhi Y, Zhou Z. Prognostic value of miR-26a and HMGA1 in urothelial bladder cancer. *Biomed Pharmacother*. (2014) 68:929–934. doi: 10.1016/j.biopha.2014.10.003
20. Frasca F, Rustighi A, Malaguarnera R, Altamura S, Vigneri P, Del Sal G, et al. HMGA1 inhibits the function of p53 family members in thyroid cancer cells. *Cancer Res*. (2006) 66:2980–9. doi: 10.1158/0008-5472.CAN-05-2637
21. Schuldenfrei A, Belton A, Kowalski J, Talbot CC, Di Cello F, Poh W, et al. HMGA1 drives stem cell, inflammatory pathway, and cell cycle progression genes during lymphoid tumorigenesis. *BMC Genomics*. (2011) 12:549. doi: 10.1186/1471-2164-12-549
22. Liu X, Wu Y, Zhou Z, Huang M, Deng W, Wang Y, et al. Celecoxib inhibits the epithelial-to-mesenchymal transition in bladder cancer via the miRNA-145/TGFBR2/Smad3 axis. *Int J Mol Med*. (2019) 44:683–93. doi: 10.3892/ijmm.2019.4241
23. Liu X, Xu X, Deng W, Huang M, Wu Y, Zhou Z, et al. CCL18 enhances migration, invasion and EMT by binding CCR8 in bladder cancer cells. *Mol Med Rep*. (2019) 19:1678–86. doi: 10.3892/mmr.2018.9791
24. Oeste CL, Seco E, Patton WF, Boya P, Pérez-Sala D. Interactions between autophagic and endo-lysosomal markers in endothelial cells. *Histochem Cell Biol*. (2013) 139:659–70. doi: 10.1007/s00418-012-1057-6
25. Fu B, Wang Y, Zhang X, Lang B, Zhou X, Xu X, et al. miR-221-induced PUMA silencing mediates immune evasion of bladder cancer cells. *Int J Oncol*. (2015) 46:1169–80. doi: 10.3892/ijo.2015.2837
26. Kenific CM, Debnath J. Cellular and metabolic functions for autophagy in cancer cells. *Trends Cell Biol*. (2015) 25:37–45. doi: 10.1016/j.tcb.2014.09.001
27. Su M, Wang J, Wang C, Wang X, Dong W, Qiu W, et al. MicroRNA-221 inhibits autophagy and promotes heart failure by modulating the p27/CDK2/mTOR axis. *Cell Death Differ*. (2015) 22:986–99. doi: 10.1038/cdd.2014.187
28. Chen Q, Zhou Y, Richards AM, Wang P. Up-regulation of miRNA-221 inhibits hypoxia/reoxygenation-induced autophagy through the DDIT4/mTORC1 and Tp53inp1/p62 pathways. *Biochem Biophys Res Commun*. (2016) 474:168–74. doi: 10.1016/j.bbrc.2016.04.090
29. Fan J, Sun Y, Wang S, Li Y, Zeng X, Cao Z, et al. Inhibition of autophagy overcomes the nanotoxicity elicited by cadmium-based quantum dots. *Biomaterials*. (2016) 78:102–14. doi: 10.1016/j.biomaterials.2015.11.029
30. Chen L, Li G, Peng F, Jie X, Dongye G, Cai K, et al. The induction of autophagy against mitochondria-mediated apoptosis in lung cancer cells by a ruthenium (II) imidazole complex. *Oncotarget*. (2016) 7:80716–34. doi: 10.18632/oncotarget.13032
31. Ng KY, Chan LH, Chai S, Tong M, Guan XY, Lee NP, et al. TP53INP1 downregulation activates a p73-dependent DUSP10/ERK signaling pathway to promote metastasis of hepatocellular carcinoma. *Cancer Res*. (2017) 77:4602–12. doi: 10.1158/0008-5472.CAN-16-3456
32. Vasaikar SV, Straub P, Wang J, Zhang B. LinkedOmics: analyzing multi-omics data within and across 32 cancer types. *Nucleic Acids Res*. (2018) 46:D956–63. doi: 10.1093/nar/gkx1090
33. Tang Z, Li C, Kang B, Gao G, Li C, Zhang Z. GEPIA: a web server for cancer and normal gene expression profiling and interactive analyses. *Nucleic Acids Res*. (2017) 45:W98–102. doi: 10.1093/nar/gkx247
34. Liu S, Wang Z, Liu Z, Shi S, Zhang Z, Zhang J, et al. miR-221/222 activate the Wnt/β-catenin signaling to promote triple-negative breast cancer. *J Mol Cell Biol*. (2018) 10:302–15. doi: 10.1093/jmcb/mjy041
35. Han J, Wang J-Z, Yang X, Yu H, Zhou R, Lu H-C, et al. METTL3 promote tumor proliferation of bladder cancer by accelerating pri-miR221/222 maturation in m6A-dependent manner. *Mol Cancer*. (2019) 18:110. doi: 10.1186/s12943-019-1036-9
36. Pradhan AK, Talukdar S, Bhoopathi P, Shen X-N, Emdad L, Das SK, et al. mda-7/IL-24 mediates cancer cell-specific death via regulation of miR-221 and the beclin-1 axis. *Cancer Res*. (2017) 77:949–59. doi: 10.1158/0008-5472.CAN-16-1731
37. Seillier M, Peuget S, Gayet O, Gauthier C, N'Guessan P, Monte M, et al. TP53INP1, a tumor suppressor, interacts with LC3 and ATG8-family proteins through the LC3-interacting region (LIR) and promotes autophagy-dependent cell death. *Cell Death Differ*. (2012) 19:1525–35. doi: 10.1038/cdd.2012.30
38. Reddy KB, Nabha SM, Atanaskova N. Role of MAP kinase in tumor progression and invasion. *Cancer Metastasis Rev*. (2003) 22:395–403. doi: 10.1023/A:1023781114568
39. Iwama H. Coordinated networks of microRNAs and transcription factors with evolutionary perspectives. *Adv Exp Med Biol*. (2013) 774:169–87. doi: 10.1007/978-94-007-5590-1_10
40. Liau SS, Jazag A, Ito K, Whang EE. Overexpression of HMGA1 promotes anoikis resistance and constitutive Akt activation in pancreatic adenocarcinoma cells. *Br J Cancer*. (2007) 96:993–1000. doi: 10.1038/sj.bjc.6603654
41. Laplante M, Sabatini DM. MTOR signaling in growth control and disease. *Cell*. (2012) 149:274–93. doi: 10.1016/j.cell.2012.03.017

Conflict of Interest: The authors declare that the research was conducted in the absence of any commercial or financial relationships that could be construed as a potential conflict of interest.

frontiers in Oncology

ORIGINAL RESEARCH
published: 19 May 2020
doi: 10.3389/fonc.2020.00755

Clinical Significance of Hotspot Mutation Analysis of Urinary Cell-Free DNA in Urothelial Bladder Cancer

Yujiro Hayashi[1], Kazutoshi Fujita[1], Kyosuke Matsuzaki[1], Marie-Lisa Eich[2,3], Eisuke Tomiyama[1], Makoto Matsushita[1], Yoko Koh[1], Kosuke Nakano[1], Cong Wang[1], Yu Ishizuya[1], Taigo Kato[1,4], Koji Hatano[1], Atsunari Kawashima[1], Takeshi Ujike[1], Motohide Uemura[1,4], Ryoichi Imamura[1], George J. Netto[2] and Norio Nonomura[1]*

[1] Department of Urology, Osaka University Graduate School of Medicine, Suita, Japan, [2] Department Pathology, University of Alabama at Birmingham, Birmingham, AL, United States, [3] Department Pathology, University Hospital Cologne, Cologne, Germany, [4] Department of Therapeutic Urologic Oncology, Osaka University Graduate School of Medicine, Suita, Japan

OPEN ACCESS

Edited by:
Masaki Shiota,
Kyushu University, Japan

Reviewed by:
Shigehiro Tsukahara,
Kyushu University, Japan
Takashi Matsumoto,
Kyushu University, Japan

***Correspondence:**
Kazutoshi Fujita
kazufujita2@gmail.com

Specialty section:
This article was submitted to Genitourinary Oncology, a section of the journal Frontiers in Oncology

Received: *05 March 2020*
Accepted: *20 April 2020*
Published: *19 May 2020*

Citation:
Hayashi Y, Fujita K, Matsuzaki K, Eich M-L, Tomiyama E, Matsushita M, Koh Y, Nakano K, Wang C, Ishizuya Y, Kato T, Hatano K, Kawashima A, Ujike T, Uemura M, Imamura R, Netto GJ and Nonomura N (2020) Clinical Significance of Hotspot Mutation Analysis of Urinary Cell-Free DNA in Urothelial Bladder Cancer. Front. Oncol. 10:755. doi: 10.3389/fonc.2020.00755

Recent studies showed the clinical utility of next-generation sequencing of urinary cell-free DNA (cfDNA) from patients with urothelial bladder cancer (UBC). In this study, we aimed to develop urinary cfDNA analysis by droplet digital PCR (ddPCR) as a high-throughput and rapid assay for UBC detection and prognosis. We analyzed urinary cfDNA of 202 samples from 2 cohorts. Test cohort was designed for investigating clinical utility of urinary cfDNA, and was composed of 74 samples from patients with UBC, and 52 samples of benign hematuria patients. Validation cohort was designed for validation and assessment of clinical utility comparing urinary cfDNA with UroVysion (Abbott, Illinois, USA), and was composed of 40 samples from patients with UBC, and 36 prospectively collected samples from patients under surveillance after surgery for urothelial carcinoma. We performed ddPCR analysis of hotspot gene mutations (*TERT* promoter and *FGFR3*). In the test cohort, the sensitivity of urinary cfDNA diagnosis was 68.9% (51/74) and the specificity was 100% in patients with UBC. The sensitivity increased to 85.9% when used in conjunction with urine cytology. In addition, patients with high *TERT* C228T allele frequency (≥14%) had significantly worse prognosis in bladder tumor recurrence than patients with low *TERT* C228T allele frequency or negative *TERT* C228T ($p = 0.0322$). In the validation cohort, the sensitivity of urinary cfDNA was 57.5% (23/40) and the specificity was 100% in UBC patients. The sensitivity of the combination of urine cytology with our hotspot analysis (77.5%) was higher than that of urine cytology with UroVysion (68.9%). In the post-surgical surveillance group, patients positive for the *TERT* C228T mutation had significantly worse prognosis for bladder tumor recurrence than mutation negative patients ($p < 0.001$). In conclusion, ddPCR analysis of urinary cfDNA is a simple and promising assay for the clinical setting, surpassing UroVysion for detection and prognosis determination in UBC.

Keywords: bladder cancer, *TERT* promoter, *FGFR3*, cell-free DNA, liquid biopsy, UroVysion, PCR, prognosis

INTRODUCTION

Urothelial bladder cancer (UBC) is one of the most common cancers in the world (1). Approximately 70% of UBC patients are diagnosed with non-muscle invasive bladder cancer at initial presentation (2). Non-muscle invasive bladder cancer is treated by transurethral resection of the bladder tumor (TURBT) and intravesical instillation therapy. Fifty to seventy percent of patients experience bladder tumor recurrence and 10–15% experience disease progression to muscle-invasive bladder cancer or distant metastasis (3, 4). For these reasons non-muscle invasive bladder cancer patients require cystoscopy, urine cytology, and computed tomography scans for a long period at regular intervals, but current follow-up methods are suboptimal due to their low sensitivity or high invasiveness (5).

Several urine-based diagnostic tools (UroVysion, NMP22, and etc) are approved for clinical use by The Food and Drug Administration. UroVysion is designed to detect aneuploidy for chromosome 3, 7, 17, and loss of 9p21 locus via fluorescence *in situ* hybridization (FISH) of cells in urinary sediments (6). Importantly, UroVysion can predict disease recurrence earlier than cystoscopy examination, suggesting that analysis of chromosomal changes by urinary analysis could predict disease recurrence in patients without visible tumors (7). However, none of these currently available tests are recommended for routine use due to their low sensitivity and high cost (2, 8).

There is an urgent need to develop useful and non-invasive assays for detection and surveillance of UBC. Several researchers have reported the utility of genomic analysis of urinary DNA from urothelial carcinoma patients by next-generation sequencing (NGS) (9–11).

NGS methods can produce a large amount of DNA data simultaneously, but a major hurdle in these methods is the data processing steps, or bioinformatics. Analysis by ddPCR can detect mutations with high sensitivity and is easy to interpret. In this study, we analyzed hotspot mutations in UBC using ddPCR analysis of urinary cfDNA focusing on *TERT* promoter and *FGFR3* mutations. Furthermore, we compared the clinical utility of cfDNA analysis with that of UroVysion.

MATERIALS AND METHODS

Patients and Samples

To select genes suitable for ddPCR analysis, 66 UBC tissues of formalin-fixed paraffin-embedded (FFPE) samples from Japanese patients were obtained by transurethral resection of bladder tumor (TURBT) performed at Osaka University Hospital. The samples were then analyzed by massively parallel sequencing as previously described (**Table S1**) (12–16).

We analyzed 202 urine samples from 2 distinct and independent cohorts: test and validation cohorts. The test cohort consisted of 74 urine samples collected before TURBT (pre-TURBT group 1), and 52 samples collected from patients with microscopic or macroscopic hematuria with no malignant findings in the urinary tract, confirmed by a urologist (hematuria group). In this group, two patients with hematuria and positive urine cytology were also included as they revealed no malignant findings in the lower and upper urinary tract after a follow-up of more than 1 year, confirmed by a detailed examination by a urologist. All the samples of the validation cohort were collected prospectively to exclude the selection bias. The validation cohort was composed of 40 urine samples collected before TURBT (pre-TURBT group 2), and 36 samples collected from patients receiving the standard surveillance protocol after TURBT or radical nephroureterectomy with negative urine cytology (surveillance group) (**Table 1**). For the validation cohort, we performed both UroVysion assay and urinary cfDNA analysis. All patients were treated at Osaka University Hospital during 2013–2019 and provided written informed consent. This study was approved by the Institutional Review Board of Osaka University (IRB #668-3).

Pathological Diagnosis

Histological diagnosis was performed by experienced pathologists according to the 8th edition of the AJCC stage classification (17), and the World Health Organization 2016 criteria (18). The urine cytology was also evaluated by pathologists according to our institutional criteria. Positive urine cytology was defined to be class IV and V. We used the highest urine cytology class for data analysis of patients receiving several cytology tests.

Sample Processing

The urine samples were processed to obtain the cfDNA following the method described in our earlier study (19). Briefly, post collection, the urine samples were centrifuged at 2,000 × g for 30 min, and the supernatants were stored at −80°C until use. Subsequently, the supernatants were thawed in a water bath at 27°C, and 12 mL of each supernatant was used for cfDNA purification after centrifugation at 16,000 × g for 10 min. The supernatant was processed by QIAamp Circulating Nucleic Acid Kit (QIAGEN, Hilden, Germany) as previously reported (19). The cell pellet was analyzed by UroVysion analysis.

Massively Parallel Sequencing

Mutation and data analysis were performed by massively parallel sequencing that assign a unique identifier to each template molecule for increasing the sensitivity as previously reported. In brief, the *TERT*SeqS (12–16) assay which targets the promoter region of *TERT*, and the UroSeqS (12–16) assay which targets 10 genes (*CDKN2A, ERBB2, FGFR3, HRAS, KRAS, MET, MLL, PIK3CA, TP53*, and *VHL*) were performed on the 66 FFPE UBC tissue samples. Multiplex PCR was used to detect these mutations. The 59 primer pairs for this PCR were listed in **Table S2**. PCR products were purified AMPure XP beads (Beckman Coulter, PA, USA) and sequenced on an Illumina Miseq (Illumina, Inc., San Diego, CA, USA). The average unique coverage depth was 27,688 × (range 667–108,370 ×) for TERTSeqs and 3,356 × (range 51–21,650 ×) for UroSeqs. These data of Japanese patients were derived from the results published before (13, 14).

TABLE 1 | Patients characteristics for urinary cell-free DNA analysis.

	Test cohort			Validation cohort		
	Pre-TURBT group1 (*n* = 74)	**Hematuria group (*n* = 52)**		**Pre-TURBT group2 (*n* = 40)**	**Surveillance group (*n* = 36)**	
	***n* (%)**	***n* (%)**	***p*-value**	***n* (%)**	***n* (%)**	***p*-value**
Age, median (range)	75 (31–91)	69 (38–89)	0.004	72.5 (47–89)	74 (44–89)	0.880
Gender						
Male	60 (81.1%)	38 (73.1%)	0.287	35 (87.5%)	31 (86.1%)	0.858
Female	14 (18.9%)	14 (26.9%)		5 (12.5%)	5 (13.9%)	
Cytology						
Positive	49 (66.2%)	2 (3.8%)	<0.0001	22 (55%)	0 (0%)	<0.0001
Negative	25 (33.8%)	50 (96.2%)		18 (45%)	36 (100%)	
UroVysion						
Positive	–	–		14 (35%)	3 (8.3%)	0.006
Negative	–	–		26 (65%)	32 (88.9%)	
Insufficient material	–	–		0 (0%)	1 (2.8%)	
Prior therapy history before urine collection						
Intravesical BCG therapy	3 (4.1%)	0 (0%)	0.142	5 (12.5%)	13 (36.1%)	0.016
Platinum-based systemic chemotherapy	1 (1.4%)	0 (0%)	0.400	2 (5.0%)	3 (8.3%)	0.558
Pathological T stage						
pTa	36 (48.6%)	–		21 (52.5%)	–	
pT1	23 (31.1%)	–		7 (17.5%)	–	
≥pT2	15 (20.3%)	–		8 (20%)	–	
No malignancy	0 (0%)	–		4 (10%)	–	
Grade						
High	56 (75.7%)	–		27 (67.5%)	–	
Low	17 (23%)	–		9 (22.5%)	–	
No malignancy	0 (0%)	–		4 (10%)	–	
Unknown	1 (1.4%)	–		0 (0%)	–	

Urine samples of validation cohort were collected prospectively to exclude selection bias.

Droplet Digital PCR (ddPCR)

Analysis of urine supernatants by ddPCR was performed on the QX100 Droplet Digital PCR System (Bio-Rad Laboratories, Hercules, CA, USA), including primers and probes (FAM, mutant type; HEX, wild type), and ddPCR Supermix for Probes (No dUTP) according to the manufacturer's protocol. Primers and probes (*TERT* promoters (g.1295228 C>T:C228T and g.1295250 C>T:C250T), and *FGFR3* S249C) for ddPCR, and PCR protocols were used as previously reported (19).

Statistical Analysis

Statistical analysis was performed using JMP Pro 14.0.0 (SAS Institute Inc., Cary, NC, USA). The patient characteristics were compared using the Mann-Whitney U test and chi-square test. A log rank test was performed for analysis of the difference between

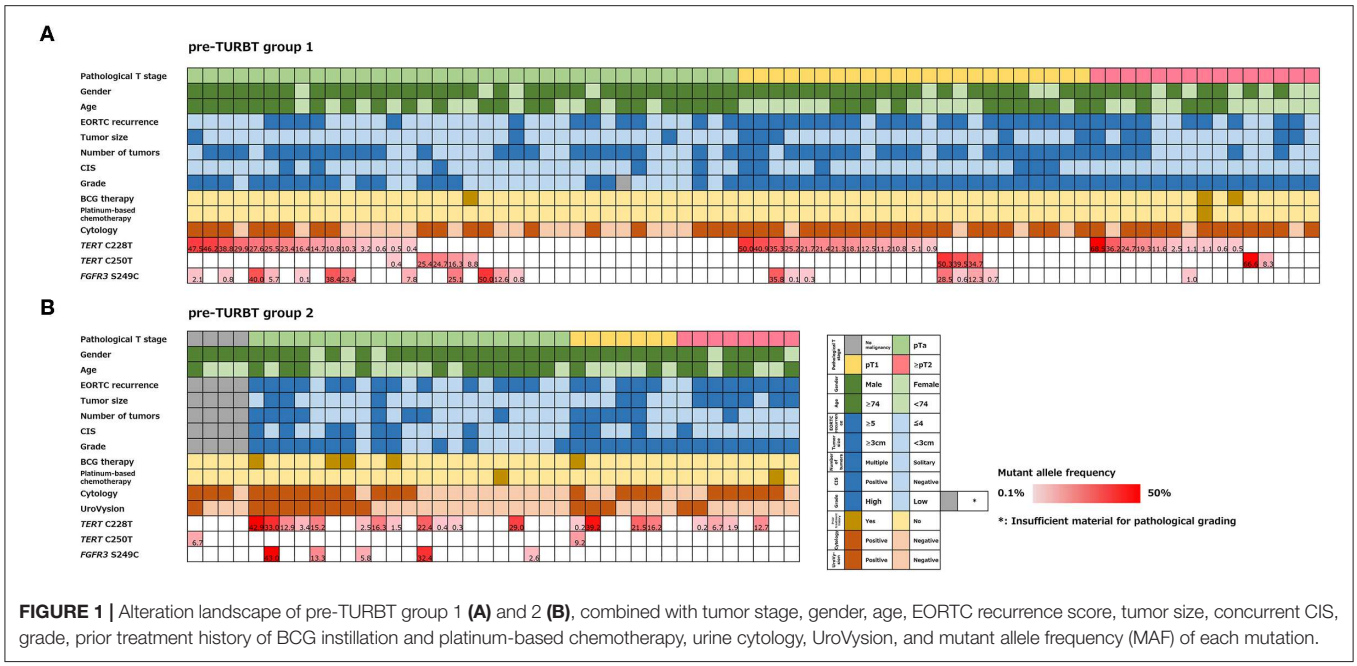

FIGURE 1 | Alteration landscape of pre-TURBT group 1 **(A)** and 2 **(B)**, combined with tumor stage, gender, age, EORTC recurrence score, tumor size, concurrent CIS, grade, prior treatment history of BCG instillation and platinum-based chemotherapy, urine cytology, UroVysion, and mutant allele frequency (MAF) of each mutation.

TABLE 2 | Positive rate of urinary cell-free DNA, urine cytology, and UroVysion for pre-TURBT group 1,2 and hematuria group.

	Pre-TURBT group 1		Hematuria group	Pre-TURBT gruop2		
	≤pT1 ($n = 59$)	≥pT2 ($n = 15$)	($n = 52$)	≤pT1 ($n = 28$)	≥pT2 ($n = 8$)	No malignancy ($n = 4$)
TERT C228T	28 (47.5%)	10 (66.7%)	0 (0%)	16 (57.1%)	4 (50%)	0 (0%)
TERT C250T	8 (13.6%)	2 (13.3%)	0 (0%)	1 (2.9%)	0 (0%)	1 (25%)
FGFR3 S249C	19 (32.2%)	1 (6.7%)	0 (0%)	5 (17.9%)	0 (0%)	0 (0%)
Overall (*TERT* promoter and *FGFR3*)	39 (66.1%)	12 (80%)	0 (0%)	18 (64.3%)	4 (5%)	1 (25%)
Cytology	37 (62.7%)	12 (80%)	2 (3.8%)	14 (50%)	5 (62.5%)	3 (75%)
UroVysion	–	–	–	11 (39.3%)	2 (25%)	1 (25%)

the two groups. The Cox proportional hazard model was used for univariate and multivariate analysis. The best cutoff value was determined by receiver-operating characteristics curve analysis. Differences were considered statistically significant when the $p < 0.05$.

RESULTS

Selection of Targeted Genes for Urinary cfDNA Analysis

At least one mutation was detected of 69.7% (46/66) of UBC tissues tested by massively parallel sequencing. *TERT* promoter mutations were detected in 48.5% (32/66) of tissues, TP53 mutations were found in 27.3% (18/66) of tissues, and *FGFR3* mutations were found in 24.2% (16/66) of tissues with high frequency. Although TP53 mutations are frequently found in UBC tissues, TP53 mutations are not suitable for ddPCR analysis because TP53 does not have hotspot mutations (**Figure S1**). However, *TERT* promoter mutations C228T and C250T, and *FGFR3* S249C are hotspot mutations with high frequency in UBC (**Figure S1**). We selected these 3 gene regions for urinary cfDNA hotspot mutation analysis by ddPCR.

Urinary cfDNA Analysis of the Test Cohort

The positive rate of urine cytology was 66.2% (49/74) in pre-TURBT group 1, and 3.8% (2/52) in hematuria group (**Table 1**). Clinical-pathological features and mutant allele frequency (MAF) of each mutation are shown in **Figure 1**. Among the patients in the pre-TURBT group 1 before urine samples were collected, three (4.1%) patients had received at least one intravesical BCG

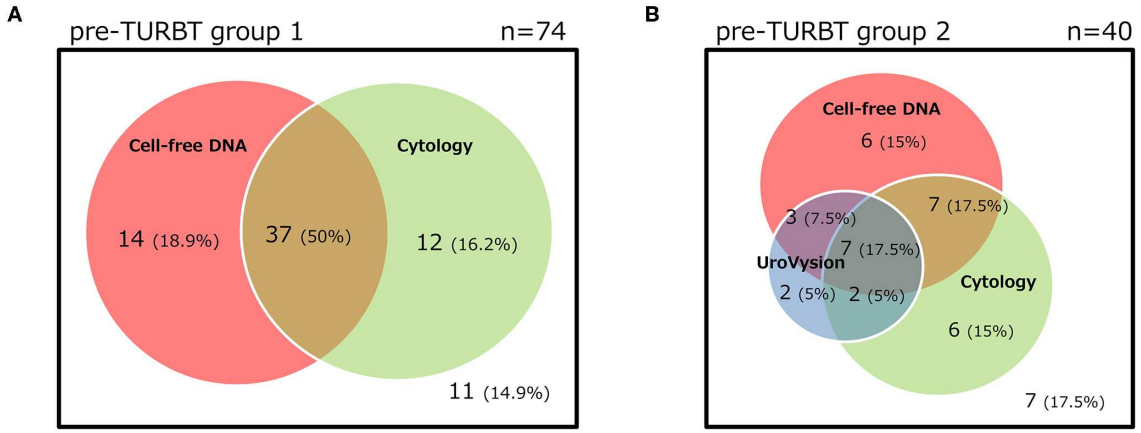

FIGURE 2 | The distribution of positive results for each test of pre-TURBT group 1 **(A)** and 2 **(B)**.

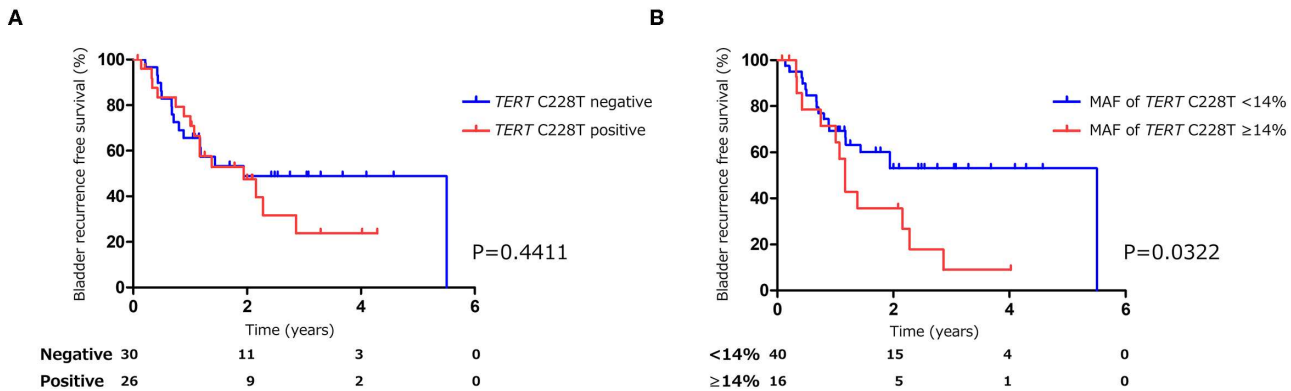

FIGURE 3 | Kaplan-Meier analysis of bladder tumor recurrence free survival of pre-TURBT group1 stratified by *TERT* C228T mutation **(A)**, and by mutant allele frequency (14%) of *TERT* C228T **(B)**.

therapy, and one (1.4%) patient had been treated with platinum-based regimens as adjuvant systemic chemotherapy for radical nephroureterectomy (**Table 1**, **Figure 1A**). The *TERT* C228T mutation was detected in both ≤pT1 tumor and ≥pT2 tumor in pre-TURBT group 1 at high frequency (**Table 2**, **Figure 1A**). The *FGFR3* S249C mutation was mainly detected in ≤pT1 tumor in pre-TURBT group 1 (**Table 2**, **Figure 1A**). There was no association between the positive rate of the three urinary cfDNA mutations and prior BCG instillation therapy history ($p = 0.235$) (**Figure 1A**). The sensitivity of urinary cfDNA analysis (*TERT* C228T, *TERT* C250T, and *FGFR3* S249C) was 68.9% in pre-TURBT 1, and the specificity was 96.2% using the hematuria group as the control cohort. When used in conjunction with urine cytology, the sensitivity increased to 85.1% in pre-TURBT group 1 (**Figure 2A**). Next, we analyzed the prognostic potential of urinary cfDNA. Although there was no association between presence of the *TERT* C228T mutation and bladder tumor recurrence, by stratifying the MAF of the *TERT* C228T at the best cut off point, the MAF of the *TERT* C228T mutation (≥14%) before TURBT was significantly associated with bladder tumor recurrence ($p = 0.0322$) (**Figure 3**). MAF of the *TERT* C228T mutation in urinary cfDNA before TURBT was an independent factor associated with bladder tumor recurrence after adjustment for European Organization for Research and Treatment of Cancer (EORTC) recurrence score and age (**Table 3**).

Urinary cfDNA Analysis of the Validation Cohort

The positive rate of urine cytology was 55% (22/40) in pre-TURBT group 2, and 0% in the surveillance group (**Table 1**). Among the patients in the pre-TURBT group 2 before urine samples were collected at the time of TURBT, five (12.5%) patients had received at least one intravesical BCG therapy, and two (5.0%) had been treated with platinum-based adjuvant chemotherapy for radical nephroureterectomy of upper tract urothelial carcinoma. Among the patients in the surveillance group, 13 (36.1%) patients had received at least one intravesical BCG therapy, and 3 (8.3%) had received platinum-based systemic chemotherapy before urine samples were collected (**Table 1**). Four patients were determined to have no evidence of tumor malignancy by pathological assessment of TURBT tissues in pre-TURBT group 2. Of these 4, one had the *TERT* C250T mutation, three had positive urine cytology, and 1 had a positive result by UroVysion (**Table 2**, **Figure 1B**). The positive rate of the 3 urinary cfDNA mutations was 57.5% in pre-TURBT group 2. There was no association between the positive rate of the three

TABLE 3 | Univariate and multivariate analysis of factors associated with bladder tumor recurrence.

	Univariate analysis			Multivariate analysis		
	Hazard ratio	**95% CI**	***p*-value**	**Hazard ratio**	**95% CI**	***p*-value**
Age						
(≥75 vs. ≤ 74)	1.82	0.87–3.93	0.1118	2.81	1.25–6.59	0.0119
EORTC recurrence score						
(≥5 vs. ≤ 4)	2.44	1.14–5.65	0.0208	2.59	1.16–6.16	0.0193
TERT C228T mutation						
(≥10% vs. <10%)	2.16	1.03–4.52	0.0417	2.28	1.03–5.01	0.0410

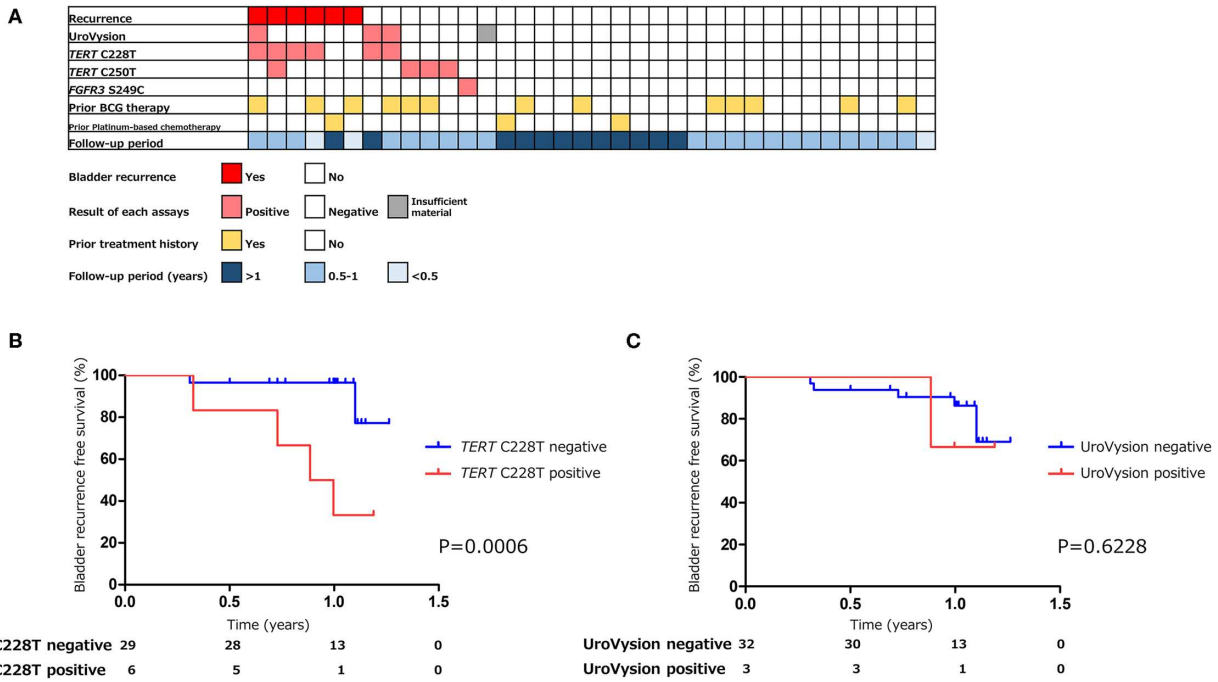

FIGURE 4 | The association of urinary markers and bladder tumor recurrence in surveillance group ($n = 36$) **(A)**. Kaplan–Meier analysis of bladder tumor recurrence free survival of surveillance group stratified by *TERT* C228T mutation **(B)**, and UroVysion **(C)**.

urinary cfDNA mutations and prior BCG instillation therapy or prior systemic chemotherapy in the pre-TURBT group 2 ($p = 0.477$), and surveillance group ($p = 0.677$) (**Figure 1B**). In addition, the sensitivity of urine cytology in conjunction with urinary cfDNA analysis (77.5%) was higher than when in conjunction with UroVysion (67.5%) (**Figure 2B**). Of the 36 patients in the surveillance group, 6 patients experienced bladder tumor recurrence during the follow-up period after sample collection (median: 364 days) (**Figure 4**). Of these 6 patients, 4 were positive for the *TERT* C228T mutation, but 1 patient tested positive by UroVysion assay. Patients in the surveillance group with the *TERT* C228T mutation had significantly worse prognosis for bladder tumor recurrence ($p = 0.0006$). This association was not detected by UroVysion assay ($p = 0.6228$) (**Figure 4**).

DISCUSSION

In this study, we showed the clinical utility of hotspot mutation analysis of urinary cell-free DNA by ddPCR for patients with UBC. This method aids in detection and surveillance of UBC in a non-invasive and simple manner. The sensitivity of urinary cfDNA analysis by ddPCR was high in both pre-TURBT groups. In combination with urine cytology, the sensitivity of urinary cfDNA assay was higher enough for clinical use than UroVysion. The mutant allele frequency of *TERT* C228T in urinary cfDNA before TURBT was significantly associated with bladder tumor recurrence. Furthermore, the utility of prognostic prediction of urinary cfDNA analysis of the TERT C228T was confirmed by samples prospectively collected in surveillance group. The *TERT* C228T mutation could predict disease recurrence more accurately than UroVysion.

Because urothelial carcinoma is directly and constantly in contact with urine, urinary cfDNA have clinical potential in cancer screening and disease monitoring of urothelial carcinoma (20, 21). There have been several studies on urinary cfDNA from UBC patients analyzed by NGS (9–11). Dudley et al. reported the usefulness of urinary cfDNA analysis by hybrid capture-based cancer personalized profiling by targeted deep sequencing (9). They reported that the sensitivity for early-stage

bladder cancer was 84% (45/54), and urinary cfDNA mutations detected by NGS were significantly associated with bladder tumor recurrence ($p < 0.0001$). The sensitivity of urinary cfDNA analysis targeting *TERT* promoter and *FGFR3* mutations by ddPCR was lower than the NGS method, but the sensitivity was comparable to the NGS method when combined with urine cytology. Hotspot mutation analysis by ddPCR is simple enough for clinical use. We also showed that hotspot mutations of *TERT* promoter and *FGFR3* are frequently identified in tumor tissues of Japanese UBC patients consistent with those in previous report in Western countries (22). This confirms that our ddPCR method can be utilized for various ethnicities. Mutations in the upstream of *TERT* gene mainly affect two hotspots (C228T and C250T) (12, 23). This region recruits transcription factor and engages in long-range chromatin interactions (24, 25). The C228T mutation in the *TERT* promoter region has been shown to increase *TERT* expression more than the C250T mutation (26). We demonstrated that the *TERT* C228T mutation was significantly associated with bladder tumor recurrence in the surveillance group, and that ≥14% MAF of *TERT* C228T, and not just a positive for *TERT* C228T, was associated with bladder tumor recurrence in pre-TURBT group 1. This observation could be due to the volume of the *TERT* C228T reflect in bladder cancer activity, playing an important biological role in recurrence of UBC.

UroVysion is a FISH assay that detects aneuploidy of urothelial cells in urine. The overall sensitivity of UroVysion in previous studies varied from 36 to 86% (27, 28). This wide range of clinical performance might be due to bias in the selection of patients. In this study, the sensitivity of UroVysion in pre-TURBT group 2, in which samples were collected prospectively to exclude selection bias, was determined to be 35%. Kim et al. reported that UroVysion can predict disease recurrence and progression in patients with non-muscle invasive bladder cancer present as negative by cystoscopy (7). Of the 6 patients who experienced bladder tumor recurrence during the follow-up period, one had tested positive by UroVysion, and four patients tested positive for *TERT* C228T. *TERT* C228T analysis has been shown to predict disease recurrence more precisely UroVysion.

In this study, the MAF of urinary cfDNA was observed to be more than 50% in some cases (**Figure 1**), and as the occurrence of SNPs in the three gene regions evaluated in this study was rare (29), the mutated genes in urinary cfDNA were thought to be mainly derived from a urothelial tumor, not from normal cells.

This study has several limitations. First, the size of each patient group was small; especially, the number of patients who experienced bladder tumor recurrence was only six in the surveillance group. Larger size and multi-institutional study are needed to warrant current method. Second, the design of the primers needs cost-benefit optimization. The analysis of three gene regions by ddPCR presented in this study is useful in a clinical setting due to its simplicity. Addition of other mutated genes analyzed could increase the sensitivity but would increase the cost per test. Currently, our *TERT* promoter and *FGFR3* mutation analysis is sufficient for clinical use in combination with urine cytology. Finally, there could be possibilities of contamination by blood cells or epithelium though we performed centrifugation to remove cellular components in processing urine samples, which might result in a lower MAF than the actual value. Therefore, careful interpretation should be made for the cases with lower MAF in urinary cfDNA.

In conclusion, we demonstrated the clinical utility of *TERT* promoter and *FGFR3* hotspot mutation analysis in urinary cfDNA from UBC patients by ddPCR. The combination of urine cytology with urinary cfDNA analysis showed a higher sensitivity than when combined with UroVysion, enough to justify utilization of ddPCR analysis in the clinic. Liquid biopsy analysis of *TERT* promoter and *FGFR3* mutations in urinary cfDNA could be a novel diagnostic and prognostic biomarker for UBC.

DATA AVAILABILITY STATEMENT

The raw data supporting the conclusions of this article will be made available by the authors, without undue reservation, to any qualified researcher.

ETHICS STATEMENT

The studies involving human participants were reviewed and approved by Osaka University. The patients/participants provided their written informed consent to participate in this study.

AUTHOR CONTRIBUTIONS

YH: conceptualization, formal analysis, methodology, investigation, and writing-original draft. KF: conceptualization, supervision, and writing-review and editing. KM: sample collection. M-LE: data analysis. ET: investigation and sample collection. MM, YK, KN, CW, and YI: investigation. TK, KH, AK, TU, MU, RI, and NN: supervision. GN: conceptualization and supervision.

FUNDING

This study was supported by Osaka University Grant.

ACKNOWLEDGMENTS

We thank all other researchers in our laboratory.

SUPPLEMENTARY MATERIAL

The Supplementary Material for this article can be found online at: https://www.frontiersin.org/articles/10.3389/fonc.2020.00755/full#supplementary-material

REFERENCES

1. Spiess PE, Agarwal N, Bangs R, Boorjian SA, Buyyounouski MK, Clark PE, et al. Bladder cancer, version 5.2017, NCCN clinical practice guidelines in oncology. *J Natl Compr Canc Netw.* (2017) 15:1240–67. doi: 10.6004/jnccn.2017.0156
2. Babjuk M, Burger M, Compérat EM, Gontero P, Mostafid AH, Palou J, et al. European association of urology guidelines on non-muscle-invasive bladder cancer (TaT1 and carcinoma *in situ*) - (2019). update. *Euro Urol.* (2019) 76:639–57 doi: 10.1016/j.eururo.2019.08.016
3. Prout GR Jr, Barton BA, Griffin PP, Friedell GH. Treated history of noninvasive grade 1 transitional cell carcinoma. The national bladder cancer group. *J Urol.* (1992) 148:1413–9. doi: 10.1016/S0022-5347(17)36924-0
4. Sylvester RJ, Van Der Meijden AP, Oosterlinck W, Witjes JA, Bouffioux C, Denis L, et al. Predicting recurrence and progression in individual patients with stage Ta T1 bladder cancer using EORTC risk tables: a combined analysis of 2596 patients from seven EORTC trials. *Eur Urol.* (2006) 49:466–5. doi: 10.1016/j.eururo.2005.12.031
5. Lotan Y, Roehrborn CG. Sensitivity and specificity of commonly available bladder tumor markers versus cytology: results of a comprehensive literature review and meta-analyses. *Urology.* (2003) 61:109–18. doi: 10.1016/S0090-4295(02)02136-2
6. Sokolova IA, Halling KC, Jenkins RB, Burkhardt HM, Meyer RG, Seelig SA, et al. The development of a multitarget, multicolor fluorescence in situ hybridization assay for the detection of urothelial carcinoma in urine. *J Mol Diagn.* (2000) 2:116–23. doi: 10.1016/S1525-1578(10)60625-3
7. Kim PH, Sukhu R, Cordon BH, Sfakianos JP, Sjoberg DD, Hakimi AA, et al. Reflex fluorescence in situ hybridization assay for suspicious urinary cytology in patients with bladder cancer with negative surveillance cystoscopy. *BJU Int.* (2014) 114:354–9. doi: 10.1111/bju.12516
8. Chang SS, Boorjian SA, Chou R, Clark PE, Daneshmand S, Konety BR, et al. Diagnosis and treatment of non-muscle invasive bladder cancer: AUA/SUO guideline. *J Urol.* (2016) 196:1021–9. doi: 10.1016/j.juro.2016.06.049
9. Dudley JC, Schroers-martin J, Lazzareschi DV, Shi WY, Chen SB, Esfahani MS, et al. Detection and surveillance of bladder cancer using urine tumor DNA. *Cancer Discov.* (2019) 9:500–9. doi: 10.1158/2159-8290.CD-18-0825
10. Satyal U, Srivastava A, Abbosh PH. Urine biopsy-liquid gold for molecular detection and surveillance of bladder cancer. *Front Oncol.* (2019) 9:1266. doi: 10.3389/fonc.2019.01266
11. Ward DG, Gordon NS, Boucher RH, Pirrie SJ, Baxter L, Ott S, et al. Targeted deep sequencing of urothelial bladder cancers and associated urinary DNA: a 23-gene panel with utility for non-invasive diagnosis and risk stratification. *BJU Int.* (2019) 124:532–44. doi: 10.1111/bju.14808
12. Kinde I, Munari E, Faraj SF, Hruban RH, Schoenberg M, Bivalacqua, et al. TERT promoter mutations occur early in urothelial neoplasia and are biomarkers of early disease and disease recurrence in urine. *Cancer Res.* (2013) 73:7162–7. doi: 10.1158/0008-5472.CAN-13-2498
13. Springer SU, Chen CH, Rodriguez Pena MDC, Li L, Douville C, Wang Y, et al. Non-invasive detection of urothelial cancer through the analysis of driver gene mutations and aneuploidy. *Elife.* (2018) 7:e43237. doi: 10.7554/eLife.32143
14. Eich ML, Rodriguez Pena MDC, Springer SU, Taheri D, Tregnago AC, Salles DC, et al. Incidence and distribution of UroSEEK gene panel in a multi-institutional cohort of bladder urothelial carcinoma. *Mod Pathol.* (2019) 32:1544–50. doi: 10.1038/s41379-019-0276-y
15. Rodriguez Pena MDC, Tregnago AC, Eich ML, Springer S, Wang Y, Taheri D, et al. Spectrum of genetic mutations in de novo PUNLMP of the urinary bladder. *Virchows Arch.* (2017) 471:761–7. doi: 10.1007/s00428-017-2164-5
16. Nguyen D, Taheri D, Springer S, Cowan M, Guner G, Mendoza Rodriguez MA, et al. High prevalence of TERT promoter mutations in micropapillary urothelial carcinoma. *Virchows Arch.* (2016) 469:427–34. doi: 10.1007/s00428-016-2001-2
17. American Joint Committee on Cancer. *AJCC Cancer Staging Manual, 8th edition*. Chicago, IL (2017).
18. *WHO Classification of Tumours of Urinary System & Male Genital Organs, 4th edition*. Geneva: World Health Organization (2016).
19. Hayashi Y, Fujita K, Matsuzaki K, Matsushita M, Kawamura K, Koh Y, et al. Diagnostic potential of TERT promoter and FGFR3 mutations in urinary cell-free DNA in upper tract urothelial carcinoma. *Cancer Sci.* (2019) 110:1771–9. doi: 10.1111/cas.14000
20. Hayashi Y, Fujita K. A new era in the detection of urothelial carcinoma by sequencing cell-free DNA. *Transl Androl Urol.* (2019) 8:S497–501. doi: 10.21037/tau.2019.08.26
21. Yoshida T, Kates M, Fujita K, Bivalacqua TJ, McConkey DJ. Predictive biomarkers for drug response in bladder cancer. *Int J Urol.* (2019) 26:1044–53. doi: 10.1111/iju.14082
22. Pietzak EJ, Bagrodia A, Cha EK, Drill EN, Iyer G, Isharwal S, et al. ext-generation sequencing of nonmuscle invasive bladder cancer reveals potential biomarkers and rational therapeutic targets. *Eur Urol:.* (2017) 72:952–9. doi: 10.1016/j.eururo.2017.05.032
23. Vinagre J, Almeida A, Pópulo H, Batista R, Lyra J, Pinto V, et al. Frequency of TERT promoter mutations in human cancers. *Nat Commun.* (2013) 4:2185. doi: 10.1038/ncomms3185
24. Stern JL, Theodorescu D, Vogelstein B, Papadopoulos N, Cech TR. Mutation of the TERT promoter, switch to active chromatin, and monoallelic TERT expression in multiple cancers. *Genes Dev.* (2015) 29:2219–24. doi: 10.1101/gad.269498.115
25. Min J, Shay JW. TERT promoter mutations enhance telomerase activation by long-range chromatin interactions. *Cancer Discov.* (2016) 6:1212–4. doi: 10.1158/2159-8290.CD-16-1050
26. Chiba K, Lorbeer FK, Shain AH, McSwiggen DT, Schruf E, Oh A, et al. Mutations in the promoter of the telomerase gene TERT contribute to tumorigenesis by a two-step mechanism. *Science.* (2017) 357:1416–20. doi: 10.1126/science.aao0535
27. Lokeshwar VB, Habuchi T, Grossman HB, Murphy WM, Hautmann SH, Hemstreet GP III, et al. Bladder tumor markers beyond cytology: international consensus panel on bladder tumor markers. *Urology.* (2005) 66:35–63. doi: 10.1016/j.urology.2005.08.064
28. van Rhijn BW, van der Poel HG, van der Kwast TH. Urine markers for bladder cancer surveillance: a systematic review. *Eur Urol.* (2005) 47:736–48. doi: 10.1016/j.eururo.2005.03.014
29. Sherry ST, Ward MH, Kholodov M, Baker J, Phan L, Smigielski EM, et al. dbSNP: the NCBI database of genetic variation. *Nucleic Acids Res.* (2001) 29:308–11. doi: 10.1093/nar/29.1.308

Conflict of Interest: GN equity or royalty from the licensed technologies from Johns Hopkins that are related to the work described in this paper.

The remaining authors declare that the research was conducted in the absence of any commercial or financial relationships that could be construed as a potential conflict of interest.

frontiers in Oncology

SYSTEMATIC REVIEW
published: 20 May 2020
doi: 10.3389/fonc.2020.00677

Prognostic Role of Serum Lactate Dehydrogenase in Patients With Urothelial Carcinoma: A Systematic Review and Meta-Analysis

Minhong Wu[1], Pengxiu Lin[1], Lifang Xu[2], Zhiling Yu[1], Qingsheng Chen[1], Hongyong Gu[1] and Cailing Liu[1]*

[1] Department of Urology, Yichun People's Hospital, Yichun, China, [2] Department of Medical Record Management, Chinese Air Force Specialty Medical Center, Beijing, China

Background: To investigate the potential prognostic role of serum lactate dehydrogenase (LDH) in patients with urothelial carcinoma (UC) using the method of systematic review and meta-analysis.

Materials and Methods: We searched PubMed, Embase, Cochrane Library, and Web of Science for eligible studies up to February 2020. Pooled hazard ratios (HRs) and 95% confidence intervals (CIs) were used to estimate the relationship.

Results: A total of 14 studies including 4,009 patients with UC were incorporated. The results showed that a high pretreatment serum LDH was associated with an inferior overall survival (OS, HR 1.61, 95% CI 1.39–1.87, $p < 0.001$), cancer-specific survival (CSS, HR 1.41, 95% CI 1.05–1.90, $p = 0.022$), and disease-free survival (DFS, HR 1.64, 95% CI 1.04–2.59, $p = 0.034$) in UC. Subgroup analyses identified that a high pretreatment serum LDH was associated with a poor OS (HR 1.97, 95% CI 1.02–3.81, $p = 0.042$) and DFS (HR 1.64, 95% CI 1.04–2.59, $p = 0.034$) in upper tract urothelial carcinoma, a short OS (HR 1.71, 95% CI 1.37–2.15, $p < 0.001$) in urothelial carcinoma of bladder.

Conclusion: Our findings indicated that a high level of pretreatment serum LDH was associated with inferior OS, CSS, and DFS in patients with UC. This biomarker can be an important factor incorporated into the prognostic models for UC.

Keywords: urothelial carcinoma, lactate dehydrogenase, prognosis, systematic review, meta-analysis

OPEN ACCESS

Edited by:
Woonyoung Choi,
The Johns Hopkins Hospital,
United States

Reviewed by:
Xin Xu,
Zhejiang University, China
Lu Yang,
Sichuan University, China

***Correspondence:**
Pengxiu Lin
lpxwmh2019@sina.com

Specialty section:
This article was submitted to Genitourinary Oncology, a section of the journal Frontiers in Oncology

Received: *13 January 2020*
Accepted: *09 April 2020*
Published: *20 May 2020*

Citation:
Wu M, Lin P, Xu L, Yu Z, Chen Q, Gu H and Liu C (2020) Prognostic Role of Serum Lactate Dehydrogenase in Patients With Urothelial Carcinoma: A Systematic Review and Meta-Analysis. Front. Oncol. 10:677. doi: 10.3389/fonc.2020.00677

INTRODUCTION

Urothelial carcinoma (UC), mainly consisting of upper tract urothelial carcinoma (UTUC) and urothelial carcinoma of the bladder (UCB), is, respectively estimated to have 85,000 new incidences and 18,000 related mortality in the United States in 2018. These made UC become the 4th and 12th most common malignance for males and females (1). Multiple lesions, high rate of recurrences, and distant metastasis are typical features of UC. Despite advances in surgical techniques and developments of preoperative and postoperative adjuvant therapy, the long-term survival of cases with UC have not significantly changed over these years (2). Especially, for patients with advanced UC, median overall survival was only 3 to 6 months without therapy, and prolonged to 13–16 months when receiving systematic chemotherapy (3). Therefore, it is important to determine prognostic factors for timely adjustment of treatment.

Previous literatures have found that cancer cells metabolize differently from normal cells, which means more lactate seems to be needed for cancer cells (4). Lactate dehydrogenase (LDH), an enzyme that catalyzes lactic acid into pyruvate, may exert a crucial role in the metabolism of tumor cells. High level of serum LDH has been reported to serve as an unfavorable prognostic factor in kinds of malignances, including prostate cancer, renal cell carcinoma, lymphoma, colorectal cancer, and lung cancer (5). Moreover, many studies have identified the prognostic role of pretreatment serum LDH in cases with UC. Because circulating blood LDH is easy to be measured clinically, it can be used as an indicator of cancer burden and a useful biomarker in clinical management. In the present study, we aimed to systematic review literatures studying the prognostic role of pretreatment LDH in UC and merged the quantitative data.

METHODS

Study Design

The present study was performed according to the PRISMA statements (**Supplementary Material**) (6). The protocol has been registered on PROSPERO (No. CRD42019147216).

Literature Searching

In order to examine the prognostic significance of serum lactate dehydrogenase in urothelial carcinoma, we searched databases PubMed, Embase, Cochrane Library, and Web of Science up to February 2020 to identify related literatures. The following major terms were used to constitute the search strategy: "lactate dehydrogenase" (e.g., "lactate dehydrogenase," "LDH," "lactic dehydrogenase"), "urothelial carcinoma" (e.g., "urothelial carcinoma," "transitional cell carcinoma," "urothelial tumor," "urothelial cancer"), and "prognosis" (e.g., "prognosis," "survival," "progression," "recurrence," "mortality," "outcome"). Additionally, we manually screened literature references to identify relevant studies. There was no language restriction in the process of literature searching.

Selection Criteria

In general, the present study included literatures investigating the prognostic role of pretreatment of serum lactate dehydrogenase (LDH) in patients with urothelial carcinoma, and detailed criteria were shown as follows. Inclusion criteria: (1) studies involving patients confirmed diagnosed with urothelial carcinoma; (2) studies that measured serum lactate dehydrogenase of patients before treatment; (3) studies that reported the results of oncological outcomes including overall survival (OS), cancer-specific survival (CSS), and disease-free survival (DFS); (4) studies that directly provided hazard ratios (HRs) and 95% confidence interval (CI) or required data for calculating them. The methods for calculation were reported by Tierney et al. (7). Exclusion criteria: (1) studies wherein we cannot extract

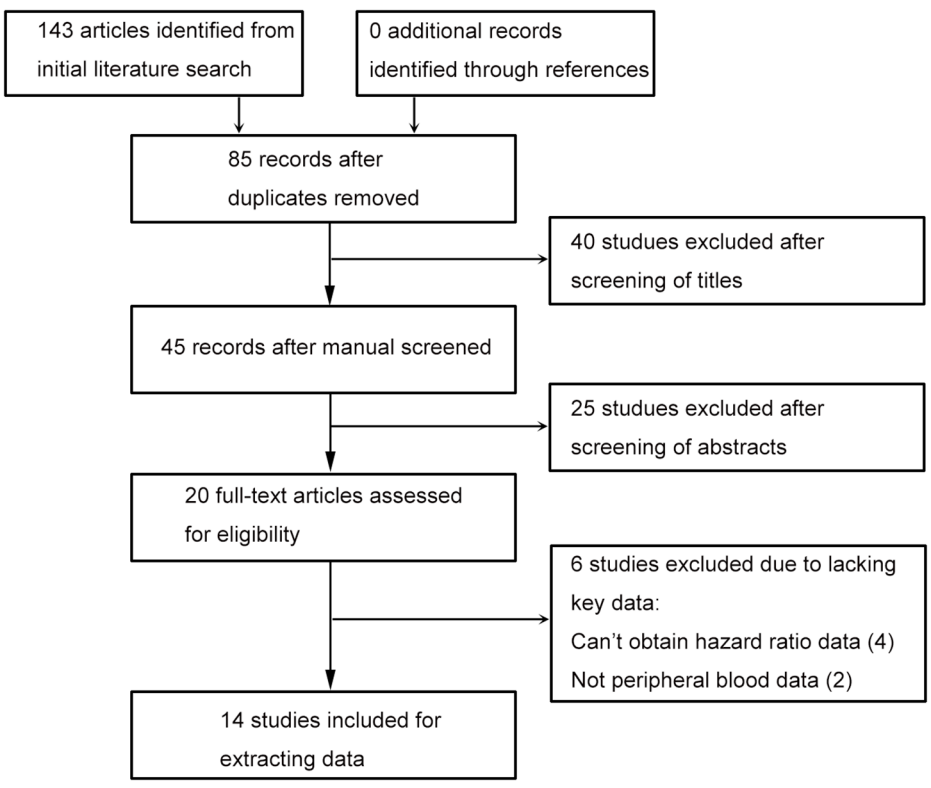

FIGURE 1 | Flowchart of study searching and screening.

HRs and 95% CI; (2) studies that did not analyze serum lactate dehydrogenase as dichotomous variable or did not clearly report the cut-off value; (3) not original article, such as review, abstract, opinion, letter, and so on; (4) duplicated results from the same cohort. Two researchers independently screened and evaluated the literature; the disputes were resolved by discussion.

TABLE 1 | Baseline features of included studies.

References	Country	Sample size	Age (years)	Cancer type	Cancer stage	Cut-off value (U/l)	Decision method	Therapy	Survival analysis
Suzuki et al. (26)	Japan	185	70 (64–76)	UC	Advanced	360	LRM	All	Multivariate
Takemura et al. (19)	Japan	125	70 (64–74)	UC	Advanced	246	Reported	All	Multivariate
Tan et al. (2)	China	668	65.8±11.4	UTUC	All	220	Normal	All	Multivariate
Nakagawa et al. (15)	Japan	1087	69 (63–75)	UCB	Recurrent	ULN	Normal	All	Multivariate
Abe et al. (16)	Japan	228	67 (30–83) R	UC	Metastatic	200	-	Chemotherapy	Univariate
Zhang et al. (17)	China	100	60.3 mean	UTUC	Localized	245	Normal	Surgery	Multivariate
Ito et al. (18)	Japan	71	-	UTUC	Localized	210	Normal	Surgery	Multivariate
Fukushima et al. (19)	Japan	88	68 (39–91)R	UC	Advanced	ULN	Normal	All	Multivariate
Nakagawa et al. (20)	Japan	114	67(32–84)R	UCB	Recurrent	ULN	Normal	All	Multivariate
Yang et al. (21)	China	310	-	UCB	Advanced	200	Reported	Surgery and chemotherapy	Univariate
Yang et al. (22)	China	535	71 (31–88) R	UC	All	200	Reported	All	Multivariate
Bellmunt et al. (23)	Spain	56	-	UC	Advanced	ULN	Normal	Chemotherapy	Univariate
Sengelov et al. (24)	Denmark	240	67 (37–86)R	UC	Recurrent or metastatic	ULN	Normal	Surgery and chemotherapy	Univariate
Hannisdal et al. (25)	Norway	202	73 (32–85)R	UCB	Localized	400	-	Radiotherapy	Multivariate

UC, urothelial carcinoma; UTUC, upper tract urothelial carcinoma; UCB, urothelial carcinoma of the bladder; ULN, upper limit of normal; LRM, linear regression model; R, range.

TABLE 2 | Follow-up and oncological outcomes.

References	Follow-up duration, month	Outcomes	Adjusted factors
Suzuki et al. (26)	12.3	OS	Age, performance status, BMI, primary tumor site, alkaline phosphatase, C-reactive protein, albumin, lymphocyte count, Pembrolizumab after chemotherapy failure
Takemura et al. (19)	12.1	OS	Age, Karnofsky performance status, primary site, neutrophil-to-lymphocyte ratio, γ-glutamyltransferase, C-reactive protein, systemic chemotherapy
Tan et al. (2)	45 (21–74)	OS, CSS, DFS	Tumor grade, concomitant variant histology, lymphovascular invasion, tumor size, tumor architecture, surgical margin status, perioperative blood transfusion, anemia, pT stage, lymph node status, alpha-hydroxybutyrate dehydrogenase, alkaline phosphatase, albumin, globulin, white blood cells, adjuvant therapy
Nakagawa et al. (15)	6.8 (3.0–15.8)	OS	Age, pT stage, lymph node density, time-to-recurrence, symptom, number of involved organs/sites, local recurrence, bone metastasis, liver metastasis, lung metastasis, hemoglobin level, leukocyte count, platelet count, total protein, albumin, alkaline phosphatase, C-reactive protein, estimated glomerular filtration rate, treatments after recurrence, era of recurrence
Abe et al. (16)	17 (14–19)	OS	-
Zhang et al. (17)	45.8 (1–151)R	OS, DFS	Pathological stage, lymph node status, subsequent bladder tumor, tumor grade, multifocality, vascular invasion, tumor necrosis, architecture
Ito et al. (18)	50.3 (1–160)R	DFS	Clinical T stage
Fukushima et al. (19)	13 (1–99)R	OS	Primary site, alkaline phosphatase, C-reactive protein, sarcopenia
Nakagawa et al. (20)	11.0 (0.2–206.7)R	OS	Time-to-recurrence, symptoms at recurrence, no metastatic organs, C-reactive protein, post-recurrent chemotherapy with platinum agent, metastasectomy
Yang et al. (21)	71 (1–132)R	CSS	-
Yang et al. (22)	81 (1–144)R	OS	Urbanization, from endemic "blackfoot disease" area, age, sex, histologic grade, T stage, lymph node metastases, distant metastases, serum creatinine level
Bellmunt et al. (23)	15.8 (11.9–19.5)	OS	-
Sengelov et al. (24)	3.6 (0.1–62.4)R	OS	-
Hannisdal et al. (25)	18	OS	T stage, ESR, age, albumin

OS, overall survival; CSS, cancer-specific survival; DFS, disease-free survival; BMI, body mass index; ESR, erythrocyte sedimentation rate; R, range.

Data Extraction and Quality Assessment

These two important steps were independently performed by two researchers, and the disputes were resolved by discussion. According to a pre-designed table, items of data extraction included the first author's last name, publication year, belonging country, number of subjects included, patient's age, cancer type (urothelial carcinoma, upper tract urothelial carcinoma, or urothelial carcinoma of bladder), cancer stage, cut-off value and decision method, therapies that patients underwent, endpoints of oncological outcomes, HRs and 95% CIs (from univariate or multivariate Cox analysis), follow-up durations, and adjusted variables in multivariate Cox analysis.

The quality of each study was evaluated using the Newcastle–Ottawa scale, which embraced three aspects including patient selection, comparability, assessment of outcome, and follow-ups.

Statistical Analysis

We extracted all HRs and 95% CIs of related endpoints from included studies. Subgroup analyses of overall survival were also conducted. The grouping variables included publication year, region, site of malignance, number of patients, cancer stage, cut-off value, and NOS score. Meta-regression was also performed to identify the resources of interstudy heterogeneity. Subgroup analyses of upper tract urothelial carcinoma (UTUC) and urothelial carcinoma of the bladder (UCB) were also performed. HRs and the corresponding 95% CI were used to assess the significance of the prognostic value of serum lactate dehydrogenase for urothelial carcinoma. A pooled value >1 was regarded as indicating an unfavorable outcome for the subjects having a high level of serum lactate dehydrogenase. Cochran's Q test and Higgins I^2 statistic were both conducted to examine inter-study heterogeneity. A random effects model was applied for all analyses. Publication bias was assessed by funnel plots, Egger's, and Begg's tests. Sensitivity analysis was performed to check the stability of the results. All statistical analyses were performed with Stata 12.0 (STATA Corporation, College Station, TX, USA).

RESULTS

Study Searching and Screening

The flowchart of this process is presented in (**Figure 1**). Database searching identified 143 articles, and no additional study was found by checking the references. Eighty-five studies were remained after excluding duplicated records. Title and abstract screening, respectively, excluded 40 and 25 literatures, then 20 studies were assessed with full text. Since there were four studies wherein hazard ratio data cannot be obtained (8–11), and two studies had no peripheral blood date (12, 13), 14 literatures were included last for data extraction (2, 14–25).

Baseline features of the included studies are shown in (**Table 1**). Nine studies were published recently (2013–2020) by Chinese and Japanese researchers (2, 14–20, 26). Five studies were published 16 years (1993–2002) ago by Chinese and European researchers (21–25). The median or mean age of patients ranged from 60.3 to 73 years, and the sample size ranged from 56 to 1,087. Seven studies focused on urothelial carcinoma (14, 16, 19,

TABLE 3 | Newcastle–Ottawa scale for risk of bias assessment.

References	Selection				Comparability	Outcome			Overall
	Representativeness of exposed cohort	Selection of nonexposed	Ascertainment of exposure	Outcome not present at start		Assessment of outcome	Adequate follow-up length	Adequacy of follow-up	
Suzuki et al. (26)	1	1	1	1	1	1	1	1	**8**
Takemura et al. (19)	0	1	1	1	1	1	1	1	**7**
Tan et al. (2)	1	1	1	1	1	1	0	1	**7**
Nakagawa et al. (15)	1	1	1	1	1	1	1	1	**8**
Abe et al. (16)	1	1	1	1	0	1	1	1	**7**
Zhang et al. (17)	0	1	1	1	1	1	0	1	**6**
Ito et al. (18)	0	1	1	1	1	1	0	1	**6**
Fukushima et al. (19)	0	1	1	1	1	1	1	1	**7**
Nakagawa et al. (20)	0	1	1	1	1	1	1	1	**7**
Yang et al. (21)	1	1	1	1	0	1	1	0	**6**
Yang et al. (22)	1	1	1	1	1	1	1	1	**8**
Bellmunt et al. (23)	0	1	1	1	0	1	1	1	**6**
Sengelov et al. (24)	1	1	1	1	0	1	1	1	**7**
Hannisdal et al. (25)	1	1	1	1	1	1	0	1	**7**

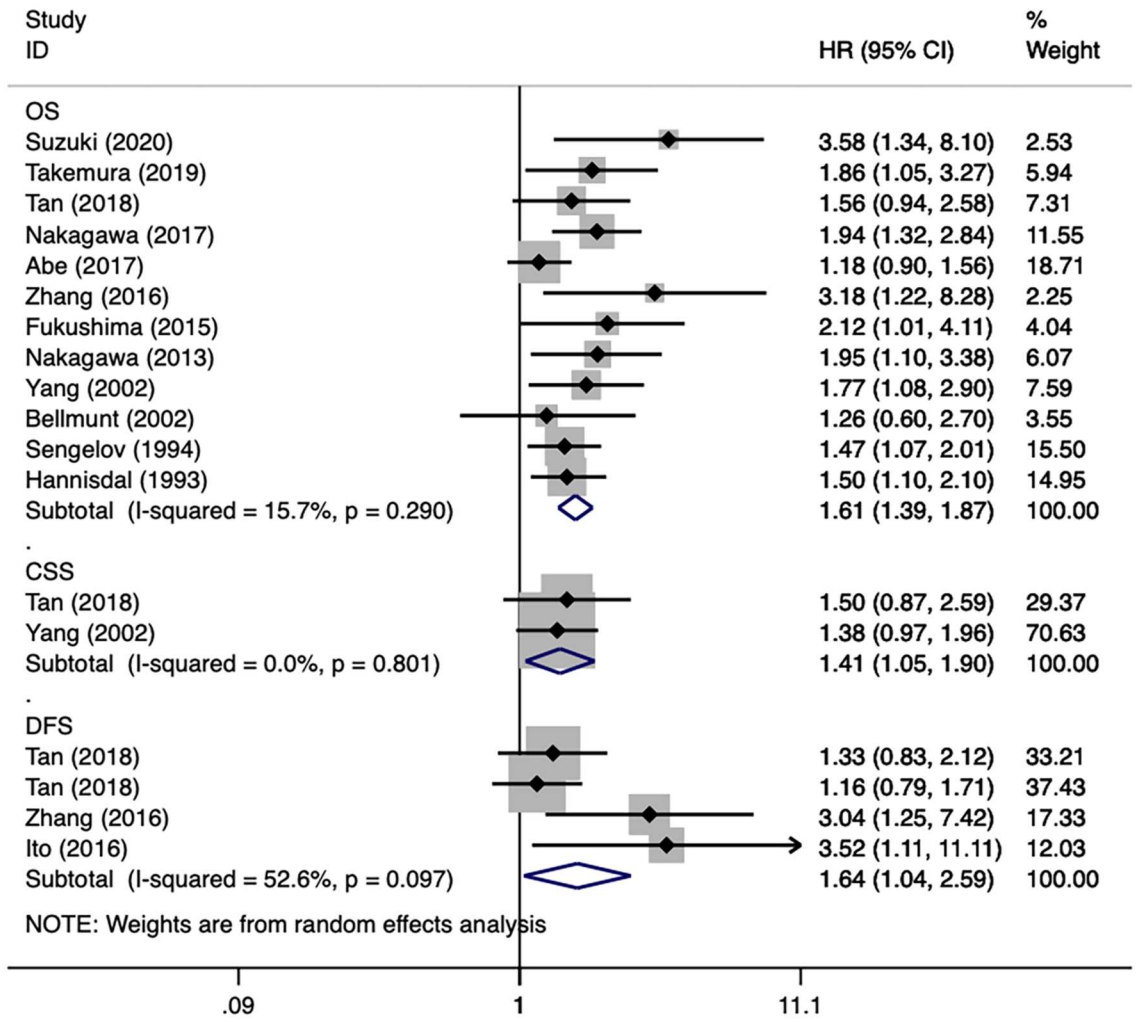

FIGURE 2 | Forest plots of studies about urothelial carcinoma.

22–24, 26), three focused on UTUC (2, 17, 18), and four focused on UCB (15, 20, 21, 25). Of all 40 studies, 10 provided results of multivariable Cox analysis (2, 14, 15, 17–20, 22, 25, 26). The adjusted factors embraced clinical, pathological, and laboratorial variables, which are detailed in (**Table 2**). All studies were of low-to-moderate risk of bias, the NOS score ranged from 6 to 8, which are presented in (**Table 3**).

Urothelial Carcinoma

First, all included studies were analyzed together. For the three endpoints (overall survival, cancer-specific survival, disease-free survival), there were 12 (2, 14–17, 19, 20, 22–26), 2 (2, 21), and 3 (2, 17, 18) studies, respectively, that reported related results. After merging HRs and 95% CIs, we identified that a high pretreatment serum LDH was associated with an inferior overall survival (HR 1.61, 95% CI 1.39–1.87, $p < 0.001$), cancer-specific survival (HR 1.41, 95% CI 1.05–1.90, $p = 0.022$), and disease-free survival (HR 1.64, 95% CI 1.04–2.59, $p = 0.034$) in patients with urothelial carcinoma (**Figure 2**). Subgroup analyses of overall survival were also conducted, and the results are presented in (**Table 4**). The subgroup variables included year of publication, region, site of carcinoma, sample size, survival analysis, and NOS score, which did not obviously change the results. Moreover, except for survival analysis ($p = 0.033$), other subgroup variables were not the resources of inter-study heterogeneity ($P > 0.05$ for all).

UTUC and UCB

Subgroup analyses of UTUC and UCB were also performed. There were three and three studies, respectively, that were included in the subgroup analyses of UTUC (2, 17, 18) and UCB (15, 20, 25). After merging HRs and 95% CIs, we identified that a high pretreatment serum LDH was associated with a poor overall survival (HR 1.97, 95% CI 1.02–3.81, $p = 0.042$) and disease-free survival (HR 1.64, 95% CI 1.04–2.59, $p = 0.034$) in patients with UTUC (**Figure 3A**). A high pretreatment serum LDH was associated with a short overall survival (HR 1.71, 95% CI 1.37–2.15, $p < 0.001$) in patients with UCB (**Figure 3B**).

TABLE 4 | Subgroup analyses for overall survival in urothelial carcinoma.

Subgroup	Studies	HR (95% CI)	*P* value	Meta-regression *P* value	Heterogeneity	
					I^2 (%)	P value
Year of publication				0.845		
2016–2020	6	1.78 (1.31–2.43)	<0.001		54.0	0.054
1993–2015	6	1.59 (1.33–1.90)	<0.001		0.0	0.846
Region				0.350		
Asia	9	1.64 (1.40–1.93)	<0.001		33.7	0.148
Non-Asia	3	1.47 (1.18–1.83)	<0.001		0.0	0.911
Site of carcinoma				0.355		
Upper urinary tract	2	1.82 (1.16–2.84)	0.009		41.3	0.192
Bladder	3	1.71 (1.37–2.15)	<0.001		0.0	0.548
All	7	1.48 (1.25–1.75)	<0.001		29.8	0.201
Sample size				0.084		
> 200	6	1.48 (1.28–1.71)	<0.001		0.0	0.425
< 200	6	2.04 (1.53–2.71)	<0.001		0.0	0.537
Survival analysis				0.033		
Multivariable	9	1.82 (1.53–2.15)	<0.001		0.0	0.695
Univariate	3	1.30 (1.06–1.59)	0.010		0.0	0.586
NOS score				0.106		
>7	3	2.00 (1.50–2.66)	<0.001		0.0	0.386
<=7	9	1.49 (1.29–1.72)	<0.001		0.0	0.457

HR, hazard ratio; CI, confidence interval; NOS, Newcastle–Ottawa Scale.

Publication Bias and Sensitivity Analysis

Since most analyses embraced insufficient literatures, we only checked publication bias and performed sensitivity analysis for overall survival of patients with urothelial carcinoma. The funnel plot showed an approximately asymmetric result, and quantitative tests identified significant differences (Begg's test: $p = 0.024$; Egger's test: $p = 0.005$) (**Figure 4A**). The result of sensitivity analysis showed that excluding any study did not significantly change the merged data (**Figure 4B**).

DISCUSSION

Previous literatures have found that cancer cells metabolize differently from normal cells. Even with sufficient oxygen, malignant cells will preferentially metabolize glucose through glycolysis to produce adequate energy for growth, which is known as the Warburg effect and is one of the major metabolic changes in the process of malignant transformation (4). The serum level of LDH, the enzyme involved in the glycolytic pathway, can reflect the metabolic alterations (27). A high level of serum LDH has been reported to serve as an unfavorable prognostic factor in several types of malignances. Several studies have examined the prognostic role of LDH in subjects with UC and have reported inconsistent results. Hence, the present systematic review and meta-analysis about this issue was performed.

After systematic literature searching and screening, 14 studies embracing 4,009 patients were included. All studies were of low-to-moderate risk of bias, and the NOS score ranged from 6 to 8. The HRs and 95% CIs extracted from these studies were merged. The results showed that a high pretreatment serum LDH was associated with an inferior overall survival, cancer-specific survival, and disease-free survival in UC. Subgroup analyses of OS showed that grouping variable did not obviously change the results. Moreover, sensitivity analysis further confirmed the stability and reliability of the results. Subgroup analyses of UTUC and UCB were also performed. We identified that a high pretreatment serum LDH was associated with a poor overall survival and disease-free survival in UTUC, a short overall survival in UCB. Since circulating blood LDH is easy to be measured clinically, it can be used as an indicator of cancer burden and a useful biomarker in management of UC.

For the prognostic significance of pretreatment LDH in cases with UC, only one meta-analysis previously was reported. In 2016, Zhang et al. (28) performed a meta-analysis to evaluate the prognostic role of LDH for cases with urological cancer. They included two studies about bladder cancer and one study about UTUC. A high level of serum LDH has been reported to serve as an unfavorable prognostic factor. With more and later studies being included, the present study may provide more comprehensive and reliable results for this issue.

Metabolically, the most prominent feature of cancer cells is an increase in lactic acid production due to their increased glucose uptake rate and reduced oxidative phosphorylation rate, regardless of the availability of oxygen. The phenomenon, called aerobic glycolysis, was first discovered 70 years ago by Otto Warburg (4). As an important substance of the Warburg effect, LDH exists in nearly all kinds of tissues, which has six different

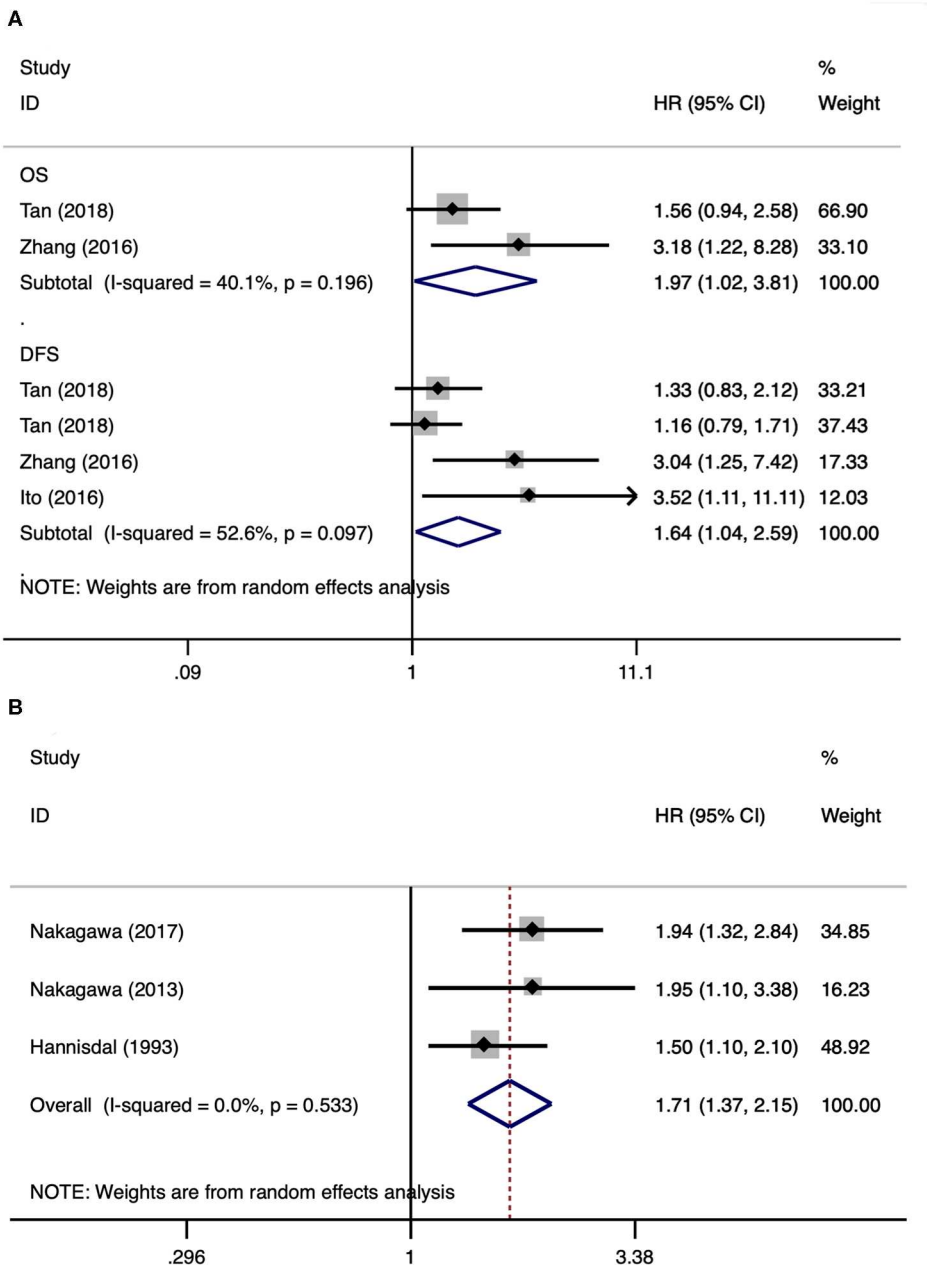

FIGURE 3 | Forest plots of studies about upper tract urothelial carcinoma and urothelial carcinoma of the bladder. **(A)** Upper tract urothelial carcinoma; **(B)** urothelial carcinoma of the bladder.

isoenzymes. These isoenzymes are assembled from two protein subunits, LDHA and LDHB, into a homo- or hetero-tetramer structure (29). The third protein subunit, called LDHC, forms the testicular specific subtype LDH-6 (30). The main function of lactate dehydrogenase is to catalyze the reversible reaction between pyruvate and lactic acid. NAD^+ is produced along with this process and is necessary for the continuous production of ATP to maintain glycolysis. Among the LDH isoforms, LDH-5 has the highest catalytic efficiency (31). When cancer tissue is necrotic, high intracellular LDH levels are released into the blood, increasing serum LDH concentrations (32). In addition, when distant metastases occur, tumor cells can damage adjacent organs, such as the lung, liver, and bone. Damage to these organs can also increase serum LDH levels (31, 33–35). In conclusion, serum LDH seems to be a significant factor in the development of malignance. Its level can reflect tumor burden and serve as cancer biomarker.

There were several limitations for the present study. First, due to limited literatures, we studied all types and stages of UC together. The differences in type, stage, and treatment for UC may be the sources of inter-study heterogeneity. Despite both belonging to UC, UTUC, and UCB may have

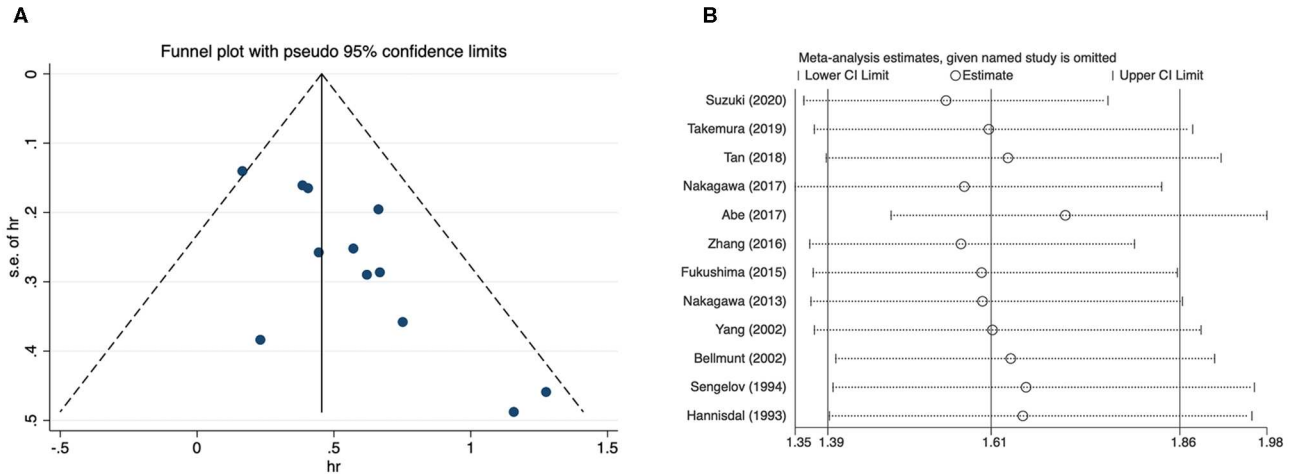

FIGURE 4 | Funnel plot and sensitivity analysis for overall survival of urothelial carcinoma. **(A)** Funnel plot; **(B)** sensitivity analysis.

different biological behaviors and disease characteristics. Hence, subgroup analyses of UTUC and UCB were also performed. Second, serum LDH may be affected by other non-tumor diseases, such as anemia, hepatic disease, muscular dystrophy, and heart failure, which have not been examined in these studies. Moreover, the present study also included results from univariable analysis. These uncontrolled factors may affect the results, and the methods of survival analysis have been found to be the source of inter-study heterogeneity. Third, taken that different cut-off values were used in the included literatures, it is a problem to choose the best one, which may affect the application of this biomarker in clinical practice. Fourth, a significant publication bias was found in the meta-analysis of overall survival, which cannot be overcome by statistical methods. Regardless, the present study represents the most comprehensive and latest systematic review and meta-analysis about the prognostic role of LDH in patients with UC.

In general, the present study proved that a high level of pretreatment serum LDH was associated with inferior OS, CSS, and DFS in patients with UC. Moreover, an elevated level of serum LDH was associated with poor OS and DFS in patients with UTUC, a short OS in patients with UCB. Despite more high-level studies were needed to verify our results, the level of serum LDH can be an important factor incorporated into the prognostic models for UC.

AUTHOR CONTRIBUTIONS

MW and PL: protocol/project development. LX, ZY, and QC: data collection or management. MW, HG, and CL: data analysis. MW and PL: manuscript writing/editing. All authors read and approved the final manuscript.

SUPPLEMENTARY MATERIAL

The Supplementary Material for this article can be found online at: https://www.frontiersin.org/articles/10.3389/fonc.2020.00677/full#supplementary-material

REFERENCES

1. Siegel RL, Miller KD, Jemal A. Cancer statistics 2018. *CA Cancer J Clin.* (2018) 68:7–30. doi: 10.3322/caac.21442
2. Tan P, Chen J, Xie N, Xu H, Ai J, Xu H, et al. Is preoperative serum lactate dehydrogenase useful in predicting the outcomes of patients with upper tract urothelial carcinoma? *Cancer Med.* (2018) 7:5096–106. doi: 10.1002/cam4.1751
3. Bellmunt J, von der Maase H, Mead GM, Skoneczna I, De Santis M, Daugaard G, et al. Randomized phase III study comparing paclitaxel/cisplatin/gemcitabine and gemcitabine/cisplatin in patients with locally advanced or metastatic urothelial cancer without prior systemic therapy: EORTC Intergroup Study 30987. *J Clin Oncol.* (2012) 30:1107–13. doi: 10.1200/JCO.2011.38.6979
4. Warburg O. On the origin of cancer cells. *Science.* (1956) 123:309–14. doi: 10.1126/science.123.3191.309
5. Zhang J, Yao YH, Li BG, Yang Q, Zhang PY, Wang HT. Prognostic value of pretreatment serum lactate dehydrogenase level in patients with solid tumors: a systematic review and meta-analysis. *Sci Rep.* (2015) 5:9800. doi: 10.1038/srep09800
6. Moher D, Liberati A, Tetzlaff J, Altman DG. Preferred reporting items for systematic reviews and meta-analyses: the PRISMA statement. *PLoS Med.* (2009) 6:e1000097. doi: 10.1371/journal.pmed.1000097
7. Tierney JF, Stewart LA, Ghersi D, Burdett S, Sydes MR. Practical methods for incorporating summary time-to-event data into meta-analysis. *Trials.* (2007) 8:16. doi: 10.1186/1745-6215-8-16
8. Inamoto T, Matsuyama H, Ibuki N, Komura K, Fujimoto K, Shiina H, et al. Risk stratification by means of biological age-related factors better predicts cancer-specific survival than chronological age in patients with upper tract urothelial carcinoma: a multi-institutional database study. *Ther Adv Urol.* (2018) 10:403–10. doi: 10.1177/1756287218811050

9. Koie T, Ohyama C, Yamamoto H, Hatakeyama S, Imai A, Yoneyama T, et al. Significance of preoperative butyrylcholinesterase as an independent predictor of survival in patients with muscle-invasive bladder cancer treated with radical cystectomy. *Urol Oncol.* (2014) 32:820–5. doi: 10.1016/j.urolonc.2014.03.010
10. Deshpande N, Mitchell IP, Hayward SW, Love S, Towler JM. Tumor enzymes and prognosis in transitional cell carcinoma of the bladder: prediction of risk of progression in patients with superficial disease. *J Urol.* (1991) 146:1247–51. doi: 10.1016/S0022-5347(17)38060-6
11. Mitchell I, Hayward S, Deshpande N, Towler JM. Enzyme studies in human transitional cell carcinoma of the urinary bladder. *J Urol.* (1989) 141:1234–7. doi: 10.1016/S0022-5347(17)41228-6
12. Wang Z, Zhou Q, Li A, Huang W, Cai Z, Chen W. Extracellular matrix protein 1 (ECM1) is associated with carcinogenesis potential of human bladder cancer. *OncoTarg Ther.* (2019) 12:1423–32. doi: 10.2147/OTT.S191321
13. Liu X, Yao D, Liu C, Cao Y, Yang Q, Sun Z, et al. Overexpression of ABCC3 promotes cell proliferation, drug resistance, and aerobic glycolysis and is associated with poor prognosis in urinary bladder cancer patients. *Tum Biol.* (2016) 37:8367–74. doi: 10.1007/s13277-015-4703-5
14. Takemura K, Fukushima H, Ito M, Kataoka M, Nakanishi Y, Sakamoto K, et al. Prognostic significance of serum gamma-glutamyltransferase in patients with advanced urothelial carcinoma. *Urol Oncol.* (2019) 37:108–15. doi: 10.1016/j.urolonc.2018.11.002
15. Nakagawa T, Taguchi S, Uemura Y, Kanatani A, Ikeda M, Matsumoto A, et al. Nomogram for predicting survival of postcystectomy recurrent urothelial carcinoma of the bladder. *Urol Oncol.* (2017) 35:457.e15-.e21. doi: 10.1016/j.urolonc.2016.12.010
16. Abe T, Ishizaki J, Kikuchi H, Minami K, Matsumoto R, Harabayashi T, et al. Outcome of metastatic urothelial carcinoma treated by systemic chemotherapy: Prognostic factors based on real-world clinical practice in Japan. *Urol Oncol.* (2017) 35:38.e1–e8. doi: 10.1016/j.urolonc.2016.08.016
17. Zhang XK, Zhang ZL, Lu X, Yang P, Cai MY, Hu WM, et al. Prognostic significance of preoperative serum lactate dehydrogenase in upper urinary tract urothelial carcinoma. *Clin Genit Cancer.* (2016) 14:341–5.e3. doi: 10.1016/j.clgc.2016.01.003
18. Ito K, Asakuma J, Kuroda K, Tachi K, Sato A, Horiguchi A, et al. Preoperative risk factors for extraurothelial recurrence in N0M0 patients with renal pelvic cancer treated by radical nephroureterectomy. *Mol Clin Oncol.* (2016) 4:530–6. doi: 10.3892/mco.2016.754
19. Fukushima H, Yokoyama M, Nakanishi Y, Tobisu K, Koga F. Sarcopenia as a prognostic biomarker of advanced urothelial carcinoma. *PLoS ONE.* (2015) 10:e0115895. doi: 10.1371/journal.pone.0115895
20. Nakagawa T, Hara T, Kawahara T, Ogata Y, Nakanishi H, Komiyama M, et al. Prognostic risk stratification of patients with urothelial carcinoma of the bladder with recurrence after radical cystectomy. *J Urol.* (2013) 189:1275–81. doi: 10.1016/j.juro.2012.10.065
21. Yang MH, Yen CC, Chen PM, Wang WS, Chang YH, Huang WJ, et al. Prognostic-factors-based risk-stratification model for invasive urothelial carcinoma of the urinary bladder in Taiwan. *Urology.* (2002) 59:232–8; discussion 8–9. doi: 10.1016/S0090-4295(01)01590-4
22. Yang MH, Chen KK, Yen CC, Wang WS, Chang YH, Huang WJ, et al. Unusually high incidence of upper urinary tract urothelial carcinoma in Taiwan. *Urology.* (2002) 59:681–7. doi: 10.1016/S0090-4295(02)01529-7
23. Bellmunt J, Albanell J, Paz-Ares L, Climent MA, Gonzalez-Larriba JL, Carles J, et al. Pretreatment prognostic factors for survival in patients with advanced urothelial tumors treated in a phase I/II trial with paclitaxel, cisplatin, and gemcitabine. *Cancer.* (2002) 95:751–7. doi: 10.1002/cncr.10762
24. Sengelov L, Kamby C, Schou G, von der Maase H. Prognostic factors and significance of chemotherapy in patients with recurrent or metastatic transitional cell cancer of the urinary tract. *Cancer.* (1994) 74:123–33. doi: 10.1002/1097-0142(19940701)74:1<123::AID-CNCR2820740121>3.0.CO;2-T
25. Hannisdal E, Fossa SD, Host H. Blood tests and prognosis in bladder carcinomas treated with definitive radiotherapy. *Radiother Oncol.* (1993) 27:117–22. doi: 10.1016/0167-8140(93)90131-Q
26. Suzuki H, Ito M, Takemura K, Nakanishi Y, Kataoka M, Sakamoto K, et al. Prognostic significance of the controlling nutritional status (CONUT) score in advanced urothelial carcinoma patients. *Urol Oncol.* (2020) 38:76.e11-76.e17. doi: 10.1016/j.urolonc.2019.10.014
27. Serganova I, Rizwan A, Ni X, Thakur SB, Vider J, Russell J, et al. Metabolic imaging: a link between lactate dehydrogenase A, lactate, and tumor phenotype. *Clin Cancer Res.* (2011) 17:6250–61. doi: 10.1158/1078-0432.CCR-11-0397
28. Zhang Y, Xu T, Wang Y, Zhang H, Zhao Y, Yang X, et al. Prognostic role of lactate dehydrogenase expression in urologic cancers: a systematic review and meta-analysis. *Oncol Res Treat.* (2016) 39:592–604. doi: 10.1159/000449138
29. Krieg AF, Rosenblum LJ, Henry JB. Lactate dehydrogenase isoenzymes a comparison of pyruvate-to-lactate and lactate-to-pyruvate assays. *Clin Chem.* (1967) 13:196–203. doi: 10.1093/clinchem/13.3.196
30. Goldberg E. Immunochemical specificity of lactate dehydrogenase-X. *Proc Natl Acad Sci USA.* (1971) 68:349–52. doi: 10.1073/pnas.68.2.349
31. Augoff K, Hryniewicz-Jankowska A, Tabola R. Lactate dehydrogenase 5: an old friend and a new hope in the war on cancer. *Cancer Lett.* (2015) 358:1–7. doi: 10.1016/j.canlet.2014.12.035
32. Gatenby RA, Gillies RJ. Why do cancers have high aerobic glycolysis? *Nat Rev Cancer.* (2004) 4:891–9. doi: 10.1038/nrc1478
33. Hermes A, Gatzemeier U, Waschki B, Reck M. Lactate dehydrogenase as prognostic factor in limited and extensive disease stage small cell lung cancer - a retrospective single institution analysis. *Resp Med.* (2010) 104:1937–42. doi: 10.1016/j.rmed.2010.07.013
34. Gatenby RA, Gawlinski ET. A reaction-diffusion model of cancer invasion. *Cancer Res.* (1996) 56:5745–53.
35. Gatenby RA. The potential role of transformation-induced metabolic changes in tumor-host interaction. *Cancer Res.* (1995) 55:4151–6.

Conflict of Interest: The authors declare that the research was conducted in the absence of any commercial or financial relationships that could be construed as a potential conflict of interest.

frontiers in Oncology

ORIGINAL RESEARCH
published: 21 May 2020
doi: 10.3389/fonc.2020.00808

Checkpoint Inhibition for Metastatic Urothelial Carcinoma After Chemotherapy—Real-World Clinical Impressions and Comparative Review of the Literature

*Christian Fuhrmann[1], Julian P. Struck[2], Philipp Ivanyi[3], Mario W. Kramer[2], Marie C. Hupe[2], Bennet Hensen[4], Alexander Fürschke[5], Inga Peters[1], Axel S. Merseburger[2], Markus A. Kuczyk[1] and Christoph-A. J. von Klot[1]**

[1] Clinic for Urology and Urological Oncology, Hanover Medical School, Hanover, Germany, [2] Department of Urology, University Hospital Schleswig-Holstein, Luebeck, Luebeck, Germany, [3] Department of Hematology, Hemostasis, Oncology and Stem Cell Transplantation, Hanover Medical School, Hanover, Germany, [4] Institute of Diagnostic and Interventional Radiology, Hanover Medical School, Hanover, Germany, [5] Clinic for Radiology and Nuclear Medicine, University Hospital Schleswig-Holstein, Luebeck, Luebeck, Germany

OPEN ACCESS

Edited by:
Ja Hyeon Ku,
Seoul National University, South Korea

Reviewed by:
Tsunenori Kondo,
Tokyo Women's Medical University Medical Center East, Japan
Benjamin Maughan,
Huntsman Cancer Institute, University of Utah, United States

***Correspondence:**
Christoph-A. J. von Klot
klot.christoph@mh-hannover.de

Specialty section:
This article was submitted to Genitourinary Oncology, a section of the journal Frontiers in Oncology

Received: 17 November 2019
Accepted: 24 April 2020
Published: 21 May 2020

Citation:
Fuhrmann C, Struck JP, Ivanyi P, Kramer MW, Hupe MC, Hensen B, Fürschke A, Peters I, Merseburger AS, Kuczyk MA and von Klot C-AJ (2020) Checkpoint Inhibition for Metastatic Urothelial Carcinoma After Chemotherapy—Real-World Clinical Impressions and Comparative Review of the Literature. Front. Oncol. 10:808. doi: 10.3389/fonc.2020.00808

Background: The introduction of checkpoint inhibitors is a long-awaited new option for a urothelial cancer with a poor prognosis. Apart from clinical studies, the data on real world experience is scarce.

Methods: Patients for monotherapy with either Atezolizumab, Nivolumab or Pembrolizumab after chemotherapy were included. Adverse events and immune related adverse events as well as survival data and imaging analyses were recorded in a prospectively designed multi-center data base. Duration of response, progression free survival (PFS), and overall survival (OS) were estimated with the Kaplan-Meier method.

Results: A total of 28 patients were included. The median follow-up was 8.0 (range, 0.7–41.7) months. Median PFS was 5.8 (95% CI, 2.3–NA) months. Median OS for all patients was 10.0 (95% CI, 8.0–NA) months. The overall response rate (ORR) was 21.4% (6 out of 28 patients). Adverse events were recorded in 20 (71.4%) of patients. Higher grade adverse events (≥Grade 3) were present in 11 (39.3%) patients. No therapy related deaths occurred during the observation period. A total of 13 (46.4%) patients had adverse events that were considered to be immune related. The most commonly affected organ was the thyroid gland with 21.4% of events.

Conclusion: Our real-world clinical series confirms an objective response for about every fifth patient, promising OS and a low incidence for severe adverse events (≥Grade 3).

Keywords: metastatic urothelial carcinoma, checkpoint inhibition, immunotherapy, atezolizumab, pembrolizumab, nivolumab

INTRODUCTION

In Europe, ∼151,000 new cases of urothelial carcinoma are diagnosed every year (1). Urothelial carcinoma is associated with a grim prognosis in the metastatic state (2). Platinum based chemotherapy is the current gold standard for metastatic disease (3), albeit the fact that median overall survival (OS) ranges between 12 to 15 months (4) and 12.8 to 14 months for patients ineligible for platinum based therapy receiving vinflunine-carboplatin or vinflunine-gemcitabine (5). Options seemed even more limited in the second line setting, with OS rates of 6.9 months for vinflunine (6). Toxicity related adverse events, the fact that only about half of patients are eligible for first line cisplatin (7), together with the poor outcome in the second line setting have emphasized the need for alternative therapeutic regimens for decades.

Currently used checkpoint inhibitors for urothelial carcinoma counteract immune evasion of cancer cells by blocking the interaction between programmed death 1 (PD-1) receptor and its ligands PD-L1 and PD-L2 (8). In Europe, Atezolizumab, Nivolumab, and Pembrolizumab have been approved for second line treatment, while Atezolizumab and Pembrolizumab may also be used in the first line setting, i.e., for patients ineligible for cisplatin based chemotherapy (9–13). Today, the use of checkpoint inhibition in the first line setting is tied to the expression of the transmembrane protein PD-L1 in cancer tissue and the presence of immune cells (14).

In this study we take a first look at real world data and first impressions on all three available substances for the treatment of advanced urothelial carcinoma. Our main goal was to evaluate clinical data on checkpoint inhibition for urothelial cancer patients in a real-world setting.

PATIENTS AND METHODS

All patients included in this study had confirmed histopathology of urothelial carcinoma. All patients received intravenous monotherapy with either Atezolizumab, Nivolumab or Pembrolizumab with the approved dosages of 1200 mg q3weeks, 3 mg/kg q2weeks, and 200 mg q3weeks, respectively. Durvalumab and Avelumab were not approved in Europe outside of clinical trials and were not used. Only patients progressing after or during chemotherapy were included. Multiple regimens ($\geq$1) of chemotherapy prior to checkpoint inhibition were allowed. Patients with both, lower and upper tract urothelial carcinoma were included. Patients with adenocarcinoma or sarcomatoid differentiation were excluded.

Routine laboratory values prior to checkpoint inhibitor administration as well as performance-status according to the Eastern Cooperative Oncology Group (ECOG) were recorded (15). The Bellmunt criteria (ECOG performance-status $>$ 0, hemoglobin concentration of less than 10 g per deciliter and presence of liver metastases) were applied for stratification of patients into risk groups (16).

All patients were followed with staging imaging. Metastatic lesions were assessed according to the Response Evaluation Criteria in Solid Tumors (RECIST, version 1.1. (17)). Adverse events in general and immune related adverse events were defined and recorded according to the National Cancer Institute Common Terminology Criteria for Adverse Events (version 4.03.). Immune-related events were counted only once per organ and per patient.

Prospective and ongoing data collection was performed in a prospectively designed, multi-center relational database. This retrospective study was carried out in accordance with the current standard of care according to the recommendations of the European Association of Urology (EAU) guidelines on treatment of metastatic urothelial carcinoma. The protocol and the retrospective analysis of anonymous data were approved by the Ethics Committee of Hanover Medical School, Hanover, Germany. All subjects gave written informed consent in accordance with the Declaration of Helsinki.

The data cutoff for the current analysis was December 12th 2018. For descriptive data presentation, categorical data was shown with absolute numbers and percentages. Continuous variables were presented with either the mean and the standard deviation or the median with range. Progression free (PFS) survival and OS were calculated with the Kaplan-Meier estimation method. R statistical software was used for statistical analysis, figures and tables (18).

RESULTS

A total of 28 patients from 3 separate institutions were included. Data was collected between 01/2016 and 02/2020. Patient characteristics are summarized in (**Table 1**). All 28 patients were given checkpoint-inhibition after prior chemotherapy. The number of patients receiving Atezolizumab, Pembrolizumab or Nivolumab were 10 (35.7%), 16 (57.1%), and 2 (7.1%), respectively. Data on PD-L1 status was scarce due to the fact, that all patients presented here were not part of any clinical trial. Duration of follow-up was defined as the time from first administration of the checkpoint-inhibitor to the date of the last clinical visit. The median follow-up was 8.0 (range, 0.7–41.7) months. Median duration of therapy for all patients was 6.05 (range, 0.7–41.8) months. Median PFS was 5.8 (95% CI, 2.3–NA, **Figure 1**) months. Median OS for all patients was 10.0 (95% CI, 8.0–NA months, **Figure 2**). OS did not differ between different scores for Bellmunt (16) risk criteria (risk score: 0, 1, $\geq$2) with estimated OS times of 8.3, 10.0, and 8.9 months ($p = 0.9$, **Figure 3**). From clinical experience we tend to see good oncological control for patients who develop immune related adverse events. We could demonstrate this difference when comparing patients with and without immune related adverse events: Patients with no event vs. grade $\geq$2 (8.3 months vs. not reached, p-value = 0.1067), however this difference was not statistically significant (**Figure 4**). At the end of data collection, a total of 8 (28.6%) patients were still under active checkpoint-inhibitory therapy. The overall response rate was 21.4% (6 out of 28 patients; 95% CI, 6.2%−36.6%). The median time to response was 13.1 weeks. The median duration of response was 16.4 weeks. At data cutoff, 5 (83.3%) out of 6 initially responding patients had an ongoing response. Change in target lesion size

TABLE 1 | Patient characteristics for 28 Patients under checkpoint inhibitor monotherapy with Atezolizumab, Pembrolizumab, or Nivolumab (ECOG = Eastern Cooperative Oncology Group; NA = not available; *ECOG performance-status >0, hemoglobin concentration <10 g/dl, presence of liver metastases (16).

Patient characteristic	Parameter	%, Range
Patients	28	100%
Age (median, range)	67.5 yrs.	53–80 yrs.
Gender		
Male	19	67.9%
Female	9	32.1%
Primary tumor		
urinary bladder	15	53.6%
upper urinary tract	5	17.9%
Unspecified	8	28.6%
Prior chemotherapy		
Gemcitabine/Cisplatin	23	82.1%
Gemcitabine/Carboplatin	3	10.7%
Carboplatin/Paclitaxel	2	7.1%
Vinflunine	2	7.1%
ECOG		
0	13	46.4%
1	5	17.9%
2	8	28.6%
3	0	0%
4	0	0%
NA	2	7.1%
Metastases		
Liver	3	10.7%
Visceral	3	10.7%
Bone	3	10.7%
Hemoglobin		
≥10 g/dl	18	64.3%
<10 g/dl	10	35.7%
Number of Bellmunt risk criteria*		
0	8	28.6%
1	12	42.9%
2	6	21.4%
3	0	0%
NA	2	7.1%

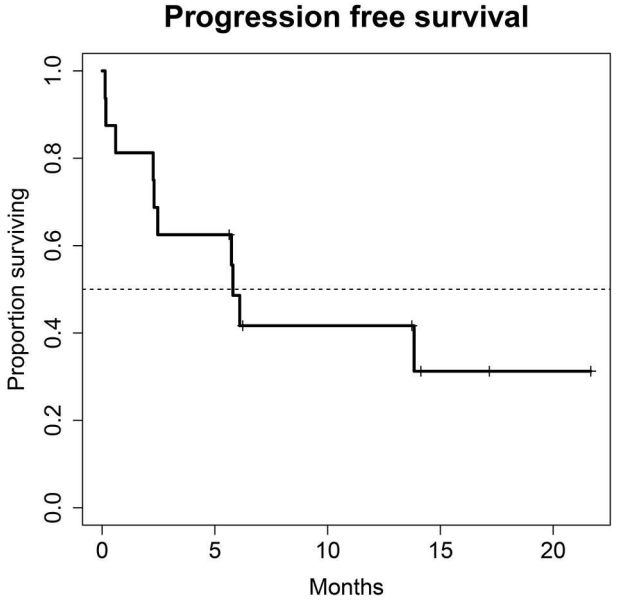

FIGURE 1 | Progression free survival (PFS) for 28 patients under second line therapy with checkpoint inhibitor monotherapy for metastatic urothelial carcinoma. Median PFS was 5.8 months (95% CI, 2.3–NA months).

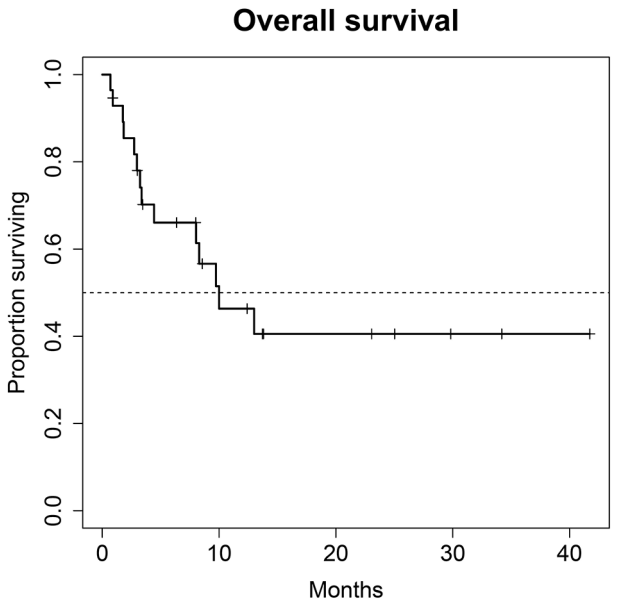

FIGURE 2 | Overall survival (OS) for 28 patients under second line therapy with checkpoint inhibitor monotherapy for metastatic urothelial carcinoma. Median OS for all patients was 10.0 months (95% CI, 8.0–NA months).

and RECIST Data are illustrated in (**Figures 5**, **6**). Adverse events were recorded in 20 (71.4%) patients. Higher grade adverse events (≥Grade 3) were present in 11 (39.3%) cases. No therapy related deaths occurred during the observation period. A total of 13 (46.4%) patients displayed adverse events that were considered to be immune related. Higher grade immune-related adverse events (≥Grade 3) were recorded in 6 (21.4%) cases. The most commonly affected organ was the thyroid gland with 21.4% of events (**Tables 2**, **3**).

DISCUSSION

This series of patients does not represent a randomized controlled trial with a defined competitor. Our main point of discussion focuses on the question whether or not real-life treatment of patients, outside of trial associated selection and restrictions, can reproduce the published data on treatment response and tolerability.

Regarding treatment response, our PFS survival almost reached 6 months. In comparison, PFS in the intention to treat population of randomized clinical phase II and III trials

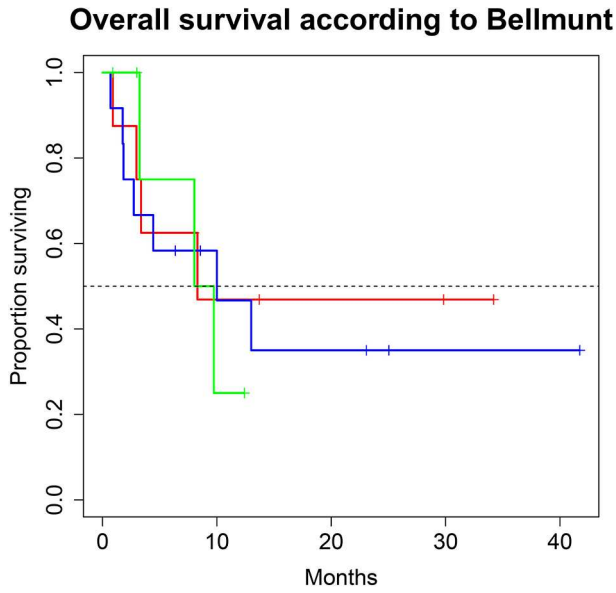

FIGURE 3 | Overall survival (OS) for 28 patients under second line therapy with checkpoint inhibitor monotherapy for metastatic urothelial carcinoma according to Bellmunt criteria [Risk score 0 (green) vs. 1 (blue), vs. ≥2 (red)]. OS did not differ between groups (8.3, 10.0 and 8.9 months; $p = 0.9$).

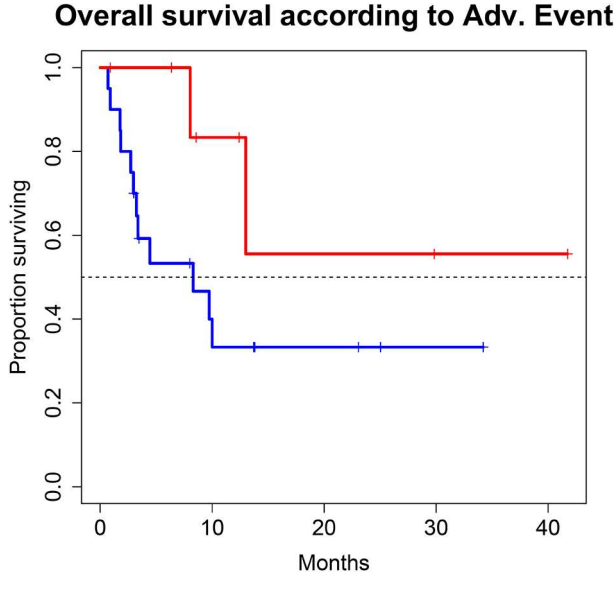

FIGURE 4 | Overall survival (OS) for 28 patients under second line therapy with checkpoint inhibitor monotherapy for metastatic urothelial carcinoma according to occurrence of immune related adverse events [Grade 0-1 (blue) vs. ≥2 (red)]. OS differed in favor for patients with immune related adverse events (8.3 months vs. not reached, p-value = 0.1067), however this difference was not statistically significant.

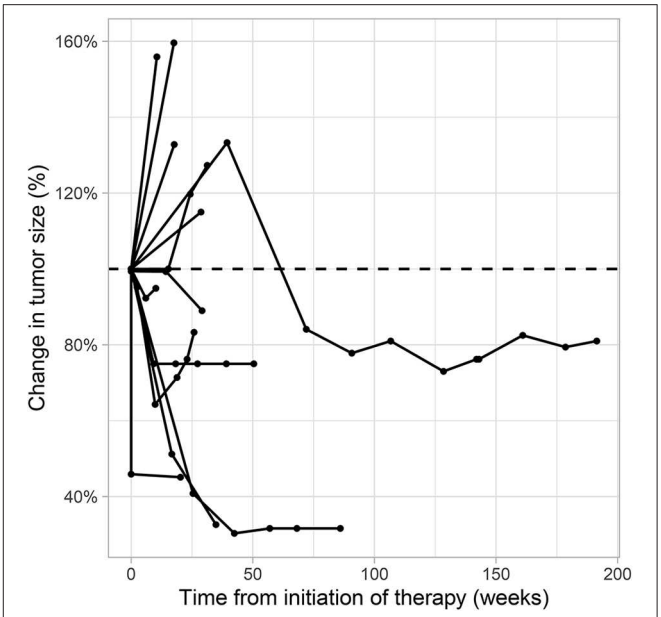

FIGURE 5 | Spider plot showing the percentage of target lesion tumor size change over time for each patient under second line therapy with checkpoint inhibitor monotherapy for metastatic urothelial carcinoma. Radiological data on tumor size change was available for 13 patients who had >1 evaluable cross-sectional imaging. Target lesion size was measured according to the Response Evaluation Criteria in Solid Tumors [RECIST v1.1 (17)].

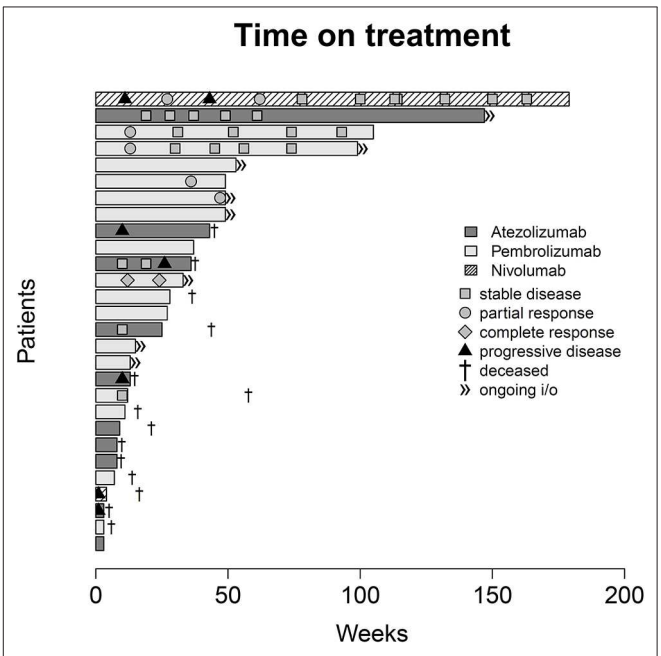

FIGURE 6 | Swimmer plot indicating duration of checkpoint inhibitor monotherapy, overall survival and radiological response according to the Response Evaluation Criteria in Solid Tumors [RECIST v1.1 (17)].

of checkpoint inhibition showed a PFS of no longer than 2.1 months in all trials (10, 12, 13, 19). This discrepancy is most likely due to the fact that our study population is still rather small. Also, in this series of real-life data, imaging did not follow the strict 3-monthly intervals as scheduled in the above-mentioned trials, also a very reasonable explanation for

TABLE 2 | Adverse events.

CTCAE Grade	Any event	Immune-related
Any Grade	20 (71.4%)	13 (46.4%)
Grade ≤2	9 (32.1%)	7 (25%)
Grade ≥3	11 (39.3%)	6 (21.4%)

Summary for patients with total adverse events and with immune-related adverse events. Numbers are shown as total number of afflicted patients per grading interval (Grade ≤2 or Grade ≥3) and percentage with regard to the total patient number of n = 28 patients (CTCAE = Common Terminology Criteria of Adverse Events).

TABLE 3 | Summary of immune-related adverse events.

Organ	Events	%
Colitis	1	3.6%
Skin	3	10.7%
Thyroid	6	21.4%
Liver	3	10.7%
Hypophysis	1	3.6%
Skeletal	1	3.6%
Pancreas	0	0%
Pharynx	0	0%
Renal	4	14.3%
Other	4	14.3%

Numbers are shown as total number of patients with immune-related adverse events per organ and as percentage of the study population of n = 28. In total, 23 immune-related events in 13 patients were recorded.

TABLE 4 | Overall response rates (ORR), progression free survival (PFS), overall survival (OS) and severe adverse events (AE, Adverse events according to the common terminology criteria for adverse events, grade ≥3) for patients treated with checkpoint inhibition monotherapy for metastatic urothelial carcinoma in the second-line setting.

Substance	Patients (*n*)	Target	ORR (%)	PFS (month)	OS (month)	Severe AE (%)
Atezolizumab *Mvigor210 [cohort 2] (10)*	310	PD-L1	15.0%	2.1	7.9	16%
Atezolizumab *IMvigor211* (19)	467	PD-L1	13.4%	2.1	8.6	20%
Nivolumab *Checkmate275 (13)*	270	PD-1	19.6%	2.0	8.73	18%
Pembrolizumab *Keynote045 (12)*	270	PD-1	21.1%	2.1	10.3	15%

All numbers refer to the intention to treat population. PD-L1 (programmed cell death ligand 1), PD-1 (programmed cell death protein 1).

the observed PFS. Therefore, progression may have been picked up late, at least in a subgroup of our patients. A systematic comparison of response rates and survival data of the current literature are shown in (**Table 4**). We were able to achieve a response rate of over 21% over all. Evaluating responses with regard to each of the three substances individually was not feasible from a statistical standpoint considering the low and uneven patient count for each group. Also, the expected variance in response rates in cohorts of 200 to 400 patients (as were evaluated in the above-mentioned trials) is rather high: Response rates from the literature show that only about every 5th patient responds to checkpoint inhibition monotherapy. Our data is consistent with this finding. However, the assumed response rates follow a binominal distribution with rather wide confidence intervals. When assuming an actual response rate of 20%, we calculated that 95% of response results would fall between 15.5% and 24.5% in a cohort of 300 patients. This explains the wide confidence intervals on response rates reported for Atezolizumab, Nivolumab and Pembrolizumab (10, 12, 13, 19). A more representative estimation on response, but only for Atezolizumab, can be extracted from the SAUL trial that comprised $n = 1004$ patients. Unfavorable conditions, such as an ECOG performance status of 2, cerebral metastases or autoimmune disease, among others, were allowed. OS in the intention-to-treat population was 8.7 months (95% CI 7.8–9.9 months), which is comparable with our results. When exclusively looking at patients ($n = 643$) from the SAUL trial who had similar inclusion criteria as in the IMvigor211 trial, median OS improved to 10.0 (95% CI 8.8–11.9) months. ORR was 13% (11–16%) months with a disease control rate of 40% (37–43%) (20).

With regard to OS, our real-world analysis reproduced the promising results from prior trials. As seen in the swimmer plot (**Figure 4**), a few patients had a short duration of treatment and died early. This may be related to the fact that most patients receiving Atezolizumab were included in the expanded access program. Some of these patients had extensive metastatic load, multiple prior regimens of chemotherapy and were given checkpoint inhibition very late in the course of the disease. Taking this into consideration, OS might improve with patients being more and more able to receive checkpoint inhibition earlier on. Gathering real life data on checkpoint inhibition is therefore important.

Regarding the safety of treatment, checkpoint inhibition exhibited a more favorable safety profile than chemotherapy, as could be expected from trials with chemotherapy as a competitor (12, 19). OS differed in favor for patients with immune related events. Albeit the fact, that this difference was not statistically significant, our data support the concept, that the presence of immune related adverse events may correlate to some extent with an increased likelihood of treatment efficacy. The thyroid gland was the most prevalently afflicted organ. Colitis, in contrast to prior trials, was not a major issue in this series. However, we did see events of immune mediated colitis in our cohort of patients with checkpoint inhibition in the first line setting (data not shown).

As a limitation, data quality may not be comparable to data derived from randomized controlled trials: In particular, RECIST evaluation was performed by multiple radiologists from 3 different institutions and imaging did not follow a strict time schedule as is the case in clinical trials. Last, a variety of inclusion and exclusion criteria do not apply in this real-world setting, hence data is less homogenous.

CONCLUSION

Our real-world clinical series confirms an objective response for about every fifth patient, promising OS and a low incidence for severe adverse events (≥Grade 3). In total, our experience with checkpoint inhibition monotherapy reflects, and to some extend surpasses, oncological efficacy and safety and is comparable with the experience from randomized trials for these substances.

DATA AVAILABILITY STATEMENT

The datasets generated for this study are available on reasonable request to the corresponding author.

AUTHOR CONTRIBUTIONS

CF: resources, data curation, writing—original draft preparation. JS and PI: validation, data curation. MWK, IP, AM, MAK, and MH: validation. BH and AF: investigation, validation, data curation. C-AK: conceptualization, methodology, formal analysis, writing—review and editing, project administration.

ACKNOWLEDGMENTS

We thank Marina Akkermann and Anna Lukanowski for their contribution in the compassionate use program for Atezolizumab.

REFERENCES

1. Ferlay J, Steliarova-Foucher E, Lortet-Tieulent J, Rosso S, Coebergh JW, Comber H, et al. Cancer incidence and mortality patterns in Europe: estimates for 40 countries in 2012. *Eur J Cancer*. (2013) 49:1374–403. doi: 10.1016/j.ejca.2012.12.027
2. Torre LA, Bray F, Siegel RL, Ferlay J, Lortet-Tieulent J, Jemal A. Global cancer statistics 2012. *CA Cancer J Clin*. (2015) 65:87–108. doi: 10.3322/caac.21262
3. De Santis M, Bellmunt J, Mead G, Kerst JM, Leahy M, Maroto P, et al. Randomized phase II/III trial assessing gemcitabine/carboplatin and methotrexate/carboplatin/vinblastine in patients with advanced urothelial cancer who are unfit for cisplatin-based chemotherapy: EORTC study 30986. *J Clin Oncol*. (2012) 30:191–9. doi: 10.1200/JCO.2011.37.3571
4. Bellmunt J, Petrylak DP. New therapeutic challenges in advanced bladder cancer. *Semin Oncol*. (2012) 65:87–108. doi: 10.1053/j.seminoncol.2012.08.007
5. De Santis M, Wiechno PJ, Bellmunt J, Lucas C, Su W-C, Albiges L, et al. Vinflunine-gemcitabine versus vinflunine-carboplatin as first-line chemotherapy in cisplatin-unfit patients with advanced urothelial carcinoma: results of an international randomized phase II trial (JASINT1). *Ann Oncol*. (2016) 27:449–54. doi: 10.1093/annonc/mdv609
6. Bellmunt J, Théodore C, Demkov T, Komyakov B, Sengelov L, Daugaard G, et al. Phase III trial of vinflunine plus best supportive care compared with best supportive care alone after a platinum-containing regimen in patients with advanced transitional cell carcinoma of the urothelial tract. *J Clin Oncol*. (2009) 27:4454–61. doi: 10.1200/JCO.2008.20.5534
7. Dash A, Galsky MD, Vickers AJ, Serio AM, Koppie TM, Dalbagni G, et al. Impact of renal impairment on eligibility for adjuvant cisplatin-based chemotherapy in patients with urothelial carcinoma of the bladder. *Cancer*. (2006) 107:506–13. doi: 10.1002/cncr.22031
8. Seidel JA, Otsuka A, Kabashima K. Anti-PD-1 and anti-CTLA-4 therapies in cancer: mechanisms of action, efficacy, and limitations. *Front Oncol*. (2018) 8:86. doi: 10.3389/fonc.2018.00086
9. Balar A V., Galsky MD, Rosenberg JE, Powles T, Petrylak DP, Bellmunt J, et al. Atezolizumab as first-line treatment in cisplatin-ineligible patients with locally advanced and metastatic urothelial carcinoma: a single-arm, multicentre, phase 2 trial. *Lancet*. (2017) 389:67–76. doi: 10.1016/S0140-6736(16)32455-2
10. Rosenberg JE, Hoffman-Censits J, Powles T, Van Der Heijden MS, Balar A V., Necchi A, et al. Atezolizumab in patients with locally advanced and metastatic urothelial carcinoma who have progressed following treatment with platinum-based chemotherapy: a single-arm, multicentre, phase 2 trial. *Lancet*. (2016) 387:1909–20. doi: 10.1016/S0140-6736(16)00561-4
11. Arjun Vasant B, Daniel E, Castellano PH, O'Donnell PG, Vuky J, Powles T, et al. *Pembrolizumab as First-Line Therapy in Cisplatin-Ineligible Advanced Urothelial Cancer: Results From the Total KEYNOTE-052 Study Population*. Genitourinary Cancers Symposium (2017).
12. Bellmunt J, de Wit R, Vaughn DJ, Fradet Y, Lee J-L, Fong L, et al. Pembrolizumab as second-line therapy for advanced urothelial carcinoma. *N Engl J Med*. (2017) 376:1015–26. doi: 10.1056/NEJMoa1613683
13. Sharma P, Retz M, Siefker-Radtke A, Baron A, Necchi A, Bedke J, et al. Nivolumab in metastatic urothelial carcinoma after platinum therapy (CheckMate 275): a multicentre, single-arm, phase 2 trial. *Lancet Oncol*. (2017) 18:312–22. doi: 10.1016/S1470-2045(17)30065-7
14. *FDA Alerts Health Care Professionals and Oncology Clinical Investigators About an Efficacy Issue Identified in Clinical Trials for Some Patients Taking Keytruda (pembrolizumab) or Tecentriq (atezolizumab) as Monotherapy to Treat Urothelial Cancer With Low* . Available online at: https://www.fda.gov/Drugs/DrugSafety/ucm608075.htm
15. Oken MM, Creech RH, Tormey DC, Horton J, Davis TE, McFadden ET, et al. Toxicity and response criteria of the Eastern Cooperative Oncology Group. *Am J Clin Oncol*. (1982) 5:649–55. doi: 10.1097/00000421-198212000-00014
16. Bellmunt J, Choueiri TK, Fougeray R, Schutz FAB, Salhi Y, Winquist E, et al. Prognostic factors in patients with advanced transitional cell carcinoma of the urothelial tract experiencing treatment failure with platinum-containing regimens. *J Clin Oncol*. (2010) 28:1850–5. doi: 10.1200/JCO.2009.25.4599
17. Eisenhauer EA, Therasse P, Bogaerts J, Schwartz LH, Sargent D, Ford R, et al. New response evaluation criteria in solid tumours: Revised RECIST guideline (version 1.1). *Eur J Cancer*. (2009) 45:228–47. doi: 10.1016/j.ejca.2008.10.026
18. Computing. *TRPFS*. (2013). Available online at: http://www.r-project.org
19. Powles T, Durán I, van der Heijden MS, Loriot Y, Vogelzang NJ, De Giorgi U, et al. Atezolizumab versus chemotherapy in patients with platinum-treated locally advanced or metastatic urothelial carcinoma (IMvigor211): a multicentre, open-label, phase 3 randomised controlled trial. *Lancet*. (2017) 391:748–57. doi: 10.1016/S0140-6736(17)33297-X
20. Sternberg CN, Loriot Y, James N, Choy E, Castellano D, Lopez-Rios F, et al. Primary results from SAUL, a multinational single-arm safety study of atezolizumab therapy for locally advanced or metastatic urothelial or nonurothelial carcinoma of the urinary tract. *Eur Urol*. (2019) 3:1-9. doi: 10.1016/j.eururo.2019.03.015

Conflict of Interest: The authors declare that the research was conducted in the absence of any commercial or financial relationships that could be construed as a potential conflict of interest.

frontiers in Oncology

REVIEW
published: 21 August 2020
doi: 10.3389/fonc.2020.01473

Role of Systemic Inflammatory Response Markers in Urothelial Carcinoma

Hyeong Dong Yuk [1,2] *and Ja Hyeon Ku* [1,2]*

[1] *Department of Urology, Seoul National University Hospital, Seoul, South Korea,* [2] *College of Medicine, Seoul National University, Seoul, South Korea*

Urothelial carcinoma (UC) can occur in various parts of the urinary tract and occurs in different stages and grades. The disease recurs frequently and is monitored through a series of invasive tests, such as cystoscopy or ureteroscopy, over the lifetime of an individual. Although many researchers have attempted to stratify the risks of UC, with the majority being based on cancer characteristics and host factors such as performance status, a risk classification system has yet to be fully developed. Cancer affects various parts of the body through the systemic immune response, including changes in hormones, the number and ratio of white blood cells and platelets, and C-reactive protein (CRP) or albumin levels under the influence of neuroendocrine metabolism, hematopoietic function, and protein and energy metabolism, respectively. Herein, we reviewed various systemic inflammatory response markers (SIRs) related to UC, including CRP, albumin-globulin ratio, albumin, Glasgow prognostic score (GPS), modified GPS, neutrophil-lymphocyte ratio, and platelet-lymphocyte ratio. Our aim was to summarize the role of various SIRs in the treatment of patients with UC.

Keywords: biomarker, C-reactive protein, neutrophil to lymphocyte ratio, systemic inflammation response, urothelial cancer

OPEN ACCESS

Edited by:
Ronald M. Bukowski,
Cleveland Clinic, United States

Reviewed by:
Ewa Czeslawa Izycka-Swieszewska,
Medical University of Gdansk, Poland
Retnagowri Rajandram,
University of Malaya, Malaysia

***Correspondence:**
Ja Hyeon Ku
kuuro70@snu.ac.kr

Specialty section:
This article was submitted to Genitourinary Oncology, a section of the journal Frontiers in Oncology

Received: *31 January 2020*
Accepted: *10 July 2020*
Published: *21 August 2020*

Citation:
Yuk HD and Ku JH (2020) Role of Systemic Inflammatory Response Markers in Urothelial Carcinoma. Front. Oncol. 10:1473. doi: 10.3389/fonc.2020.01473

INTRODUCTION

Urothelial carcinoma (UC) is the fourth most common cancer (1). The cancer is classified based on the site of occurrence as bladder UC (BC) and upper urinary tract UC (UTUC) (1–4). BC accounts for 90–95% of all UCs, (1–4) and is the fourth most common cancer among men in the United States, ranking eighth in terms of mortality (4). UC can occur in various parts of the urinary tract and in different stages and grades (2–4). Most UCs start in the bladder, and 75% of the patients are initially diagnosed with non-muscle invasive bladder cancer (NMIBC) (3, 4). Endoscopic surgery, intravesical therapy, and immunotherapy can be performed for the treatment of NMIBC (3). A combination of radical cystectomy (RC), radiation therapy (RT), chemotherapy, and immunotherapy among other treatments have been considered in the standard management of MIBC (2). UTUC demonstrates twice as many pyelocalyx as ureters. More than 60% of the patients have been reported to present with invasive cancer at the time of diagnosis and 15–25% have BC (4). Radical nephroureterectomy (RNU) is the standard treatment of UTUC. A 22–47% recurrence rate of the cancer has been reported in the bladder in contrast to 2–6% in the opposite upper tract (4). Local and distant metastases are associated with a poor prognosis despite the availability of various treatment options (2–4). A study reported that the 5-years relative survival rate of patients with BC, diagnosed from 2009 to 2015, was ∼77%, with the occurrence of regional and distant metastases in 38 and 5% of the cases, respectively (1). In contrast, the upper tract variant is a relatively rare disease

that accounts for 5–10% of all UCs (4). Considering the high relapse rate, the cost of treatment of BC from diagnosis to death, with repeated surgeries and investigations, is the highest among all UCs (2–4). Appropriate risk stratification and prediction of prognosis are important to determine the necessary treatment protocols based on the characteristics of UC (2–4). Accordingly, several studies have assessed the role of systemic inflammatory response markers (SIRs) in the prediction of the progression and prognosis of UC. C-reactive protein (CRP), albumin, albumin-globulin ratio (AGR), Glasgow prognostic score (GPS), modified GPS (mGPS), neutrophil-lymphocyte ratio (NLR), and platelet-lymphocyte ratio (PLR) have been studied as potential prognostic factors. Herein, we reviewed studies on different SIRs for the diagnosis and treatment of UC.

SIR MARKERS IN CANCER

Cancer progression and prognosis are affected by a variety of factors. Representative parameters in the treatment of cancers are the characteristics of the tumor associated with prognosis. These include the pathological variant, stratified grade and stage, and the imaging stage, which are considered in the measurement of disease progression. However, in addition to these characteristics, status of the patient, including performance status, degree of systemic inflammatory response, muscle mass, and weight status (sarcopenia or cachexia) are also important parameters to be considered. Inflammation plays an important role in the development and progression of cancers as well as in the patients' response to therapy (5). Tumors consist of various types of inflammatory and immune cells (6), which can activate immune cells to produce cytokines, chemokines, growth factors, and prostaglandins (6, 7). The inflammatory microenvironment is an essential component of tumorigenesis since most cancers trigger an inflammatory response by building a pro-tumorigenic microenvironment (6, 8). The resultant inflammation affects the host immune response to the tumor (6, 8). Potential SIR-related biomarkers in cancer patients include as CRP, NLR, PLR, albumin and GPS.

Level of CRP increases blood circulation in various immunologically mediated inflammatory conditions, including trauma, infection, surgery, burns, allergic reactions, and cancer (9). CRP is primarily synthesized in the liver and is a major component of the innate immune system. It is involved in the initial immunity during infection and in the process of cell death (10). CRP binds to phosphocholine on the surface of damaged and foreign cells and bacteria, activating phagocytosis by macrophages (10). The normal concentration of CRP in healthy adults is between 0.8 and 3.0 mg/L. However, the level of this protein increases during the acute phase of inflammation (10). Depending on the cause, levels of CRP increase to over 50–100 mg/L in 4–6 h and have also been reported to increase over 1000-fold (10). The concentration of CRP is typically maintained in the range of 2–10 mg/L in individuals with chronic inflammation (10).

It is known that secretion of CRP is primarily regulated by IL-6; however, its mechanism has not been fully elucidated. There is lack of clarity on whether elevation of CRP is related to the inflammatory factors released by the tumor or due to a compromised host immune response. Although there is no clear evidence of the diagnostic or etiological role of CRP in cancer, several studies have reported higher levels of this protein in cancer patients than in healthy individuals (11). Moreover, high baseline levels and specific single nucleotide polymorphisms of CRP have been previously associated with an increased risk of cancer (11). Many recent studies have reported an association between high CRP levels and poor prognosis as well as progressive disease in patients with a variety of cancers, including lung, kidney, colorectal, breast, and ovarian cancers (11).

NLR, another marker of reactions to inflammatory conditions. An absolute NLR ratio has not yet been defined owing to the lack of clarity of the association between high NLR and poor survival in cancer patients. In general, neutrophils provide rapid defense against microorganisms in the infected area during a superficial infection (12). Similarly, in cancers, neutrophils are displaced around tumor cells in response to cytokines and chemical attractants to participate in the initial inflammatory response (12). They recruit CD8+ T cells and promote an anti-tumor response by inducing the production of cytokines, such as TNF-α or IL-12 (12). In contrast, several phenotypes of neutrophil exist, which can promote the formation of tumors *via* their involvement in immunosuppression mediated by TGF-β (12). Neutrophils stimulated with G-CSF were found to improve the growth of circulating tumor cells in metastatic sites and were involved in angiogenesis caused by cancer (12). Many studies have been published recently on the role of NLR in patients with UC (12). A high NLR was reported to be associated with poor prognosis in cancer patients (12).

Albumin, another marker of reactions to inflammatory conditions. Serum albumin and globulin are the major components of blood plasma (13). Albumin is predominantly produced by the liver. Globulins are produced by the liver as well as the immune system. The main function of albumin is to regulate the volume of blood by maintaining the colloid pressure of blood (13). Infections, burns, liver disease, nephrotic syndrome, and malignant tumors decrease serum albumin levels (13). Normal serum albumin levels range from 3.5 to 5 g/dL and that of serum globulin are 2.6–4.6 g/dL (13). The association between albumin levels and the prognosis of patients has been reported in various cancers, including ovarian, colorectal, and lung cancers, in addition to UC (14). Globulin is composed of various pro-inflammatory proteins such as complement components and immunoglobulins and plays an important role in immunity and inflammation (14). Levels of globulin increase in patients with chronic inflammation or cancer. Albumin and globulin are associated with immune responses in cancer patients as well as the nutritional status (14). Low albumin levels reflect a decline in the status of nutrients, which is common in cancer patients, and is known to interfere with immune mechanisms such as humoral and cellular immunity and phagocytic function (14). Hypoalbuminemia in cancer patients has been reported to result from a reduction in albumin synthesis mediated by secretion of pro-inflammatory cytokines, increased catabolism,

and cachexia (14). Increased vascular permeability in these patients also reduces blood albumin levels due to redistribution of the protein from the intravascular to the interstitial areas (14).

Inflammatory cytokines or chemokines are responsible for the activation of platelets (15). Activated platelets induce leukocytes to accumulate in inflamed regions (15). Platelets interact with leukocytes and induce a bidirectional cell activation process, wherein the platelets activate leukocytes, and various leukocyte-derived molecules activate platelets (15). Activated platelets stimulate neutrophils, which in turn release chromatin (15). Chromatin further recruits and activates platelets (15). Cancer cells in the bloodstream induce platelet-mediated recognition (16). Platelets are amplified by a variety of immune cells, cell products, cell surface receptors, and extracellular factors (16). Under certain circumstances, the interaction between cancer cells and platelets can suppress the recognition or removal of cancer cells by immune cells (16).

C-REACTIVE PROTEIN

Several studies on UC have reported that elevated CRP levels before surgery or chemotherapy were associated with poor prognosis (**Table 1**) (17–36). The cutoff value for CRP varies from 3.4 to 10 mg/L. While most studies have compared their results with the prognosis for RNU or RC preoperative evaluation (21–24, 28–34), Yoshida et al. (24), and Egger et al. (25) compared the prognosis with a pre-cancer evaluation. Yoshida et al. included 88 patients with MIBC and reported that a high level of CRP before treatment was a factor in predicting the 5-years cancer specific survival (CSS) after chemoradiotherapy (24). Egger et al. showed that CRP levels before chemotherapy in patients with metastatic BC correlated with patient- and cancer-specific characteristics. The median progression-free survival (PFS) in patients with high CRP levels was extended by 1.5 months compared to patients with low CRP levels. Furthermore, the 1-year overall survival (OS) rate was higher at 60.4% (25). Nakagawa et al. evaluated the prognosis of patients with metastatic UC based on preoperative levels of CRP (34). The study reported that higher pre-metastasectomy levels of CRP was associated with worse prognosis [hazard ratio (HR) 0.24, $P = 0.005$]. Therefore, the authors suggested evaluation of CRP levels when considering metastasectomy (34).

CRP is considered a clinically significant biomarker based on current evidence and a static variable in predicting prognosis. However, CRP kinetics has been considered a variable to measure prognosis; therefore, its potential as a dynamic variable has also been reported. Saito et al. measured CRP levels before and after second-line chemotherapy and not before surgery (35). The prognosis was evaluated based on the kinetics of CRP. In the umbilical evaluation, patients were divided into groups based on CRP levels greater or lesser than 5 mg/L. Patients with preoperative CRP levels of $\geq$5 mg/L were categorized as the non-normalized group, and those with levels $\leq$5 mg/L were considered the normalized group. The study reported that patients in the non-normalized group demonstrated poor prognosis before and after surgery (HR 2.21, $P = 0.001$). Tanaka et al. also compared the prognosis of individuals with CRP levels $\leq$5, 5.1–20, and $\geq$20 mg/L. Patients with CRP levels >20 mg/L had poor CSS and recurrence-free survival (RFS) compared to those with values $\leq$5 mg/L (HR 1.74, 1.47, $P = 0.0009$ and 0.007, respectively) (31).

NEUTROPHIL-TO-LYMPHOCYTE RATIO

Several papers have reported on the prognostic role of NLR in NMIBC (**Table 2**) (19, 37–46). Most of these studies have reported on the relationship between NLR, RFS, and PFS before transurethral resection of bladder tumor (TURBT) (19, 37–45). Vartolomei et al. and Mbeutcha et al. analyzed NLR in more than 1,000 patients (19, 43). Mbeutcha et al. reported that a high NLR was associated with RFS (HR 1.27, $P = 0.013$), which was reported to be related to PFS (HR 1.72, $P = 0.007$) (19). Similarly, Vartolomei et al. demonstrated high NLR and low NLR (58.8 and 9.4%) for 5-years RFS ($P < 0.001$), 79.2 and 57.1%) for 5-years PFS ($P < 0.001$), and 84.3 and 77.4% for 10-years CSS ($P = 0.004$) (43). A high NLR was associated with RFS (HR 3.34, $P < 0.001$), PFS (HR 2.18, $P < 0.001$), and CSS (HR 1.65, $P = 0.030$) (68). In addition, Yuk et al. reported on the relationship between OS (HR 2.24, $P = 0.005$) and CSS (HR 2.03. $P = 0.039$) based on the NLR in patients before BCG treatment (46).

Several studies have reported on the prognostic role of NLR in MIBC and metastatic BC (**Table 2**) (24, 41, 47–60). Furthermore, several studies have reported on the role of prognostic factors in survival outcomes of MIBC and metastatic UC (24, 41, 47, 48, 50, 52–56, 59, 60), while other studies have suggested that the postoperative stages or disease severity can be predicted (**Table 3**) (41, 48, 49, 58, 69–73). The majority of the studies reported a positive role of a high NLR on the prediction of worse OS and CSS rates. Furthermore, elevated NLR has been reported as an independent predictor of recurrence in several studies (32, 41, 50, 52, 55), with some reporting higher NLR values in patients with MIBC compared to those with NMIBC (69, 70). Other studies have reported on considering the NLR in predicting disease severity, such as extravesical involvement, upstaging, or LN involvement (48, 49, 55). Furthermore, some studies have considered the NLR to predict the pathologic complete response after chemotherapy or surgery (58, 72, 73). Seah et al. analyzed NLR kinetics before, during, and after NAC and reported differences in the patterns between the CR and non-responder groups (72). Although the role of the preoperative evaluation of NLR has been commonly discussed, some studies have assessed the prognostic value of changes in the ratio through repeated measurements over time (56). Kang et al. reported that postoperative NLR increases were associated with adverse pathological outcomes and were predictors of worse OS and CSS (51). Patients with consistently elevated NLR before and after surgery had worse OS and CSS compared to other patients (51). Yoshida et al. predicted patient prognosis by comparing the NLR before and after surgery (24). Patients

TABLE 1 | The studies evaluating the role of C-reactive protein in urothelial cancer.

Study	Year	Case	Site	Stage	Assessment and Treatment	Threshold	Outcomes
Ishioka et al. (17)	2012	232	Bladder + Ureter	pT4 or N+ or M+	At diagnosis	5.15 mg/L	OS, HR 1.68 (1.27–2.30), $P < 0.001$ Median OS, 16.0 m (CRP ≤ 5), 6.5 m(5 < CRP ≤ 10), 3.8 m (10 ≤ CRP < 30), 2.6 m (30 ≤ CRP)
Hilmy et al. (18)	2005	105	Bladder	pTa-2	Pre-TURBT	10.0 mg/L	CSS, HR 3.31 (1.09–10.09), $P = 0.035$ OS, HR 2.73 (1.23–6.07), $P = 0.014$
Mbeutcha et al. (19)	2016	1117	Bladder	pT1N0M0	Pre-TURBT	5 mg/L	PFS, HR 1.72 (1.05–2.81), $P = 0.031$
Gakis et al. (20)	2011	246	Bladder	pT2-4N0/+	Pre-RC	5 mg/L	CSS, HR 1.18 (1.09–1.27), $P = 0.001$ 3 yr CSS 44 vs. 74%, $P < 0.0014$ (high vs. low)
Kramer et al. (21)	2013	194	Bladder	pT3-4	Pre-RC	5 mg/L	CSS, HR 1.68 (1.17–2.09)
Nakagawa et al. (22)	2013	114	Bladder	pT0-4N1-3	Pre-RC	5 mg/L	OS, HR 2.63 (1.58–4.39), $P < 0.001$
Sejima et al. (23)	2014	249	Bladder	pT0-4N0/+M0	Pre-RC	5 mg/L	DSS, HR 1.99 (1.13–3.52), $P = 0.016$
Yoshida et al. (24)	2008	88	Bladder	cT2-4N0M0	Pre-Radiochemotherapy	5 mg/L	CSS, HR 1.80 (1.01–2.97), $P = 0.046$
Eggers et al. (25)	2013	34	Bladder	M+	Pre-Chemotherapy	80 mg/L	OS, HR 14.8 (3.7–60.0), $P < 0.001$ 1 yr-OS: 22.2 vs. 82.6%, $P < 0.001$ (high vs. low)
Nakagawa et al. (26)	2017	1087	Bladder	pT0-4N0-3M0	Pre-Treatment	5 mg/L	OS, HR 1.48 (1.00–2.19), $P = 0.049$
Saito et al. (27)	2007	130	Ureter	pTa-4N0M0	Pre-RNU and Partial ureterectomy	5 mg/L	RFS, HR 1.45(1.05–1.97), $P = 0.023$ DSS, HR 1.78 (1.21–2.68), $P = 0.004$
Obata et al. (28)	2013	183	Ureter	pTa-4N0M0	Pre-RNU	5 mg/L	RFS, 2.83 (1.41–5.68), $P < 0.001$ CSS, 2.65 (1.24–5.65), $P < 0.012$
Stein et al. (29)	2014	115	Ureter	pTa-4N0/+M0/+	Pre-RNU	5 mg/L	5 yr CSS 26.4 vs. 54.2%, $P = 0.006$ (high vs. low) CSS, HR 2.67 (1.28–5.54), $P = 0.009$
Aziz et al. (30)	2014	265	Ureter	pTa-4N0/+M0	Pre-RNU	9 ml/L	RFS 1.18 (0.71–1.97), $P = 0.050$ DSS 1.61 (0.95–2.73), $P = 0.026$
Tanaka et al. (31)	2014	564	Ureter	pTa-4N0/+M0	Pre-RNU	≤5 mg/L /5.1–20 mg/L/>20 mg/L	CSS, HR 1.74 (1.15–2.64), $P = 0.009$, (5.1–20 vs. ≤5); HR 2.31 (1.41–3.82), $P = 0.001$, (>20 vs. ≤5) RFS, HR 1.47 (1.01–2.13), $P = 0.007$, (>20 vs. ≤5)
Morizane et al. (32)	2015	345	Ureter	pTa-4N0/+M0	Pre-RNU	5 mg/L	CSS, HR 2.43 (1.30–4.54), $P = 0.006$
Fujita et al. (33)	2015	45	Ureter	pTa-4N1-3M0	Pre-RNU / ACT	2.8 mg/L	CSS, HR 3.20 (1.21–8.43), $P = 0.018$
Nakagawa et al. (34)	2017	37	Bladder + Ureter	pT0-4N0/+M1 with metasectomy	Pre-Metasectomy	5 mg/L	CSS, HR 0.24 (0.09–0.64), $P = 0.005$ (low)
Saito et al. (35)	2012	80	Bladder + Ureter	M+	Pre-2nd line chemotherapy	Kinetics	OS, HR 2.21 (1.41–3.28), $P = 0.001$ (non-normalized)
Matsumoto et al. (36)	2018	114	Bladder + Ureter+Urethra/ Prostate	M+	Pre-2nd line chemotherapy	10 mg/L	OS, HR 2.63 (1.43–4.76), $P = 0.002$

ACT, adjuvant chemotherapy; CRP, C-reactive protein; CSS, cancer specific survival; DSS, disease specific survival; HR, hazard ratio; OM, overall morbidity; OS, overall survival; RC, radical cystectomy; RFS, recurrence free survival; RNU, radical nephroureterectomy; TURBT, transurethral resection of bladder tumor.

with high and low NLRs were categorized based on their preoperative and postoperative values, respectively. Patients were divided into four groups according to the change in NLR before and after surgery. Patients with consistently high NLR before and after surgery demonstrated worse prognosis compared to other patients (24). The degree of change in the NLR before and after surgery was reported to be related to OS (24). In addition, Kiser et al. measured and analyzed the NLR at the beginning of and intermediately during NAC and reported differences in median DSS (12.6 vs. 34.8 m, $P = 0.002$) and median OS (19.4 vs. 44.0 m, $P = 0.001$) (59). One study analyzed the differences in the NLR over a period of 1–5 years after surgery and reported significant results of 1-year OS ($P = 0.018$) and 1-year CSS ($P = 0.001$) rates; however, there was no difference in the rates due to differences in the NLR from the 2nd year onwards (56). The majority of the studies have reported that the NLR before and after surgery or chemotherapy can be used to predict survival outcomes, pathological findings, and disease progression. Thus, measurement of the NLR before and after treatment is a reliable

TABLE 2 | The studies evaluating the role of neutrophil to lymphocyte in urothelial cancer.

Study	Year	Cases	Stage	Grade	Assessment and treatment	Threshold	Outcomes
Non-muscle invasive bladder cancer							
Mano et al. (37)	2015	107	pTa-1	G1-3	Pre-TURBT	2.41	3 yr-PFS, 84 vs. 61%, $P = 0.004$ PFS, HR 3.52 (1.33–9.33), $P = 0.012$
Favilla et al. (38)	2016	178	pTa-1	LG/HG	Pre-TURBT	3	RFS, HR 2.84 (1.5–5.75), $P < 0.010$ PFS, HR 5.35 (0.39–73.7), $P < 0.210$
Mbeutcha et al. (19)	2016	1117	pTa-1	G1-3	Pre-TURBT	2.5	RFS, HR 1.27 (1.05–1.53), $P = 0.013$ PFS, HR 1.72 (1.16–2.54), $P = 0.007$
Ogihara et al. (39)	2016	605	pTa-1	LG/HG	Pre-TURBT	2.2	5 yr-RFS, 66.3 vs. 31.7%, $P < 0.001$ 5 yr-PFS, 97.5 vs. 90.4%, $P < 0.001$ RFS, HR 2.08 (1.6–2.7), $P < 0.001$ PFS, HR 2.37 (1.17–4.78), $P = 0.016$
Ozyalvacli et al. (40)	2016	166	pT1	HG 1	Pre-TURBT	2.43	RFS, HR 3.81 (1.5–9.67), $P = 0.005$
D'Andrea et al. (41)	2017	918	pTa-1	G1-3	Pre-TURBT	3	5 yr-RFS, 55.5 vs. 45.9%, $P < 0.010$ 5 yr-PFS, 94.9 vs. 89.9%, $P = 0.004$ RFS, HR 1.3 (1.1–1.6), $P = 0.004$ PFS, HR 1.9 (1.2–3.0), $P = 0.006$
Kang et al. (42)	2017	1698	pTis-1	PUNLMP/LH-HG	Pre-TURBT	2.0	OS, HR 1.52 (1.19–1.95), $P = 0.001$ CSS, HR 1.12 (1.01–1.25). $P = 0.030$
Vartolomei et al. (43)	2018	1046	pT1	HG/G3	Pre-TURBT		5 yr-RFS 58.8 vs. 9.4%, $P < 0.001$ 5 yr-PFS 79.2 vs. 57.1%, $P < 0.001$ 10 yr-OS 66.5 vs. 63.6%, $P = 0.030$ 10 yr-CSS 84.3 vs. 77.4%, $P = 0.004$ RFS, HR 3.34 (2.82–3.95), $P < 0.001$ PFS, HR 2.18 (1.71–2.78), $P < 0.001$ CSS, HR 1.65 (1.02–2.66), $P = 0.030$
Getzler et al. (44)	2018	113	pTa-1	G1-3	Pre-TURBT	2.5	RFS, HR 2.10 (1.17–3.75). $P = 0.012$ RFS HR 3.96 (1.19–13.16). $P = 0.025$, (BCG subgroup)
Racioppi et al. (45)	2019	100	high-risk NMIBC, pTa-1	HG	Pre-TURBT	3	Recurrence risk score ($r = 0.55$, $p = 0.01$) Progression risk score ($r = 0.49$, $p = 0.01$) BCG response, OR0.08 (0.008–0.147), $P = 0.02$
Yuk et al. (46)	2019	385	pTis-1	LG/HG	Pre-BCG treatment	1.5	OS, HR 2.24 (1.26–3.96), $P = 0.005$ CSS, HR 2.03 (1.03–3.99). $P = 0.039$
Study	**Year**	**Cases**	**Stage**		**Assessment and treatment**	**Threshold**	**Outcomes**
Muscle Invasive Bladder Cancer							
Gondo et al. (47)	2012	189	cTa-4		Pre-RC	2.5	DSS, HR 1.95 (1.03–3.67). $P = 0.038$
Viers et al. (48)	2014	889	pT0-4/Nx-3		Pre-RC	2.7	RFS, HR 1.04 (1.01–1.08). $P = 0.02$ CSS, HR 1.04 (1.01–1.08). $P = 0.01$ OS, HR 1.03 (1.01–1.06), $P = 0.01$
Krane et al. (49)	2013	68	Recurrent T1HG and MIBC		Pre-RC	2.5	OS, HR 2.49 (1.14–6.09),
Hermanns et al. (50)	2014	424	pT0-4Nx/+M0		Pre-RC	3	5 y-RFS: 64 vs. 53%, $P = 0.013$ 5 y-CSS: 75 vs. 57%, $P < 0.001$ 5 y-OS: 64 vs. 43%, $P < 0.001$ RFS, HR 1.49 (1.12–2.00), $P = 0.007$ CSS, HR 1.88 (1.39–2.54), $P < 0.001$ OS, HR 1.67 (1.17–2.39), $P = 0.005$
Kang et al. (51)	2015	385	pT0-4N0-3M0		Pre-RC	2	CSS, HR 0.81 (0.38–1.7) OS, HR 0.97 (0.51–1.84)
Bhindi et al. (52)	2016	418	pT0-4Nx/+M0		Pre-RC	2.9	RFS, HR 1.52 (1.17–1.98), $P = 0.002$ CSS, HR 1.47 (1.20–1.80), $P < 0.001$ OS, HR 1.56 (1.16–2.10), $P = 0.004$

(Continued)

TABLE 2 | Continued

Study	Year	Cases	Stage	Grade	Assessment and treatment	Threshold	Outcomes
Kawahara et al. (53)	2016	74	pT0-4Nx/+M0		Pre-RC	2.38	OS, HR 4.62 (1.16–18.34), $P = 0.030$
Hirasawa et al. (54)	2016	136	cT1-4		Pre-RC	Continuous	CSS, HR 1.3 (1.1–1.5), $P = 0.005$
D'Andrea et al. (41)	2017	4435	pT0-4Nx/+M0		Pre-RC	2.7	RFS, HR 1.2 (1.1–1.3), $P < 0.001$ CSS, HR 1.2 (1.1–1.4), $P < 0.001$ OS, HR 1.1 (1.0–1.2), $P = 0.01$
Tan et al. (55)	2017	84	pT0-4Nx/+M0		Pre-RC	2.7	5 yr-DFS: 58 vs. 22%, $P = 0.017$ 5 yr-OS: 60 vs. 23%, $P = 0.008$ RFS, HR 7.00 (1.71–28.60), $P = 0.007$
Kang et al. (56)	2017	385	pT0-4N0-3M0		Pre-RC	2.5	1 yr-OS, $P = 0.018$, 1 yr-CSS $P = 0.001$
Morizawa et al. (57)	2016	110	pT0-4Nx/+M0		Pre/Post-RC	2.6	RFS, HR 2.6 (1.1–6.0), $P = 0.02$ CSS, HR 2.6 (1.2–5.6), $P= 0.01$ OS, HR 2.8 (1.4–5.4), $P < 0.01$
Yoshida et al. (24)	2016	323	pT0-4N0/+M0		Pre/Post-RC	2.7/Kinetics	OS $P < 0.001$, (High < Low), OS $P < 0.001$, (HH<LL+HK+LH) OS, HR 2.56 (1.75–3.73) $P < 0.001$ (NLR change)
Buisan et al. (58)	2016	205	pT0-4Nx-2M0		Pre-RC/with NAC	2.26/Continuous	PFS, HR 1.25 (1.10–1.42), $P < 0.001$ CSS, HR 1.27 (1.11–1.44), $P < 0.001$ OS, HR 1.12 (1.01–1.23), $P < 0.021$
Kaiser et al. (59)	2018	296	cT2-4aN0M0		Pre-NAC/ mid-NAC	3	Median DSS, 12.6 vs. 34.8 m, $P = 0.002$ Median OS, 19.4 vs. 44.0 m, $P = 0.001$
Ohtake et al. (60)	2016	23	M+		Pre-Chemotherapy/ Gemcitabine + Nedaplatin	4.14	PFS, $P = 0.011$ and OS, $P = 0.045$, (High < Low)
Upper Urinary Tract Urothelial Cancer							
Azuma et al. (61)	2013	137	pTa-4N0M0		Pre-RNU	2.5	5 yr-RFS, 74.3 vs. 30.45%, $P < 0.001$ 5 yr-CSS, 81.3 vs. 29.4%, $P < 0.001$ RFS, HR 2.11 (1.02–4.46), $P = 0.045$ CSS, HR 3.06 (1.44–6.83), $P = 0.003$
Tanaka et al. (62)	2014	665	pTa-4Nx/+M0		Pre-RNU	3	5 yr-RFS, 69.2 vs. 57.0%, $P < 0.001$ 5 yr-CSS, 77.3 vs. 60.2%, $P < 0.001$ RFS, HR 1.38 (1.02–1.87), $P = 0.037$ CSS, HR 1.47 (1.03–2.11), $P = 0.036$
Luo et al. (63)	2014	234	pTa-4N0M0		Pre-RNU	3	RFS, HR 2.47 (1.16–5.29), $P = 0.020$ CSS, HR 6.38 (1.75–23.31), $P = 0.006$
Dalpiaz et al. (64)	2014	202	pTa-4N0M0		Pre-RNU or segmental ureterectomy	2.7	CSS, HR 2.72 (1.25–5.93), $P = 0.012$ OS, HR 2.48 (1.31–4.70), $P = 0.005$
Altan et al. (65)	2017	113	pTa-4N0M0		Pre-RNU	2.9	5 yr-DFS, 83.2 vs. 30%, $P < 0.001$ 5 yr-PFS, 53.7 vs. 18.3%. $P < 0.001$ DFS, HR 1.84 (1.10–3.09), $P = 0.021$ PFS, HR 2.90 (1.35–6.22), $P = 0.006$
Kishimoto et al. (66)	2017	100	pTa-4Nx/+M0		Pre-RNU	3.8	Intravesical-RFS, HR 2.49 (1.20–5.20), $P = 0.015$
Tan et al. (67)	2018	717	pTa-4Nx/+M0		Pre-RNU	2.5	RFS, HR 1.70 (1.31–2.20), $P < 0.001$ MFS, HR 1.67 (1.22–2.31), $P = 0.002$ CSS, HR 1.95 (1.42–2.69), $P < 0.001$ OS, HR 1.88 (1.42–2.50), $P < 0.001$

BCG, Bacillus Calmette-Guérin; CSS, cancer specific survival; DFS, disease free survival; DSS, disease specific survival; HG, high grade; HR, hazard ratio; LG, low grade; MFS, metastatic free survival; MIBC, muscle invasive bladder cancer; OS, overall survival; PFS, progression free survival; PUNLMP, papillary urothelial neoplasm of low malignant potential; RC, radical cystectomy; RFS, recurrence free survival; RNU, radical nephroureterectomy; TURBT, transurethral resection of bladder tumor.

tool for predicting postoperative survival outcomes in patients with MIBC.

Several studies have reported that preoperative assessment of the NLR can be considered to predict the survival outcomes in patients with UTUC (**Table 2**) (61–67), with a cutoff value between 2.5 and 3. Kishimoto et al. evaluated the predictive ability of the NLR before RNU on intra-bladder recurrence (66). The study reported that a high preoperative NLR was associated with an increased risk of recurrence of BC (HR 2.49, $P = 0.015$). The majority of the studies have reported

TABLE 3 | The studies evaluating the role of neutrophil to lymphocyte of urothelial cancer pathologic staging.

Study	Year	Cases	Stage	Assessment and treatment	Threshold	Predictable variable	Outcomes
Can et al. (69)	2012	182	pT0-4N0M0	Pre-TURBT	2.57	MIBC possibility	OR 2.78 (1.38–5.59), $P = 0.004$
Lee et al. (70)	2015	226	pT0-4N0M0	Pre-TURBT	3.89	MIBC possibility	OR 8.24 (2.49–27.32), $P = 0.001$
Krane et al. (49)	2013	68	Recurrent T1 + MIBC	Pre-RC	2.5	Extravesical disease	OR 3.18 (1.09–9.79)
Potretzke et al. (71)	2014	102	pT0-4N0M0	Pre-RC	Continuous	≥pT3 upstaging Extravesical disease	OR 1.36 (1.01–1.84), $P = 0.040$ OR 1.5 (1.07–2.10), $P = 0.020$
Viers et al. (48)	2014	889	pT0-4N0M0	Pre-RC	2.7	Extravesical disease LN involvement	OR 1.07 (1.01–1.15), $P = 0.030$ OR 1.09 (1.02–1.16), $P = 0.020$
Buisan et al. (58)	2016	205	pT0-4Nx-2M0	Pre-RC	Continuous	pCR	OR 0.80 (0.64–0.99), $P = 0.04$
D'Andrea et al. (41)	2017	4435	pT0-4N0M0	Pre-RC	2.7	LN involvement	OR 1.9 (1.7–2.3), $P < 0.001$
Seah et al. (72)	2015	26	pT0-4N0-3	Pre-NAC/Mid/Pre-RC	Kinetics	NLR pattern during NAC	Different between pCR and non-responder, $P = 0.038$
Leibowitz-Amit et al. (73)	2016	55	pT2-4N0M0	Pre-NAC	Continuous	pCR	OR 0.48 (0.23–0.98), $P = 0.05$

LN, lymph node; NLR, neutrophil to lymphocyte ratio; MIBC, muscle invasive bladder cancer; OR, odd ratio; OS, overall survival; pCR, pathologic complete response; RC, radical cystectomy; TURBT, transurethral resection of bladder tumor.

TABLE 4 | The studies evaluating the role of neutrophil to lymphocyte in urothelial cancer on chemotherapy.

Study	Year	Cases	Site	Stage	Assessment and treatment	Threshold	Outcomes
Rossi et al. (74)	2015	292	Bladder + Ureter	Advanced or Metastatic	Pre/Follow up-Chemotherapy	3/Kinetics	PFS, 2.76 (1.92–3.96), $P < 0.001$ OS, 3.15 (2.13–4.66), $P < 0.001$
Taguchi et al. (75)	2015	185	Bladder + Ureter	Metastatic	Pre-Chemotherapy	3	CSS, 1.48 (1.01–2.17), $P = 0.043$ OS, 1.49 (1.02–2.18), $P = 0.040$
Auvray et al. (76)	2017	280	Bladder + Ureter	Metastatic	Pre-Chemotherapy	3.2	OS, 1.36 (1.23–1.51), $P < 0.001$ PFS, 1.18 (1.05–1.33), $P = 0.005$
Su et al. (77)	2017	256	Bladder + Ureter	Metastatic	Pre-Chemotherapy	3	OS 1.60 (1.21–2.31), $P = 0.001$
Tan et al. (55)	2018	150	Bladder	Advanced or Metastatic (cT4bN0M0 or TxN1-3M0 or TxNxM1)	Pre-Chemotherapy	3	OS 5.06 (2.88–8.88), $P < 0.001$

CSS, cancer specific survival; HR, hazard ratio; OS, overall survival; PFS, progression free survival; RC, radical cystectomy; RFS, recurrence free survival; RNU, radical nephroureterectomy.

a link between the CSS and RFS (101, 103, 105, 106). The European Association of Urology proposes the NLR as a prognostic factor for CSS in patients with UTUC (4). However, the evidence supporting prognostic role of NLR in UTUC remains low, and currently there are no guidelines of risk stratification (4).

Studies that evaluated the prognostic value of the NLR before chemotherapy for advanced or metastatic disease, wherein surgery was inappropriate, mainly reported on patients with BC and UTUC (**Table 4**) (55, 74–77), with a cutoff value of 3. Interestingly, one study evaluated the prognostic value of NLR kinetics before and after chemotherapy. A high NLR before chemotherapy helped predict poor survival outcomes (76).

ALBUMIN AND ALBUMIN-GLOBULIN RATIO

Several studies have reported on the association of hypoalbuminemia with poor prognosis in patients with UC (**Table 5**) (49, 68, 72, 78–91). The cutoff value of albumin varies from 2 to 4 mg/L, although it is normally around 3.5 mg/L. Many

TABLE 5 | The studies evaluating the role of albumin and Glasgow prognostic score in urothelial cancer.

Study	Year	Case	Site	Stage	Assessment and treatment	Threshold	Outcomes
Albumin							
Caras et al. (78)	2017	1374/4200	Bladder	NA	Pre-RC/Pre-TURBT	3.5 g/dL	OM, HR 1.49, $P = 0.006$ (RC); HR 2.71, $P < 0.001$(TURBT) OS, HR 4.0, $P < 0.001$(TURBT)
Lambert et al. (79)	2012	187	Bladder	pT0-4pN0-3M0	Pre-RC	3.5 g/dL	OS, HR 1.76, $P = 0.04$
Krane et al. (49)	2013	68	Bladder	Recurrent T1HG and MIBC	Pre-RC	3.5 g/dL	OS, HR 4.96 (2.18–11.67)
Ku et al. (80)	2015	419	Bladder	pT0-4N0/+M0	Pre-RC	3.5 g/dL	DSS, HR 1.79 (10.1–3.19), $P = 0.046$ OS, HR 1.67 (10.1–2.77), $P = 0.047$
Djaladat et al. (81)	2014	1964	Bladder	pT0-4N0-3M0	Pre-RC	3.5 g/dL	RFS, HR 1.68 (1.16–2.43), $P < 0.001$ OS, HR 1.93 (1.43–2.63), $P < 0.006$
Laurent et al. (82)	2017	197	Bladder	pT2-4N0/+M0/+	Pre-Chemotherapy	3.5 g/dL	1yr-mortality, HR 3.06 (1.81–5.17), $P < 0.001$
Hwang et al. (83)	2012	67	Bladder	M1	Pre-Chemotherapy	3.5 g/dL	DFS, HR 2.04 (1.10–3.78), $P = 0.023$
Ku et al. (68)	2014	181	Ureter	pTa-4N0/+M0	Pre-RNU	3.5 g/dL	DSS, HR 2.97 (1.25–7.03), $P = 0.013$ OS, HR 2.48 (1.18–5.21), $P = 0.016$
Seah et al. (72)	2016	101	Ureter	pTa-4N0/+M0	Pre-RNU	4.0g/dL	RFS, HR 4.40 (2.04–9.30), $P < 0.001$ OS, HR 3.37 (1.43–7.92), $P = 0.005$
Huang (84)	2017	425	Ureter	pTa-4N0/+M0	Pre-RNU	2.0 g/dL	CSS, HR 1.85 (1.14–3.00), $P = 0.013$ OS, HR 1.73 (1.12–2.70), $P = 0.015$
Albumin/Globulin Ratio (AGR)							
Niwa et al. (85)	2018	364	Bladder	pTa-T1N0M0	Pre-TURBT	1.6	RFS, HR 0.53 (0.36–0.78), $P < 0.010$ (low)
Liu et al. (86)	2016	296	Bladder	pT0-4N0/+M0	Pre-RC	1.60	5 yr-RFS 87.0 vs. 48.0%, $P < 0.001$ (high vs. low) Median CSS: 156.0 vs. 71.1 m $P = 0.005$ (high vs. low) RFS, HR 0.36 (0.17–0.75), $P = 0.006$ (low) CSS, HR 0.28 (0.11–0.68), $P = 0.005$
Liu et al. (87)	2018	189	Bladder	pT1-4N0/+M0	Pre-RC	1.55	PFS, HR 0.30 (0.15–0.61), $P = 0.001$ (low) CSS, HR 0.25 (0.10–0.58), $P = 0.001$ OS, HR 0.20 (0.09–0.47), $P < 0.001$
Zhang et al. (88)	2015	187	Ureter	pTa-4N0/+M0	Pre-RNU	1.45	OS, HR 0.45 (0.27–0.75), $P = 0.002$ (low) CSS, HR 0.47 (0.26–0.86), $P = 0.015$
Fukushima et al. (89)	2018	105	Ureter	pTa-4N0/+ M0	Pre-RNU	1.24	5 yr DFS, 90 vs. 60%, $P < 0.001$ (high vs. low) 5 yr OS, 89 vs. 65%, $P < 0.001$ DFS, 0.34 (0.10–0.95), $P = 0.038$ (low) OS, 0.24 (0.07–0.67), $P = 0.006$
Xu et al. (90)	2018	620	Ureter	pTa-4N0/+M0	Pre-RNU	1.45	5 yr-RFS, 58.4 vs. 38.3%, $P < 0.001$ (low vs. high) 5 yr-CSS, 72.8 vs. 48.9%, $P < 0.001$ 5 yr-OS, 67.0 vs. 41.3%, $P < 0.001$ RFS, HR 1.32 (1.028–1.697), $P = 0.029$ (high) CSS, HR 1.50 (1.11–2.04), $P = 0.010$ OS, HR 1.40 (1.07–1.84), $P = 0.015$
Otsuka et al. (91)	2018	124	Ureter	pTa-4 N0/+M0	Pre-RNU	1.40	RFS, HR 3.96 (1.65–10.11), $P = 0.002$ (high) CSS, HR 5.69 (2.13–17.22), $P < 0.001$ OS, HR 3.12 (1.47–6.28), $P = 0.003$
Glasgow Prognostic Score/Modified Glasgow Prognostic Score							
Hwang et al. (83)	2012	67	Bladder	M1	Pre-Chemotherapy	GPS	OS, HR 7.00 (2.53–19.36), $P = 0.001$ (GPS2)
Qayyum et al. (92)	2013	68	Bladder	pTa-4N0M0	NA	mGPS	CSS, HR 1.78 (1.09–2.90), $P = 0.020$

(Continued)

TABLE 5 | Continued

Study	Year	Case	Site	Stage	Assessment and treatment	Threshold	Outcomes
Cho et al. (93)	2014	147	Ureter	NA	Pre-RNU	GPS	RFS, HR 6.86 (3.69–12.7), $P = 0.001$ (GPS1); HR 5.96 (3.10–11.4), $P = 0.001$ (GPS2)
Ferro et al. (94)	2015	1037	Bladder	pTa-4N0/+M0	Pre-RC	mGPS	5 yr-RFS 36 vs. 18 vs. 5%, $P < 0.001$ RFS, HR 1.54 (1.31–1.81), $P < 0.001$ (GPS1 vs. 2); HR 2.38 (1.86–3.05), $P < 0.001$ (GPS2)
Lucca et al. (95)	2016	310	Bladder	cTa-2N0M0	Pre-RC	GPS	NOC-UCB, HR 2.78 (1.52–5.09), $P = 0.001$ (GPS1); HR 5.37 (1.59–20.85), $P = 0.008$ (GPS2)
Wuethrich et al. (96)	2016	224	Bladder	pT0-4N0-3M0	Pre-RC	GPS	90-days mortality, HR 3.79 (1.29–11.14), $P = 0.016$ (GPS2)
Miyake et al. (97)	2017	117	Bladder	pT0-4N0/+M0	Pre-RC	mGPS	OS, HR 2.9 (1.5–5.8) *P*-0.002 (GPS1-2)
Inamoto et al. (98)	2017	574	Ureter	pT0-4N0M0	Pre-RNU	GPS	10 yr-CSS, 99.5 vs. 75.9%, $P < 0.001$ (GPS0 vs. 2) 10 yr-OS, 93.8 vs. 81.8%, $P < 0.006$ (GPS0 vs. 1); 93.8 vs. 67.6%, $P = 0.001$ (GPS0 vs. 2) OS, HR 1.54 (1.24–1.91), $P < 0.01$
Kimura et al. (99)	2019	1096	Bladder	pTa-1 N0M0	Pre-TURBT	mGPS	PFS, HR 2.06 (1.37–3.12), $P = 0.001$ (GPS1); HR 3.31 (1.40–7.87), $P = 0.007$ (GPS2)
Suyama et al. (100)	2019	74	Ureter	NA	Pre-RNU	GPS	OS, HR 2.28 (1.33–3.91), $P = 0.003$

CSS, cancer specific survival; DFS, disease free survival; DSS, disease specific survival; GPS, Glasgow prognostic score; HR, hazard ratio; mGPS, modified Glasgow prognostic score; NOC-UCB, nomogram-confined urothelial carcinoma of the bladder; OM, overall morbidity; OS, overall survival; PFS, progression free survival; RC, radical cystectomy; RFS, recurrence free survival; RNU, radical nephroureterectomy; TURBT, transurethral resection of bladder tumor.

studies have reported on the role of preoperative evaluation of albumin levels on the prognosis of patients. Hwang et al. reported that presence of hypoalbuminemia before chemotherapy was associated with a worse DFS (HR 2.04, $P = 0.023$) in patients with metastatic BC (83). Laurent et al. reported an increase in the 1-year mortality rate after chemotherapy (HR 3.06, $P < 0.001$) in patients with hypoalbuminemia before the treatment (82).

AGR is the ratio of albumin and total proteins to albumin. The assessment of both albumin and globulin is believed to provide a greater prognostic insight than albumin alone. However, considering the limited number of studies, the utility of this combination remains to be established. Recent studies have reported on the prognostic effect of AGR in patients with UC (85–91).

GLASGOW PROGNOSTIC SCORE AND MODIFIED GLASGOW PROGNOSTIC SCORE

The GPS and mGPS are a combination of CRP and albumin scores, representing methods designed to predict the prognosis of cancer patients. The GPS system is an indicator of the nutritional status of an individual based on systemic inflammation. McMillan et al. first introduced GPS for predicting the prognosis of patients with non-small cell lung cancer (101). Since then, GPS has proved to be useful in predicting the prognosis of patients with a variety of cancers, including colorectal, esophageal, lung, gastric, pancreatic, and liver cancers (101). Recently, few studies recorded the aforementioned scores before chemotherapy and surgery in patients with UC (**Table 5**) (83, 92–100). The majority of the preoperative evaluation studies were performed on patients undergoing RC and RNU. Preoperative GPS or mGPS were reported as factors predicting survival outcomes such as OS, CSS, and RFS. Ferro et al. conducted a study on 1,037 patients undergoing RC and reported longer RFS in the group with higher preoperative mGPS. Furthermore, the group with the highest mGPS demonstrated ∼30% longer RFS compared to those with the lowest scores (94). Inamoto et al. conducted a study on 574 patients undergoing RNU and reported that patients with high GPS before surgery demonstrated 23.6% longer 10-years CSS and 12% longer 10-years OS compared to patients with low GPS (98). One study recorded preoperative GPS in patients undergoing TURB. Kimura et al. conducted a study on 1,096 patients undergoing TURB and reported that preoperative mGPS helped in the prediction of PFS after surgery (99). Another study recorded GPS before chemotherapy in patients with M1 BC. Hwang et al. reported that high GPS levels before chemotherapy were indicative of poor survival (HR 7.0, $P = 0.001$) (83).

PLATELET-TO-LYMPHOCYTE RATIO

Several studies have reported on the prognostic value of the preoperative assessment of the PLR (**Table 6**) (12, 42, 52, 64,

TABLE 6 | The studies evaluating the role of platelet to lymphocyte in urothelial cancer.

Study	Year	Cases	Site	Stage	Assessment and treatment	Threshold	Outcomes
Kang et al. (42)	2017	1551	Bladder	pTa-1N0M0	Pre-TURBT	124	OS, CSS: Not significant
Lee et al. (52)	2015	226	Bladder	pTa-1N0M0	Pre-TURBT	218	OS: Not significant
Bhindi et al. (70)	2016	418	Bladder	pT0-4Nx/+M0	Pre-RC	150	RFS, CSS, OS: Not significant
Schulz et al. (102)	2017	665	Bladder	pT0-4N0/+M0	Pre-RC	28	CSS, HR, 1.4 (1.1–1.9), $P = 0.022$ OS, HR, 1.4 (1.0–1.8), $P = 0.025$
Son et al. (103)	2018	1137	Ureter	pTa-4N0/+M0	Pre-RNU	150	RFS, HR 1.32 (1.08–1.62), $P = 0.007$ CSS, HR 1.87 (1.21–2.92), $P = 0.005$
Kim and Ku (12)	2015	277	Ureter	pTa-4N0M0	Pre-RNU	<150, 150–300, >300	RFS, DFS: Not significant
Dalpiaz et al. (64)	2017	180	Ureter	pTa-4N0M0	Pre-RNU	150	CSS, HR 2.03 (1.04–3.93), $P = 0.037$ OS, HR 1.78 (1.04–3.05), $P = 0.035$
Altan et al. (65)	2017	113	Ureter	pTa-4N0M0	Pre-RNU	150	PFS, DFS: Not significant

CSS, cancer specific survival; HR, hazard ratio; OS, overall survival; PFS, progression free survival; RC, radical cystectomy; RFS, recurrence free survival; RNU, radical nephroureterectomy.

65, 70, 102, 103), wherein a high ratio has been reported to be associated with poor OS, CSS, and RFS. The cutoff value for PLR varies from 123 to 218. Interestingly, Kim and Ku categorized the PLR into three sections with two values, 150 and 300, but did not observe any relationship with the OS of the patients (12).

DISCUSSION

Since hematologic tests in cancer patients are basic and frequently repeated, SIR biomarkers using them can be easily obtained in cancer patients and used as economic and objective parameters. In the UC, in the system for predicting the existing prognosis or in nomogram and risk stratification studies, hematologic factors predicting pathological prognoses such as the number of tumors, tumor diameter, tumor grade, T stage, CIS, and LIV rather than biomarkers I mainly used them (12, 17, 26, 47, 95). However, in the case of clinical staging, the upstaging rate in pathological results after RC reaches 50%, and its accuracy is still low (12). Therefore, there is a need for other biomarkers to predict the prognosis of patients before treatment and to stratify risk, and for this purpose, SIR-related hematologic biomarkers can be a potential and effective factor. In the UC, the SIR biomarker is known to play an essential role in the progression and various oncologic outcomes, even though the inflammatory process develops cancer. In particular, CRP and NLR seem to be particularly useful for these oncologic outcomes and as predictors. And Albumin, AGP GPS, mGPS, PLR, etc. are potential factors, but they still lack data. The standard treatment for NMIBC is TURBT (2). However, due to frequent relapses and progression to MIBC after TURBT, regular examinations, and long-term follow-up are required (2). This repeated and long-term follow-up is putting a high economic burden on the patient (2). In addition, cystoscopy, the most representative test method, is an invasive test that causes significant pain and discomfort to the patient. Based on previous study results, patients with high CRP before surgery in NMIBC have a significant correlation with adverse outcomes in treatment outcomes and survival (18, 19). NLR had a high rate of pathologic upstaging in patients with increased NLR before TURBT (37–45), and the risk of progression to MIBC was also high (69, 70). SIR biomarkers can also be of great help in predicting the prognosis of NMIBC patients and determining the duration or method of follow-up and re-TURB. For MIBC, the standard treatment is RC. There are also various supplementary treatments such as chemotherapy, RT, and immunotherapy. In MIBC (3), patients with high CRP before surgery have a significant correlation with adverse outcomes in treatment outcomes and survival. And NLR was relatively low in complete response and pathologic T0 in patients with high NLR before RC or before NAC (47–60). And increased NLR levels during 1–3 months post RC were associated with adverse survival outcomes (12). The SIR biomarker may be helpful in MIBC patients considering the sequence and timing of treatment such as immediate RC and NAC after prognosis. And the patterns of change in NLRs before and after surgery can also provide useful information for determining additional target groups, such as adjuvant chemotherapy, radiation therapy, and immunotherapy.

In addition to the systemic inflammatory response, CRP is a biomarker that predicts the outcome of IL-2 or IFN-α immunotherapy and has been considered in the evaluation of patients with renal cancer (104). Patients with normal CRP have been reported to demonstrate good tolerance and adherence to immunotherapy (104). The scope of immunotherapy is expanding in patients with UC, and CRP could be considered a factor in predicting the prognosis and compliance to treatment.

The limitations of SIR biomarker's research at UC are: First, there is no objective and clear cut off value. Second, unlike pathological prognostic factors, SIR biomarkers may be affected by other inflammatory diseases or physical conditions other than the patient's cancer. And third, due to the nature of the research,

most studies are retrospective and lack of large-scale prospective research results.

CONCLUSION

In this review, we discussed the applicability of CRP, AGR, albumin, GPS, mGPS, NLR, and PLR as SIRs in patients with UC. These SIRs have proven to be useful during preoperative evaluations in the treatment and risk assessment of patients with UC. However, there is a need to develop uniform classification criteria with a consensus regarding the use of these SIRs in clinical settings. We believe that large prospective studies are needed on this subject based on observations of this retrospective review.

AUTHOR CONTRIBUTIONS

HY and JK contributed to the concept, project planning, and contributed significantly to the writing of the manuscript. JK contributed significantly in the editing of the final manuscript. All authors contributed to the article and approved the submitted version.

FUNDING

This work was supported by the Basic Science Research Program through the National Research Foundation of Korea (NRF) funded by the Ministry of Education (NRF-2019 R1F1A1050507).

REFERENCES

1. Siegel RL, Miller KD, Jemal A. Cancer statistics, 2020. *CA Cancer J Clin.* (2020) 70:7–30. doi: 10.3322/caac.21590
2. Alfred Witjes J, Lebret T, Comperat EM, Cowan NC, De Santis M, Bruins HM, et al. Updated 2016 EAU guidelines on muscle-invasive and metastatic bladder cancer. *Eur Urol.* (2017) 71:462–75. doi: 10.1016/j.eururo.2016.06.020
3. Babjuk M, Burger M, Comperat EM, Gontero P, Mostafid AH, Palou J, et al. European association of urology guidelines on non-muscle-invasive bladder cancer. (TaT1 and carcinoma *in situ*) - 2019 update. *Eur Urol.* (2019) 76:639–57. doi: 10.1016/j.eururo.2019.08.016
4. Roupret M, Babjuk M, Comperat E, Zigeuner R, Sylvester RJ, Burger M, et al. European association of urology guidelines on upper urinary tract urothelial carcinoma: 2017 update. *Eur Urol.* (2018) 73:111–22. doi: 10.1016/j.eururo.2017.07.036
5. Liccardi G, Pentimalli F. Cancer, immunity and inflammation. report from the CDD cambridge conferences 2018 and 2019. *Cell Death Dis.* (2019) 10:798. doi: 10.1038/s41419-019-2032-0
6. Grivennikov SI, Greten FR, Karin M. Immunity, inflammation, and cancer. *Cell.* (2010) 140:883–99. doi: 10.1016/j.cell.2010.01.025
7. Germano G, Allavena P, Mantovani A. Cytokines as a key component of cancer-related inflammation. *Cytokine.* (2008) 43:374–9. doi: 10.1016/j.cyto.2008.07.014
8. Mantovani A, Allavena P, Sica A, Balkwill F. Cancer-related inflammation. *Nature.* (2008) 454:436–44. doi: 10.1038/nature07205
9. Gabay C, Kushner I. Acute-phase proteins and other systemic responses to inflammation. *N Engl J Med.* (1999) 340:448–54. doi: 10.1056/NEJM199902113400607
10. Bray C, Bell LN, Liang H, Haykal R, Kaiksow F, Mazza JJ, et al. Erythrocyte sedimentation rate and C-reactive protein measurements and their relevance in clinical medicine. *WMJ.* (2016) 115: 317–21.
11. Shrotriya S, Walsh D, Bennani-Baiti N, Thomas S, Lorton C. C-Reactive protein is an important biomarker for prognosis tumor recurrence and treatment response in adult solid tumors: a systematic review. *PLoS ONE.* (2015) 10:e0143080. doi: 10.1371/journal.pone.0143080
12. Kim HS, Ku JH. Systemic inflammatory response based on neutrophil-to-lymphocyte ratio as a prognostic marker in bladder cancer. *Dis Markers.* (2016) 2016:8345286. doi: 10.1155/2016/8345286
13. Farrugia A. Albumin usage in clinical medicine: tradition or therapeutic? *Transfus Med Rev.* (2010) 24:53–63. doi: 10.1016/j.tmrv.2009.09.005
14. Moujaess E, Fakhoury M, Assi T, Elias H, El Karak F, Ghosn M, et al. The therapeutic use of human albumin in cancer patients' management. *Crit Rev Oncol Hematol.* (2017) 120:203–9. doi: 10.1016/j.critrevonc.2017.11.008
15. Thomas MR, Storey RF. The role of platelets in inflammation. *Thromb Haemost.* (2015) 114:449–58. doi: 10.1160/TH14-12-1067
16. Menter DG, Tucker SC, Kopetz S, Sood AK, Crissman JD, Honn KV. Platelets and cancer: a casual or causal relationship: revisited. *Cancer Metastasis Rev.* (2014) 33:231–69. doi: 10.1007/s10555-014-9498-0
17. Ishioka J, Saito K, Sakura M, Yokoyama M, Matsuoka Y, Numao N, et al. Development of a nomogram incorporating serum C-reactive protein level to predict overall survival of patients with advanced urothelial carcinoma and its evaluation by decision curve analysis. *Br J Cancer.* (2012) 107:1031–6. doi: 10.1038/bjc.2012.254
18. Hilmy M, Bartlett JM, Underwood MA, McMillan DC. The relationship between the systemic inflammatory response and survival in patients with transitional cell carcinoma of the urinary bladder. *Br J Cancer.* (2005) 92:625–7. doi: 10.1038/sj.bjc.6602406
19. Mbeutcha A, Shariat SF, Rieken M, Rink M, Xylinas E, Seitz C, et al. Prognostic significance of markers of systemic inflammatory response in patients with non-muscle-invasive bladder cancer. *Urol Oncol.* (2016) 34:483.e17–24. doi: 10.1016/j.urolonc.2016.05.013
20. Gakis G, Todenhofer T, Renninger M, Schilling D, Sievert KD, Schwentner C, et al. Development of a new outcome prediction model in carcinoma invading the bladder based on preoperative serum C-reactive protein and standard pathological risk factors: the TNR-C score. *BJU Int.* (2011) 108:1800–5. doi: 10.1111/j.1464-410X.2011.10234.x
21. Kramer MW, Heinisch A, Wegener G, Abbas M, von Klot C, Peters I, et al. [C-reactive protein prior to radical cystectomy: preoperative determination of CRP]. *Urologe A.* (2014) 53:222–7. doi: 10.1007/s00120-013-3299-x
22. Nakagawa T, Hara T, Kawahara T, Ogata Y, Nakanishi H, Komiyama M, et al. Prognostic risk stratification of patients with urothelial carcinoma of the bladder with recurrence after radical cystectomy. *J Urol.* (2013) 189:1275–81. doi: 10.1016/j.juro.2012.10.065
23. Sejima T, Morizane S, Yao A, Isoyama T, Saito M, Amisaki T, et al. Prognostic impact of preoperative hematological disorders and a risk stratification model in bladder cancer patients treated with radical cystectomy. *Int J Urol.* (2014) 21:52–7. doi: 10.1111/iju.12161
24. Yoshida S, Saito K, Koga F, Yokoyama M, Kageyama Y, Masuda H, et al. C-reactive protein level predicts prognosis in patients with muscle-invasive bladder cancer treated with chemoradiotherapy. *BJU Int.* (2008) 101:978–81. doi: 10.1111/j.1464-410X.2007.07408.x
25. Eggers H, Seidel C, Schrader AJ, Lehmann R, Wegener G, Kuczyk MA, et al. Serum C-reactive protein: a prognostic factor in metastatic urothelial cancer of the bladder. *Med Oncol.* (2013) 30:705. doi: 10.1007/s12032-013-0705-6
26. Nakagawa T, Taguchi S, Uemura Y, Kanatani A, Ikeda M, Matsumoto A, et al. Nomogram for predicting survival of postcystectomy recurrent urothelial carcinoma of the bladder. *Urol Oncol.* (2017) 35:457.e15–21. doi: 10.1016/j.urolonc.2016.12.010
27. Saito K, Kawakami S, Ohtsuka Y, Fujii Y, Masuda H, Kumagai J, et al. The impact of preoperative serum C-reactive protein on the prognosis of patients with upper urinary tract urothelial carcinoma treated surgically. *BJU Int.* (2007) 100:269–73. doi: 10.1111/j.1464-410X.2007.06934.x

28. Obata J, Kikuchi E, Tanaka N, Matsumoto K, Hayakawa N, Ide H, et al. C-reactive protein: a biomarker of survival in patients with localized upper tract urothelial carcinoma treated with radical nephroureterectomy. *Urol Oncol.* (2013) 31:1725–30. doi: 10.1016/j.urolonc.2012.05.008
29. Stein B, Schrader AJ, Wegener G, Seidel C, Kuczyk MA, Steffens S. Preoperative serum C- reactive protein: a prognostic marker in patients with upper urinary tract urothelial carcinoma. *BMC Cancer.* (2013) 13:101. doi: 10.1186/1471-2407-13-101
30. Aziz A, Rink M, Gakis G, Kluth LA, Dechet C, Miller F, et al. Preoperative C-reactive protein in the serum: a prognostic biomarker for upper urinary tract urothelial carcinoma treated with radical nephroureterectomy. *Urol Int.* (2014) 93:352–60. doi: 10.1159/000362248
31. Tanaka N, Kikuchi E, Shirotake S, Kanao K, Matsumoto K, Kobayashi H, et al. The predictive value of C-reactive protein for prognosis in patients with upper tract urothelial carcinoma treated with radical nephroureterectomy: a multi-institutional study. *Eur Urol.* (2014) 65:227–34. doi: 10.1016/j.eururo.2012.11.050
32. Morizane S, Yumioka T, Yamaguchi N, Masago T, Honda M, Sejima T, et al. Risk stratification model, including preoperative serum C-reactive protein and estimated glomerular filtration rate levels, in patients with upper urinary tract urothelial carcinoma undergoing radical nephroureterectomy. *Int Urol Nephrol.* (2015) 47:1335–41. doi: 10.1007/s11255-015-1033-x
33. Fujita K, Inamoto T, Yamamoto Y, Tanigawa G, Nakayama M, Mori N, et al. Role of adjuvant chemotherapy for lymph node-positive upper tract urothelial carcinoma and the prognostic significance of C-reactive protein: a multi-institutional, retrospective study. *Int J Urol.* (2015) 22:1006–12. doi: 10.1111/iju.12868
34. Nakagawa T, Taguchi S, Kanatani A, Kawai T, Ikeda M, Urakami S, et al. Oncologic outcome of metastasectomy for urothelial carcinoma: who is the best candidate? *Ann Surg Oncol.* (2017) 24:2794–800. doi: 10.1245/s10434-017-5970-8
35. Saito K, Urakami S, Komai Y, Yasuda Y, Kubo Y, Kitsukawa S, et al. Impact of C-reactive protein kinetics on survival of patients with advanced urothelial carcinoma treated by second-line chemotherapy with gemcitabine, etoposide and cisplatin. *BJU Int.* (2012) 110:1478–84. doi: 10.1111/j.1464-410X.2012.11153.x
36. Matsumoto R, Abe T, Ishizaki J, Kikuchi H, Harabayashi T, Minami K, et al. Outcome and prognostic factors in metastatic urothelial carcinoma patients receiving second-line chemotherapy: an analysis of real-world clinical practice data in Japan. *Jpn J Clin Oncol.* (2018) 48:771–6. doi: 10.1093/jjco/hyy094
37. Mano R, Baniel J, Shoshany O, Margel D, Bar-On T, Nativ O, et al. Neutrophil-to-lymphocyte ratio predicts progression and recurrence of non-muscle-invasive bladder cancer. *Urol Oncol.* (2015) 33:67 e1–7. doi: 10.1016/j.urolonc.2014.06.010
38. Favilla V, Castelli T, Urzi D, Reale G, Privitera S, Salici A, et al. Neutrophil to lymphocyte ratio, a biomarker in non-muscle invasive bladder cancer: a single-institutional longitudinal study. *Int Braz J Urol.* (2016) 42:685–93. doi: 10.1590/S1677-5538.IBJU.2015.0243
39. Ogihara K, Kikuchi E, Yuge K, Yanai Y, Matsumoto K, Miyajima A, et al. The preoperative neutrophil-to-lymphocyte ratio is a novel biomarker for predicting worse clinical outcomes in non-muscle invasive bladder cancer patients with a previous history of smoking. *Ann Surg Oncol.* (2016) 23(Suppl.5):1039–47. doi: 10.1245/s10434-016-5578-4
40. Ozyalvacli ME, Ozyalvacli G, Kocaaslan R, Cecen K, Uyeturk U, Kemahli E, et al. Neutrophil-lymphocyte ratio as a predictor of recurrence and progression in patients with high-grade pT1 bladder cancer. *Can Urol Assoc J.* (2015) 9:E126–31. doi: 10.5489/cuaj.2523
41. D'Andrea D, Moschini M, Gust K, Abufaraj M, Ozsoy M, Mathieu R, et al. Prognostic role of neutrophil-to-lymphocyte ratio in primary non-muscle-invasive bladder cancer. *Clin Genitourin Cancer.* (2017) 15:e755–64. doi: 10.1016/j.clgc.2017.03.007
42. Kang M, Jeong CW, Kwak C, Kim HH, Ku JH. Preoperative neutrophil-lymphocyte ratio can significantly predict mortality outcomes in patients with non-muscle invasive bladder cancer undergoing transurethral resection of bladder tumor. *Oncotarget.* (2017) 8:12891–901. doi: 10.18632/oncotarget.14179
43. Vartolomei MD, Ferro M, Cantiello F, Lucarelli G, Di Stasi S, Hurle R, et al. Validation of neutrophil-to-lymphocyte ratio in a multi-institutional cohort of patients with T1G3 non-muscle-invasive bladder cancer. *Clin Genitourin Cancer.* (2018) 16:445–52. doi: 10.1016/j.clgc.2018.07.003
44. Getzler I, Bahouth Z, Nativ O, Rubinstein J, Halachmi S. Preoperative neutrophil to lymphocyte ratio improves recurrence prediction of non-muscle invasive bladder cancer. *BMC Urol.* (2018) 18:90. doi: 10.1186/s12894-018-0404-x
45. Racioppi M, Di Gianfrancesco L, Ragonese M, Palermo G, Sacco E, Bassi PF. Can neutrophil-to-Lymphocyte ratio predict the response to BCG in high-risk non muscle invasive bladder cancer? *Int Braz J Urol.* (2019) 45:315–24. doi: 10.1590/s1677-5538.ibju.2018.0249
46. Yuk HD, Jeong CW, Kwak C, Kim HH, Ku JH. Elevated neutrophil to lymphocyte ratio predicts poor prognosis in non-muscle invasive bladder cancer patients: initial intravesical bacillus calmette-guerin treatment after transurethral resection of bladder tumor setting. *Front Oncol.* (2018) 8:642. doi: 10.3389/fonc.2018.00642
47. Gondo T, Nakashima J, Ohno Y, Choichiro O, Horiguchi Y, Namiki K, et al. Prognostic value of neutrophil-to-lymphocyte ratio and establishment of novel preoperative risk stratification model in bladder cancer patients treated with radical cystectomy. *Urology.* (2012) 79:1085–91. doi: 10.1016/j.urology.2011.11.070
48. Viers BR, Boorjian SA, Frank I, Tarrell RF, Thapa P, Karnes RJ, et al. Pretreatment neutrophil-to-lymphocyte ratio is associated with advanced pathologic tumor stage and increased cancer-specific mortality among patients with urothelial carcinoma of the bladder undergoing radical cystectomy. *Eur Urol.* (2014) 66:1157–64. doi: 10.1016/j.eururo.2014.02.042
49. Krane LS, Richards KA, Kader AK, Davis R, Balaji KC, Hemal AK. Preoperative neutrophil/lymphocyte ratio predicts overall survival and extravesical disease in patients undergoing radical cystectomy. *J Endourol.* (2013) 27:1046–50. doi: 10.1089/end.2012.0606
50. Hermanns T, Bhindi B, Wei Y, Yu J, Noon AP, Richard PO, et al. Pre-treatment neutrophil-to-lymphocyte ratio as predictor of adverse outcomes in patients undergoing radical cystectomy for urothelial carcinoma of the bladder. *Br J Cancer.* (2014) 111:444–51. doi: 10.1038/bjc.2014.305
51. Kang M, Jeong CW, Kwak C, Kim HH, Ku JH. The prognostic significance of the early postoperative neutrophil-to-lymphocyte ratio in patients with urothelial carcinoma of the bladder undergoing radical cystectomy. *Ann Surg Oncol.* (2016) 23:335–42. doi: 10.1245/s10434-015-4708-8
52. Bhindi B, Hermanns T, Wei Y, Yu J, Richard PO, Wettstein MS, et al. Identification of the best complete blood count-based predictors for bladder cancer outcomes in patients undergoing radical cystectomy. *Br J Cancer.* (2016) 114:207–12. doi: 10.1038/bjc.2015.432
53. Kawahara T, Furuya K, Nakamura M, Sakamaki K, Osaka K, Ito H, et al. Neutrophil-to-lymphocyte ratio is a prognostic marker in bladder cancer patients after radical cystectomy. *BMC Cancer.* (2016) 16:185. doi: 10.1186/s12885-016-2219-z
54. Hirasawa Y, Nakashima J, Yunaiyama D, Sugihara T, Gondo T, Nakagami Y, et al. Sarcopenia as a novel preoperative prognostic predictor for survival in patients with bladder cancer undergoing radical cystectomy. *Ann Surg Oncol.* (2016) 23(Suppl.5):1048–54. doi: 10.1245/s10434-016-5606-4
55. Tan YG, Eu EWC, Huang HH, Lau WKO. High neutrophil-to-lymphocyte ratio predicts worse overall survival in patients with advanced/metastatic urothelial bladder cancer. *Int J Urol.* (2018) 25:232–8. doi: 10.1111/iju.13480
56. Kang M, Balpukov UJ, Jeong CW, Kwak C, Kim HH, Ku JH. Can the preoperative neutrophil-to-lymphocyte ratio significantly predict the conditional survival probability in muscle-invasive bladder cancer patients undergoing radical cystectomy? *Clin Genitourin Cancer.* (2017) 15:e411–20. doi: 10.1016/j.clgc.2016.10.015
57. Morizawa Y, Miyake M, Shimada K, Hori S, Tatsumi Y, Nakai Y, et al. Neutrophil-to-lymphocyte ratio as a detection marker of tumor recurrence in patients with muscle-invasive bladder cancer after radical cystectomy. *Urol Oncol.* (2016) 34:257 e11–7. doi: 10.1016/j.urolonc.2016.02.012
58. Buisan O, Orsola A, Areal J, Font A, Oliveira M, Martinez R, et al. Low pretreatment neutrophil-to-lymphocyte ratio predicts for good outcomes in patients receiving neoadjuvant chemotherapy before radical cystectomy for

muscle invasive bladder cancer. *Clin Genitourin Cancer.* (2017) 15:145–51 e2. doi: 10.1016/j.clgc.2016.05.004
59. Kaiser J, Li H, North SA, Leibowitz-Amit R, Seah JA, Morshed N, et al. The prognostic role of the change in neutrophil-to-lymphocyte ratio during neoadjuvant chemotherapy in patients with muscle-invasive bladder cancer: a retrospective, multi-institutional study. *Bladder Cancer.* (2018) 4:185–94. doi: 10.3233/BLC-170133
60. Ohtake S, Kawahara T, Kasahara R, Ito H, Osaka K, Hattori Y, et al. Pretreatment neutrophil-to-lymphocyte ratio can predict the prognosis in bladder cancer patients who receive gemcitabine and nedaplatin therapy. *Biomed Res Int.* (2016) 2016:9846823. doi: 10.1155/2016/9846823
61. Azuma T, Matayoshi Y, Odani K, Sato Y, Sato Y, Nagase Y, et al. Preoperative neutrophil-lymphocyte ratio as an independent prognostic marker for patients with upper urinary tract urothelial carcinoma. *Clin Genitourin Cancer.* (2013) 11:337–41. doi: 10.1016/j.clgc.2013.04.003
62. Tanaka N, Kikuchi E, Kanao K, Matsumoto K, Shirotake S, Miyazaki Y, et al. A multi-institutional validation of the prognostic value of the neutrophil-to-lymphocyte ratio for upper tract urothelial carcinoma treated with radical nephroureterectomy. *Ann Surg Oncol.* (2014) 21:4041–8. doi: 10.1245/s10434-014-3830-3
63. Luo HL, Chen YT, Chuang YC, Cheng YT, Lee WC, Kang CH, et al. Subclassification of upper urinary tract urothelial carcinoma by the neutrophil-to-lymphocyte ratio. (NLR) improves prediction of oncological outcome. *BJU Int.* (2014) 113:E144–9. doi: 10.1111/bju.12582
64. Dalpiaz O, Ehrlich GC, Mannweiler S, Hernandez JM, Gerger A, Stojakovic T, et al. Validation of pretreatment neutrophil-lymphocyte ratio as a prognostic factor in a European cohort of patients with upper tract urothelial carcinoma. *BJU Int.* (2014) 114:334–9. doi: 10.1111/bju.12441
65. Altan M, Haberal HB, Akdogan B, Ozen H. A critical prognostic analysis of neutrophil-lymphocyte ratio for patients undergoing nephroureterectomy due to upper urinary tract urothelial carcinoma. *Int J Clin Oncol.* (2017) 22:964–71. doi: 10.1007/s10147-017-1150-x
66. Kishimoto N, Takao T, Kuribayashi S, Yamamichi G, Nakano K, Kawamura M, et al. The neutrophil-to-lymphocyte ratio as a predictor of intravesical recurrence in patients with upper urinary tract urothelial carcinoma treated with radical nephroureterectomy. *Int J Clin Oncol.* (2017) 22:153–8. doi: 10.1007/s10147-016-1040-7
67. Tan P, Xu H, Liu L, Ai J, Xu H, Jiang Y, et al. The prognostic value of preoperative neutrophil-to-lymphocyte ratio in patients with upper tract urothelial carcinoma. *Clin Chim Acta.* (2018) 485:26–32. doi: 10.1016/j.cca.2018.06.019
68. Ku JH, Kang M, Kim HS, Jeong CW, Kwak C, Kim HH. The prognostic value of pretreatment of systemic inflammatory responses in patients with urothelial carcinoma undergoing radical cystectomy. *Br J Cancer.* (2015) 112:461–7. doi: 10.1038/bjc.2014.631
69. Can C, Baseskioglu B, Yilmaz M, Colak E, Ozen A, Yenilmez A. Pretreatment parameters obtained from peripheral blood sample predicts invasiveness of bladder carcinoma. *Urol Int.* (2012) 89:468–72. doi: 10.1159/000343278
70. Lee SM, Russell A, Hellawell G. Predictive value of pretreatment inflammation-based prognostic scores. (neutrophil-to-lymphocyte ratio, platelet-to-lymphocyte ratio, and lymphocyte-to-monocyte ratio) for invasive bladder carcinoma. *Korean J Urol.* (2015) 56:749–55. doi: 10.4111/kju.2015.56.11.749
71. Potretzke A, Hillman L, Wong K, Shi F, Brower R, Mai S, et al. NLR is predictive of upstaging at the time of radical cystectomy for patients with urothelial carcinoma of the bladder. *Urol Oncol.* (2014) 32:631–6. doi: 10.1016/j.urolonc.2013.12.009
72. Seah JA, Leibowitz-Amit R, Atenafu EG, Alimohamed N, Knox JJ, Joshua AM, et al. Neutrophil-Lymphocyte ratio and pathological response to neoadjuvant chemotherapy in patients with muscle-invasive bladder cancer. *Clin Genitourin Cancer.* (2015) 13:e229–33. doi: 10.1016/j.clgc.2015.02.001
73. Leibowitz-Amit R, Israel A, Gal M, Atenafu EA, Symon Z, Portnoy O, et al. Association between the absolute baseline lymphocyte count and response to neoadjuvant platinum-based chemotherapy in muscle-invasive bladder cancer. *Clin Oncol.* (2016) 28:790–6. doi: 10.1016/j.clon.2016.07.007
74. Rossi L, Santoni M, Crabb SJ, Scarpi E, Burattini L, Chau C, et al. High neutrophil-to-lymphocyte ratio persistent during first-line chemotherapy predicts poor clinical outcome in patients with advanced urothelial cancer. *Ann Surg Oncol.* (2015) 22:1377–84. doi: 10.1245/s10434-014-4097-4
75. Taguchi S, Nakagawa T, Matsumoto A, Nagase Y, Kawai T, Tanaka Y, et al. Pretreatment neutrophil-to-lymphocyte ratio as an independent predictor of survival in patients with metastatic urothelial carcinoma: a multi-institutional study. *Int J Urol.* (2015) 22:638–43. doi: 10.1111/iju.12766
76. Auvray M, Elaidi R, Ozguroglu M, Guven S, Gauthier H, Culine S, et al. Prognostic value of baseline neutrophil-to-lymphocyte ratio in metastatic urothelial carcinoma patients treated with first-line chemotherapy: a large multicenter study. *Clin Genitourin Cancer.* (2017) 15:e469–e76. doi: 10.1016/j.clgc.2016.10.013
77. Su YL, Hsieh MC, Chiang PH, Sung MT, Lan J, Luo HL, et al. Novel inflammation-based prognostic score for predicting survival in patients with metastatic urothelial carcinoma. *PLoS ONE.* (2017) 12:e0169657. doi: 10.1371/journal.pone.0169657
78. Caras RJ, Lustik MB, Kern SQ, McMann LP, Sterbis JR. Preoperative albumin is predictive of early postoperative morbidity and mortality in common urologic oncologic surgeries. *Clin Genitourin Cancer.* (2017) 15:e255–62. doi: 10.1016/j.clgc.2016.09.008
79. Lambert JW, Ingham M, Gibbs BB, Given RW, Lance RS, Riggs SB. Using preoperative albumin levels as a surrogate marker for outcomes after radical cystectomy for bladder cancer. *Urology.* (2013) 81:587–92. doi: 10.1016/j.urology.2012.10.055
80. Ku JH, Kim M, Choi WS, Kwak C, Kim HH. Preoperative serum albumin as a prognostic factor in patients with upper urinary tract urothelial carcinoma. *Int Braz J Urol.* (2014) 40:753–62. doi: 10.1590/S1677-5538.IBJU.2014.06.06
81. Djaladat H, Bruins HM, Miranda G, Cai J, Skinner EC, Daneshmand S. The association of preoperative serum albumin level and American Society of Anesthesiologists. (ASA) score on early complications and survival of patients undergoing radical cystectomy for urothelial bladder cancer. *BJU Int.* (2014) 113:887–93. doi: 10.1111/bju.12240
82. Laurent M, Brureau L, Demery ME, Flechon A, Thuaut AL, Carvahlo-Verlinde M, et al. Early chemotherapy discontinuation and mortality in older patients with metastatic bladder cancer: the AGEVIM multicenter cohort study. *Urol Oncol.* (2017) 35:34 e9–16. doi: 10.1016/j.urolonc.2016.08.003
83. Hwang EC, Hwang IS, Yu HS, Kim SO, Jung SI, Hwang JE, et al. Utility of inflammation-based prognostic scoring in patients given systemic chemotherapy first-line for advanced inoperable bladder cancer. *Jpn J Clin Oncol.* (2012) 42:955–60. doi: 10.1093/jjco/hys124
84. Huang J, Wang Y, Yuan Y, Chen Y, Kong W, Chen H, et al. Preoperative serum pre-albumin as an independent prognostic indicator in patients with localized upper tract urothelial carcinoma after radical nephroureterectomy. *Oncotarget.* (2017) 8:36772–9. doi: 10.18632/oncotarget.13694
85. Niwa N, Matsumoto K, Ide H, Nagata H, Oya M. Prognostic value of pretreatment albumin-to-globulin ratio in patients with non-muscle-invasive bladder cancer. *Clin Genitourin Cancer.* (2018) 16:e655–e61. doi: 10.1016/j.clgc.2017.12.013
86. Liu J, Dai Y, Zhou F, Long Z, Li Y, Liu B, et al. The prognostic role of preoperative serum albumin/globulin ratio in patients with bladder urothelial carcinoma undergoing radical cystectomy. *Urol Oncol.* (2016) 34:484 e1–8. doi: 10.1016/j.urolonc.2016.05.024
87. Zhang B, Yu W, Zhou LQ, He ZS, Shen C, He Q, et al. Prognostic significance of preoperative albumin-globulin ratio in patients with upper tract urothelial carcinoma. *PLoS ONE.* (2015) 10:e0144961. doi: 10.1371/journal.pone.0144961
88. Fukushima H, Kobayashi M, Kawano K, Morimoto S. Prognostic value of albumin/globulin ratio in patients with upper tract urothelial carcinoma patients treated with radical nephroureterectomy. *Anticancer Res.* (2018) 38:2329–34. doi: 10.21873/anticanres.12478
89. Xu H, Tan P, Ai J, Huang Y, Lin T, Yang L, et al. Prognostic impact of preoperative albumin-globulin ratio on oncologic outcomes in upper tract urothelial carcinoma treated with radical nephroureterectomy. *Clin Genitourin Cancer.* (2018) 16:e1059–68. doi: 10.1016/j.clgc.2018.06.003
90. Otsuka M, Kamasako T, Uemura T, Takeshita N, Shinozaki T, Kobayashi M, et al. Prognostic role of the preoperative serum albumin : globulin ratio after radical nephroureterectomy for upper tract urothelial carcinoma. *Int J Urol.* (2018) 25:871–8. doi: 10.1111/iju.13767

91. Liu J, Wang F, Li S, Huang W, Jia Y, Wei C. The prognostic significance of preoperative serum albumin in urothelial carcinoma: a systematic review and meta-analysis. *Biosci Rep.* (2018) 38(4) doi: 10.1042/BSR20180214
92. Qayyum T, McArdle P, Hilmy M, Going J, Orange C, Seywright M, et al. A prospective study of the role of inflammation in bladder cancer. *Curr Urol.* (2013) 6:189–93. doi: 10.1159/000343537
93. Cho YH, Seo YH, Chung SJ, Hwang I, Yu HS, Kim SO, et al. Predictors of intravesical recurrence after radical nephroureterectomy for upper urinary tract urothelial carcinoma: an inflammation-based prognostic score. *Korean J Urol.* (2014) 55:453–9. doi: 10.4111/kju.2014.55.7.453
94. Ferro M, De Cobelli O, Buonerba C, Di Lorenzo G, Capece M, Bruzzese D, et al. Modified glasgow prognostic score is associated with risk of recurrence in bladder cancer patients after radical cystectomy: a multicenter experience. *Medicine.* (2015) 94:e1861. doi: 10.1097/MD.0000000000001861
95. Lucca I, Hofbauer SL, Leitner CV, de Martino M, Ozsoy M, Susani M, et al. Development of a preoperative nomogram incorporating biomarkers of systemic inflammatory response to predict nonorgan-confined urothelial carcinoma of the bladder at radical cystectomy. *Urology.* (2016) 95:132–8. doi: 10.1016/j.urology.2016.06.007
96. Wuethrich PY, Vidal A, Burkhard FC. There is a place for radical cystectomy and urinary diversion, including orthotopic bladder substitution, in patients aged 75 and older: results of a retrospective observational analysis from a high-volume center. *Urol Oncol.* (2016) 34:58 e19–27. doi: 10.1016/j.urolonc.2015.08.011
97. Miyake M, Morizawa Y, Hori S, Marugami N, Iida K, Ohnishi K, et al. Integrative assessment of pretreatment inflammation-, nutrition-, and muscle-based prognostic markers in patients with muscle-invasive bladder cancer undergoing radical cystectomy. *Oncology.* (2017) 93:259–69. doi: 10.1159/000477405
98. Inamoto T, Matsuyama H, Sakano S, Ibuki N, Takahara K, Komura K, et al. The systemic inflammation-based glasgow prognostic score as a powerful prognostic factor in patients with upper tract urothelial carcinoma. *Oncotarget.* (2017) 8:113248–57. doi: 10.18632/oncotarget.22641
99. Kimura S, D DA, Soria F, Foerster B, Abufaraj M, Vartolomei MD, et al. Prognostic value of modified glasgow prognostic score in non-muscle-invasive bladder cancer. *Urol Oncol.* (2019) 37:179 e19–28. doi: 10.1016/j.urolonc.2018.11.005
100. Suyama T, Kanbe S, Maegawa M, Shimizu H, Nakajima K. Prognostic significance of inflammation-based prognostic scoring in patients with upper urinary tract urothelial carcinoma. *Int Braz J Urol.* (2019) 45:541–8. doi: 10.1590/s1677-5538.ibju.2018.0251
101. McMillan DC. The systemic inflammation-based glasgow prognostic score: a decade of experience in patients with cancer. *Cancer Treat Rev.* (2013) 39:534–40. doi: 10.1016/j.ctrv.2012.08.003
102. Schulz GB, Grimm T, Buchner A, Jokisch F, Grabbert M, Schneevoigt BS, et al. Prognostic value of the preoperative platelet-to-leukocyte ratio for oncologic outcomes in patients undergoing radical cystectomy for bladder cancer. *Clin Genitourin Cancer.* (2017) 15:e915–21. doi: 10.1016/j.clgc.2017.05.009
103. Son S, Hwang EC, Jung SI, Kwon DD, Choi SH, Kwon TG, et al. Prognostic value of preoperative systemic inflammation markers in localized upper tract urothelial cell carcinoma: a large, multicenter cohort analysis. *Minerva Urol Nefrol.* (2018) 70:300–9.
104. Casamassima A, Picciariello M, Quaranta M, Berardino R, Ranieri C, Paradiso A, et al. C-reactive protein: a biomarker of survival in patients with metastatic renal cell carcinoma treated with subcutaneous interleukin-2 based immunotherapy. *J Urol.* (2005) 173:52–5. doi: 10.1097/01.ju.0000146713.50673.e5

Conflict of Interest: The authors declare that the research was conducted in the absence of any commercial or financial relationships that could be construed as a potential conflict of interest.

frontiers in Oncology

ORIGINAL RESEARCH
published: 02 October 2020
doi: 10.3389/fonc.2020.532924

Development and Validation of a Nomogram to Predict Lymph Node Metastasis in Patients With T1 High-Grade Urothelial Carcinoma of the Bladder

Ningjing Ou[1†], Yuxuan Song[1†], Mohan Liu[2†], Jun Zhu[1], Yongjiao Yang[3] and Xiaoqiang Liu[1]*

[1] Department of Urology, Tianjin Medical University General Hospital, Tianjin, China, [2] State Key Laboratory of Biotherapy and Cancer Center, West China Hospital, Sichuan University and Collaborative Innovation Center, Chengdu, China, [3] Department of Urology, The Second Hospital of Tianjin Medical University, Tianjin, China

OPEN ACCESS

Edited by:
Ja Hyeon Ku, Seoul National University, South Korea

Reviewed by:
Matteo Ferro, European Institute of Oncology (IEO), Italy
Luis Alex Kluth, University Hospital Frankfurt, Germany

***Correspondence:**
Xiaoqiang Liu
15122926116@163.com

[†] These authors have contributed equally to this work

Specialty section:
This article was submitted to Genitourinary Oncology, a section of the journal Frontiers in Oncology

Received: *06 February 2020*
Accepted: *01 September 2020*
Published: *02 October 2020*

Citation:
Ou N, Song Y, Liu M, Zhu J, Yang Y and Liu X (2020) Development and Validation of a Nomogram to Predict Lymph Node Metastasis in Patients With T1 High-Grade Urothelial Carcinoma of the Bladder. Front. Oncol. 10:532924. doi: 10.3389/fonc.2020.532924

Purpose: This study aims to develop and validate a nomogram to predict lymph node (LN) metastasis preoperatively in patients with T1 high-grade urothelial carcinoma.

Methods: We retrospectively evaluated the data of 2,689 patients with urothelial carcinoma of the bladder (UCB) treated with radical cystectomy (RC) and bilateral lymphadenectomy in two medical centers. Eventually, 412 patients with T1 high-grade urothelial carcinoma were enrolled in the primary cohort to develop a prognostic nomogram designed to predict LN status. An independent validation cohort (containing 783 consecutive patients during the same period) was subjected to validate the predicting model. Binary regression analysis was used to develop the predicting nomogram. We assessed the performance of the nomogram concerning its clinical usefulness, calibration, and discrimination.

Results: Overall, 69 (16.75%), and 135 (17.24%) patients had LN metastasis in the primary cohort and external validation cohort, respectively. The final nomogram included information on tumor number, tumor size, lymphovascular invasion (LVI), fibrinogen, and monocyte-to-lymphocyte ratio (MLR). The nomogram showed good predictive accuracy and calibration with a concordance index in the primary cohort of 0.853. The application of the nomogram in the external validation cohort still gave good discrimination (C-index, 0.845) and good calibration. The analysis of the decision curve shows that the nomogram has clinical application value.

Conclusion: The nomogram that incorporated the tumor number, tumor size, LVI, fibrinogen, and MLR showed favorable predictive accuracy for LN metastasis. It may be conveniently used to predict LN metastasis in patients with T1 high-grade urothelial carcinoma and be helpful in guiding treatment decisions.

Keywords: nomogram, lymph node metastasis, MLR, bladder cancer, T1 high grade urothelial carcinoma

INTRODUCTION

Urothelial carcinoma of the bladder (UCB) is the ninth most common tumor worldwide (1). It is also the most prevalent cancer of the urinary tract and the fourth cause of cancer-related death in men (2). Approximately 75% of patients with UCB are diagnosed as non-muscle-invasive bladder cancer (NMIBC) at the first time in seeking medical care. Most of the NMIBC patients will choose to retain bladder therapy: transurethral resection of the bladder (TURBT) combined with maintenance bacillus Calmette–Guérin (BCG), but some patients (especially T1 high grade) are very likely to fail BCG therapy alone (3). Approximately 22% of the UCB patients finally found positive lymph nodes, and this number will increase with pathologic stage progressing (13% for pT1 and 45% for pT4). To date, extended pelvic lymph node (LN) dissection is suggested in some clinical trials for UCB patients with LN metastasis. It can prolong the lifetime of these patients (4, 5). Immediate radical cystectomy (RC) and LN dissection should be considered in selected cases such as those patients with pT1 high-grade disease and other risk factors such as lymphovascular invasion (LVI), histological variants, and size of the tumor (6). However, some patients with T1 high-grade bladder cancer have a low risk of metastasis and progression, and conservative treatment can be tried. In these cases, RC may be an overtreatment (7). Some researchers found that even muscle-invasive bladder tumor can be treated with trigeminal therapy that can preserve the bladder and improve the quality of the patient's life (8). At the same time, some scholars believe that extended lymph dissection should be performed during RC for patients with higher risk of LN metastasis. However, others thought that the extent of pelvic LN dissection (PLND) of T1 high-grade UCB remains highly disputed if there has no evidence of LN metastasis (9–11). A good preoperative prediction about LN metastasis can be helpful in making a decision on PLND (10, 12). There is no validated project to decide which treatment program is optimal for each patient with T1 high-grade disease. Current evidence demonstrate that clinicopathological and molecular risk classifiers together may help to select the optimal management strategy for each patient with T1 high-grade disease (7).

Recently, several researches have found that systemic inflammatory response is highly related to LN metastasis and tumor progression (13, 14). Some studies have found that preoperative neutrophil-to-lymphocyte ratio (NLR), platelet-to-lymphocyte ratio (PLR), monocyte-to-lymphocyte ratio (MLR), and fibrinogen are directly associated with nodal involvement status of tumors (15–19). Kilian et al. found that decreased cholinesterase (ChE) is associated with poor prognosis in patients with NMIBC undergoing TURBT (8). Ferro et al. found that type 2 diabetes mellitus predicts worse outcomes in patients with high-grade T1 bladder cancer (20). These results indicate that many routine laboratory reports will be helpful to predict the prognosis of tumors.

Hence, this study was aimed to detect the relationship between inflammation biomarkers, clinicopathological features, and LN metastasis in patients with T1 high-grade UCB treated with RC. This study also aimed to develop and validate a nomogram to predict LN metastasis preoperatively in patients with T1 high-grade urothelial carcinoma.

Abbreviations: LN, lymph node; UCB, urothelial carcinoma of the bladder; NLR, neutrophil-to-lymphocyte ratio; PLR, platelet-to-lymphocyte ratio; MLR, monocyte-to-lymphocyte ratio; NMIBC, non-muscle invasive bladder cancer; PLND, pelvic LN dissection; ChE, cholinesterase; TURBT, transurethral resection of the bladder; RC, radical cystectomy; TNM, tumor node metastasis; HB, hemoglobin; ALB, albumin; WBC, white blood cell; AUC, area under the curve; CSS, cancer-specific survival; OS, overall survival.

MATERIALS AND METHODS

We retrospectively evaluated the data of 2,689 patients with UCB treated with RC and bilateral lymphadenectomy at the Second Hospital of Tianjin Medical University and Tianjin Medical University General Hospital between January 2010 and December 2019. Eventually, we enrolled 1,195 patients (412 in the primary cohort and 783 in the validation cohort) with T1 high-grade UCB in this study (**Figure 1**). All patients enrolled had RC immediately (no more than 1 month) after histologically confirmed pT1 high-grade disease. Approximately 35% of the patients had repeated TURBT. The tumor was graded according to the World Health Organization—International Society of Urologic Pathology 2004 guidelines and the tumor node metastasis (TNM) 2002 staging system. All patients were histologically confirmed, and the exclusion criteria were as follows: (a) patients without muscle in the TURBT specimen, (b) patients received radiation therapy or neoadjuvant chemotherapy, (c) liver cirrhosis, (d) patients had distant metastatic disease at the time of RC, (e) severe inflammation, (f) immune system or severe bleeding disease, (g) patients had concomitant carcinoma *in situ* (CIS), and (h) patients received adjuvant intravesical chemo before RC.

Sex, age, lymphatic invasion, LN status, tumor number, tumor size, TNM stage, and routine preoperative laboratory measurements including white blood cell (WBC) count, neutrophil count, lymphocyte count, monocyte count, hemoglobin (HB), albumin (ALB), and fibrinogen were recorded in our study. Two doctors independently reviewed the medical data and pathological data of all patients.

PLR, NLR, and MLR Evaluation

Blood count test was a routine part of the preoperative inspection before the surgery. All blood samples were obtained within 14 days (median 6.3 days) before RC. The definition of PLR, NLR, and MLR was platelet count divided by lymphocyte count, neutrophil count divided by lymphocyte count, and monocyte count divided by lymphocyte count, respectively.

Statistical Analysis

Our patients were divided into two groups on the basis of LN status. Continuous data were presented as means ± standard deviations. Mann–Whitney *U*-test was conducted for all variables with non-normal distribution. The features of clinicopathological and categorical variables associated with LN status were analyzed using the $\chi 2$ test. Statistical analyses were performed using IBM

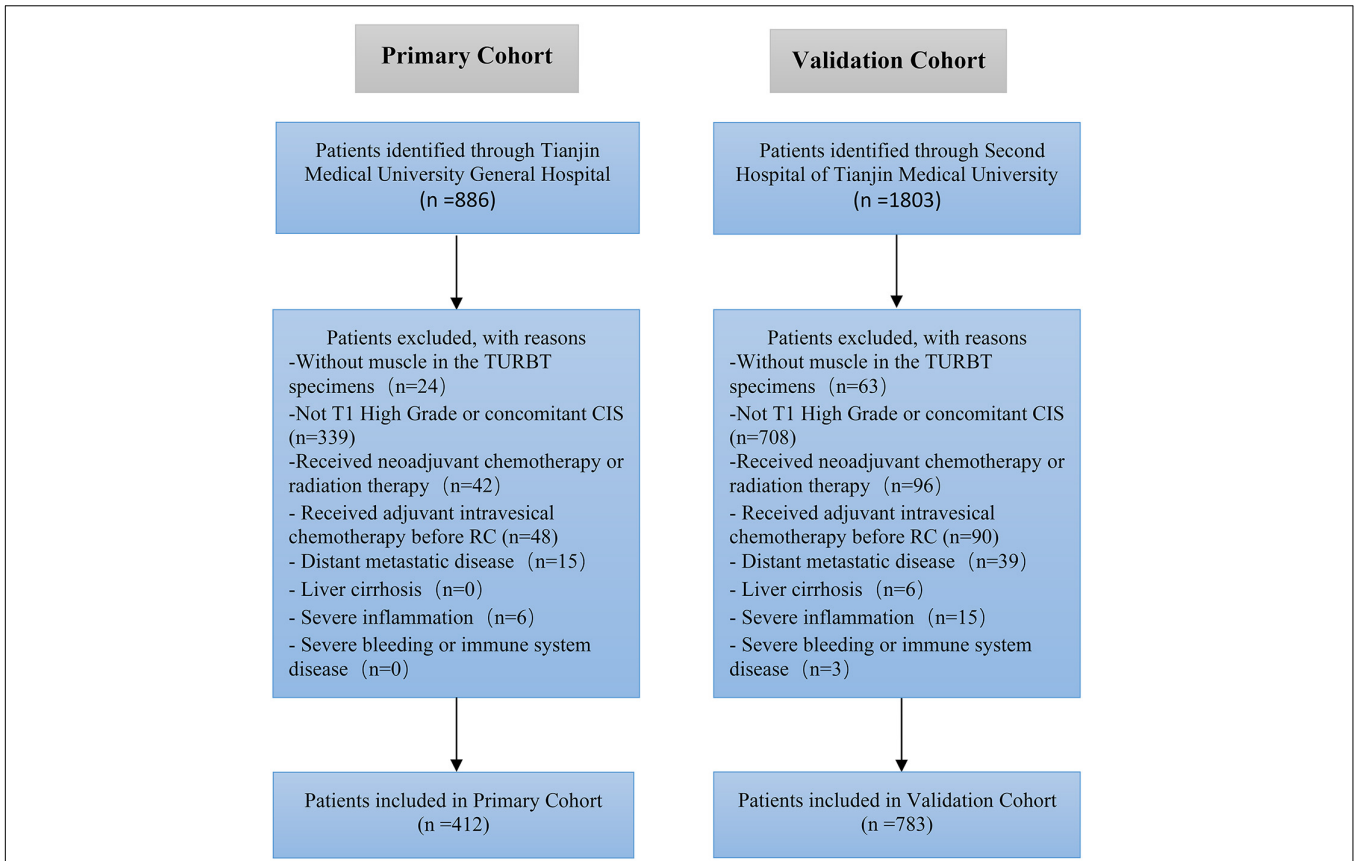

FIGURE 1 | Flow chart of the enrollment of patients.

SPSS (version 22.0) and R software (version 3.5.2). $P < 0.05$ was accepted as statistically significant.

Development of Prediction Model

Binary logistic regression analysis was conducted with the following clinical candidate predictors: tumor number, tumor size, LVI, fibrinogen, NLR, PLR, and MLR. Then, tumor number, tumor size, LVI, fibrinogen, and MLR were applied to develop a diagnostic model for LN metastasis by using the primary cohort. Backward step-wise selection was applied by using the likelihood ratio test with Akaike's information criterion as the stopping rule to develop and validate the nomogram.

Performance of the Nomogram in the Primary Cohort

Calibration curves and Hosmer–Lemeshow test were conducted to assess the calibration of the nomogram. To quantify the discrimination performance of the nomogram, Harrell's C-index was used. Bootstrapping validation (1,000 bootstrap resample) was used to calculate a relatively corrected C-index.

Validation of the Nomogram

Internal validation was performed. The logistic regression formula was built with the primary cohort and was applied to the validation cohort, with total points for each patient evaluated. The total points were then subjected to logistic regression as a factor. Decision curve analysis was performed to assess the clinical usefulness of the nomogram.

RESULTS

Characteristics

Patients' characteristic of the primary cohort and validation cohort showed in **Table 1**. No significant difference was found between primary cohort (16.75%, 69/412) and validation cohort (17.24%, 135/783) in regard to lymph node-positive rate ($P = 0.462$). Patients with LN metastasis in both primary and validation cohorts were more likely to have bigger tumor (≥3 cm), multiple tumors, hydronephrosis, and LVI than the patients without LN metastasis. There is no significant difference association with LN status for other parameters, such as gender, age, body mass index (BMI), and ALB.

Features of Preoperative Inflammatory Indicators

As shown in **Table 2**, although the WBC count did not show any difference between the two groups ($P = 0.393$) concerning

TABLE 1 | Clinicopathologic features of patients according to the lymph node status.

Parameters	Primary cohort				Validation cohort			
	Overall *n* = 412	LN (+) *n* = 69	LN (–) *n* = 343	*P*	Overall *n* = 783	LN (+) *n* = 135	LN (–) *n* = 648	*P*
Gender				0.481				0.189
Male	372	63(16.9)	309(83.1)		487	123(25.3)	564(74.7)	
Female	40	6(15.0)	34(85.0)		96	12(12.5)	84(87.5)	
Age (years)				0.184				0.526
≥60	264	48(18.2)	216(77.8)		574	96(16.7)	478(83.3)	
<60	148	21(14.2)	127(85.8)		209	39(18.7)	170(80.3)	
BMI				0.143				0.273
≥28	45	11(24.4)	34(65.6)		69	18(26.1)	51 (73.9)	
<28	367	58(15.8)	309(84.2)		728	149(20.4)	579(79.6)	
Hydronephrosis				0.011				0.001
Present	64	18(28.1)	47(61.9)		114	36(31.6)	78(68.4)	
Absent	347	51(14.7)	296(85.3)		669	99(14.8)	570(85.2)	
ALB(g/l)				0.125				0.189
≥35	324	49(15.1)	275(84.9)		624	102(16.3)	522(83.7)	
<35	88	20(22.2)	68(77.8)		159	33(20.8)	126(79.2)	
Pathological stage				0.001*				<0.001*
pTa	21	0(0.0)	21(100.0)		27	0(0.00)	27(100.0)	
pT1	98	9(9.2)	89(90.8)		337	39(11.6)	288(88.4)	
pT2	149	18(12.1)	131(87.9)		343	39(11.3)	204(88.7)	
pT3	101	21(20.1)	80(79.9)		121	33(27.3)	88(72.7)	
pT4	39	18(46.2)	21(53.8)		65	24(36.9)	41(63.1)	
≥pT1	293	60(20.5)	233(79.5)		429	96(22.3)	333(77.5)	
LVI, no. (%)				<0.001				<0.001
Present	135	42(38.9)	93(61.1)		303	99(32.7)	204(67.3)	
Absent	277	27(13.2)	250(86.8)		480	36(7.5)	444(92.5)	
Tumor size (cm)				<0.001				<0.001
≥3	114	42(36.8)	72(53.2)		364	99(27.2)	265(72.7)	
<3	341	27(7.9)	271(92.1)		419	36(8.5)	383(91.5)	
Tumor number				<0.001				0.012
Multiple	174	51(29.3)	123(70.7)		362	87(24.0)	275(76.0)	
Single	264	18(6.8)	246(93.2)		421	48(11.4)	373(88.6)	

*BMI, body mass index; ALB, albumin; and LVI, lymphovascular invasion. *Chi-square tests of pT1 and ≥pT1.*

TABLE 2 | Inflammation indicators according to lymph node status.

Parameters	Primary cohort			Validation cohort		
	LN (+)	LN (–)	*P*	LN (+)	LN (–)	*P*
WBC count	6.78 ± 1.92	7.31 ± 4.17	0.393	7.47 ± 1.99	7.00 ± 1.68	0.311
Neutrophil count	4.67 ± 1.76	4.60 ± 178	0.792	5.15 ± 1.85	4.53 ± 1.54	0.153
Lymphocyte count	1.42 ± 0.66	1.82 ± 0.66	<0.001	1.34 ± 0.71	1.82 ± 0.58	0.006
Monocyte count	0.42 ± 0.16	0.44 ± 0.17	0.523	0.49 ± 0.16	0.45 ± 0.20	0.395
Platelet count	229.38 ± 66.32	237.50 ± 71.24	0.486	233.09 ± 40.03	254.60 ± 65.916	0.140
HB	124.58 ± 21.47	133.58 ± 20.38	0.009	123.61 ± 20.71	133.10 ± 22.53	0.073
ALB	38.91 ± 6.30	39.58 ± 6.22	0.522	37.09 ± 7.00	39.24 ± 6.69	0.198
Fibrinogen	3.87 ± 0.76	3.36 ± 0.87	<0.001	4.25 ± 0.76	3.35 ± 0.86	0.001
NLR	3.98 ± 3.09	3.01 ± 2.65	0.033	4.67 ± 2.29	2.81 ± 1.42	0.001
PLR	193.85 ± 119.73	148.40 ± 80.30	0.019	248.92 ± 167.54	157.37 ± 73.53	0.017
MLR	0.34 ± 0.15	0.27 ± 0.14	0.012	0.48 ± 0.24	0.28 ± 0.17	0.001

WBC, white blood cell; HB, hemoglobin; ALB, albumin; NLR, neutrophil-to-lymphocyte ratio; PLR, platelet-to-lymphocyte ratio; and MLR, monocyte-to-lymphocyte ratio.

TABLE 3 | Risk factors for LN metastasis.

Variable and intercept	Univariate logistic regression		Multivariate logistic regression	
	Adjusted OR (95% CI)	*P*	Adjusted OR (95% CI)	*P*
Hydronephrosis	2.66 (1.20–5.86)	0.016		
Lymphocyte count	0.35 (0.19–0.66)	0.01		
HB	0.98 (0.965–1.00)	0.10		
Fibrinogen	1.89 (1.31–2.73)	<0.001	1.88 (1.18–2.99)	0.008
NLR	1.12 (0.99–1.24)	0.074		
PLR	1.004 (0.961–1.008)	0.236		
MLR	5.81 (1.69–52.13)	0.007	7.79 (1.94–60.06)	0.003
Lymphovascular invasion	6.00 (2.89–12.43)	<0.001	8.50 (3.66–19.74)	<0.001
Tumor size	4.28 (2.19–8.36)	<0.001	4.71 (2.06–10.78)	<0.001
Tumor number	2.8 (1.5–5.24)	0.001	3.50 (1.53–8.06)	0.001

NLR, neutrophil-to-lymphocyte ratio; PLR, platelet-to-lymphocyte ratio; and MLR, monocyte-to-lymphocyte ratio.

the nodal status, fibrinogen ($P < 0.001$), and lymphocyte count ($P < 0.001$) were significantly higher in patients with nodal involvement than those without. The differences between the lymph node-positive and lymph node-negative groups were statistically significant in regard to HB ($P = 0.009$), PLR ($P = 0.019$), NLR ($P = 0.033$), and MLR ($P = 0.012$). Other parameters like neutrophil count, monocyte count, platelet count, and ALB did not show an association with LN status.

Development of the Prediction Model

Binary regression analysis identified tumor number, tumor size, LVI, fibrinogen, and MLR as independent predictors (**Table 3**). These independent predictors were pooled to develop the prediction model. The prediction model was demonstrated as a nomogram (**Figure 2**).

Performance of the Nomogram

The area under the curve (AUC) of the receiver operating characteristic (ROC) curve (**Figure 3**) of the nomogram was 0.853 (95% CI, 0.785 to 0.906), indicating that the nomogram is powerful to differentiate LN metastasis. The calibration curve of the nomogram demonstrated a good agreement between the observation cases and prediction cases both in the primary cohort and validation cohort (**Figure 4**). The Hosmer–Lemeshow test of the nomogram harvested a non-significant statistic in the primary cohort ($P = 0.381$) and validation cohort ($P = 0.236$). The C-index of the nomogram was 0.853 (95% CI, 0.77 to 0.91) in the primary cohort, which was confirmed to be 0. 845 (95% CI, 0.76 to 0.98) in the validation cohort.

Clinical Use

The result of the decision curve (**Figure 5**) in regard to the primary cohort demonstrated that when the threshold probability was 0.15–0.80, the nomogram will be helpful to predict LN metastases. Correspondingly, if the threshold probability was 0.20–0.60 in the validation cohort, using the nomogram to predict LN metastases and make treatment decision adds more benefit than either the treat-all-patients scheme or the treat-none scheme.

DISCUSSION

As is known to all, cancer-specific survival (CSS) and overall survival (OS) of patients with UCB were associated with pathologic stage and LN status at the time of cystectomy. The potential of LN metastasis plays an important role when considering an operation (21). Fritsche et al. reported that 16.2% of the patients treated with RC for T1 high-grade UCB had LN metastasis (22). If we can identify patients who may have LN metastasis with T1 high-grade UCB before surgical treatment, it will facilitate individualized treatment of the disease.

Nowadays, plenty of methods including quantitative comparative proteomic, imaging techniques (such as PET-CT and MRI) (23, 24), and histological analysis have been used to identify new markers predicting LN metastasis. Brunocilla et al. evaluated the role of PET-CT in the preoperative evaluation of the nodal involvement of patients with BC suitable for RC and found that PET-CT showed a sensitivity of 42% and a specificity of 84%, whereas contrast-enhanced CT showed a sensitivity of 14% and a specificity of 89% (24). Birkhäuser et al. assessed the diagnostic accuracy of combined ultrasmall superparamagnetic particles of iron oxide (USPIO) MRI and diffusion-weighted (DW) MRI in staging of normal-sized pelvic LNs in bladder cancer patients. The results showed that per-patient sensitivity and specificity for detection of LN metastases by the three readers ranged from 65% to 75% and 93% to 96%, respectively (25). All of the above results indicate that it is difficult to predict LN metastasis accurately even using the most advanced imaging techniques. Therefore, we wanted to explore a more accurate model to predict LN metastasis of T1 high-grade BC by combining the pathological characteristics of TURBT specimens with inflammation indicators in peripheral blood. Cantiello et al. investigated 1,151 NMIBC patients who underwent first TURBT at 13 academic institutions and found that NLR, PLR, and LMR are factors predictive of recurrence, progression, cancer-specific mortality, and overall mortality (26). Previous studies have demonstrated that NLR, PLR, and fibrinogen are

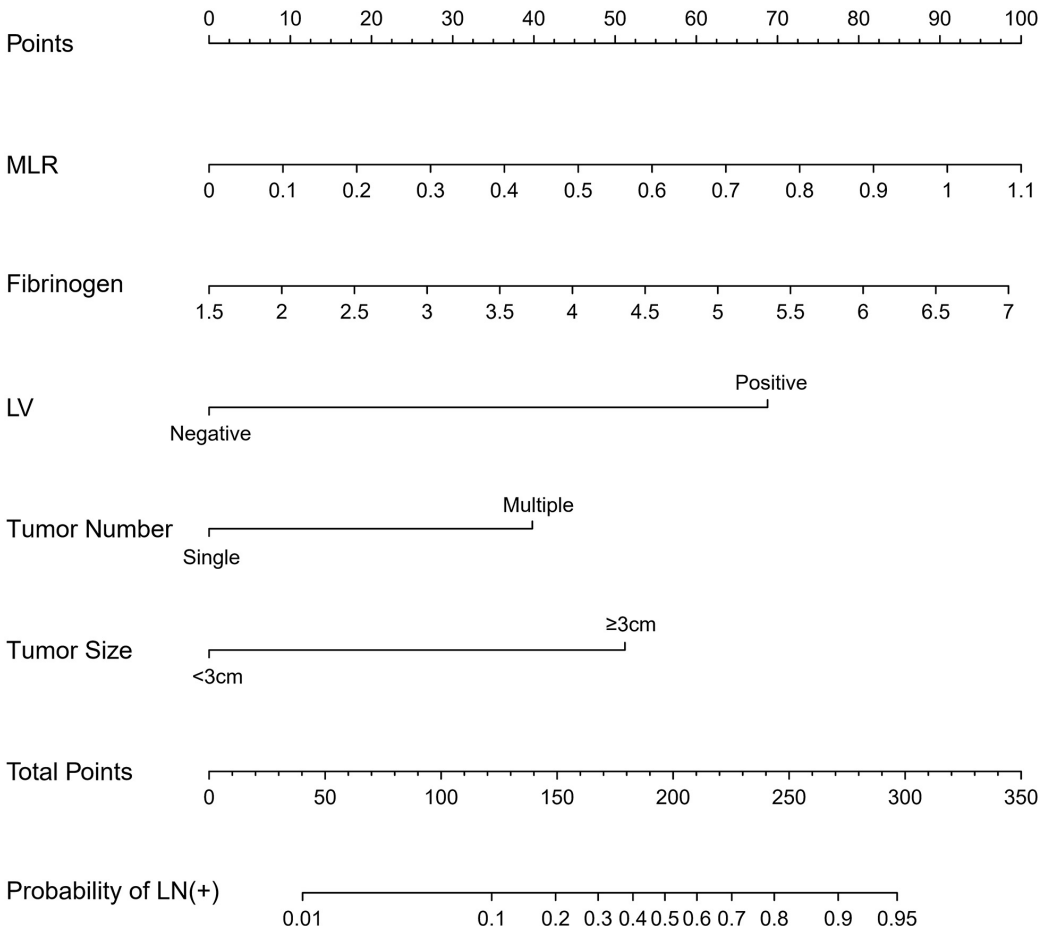

FIGURE 2 | The nomogram was developed in the primary cohort, with tumor number, tumor size, lymphovascular invasion, fibrinogen, and MLR.

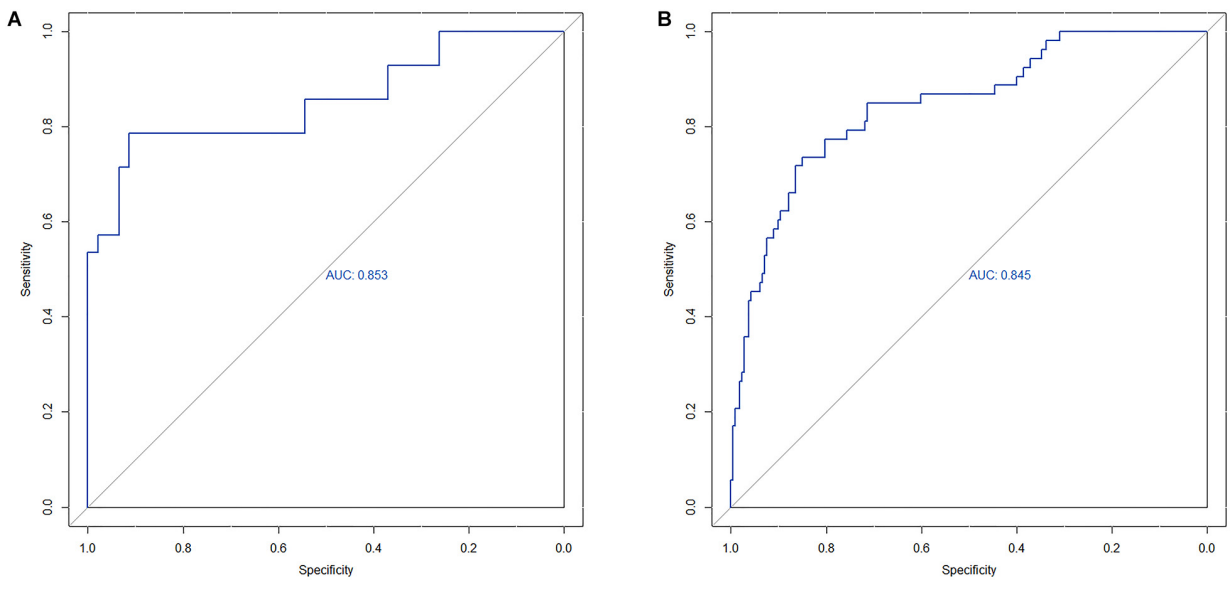

FIGURE 3 | (A) The ROC curve of nomogram in the primary cohort. **(B)** The ROC curve of nomogram in the validation cohort.

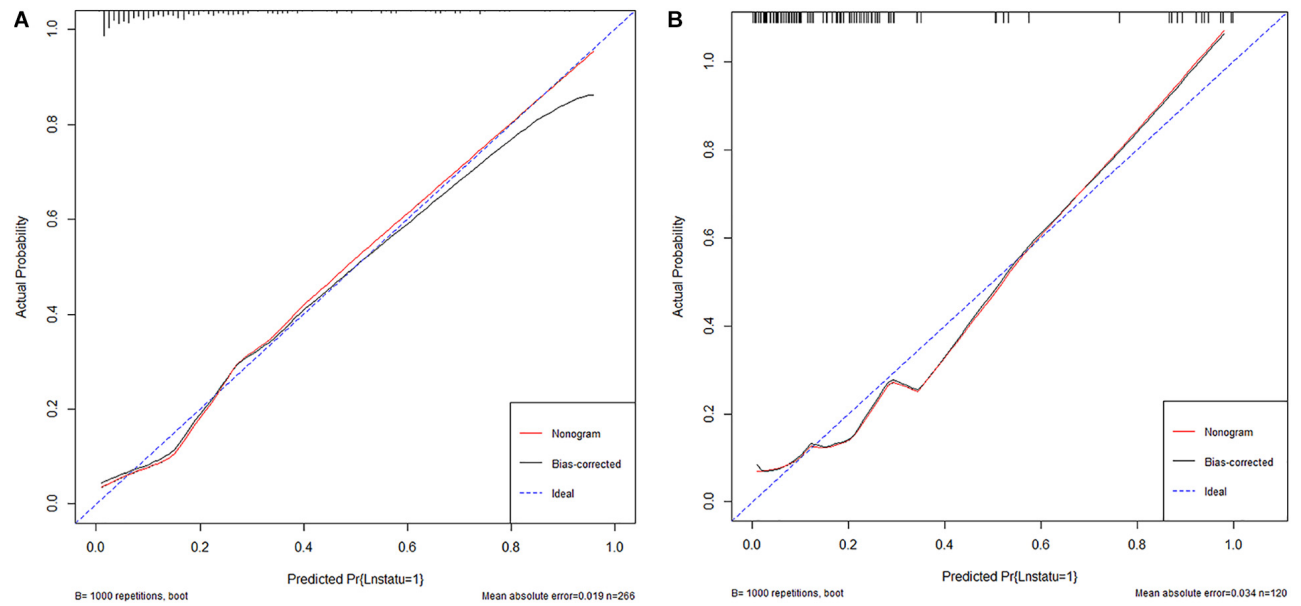

FIGURE 4 | (A) The calibration curve of nomogram in the primary cohort. **(B)** The calibration curve of nomogram in the validation cohort.

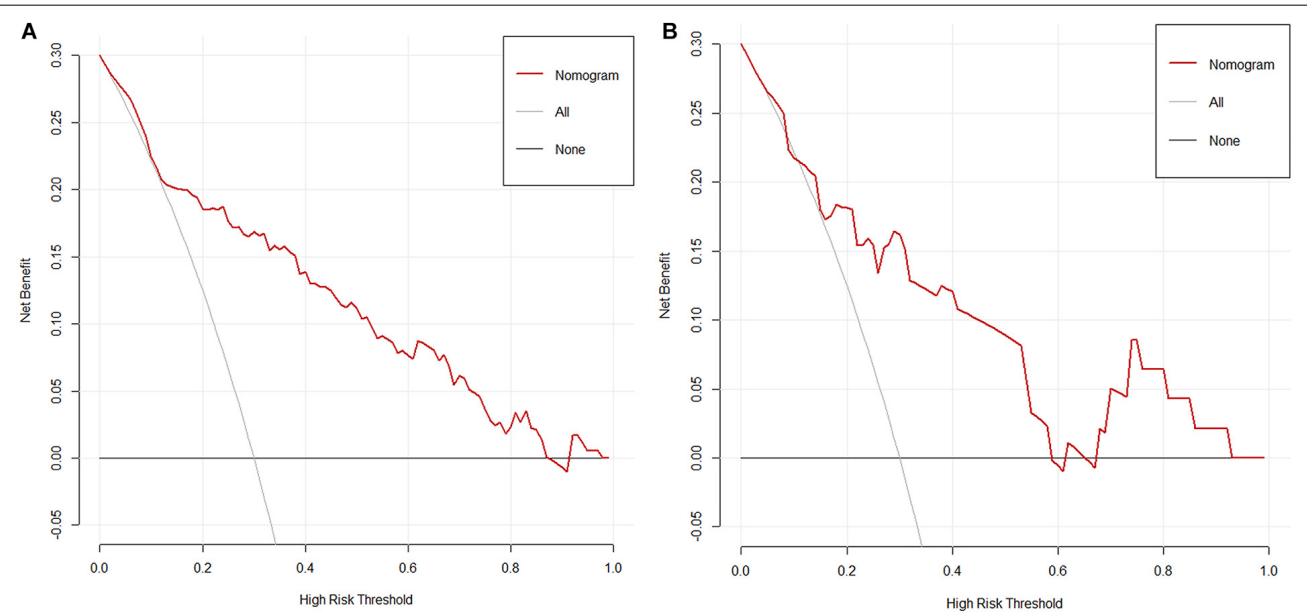

FIGURE 5 | (A) The decision curve of nomogram in the primary cohort. **(B)** The decision curve of nomogram in the validation cohort. Net benefit can be interpreted as the proportion of all patients who have lymph node metastases and are recommended for extended pelvic lymph node dissection if no patients with negative lymph nodes were treated.

available biomarkers to predict LN metastasis (21, 27), and other hematological indicators, like MLR and ALB, have been shown to be associated with pathologic stage or LN status of bladder carcinoma (17, 27–29). A study involving patients with high-grade T1 bladder cancer also showed that absolute basophil count is associated with time to recurrence in patients receiving BCG after TURBT tumor (30). Hematological indicators are cheap and accessible. However, their clinical applications are unrealistic because there is no good sensitivity and specificity to use them solely.

In our study, we found LN metastasis in about 20% of the patients who underwent RC for T1 high-grade UCB. It is higher than the previous study conducted by Fritsche et al. We suspect that the difference may come from the different ethnicity of patients or may have resulted from the different treatment strategies (our patients received less repeated

TURBT and adjuvant intravesical chemotherapy before RC). In our results, there is no significant difference in lymphocyte and monocyte counts between the two groups, but both lymphocyte count and monocyte count were increased in the lymph node-positive group. Monocytes and tumor-associated macrophages (differentiated by monocytes) were thought to have an impact on tumorigenesis and will be recruited to the tumor site (31). The main function of lymphocytes is suppressing proliferation and migration of cancer cell (32). Therefore, monocyte and lymphocyte count (to suppress migration of cancer cells) may increase or decrease in patients having tumor. Besides, after calculating the ratio of platelet count, neutrophil count, and monocyte count to lymphocyte count, we found that NLR, PLR, and MLR were significantly correlated with LN metastasis in bladder tumors, which is consistent with previous studies.

According to our results, there were significant differences about the means of PLR, NLR, MLR, and fibrinogen between the lymph node-positive and lymph node-negative groups. Also, the tumor number, tumor size, LVI, fibrinogen, and MLR, according to the logistic regression analysis, are independent predictors of LN metastasis in patients with T1 high-grade urothelial carcinoma. It suggests that there is a close relationship between cancer and inflammation (33).

Pathologic features, such as tumor number, tumor size, and LVI are widely accepted as an indicator of tumor prognosis. Thus, we attempted to develop a model including tumor number, tumor size, LVI, fibrinogen, PLR, NLR, and MLR for the prediction of LN metastasis. Then, we found that the tumor number, tumor size, LVI, fibrinogen, and MLR are independent predictors of LN metastasis in patients with T1 high-grade urothelial carcinoma. Our results are consistent with previous research. Ferro et al. found that tumor size and the presence of carcinoma *in situ* are independent predictors to identify patients at risk of residual T1 high-grade bladder cancer after a complete TUR (34). This suggests that the combination of pathological features and inflammatory status is a good predictor of LN metastasis in patients with T1 high-grade urothelial carcinoma (12).

Therefore, we developed a nomogram of tumor number, tumor size, LVI, fibrinogen, and MLR to help doctors and patients make better decisions on the treatment of T1 high-grade urothelial carcinoma. The Hosmer–Leme show test of the nomogram shows that this model has a good fit. The nomogram of this combination was conducted to present it. The AUC (0.843) of the ROC curve of the nomogram indicated that the nomogram is powerful to differentiate LN metastasis. The calibration curve demonstrated good consistency in the primary cohort and validation cohort. To justify the clinical usefulness of the nomogram, we assessed whether nomogram-assisted decisions would improve patient outcomes. The decision curve showed that the nomogram will be helpful to predict LN metastases. All of the measurements above indicate that the nomogram of tumor number, tumor size, LVI, fibrinogen, and MLR can help doctors and patients make better decisions on the treatment of T1 high-grade urothelial carcinoma.

Nevertheless, our study has many limitations. First, even if we collected two institutions' data, the sample size remains small. More and more patients with T1 high-grade bladder tumor choose to retain the bladder, and fewer and fewer patients receive RC in the early stage. We believe that even if we wait a few more years, the number of cases will not increase significantly. However, considering that 20% of the patients will still benefit from the early standard full cut, we believe that more patients will benefit from using this model to assist in clinical decision making. Second, although we have tried our best to control potential confounders, we could not control surgeon and pathologist experience, treatment decisions, including patient and surgeon preferences. Fortunately, we have two pathologists to review to identify LNs. Third, the data were collected retrospectively. However, for now, the model was developed by the best data we can achieve, and it may provide some reference for clinical decision making. In future studies, we will design a prospective randomized controlled study with a higher level of evidence to further validate our model.

CONCLUSION

The nomogram that incorporated the tumor number, tumor size, LVI, fibrinogen, and MLR showed favorable predictive accuracy for LN metastasis. It may be conveniently used to predict LN metastasis in patients with T1 high-grade urothelial carcinoma and be helpful in guiding treatment decisions. Large-sample multicenter validation is needed for its clinical application.

DATA AVAILABILITY STATEMENT

The datasets generated for this study are available on request to the corresponding author.

ETHICS STATEMENT

The study protocol was approved by the internal research Ethics Committee of Tianjin Medical University General Hospital. The patients/participants provided their written informed consent to participate in this study.

AUTHOR CONTRIBUTIONS

The project was designed by XL and JZ. YS and ML congregated data and analyzed it. YY and NO wrote the manuscript. All authors have read and approved the final manuscript.

FUNDING

This work was supported by the Natural Science Foundation of Tianjin City (16JCZDJC34600) and Zhao Yi-Cheng Medical Science Foundation (ZYYFY2018031).

REFERENCES

1. Antoni S, Ferlay J, Soerjomataram I, Znaor A, Jemal A, Bray F. Bladder cancer incidence and mortality: a global overview and recent trends. *Eur Urol*. (2017) 71:96–108. doi: 10.1016/j.eururo.2016.06.010
2. Siegel R, Ma J, Zou Z, Jemal A. Cancer statistics, 2014. *CA Cancer J Clin*. (2014) 64:9–29. doi: 10.3322/caac.21208
3. Ferro M, Vartolomei MD, Cantiello F, Lucarelli G, Di Stasi SM, Hurle R, et al. High-grade T1 on re-transurethral resection after initial high-grade T1 confers worse oncological outcomes: results of a multi-institutional study. *Urol Int*. (2018) 101:7–15. doi: 10.1159/000490765
4. Karl A, Carroll PR, Gschwend JE, Knuchel R, Montorsi F, Stief CG, et al. The impact of lymphadenectomy and lymph node metastasis on the outcomes of radical cystectomy for bladder cancer. *Eur Urol*. (2009) 55:826–35. doi: 10.1016/j.eururo.2009.01.004
5. Ghodoussipour S, Daneshmand S. Current controversies on the role of lymphadenectomy for bladder cancer. *Urol Oncol*. (2019) 37:193–200. doi: 10.1016/j.urolonc.2018.05.005
6. Babjuk M, Bohle A, Burger M, Capoun O, Cohen D, Comperat EM, et al. EAU guidelines on non-muscle-invasive urothelial carcinoma of the bladder: update 2016. *Eur Urol*. (2017) 71:447–61. doi: 10.1016/j.eururo.2016.05.041
7. Yun SJ, Kim SK, Kim WJ. How do we manage high-grade T1 bladder cancer? Conservative or aggressive therapy? *Investig Clin Urol*. (2016) 57(Suppl. 1):S44–51. doi: 10.4111/icu.2016.57.S1.S44
8. Royce TJ, Feldman AS, Mossanen M, Yang JC, Shipley WU, Pandharipande PV, et al. Comparative effectiveness of bladder-preserving tri-modality therapy versus radical cystectomy for muscle-invasive bladder cancer. *Clin Genitourin Cancer*. (2019) 17:23–31.e3. doi: 10.1016/j.clgc.2018.09.023
9. Zehnder P, Studer UE, Daneshmand S, Birkhauser FD, Skinner EC, Roth B, et al. Outcomes of radical cystectomy with extended lymphadenectomy alone in patients with lymph node-positive bladder cancer who are unfit for or who decline adjuvant chemotherapy. *BJU Int*. (2014) 113:554–60. doi: 10.1111/bju.12520
10. Zargar-Shoshtari K, Zargar H, Lotan Y, Shah JB, van Rhijn BW, Daneshmand S, et al. A multi-institutional analysis of outcomes of patients with clinically node positive urothelial bladder cancer treated with induction chemotherapy and radical cystectomy. *J Urol*. (2016) 195:53–9. doi: 10.1016/j.juro.2015.07.085
11. Shariat SF, Karakiewicz PI, Palapattu GS, Lotan Y, Rogers CG, Amiel GE, et al. Outcomes of radical cystectomy for transitional cell carcinoma of the bladder: a contemporary series from the Bladder Cancer Research Consortium. *J Urol*. (2006) 176:2414–22; discussion 22. doi: 10.1016/j.juro.2006.08.004
12. Kluth LA, Black PC, Bochner BH, Catto J, Lerner SP, Stenzl A, et al. Prognostic and prediction tools in bladder cancer: a comprehensive review of the literature. *Eur Urol*. (2015) 68:238–53. doi: 10.1016/j.eururo.2015.01.032
13. Balkwill F, Mantovani A. Inflammation and cancer: back to Virchow? *Lancet*. (2001) 357:539–45. doi: 10.1016/S0140-6736(00)04046-0
14. Shariat SF, Rink M, Ehdaie B, Xylinas E, Babjuk M, Merseburger AS, et al. Pathologic nodal staging score for bladder cancer: a decision tool for adjuvant therapy after radical cystectomy. *Eur Urol*. (2013) 63:371–8. doi: 10.1016/j.eururo.2012.06.008
15. Yoshida T, Kinoshita H, Yoshida K, Mishima T, Yanishi M, Inui H, et al. Prognostic impact of perioperative lymphocyte-monocyte ratio in patients with bladder cancer undergoing radical cystectomy. *Tumour Biol*. (2016) 37:10067–74. doi: 10.1007/s13277-016-4874-8
16. Ma C, Lu B, Diao C, Zhao K, Wang X, Ma B, et al. Preoperative neutrophil-lymphocyte ratio and fibrinogen level in patients distinguish between muscle-invasive bladder cancer and non-muscle-invasive bladder cancer. *Onco Targets Ther*. (2016) 9:4917–22. doi: 10.2147/OTT.S107445
17. D'Andrea D, Moschini M, Gust KM, Abufaraj M, Ozsoy M, Mathieu R, et al. Lymphocyte-to-monocyte ratio and neutrophil-to-lymphocyte ratio as biomarkers for predicting lymph node metastasis and survival in patients treated with radical cystectomy. *J Surg Oncol*. (2017) 115:455–61. doi: 10.1002/jso.24521
18. Vartolomei MD, Ferro M, Cantiello F, Lucarelli G, Di Stasi S, Hurle R, et al. Validation of neutrophil-to-lymphocyte ratio in a multi-institutional cohort of patients with T1G3 non-muscle-invasive bladder cancer. *Clin Genitourin Cancer*. (2018) 16:445–52. doi: 10.1016/j.clgc.2018.07.003
19. Hermanns T, Bhindi B, Wei Y, Yu J, Noon AP, Richard PO, et al. Pre-treatment neutrophil-to-lymphocyte ratio as predictor of adverse outcomes in patients undergoing radical cystectomy for urothelial carcinoma of the bladder. *Br J Cancer*. (2014) 111:444–51. doi: 10.1038/bjc.2014.305
20. Ferro M, Katalin MO, Buonerba C, Marian R, Cantiello F, Musi G, et al. Type 2 diabetes mellitus predicts worse outcomes in patients with high-grade T1 bladder cancer receiving bacillus Calmette-Guérin after transurethral resection of the bladder tumor. *Urol Oncol*. (2020) 38:459–64. doi: 10.1016/j.urolonc.2020.02.016
21. Pang W, Lou N, Jin C, Hu C, Arvine C, Zhu G, et al. Combination of preoperative platelet/lymphocyte and neutrophil/lymphocyte rates and tumor-related factors to predict lymph node metastasis in patients with gastric cancer. *Eur J Gastroenterol Hepatol*. (2016) 28:493–502. doi: 10.1097/MEG.0000000000000563
22. Fritsche HM, Burger M, Svatek RS, Jeldres C, Karakiewicz PI, Novara G, et al. Characteristics and outcomes of patients with clinical T1 grade 3 urothelial carcinoma treated with radical cystectomy: results from an international cohort. *Eur Urol*. (2010) 57:300–9.
23. Kiss B, Thoeny HC, Studer UE. Current status of lymph node imaging in bladder and prostate cancer. *Urology*. (2016) 96:1–7. doi: 10.1016/j.urology.2016.02.014
24. Brunocilla E, Ceci F, Schiavina R, Castellucci P, Maffione AM, Cevenini M, et al. Diagnostic accuracy of. (11)C-choline PET/CT in preoperative lymph node staging of bladder cancer: a systematic comparison with contrast-enhanced CT and histologic findings. *Clin Nucl Med*. (2014) 39:e308–12. doi: 10.1097/RLU.0000000000000342
25. Birkhäuser FD, Studer UE, Froehlich JM, Triantafyllou M, Bains LJ, Petralia G, et al. Combined ultrasmall superparamagnetic particles of iron oxide-enhanced and diffusion-weighted magnetic resonance imaging facilitates detection of metastases in normal-sized pelvic lymph nodes of patients with bladder and prostate cancer. *Eur Urol*. (2013) 64:953–60. doi: 10.1016/j.eururo.2013.07.032
26. Cantiello F, Russo GI, Vartolomei MD, Farhan ARA, Terracciano D, Musi G, et al. Systemic inflammatory markers and oncologic outcomes in patients with high-risk non-muscle-invasive urothelial bladder cancer. *Eur Urol Oncol*. (2018) 1:403–10.
27. Xiang J, Zhou L, Li X, Bao W, Chen T, Xi X, et al. Preoperative monocyte-to-lymphocyte ratio in peripheral blood predicts stages, metastasis, and histological grades in patients with ovarian cancer. *Transl Oncol*. (2017) 10:33–9. doi: 10.1016/j.tranon.2016.10.006
28. Viers BR, Boorjian SA, Frank I, Tarrell RF, Thapa P, Karnes RJ, et al. Pretreatment neutrophil-to-lymphocyte ratio is associated with advanced pathologic tumor stage and increased cancer-specific mortality among patients with urothelial carcinoma of the bladder undergoing radical cystectomy. *Eur Urol*. (2014) 66:1157–64. doi: 10.1016/j.eururo.2014.02.042
29. Ferro M, De Cobelli O, Buonerba C, Di Lorenzo G, Capece M, Bruzzese D, et al. Modified glasgow prognostic score is associated with risk of recurrence in bladder cancer patients after radical cystectomy: a multicenter experience. *Medicine*. (2015) 94:e1861. doi: 10.1097/MD.0000000000001861
30. Ferro M, Di Lorenzo G, Vartolomei MD, Bruzzese D, Cantiello F, Lucarelli G, et al. Absolute basophil count is associated with time to recurrence in patients with high-grade T1 bladder cancer receiving bacillus Calmette-Guérin after transurethral resection of the bladder tumor. *World J Urol*. (2020) 38:143–50. doi: 10.1007/s00345-019-02754-2
31. Chanmee T, Ontong P, Konno K, Itano N. Tumor-associated macrophages as major players in the tumor microenvironment. *Cancers*. (2014) 6:1670–90. doi: 10.3390/cancers6031670

32. Bastid J, Bonnefoy N, Eliaou JF, Bensussan A. Lymphocyte-derived interleukin-17A adds another brick in the wall of inflammation-induced breast carcinogenesis. *Oncoimmunology*. (2014) 3:e28273. doi: 10.4161/onci.28273
33. Diakos CI, Charles KA, McMillan DC, Clarke SJ. Cancer-related inflammation and treatment effectiveness. *Lancet Oncol*. (2014) 15:e493–503. doi: 10.1016/S1470-2045(14)70263-3
34. Ferro M, Di Lorenzo G, Buonerba C, Lucarelli G, Russo GI, Cantiello F, et al. Predictors of residual T1 high grade on re-transurethral resection in a large multi-institutional cohort of patients with primary T1 high-grade/grade 3 Bladder cancer. *J Cancer*. (2018) 9:4250–4. doi: 10.7150/jca.26129

Conflict of Interest: The authors declare that the research was conducted in the absence of any commercial or financial relationships that could be construed as a potential conflict of interest.

frontiers in Oncology

ORIGINAL RESEARCH
published: 09 November 2020
doi: 10.3389/fonc.2020.491129

ADNP Upregulation Promotes Bladder Cancer Cell Proliferation *via* the AKT Pathway

*Shuai Zhu[1], Zhenzhou Xu[1], Yong Zeng[2], Ying Long[2], Gang Fan[3], Qi Ding[2], Yuheng Wen[1], Jian Cao[1], Tao Dai[1], Weiqing Han[1] and Yu Xie[1]**

[1] Department of Urology, The Affiliated Cancer Hospital of Xiangya School of Medicine, Central South University, Hunan Cancer Hospital, Changsha, China, [2] Clinical Translational Research Center, The Affiliated Cancer Hospital of Xiangya School of Medicine, Central South University, Hunan Cancer Hospital, Changsha, China, [3] Department of Urology, Huazhong University of Science and Technology Union Shenzhen Hospital, The 6th Affliated Hospital of Shenzhen University Health Science Center, Shenzhen, China

Background: Activity-dependent neuroprotective protein (ADNP), which is involved in embryonic development and neurogenesis, has been proven to be upregulated in some human tumors. However, its role in bladder cancer (BC) has never been studied.

Objective: We aimed to investigate the mechanisms by which ADNP promotes the progression of BC.

Methods: ADNP expressions in BC cell lines and paired BC and adjacent normal tissues were measured by quantitative real-time PCR (qRT-PCR), Western blot, and immunohistochemistry. Colony formation, Cell Counting Kit-8 (CCK-8), trypan blue exclusion assay, flow cytometry, and nude mice tumorigenesis assay were performed to explore the effects of ADNP on growth of BC *in vivo* and *in vitro*. The impacts of ADNP on AKT signaling pathways were measured by Western blot.

Results: The expression of ADNP mRNA and protein was significantly upregulated in BC tissues compared with adjacent normal tissues. Immunohistochemical analysis of 221 BC and 51 adjacent normal tissue paraffin sections indicated that ADNP expression was significantly associated with histological classification and pathological T and N stages. Survival analysis revealed that patients with high ADNP expression have worse prognosis with respect to overall survival and progression-free disease. ADNP knockdown markedly delayed propagation of BC *in vitro* and the development of BC *in vivo.* ADNP overexpression showed the opposite effect. In addition, ADNP can markedly promote G1-S cell cycle transition in BC cells. On the molecular level, we confirmed that ADNP mediated acceleration of G1-S transition was associated with activation of the AKT pathways in BC.

Conclusion: ADNP is overexpressed in BC and promotes BC growth partly through AKT pathways. ADNP is crucial in predicting the outcome of BC patients and may be a potential therapeutic target in BC.

Keywords: activity-dependent neuroprotective protein, cell cycle, proliferation, bladder cancer, AKT pathway

OPEN ACCESS

Edited by:
Woonyoung Choi,
Johns Hopkins Medicine,
United States

Reviewed by:
Mingwei Chen,
The First Affiliated Hospital of Soochow University, China
Chunhua Wan,
Nantong University, China

***Correspondence:**
Yu Xie
xieyu420@sina.com

Specialty section:
This article was submitted to Genitourinary Oncology, a section of the journal Frontiers in Oncology

Received: *12 August 2019*
Accepted: *18 September 2020*
Published: *09 November 2020*

Citation:
Zhu S, Xu Z, Zeng Y, Long Y, Fan G, Ding Q, Wen Y, Cao J, Dai T, Han W and Xie Y (2020) ADNP Upregulation Promotes Bladder Cancer Cell Proliferation via the AKT Pathway. Front. Oncol. 10:491129. doi: 10.3389/fonc.2020.491129

INTRODUCTION

Bladder cancer (BC), particularly urothelial carcinoma, is one of the most prevalent urinary system malignancies (1). Despite significant improvements in surgical and chemotherapeutic treatment, incident cases and recurrence rates continue to increase by 5% (2). Approximately 70% of all incident cases are non-muscle-invasive bladder cancer (NMBC), while 30% are muscle-invasive bladder cancer (MIBC) (3). NMBC rarely progresses but recurs easily, leading to high treatment costs because of the need for long-term monitoring (4). Meanwhile, MIBC, to some extent, is more aggressive and prone to metastasis, and thus the 5-year survival rate is only 50% (5). This dismal prognosis highlights the urgent need for accurate prognostic markers for BC that can be used for both treatment planning and follow-up.

Activity-dependent neuroprotective protein (ADNP), which locates in the chromosome 20q12–13.2 and encodes a protein with nine zinc fingers and a bipartite nuclear localization signal (6), has been found to protect neural activity against external stimuli in glial cells (7). As a transcription factor, ADNP is extremely conserved and highly expressed in antenatal life. It interacts with some components of the SWI/SNF chromatin remodeling complex such as BAF250a, BRG1, and BAF170 and mediates genes involved in brain formation and neurodevelopment (8, 9). The ADNP-deficient mouse model showed an inability to close neural tube and died at the embryonic stage (9). Previous studies have also identified that ADNP functions as a responsive genetic factor of vasoactive intestinal peptide and has a critical role in axonal transport, dendritic spine plasticity, and autophagy (10, 11). Importantly, ADNP is closely associated with various clinical illnesses, such as epilepsy, intellectual disabilities, and autism spectrum disorders (12).

The role of ADNP in tumorigenesis has recently gained profound research attention, and ADNP is closely linked with tumor growth, particularly in various cancers, including breast, ovarian, pancreatic, and colon cancer (13). According to the previous research, ADNP loss-of-function mutations have been found to be related to carcinogenesis (14). It was reported that ADNP can suppress cellular migration, invasion, and proliferation *via* the WNT signaling pathway in colon carcinoma (15) and triple-negative breast cancer (16). By contrast, the activation of the ADNP signaling system, mediated by an endogenous pituitary adenylate cyclase-activating polypeptide, can increase the resistance of malignant peripheral nerve sheath tumor to H_2O_2-induced death with serum starvation (17). It suggests that ADNP may also act as an oncogene in certain cellular contexts. Pascual et al. reported that ADNP overexpression could induce activation of the AKT pathway (18), which plays a major role in cancer cell proliferation and cell cycle development (19). Moreover, p53 protein, regulated by ADNP/SWI/SNF complex, is inactivated in cancer (20), leading to unlimited cell growth (21). Owing to this dual characteristic, the mechanisms of ADNP in BC are poorly understood. Our previous study showed that ADNP was significantly upregulated in BC. Therefore, we hypothesize that ADNP can stimulate the proliferation of BC cells *via* AKT pathway.

In this study, we investigate the role of ADNP in BC growth and identify the underlying mechanism whether ADNP can regulate the proliferation and cell cycle in BC cells *via* activating AKT signaling pathway. By activating AKT signaling pathway, ADNP enhance the proliferation of BC cell *in vitro* and *in vivo*. These findings establish evidence that ADNP have an important role in BC tumorigenesis.

MATERIALS AND METHODS

Cell Lines and Tissue

We analyzed 221 paraffin-fixed specimens of human bladder urothelial carcinoma tissues as well as 51 neighboring conventional bladder transitional cell tissues collected between January 2005 and December 2007 at the Affiliated Cancer Hospital of Xiangya School of Medicine, Central South University. In addition, 20 cases of BC fresh surgical specimens were collected from patients hospitalized in our hospital from September to December in 2017. The adjacent normal control was collected at least 2 cm away from the tumor margin (22). The collected cancer tissue and its adjacent normal tissue have been identified under the microscope. All patients with BC were diagnosed by histopathology and treated with radical cystectomy or tumor resection. Human BC cell lines (BIU87, T24, 5637, and TCCSUP) were acquired from the Institute of Cancer Prevention and Treatment, Sun Yat-Sen University (Guangzhou, China) and human normal urothelial cells (SV-HUC-1) were acquired from Department of life science, Hunan Normal University (Changsha, China). BC cell lines were cultivated in RPMI-1640 media (Gibco, USA) supplemented with 10% fetal bovine serum (Gibco, USA), 1% streptomycin, and penicillin, and the SV-HUC-1 cells were cultivated in F-12k media (Gibco, USA) supplemented with 10% fetal bovine serum (Gibco, USA), 1% streptomycin, and penicillin. All the cells were cultured under 5% atm CO_2 at 37°C.

Quantitative Real-Time PCR (qRT-PCR)

RNA extraction was performed using TRIzol reagent (Invitrogen, USA) according to the manufacturer's instructions. RNA purity was assessed *via* spectrophotometry (A260/A280 = 1.8–2.0). M-MLV transcriptase (BioRAD, USA) was used to generate cDNAs according to the manufacturer's instructions. Quantitative real-time polymerase chain reaction (RT-PCR) was performed using 1 μg cDNA, 0.4 μl primer pairs for the interest gene, and 5 μl 2X SYBR green (BioRAD, USA) *via* LightCycler480 RT-PCR System (BioRAD, USA) under these amplification conditions: one cycle of 95° for 30 s, followed by 35 cycles in 95° for 15 s, 95° in 10 s, 65° in 60 s, and a final cycle of 97° for 1s. The comparative threshold cycle method ($2^{-\Delta\Delta CT}$) was applied for estimating the relative gene expression among BC tissues and corresponding normal bladder urothelial tissues. Triplicate PCR amplifications were performed for each sample. The primer sequences for ADNP amplification were as follows: forward: 5′-CATCCTGCGTCTGGACCTGG-3′; reverse: 5′-TAATGTCACGCACGATTTCC-3′.

Western Blot Analysis

The cells and tissues were washed with phosphate-buffered saline (PBS) and then lysed using RIPA buffer (0.5% sodium deoxycholate, 0.1% SDS, 50 mM Tris, and 150 mM NaCl, pH 8.0) with protease inhibitor mixture (Roche, USA) and phosphatase inhibitors (Roche, USA) at freezing condition for 15 min. The protein levels were measured with BCA Protein Assay Reagent kit (Thermo Scientific, USA). A 10% SDS-polyacrylamide gel was used to separate tissue lysate aliquots containing 20 μg protein. These were subsequently moved to PVDF membranes (Millipore), and the membranes were consequently blocked for 2 hours with TBST buffer with 5% skim milk at 22°C, and incubated at 4°C with primary antibodies overnight. We then added peroxidase-conjugated secondary antibodies and performed ECL (Cell Signaling Technology, 12757) visualization. Band enumeration was conducted using densitometric analysis software (Bio-Rad). GAPDH expression was used as the internal standard to standardize expression of the supplementary proteins. The primary antibodies were as follows: anti-ADNP (1:1000, Proteintech, USA), anti-GAPDH, CDK4, CDK6, Cyclin D1, Cyclin B1, p-cdc-2, p-Rb, E2F1, p53, MDM2, AKT, p-AKT, and p21 (1:1000, Cell Signaling Technology, USA). The secondary antibodies were HRP-Goat-anti-Rabbit Ig G and HRP-Goat-anti-Mouse Ig G (1:1000, Cell Signaling Technology, USA).

Immunostaining

The paraffin-fixed tissues were cut into 5 μm sections and heated for 2 h at 60°C. Slices were deparaffinized using xylene, rehydrated in graded alcohols, and then treated with 0.3% hydrogen peroxide in methanol. Subsequently, they were immersed in antigenic recovery buffer of EDTA and heated in a microwave for antigen retrieval. Thereafter, the slices were blocked using 1% BSA and anti-ADNP (1:200, Abcam, ab199120) and then incubated for 12 h at 4°C. After washing in PBS, we added anti-rabbit secondary antibody (Zymed, USA) onto the tissue slices and then incubated them with peroxidase-tagged streptavidin (Zymed, USA). Thereafter, the slices were submerged in 3.3′-diaminobenzidine and subsequently counterstained, dried, and fixed using hematoxylin.

Two independent experienced observers blinded to the histopathological diagnosis and clinical information reviewed and rated the extent of formalin- and paraffin-fixed immunostaining. They had been exposed to professional training in immunohistochemical staining scoring. Scores were based on combination of the ratio of completely stained cancer cells to the staining power. Tumor cell ratio was graded as 0 for no positive tumor cells; 1, < 10%; 2, 10%–25%; 3, 26–75%; and 4, > 75% positive tumor cells. Meanwhile, the extent of staining was rated as 1 for negative staining; 2, weak staining (light yellow); 3, adequate staining (yellow brown); and 4, heavy staining (brown). The staining index was calculated by multiplying the fraction of positive tumor cells by the staining power score. The staining index (total 0, 1, 2, 3, 4, 6, 8, 9, and 12) was used to estimate ADNP expression in bladder tissues, with scores ≥ 6 and < 6 considered as high and low expression, respectively. Five areas at a magnification of 400× were chosen randomly, and each area was scored separately according to the staining index (23). The score of a paraffin slide was obtained by the average score of these five areas.

Cell Transfection

The plasmids overexpressing ADNP (ViGene, Shandong, China) and vector (ViGene, Shandong, China) were used to target the ADNP gene. Through subcloning whole cDNA human ADNP to a pMSCV-retro-puro vector (Clontech, Palo Alto, CA), an ADNP construct was expressed. For the ADNP knockdown, three ADNP-shRNA (KD-1: CAACATGACTGATGGAGTA; KD-2: GCAAATGCCTCTACTGTAA; KD-3: TAGTAA GACTGCTGACAAA) and a non-silencing shRNA (NC) were purchased from GeneChem, Shanghai, China. Cells were transfected with shRNA when they reached 30%–50% confluence. The cells were then incubated for 72 h in a 1 μg/mL puromycin (Sigma-Aldrich) medium for selection before transfection. After selection, cell replicas were confirmed *via* western blot analysis. The fabricated stable cell lines were preserved in 0.1 μg/mL puromycin medium.

Cell Proliferation Assay

Approximately 2,000 stably transfected cells were distributed onto 96-well plates. Once attached, they were prepared as per their individual study procedure. Subsequently, 20 μl Cell Counting Kit–8 reagent (CK04, Dojindo Kumamoto, Japan) was supplemented to individual wells and retained for 2 h. Vmax microplate spectrophotometer (Molecular Devices, Sunnyvale, CA, USA) was used to measure the absorbance at 450 nm wavelength. These assays were performed in triplicate.

Colony Growth Assay

Approximately 2,000 stably transfected cells were planted on 6-mm plates in each well and nurtured for 15 days. The media was replaced after every 3 days. Cells were washed with PBS twice before harvest and then subjected to hematoxylin staining. Cell colonies were counted using imagej software (Co. Bharti Airtel Ltd, Version. 1.52n) and colonies with > 100 cells were counted. Every assay was executed in triplicate.

Cell Viability Assay

Cell viability was determined by the trypan blue exclusion assay. The cell suspension was mixed with trypan blue dye (Sigma, USA) and observed under the microscope within 3 minutes. Cell viability was determined by dividing the number of non-stained (viable) cells by the number of total cells counted. In addition, flow cytometry analysis were also used to test the cell viability. Cells were stained with Annexin-FITC and propidium iodide (PI) for 15 min (Biolegend, USA) according to the manufacturer's protocol. Cells were placed in ice and analyzed using a Beckman Coulter Cytoflex.

Cell Cycle Analysis

The stably transfected cells ($1*10^6$) were seeded at 6-well plates until 60%–70% confluence with the culture medium. The cells were then collected *via* trypsinization, suspended again in PBS, and immobilized overnight at 4°C in 70% cold alcohol. Before cell cycle analysis, bovine pancreatic RNase (2 μg/ml; Sigma) was added to the cells at 37°C for 30 min, and the cells were then incubated in propidium iodide (20 μg/ml; Sigma) for 20 min. BD LSRII Flow Cytometry System and FACSDiva software (BD Bioscience, Franklin Lakes, USA) were used for analysis. NovoExpress software package was also used to assess the information, and the cell cycle distribution was presented as percentage of cells in G0/G1, S, and G2/M populations. These assays were repeated in triplicate.

Tumor Xenograft Experiments

Four-week-old male NOD/SCID nude mice were acquired from Hunan SJA Laboratory Animal Co., Ltd., Changsha, Hunan, China. The animals were kept in a pathogen-free environment at The Institutional Animal Care and Use Committee of Affiliated Cancer Hospital, Xiangya School of Medicine, Central South University. Stable transfected T24-ADNP-knockdown/T24-ADNP-negative control and TCCSUP-ADNP-overexpression/TCCSUP-ADNP-vector was hypodermically introduced (1×10^6 cells per injected) in the right axillary fossa of the NOD/SCID nude mice respectively (5 mice in each group). The tumor length (L) and width (W) were measured using a caliper, and then the individual volume was computed as per (L×W2)/2 equation. The mice injected with T24 were sacrificed on the 28th day and the others on the 42nd days, and the tumors were resected, measured, segmented, and then stained with anti-ADNP antibody, anti-Ki67, anti-cyclin D1, anti-CDK4, and anti-CDK6. Concurrently, the expression of ADNP, Ki-67, cyclin D1, CDK4, and CDK6 in isolated tissue were detected.

Statistical Analysis

The obtained data were resultant of at least 3 separate assessments and were presented as mean ± S.D. The significance of immunostaining scores in human paraffin-fixed tissues were tested using one-way ANOVA followed post hoc Bonferroni test. Two-way ANOVA tests were used to identify the significance of cell proliferation curve and mice tumorigenesis curve among the various groups, and the post hoc Bonferroni test was used for pairwise comparisons. The group comparisons of mRNA and protein expression, cell colonies, cell cytometry, the final weight and volume of mice tumor, and the immunostaining scores of mice tumor were performed using Student's t test. The weighted Fleiss-Cohen (quadratic) kappa statistics were used to assess the inter-observer agreement (24). The correlation between ADNP expression and clinicopathological features was examined *via* Chi-squared test. Survival arcs were drawn according to Kaplan-Meier analysis and evaluated using log-rank test. Survival data were analyzed using univariate and multivariate Cox regression analysis. All statistical analyses were performed using SPSS 21.0 (SPSS Incorporated, Chicago) statistical software package, and $P < 0.05$ was considered statistically significant.

RESULT

High ADNP Expression in Human BC

To detect ADNP expression in BC tissue samples, we analyzed BC tissue pairing (T) and the pair of adjacent normal BC tissue (A) *via* RT-PCR. Compared with normal bladder urothelial tissue, the ADNP mRNA expression of BC tissues tended to be upregulated ($P < 0.05$, **Figure 1A**). Similarly, western blot analysis revealed that ADNP protein expression in human primary bladder tumor was also significantly upregulated (**Figure 1B**). These findings indicate that ADNP is highly expressed in BC.

Upregulated ADNP Expression Is Associated With Advanced Clinicopathological Characteristics of BC

We examined the relationship between ADNP and the clinicopathological characteristics of bladder urothelial carcinoma. The weighted Fleiss-Cohen (quadratic) kappa value was 0.893. **Table 1** describes the medical data of 221 paraffin-embedded BC specimens. ADNP expression was significantly associated with pathological level ($P = 0.009$), T stage ($P < 0.001$), N stage ($P= 0.007$), and mortality status ($P < 0.001$) (**Table 1**), but not with age ($P = 0.832$), sex ($P = 0.214$), multifocal growth ($P = 0.196$), and tumor size ($P = 0.508$). Furthermore, immunohistochemical quantitative results indicated that ADNP expression was higher in the 221 cases of BC than in the 51 samples of normal bladder tissues (**Figures 1C, D**). Further, ADNP expression was higher in advanced clinical stage (MIBC) and pathological grade (Level III) BC than the early clinical stage (NMBC) and low pathological grade (Levels I and II) BC (**Figure 1D**). These results show that high ADNP expression is significantly associated with advanced clinicopathological features.

High ADNP Expression Is Associated With Poor Outcome

Immunohistochemistry was used to detect ADNP expression in 221 samples of paraffin-embedded tissues to determine the frequency of ADNP overexpression in BC tissues. In the 221 samples, 108 were pathological grade I; 52, pathological grade II; and 61, pathological grade III (**Table 1**). We found there was higher ADNP expression in BC specimens when compared with normal bladder urothelial tissues. Quantitative analysis showed that the expression of ADNP was highly upregulated in the 221 BC specimens. In Cox regression analysis, we evaluated the potential of ADNP as a predictive factor of prognosis; it showed high ADNP expression significantly increased the risk of mortality in both univariate ($P < 0.001$; **Table 2**) and multivariate analyses ($P = 0.001$). The Kaplan-Meier survival curve showed that the overall survival of patients with high ADNP expression was lower than that of patients with low ADNP expression, and the survival without disease progression show the same (**Figure 1E**, $P < 0.001$). These results support that upregulated ADNP expression is related to poor prognosis in BC.

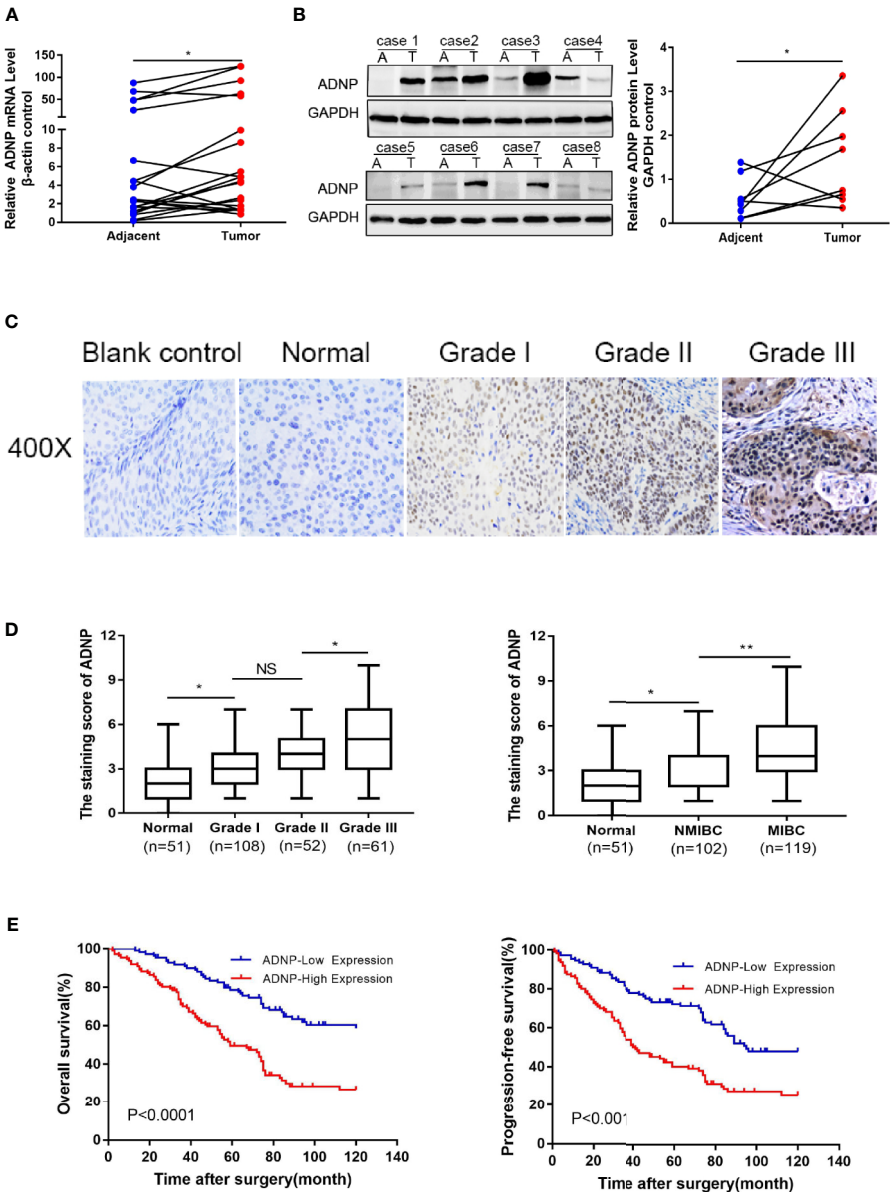

FIGURE 1 | ADNP is upregulated in bladder cancer. **(A)** Real-time PCR analysis of ADNP mRNA expression in 20 paired bladder tumor tissues (Tumor) and their adjacent normal tissues (Adjacent). The average ADNP mRNA expression was normalized to the expression of β-actin. **(B)** ADNP protein expression in 8 paired bladder tumor tissues (T) and their adjacent normal tissues (A) determined *via* western blot analysis. GAPDH was detected as a loading control in the western blot analysis. **(C)** Representative images of ADNP expression in normal bladder tissues and different grades of bladder cancer (scale bar: 50 μm; magnification: ×400). **(D)** Quantification of immunohistochemical analysis of ADNP expression in 51 normal bladder mucosa and in 108 Grade I, 52 Grade II, and 61 Grade III bladder cancer tissues (left). Quantification of the average staining score for ADNP in 51 normal bladder mucosa and in different clinical stages of bladder cancer (102 NMBC, 119 MIBC) (right). **(E)** Kaplan-Meier curves of overall survival (left) and progression free survival (right) for the 221 patients with bladder cancer stratified by high and low expression of ADNP. **P < 0.01, *P < 0.05. NS, no significance.

ADNP Regulates Bladder Cancer Cell Proliferation

In western blot analysis to detect ADNP protein expression in BC cell lines and normal urothelial cell line, ADNP was significantly increased in T24 and BIU87 cells and had relatively low expression in 5637, TCCSUP, and SV-HUC-1 cells (**Figure 2A**). Therefore, we constructed ADNP-knockdown cells with three specific sites by lentivirus, verified the knockdown efficiency with western blot analysis, and selected the lowest-knockdown-degree cell for a series of functional experiments (**Figure 2B**). In addition, we overexpressed ADNP in 5637, TCCSUP, and SV-HUC-1 cells (**Figure 2C**). Trypan

TABLE 1 | ADNP expression in bladder cancer and its correlation with clinicopathological characteristics.

Characteristics ADNP	n (%)	ADNP		Pearson correlation	*P*-value
		Low (n = 110)	High (n = 111)		
Age (y)				0.014	0.832
≥ 60	96 (43.4%)	47	62		
< 60	125 (56.6%)	63	49		
Sex				-0.084	0.214
Male	180 (81.4%)	86	94		
Female	41 (18.6%)	24	17		
pathological grade				0.199	0.009
1	108 (48.9%)	65	43		
2	52 (23.5%)	22	30		
3	61 (27.6%)	23	38		
T stage				0.363	<0.001
Ta	49 (22.2%)	46	2		
T1	53 (24.0%)	20	33		
T2	88 (39.8%)	34	54		
T3	16 (7.2%)	5	11		
T4	15 (6.8%)	5	10		
N stage				0.182	0.007
Negative	179 (81.0%)	97	82		
Positive	42 (19.0%)	13	29		
Tumor multiplicity				-0.087	0.196
Unifocal	134 (60.6%)	62	72		
Multifocal	87 (39.4%)	48	39		
Tumor size(cm)				0.045	0.508
≥ 3	75 (33.9%)	75	71		
< 3	146 (66.1%)	35	40		
Mortality status				0.285	<0.001
Alive	77 (34.8%)	53	24		
Dead	102 (46.2%)	37	65		
Lost to follow-up	32 (14.5%)	10	22		

TABLE 2 | Univariate and multivariate Cox regression analyses of prognostic factors in bladder cancer.

Variables	Univariate analysis			Multivariate analysis		
	HR	95% CI	*p*-Value	HR	95% CI	*p*-Value
Age	0.863	0.591–1.256	0.863	–	–	–
Sex	0.862	0.499–1.368	0.458	–	–	–
Pathological grade	1.833	1.461–2.299	<0.001	1.364	1.059–1.759	0.016
T stage	1.980	1.668–2.350	<0.001	1.882	1.321–2.680	<0.001
N stage	1.774	1.147–2.744	0.010	1.899	1.223–2.948	0.004
Tumor multiplicity	0.956	0.653–1.399	0.817	–	–	–
Tumor size	1.970	1.354–2.864	<0.001	2.113	1.427–3.129	<0.001
ADNP	2.627	1.779–3.879	<0.001	1.944	1.330–2.990	0.001

HR, hazard ratio; CI, confidence interval.

blue exclusion test and flow cytometry showed the downregulation of ADNP significantly decreased the cell viability in T24 and BIU87 cells, while overexpressed ADNP markedly increased the proportion of viable cells in TCCSUP, 5637, and SV-HUC-1 cells (**Figures 2D, E**). CCK8 assay showed that ADNP knockdown significantly slowed down the growth speed of T24 and BIU87, while overexpressed ADNP significantly increased the growth rate of BC cells and normal urothelial cells (**Figure 2F**). Further, compared with blank transfected cells, the downregulation of ADNP markedly reduced the average quantity of colonies in the colony growth experiment, while the overexpression of ADNP increased the clone number in TCCSUP, 5637, and SV-HUC-1 cells (**Figure 2G**). These findings show that ADNP can stimulate proliferation of BC cells.

ADNP Accelerated G1-to-S Cell Cycle Transformation

To further explore the role of ADNP in stimulating cell propagation, flow cytometry was applied in cell analysis. ADNP knockdown markedly lowered the percentage of G0/G1 peak cells and improved the percentage of S peak cells (**Figure 3A**).

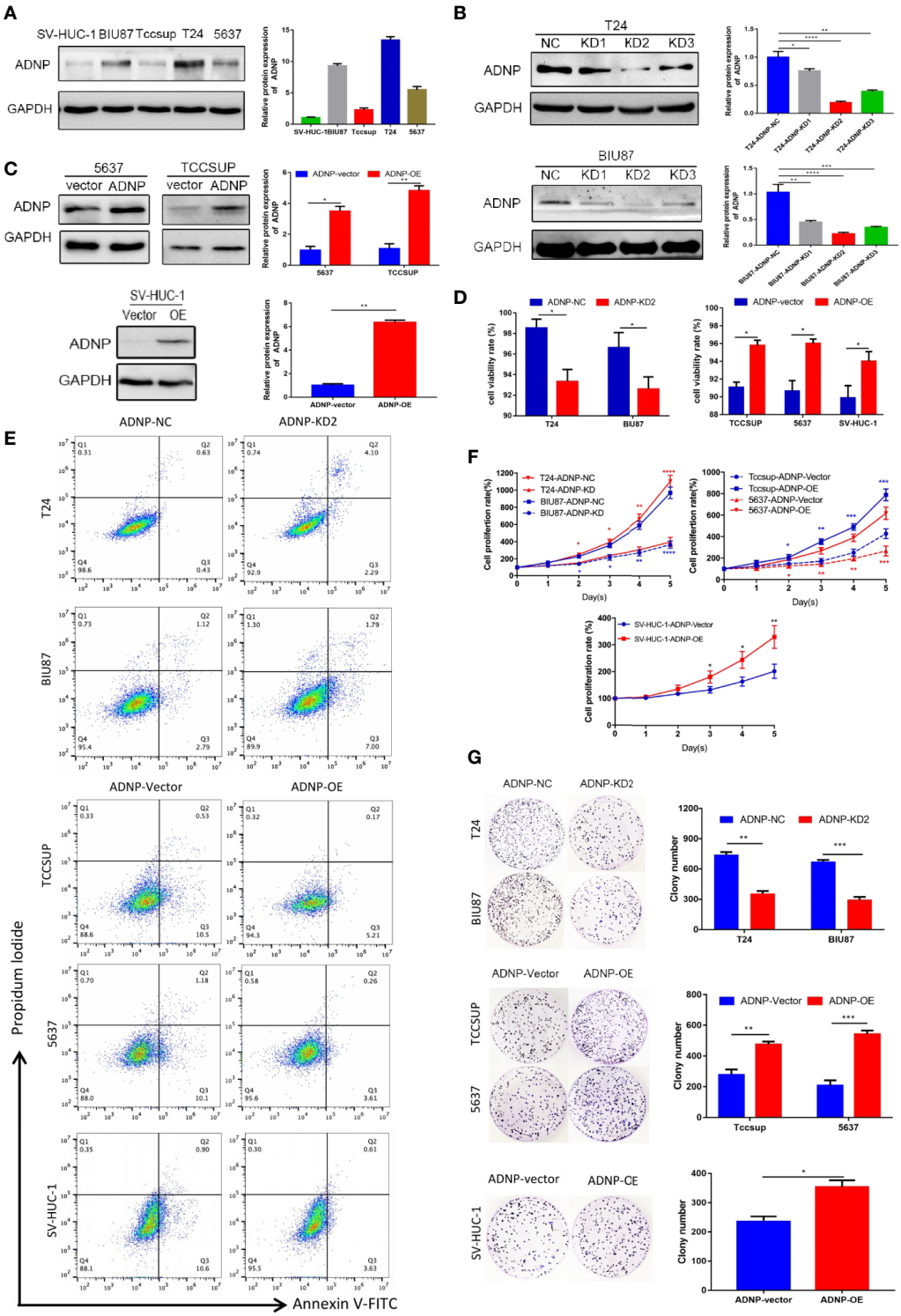

FIGURE 2 | ADNP modulates proliferation of bladder cancer cells. **(A)** Western blot analysis of ADNP basic expression in 4 different bladder cancer cell lines (T24, BIU87, TCCSUP, 5637) and 1 normal urothelial cell line (SV-HUC-1). **(B)** The efficiency of ADNP knockdown in T24 and BIU87 cells were determined by Western blot **(C)** The efficiency of ADNP overexpression in 5637, TCCSUP, and SV-HUC-1 cells were determined by Western blot. **(D)** Cell viability of bladder cells and SV-HUC-1 cells were determined by the trypan blue exclusion assay. **(E)** Representative images of flow cytometric analysis were used to show viability rates after ADNP knockdown or overexpression. **(F)** CCK8 assays revealed the proliferation of indicated bladder cancer cells. **(G)** Colony formation assay test for tumorigenesis in indicated bladder cancer cells. The results are presented as the mean ± SD. ****P < 0.0001, ***P < 0.001, **P < 0.01, *P < 0.05.

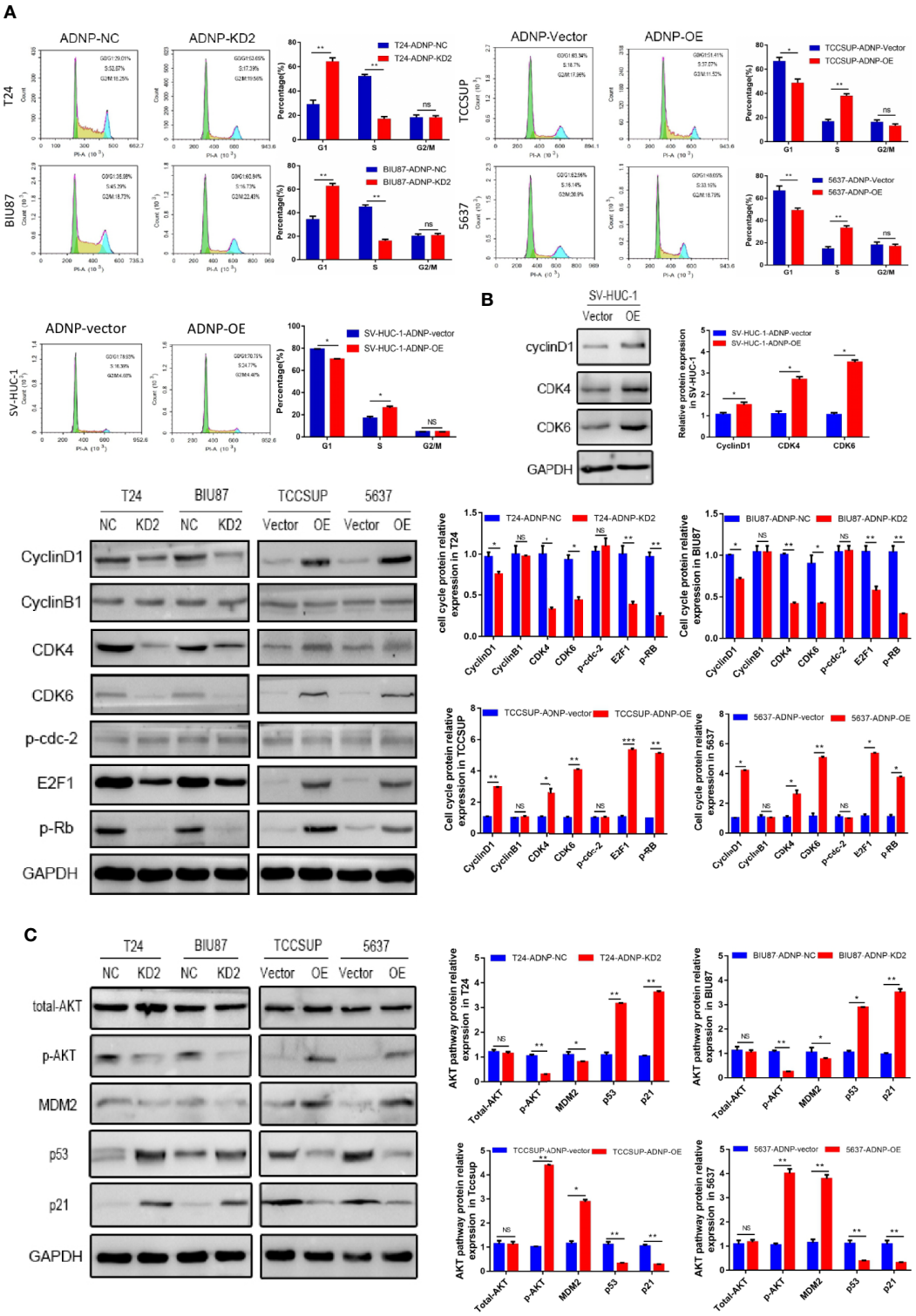

FIGURE 3 | ADNP is involved in transition from G1 phase to S phase in the cell cycle and regulates proliferation of bladder cancer cells through the activation of the AKT-MDM2-p53 signaling pathway. **(A)** Representative images of flow cytometry analysis in indicated bladder cancer cell lines, and quantification of cell cycle analysis in indicated bladder cancer cell lines. **(B)** Western blot analysis of cyclin B1, cyclin D1, CDK4, CDK6, p-cdc-2, E2F1, and p-Rb expression in indicated cells. **(C)** Western blot analysis of phosphorylated Akt (p-Akt), total Akt, MDM2, p53, and p21 protein in the indicated bladder cancer cell lines. ***P < 0.001, **P < 0.01, *P < 0.05. NS, no significance.

However, there was no significant difference in G2/M phase ratio, and ADNP overexpression showed the opposite result, suggesting that ADNP can accelerate the G1 to S phase conversion of BC and normal urothelial cells (**Figure 3A**). In addition, western blot analysis showed that the expression of Cyclin D1, CDK4, CDK6, p-RB, and E2F1 in ADNP-overexpressed bladder cell lines was upregulated, while the expression of them was downregulated in ADNP-knockdown cells. Overexpressing ADNP also led to the significant increase of CyclinD1, CDK4, and CDK6 in SV-HUC-1 cells. In addition, changing ADNP expression did not have a significant impact on Cyclin B1 and p-cdc-2 expression (**Figure 3B**), both of which were promoters of G2-to-M transformation, suggesting that ADNP further increased BC cell propagation by accelerating the G1-S phase transformation.

ADNP Activates AKT-MDM2-p53 Signaling Pathways

To determine the molecular dynamics regulating the cell cycle, several key proteins of classical signaling pathways were detected. After altering ADNP expression, p-AKT expression was higher in T24 and BIU87 cells, but lower in 5637 and in TCCSUP cells. Meanwhile, there were no significant changes in total AKT expression (**Figure 3C**). In addition, the activation of downstream target protein MDM2 was correlated with the degree of AKT phosphorylation, and the upregulation of MDM2 mediated the decrease of p53 and its downstream protein p21. These results suggest that ADNP may regulate p21-induced cell cycle transformation by activating the AKT/MDM2/p53 pathway, thereby promoting the propagation of BC cells.

ADNP Regulates Bladder Cancer Tumorigenesis In Vivo

To verify the outcome of tumorigenesis experiments in vitro, xenograft bladder tumor models were constructed in NOD/SCID nude mice using T24.The final volume, weight, and tumor growth curve of the transplanted tumor (**Figures 4A–C**) revealed that compared with the negative control group, T24 cells with ADNP knockdown had significantly lower capability of tumor formation. In addition, western blot analysis confirmed that the expression of ADNP, Ki-67, Cyclin D1, CDK4, and CDK6 in T24 BC cells with ADNP knockdown was considerably lower than those in the negative control (**Figure 4D**). Similarly, immunohistochemical results showed that ADNP knockdown group had lower expression of ADNP, Ki-67, CyclinD1, CDK4, and CDK6 compared with the control group (**Figure 4E**). These in vivo results indicate that ADNP might play a key role in BC tumorigenesis.

Effect of ADNP on Proliferation and Cell Cycle Could Be Rescued by MK-2206 2HCl

To elucidate the role of AKT in ADNP-induced cycle acceleration and proliferation of BC cells, the AKT-specific inhibitor MK-2206 2HCI was used to treat 5637 and TCCSUP BC cells that overexpressed ADNP. CCK8 experiment and clone growth experiment results show that the AKT inhibitor can inhibit the proliferation in BC cells (**Figures 5A, B**). Moreover, compared with the blank group, the percentage of S phase cells was significantly lower in the AKT inhibitor treatment group (**Figure 5C**). Further, we found that MK-2206 2HCI can reverse the effect of ADNP on p-AKT, MDM2, p53, p21, cyclinD1, and CDK4 and CDK6 (**Figure 5D**). In vivo experiment, the final volume, weight and tumor growth curve of the transplanted tumor (**Figures 5E–G**) showed that TCCSUP cells treated with MK-2206 2HCI had significantly lower capability of tumor formation compared with the control group. Moreover, immunohistochemical results confirmed that the expression of Ki-67, Cyclin D1, CDK4, and CDK6 in the TCCSUP cells handled with MK-2206 2HCI was considerably lower than those in the control; there was no significant difference on the expression of ADNP between the two groups (**Figure 5H**). Collectively, these results suggest that the changes in cell cycle and proliferation mediated by ADNP expression are related to the AKT-MDM2-p53 signaling pathway in BC cells.

DISCUSSION

Here, we found that ADNP expression was upregulated in BC, and significantly correlated with high pathological grade and advanced clinical stage. ADNP stimulates the AKT-MDM2-p53 pathway and enhances binding of cyclin D1 to CDK4 or CDK6, accelerating the cell cycle transition from G1 phase to S phase. Furthermore, we demonstrate that ADNP can promote the growth of bladder cancer in vivo.

The significance of ADNP expression in BC is unclear. Although the copy number of the ADNP gene has been reported to be amplified in BC (13), no study has explored the significance of ADNP mRNA and protein expression in the clinicopathology of BC. In this study, we found that the mRNA and protein expression of ADNP were upregulated compared with normal bladder urothelial tissues, and overexpression of ADNP protein was significantly associated with higher pathological grade, advanced clinical stage, and poor prognosis in BC patients. Consistent with our observations, DNA amplification and overexpression of the transcription factor ADNP were identified in high-grade and poorly prognostic ovarian cancer (25).

ADNP encodes a protein involved in embryonic development and brain formation (9). In previous studies, ADNP was associated with the de novo mutation that leads to autism-like spectrum disorder (18). However, a recent study suggested that negative ADNP expression in the colon activates the WNT signaling pathway, promoting colon cancer cell migration, invasion, and proliferation (15). We found that ADNP expression was significantly correlated with high pathological grade and advanced clinical stage, indicating that ADNP may be an oncogene of BC that can lead to tumor cell proliferation and tumorigenesis.

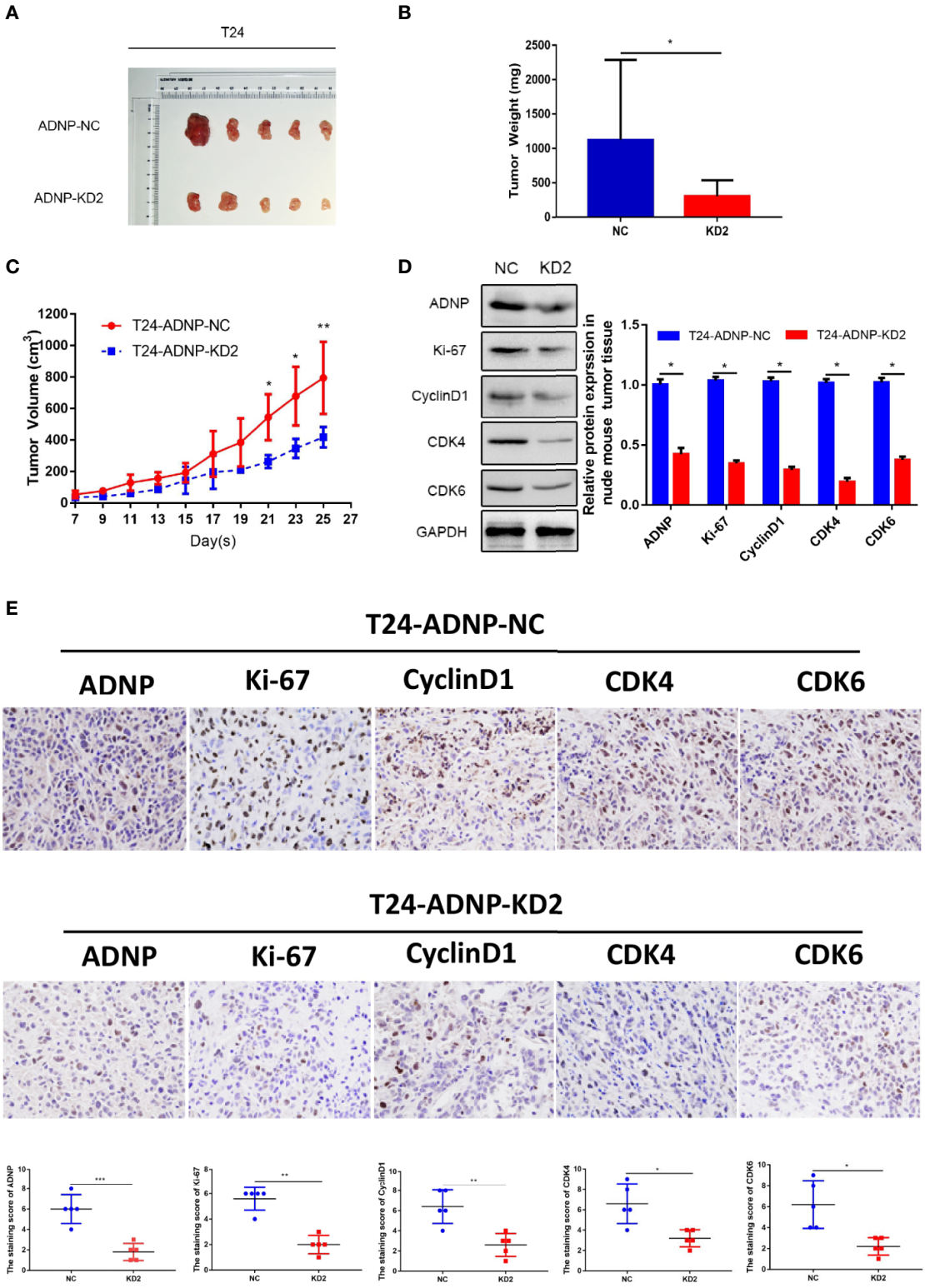

FIGURE 4 | ADNP modulates growth of bladder cancer in vivo. **(A)** Images of excised tumors from five NOD/SCID mice at 25 days after injection with non-silencing shRNA cells (NC) and ADNP-sh2-transfected cells (KD2). **(B)** Average weight of excised tumors. **(C)** Tumor volumes were measured every 2 days. **(D)** Western blot analysis of ADNP, Ki-67, Cyclin D1, CDK4, and CDK6 expression in excised xenograft tumors. **(E)** Representative images of sections sliced from indicated tumors and stained with anti-ADNP, anti-Ki67, anti-Cyclin D1, anti-CDK4, and anti-CDK6. $^{**}P < 0.01$, $^{*}P < 0.05$.

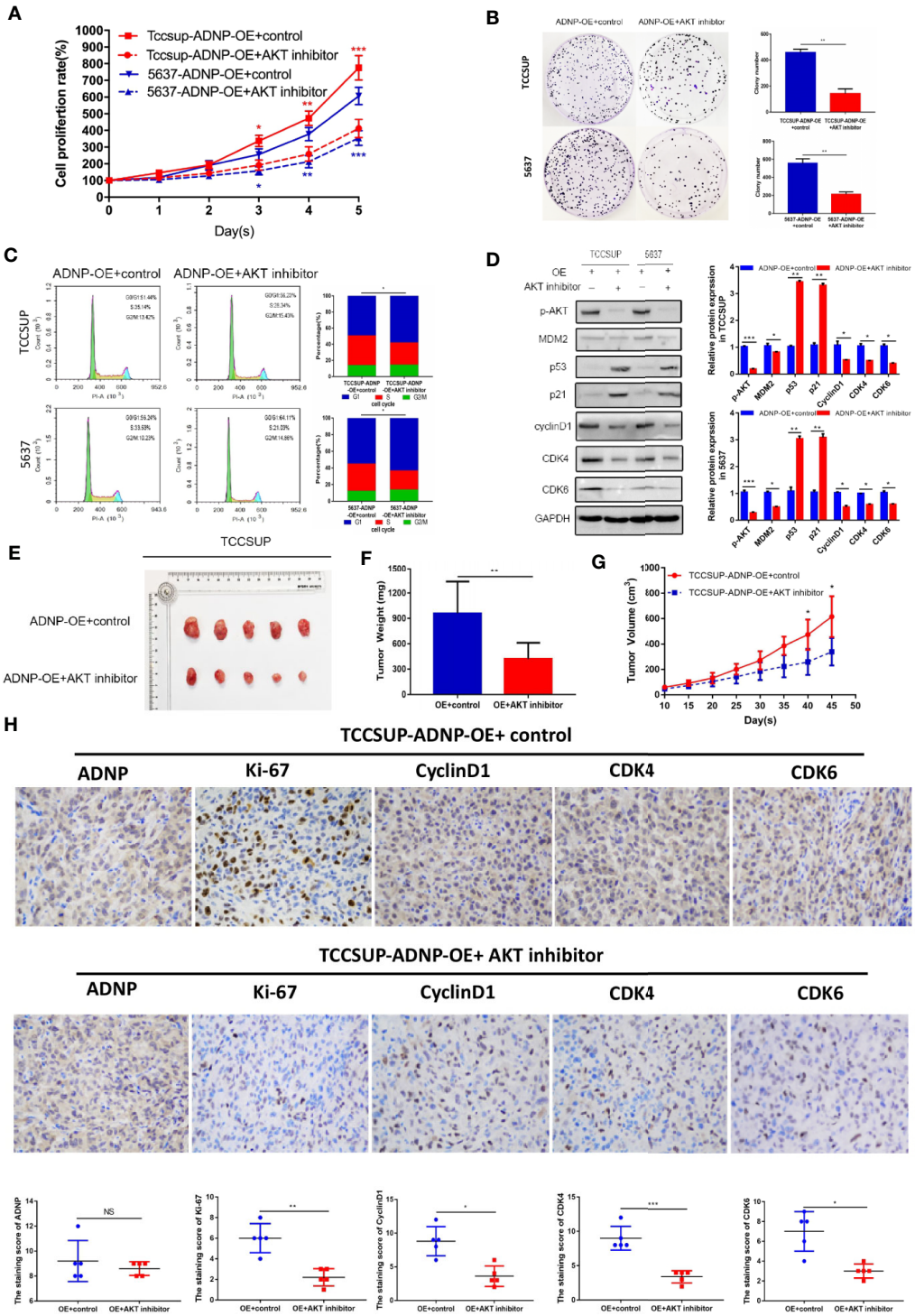

FIGURE 5 | Effect of ADNP on proliferation and cell cycle could be rescued by MK-2206 2HCl. **(A)** TCCSUP cells with ADNP overexpression were treated with the AKT inhibitor MK-2206 for 24 h, and CCK8 assays revealed the role of AKT in the proliferation of ADNP-transduced cells. **(B)** Colony formation assays revealed the role of AKT in the tumorigenesis of ADNP-transduced cells. **(C)** Flow cytometric assays revealed the role of AKT in the G1-to-S transition of ADNP-transduced cells. **(D)** Western blot analysis revealed the role of AKT in the downstream cell cycle-associated genes of ADNP-transduced cells. **(E)** Images of excised tumors from five NOD/SCID mice at 45 days after being handled with MK-2206 2HCl and PBS (control). **(F)** Average weight of excised tumors. **(G)** Tumor volumes were measured every 5 days. **(H)** Representative images of sections sliced from indicated tumors and stained with anti-ADNP, anti-Ki67, anti-cyclin D1, anti-CDK4, and anti-CDK6. ***P < 0.001, **P < 0.01, *P < 0.05. NS, no significance.

To test our hypothesis, we studied ADNP function in BC in vivo and in vitro. We found the evidence in our study that ADNP can significantly promote tumor cell growth and proliferation. The infinite proliferation in cells is an important factor leading to the development of tumors. Alessandro et al. (17) showed that the activation of the ADNP signaling pathway increases the survival ability of malignant glioma cells in harsh environments and participates in the resistance to cell death, which is consistent with our experimental results.

In general, infinite growth is caused by the increase of cell viability or the disruption of cell cycle checkpoints (26). To investigate whether this effect is related to cell viability, we performed trypan blue exclusion tests and flow cytometry, which showed ADNP lead to increased cell viability. In line with our study, ADNP was also proved to increase the cell viability to resist the toxicity induced by H_2O_2 in malignant peripheral nerve sheath tumor (17). The disorder of cell cycle is the initial cause of abnormal growth of tumor cells and the important step of obtaining infinite proliferation ability of tumor (26). After the cell cycle is disturbed, cell division is no longer regulated by G1/S and G2/M checkpoints, and cells can obtain stronger proliferation capacity (27, 28). A study recently showed that the mice with ADNP haplo-insufficiency exhibit the decrease ability of wound healing due to the broken cell cycle progression, and the reactivation of ADNP in mouse models increased the ability of wound healing and accelerated cell cycle progression (29). Moreover, ADNP was identified to be an oncogenic mediator of cell proliferation through dysregulation of cell cycle checkpoints in high-grade serous ovarian cancer (25). In our study, flow cytometry showed that ADNP significantly accelerated transition of BC cells from G1 phase to S phase. Meanwhile, our Western blot analysis indicated that ADNP significantly increased the expression of Cyclin D1, CDK4, CDK6, phosphorylating retinoblastoma (p-Rb), and E2F1. Cyclin D1 is mainly expressed in the G1 phase of the cell cycle, and it can combine with cell cycle protein CDK4 or CDK6 to form active cell cycle protein complexes, such as p-Rb protein and E2F, which crosses the cell cycle checkpoint of the G1 phase to S phase (30, 31).

In many types of tumor cells, AKT can be activated by growth factor receptors, tenin homologous proteins, and mutations in tumor suppressor phosphatase signals, transmitting effective proliferation signals (32). AKT can promote tumor cell proliferation by accelerating the progress of cell cycle G1-S by isolating p21 in the cytoplasm and stabilization of cyclin D1 (33, 34). Previous studies show p-AKT can directly promote the degradation of p53 protein by nuclear MDM2 and downregulate the activity of p53, resulting in an imbalanced microenvironment that promotes cancer cell proliferation but inhibits apoptosis (35, 36). Our study shows that ADNP activated the AKT-MDM2-p53 signaling pathway, mediated the degradation of p21 and the stability of cyclin D1, and promoted the proliferation of tumor cells. Consistent with our research, a number of studies have reported that ADNP plays an important role in regulating cell growth, proliferation in some types of sarcomas and neuronal tissue as well as modulating AKT signaling pathway (25). AKT signaling also plays an important role in $CD8^+$T cell differentiation and regulatory T cell survival (37–39). Loss or weakening of AKT signaling would result in transcriptional rearrangement of differentiated cytotoxic T lymphocytes, transforming effector cells into memory cells to enhance the anti-tumor effects in the immune system (40, 41). In a xenograft study, MK-2206 2HCI treatment in mice with ovarian cancer cell lines resulted in 60% growth inhibition (42). Meanwhile, the addition of AKT inhibitor blocked the radiation-induced Treg cell survival in bladder cancer cell, which can inhibit $CD8^+$ T cells in the tumor tissue to compromise the antitumor activities (43). We found that the effect of ADNP on tumor proliferation was rescued by AKT inhibitors, suggesting that ADNP promotes cell proliferation mainly through activation of the AKT pathway in BC. Previous studies have reported that ADNP can activate the AKT pathway to promote the neuronal growth and differentiation, which is related to the up-regulation of the expression of AKT phosphorylated kinase (19), and this mechanism may also exist in bladder cancer. Nevertheless, further studies are warranted to replicate and extend these findings.

In conclusion, the mRNA and protein expressions of ADNP were up-regulated in human bladder cancer and reveal its role as a tumor promoter with effects on tumor cell proliferation as well as cell cycle with the activation of AKT pathway. Accordingly, these findings provide the evidences that ADNP expression can be an independent predictor of poor prognosis in patients with BC, and a candidate therapeutic target for novel molecular therapy.

DATA AVAILABILITY STATEMENT

All datasets generated for this study are included in the article/supplementary material.

ETHICS STATEMENT

The studies involving human participants were reviewed and approved by The study involving human participants was approved by the ethics committee of the Affiliated Cancer Hospital of Xiangya School of Medicine, Central South University. Patients/participants provided written informed consent for their participation in this study. The patients/participants provided their written informed consent to participate in this study. The animal study was reviewed and approved by The animal research was examined and approved by the animal ethics committee of the Affiliated Cancer Hospital of Xiangya School of Medicine, Central South University.

AUTHOR CONTRIBUTIONS

YX and SZ designed the research. YL and QD collected the data. GF and JC interpreted the data. SZ, ZX, and YW carried out the experiment. SZ drafted the manuscript. YX, YZ, and WH

critically revised the manuscript. All authors contributed to the article and approved the submitted version.

FUNDING

This study was funded by the Key Research and Development Projects of Hunan Province (grant number 2018SK2125 and 2018SK2120) and the Key Research Project of National Cancer Center (grant number NCC201818A55).

ACKNOWLEDGMENTS

The authors thank Prof. Xiaofeng Ding for helping with the data analysis.

REFERENCES

1. Bray F, Ferlay J, Soerjomataram I, Siegel RL, Torre LA, Jemal A. Global cancer statistics 2018: GLOBOCAN estimates of incidence and mortality worldwide for 36 cancers in 185 countries. *CA Cancer J Clin* (2018) 6:394–424. doi: 10.3322/caac.21492
2. Chen W, Zheng R, Baade PD, Zhang S, Zeng H, Bray F, et al. Cancer statistics in China, 2015. *CA Cancer J Clin* (2016) 2:115–32. doi: 10.3322/caac.21338
3. Wu XR. Urothelial tumorigenesis: a tale of divergent pathways. *Nat Rev Cancer* (2005) 9:713–25. doi: 10.1038/nrc1697
4. Sangar VK, Ragavan N, Matanhelia SS, Watson MW, Blades RA. The economic consequences of prostate and bladder cancer in the UK. *BJU Int* (2005) 1:59–63. doi: 10.1200/JCO.2001.19.3.666
5. Stein JP, Lieskovsky G, Cote R, Groshen S, Feng AC, Boyd S, et al. Radical cystectomy in the treatment of invasive bladder cancer: long-term results in 1,054 patients. *J Clin Oncol* (2001) 3:666–75. doi: 10.1200/JCO.2001.19.3.666
6. Mandel S, Gozes I. Activity-dependent neuroprotective protein constitutes a novel element in the SWI/SNF chromatin remodeling complex. *J Biol Chem* (2007) 47:34448–56. doi: 10.1016/j.ydbio.2006.11.039
7. Gozes I, Bassan M, Zamostiano R, Pinhasov A, Davidson A, Giladi E, et al. A novel signaling molecule for neuropeptide action: activity-dependent neuroprotective protein. *Ann N Y Acad Sci* (1999) 897:125–35. doi: 10.1111/j.1749-6632.1999.tb07884.x
8. Mandel S, Rechavi G, Gozes I. Activity-dependent neuroprotective protein (ADNP) differentially interacts with chromatin to regulate genes essential for embryogenesis. *Dev Biol* (2007) 2:814–24. doi: 10.1074/jbc.M704756200
9. Pinhasov A, Mandel S, Torchinsky A, Giladi E, Pittel Z, Goldsweig AM, et al. Activity-dependent neuroprotective protein: a novel gene essential for brain formation. *Brain Res Dev Brain Res* (2003) 1:83–90. doi: 10.1016/s0165-3806(03)00162-7
10. Kanki T, Wang K, Cao Y, Baba M, Klionsky DJ. Atg32 is a mitochondrial protein that confers selectivity during mitophagy. *Dev Cell* (2009) 1:98–109. doi: 10.1016/j.devcel.2009.06.014
11. Gozes I, Werner H, Fawzi M, Abdelatty A, Shani Y, Fridkin M, et al. Estrogen regulation of vasoactive intestinal peptide mRNA in rat hypothalamus. *J Mol Neurosci* (1989) 1:55–61. doi: 10.1007/BF02896857
12. Sragovich S, Merenlender-Wagner A, Gozes I. ADNP Plays a Key Role in Autophagy: From Autism to Schizophrenia and Alzheimer's Disease. *Bioessays* (2017) 11:170005401-10. doi: 10.1002/bies.201700054
13. Zamostiano R, Pinhasov A, Gelber E, Steingart RA, Seroussi E, Giladi E, et al. Cloning and characterization of the human activity-dependent neuroprotective protein. *J Biol Chem* (2001) 1:708–14. doi: 10.1074/jbc.M007416200
14. Jo YS, Kim MS, Yoo NJ, Lee SH, Song SY. ADNP encoding a transcription factor interacting with BAF complexes exhibits frameshift mutations in gastric and colorectal cancers. *Scand J Gastroenterol* (2016) 10:1269–71. doi: 10.1080/00365521.2016.1193220
15. Blaj C, Bringmann A, Schmidt EM, Urbischek M, Lamprecht S, Frohlich T, et al. ADNP Is a Therapeutically Inducible Repressor of WNT Signaling in Colorectal Cancer. *Clin Cancer Res* (2017) 11:2769–80. doi: 10.1158/1078-0432.CCR-16-1604
16. Rangel R, Guzman-Rojas L, Kodama T, Kodama M, Newberg JY, Copeland NG, et al. Identification of new tumor suppressor genes in triple-negative breast cancer. *Cancer Res* (2017) 77:4089–101. doi: 10.1158/0008-5472.CAN-17-0785
17. Castorina A, Giunta S, Scuderi S, D'Agata V. Involvement of PACAP/ADNP signaling in the resistance to cell death in malignant peripheral nerve sheath tumor (MPNST) cells. *J Mol Neurosci* (2012) 3:674–83. doi: 10.1007/s12031-012-9755-z
18. Helsmoortel C, Vulto-van Silfhout AT, Coe BP, Vandeweyer G, Rooms L, van den Ende J, et al. A SWI/SNF-related autism syndrome caused by de novo mutations in ADNP. *Nat Genet* (2014) 4:380–4. doi: 10.1038/ng.2899
19. Pascual M, Guerri C. The peptide NAP promotes neuronal growth and differentiation through extracellular signal-regulated protein kinase and Akt pathways, and protects neurons co-cultured with astrocytes damaged by ethanol. *J Neurochem* (2007) 2:557–68. doi: 10.1111/j.1471-4159.2007.04761.x
20. Sasaki T, Kuniyasu H, Luo Y, Kitayoshi M, Tanabe E, Kato D, et al. Increased phosphorylation of AKT in high-risk gastric mucosa. *Anticancer Res* (2013) 8:3295–300. doi: 10.3109/0284186X.2013.806820
21. Gozes I, Yeheskel A, Pasmanik-Chor M. Activity-dependent neuroprotective protein (ADNP): a case study for highly conserved chordata-specific genes shaping the brain and mutated in cancer. *J Alzheimers Dis* (2015) 1:57–73. doi: 10.3233/JAD-142490
22. Zhou X, Liu N, Zhang J, Ji H, Liu Y, Yang J, et al. Increased expression of EZH2 indicates aggressive potential of urothelial carcinoma of the bladder in a Chinese population. *Sci Rep* (2018) 1:17792. doi: 10.1038/s41598-018-36164-y
23. Jain AK, Tewari-Singh N, Inturi S, Orlicky DJ, White C W, Agarwal R. Histopathological and immunohistochemical evaluation of nitrogen mustard-induced cutaneous effects in SKH-1 hairless and C57BL/6 mice. *Exp Toxicol Pathol* (2014) 2-3:129–38. doi: 10.1016/j.etp.2013.11.005
24. Detrano R, Guerci AD, Carr JJ, Bild DE, Burke G, Folsom AR, et al. Coronary calcium as a predictor of coronary events in four racial or ethnic groups. *New Engl J Med* (2008) 358(13):1336–45. doi: 10.1056/NEJMoa072100
25. Karagoz K, Mehta GA, Khella CA, Khanna P, Gatza ML. Integrative proteogenomic analyses of human tumours identifies ADNP as a novel oncogenic mediator of cell cycle progression in high-grade serous ovarian cancer with poor prognosis. *EBioMedicine* (2019) 50:191–202. doi: 10.1016/j.ebiom.2019.11.009
26. Ivy SP, Kunos CA, Arnaldez F I, Kohn EC. Defining and targeting wild-type BRCA high-grade serous ovarian cancer: DNA repair and cell cycle checkpoints. *Expert Opin Invest Drugs* (2019) 9:771–85. doi: 10.1080/13543784.2019.1657403
27. Dong Y, Zhao X, Feng X, Zhou Y, Yan X, Zhang Y, et al. SETD2 mutations confer chemoresistance in acute myeloid leukemia partly through altered cell cycle checkpoints. *Leukemia* (2019) 11:2585–98. doi: 10.1038/s41375-019-0456-2
28. Sun B, Qin W, Song M, Liu L, Yu Y, Qi X, et al. Neutrophil Suppresses Tumor Cell Proliferation *via* Fas /Fas Ligand Pathway Mediated Cell Cycle Arrested. *Int J Biol Sci* (2018) 14:2103–13. doi: 10.7150/ijbs.29297
29. Mollinedo P, Kapitansky O, Gonzalez-Lamuno D, Zaslavsky A, Real P, Gozes I, et al. Cellular and animal models of skin alterations in the autism-related ADNP syndrome. *Sci Rep* (2019) 1:736. doi: 10.1038/s41598-018-36859-2
30. Dozier C, Mazzolini L, Cenac C, Froment C, Burlet-Schiltz O, Besson A, et al. CyclinD-CDK4/6 complexes phosphorylate CDC25A and regulate its stability. *Oncogene* (2017) 26:3781–8. doi: 10.1038/onc.2016.506
31. Giacinti C, Giordano A. RB and cell cycle progression. *Oncogene* (2006) 38:5220–7. doi: 10.1038/sj.onc.1209615
32. Hennessy BT, Smith DL, Ram PT, Lu Y, Mills GB. Exploiting the PI3K/AKT pathway for cancer drug discovery. *Nat Rev Drug Discovery* (2005) 12:988–1004. doi: 10.1038/nrd1902

33. West KA, Castillo SS, Dennis PA. Activation of the PI3K/Akt pathway and chemotherapeutic resistance. *Drug Resist Update* (2002) 6:234–48. doi: 10.1016/S1368-7646(02)00120-6
34. Parsons CM, Muilenburg D, Bowles TL, Virudachalam S, Bold RJ. The role of Akt activation in the response to chemotherapy in pancreatic cancer. *Anticancer Res* (2010) 9:3279–89. doi: 10.1097/CAD.0b013e32833d19f0
35. Ogawara Y, Kishishita S, Obata T, Isazawa Y, Suzuki T, Tanaka K, et al. Akt enhances Mdm2-mediated ubiquitination and degradation of p53. *J Biol Chem* (2002) 24:21843–50. doi: 10.1074/jbc.M109745200
36. Mayo LD, Donner DB. A phosphatidylinositol 3-kinase/Akt pathway promotes translocation of Mdm2 from the cytoplasm to the nucleus. *Proc Natl Acad Sci USA* (2001) 20:11598–603. doi: 10.1073/pnas.181181198
37. Crompton JG, Sukumar M, Roychoudhuri R, Clever D, Gros A, Eil RL, et al. Akt inhibition enhances expansion of potent tumor-specific lymphocytes with memory cell characteristics. *Cancer Res* (2015) 2:296–305. doi: 10.1158/0008-5472.CAN-14-2277
38. Li CG, He MR, Wu FL, Li Y J, Sun AM. Akt promotes irradiation-induced regulatory T-cell survival in hepatocellular carcinoma. *Am J Med Sci* (2013) 2:123–7. doi: 10.1097/MAJ.0b013e31826ceed0
39. Macintyre AN, Finlay D, Preston G, Sinclair LV, Waugh CM, Tamas P, et al. Protein kinase B controls transcriptional programs that direct cytotoxic T cell fate but is dispensable for T cell metabolism. *Immunity* (2011) 2:224–36. doi: 10.1016/j.immuni.2011.01.012
40. Klebanoff CA, Gattinoni L, Palmer DC, Muranski P, Ji Y, Hinrichs CS, et al. Determinants of successful CD8+ T-cell adoptive immunotherapy for large established tumors in mice. *Clin Cancer Res* (2011) 16:5343–52. doi: 10.1158/1078-0432.CCR-11-0503
41. Guo J, Muse E, Christians AJ, Swanson S J, Davila E. An Anticancer Drug Cocktail of Three Kinase Inhibitors Improved Response to a Dendritic Cell-Based Cancer Vaccine. *Cancer Immunol Res* (2019) 9:1523–34. doi: 10.1158/2326-6066.CIR-18-0684
42. Xu B, Yuan L, Chen G, Li T, Zhou J, Zhang C, et al. S-15 in combination of Akt inhibitor promotes the expansion of CD45RA(-)CCR7(+) tumor infiltrating lymphocytes with high cytotoxic potential and downregulating PD-1(+)Tim-3(+) cells as well as regulatory T cells. *Cancer Cell Int* (2019) 19:32201–11. doi: 10.1186/s12935-019-1043-3
43. Wang M, Gou X, Wang L. Protein kinase B promotes radiation-induced regulatory T cell survival in bladder carcinoma. *Scand J Immunol* (2012) 1:70–4. doi: 10.1111/j.1365-3083.2012.02707.x

Conflict of Interest: The authors declare that the research was conducted in the absence of any commercial or financial relationships that could be construed as a potential conflict of interest.

frontiers in Oncology

ORIGINAL RESEARCH
published: 07 December 2020
doi: 10.3389/fonc.2020.527385

PD-L1 Expression in Muscle-Invasive Urinary Bladder Urothelial Carcinoma According to Basal/Squamous-Like Phenotype

Bohyun Kim[1], *Cheol Lee*[1], *Young A. Kim*[2] *and Kyung Chul Moon*[1,3]*

[1] *Department of Pathology, Seoul National University College of Medicine, Seoul, South Korea,* [2] *Department of Pathology, Seoul Metropolitan Government-Seoul National University Boramae Medical Center, Seoul, South Korea,* [3] *Kidney Research Institute, Medical Research Center, Seoul National University College of Medicine, Seoul, South Korea*

OPEN ACCESS

Edited by:
Woonyoung Choi, Johns Hopkins Medicine, United States

Reviewed by:
Francesca Sanguedolce, Azienda Ospedaliero-Universitaria Ospedali Riuniti di Foggia, Italy
Carlo Terrone, San Martino Hospital (IRCCS), Italy

***Correspondence:**
Kyung Chul Moon
blue7270@gmail.com

Specialty section:
This article was submitted to Genitourinary Oncology, a section of the journal Frontiers in Oncology

Received: *16 January 2020*
Accepted: *03 November 2020*
Published: *07 December 2020*

Citation:
Kim B, Lee C, Kim YA and Moon KC (2020) PD-L1 Expression in Muscle-Invasive Urinary Bladder Urothelial Carcinoma According to Basal/Squamous-Like Phenotype. Front. Oncol. 10:527385. doi: 10.3389/fonc.2020.527385

Urothelial carcinoma (UC) is the most common histologic type of urinary bladder cancer, and muscle-invasive UC shows aggressive behaviors. Programmed cell death-1 (PD-1)/programmed cell death-ligand 1 (PD-L1) blockades have been approved as standard treatments for patients with advanced stage UC. A total of 166 muscle-invasive urinary bladder cancer (MIBC) patients, who underwent transurethral resection of the bladder or cystectomy from 2004 to 2010 were included. We evaluated PD-L1 expression by the SP142 and SP263 assays and classified the cases "positive" or "negative" according to the manufacturer's recommendations. We performed immunohistochemistry (IHC) for cytokeratin (CK) 5/6, CK14, GATA3, FOXA1, and CK20 and classified samples as Basal-Squamous-like (BASQ) or non-BASQ subtype. The overall concordance rate for PD-L1 expression is 91.6% (152/166) (kappa = 0.732). The SP142 assay showed 15.1% positivity; the SP263 assay showed 23.5%. The high positivity in the SP142 and SP263 assay was significantly correlated with positive CK5/6, CK14 expression, negative GATA3, FOXA1, and CK20 expression. Classification according to IHC expression resulted in 12.0% (20/166) of samples being classified as BASQ subtype and 88.0% (146/166) of samples being classified as non-BASQ subtype. High positivity in the SP142 and SP263 assay was significantly correlated with the BASQ subtype ($p < 0.001$, both). Our study is the first to analyze the association of immunohistochemically defined BASQ and non-BASQ subtypes with two PD-L1 assays in MIBC. In conclusion, we revealed that a high PD-L1 positive rate in all PD-L1 assays was significantly associated with the BASQ-subtype, and these results suggest that the BASQ classification may be important to apply the PD-1/PD-L1 blockades in MIBC.

Keywords: programmed cell death-ligand 1, muscle-invasive bladder cancer, basal/squamous-like, cytokeratin 5/6, cytokeratin 14, GATA3, FOXA1, immunohistochemistry

INTRODUCTION

Urinary bladder cancer is the 10th most common cancer and 14th most common cause of cancer-related death worldwide (1). Urothelial carcinoma (UC) is the most common malignant urinary bladder tumor. Programmed cell death-1 (PD-1)/programmed cell death-ligand 1 (PD-L1) blockades have shown clinical treatment efficacy in patients with advanced or metastatic UC (2, 3). Atezolizumab was approved for locally advanced or metastatic UC, and the SP142 assay was approved as a companion diagnostic test. Durvalumab was approved for inoperable or metastatic disease, and the SP263 assay was approved as a complementary diagnostic test (4).

Immune checkpoint inhibitors have been a promising and effective treatment option for various malignant tumors (5–8). Blockade of the PD-1/PD-L1 signaling pathway has been the main focus of treatment strategies, and PD-L1 immunohistochemical expression has been shown to be involved in predicting immune checkpoint inhibitor therapy efficacy (9).

Various previous studies identified the gene expression profiles and molecular characteristics of UC (10–14). From these studies, UC can be classified into several intrinsic molecular subtypes. Each research group uses different subtype classifications, among which there are many similarities, and classification into a basal subtype and a luminal subtype is common. The basal subtype expresses high levels of KRT5, KRT6, KRT14, and CD44. The luminal subtype expresses high levels of UPKs, KRT20, GATA3, and FOXA1 (11, 12). Additionally, in a consensus meeting urinary bladder cancers with high expression of KRT5/6 and KRT14 and low expression of FOXA1 and GATA3 were designated as the Basal-Squamous-like (BASQ) subtype (15). In addition to these mRNA expression-based subtype classifications, a few studies have reported immunohistochemistry (IHC)-based subtype classifications (16, 17). In one study, the IHC expression of basal (KRT5/6) and luminal (GATA3) markers reportedly reflected the molecular subtype with high accuracy (16). In another study, the basal/squamous cell carcinoma-like group was reported to show a tumor phenotype with high KRT6 and KRT14 and low FOXA1 and GATA3 expression by IHC (17).

The IMvigor210 phase II trial and another study reported that in locally advanced UC patients, molecular subtypes showed different clinical prognoses and clinical responses to the PD-L1 inhibitor atezolizumab (18–20). TCGA molecular subtypes showed different tumor cell (TC) PD-L1 expression and immune cell (IC) PD-L1 expression and different responses to atezolizumab (18, 19). In addition, Hodgson et al. suggested distinguishing luminal and basal subtypes of muscle-invasive urinary bladder UC (MIBC) using cytokeratin (CK) 5/6 and GATA3 IHC, and after such classification, the basal subtype showed a significant association with the abundance of CD8+ T cell expression and with high PD-L1 positivity identified by the SP263 assay (21).

Based on these findings, in this study, we classified MIBC into either BASQ or non-BASQ subtypes according to the expression profile of the CK5/6, CK14, GATA3, and FOXA1 and investigated PD-L1 expression in MIBC in BASQ and non-BASQ subtypes.

MATERIALS AND METHODS

Patients and Tissue Samples

In total, MIBC tissues were from 163 patients who underwent transurethral resection of the bladder and 42 patients who underwent cystectomy. 104 patients were retrieved from Seoul National University Hospital (SNUH), 101 patients from Seoul Metropolitan government-Seoul National University Boramae Medical Center between 2004 and 2010. Patients without prior history of preoperative treatment were selected, and only 166 pure UCs showing no specific differentiation or variant histology were included in the study. Clinicopathologic data, including histologic subtype, were collected by reviewing medical records. We reviewed hematoxylin and eosin (H&E)-stained slides to confirm the diagnosis and identify various pathologic parameters.

A tissue microarray (TMA) block was prepared from formalin-fixed paraffin-embedded tissue blocks (SuperBio-Chips Laboratories, Seoul, South Korea). Two cores (2 mm in diameter) containing the invasive tumor area were obtained from each patient.

This study was approved by the Institutional Review Board (IRB) of SNUH (IRB No H-1909-033-1062) and was performed in accordance with the principles of the Declaration of Helsinki. Informed consent was waived by the IRB.

Immunohistochemical Staining

For immunohistochemical analyses, the TMA blocks were cut at 4 μm thickness. All PD-L1 immunohistochemical staining was carried out on a Benchmark Ultra System (Ventana Medical Systems, Tucson, AZ). Clone SP142 (Ventana Medical Systems; retrieval: CC1 48′; incubation: 16′; RTU dilution) and clone SP263 [Ventana Medical Systems; retrieval: CC1 40′; incubation: 32′; ready to use (RTU) dilution] were used in accordance with the manufacturer's guidelines. The SP142 assay used tonsil tissue, and the SP263 assay used placenta tissue as control tissue. Two control tissues were used for each staining run, one as a positive control using an antibody reagent and one as a negative control using a negative reagent.

Additional immunohistochemical staining for CK5/6, CK14, GATA3, FOXA1, and CK20 was performed using a Ventana Benchmark XT automated staining system (Ventana Medical Systems). Mouse monoclonal antibodies against CK5/6 (1:100; D5/16 B4; Dako, Glostrup, Denmark), CK14 (1:300; LL002; Cell Marque, Rocklin, CA), GATA3 (1:500; L50-823; Cell Marque), FOXA1 (1:500; PA5-27157; Thermo Fisher, Waltham, MA), and CK20 (1:50; Ks 20.8; Dako) were used.

Immunohistochemical Scoring

PD-L1 expression of TC was evaluated based on the proportion of tumor cells exhibiting membranous staining of any intensity. PD-L1 expression of IC was evaluated based on the proportion of tumor-associated immune cells with membranous, cytoplasmic, or punctate staining at any intensity and the proportion of tumor area that was occupied by PD-L1 staining IC of any intensity. Each PD-L1 expression type was dichotomized as "positive" or "negative" according to the manufacturer's recommendations.

Cut-off criteria for PD-L1 expression positivity are summarized in **Table 1**. For CK5/6, CK14, and CK20, >20% expression was defined as positive expression status. 20% cut-off value was

reported in previous studies to be ideal for classification of molecular subtypes in bladder cancer (16, 21). So, we also applied the same criteria. GATA3 and FOXA1 were based on nuclear staining, and percentage of stained cells and staining intensity were also considered. Staining intensity was scored 0 to 3+ (0: no staining, 1+: weak staining, 2+: moderate staining, 3+: strong staining). 3+ staining intensity on more than 20% of tumor cells was defined as positive expression. The average of the two core values was evaluated as the final result.

We classified all cases as either BASQ or non-BASQ based on CK5/6, CK14, GATA3, and FOXA1 IHC expression. The BASQ subtype included cases with both positive CK5/6 and CK14 expression and both negative GATA3 and FOXA1 expression. The remaining cases were classified as non-BASQ subtype.

Two pathologists (BK and CL) evaluated the IHC staining at two different time points, without awareness of previous results at the second evaluation. The discrepant cases were evaluated by another pathologist (KM) for the final consensus results.

TABLE 1 | Positive criteria of PD-L1 assays.

	Cutoff for positivity
PD-L1 (SP142)	Presence of discernible PD-L1 staining of any intensity in tumor-infiltrating immune cells covering ≥ 5% of tumor area occupied by tumor cells, associated intratumoral, and contiguous peritumoral stroma
PD-L1 (SP263)	≥25% of tumor cells exhibit membrane staining; or, ICP > 1% and IC+ ≥ 25%; or, ICP = 1% and IC+ = 100%

IC+, Percentage of tumor-associated immune cells with staining; ICP, Percent of tumor area occupied by any tumor-associated immune cells.

TABLE 2 | Clinicopathologic characteristics of patients and association with BASQ classification.

	Non-BASQ N(%)	BASQ N(%)	Total	p value
Age (years)				
≤69	62 (42.5%)	12 (60.0%)	74	0.139
>69	84 (57.5%)	8 (40.0%)	92	
Gender				
Male	121 (82.9%)	18 (90.0%)	139	0.418*
Female	25 (17.1%)	2 (10.0%)	27	
Nuclear grade				
Low	6 (4.1%)	1 (5.0%)	7	0.853*
High	140 (95.9%)	19 (95.0%)	159	
T category				
T 2	132 (90.4%)	18 (90.0%)	150	0.953*
T 3–4	14 (9.6%)	2 (10.0%)	16	

**Fisher's exact test.*
BASQ, Basal-Squamous-like tumors.

Statistical Analysis

The concordance rate of PD-L1 expression between the SP142 assay and the SP263 assay was evaluated. Cohen's kappa coefficient of agreement was calculated: the level of concordance could be classified as poor (kappa = 0.00), slight (kappa = 0.00–0.20), fair (kappa = 0.21–0.40), moderate (kappa = 0.41–0.60), substantial (kappa = 0.61–0.80) or almost perfect (kappa = 0.81–1.00) (22). The association between PD-L1 expression and immunohistochemical results was evaluated by the chi-square test or Fisher's exact test. Statistical analyses were performed using SPSS software (version 23; IBM, Armonk, NY, USA). Two-sided p values of <0.05 were considered to be statistically significant.

RESULTS

Clinicopathologic Characteristics of Patients

Overall, 166 patients were included in this study, including 139 males and 27 females. The age at the time of diagnosis ranged from 37 to 87 years, with a mean age of 76 years. According to the 8th edition of the TNM staging system of the AJCC, 150 patients were in pT2, 10 patients were in pT3, and six patients in pT4. According to the WHO/ISUP grading system, seven cases were classified as low grade, and 159 cases as high grade. The association of BASQ classification with clinicopathologic characteristics was summarized in **Table 2**. The BASQ subtype was not correlated with old age (>69 years), gender, high WHO/ISUP grade, and high T category.

PD-L1 Assays

The results of the SP142 and SP263 assays are summarized in **Table 3**. The overall concordance rate for PD-L1 expression between SP 142 and SP 263 was 91.6% (152/166) (kappa = 0.732). The SP142 assay showed 15.1% (25/166) positivity at the IC 5% cut-off. The mean percentage of IC expression was 2.7% (range, 0–80), and the mean percentage of TC expression was 3.1% (range, 0–80). The SP263 assay showed 23.5% (39/166) positivity at the TC or IC 25% cut-off. When further subdivided, 11 cases met only the TC criteria, 10 cases met only the IC criteria, and 18 cases met both TC and IC criteria. The mean percentage of IC expression was 9.7% (range, 0–80), and the mean percentage of TC expression was 11.3% (range, 0–95). The union with either SP142 or SP263 assays of

TABLE 3 | Distribution of PD-L1 expression in MIBC.

PD-L1 assay	Positive cell	Positive rate					
		0%	1–4%	5–9%	10–24%	25–49%	50–100%
SP142	TC	119 (71.7%)	21 (12.7%)	9 (5.4%)	11 (6.6%)	4 (2.4%)	2 (1.2%)
	IC	88 (53.0%)	53 (32.0%)	11 (6.6%)	10 (6.0%)	2 (1.2%)	2 (1.2%)
SP263	TC	99 (59.6%)	22 (13.3%)	8 (4.8%)	8 (4.8%)	10 (6.0%)	19 (11.5%)
	IC	58 (34.9%)	41 (24.7%)	20 (12.0%)	19 (11.5%)	19 (11.5%)	9 (5.4%)

MIBC, Muscle-invasive urinary bladder urothelial cell carcinoma; TC, tumor cell; IC, immune cell.

TABLE 4 | PD-L1 assays values of the 39 positive results cases.

Positive cases No.	SP142			SP263		
	IC positive (%)	TC positive (%)	Result	IC positive (%)	TC positive (%)	Result
1	0	1	Neg	30	5	Pos
2	0	3	Neg	10	57.5	Pos
3	0	5	Neg	5	30	Pos
4	0.5	0	Neg	0	80	Pos
5	0.5	0	Neg	25	5	Pos
6	1	0	Neg	6	75	Pos
7	1	0	Neg	25	5	Pos
8	1	0	Neg	27.5	25	Pos
9	1	0	Neg	30	35	Pos
10	1	0	Neg	40	1	Pos
11	1	0	Neg	40	5	Pos
12	1	1	Neg	15	75	Pos
13	2	0	Neg	27.5	5	Pos
14	2.5	0.5	Neg	1	77.5	Pos
15	5	0	Pos	0	25	Pos
16	5	0	Pos	25	25	Pos
17	5	1	Pos	25	1	Pos
18	5	1	Pos	25	22.5	Pos
19	5	1	Pos	30	25	Pos
20	5	5	Pos	7.5	90	Pos
21	5	15	Pos	30	80	Pos
22	6	12.5	Pos	10	85	Pos
23	7.5	20	Pos	5	95	Pos
24	7.5	25	Pos	30	0	Pos
25	7.5	35	Pos	72.5	75	Pos
26	10	1	Pos	10	50	Pos
27	10	1	Pos	45	82.5	Pos
28	10	5	Pos	40	27.5	Pos
29	10	5	Pos	42.5	30	Pos
30	10	5	Pos	75	70	Pos
31	10	10	Pos	40	50	Pos
32	15	1	Pos	80	20	Pos
33	15	5	Pos	57.5	60	Pos
34	17.5	10	Pos	70	55	Pos
35	17.5	20	Pos	30	80	Pos
36	20	20	Pos	55	40	Pos
37	30	25	Pos	50	42.5	Pos
38	55	75	Pos	55	50	Pos
39	80	80	Pos	80	92.5	Pos

IC, immune cell; Neg, negative; No., number; Pos, positive; TC, tumor cell.

positive cases was 39 cases. The PD-L1 IHC expression values of the 39 positive results cases are summarized in **Table 4**. Among them, all 25 cases positive for the SP142 assay were also positive for the SP 263 assay, and 14 cases were positive for SP263 assay only. The SP263 assay showed higher PD-L1 expression than the SP142 assay in both tumor cells and immune cells.

Comparisons of PD-L1 IHC expression with the SP142 and SP263 assays between positive and negative groups classified according to CK5/6, CK14, GATA3, FOXA1 and CK20 expression levels are summarized in **Table 5**. High positivity in both the SP142 and SP263 assays was significantly correlated with positive CK5/6, positive CK14, negative GATA3, negative FOXA1 and negative CK20 expression.

PD-L1 Expression in BASQ or Non-BASQ Subtype

Classification according to CK5/6, CK14, GATA3 and FOXA1 IHC expression resulted in 12.0% (20/166) of samples being classified as the BASQ-subtype and 88.0% (146/166) of samples being classified as the non-BASQ subtype. High positivity in both the SP142 and SP263 assays was significantly correlated with the BASQ subtype ($p < 0.001$, both) (**Figure 1** and **Table 6**).

DISCUSSION

Great progress has been reported in research on the molecular classification of UC. Molecular classification of bladder cancer based on mRNA expression has been suggested by The Cancer Genome Atlas (10), the MD Anderson group (11), the University of North Carolina group (12), and the Lund Bladder Cancer Research group (17). Each group suggested different classifications, but the most basic classification scheme includes classification into basal and luminal subtypes. Additionally, IHC based classifications that reflect mRNA expression and are also easy and accessible in practical settings have been suggested. Dadhania et al. suggested IHC positivity for CK 5/6 and CK14 as basal subtype markers and IHC positivity of GATA3, CK20, and uroplakin as luminal subtype markers and suggested CK5/6 and GATA3 to be representative IHC markers (16). In

TABLE 5 | Relationship between PD-L1 positivity and CK5/6, CK14, GATA3, FOXA1, and CK20 expression.

		SP142			SP263		
		Neg (n = 80)	Pos (n = 24)	p	Neg (n = 75)	Pos (n = 28)	p
CK5/6	Neg	102 (72.3%)	5 (20.0%)	<0.001	99 (78.0%)	8 (20.5%)	<0.001
	Pos	39 (27.7%)	20 (80.0%)		28 (22.0%)	31 (79.5%)	
CK14	Neg	129 (91.5%)	15 (60.0%)	<0.001*	121 (95.3%)	23 (59.0%)	<0.001
	Pos	12 (8.5%)	10 (40.0%)		6 (4.7%)	16 (41.0%)	
GATA3	Neg	55 (39.0%)	19 (76.0%)	0.001	44 (34.6%)	30 (76.9%)	<0.001
	Pos	86 (61.0%)	6 (24.0%)		83 (65.4%)	9 (23.1%)	
FOXA1	Neg	81 (57.4%)	21 (84.0%)	0.012	69 (54.3%)	33 (84.6%)	0.001
	Pos	60 (42.6%)	4 (16.0%)		58 (45.7%)	6 (15.4%)	
CK20	Neg	67 (47.5%)	22 (88.0%)	<0.001	55 (43.3%)	34 (87.2%)	<0.001
	Pos	74 (52.5%)	3 (12.0%)		72 (56.7%)	5 (12.8%)	

**Fisher's exact test.*

CK, cytokeratin; Neg, negative; Pos, positive.

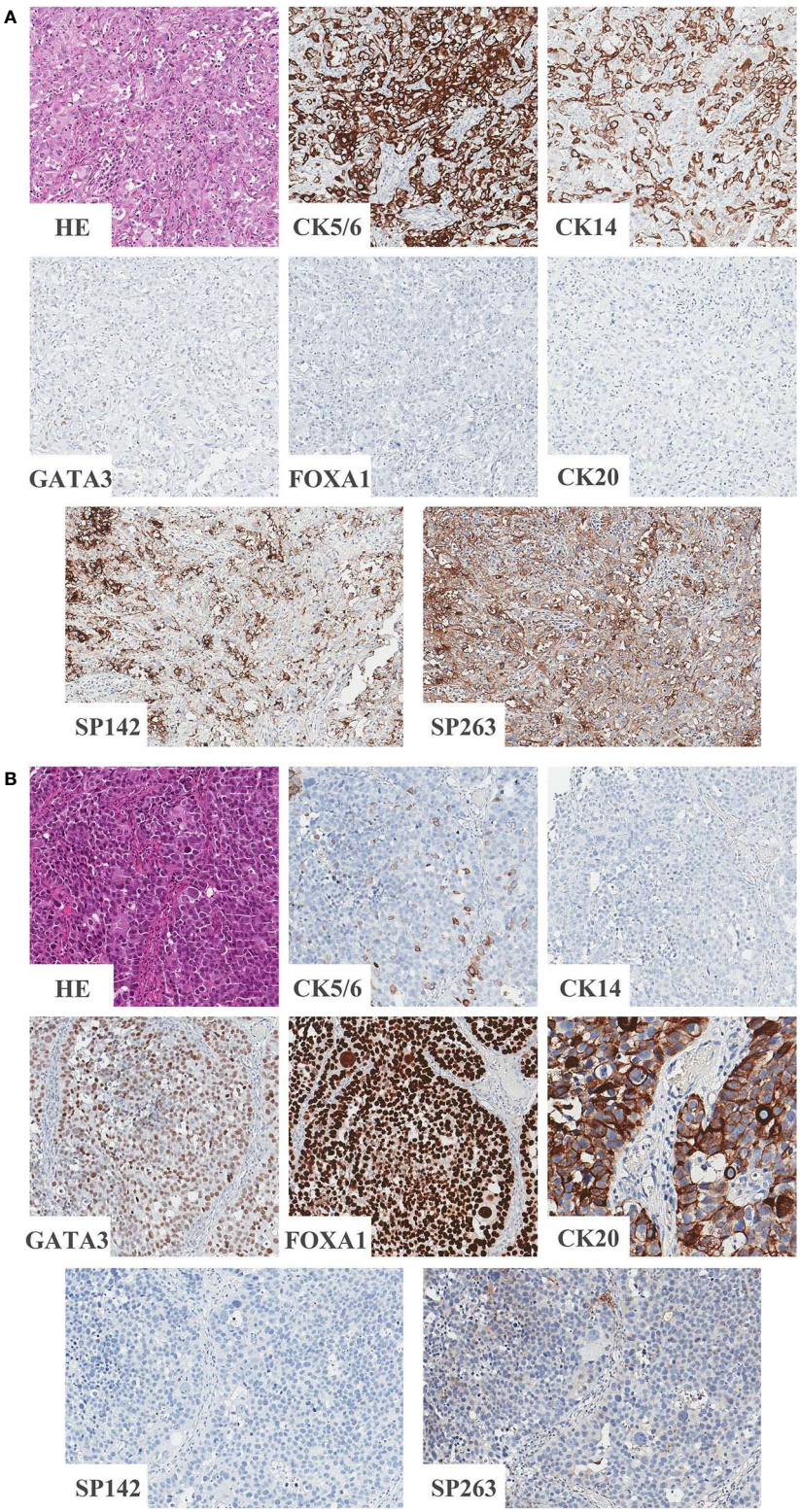

FIGURE 1 | Representative images of BASQ and non-BASQ subtype. **(A)** BASQ subtype is positive for CK5/6, CK14 and negative for GATA3, FOXA1, CK20. This subtype is highly correlated with positivity of PD-L1 assays (SP142 and SP263). **(B)** Non-BASQ subtype is negative for CK5/6, CK14 and positive for GATA3, FOXA1, CK20. PD-L1 assays (SP142, SP263) are negative.

TABLE 6 | Comparison of PD-L1 positivity and BASQ phenotype.

	SP142			SP263		
	Neg (n = 80)	Pos (n = 24)	p	Neg (n = 75)	Pos (n = 28)	p
Non-BASQ	131 (92.9%)	15 (60.0%)	<0.001*	123 (96.9%)	23 (59.0%)	<0.001*
BASQ	10 (7.1%)	10 (40.0%)		4 (3.1%)	16 (41.0%)	

Fisher's exact test.
BASQ, Basal-Squamous-like; Neg, negative; Pos, positive.

addition, Choi et al. suggested a BASQ subtype with the immunohistochemical expression pattern of CK5/6 (+), CK14 (+), GATA3 (−) and FOXA1 (−) (11).

Different molecular subtypes have been reported to have different prognoses and chemotherapy sensitivities. Additionally in phase II clinical trial of CheckMate, 275 different Nivolumab immunotherapy responses were reported among molecular subtypes in patients with metastatic UC, of which it was highest in the TCGA cluster III (23). Additionally, in a clinical trial using the SP142 assay, mRNA based TCGA clusters III and IV, which correspond to the basal type, showed highly enriched PD-L1 IC and TC expression, and TCGA cluster II, which corresponds to the luminal type, showed a significantly higher response to atezolizumab, a humanized monoclonal anti PD-L1 antibody, than clusters III and IV (18). Our present results showing high PD-L1 expression in BASQ subtype are in line with previous research.

In a previous study, Hodgson et al. suggested that MIBC could be classified into luminal and basal subtypes using CK5/6 and GATA3 IHC, and each subtype was analyzed for its PD-L1 SP263 expression and tumor infiltrating lymphocytes. The results showed that PD-L1 positivity was more common in the basal subtype and that CD8+ T cells and PD-1 expression were also significantly associated with the basal subtype (21).

In this study, we additionally analyzed the PD-L1 expression status using SP142 as well as SP263 in MIBC immunohistochemically defined molecular subtypes. We performed IHC with five antibodies to classify the BASQ subtype which was defined at a previous consensus meeting. We designated cases with positive CK5/6 and CK14 IHC expression and negative GATA3 and FOXA1 IHC expression as BASQ subtype. We evaluated PD-L1 expression using two PD-L1 assays (SP142 and SP263), and the overall concordance rate of PD-L1 positive status was substantial, in line with previous studies (24). We demonstrated that a high PD-L1 positive rate was significantly associated with the BASQ subtype. Furthermore, we demonstrated that a high PD-L1 positive rate was significantly associated with positive CK5/6 and CK14 expression and negative GATA3, FOXA1 and CK20 expression.

T lymphocytes eliminate tumor cells through immune surveillance using T cell receptor and major histocompatibility complex interaction. The interaction of PD-1 expressed in T lymphocyte with PD-L1 expressed in tumor cell leads to obstacles in immune regulation described above. PD-1/PD-L1 pathway is used by tumor cells as a method of immune evasion. But, PD-L1 expression on clinical prognosis is poorly defined in UC. Some studies have suggested that PD-L1 overexpression was correlated with poor prognosis in bladder cancer (25–27). On the other hand, some studies reported that PD-L1 expression has no correlation with clinical outcome in UC (28, 29).

The role of PD-L1 expression as a predictive biomarker also has many points to consider. There are clinical trial results that show that PD-L1 expression and response rate of PD-1/PD-L1 blockades are insufficiently related (30). However, currently, it is clear that PD-L1 expression is a companion or complementary diagnostic test of PD-1/PD-L1 blockades and a potential predictive biomarker. And it is generally accepted that PD-1/PD-L1 blockades has been known to have a higher efficacy in patients whose immune cells express PD-L1. The positive PD-L1 expression rate in BASQ and non-BASQ subtype UC can help to determine a treatment strategy in MIBC. Classification of MIBC according to the BASQ/non-BASQ classification could be suggested as a potential marker for PD-1/PD-L1 blockade treatment.

There are several limitations to this study. First, PD-L1 expression may show intratumoral heterogeneity. To compensate for this deficiency, two different tumor cores were used for each case, but there is a possibility that this result may not represent the overall tumor expression rate. Next, the cut-off value of the CK5/6, CK14, GATA3, and FOXA1 expression for BASQ classification has not been clearly established. For accurate analysis, we investigated various previous studies, identified cut-off values that were proved appropriate, and applied them to our study.

In conclusion, we demonstrated that BASQ subtype is highly associated with the positivity of the PD-L1 assays. To the best of our knowledge, our study is the first to analyze the association of immunohistochemically defined BASQ or non-BASQ subtype with two PD-L1 assays (SP142 and SP263) in MIBC. The significant difference of positive rate of PD-L1 assays according to BASQ classification suggests that BASQ classification may be important to apply the PD-1/PD-L1 blockade treatment in patients with MIBC.

DATA AVAILABILITY STATEMENT

The datasets generated for this study are available on request to the corresponding author.

ETHICS STATEMENT

The studies involving human participants were reviewed and approved by Institutional Review Board (IRB) of Seoul National University Hospital. Written informed consent for participation

was not required for this study in accordance with the national legislation and the institutional requirements.

AUTHOR CONTRIBUTIONS

CL and KM designed and performed the experiments. BK, CL, and YK analyzed the data. BK wrote the manuscript. KM supervised the entire process. All authors contributed to the article and approved the submitted version.

FUNDING

This research was supported by Basic Science Research Program through the National Research Foundation of Korea (NRF) funded by the Ministry of Education (2018R1D1A1B07045763).

REFERENCES

1. Bray F, Ferlay J, Soerjomataram I, Siegel RL, Torre LA, Jemal A. Global cancer statistics 2018: GLOBOCAN estimates of incidence and mortality worldwide for 36 cancers in 185 countries. *CA Cancer J Clin* (2018) 68:394–424. doi: 10.3322/caac.21492
2. Apolo AB, Infante JR, Balmanoukian A, Patel MR, Wang D, Kelly K, et al. Avelumab, an Anti-Programmed Death-Ligand 1 Antibody, In Patients With Refractory Metastatic Urothelial Carcinoma: Results From a Multicenter, Phase Ib Study. *J Clin Oncol* (2017) 35:2117–24. doi: 10.1200/JCO.2016.71.6795
3. Bellmunt J, Bajorin DF. Pembrolizumab for Advanced Urothelial Carcinoma. *N Engl J Med* (2017) 376:2304. doi: 10.1056/NEJMc1704612
4. Alhalabi O, Shah AY, Lemke EA, Gao J. Current and Future Landscape of Immune Checkpoint Inhibitors in Urothelial Cancer. *Oncol (Williston Park)* (2019) 33:11–8. doi: 10.1111/his.13696
5. Hodi FS, O'Day SJ, McDermott DF, Weber RW, Sosman JA, Haanen JB, et al. Improved survival with ipilimumab in patients with metastatic melanoma. *N Engl J Med* (2010) 363:711–23. doi: 10.1056/NEJMoa1003466
6. Ansell SM, Lesokhin AM, Borrello I, Halwani A, Scott EC, Gutierrez M, et al. PD-1 blockade with nivolumab in relapsed or refractory Hodgkin's lymphoma. *N Engl J Med* (2015) 372:311–9. doi: 10.1056/NEJMoa1411087
7. Nayak L, Iwamoto FM, LaCasce A, Mukundan S, Roemer MGM, Chapuy B, et al. PD-1 blockade with nivolumab in relapsed/refractory primary central nervous system and testicular lymphoma. *Blood* (2017) 129:3071–3. doi: 10.1182/blood-2017-01-764209
8. Garon EB, Rizvi NA, Hui R, Leighl N, Balmanoukian AS, Eder JP, et al. Pembrolizumab for the treatment of non-small-cell lung cancer. *N Engl J Med* (2015) 372:2018–28. doi: 10.1056/NEJMoa1501824
9. Aguiar PN Jr., Santoro IL, Tadokoro H, de Lima Lopes G, Filardi BA, Oliveira P, et al. The role of PD-L1 expression as a predictive biomarker in advanced non-small-cell lung cancer: a network meta-analysis. *Immunotherapy* (2016) 8:479–88. doi: 10.2217/imt-2015-0002
10. Cancer Genome Atlas Research N. Comprehensive molecular characterization of urothelial bladder carcinoma. *Nature* (2014) 507:315–22. doi: 10.1038/nature12965
11. Choi W, Porten S, Kim S, Willis D, Plimack ER, Hoffman-Censits J, et al. Identification of distinct basal and luminal subtypes of muscle-invasive bladder cancer with different sensitivities to frontline chemotherapy. *Cancer Cell* (2014) 25:152–65. doi: 10.1016/j.ccr.2014.01.009
12. Damrauer JS, Hoadley KA, Chism DD, Fan C, Tiganelli CJ, Wobker SE, et al. Intrinsic subtypes of high-grade bladder cancer reflect the hallmarks of breast cancer biology. *Proc Natl Acad Sci U.S.A.* (2014) 111:3110–5. doi: 10.1073/pnas.1318376111
13. Sjodahl G, Lauss M, Lovgren K, Chebil G, Gudjonsson S, Veerla S, et al. A molecular taxonomy for urothelial carcinoma. *Clin Cancer Res* (2012) 18:3377–86. doi: 10.1158/1078-0432.CCR-12-0077-T
14. Sjodahl G, Lovgren K, Lauss M, Patschan O, Gudjonsson S, Chebil G, et al. Toward a molecular pathologic classification of urothelial carcinoma. *Am J Pathol* (2013) 183:681–91. doi: 10.1016/j.ajpath.2013.05.013
15. Lerner SP, McConkey DJ, Hoadley KA, Chan KS, Kim WY, Radvanyi F, et al. Bladder Cancer Molecular Taxonomy: Summary from a Consensus Meeting. *Bladder Cancer* (2016) 2:37–47. doi: 10.3233/BLC-150037
16. Dadhania V, Zhang M, Zhang L, Bondaruk J, Majewski T, Siefker-Radtke A, et al. Meta-Analysis of the Luminal and Basal Subtypes of Bladder Cancer and the Identification of Signature Immunohistochemical Markers for Clinical Use. *EBioMedicine* (2016) 12:105–17. doi: 10.1016/j.ebiom.2016.08.036
17. Sjodahl G, Eriksson P, Liedberg F, Hoglund M. Molecular classification of urothelial carcinoma: global mRNA classification versus tumour-cell phenotype classification. *J Pathol* (2017) 242:113–25. doi: 10.1002/path.4886
18. Rosenberg JE, Hoffman-Censits J, Powles T, van der Heijden MS, Balar AV, Necchi A, et al. Atezolizumab in patients with locally advanced and metastatic urothelial carcinoma who have progressed following treatment with platinum-based chemotherapy: a single-arm, multicentre, phase 2 trial. *Lancet* (2016) 387:1909–20. doi: 10.1016/S0140-6736(16)00561-4
19. Kim J, Kwiatkowski D, McConkey DJ, Meeks JJ, Freeman SS, Bellmunt J, et al. The Cancer Genome Atlas Expression Subtypes Stratify Response to Checkpoint Inhibition in Advanced Urothelial Cancer and Identify a Subset of Patients with High Survival Probability. *Eur Urol* (2019) 75:961–4. doi: 10.1016/j.eururo.2019.02.017
20. Tan TZ, Rouanne M, Tan KT, Huang RY, Thiery JP. Molecular Subtypes of Urothelial Bladder Cancer: Results from a Meta-cohort Analysis of 2411 Tumors. *Eur Urol* (2019) 75:423–32. doi: 10.1016/j.eururo.2018.08.027
21. Hodgson A, Liu SK, Vesprini D, Xu B, Downes MR. Basal-subtype bladder tumours show a 'hot' immunophenotype. *Histopathology* (2018) 73:748–57. doi: 10.1111/his.13696
22. Kundel HL, Polansky M. Measurement of observer agreement. *Radiology* (2003) 228:303–8. doi: 10.1148/radiol.2282011860
23. Sharma P, Retz M, Siefker-Radtke A, Baron A, Necchi A, Bedke J, et al. Nivolumab in metastatic urothelial carcinoma after platinum therapy (CheckMate 275): a multicentre, single-arm, phase 2 trial. *Lancet Oncol* (2017) 18:312–22. doi: 10.1016/S1470-2045(17)30065-7
24. Rijnders M, van der Veldt AAM, Zuiverloon TCM, Grunberg K, Thunnissen E, de Wit R, et al. PD-L1 Antibody Comparison in Urothelial Carcinoma. *Eur Urol* (2019) 75:538–40. doi: 10.1016/j.eururo.2018.11.002
25. Ding X, Chen Q, Yang Z, Li J, Zhan H, Lu N, et al. Clinicopathological and prognostic value of PD-L1 in urothelial carcinoma: a meta-analysis. *Cancer Manag Res* (2019) 11:4171–84. doi: 10.2147/CMAR.S176937
26. Zhu L, Sun J, Wang L, Li Z, Wang L, Li Z. Prognostic and Clinicopathological Significance of PD-L1 in Patients With Bladder Cancer: A Meta-Analysis. *Front Pharmacol* (2019) 10:962:962. doi: 10.3389/fphar.2019.00962
27. Wang B, Pan W, Yang M, Yang W, He W, Chen X, et al. Programmed death ligand-1 is associated with tumor infiltrating lymphocytes and poorer survival in urothelial cell carcinoma of the bladder. *Cancer Sci* (2019) 110:489–98. doi: 10.1111/cas.13887
28. Faraj SF, Munari E, Guner G, Taube J, Anders R, Hicks J, et al. Assessment of tumoral PD-L1 expression and intratumoral CD8+ T cells in urothelial carcinoma. *Urology* (2015) 85:703 e1–6. doi: 10.1016/j.urology.2014.10.020
29. Bellmunt J, Mullane SA, Werner L, Fay AP, Callea M, Leow JJ, et al. Association of PD-L1 expression on tumor-infiltrating mononuclear cells and overall survival in patients with urothelial carcinoma. *Ann Oncol* (2015) 26:812–7. doi: 10.1093/annonc/mdv009
30. Aggen DH, Drake CG. Biomarkers for immunotherapy in bladder cancer: a moving target. *J Immunother Cancer* (2017) 5:94. doi: 10.1186/s40425-017-0299-1

Conflict of Interest: The authors declare that the research was conducted in the absence of any commercial or financial relationships that could be construed as a potential conflict of interest.

Advantages of publishing in Frontiers

OPEN ACCESS
Articles are free to read for greatest visibility and readership

FAST PUBLICATION
Around 90 days from submission to decision

HIGH QUALITY PEER-REVIEW
Rigorous, collaborative, and constructive peer-review

TRANSPARENT PEER-REVIEW
Editors and reviewers acknowledged by name on published articles

Frontiers
Avenue du Tribunal-Fédéral 34
1005 Lausanne | Switzerland

Visit us: www.frontiersin.org
Contact us: frontiersin.org/about/contact

REPRODUCIBILITY OF RESEARCH
Support open data and methods to enhance research reproducibility

DIGITAL PUBLISHING
Articles designed for optimal readership across devices

FOLLOW US
@frontiersin

IMPACT METRICS
Advanced article metrics track visibility across digital media

EXTENSIVE PROMOTION
Marketing and promotion of impactful research

LOOP RESEARCH NETWORK
Our network increases your article's readership